NASA/TM–2020–5003178

Investigation of a Tandem Tilt-wing VTOL Aircraft in the NASA Langley 12-Foot Low-Speed Tunnel

Steven C. Geuther, David D. North and Ronald C. Busan
Langley Research Center, Hampton, Virginia

June 2020

NASA STI Program. . . in Profile

Since its founding, NASA has been dedicated to the advancement of aeronautics and space science. The NASA scientific and technical information (STI) program plays a key part in helping NASA maintain this important role.

The NASA STI Program operates under the auspices of the Agency Chief Information Officer. It collects, organizes, provides for archiving, and disseminates NASA's STI. The NASA STI Program provides access to the NASA Aeronautics and Space Database and its public interface, the NASA Technical Report Server, thus providing one of the largest collection of aeronautical and space science STI in the world. Results are published in both non-NASA channels and by NASA in the NASA STI Report Series, which includes the following report types:

- TECHNICAL PUBLICATION. Reports of completed research or a major significant phase of research that present the results of NASA programs and include extensive data or theoretical analysis. Includes compilations of significant scientific and technical data and information deemed to be of continuing reference value. NASA counterpart of peer-reviewed formal professional papers, but having less stringent limitations on manuscript length and extent of graphic presentations.
- TECHNICAL MEMORANDUM. Scientific and technical findings that are preliminary or of specialized interest, e.g., quick release reports, working papers, and bibliographies that contain minimal annotation. Does not contain extensive analysis.
- CONTRACTOR REPORT. Scientific and technical findings by NASA-sponsored contractors and grantees.
- CONFERENCE PUBLICATION. Collected papers from scientific and technical conferences, symposia, seminars, or other meetings sponsored or co-sponsored by NASA.
- SPECIAL PUBLICATION. Scientific, technical, or historical information from NASA programs, projects, and missions, often concerned with subjects having substantial public interest.
- TECHNICAL TRANSLATION. English-language translations of foreign scientific and technical material pertinent to NASA's mission.

Specialized services also include organizing and publishing research results, distributing specialized research announcements and feeds, providing information desk and personal search support, and enabling data exchange services.

For more information about the NASA STI Program, see the following:

- Access the NASA STI program home page at `http://www.sti.nasa.gov`
- E-mail your question to `help@sti.nasa.gov`
- Phone the NASA STI Information Desk at 757-864-9658
- Write to:
  NASA STI Information Desk
  Mail Stop 148
  NASA Langley Research Center
  Hampton, VA 23681-2199

NASA/TM–2020–5003178

Investigation of a Tandem Tilt-wing VTOL Aircraft in the NASA Langley 12-Foot Low-Speed Tunnel

Steven C. Geuther, David D. North and Ronald C. Busan
Langley Research Center, Hampton, Virginia

National Aeronautics and
Space Administration

June 2020

Acknowledgments

This work was funded by NASA's Aeronautics Research Mission Directorate (ARMD) under the Transformative Aeronautics Concepts Program. In particular, this research was part of the Convergent Aeronautics Solutions (CAS) and Transformational Tools and Technologies (TTT) Projects. The authors thank the Flight Dynamics Branch at NASA Langley Research Center for the operation of the 12 Foot Low-Speed Tunnel and discussions throughout the testing. The authors thank NASA for their support of the LA-8.

Available from:

NASA STI Program / Mail Stop 148
NASA Langley Research Center
Hampton, VA 23681-2199
Fax: 757-864-6500

Abstract

The emerging Urban Air Mobility market imposes new design requirements on aircraft, including the ability to have vertical take-off and landing (VTOL) capabilities with the ability to transition into fast and efficient forward flight. Industry has proposed many different vehicle configurations, which have many different challenges. A primary challenge facing many of these concepts is flight through the transition corridor from vertical to horizontal flight and back. In an effort to better understand and help improve vehicle safety in the complex transition corridors, NASA Langley Research Center has proposed to characterize the transition corridor with wind tunnel and flight tests for a variety of unmanned aircraft system sized VTOL configurations. The first vehicle of this series is the Langley Aerodrome 8 (LA-8). LA-8 is a high-risk/high-reward tandem tilt-wing vehicle with distributed electric propulsion and a partially deflected slipstream aircraft. The LA-8 vehicle has gone through a preliminary wind tunnel test in NASA Langley's 12-Foot Low-Speed Wind Tunnel. The results of the aerodynamic data collected, including the longitudinal, lateral, and directional force and moment aerodynamic coefficients, from these tests during different phases of flight are presented.

Contents

List of Figures

List of Tables

Nomenclature

α	Angle of Attack, deg
β	Angle of Sideslip, deg
ρ	Density, slug/ft^3
b	Wing Span, ft
c	Wing Chord, ft
C_D	Drag Coefficient, Axial Force/Q*S
C_D	Thrust Coefficient, Axial Force/ρ*n^2*D^4
C_{l_β}	Variation of Rolling-moment Coefficient with Sideslip Angle, C_l per deg
C_L	Lift Coefficient, Normal Force/Q*S
C_l	Rolling-moment Coefficient, Rolling Moment/Q*S*b
C_m	Pitching-moment Coefficient, Pitching Moment/Q*S*b
C_{n_β}	Variation of Yawing-moment Coefficient with Sideslip Angle, C_n per deg
C_n	Yawing-moment Coefficient, Yawing Moment/Q*S*b
CG	Center of Gravity
D	Propeller Diameter, ft
DEP	Distributed Electric Propulsion
DOE	Design of Experiments
ESC	Electronic Speed Controller
LA-8	Langley Aerodrome 8
n	Propeller Speed, Rev/s
PWM	Pulse Width Modulation
Q	Free-stream Dynamic Pressure, lb/ft^2
S	Wing area, ft^2
TED	Trailing Edge Down
TEI	Trailing Edge In
TEO	Trailing Edge Out
TEU	Trailing Edge Up

UAM Urban Air Mobility

UAS Unmanned Aircraft System

$VTOL$ Vertical Takeoff and Landing

1 Introduction

The Langley Aerodrome 8 (LA-8) unmanned aircraft system (UAS) is the first in a planned series of electric vertical takeoff and landing (VTOL) high-risk/high-reward testbeds from NASA Langley Research Center to support Urban Air Mobility (UAM) research [1]. Because of the large number of control features inherent to VTOL aircraft and the interaction of the propulsion system with aerodynamic surfaces in distributed electric propulsion (DEP) designs, there are a corresponding large number of unknowns in the performance and control characteristics of these vehicles. These unknowns are often difficult to model and analyze with current techniques. In an effort to assist industry in both the development of aircraft configurations and validation of tools for unconventional aircraft, NASA has developed the capability to rapidly produce electric VTOL wind tunnel and flight models to gather the data necessary to characterize these vehicles. The first wind tunnel test of LA-8 is described in this report, with additional configurations of the vehicle and subsequent wind tunnel tests planned to be performed at a later date. The wind tunnel data and experimentation in this first test helps inform upcoming wind tunnel test limits and best practices. In addition, this initial wind tunnel test provides information on characterizing the vehicle in order to understand the control power and stability to prepare for flight testing. With this data, conceptual design tools can be validated for complex configurations, including post-stall conditions and blown wings for DEP aircraft. Finally, the wind tunnel test data provides insight into the stability and performance of LA-8 in order to inform design iterations or modifications prior to a second wind tunnel entry.

2 Langley Aerodrome 8 Configuration Description

Langley Aerodrome 8 is a tandem tilt-wing UAS with DEP that can be utilized as a wind tunnel model and free flight testbed. The LA-8 is not a scale model of a full scale UAM concept. However, non-dimensional scaling laws can be used for prediction of the behavior of larger scale, similar vehicles. The vehicle can be seen in Figure 1. The LA-8 geometry, build characteristics, and development can be found in Reference [2]. For all data presented in this report, the reference center of gravity (CG) of the wind tunnel model remains constant at a location of 1.9 feet aft of (positive x-direction) the nose of the fuselage and 0.65 feet vertically (positive z-direction) from the waterline of the nose of the aircraft. This CG location is the analytically determined CG for static stability in forward flight in all three axes. The vehicle has two rotatable wings, eight propellers and motors, four single-slotted Fowler flaps, four hinged elevons, and two hinged ruddervators. The top view of the vehicle with all of the controllable features, except for ruddervators, can be seen in Figure 2. The elevons and flaps are approximately drawn to scale. Throughout this paper, the referencing of each controllable feature will be identical to the numbering in Figure 2. Additionally, the numbering convention for the ruddervators is identical, where ruddervator 1, which can be seen in Figure 3, is located on the left side of the vehicle under wing 2. Ruddervator 2 is located on the right side in a similar manner for symmetry. Additionally, in Figures 4 and 5 the LA-8 can be seen in its hovering mode configuration.

Figure 1. LA-8 UAS in the 12-foot low-speed tunnel.

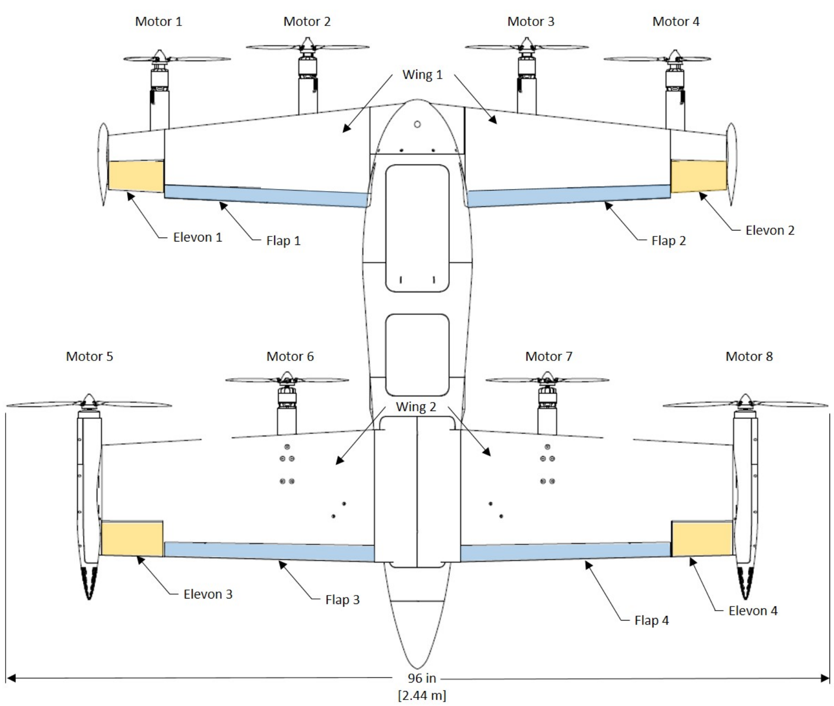

Figure 2. LA-8 top view, forward flight mode configuration.

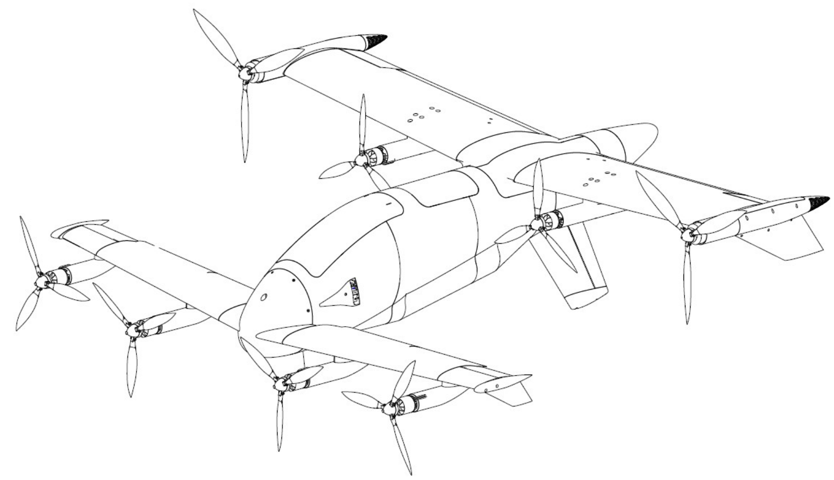

Figure 3. LA-8 isometric view, forward flight mode configuration.

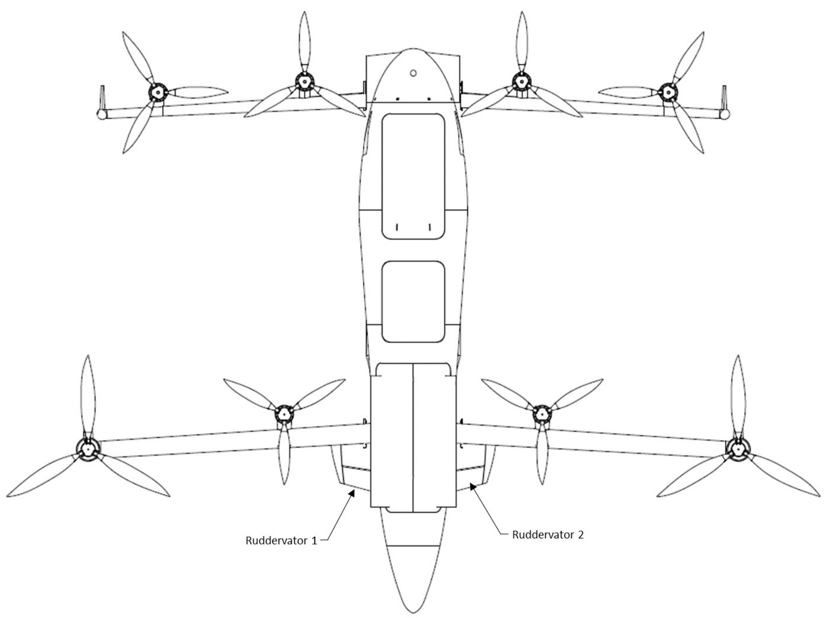

Figure 4. LA-8 top view, hover mode configuration.

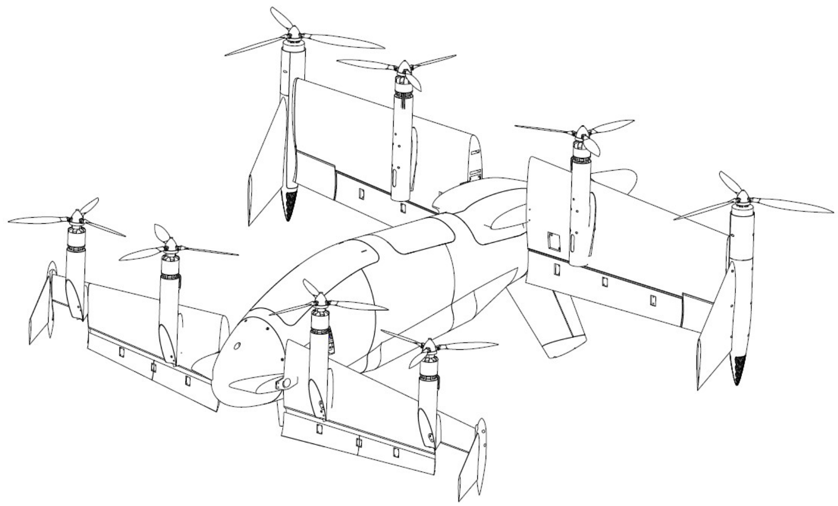

Figure 5. LA-8 isometric view, hover mode configuration.

All propellers on the vehicle are 3-bladed. Propellers on motors 5 and 8 are 21.5 inch diameter with a 7.5 inch pitch and were purchased through commercial vendors. These two propellers were implemented to solely propel the vehicle in the cruise configuration. The motors used in conjunction with these propellers were commercially available 220 KV brushless motors. The remaining propellers are 16 inch diameter with an 8 inch pitch (16x8). These propellers could only be procured in the clockwise (aft looking forward) configuration. Custom propellers, which are geometrically mirrored versions of the clockwise propellers, were designed and manufactured for the counter-clockwise propellers. Motors 1-4, 6, and 7, which have the 16x8 propellers, are commercially available 450 KV brushless motors. For this wind tunnel test, motors 1, 2, 5, and 6 used counter-clockwise propellers and motors 3, 4, 7, and 8 used clockwise propellers. In order to maintain proper and consistent terminology of the wing reference and vehicle reference, both wing angles are specified by a wing incidence or wing angle taxonomy, while the vehicle will use angle of attack, α, which is referenced from the waterline of the nose of the fuselage. The sideslip angle, β, is referenced from the symmetry plane of the vehicle. For all wings, flaps, and elevons, the sign convention for deflections is trailing edge up (TEU) as negative and trailing edge down (TED) as positive. Due to the construction of the wings and flaps, these surfaces will not exhibit a TEU. At zero degrees, the wings are positioned into forward flight conditions, and at approximately 90 degrees incidence angle the wings are in hover conditions. The ruddervators follow the convention of trailing edge in (TEI) and trailing edge out (TEO), which indicates the direction of the trailing edge compared to the symmetry plane of the aircraft. Therefore, the ruddervators are in positive deflection when they are TEI and negative for TEO.

For this aircraft and due to the design of the single-slotted Fowler flaps, flaps are not used for control of the vehicle. The convention of controlling the aircraft in the hover configuration with wing incidence angles at approximately 90 degrees is done by traditional means. In order to roll the vehicle, differential thrust is used on the left and right side of the vehicle. Yaw control utilizes differential elevons and ruddervators on the left and right side of the vehicle as well as differential thrust on the clockwise and counterclockwise rotating propellers. The vehicle has the ability to use either differential thrust on the front and back wing or the ruddervators in unison to produce a pitching moment in hover. In forward flight, the vehicle utilizes differential elevon on the left and right side of the vehicle to roll. To pitch the vehicle in forward flight, differential elevons and thrust between the front and aft wing along with ruddervators are used. Finally, yaw control uses left and right differential ruddervator and thrust inputs. All transition points and wing angles in between 0 and 90 degrees utilize a mixing of the control effectors based upon the percentage of the transition in order to control the vehicle.

3 NASA Langley 12-Foot Low-Speed Tunnel Test Setup

The Langley 12-Foot Low-Speed Tunnel (12-ft LST) is an atmospheric pressure, open circuit tunnel enclosed in a 60-foot diameter sphere (Figures 6 and 7) [3]. The test section is octagonal with a width and height of 12 feet and a length of 15 feet with each octagonal side measuring 5 feet. The maximum operating dynamic pressure (Q) is seven pounds per square foot (psf) (V=77 ft/sec at standard sea level conditions), which corresponds to a Reynolds number of approximately 492,000 per foot. However, for the LA-8 tests the dynamic pressure was limited to 6 psf to keep the tunnel's main fan motor heating within bounds for the longer runs. The longitudinal center-line-flow in the test section has a turbulence level of about 0.6 percent. Test section airflow is produced by a 15.8 ft diameter, 6-blade drive fan powered by a 280 HP, 600 volt, 600 RPM DC motor which is controlled by a 500 HP AC motor that drives a field controlled generator.

The size of the model was limited to an 8 foot span, as measured from left propeller tip to right propeller tip, to avoid blockage issues in the 12-Foot Low-Speed Tunnel. Electrical power, at 32 volts, was supplied to the model through electrical lines attached to the tunnel sting. Power was supplied to the eight motor electronic speed controllers (ESCs) at that voltage. Additional voltage regulators within the model supplied power to the twelve model servos, control board, and data recording systems. Motor ESCs and servos were sent pulse width modulation (PWM) commands from an Arduino Mega microcontroller within the model, which were connected via Ethernet to a computer in the control room. The motor RPM values were recorded from each ESC using a Teensy microcontroller board. The tunnel sting mechanism can move the model in both the pitch (α) and yaw (β) planes. In total, there were 23 control parameters for testing (α, β, Q, 12 servo signals, and 8 motor signals).

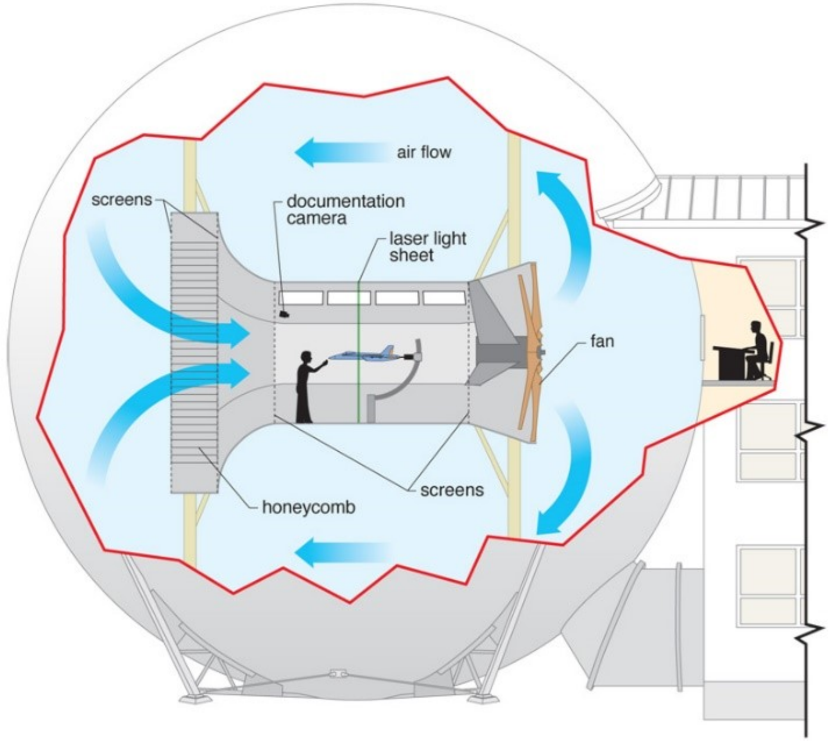

Figure 6. NASA Langley 12-foot low-speed tunnel cutaway.

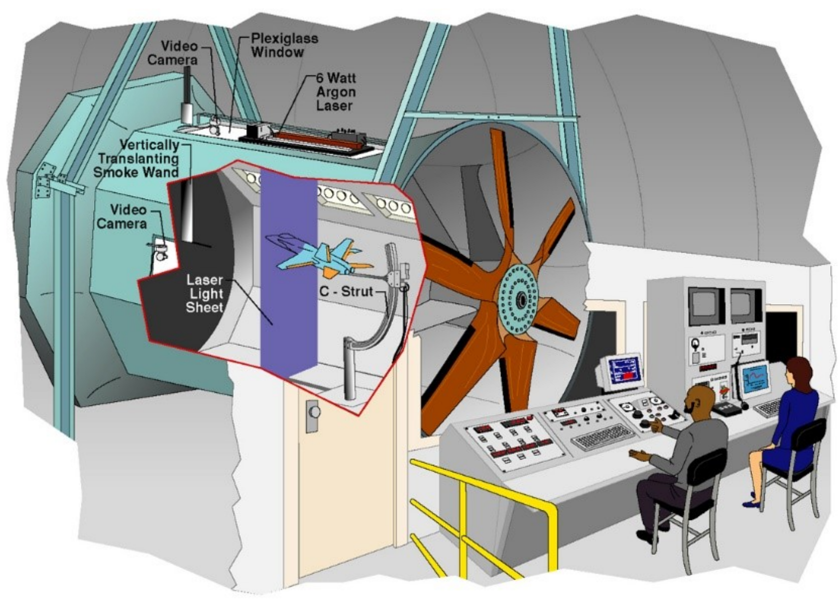

Figure 7. NASA Langley 12-foot low-speed tunnel view of tunnel and control room.

The model balance measured forces in the X, Y, and Z directions and measures torques around the same three axes. The balance is limited to normal forces of

400 lb and axial and side forces of 200 lb. Pitch and yaw moments are limited to 2000 lb-inch and roll moments to 1248 lb-inch. With this balance, the associated resolutions are 0.48 lb for normal force, 0.20 lb for axial force, 0.32 lb for side force, 2.40 lb-inch for pitching moment, 2.46 lb-inch for rolling moment, and 2.00 lb-inch for yawing moment all with a 95% confidence. The maximum balance loads set constraints on model operating conditions, such as high wing angles with high dynamic pressures. Non-flight mounting hardware was used to mount the balance. The additional mounting structure allowed the transfer of model loads through the balance to a "dog leg" sting, which exited through a clearance hole in the bottom of the model and can be seen in Figure 8. The sting positioning mechanism allows rotation of the model in both the longitudinal and lateral planes.

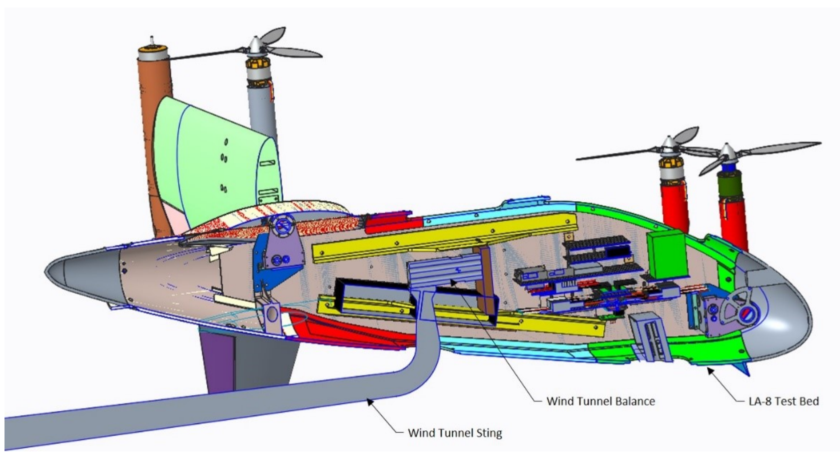

Figure 8. Model balance and sting arrangement.

The tunnel data recording system in the control room records all model command signals (20 total), tunnel dynamic pressure, alpha, beta, and balance force and moments. Wind tunnel dynamic pressure is set manually and all other model control parameters can be set up to run a series of model settings automatically from a spreadsheet. Data is recorded automatically at each test point after a five second period for model movement and two seconds of flow settling.

4 Langley Aerodrome 8 Wind Tunnel Tests

In order to characterize the vehicle performance and stability, the wind tunnel test matrix was split up into 4 main sections. The first section included test points with the propellers removed from the vehicle in order to examine the airframe aerodynamics independently from the propulsion system. The propellers were then installed on the vehicle and the next three sections used propulsion to achieve hover, transition, and forward flight conditions. For all of these tests, the vehicle went through a tare run to remove the change in moments and forces from the shifting of the CG while varying wing and control surface angles.

4.1 Airframe Performance and Stability

With the propellers removed from the vehicle, the test matrix investigated controllability and stability using control surface deflections with both wings in the forward flight configuration. LA-8 has a nominal 3.5 degrees incidence on the root of wing 1 and 1 degree incidence on the root of wing 2 when the vehicle fuselage angle of attack is at zero degrees. Additionally, both wings have a 2 degree washout at the tips. However, when the vehicle's wing angles are physically at these incidence angles, the angles are referenced as an angle of "zero" in all plots. Vehicle fuselage angle is measured from the flat portion of the fuselage just forward of wing 2. The vehicle design creates a vertical spacing of 12 inches between wing 1 and wing 2 in forward flight. The test matrix also included several angle of attack sweeps at different dynamic pressures and sideslip angles. Finally, the transition corridor was investigated by preforming an incidence angle sweep on both wings at the same time. This data allows for a better understanding of non-propulsive flight. In addition, this set of testing benefits tool validation for basic aerodynamics and performance. The results from this test block can be seen in Section 5.1.

4.2 Hover Performance and Stability

In order to determine the hover performance and stability of LA-8, the wing angle and motor RPM had to be determined. For hover performance and stability, where dynamic pressure is zero, angle of attack is used to describe the fuselage angle relative to the ground. In these discovery runs, both wing 1 and wing 2 were set to equal incidence angles. Initially, all motors and propellers were set to an approximately equal thrust output in order to find an acceptable wing angle, where net axial force is approximately equal to zero. Next, the constraint of normal force equal to model weight was examined in order to determine the average propeller thrust combination for the specific wing angles. Finally, the average thrust on each wing was varied, while maintaining the total average thrust on the aircraft, to provide differential thrust in order to satisfy a requirement of zero pitching moment. The tests resulted in an aircraft where lift was approximately equal to the estimate flight weight of the vehicle (60 lbs), the thrust of the propellers was approximately equal to the drag of the vehicle, and the pitching moment coefficient was approximately zero at a fuselage angle between zero and 2 degrees for a specific dynamic pressure. In addition, the thrust from all of the propellers were approximately equal. This configuration of the vehicle is referred to as the hover trim point. After these vehicle settings were determined, control power, performance and stability of the vehicle were measured by varying angle of attack, sideslip angle, and control surface deflections in a dynamic pressure of zero. The results of the performance and stability after determining the hover trim point are presented in Section 5.2.

4.3 Transition Performance and Stability

Similar to the hover trim points, the investigatory tests were performed for the transition corridor to determine the correct trim RPMs of forward motors (1-4) relative to rear motors (5-8). A number of wing angle settings were investigated to characterize the transition corridor. It was assumed that wing incidence angles above 60 degrees were considered a hover condition due to the dominance in propulsion control and, therefore, were not investigated. Fourteen transition trim points were investigated in this wind tunnel test including and between 56 and 14 degrees incidence angle on the wings. Each transition trim point maintained the requirements of lift approximately equal to weight, thrust approximately equal to drag, and C_m equal to zero with all propellers on a given wing providing approximately equal thrust. (The differential between the wing 1 and wing 2 total thrusts was adjusted to achieve C_m equal to zero.) As previously stated, wing 1 and wing 2 incidence angles remain equal throughout the transition. During these tests, the dynamic pressure was estimated for each of the transition trim points based upon the expected flight speed at that transition point. After the transition trim points were determined for the respective dynamic pressures, angle of attack and sideslip sweeps, and control surface deflections were performed. The performance and stability results of the transition trim points can be seen in Section 5.3.

4.4 Forward Flight Performance and Stability

Incidence angles below 14 degrees on both wings were considered to be within the forward flight regime. Therefore, the next wing angle settings would be the forward flight trim point. The tunnel was briefly taken to a dynamic pressure of 6 psf and an exploratory test was performed to assure the vehicle could maintain level flight at the predicted required cruise speed. However, a comprehensive investigation of forward flight trim points could not be performed due to wind tunnel motor overheating concerns at that dynamic pressure. Therefore, a full investigation was performed at a dynamic pressure of 4 psf. This exploration at a lower dynamic pressure is considered the forward flight trim point for this report. It should be noted that in order to achieve the necessary constraints of lift approximately equal to weight and drag equal to thrust with minimal pitching moment, the dynamic pressure needs to be above the tunnel limitations. The actual cruise Reynolds number is approximately 550,000, while the testing of the vehicle is at a Reynolds number of approximately 425,000, with respect to the aft wing. Also, due to limitations on the balance, angles of attack in stall and post-stall conditions could not be explored. For completeness of the control power, stability, and performance investigation, the vehicle performed control surface deflections, angle of attack and sideslip sweeps at the lower dynamic pressure. The results of this test are presented in Section 5.4.

5 Wind Tunnel Test Results

In these wind tunnel tests, a single force balance was used as described in Section 3. The forces and moments were used to calculate the coefficients that are presented in this section. The use of DEP, custom built propellers, and two differently sized propellers prevented non-dimensional coefficient derivation for individual propellers. The thrust or axial force measured by the balance uses all force components in the x-axis. Therefore at different wing incidence angles, angles of attack, and side slip angles, the axial force is a component of the wing lift from the freestream velocity (i.e. induced drag), thrust from the propeller, and blowing of the wing from the propeller, which creates difficulty in determining the contribution of each force with a single force balance. In subsections 5.2-5.4, the RPMs for each motor and propeller combination at all wing incidence angles will be provided for the trimmed configuration due to this complexity. For each plot, if the vehicle attitude is not being varied, the vehicle angle is zero degrees.

For the control surfaces, standard airplane convention was used. When looking at maximum control authority with the elevons only, there is a differential elevon deflection input (left elevons and right elevons go in opposite directions) in order to create maximum rolling capability, which is typically done in a fixed wing aircraft. Similarly for ruddervators, maximum yawing capability was determined using the opposite deflection angle on each ruddervator. Finally, symmetric elevon and ruddervator deflections were used to investigate maximum pitching capability. The x-axes on each plot determine the combination and type of control surface deflections being tested. If ruddervator is the only control surface shown, the ruddervators are being deflected for a yawing moment (in forward flight) and the elevons are neutral. This is the same case for the elevons and rolling moment. Finally, some plots will show both elevon (on the lower x-axis) and ruddervator (on the upper x-axis) control surfaces in order to showcase pitching moment ability. However, it should be noted, as the angle of the wings increase or decrease, the axis of importance changes and there will be coupling between all axes. Therefore, lateral, longitudinal, and directional plots will be shown for all wing angles. If the control surface (ruddervator, elevon, or flap) is not being deflected in the results, the surface is set to nominal zero degrees. This was performed at an angle of attack of zero degrees , negative six degrees, and positive six degrees. Both the nominal control power with deflecting the control surfaces at zero degrees angle of attack and the maximum control delta through the range of angles of attack is presented in this paper. Maximum control delta is defined as the change in moment or moment coefficient with a maximum control surface deflection angle and of a minimum control surface deflection angle (e.g. [C_m with -25 degrees elevon deflection] - [C_m with +25 degrees elevon deflection]). The maximum control delta is plotted versus angle of attack to show the influence of angle of attack and control power.

5.1 Airframe Performance and Stability

In Appendix A, a full set of plots referencing only the airframe testing can be seen. The plots include the coefficients of lift, drag, pitching moment, rolling moment with sideslip angle and yawing moment with sideslip angle (C_L, C_D, C_m, C_{l_β}, C_{n_β}) vs angle of attack at different dynamic pressures. This study was performed to check for data consistency. The C_L is investigated to determine the stall characteristics of the vehicle. The C_L vs angle of attack curves in Figure 9 indicate that there is a soft stall at approximately 15 degrees angle of attack and then a second stall at approximately 25 degrees. Figure 10 shows consistent C_D values throughout the dynamic pressures. Due to the design of LA-8 using a tandem wing, wing 1 stalls first at 15 degree angle of attack and then wing 2 at 25 degrees. It is known that the first wing stalls by referencing the large pitch down moment at 15 degrees angle of attack and then a pitch break for the second stall at approximately 25 degrees angle of attack as seen in Figure 11. The stability of the vehicle in the lateral, longitudinal, and directional directions are all examined. Figure 11 indicates a negative slope for pitching moment, however, the trim point of the vehicle approaches -20 degrees angle of attack. In terms of lateral and directional stability, the format of these plots include C_{n_β} vs α and C_{l_β} vs α which follows the format for future work in order to contribute to handling qualities similar to Reference [4]. The C_{l_β} values that are negative prove a stable aircraft laterally for a range of angles of attacks up to the second stall point as seen in Figure 12. Similarly, positive C_{n_β} values indicate a stable aircraft directionally for a range of angles of attack. Nearing 10 degrees angle of attack, the aircraft begins to approach directional instability as seen in Figure 13. The remainder of the plots in Appendix A show the control power of each control surface (with and without flap deflections) and performance and stability for a variation of wing angles between zero and 50 degrees. When there is an indicated flap deflection in the airframe performance plot, all flaps are being actuated identically on both wings. The wing variation assumes that wing 1 and wing 2 are at the same incidence angle.

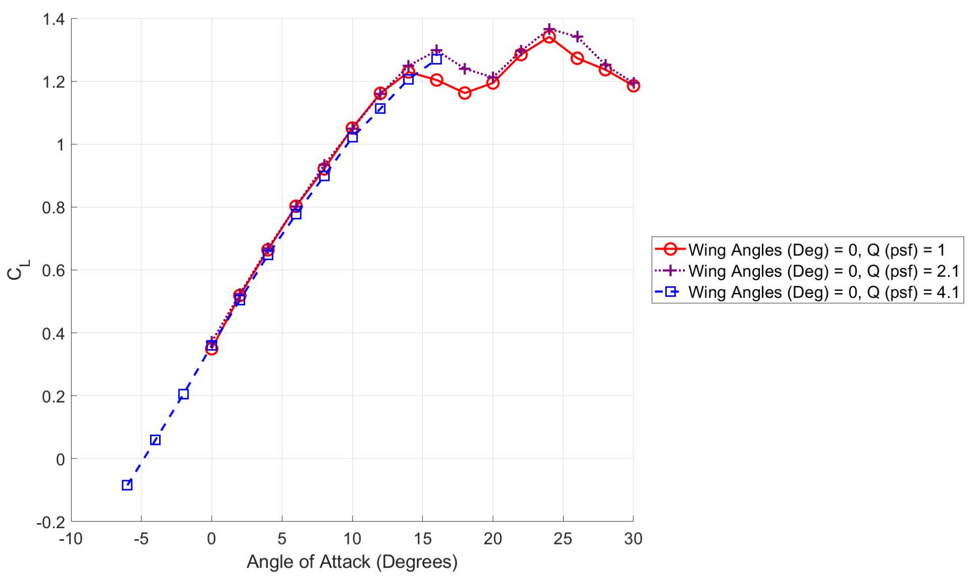

Figure 9. Propellers off C_L vs angle of attack.

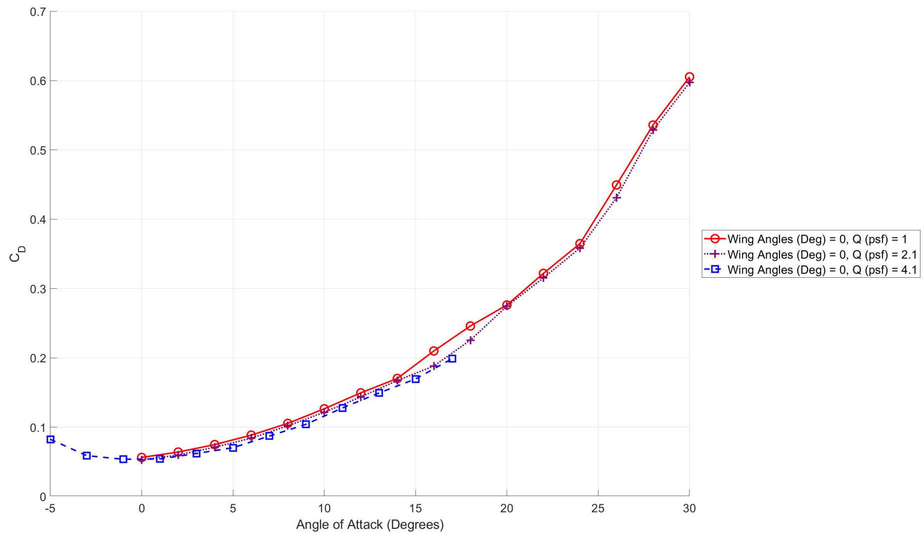

Figure 10. Propellers off C_D vs angle of attack.

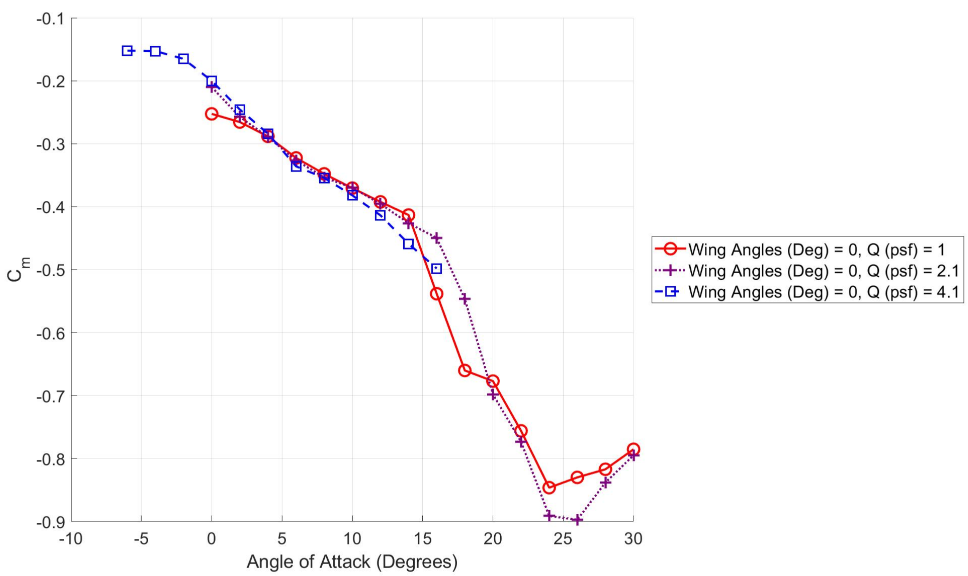

Figure 11. Propellers off C_m vs angle of attack.

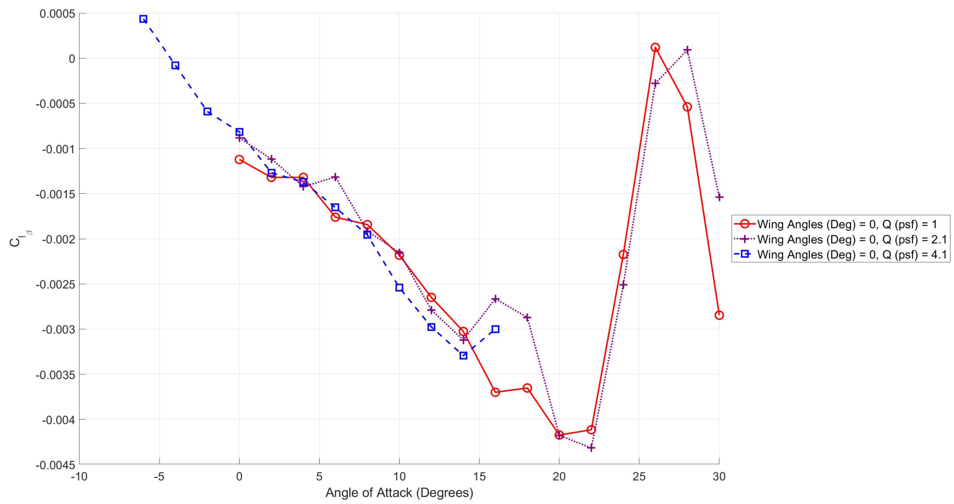

Figure 12. Propellers off C_{l_β} vs angle of attack with Q variation.

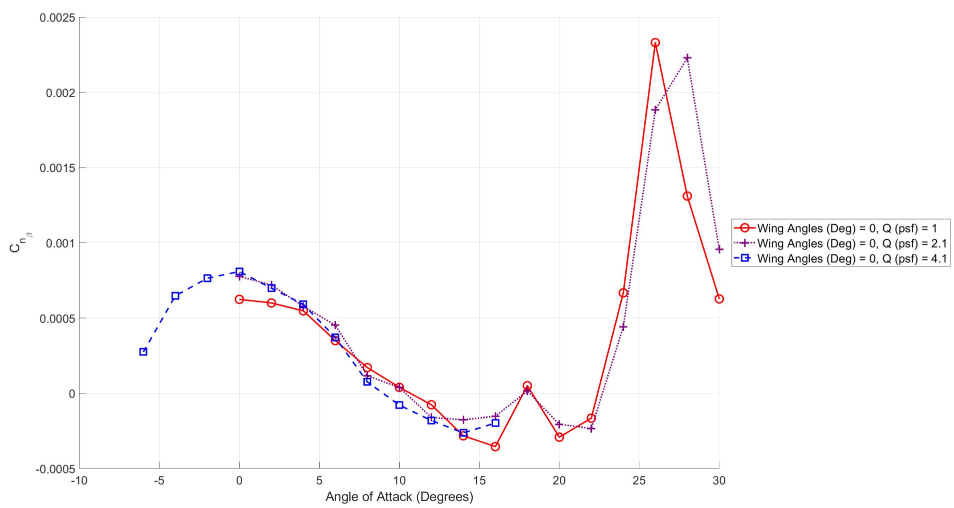

Figure 13. Propellers off C_{n_β} vs angle of attack with Q variation.

In addition to gathering data based upon the current design, flight conditions were considered including a non-propulsive landing. In this case, the intent was being able to correct the C_m vs angle of attack to have a reasonable trim point by either using flaps or by trimming one wing to a different incidence angle for a given CG. A CG shift was also considered, with the knowledge that the CG will be shifting forward approximately 1.5 inches during the full transition from hover to forward flight from the rotation of the wings and motors with the actual flight model. Using the front wing to trim the aircraft, the wing 1 incidence angle would need to be set to approximately 10 degrees. The results of this investigation can be seen in Figure 14. Changing the wing 1 incidence angle can be used in extreme conditions, but should not be used for any non-propulsive flight due to the proximity to the stall point, which can be seen in the extreme pitching moment change in the figure. A more appropriate approach would be to use flaps 1 and 2 or a combination of wing incidence angle and flaps.

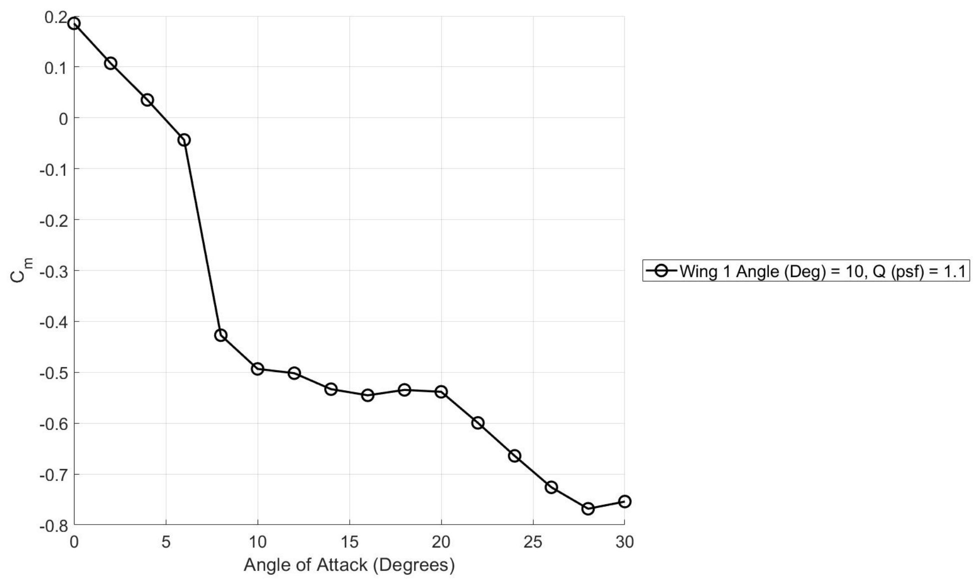

Figure 14. Propellers off C_m vs angle of attack with wing 1 incidence at 10 degrees.

5.2 Hover Performance and Stability

At the hover trim point, the dynamic pressure is set to zero for the wind tunnel. Both wing incidence angles and RPMs were varied until the conditions explained in subsection 4.2 were met. The resultant RPMs can be seen in Table 1 for wing incidence angles of 82 and zero degrees angle of attack. Due to the propulsion dominated configuration, the hover static stability criteria were loosely defined with knowledge that a flight controller would typically be used for active stability control, similar to a multirotor. The main driving constraints were providing a configuration that met the approximately 60 lb normal force with no forward or backwards movement (i.e. axial force on the balance equals zero). Results are shown in Figures 15 and 16. The y-axis scales on both figures are finely numerated and may mislead results, however, these results show that there was an approximately constant normal and axial force on the model through the range of angles of attack. It is important to note that the y-axis on all plots in the hover section use forces and moments instead of aerodynamic coefficients due to the dynamic pressure of zero psf. The aerodynamic coefficient values are computed from the balance force and moments due to a single force balance and therefore cannot be calculated for a dynamic pressure of zero psf. The full performance, stability, and control power during this mode of flight is presented in Appendix B. The control surface deflection figures are all performed at an angle of attack of zero degrees.

Table 1. Hover Trim Motor RPMs at 0 Degrees Angle of Attack

	Dynamic Pressure (psf)	Motor 1 RPM	Motor 2 RPM	Motor 3 RPM	Motor 4 RPM
Hover Trim	0	6111	5841.69	6026.31	5969.63
	Dynamic Pressure (psf)	**Motor 5 RPM**	**Motor 6 RPM**	**Motor 7 RPM**	**Motor 8 RPM**
Hover Trim	0	3004	6381.25	5976.88	3112.25

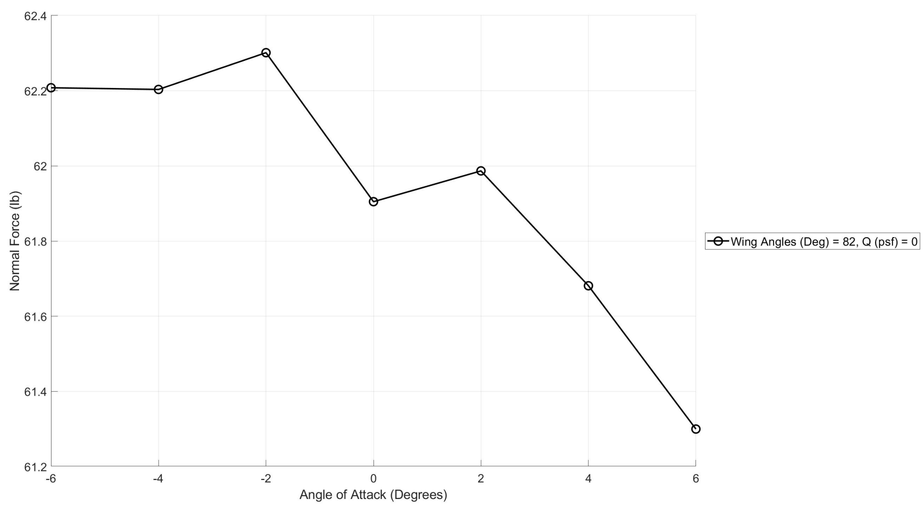

Figure 15. Hover trim point normal force vs angle of attack.

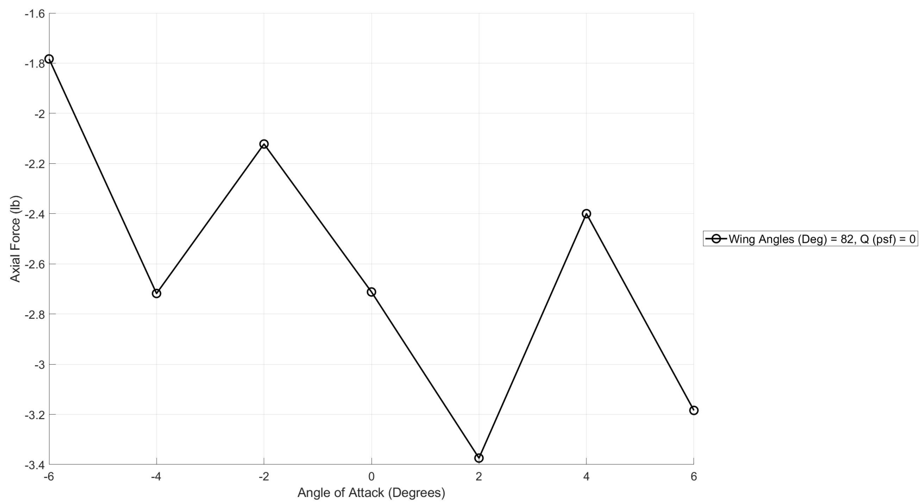

Figure 16. Hover trim point axial force vs angle of attack.

5.3 Transition Performance and Stability

In this section, figures are presented with multiple wing incidence angles for easy trend comparison. Appendix C includes additional wing incidence angles individually for more resolution on the data. Table 2 lists motor RPMs for all 14 trim combinations of wing incidence angles and dynamic pressures that are presented in Appendix C and this section. The summary results of performance and stability, shown in this section in Figures 17 - 39, show the general trend of performance and stability throughout the transition corridor. In general, the plots show that throughout the transition corridor, the aircraft maintains lateral, longitudinal, and directional stability. There is a small instability at high wing incidence angles for lateral stability, where the propellers have a significant influence on the roll of the vehicle. As explained prior in subsection 5.2, the C_L values that are provided at high wing incidence angles utilize the normal force to calculate the aerodynamic coefficient due to a single force balance. Therefore, at 56 degrees wing incidence angle, the vehicle has a large C_L, which is mostly contributed by the thrust of the propellers. The same coefficient plots for an α of zero degrees were performed by deflecting the control surface in order to achieve a specific command on the vehicle, as discussed earlier in Section 5, and to investigate the control surface influence and determine the control power throughout the transition corridor. Finally, the trends of the maximum control surface deflections show the influence of angle of attack on the control power in each axis in Figures 40 - 48.

Table 2. Transition Trim Motors RPMs at 0 Degrees Angle of Attack

	Dynamic Pressure (psf)	Motor 1 RPM	Motor 2 RPM	Motor 3 RPM	Motor 4 RPM
56° Incidence Trim	0.5	5184.94	4889.69	5170.94	5118.62
51° Incidence Trim	0.75	5190.12	4898.12	5181.38	5129.38
47° Incidence Trim	1.0	5042.25	4750.56	5025.5	4986.31
43° Incidence Trim	1.25	4975.5	4675.75	4926	4902.19
38° Incidence Trim	1.5	4847.75	4526.69	4768.81	4765.94
35° Incidence Trim	1.75	4818.69	4490.62	4733.94	4730.56
32° Incidence Trim	2.0	4820.38	4496.44	4742.81	4739.75
30° Incidence Trim	2.25	4699.25	4377.38	4630	4635.31
27° Incidence Trim	2.5	4700.69	4365.19	4613.12	4630
23° Incidence Trim	2.75	4716.31	4374.06	4625	4643.19
21° Incidence Trim	3.0	4638.19	4292.94	4543.75	4564.31
18° Incidence Trim	3.25	4673	4324.25	4571	4594.69
16° Incidence Trim	3.5	4723.31	4394.62	4628.06	4662.81
14° Incidence Trim	4.0	4876	4532.69	4772.06	4796.62

	Dynamic Pressure (psf)	Motor 5 RPM	Motor 6 RPM	Motor 7 RPM	Motor 8 RPM
56° Incidence Trim	0.5	2712.62	5712.69	5402.88	2798.44
51° Incidence Trim	0.75	2680.94	5619.56	5315.88	2749.06
47° Incidence Trim	1.0	2569.25	5342.31	5085.19	2653.56
43° Incidence Trim	1.25	2547.75	5259.31	5005.62	2627.87
38° Incidence Trim	1.5	2530.94	5158.44	4919.5	2608.38
35° Incidence Trim	1.75	2532.31	5090.81	4855.88	2609.75
32° Incidence Trim	2.0	2564.12	5048.44	4822.06	2630.81
30° Incidence Trim	2.25	2638.94	4993.19	4776.69	2693.62
27° Incidence Trim	2.5	2722.06	4601.19	4397.37	2749
23° Incidence Trim	2.75	2873.56	4474.69	4242.06	2900.25
21° Incidence Trim	3.0	2977.25	4349.38	4052.94	2999.81
18° Incidence Trim	3.25	3111.44	4442.5	4092.31	3134.56
16° Incidence Trim	3.5	3165	4492.94	4129.81	3193.06
14° Incidence Trim	4.0	3403.12	4782.56	4406	3412.5

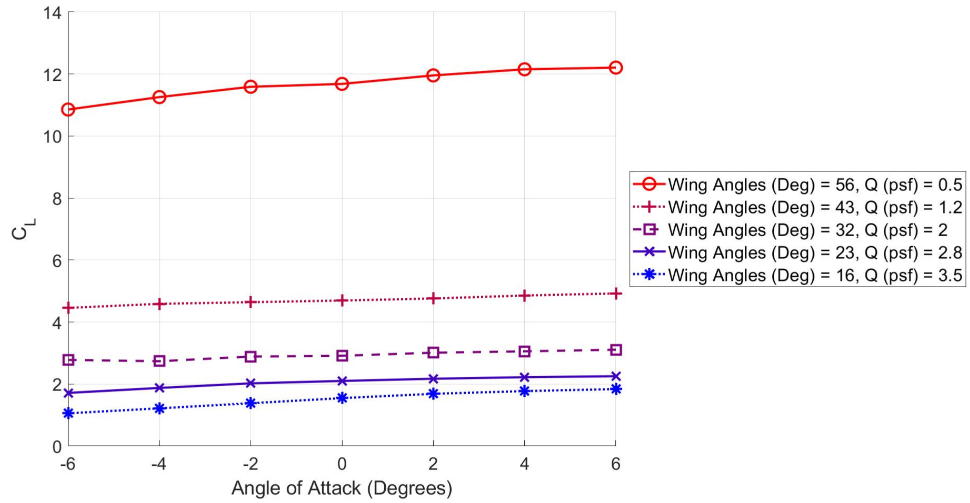

Figure 17. Trimmed wing sweep C_L vs angle of attack.

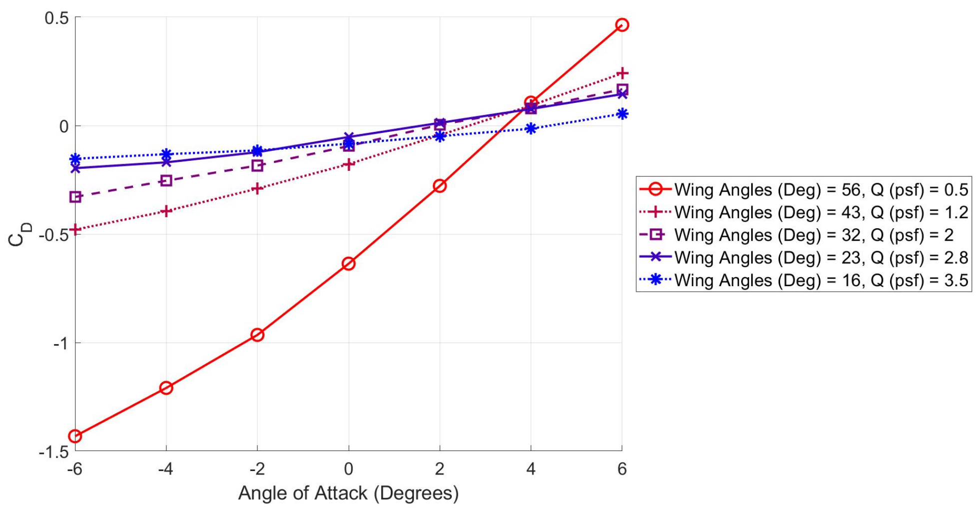

Figure 18. Trimmed wing sweep C_D vs angle of attack.

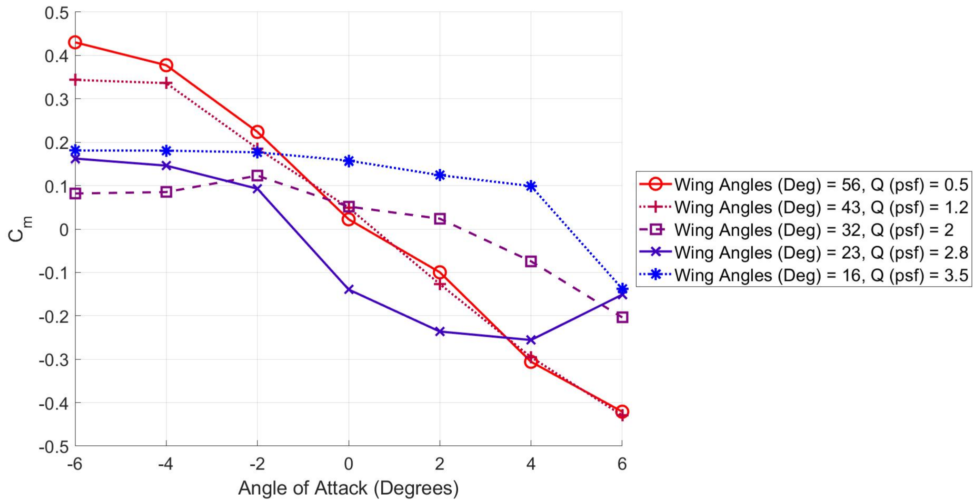

Figure 19. Trimmed wing sweep C_m vs angle of attack.

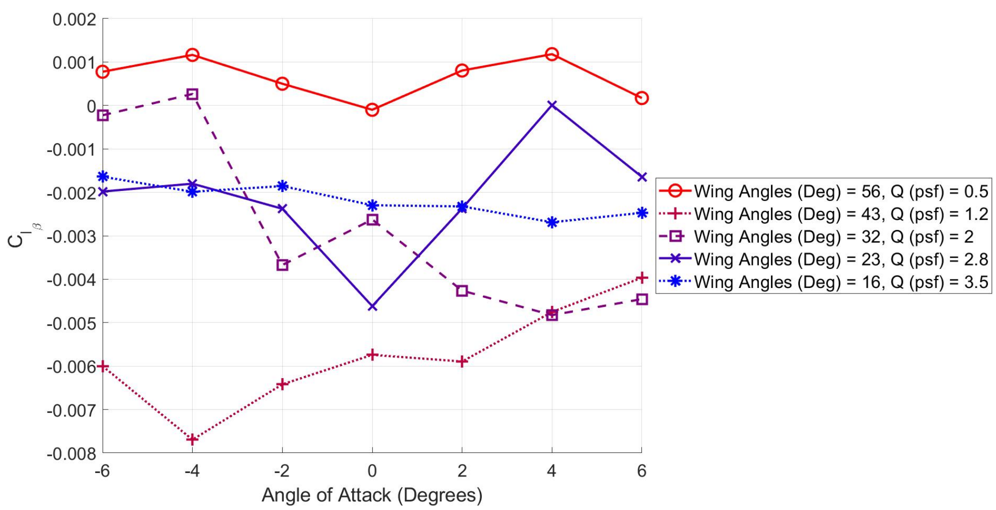

Figure 20. Trimmed wing sweep C_{l_β} vs angle of attack.

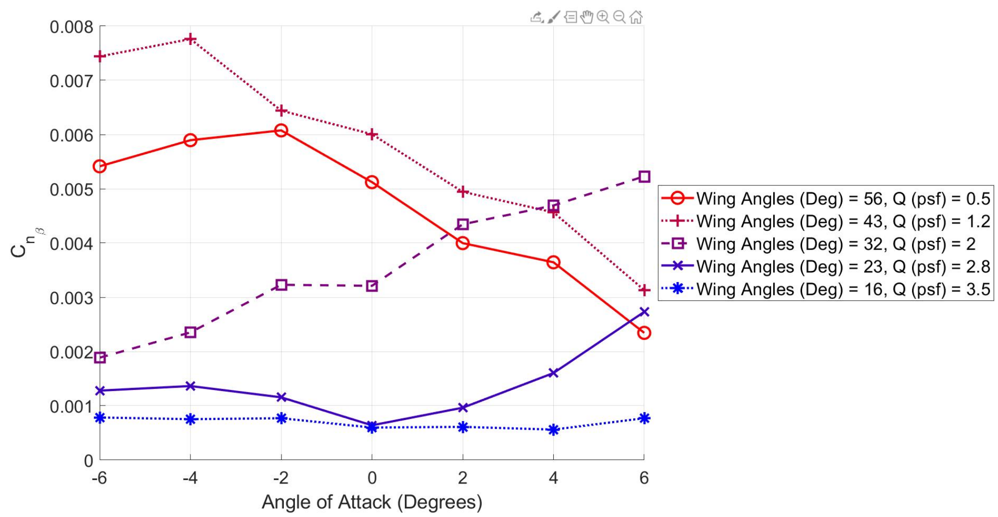

Figure 21. Trimmed wing sweep C_{n_β} vs angle of attack.

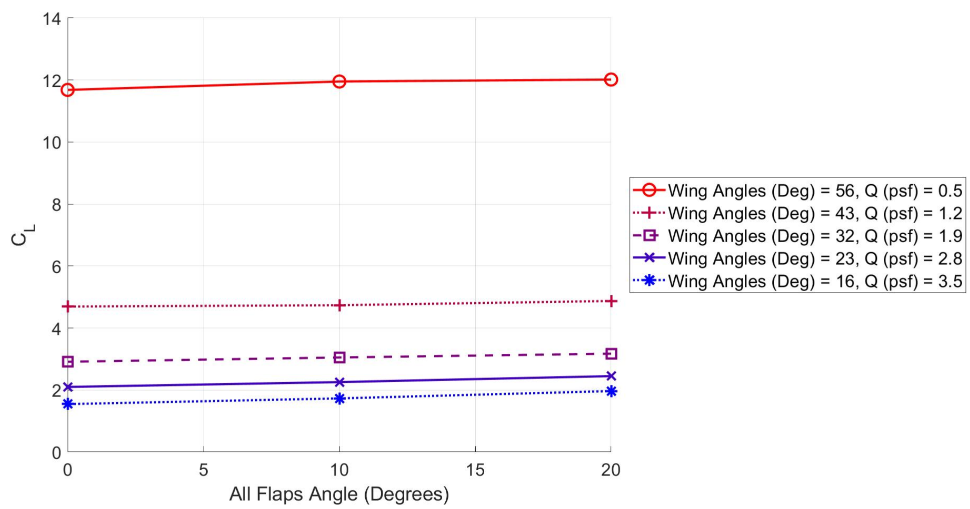

Figure 22. Trimmed wing sweep C_L vs all flap deflection angle.

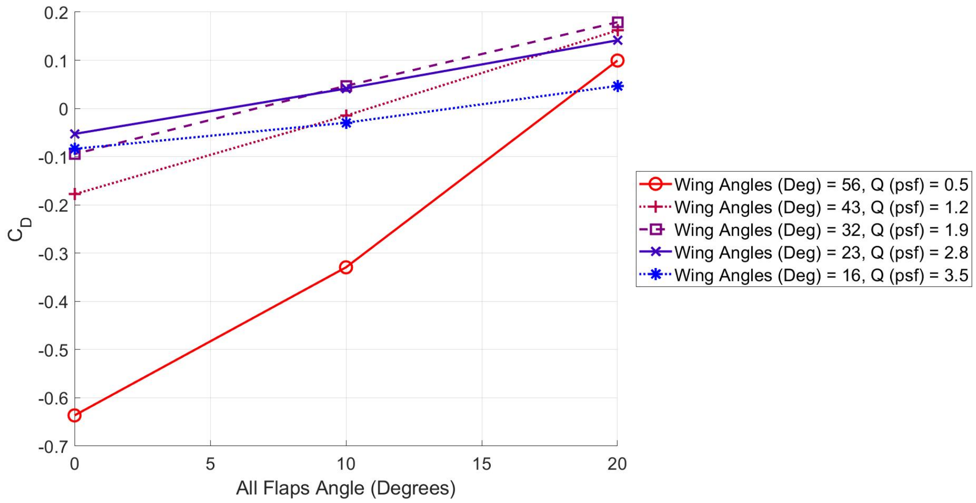

Figure 23. Trimmed wing sweep C_D vs all flap deflection angle.

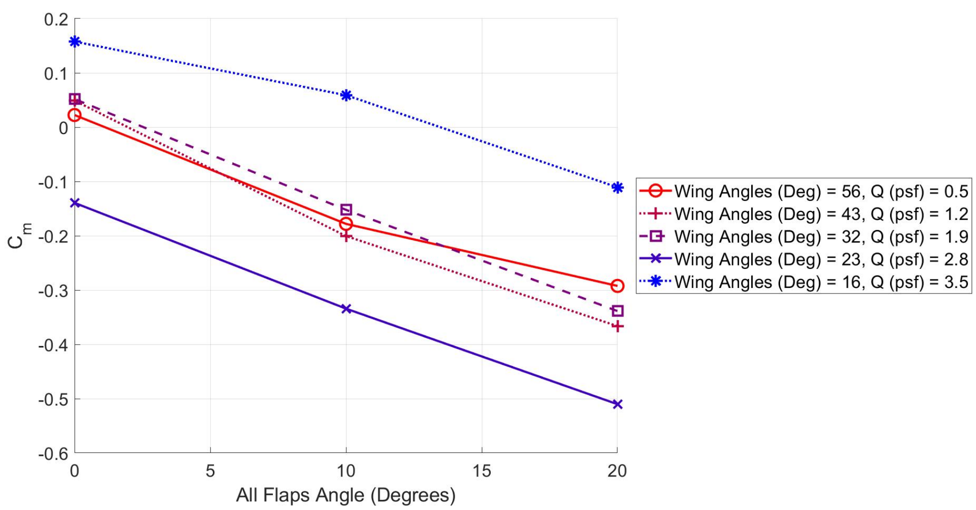

Figure 24. Trimmed wing sweep C_m vs all flap deflection angle.

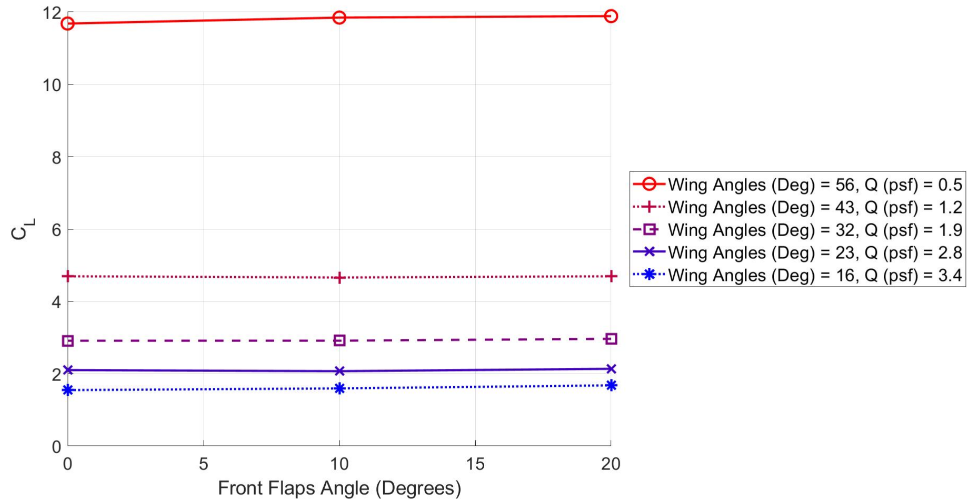

Figure 25. Trimmed wing sweep C_L vs front flap deflection angle.

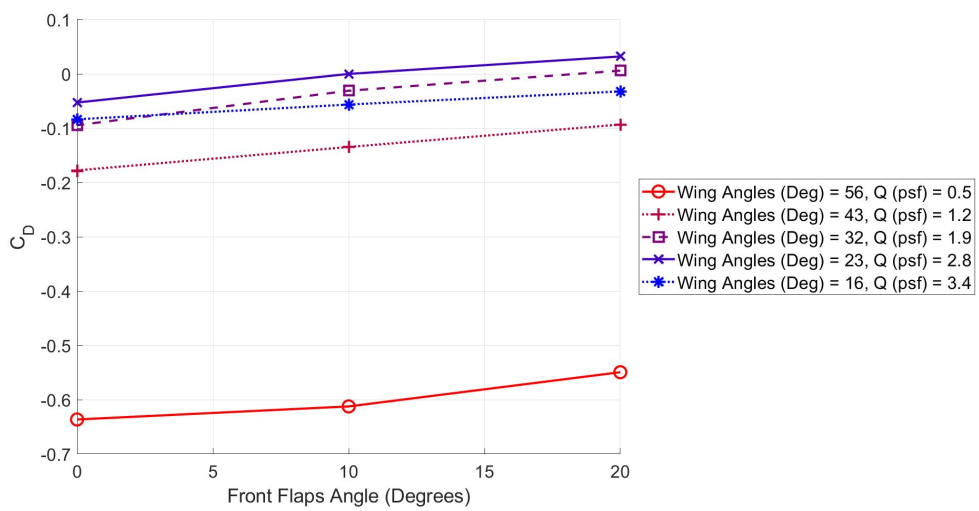

Figure 26. Trimmed wing sweep C_D vs front flap deflection angle.

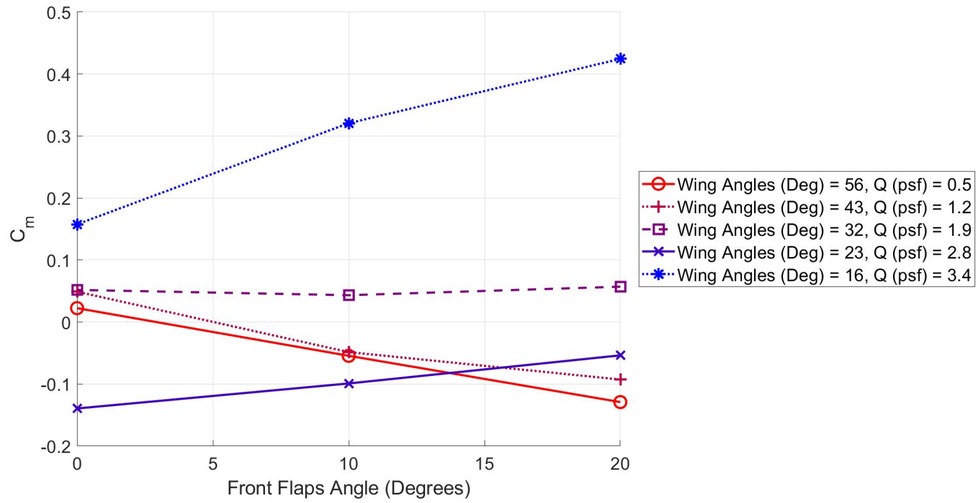

Figure 27. Trimmed wing sweep C_m vs front flap deflection angle.

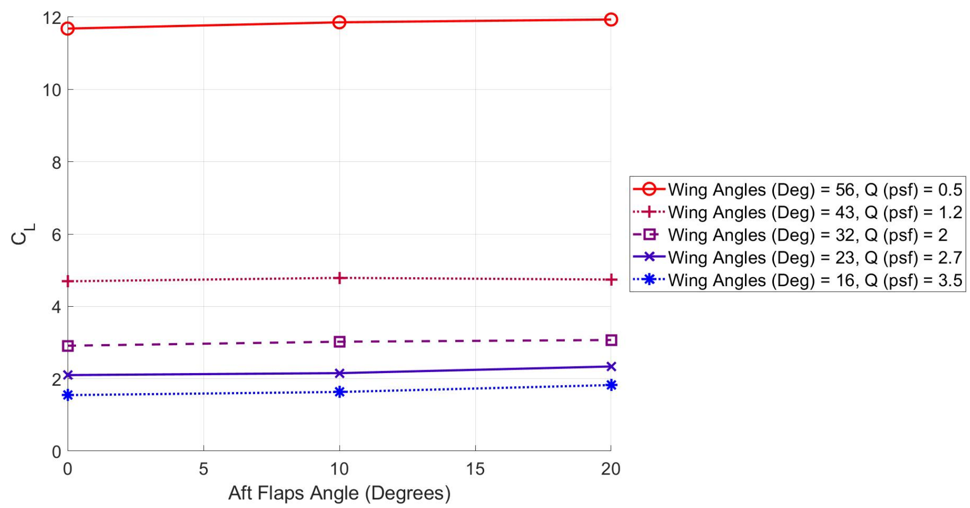

Figure 28. Trimmed wing sweep C_L vs aft flap deflection angle.

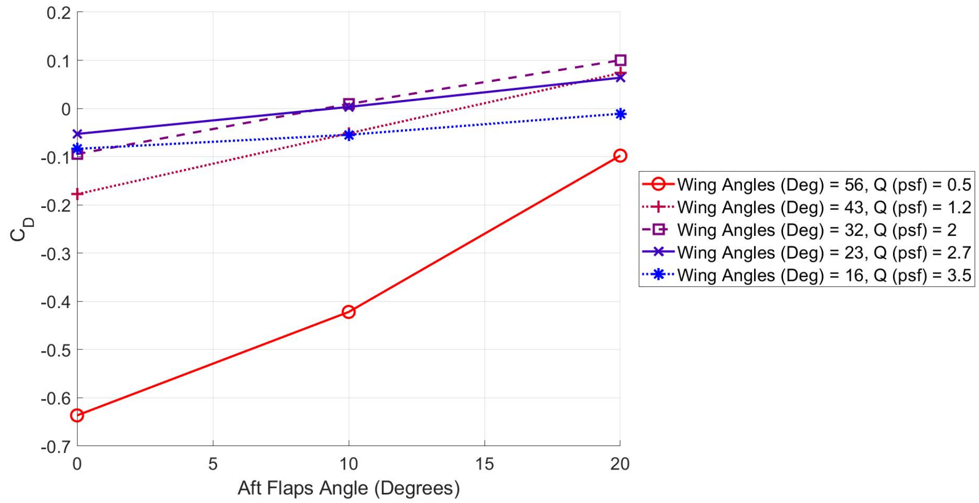

Figure 29. Trimmed wing sweep C_D vs aft flap deflection angle.

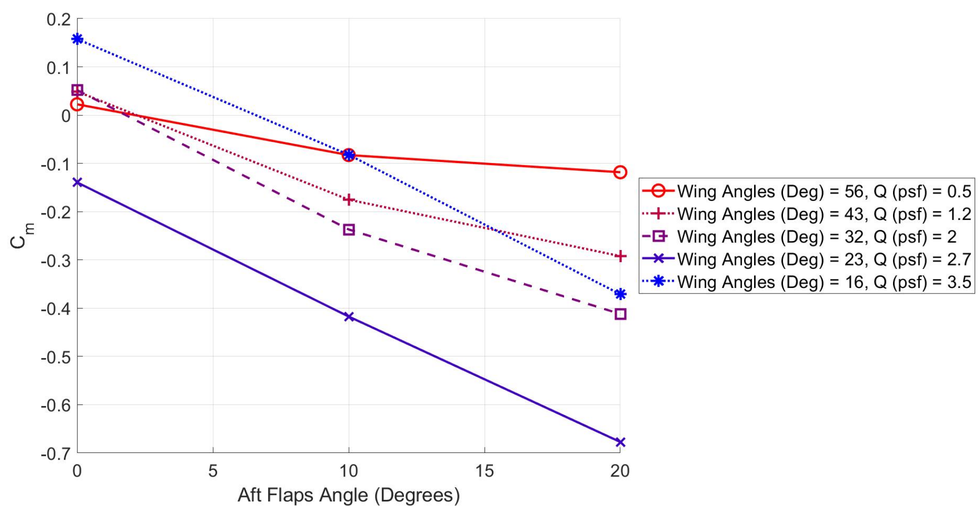

Figure 30. Trimmed wing sweep C_m vs aft flap deflection angle.

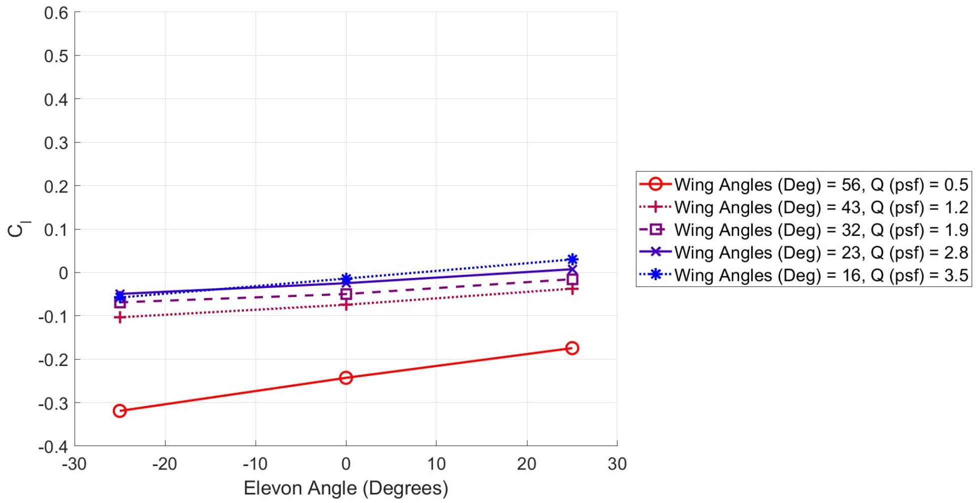

Figure 31. Trimmed wing sweep C_l vs elevon deflection angle.

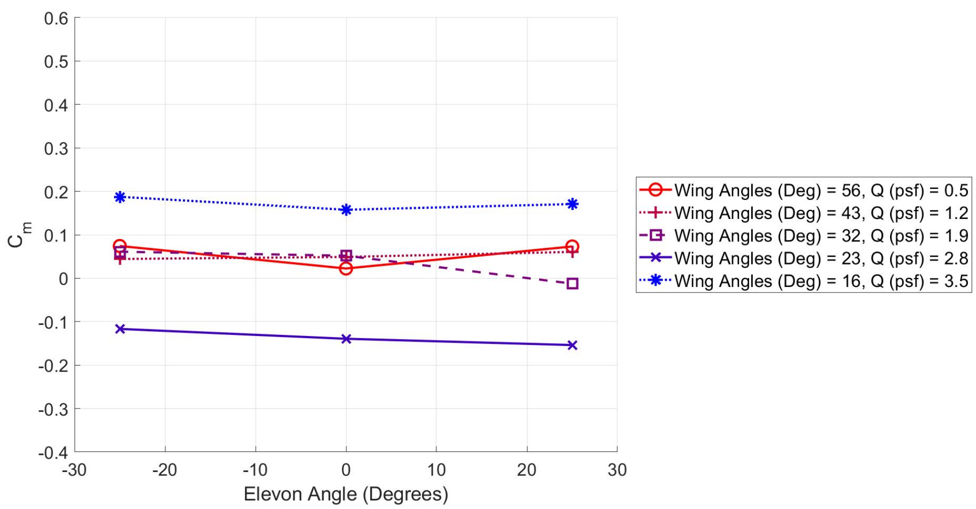

Figure 32. Trimmed wing sweep C_m vs elevon deflection angle.

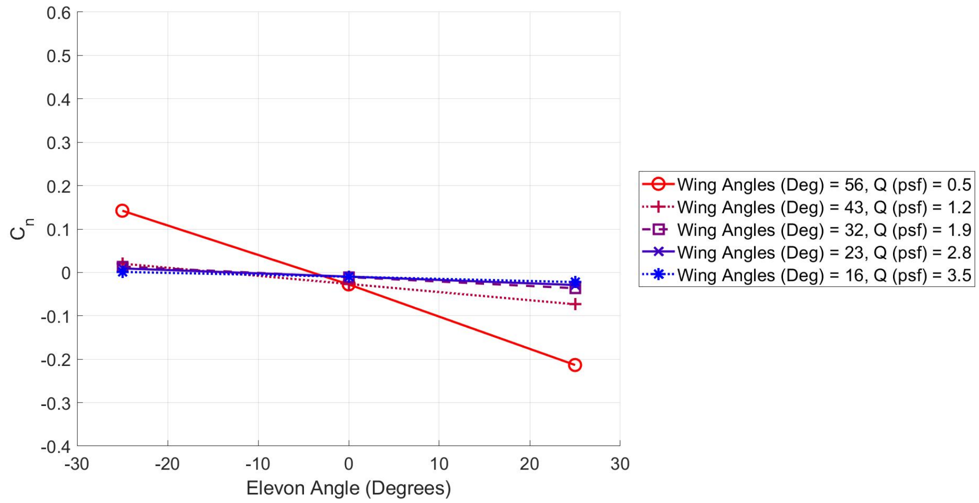

Figure 33. Trimmed wing sweep C_n vs elevon deflection angle.

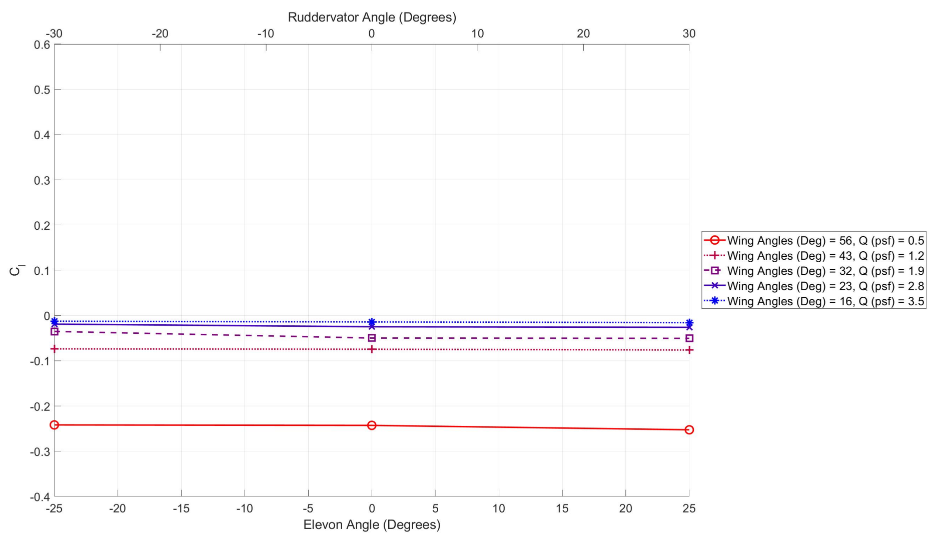

Figure 34. Trimmed wing sweep C_l vs elevon and ruddervator deflection angles.

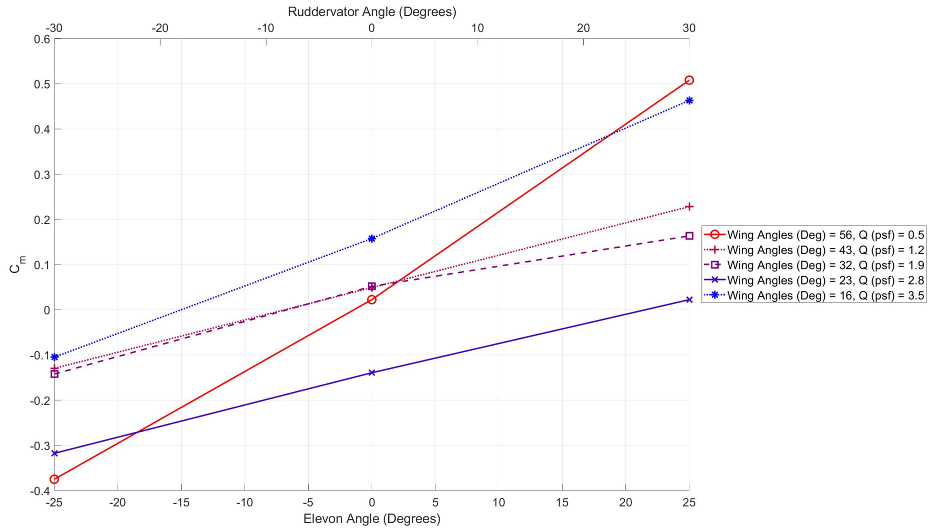

Figure 35. Trimmed wing sweep C_m vs elevon and ruddervator deflection angles.

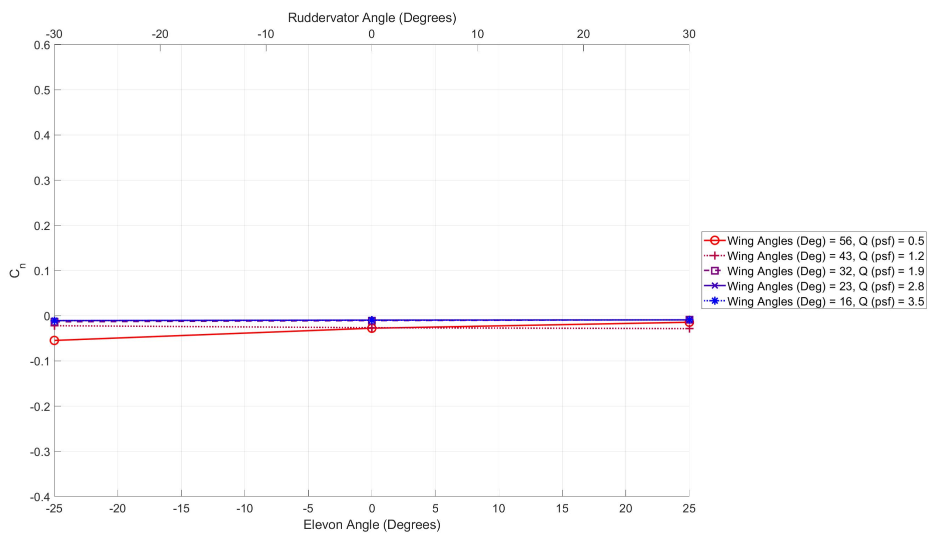

Figure 36. Trimmed wing sweep C_n vs elevon and ruddervator deflection angles.

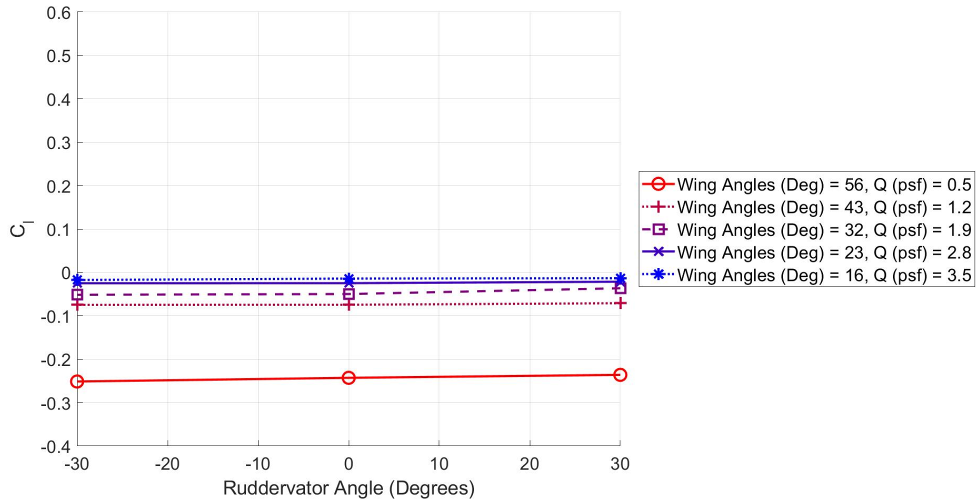

Figure 37. Trimmed wing sweep C_l vs ruddervator deflection angle.

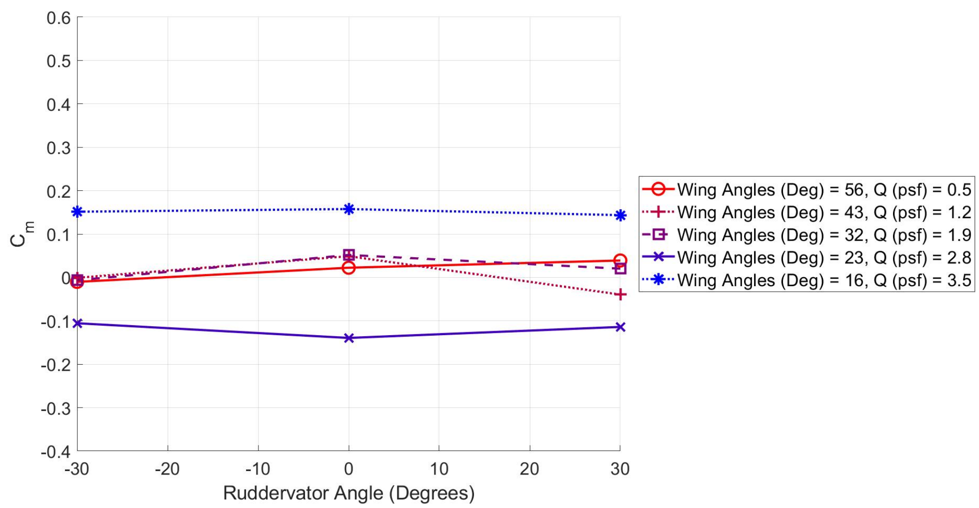

Figure 38. Trimmed wing sweep C_m vs ruddervator deflection angle.

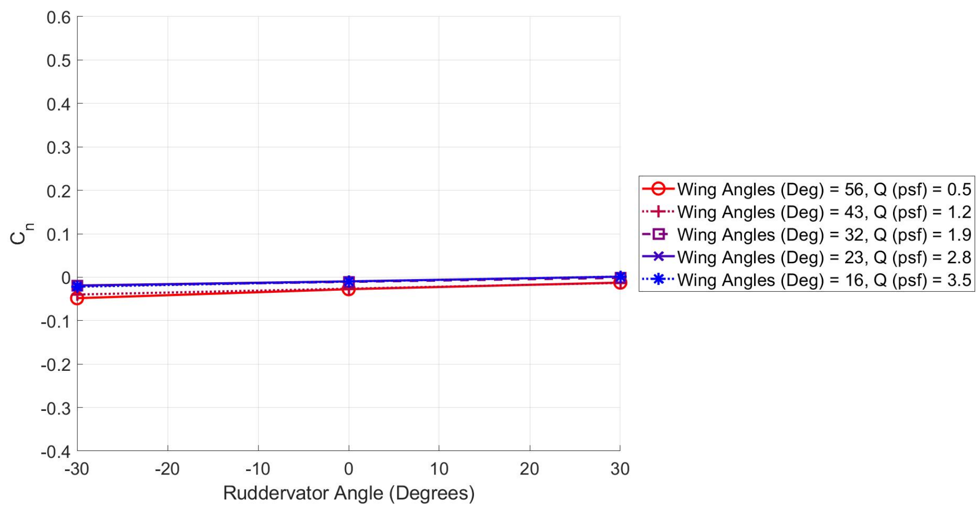

Figure 39. Trimmed wing sweep C_n vs ruddervator deflection angle.

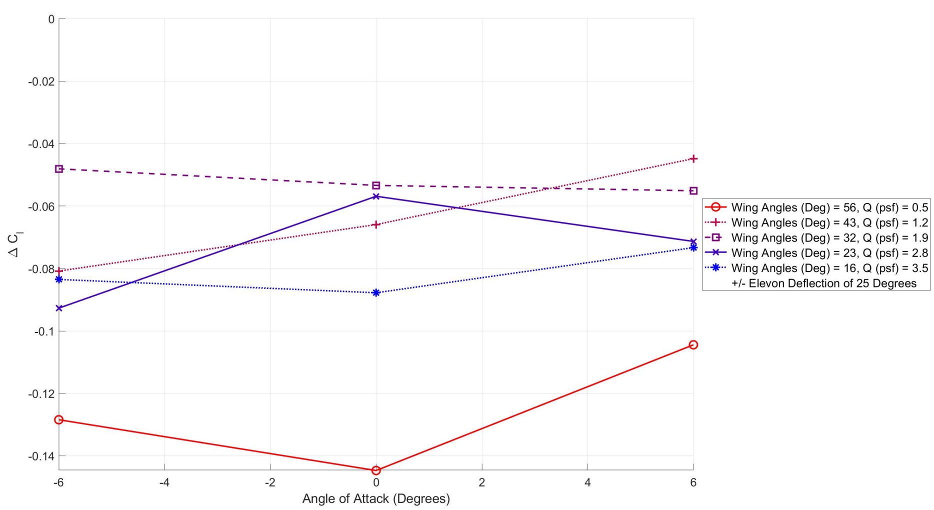

Figure 40. Trimmed wing sweep Δ C_l vs angle of attack for elevon deflection.

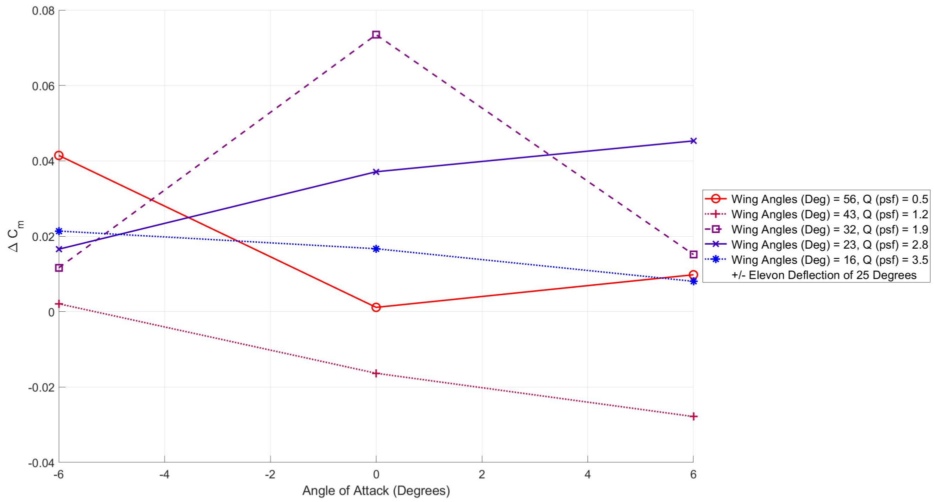

Figure 41. Trimmed wing sweep Δ C_m vs angle of attack for elevon deflection.

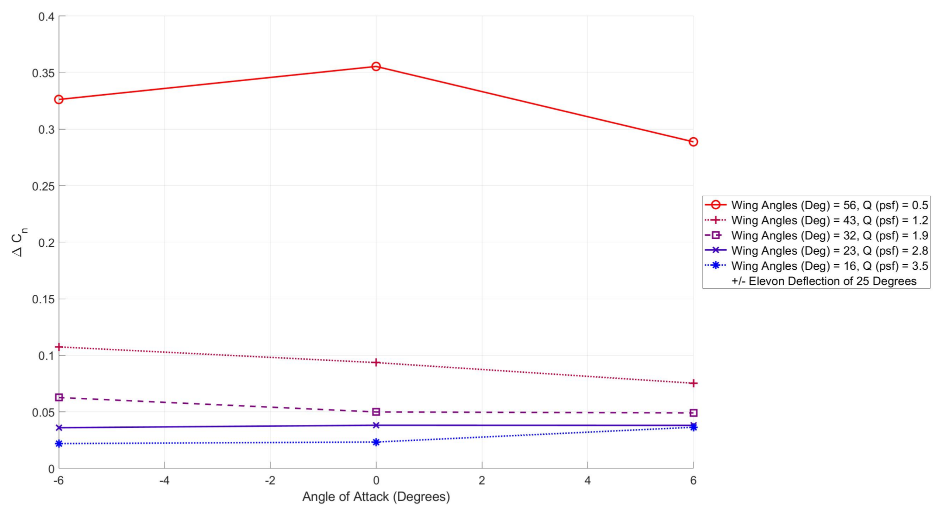

Figure 42. Trimmed wing sweep Δ C_n vs angle of attack for elevon deflection.

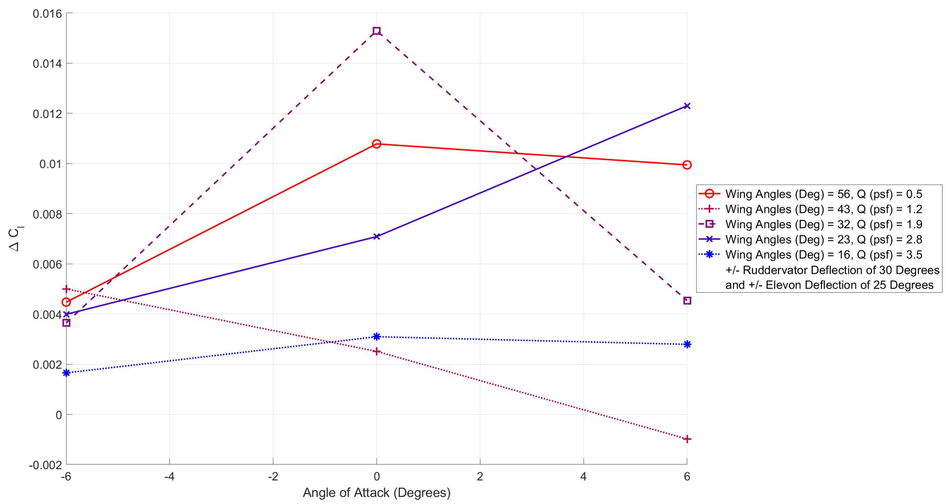

Figure 43. Trimmed wing sweep Δ C_l vs angle of attack for elevon and ruddervator deflection.

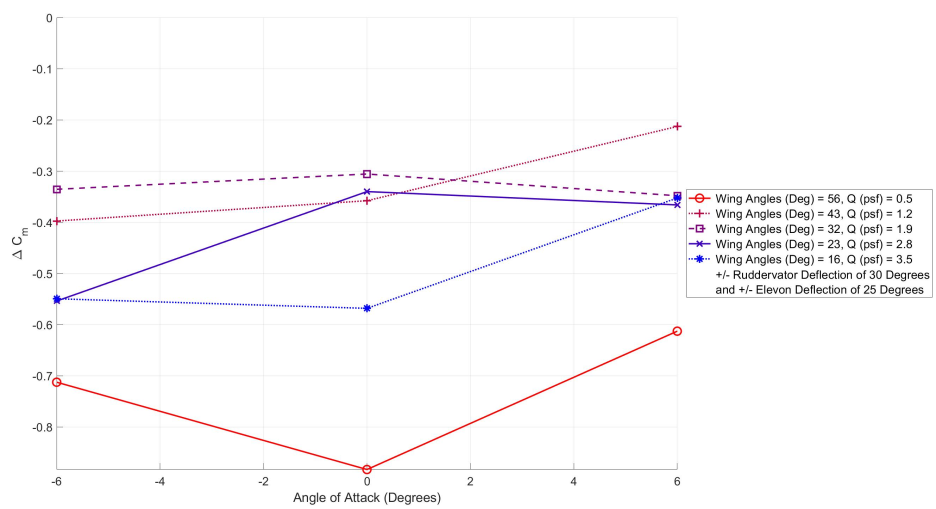

Figure 44. Trimmed wing sweep Δ C_m vs angle of attack for elevon and ruddervator deflection.

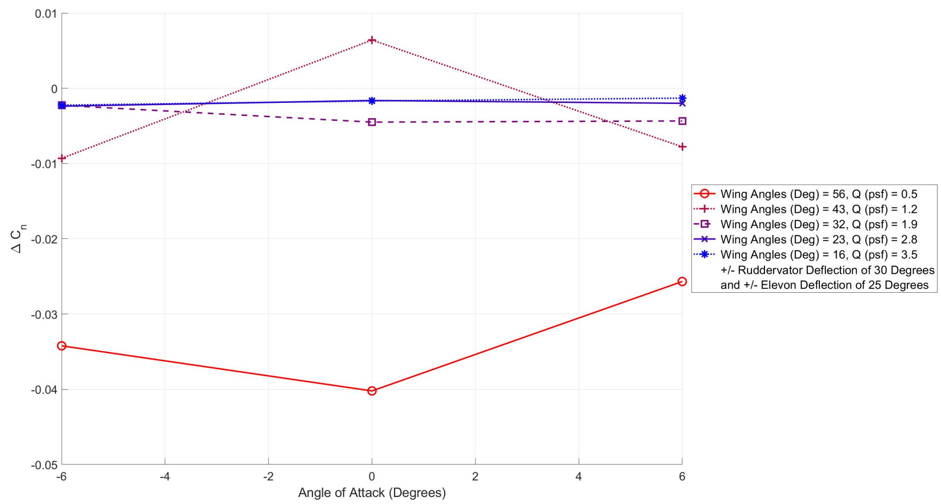

Figure 45. Trimmed wing sweep Δ C_n vs angle of attack for elevon and ruddervator deflection.

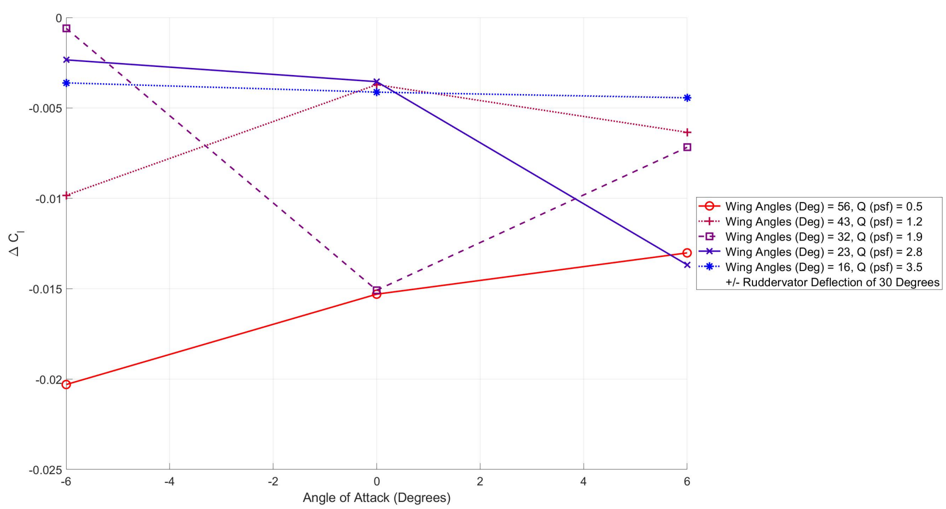

Figure 46. Trimmed wing sweep Δ C_l vs angle of attack for ruddervator deflection.

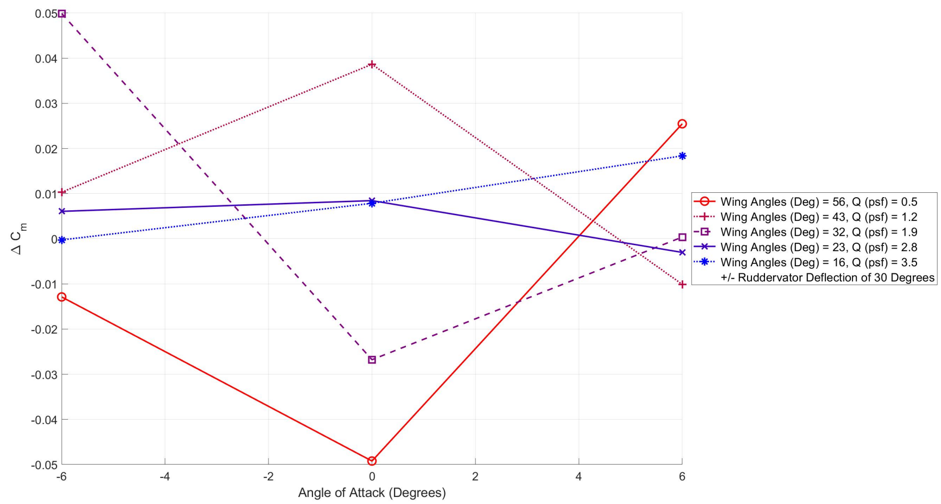

Figure 47. Trimmed wing sweep Δ C_m vs angle of attack for ruddervator deflection.

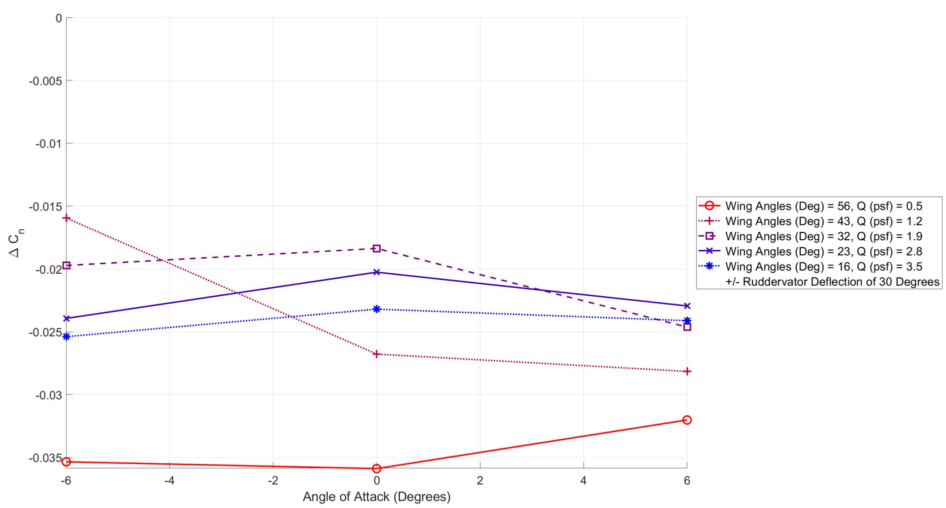

Figure 48. Trimmed wing sweep Δ C_n vs angle of attack for ruddervator deflection.

5.4 Forward Flight Performance and Stability

Due to the limitations of the 12-Foot Low-Speed Wind Tunnel at NASA Langley Research Center, the performance and stability of the vehicle at a representative flight speed while matching Reynolds number and Mach number could not be examined. Alternatively, testing was completed at a dynamic pressure of 4 psf. The basic aerodynamic coefficients for no control surface deflections can be seen in Figures 49 - 53. The remainder of the forward flight performance, stability, and control power plots can be seen in Appendix D. The plots in Appendix D are all with the LA-8 vehicle in a dynamic pressure of 4 psf. The associated motor RPMs can be seen in Table 3. The average C_T with these RPMs is 0.32. With an average C_T of 0.32, the vehicle would be in a state of accelerating, climbing flight. With an average C_T of 0.16, the vehicle would be in a state of steady, non-accelerating flight. A single thrust coefficient is being used as an average of the propeller RPMs and diameters due to the variation in diameters on the vehicle and measured RPMs from similar propellers. The thrust coefficients are using the assumption that the propeller blowing effect on the wing has no additional benefit to the axial force. This average C_T of 0.32 is used for all forward flight figures unless otherwise noted in the legend of the figure. None of these runs were taken to stall due to constraints on the model and balance.

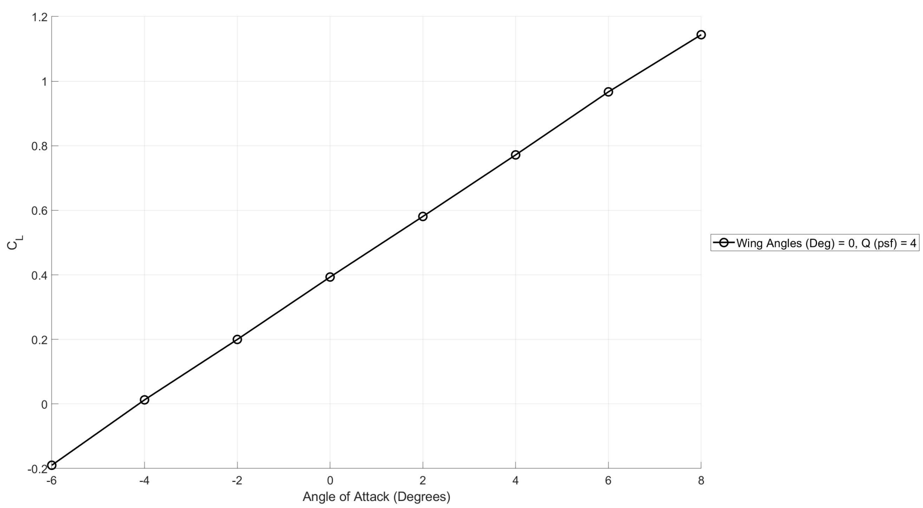

Figure 49. Forward flight trim point C_L vs angle of attack.

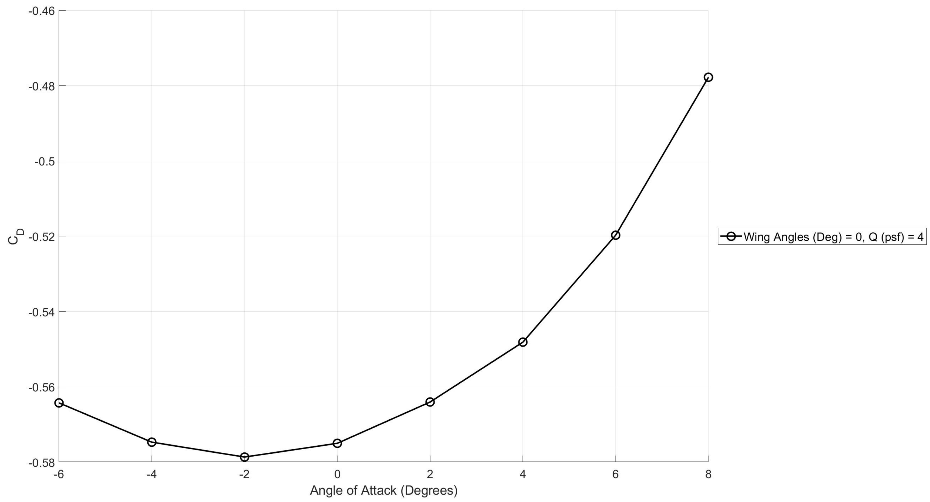

Figure 50. Forward flight trim point C_D vs angle of attack.

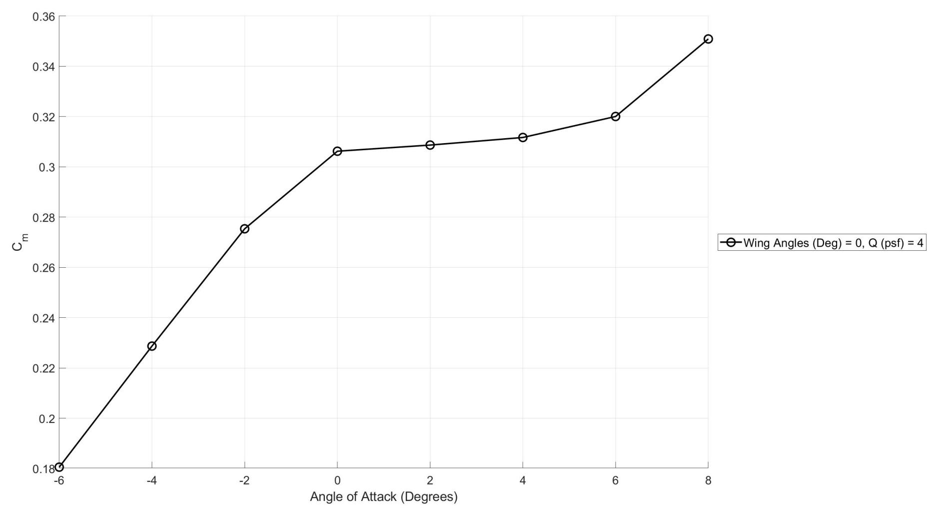

Figure 51. Forward flight trim point C_m vs angle of attack.

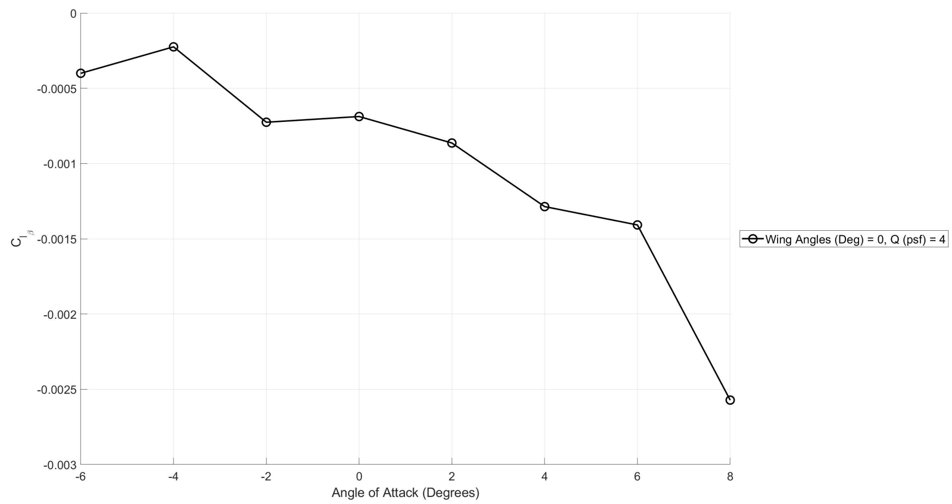

Figure 52. Forward flight trim point C_{l_β} vs angle of attack.

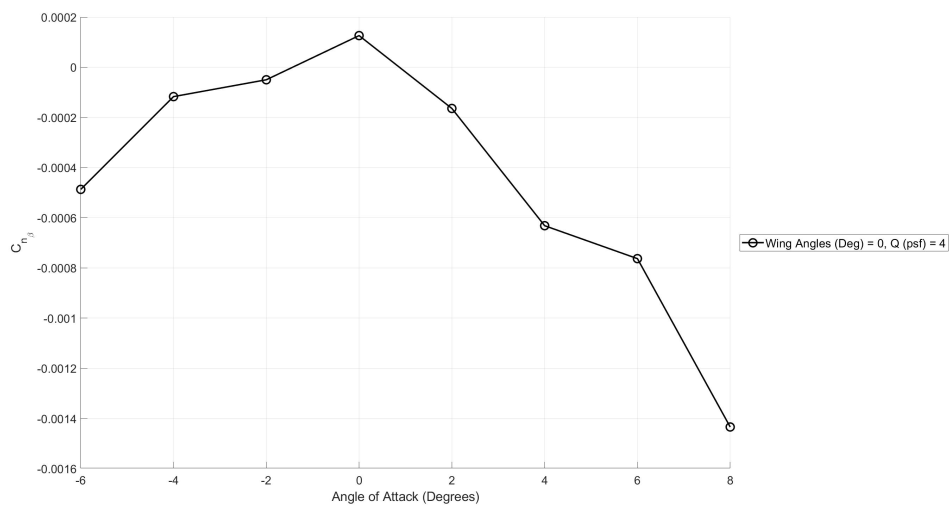

Figure 53. Forward flight trim point C_{n_β} vs angle of attack.

Table 3. Forward Flight Trim Motor RPMs at 0 Degrees Angle of Attack

	Dynamic Pressure (psf)	Motor 1 RPM	Motor 2 RPM	Motor 3 RPM	Motor 4 RPM
Forward Flight Trim	4.0	6199	5892.12	6109.12	6071.25
	Dynamic Pressure (psf)	Motor 5 RPM	Motor 6 RPM	Motor 7 RPM	Motor 8 RPM
Forward Flight Trim	4.0	3606.69	6137.31	5757.25	3638

The most notable concern in the forward flight stability and performance is that the vehicle is unstable longitudinally and directionally. Comparing the airframe-only result, which is indicated by the "Propellers Off" curve in Figures 54 and 55, with the propeller RPMs at two different settings, where the forward flight trim motor RPMs run is labeled as "Average $C_T = 0.32$", it can be seen that the propellers and the blowing over the wing can change the stability and the trim point unfavorably. Additional plots 56 - 58 show the lift, drag, and lateral stability with the influence of different propeller settings. In all of these figures, the "Average $C_T = 0.32$" tests were only taken to an angle of attack of eight degrees due to balance limitations.

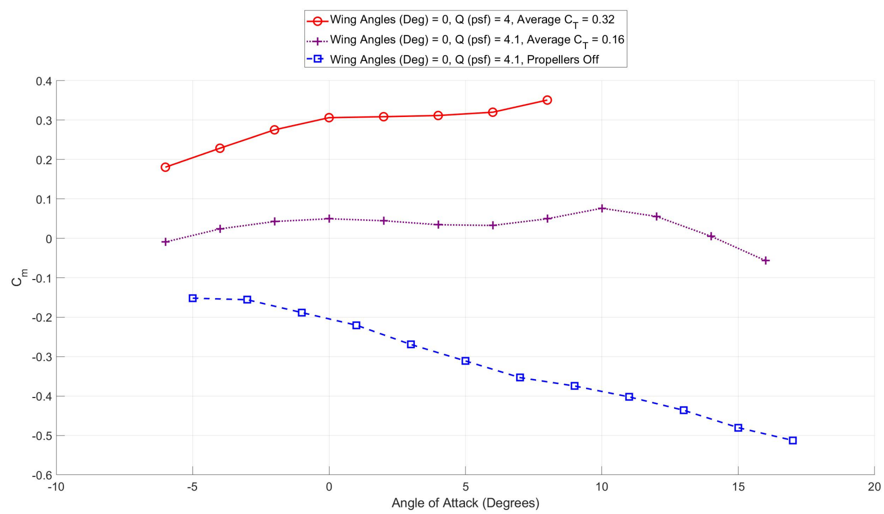

Figure 54. Forward flight pitch stability with motor RPM.

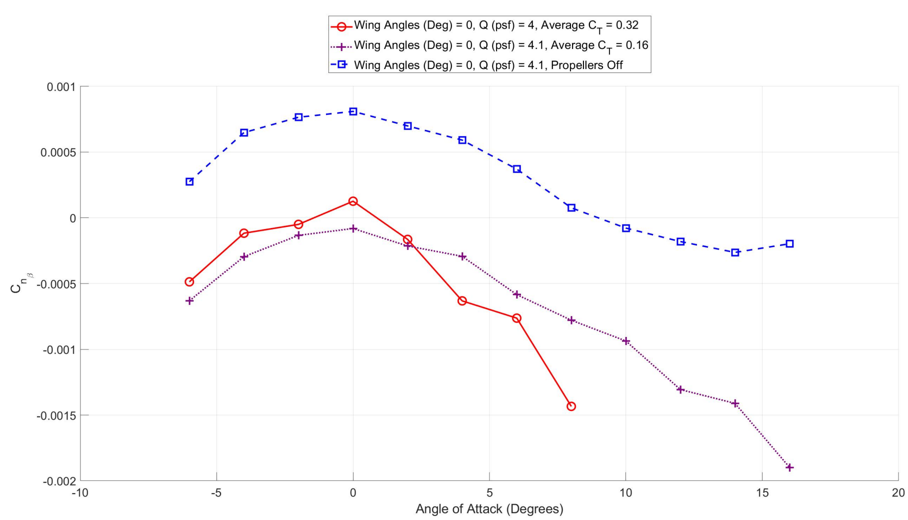

Figure 55. Forward flight yaw stability with motor RPM.

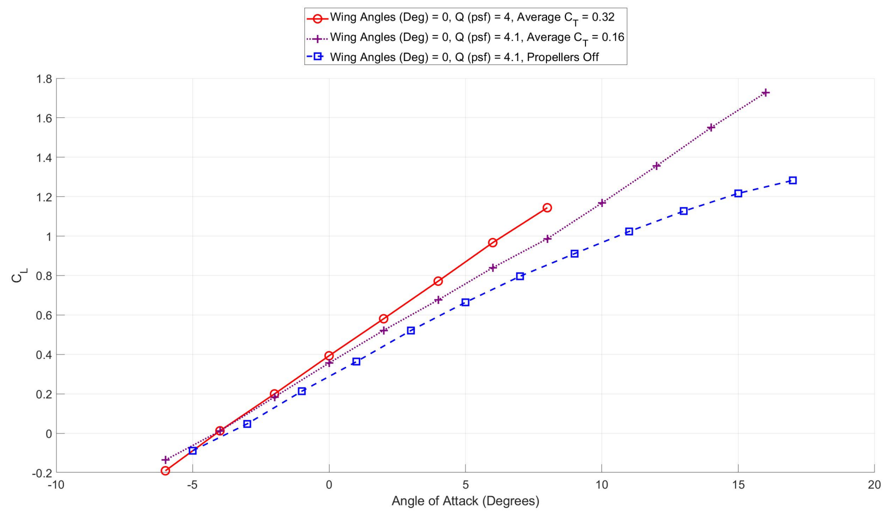

Figure 56. Forward flight lift coefficient with motor RPM.

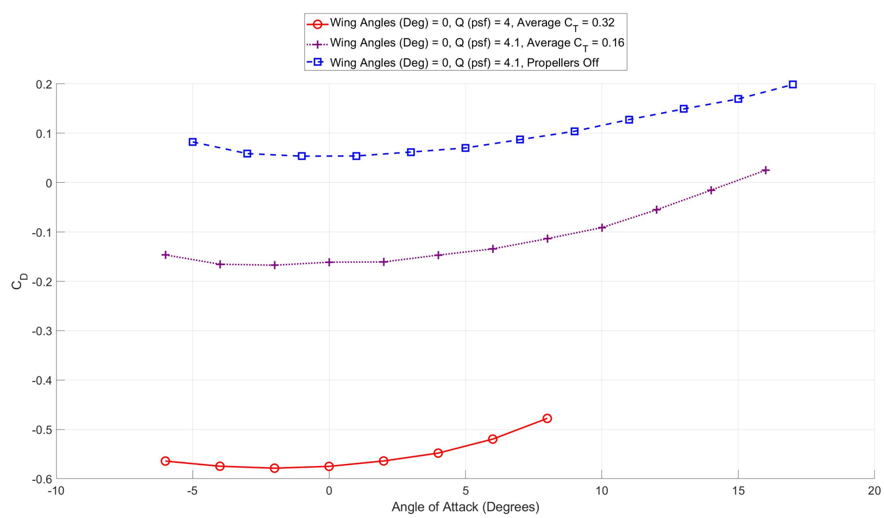

Figure 57. Forward flight drag coefficient with motor RPM.

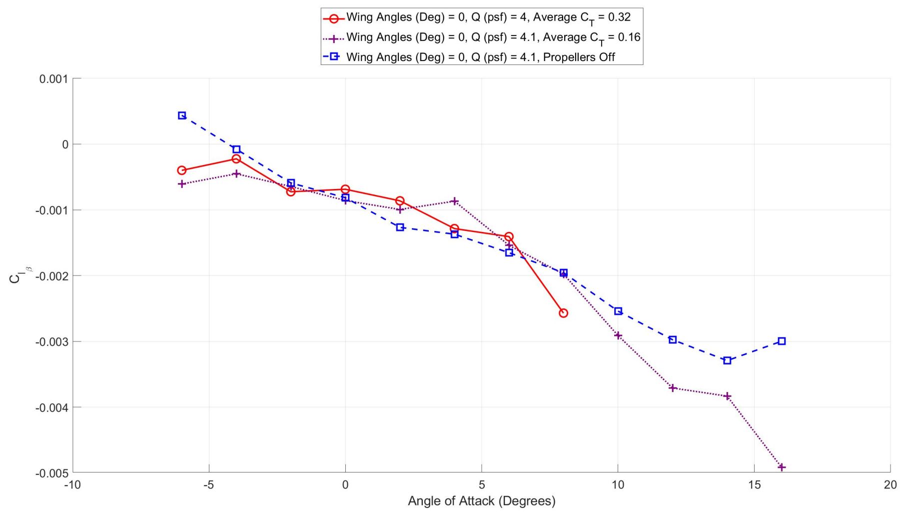

Figure 58. Forward flight roll stability with motor RPM.

In order to achieve a longitudinally and directionally stable aircraft in forward flight, a change in the CG was considered. In Figures 59 - 61, using the raw aerodynamic forces and moments from the balance, the moment coefficients were recalculated based upon two different offsets, 0.2 and 0.4 ft forward in the x-direction (towards the nose of the aircraft). With a shift of the CG 0.4 ft forward, the vehicle becomes stable and trims at a more appropriate angle of attack. As previously stated in Section 4, the tare from the tunnel procedures removes the physical CG shifting from the wind tunnel data and therefore the reference CG is held constant for all of the wing angles throughout this report. This reference CG can be post-processed to represent a different CG. If the CG location for hover is the reference CG of 1.9 ft in the x-direction from the nose, then the CG location for forward flight would land approximately at the results of the CG offset of 0.2 ft from the rotation of the wings and motors, which provides marginal amounts of longitudinal stability. This shift does not impact the lateral stability and corrects the directional stability for angles of attack between -6 and 6 degrees as seen in Figures 60 and 61. All three of these plots use the forward flight trim motor RPMs presented in Table 3.

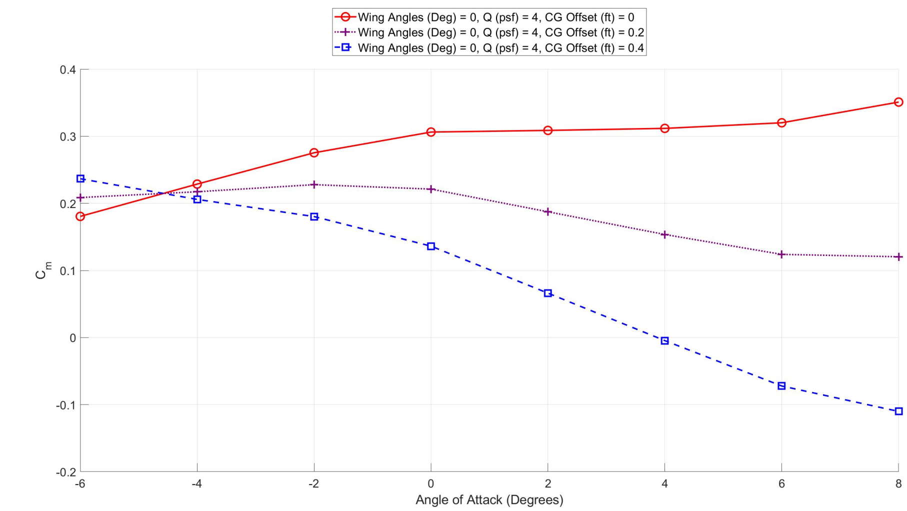

Figure 59. Center of gravity change in forward flight for C_m vs angle of attack.

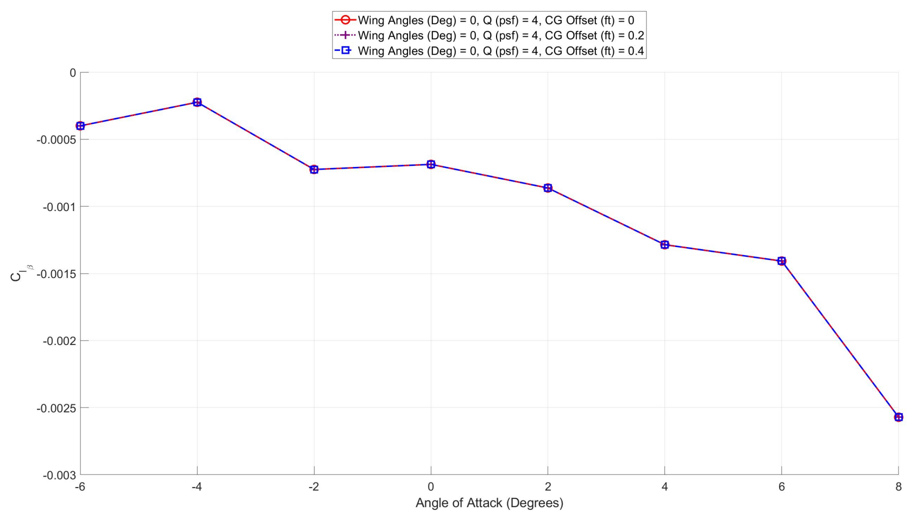

Figure 60. Center of gravity change in forward flight for C_{l_β} vs angle of attack.

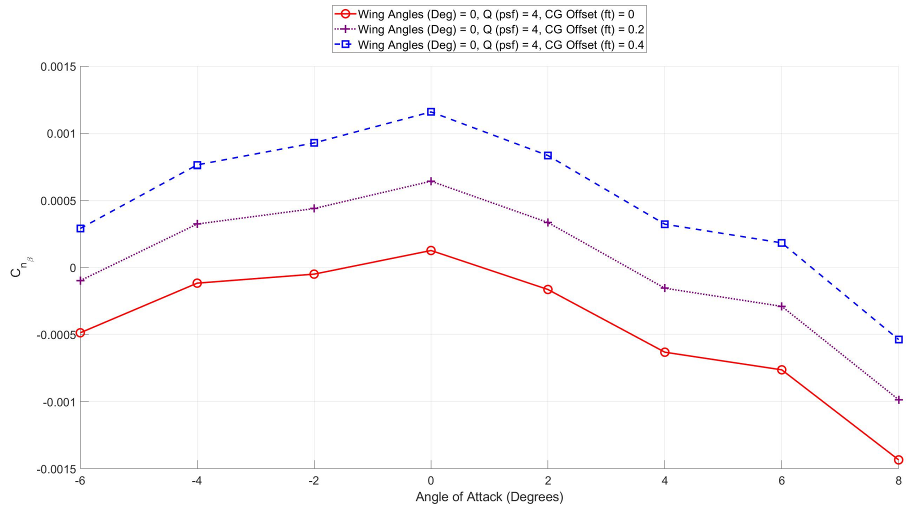

Figure 61. Center of gravity change in forward flight for C_{n_β} vs angle of attack.

6 Concluding Remarks

Significant investigation of the LA-8 flight characteristics took place in the NASA Langley 12-Foot Low-Speed Wind Tunnel. The major findings from this initial wind tunnel testing of the LA-8 electric VTOL UAS are:

1) Longitudinal and directional stability is influenced significantly by the inclusion of a blown wing and can cause the vehicle to become unstable in the longitudinal (pitch) and directional (yaw) axis at cruise thrust conditions.

2) While using constant pitch propellors, there is a trade-off of maintaining static stability and obtaining a favorable trim point without control surface deflections. For the LA-8, there are potential issues with non-propulsive forward flight landings as the pitch trim angle is approximately -20 degrees without the propellers installed on the aircraft. This would require a very high speed descent and a precision flare to safely land the vehicle.

3) Lift on the vehicle is created by a) direct lift from propellers b) lift from wings, and c) lift from wing sections blown by propellers. Additional testing of motors and propellers not attached to the airframe is needed to accurately determine the contributions from each component.

4) The center of gravity location as determined by analysis tools for the initial LA-8 design does not support the required stability in forward flight conditions. Therefore, the stability can be corrected through a combination of wing angle, flap deployment, and differential RPM. An alternative solution is to move the center of gravity approximately 0.4 ft forward from the design location in order to achieve longitudinal and directional stability.

7 Future Work

A second tunnel entry for LA-8, with slight modifications[1], in the NASA Langley 12-Foot Low-Speed Tunnel has been completed and will be documented. This second entry used a design of experiments approach to investigate the performance and control characteristics of the vehicle in a more detailed but concise test matrix. A future free flight test of the LA-8 is also planned that will use the data from these wind tunnel tests and will investigate the dynamic performance of the vehicle. In addition, future configurations will be built and tested in order to support the vast array of designs and technologies from industry.

References

1. Meade, D., *Langley Aerodrome Created to Explore Urban Air Mobility*, `https://www.nasa.gov/feature/langley/langley-aerodrome-created-to-explore-urban-air-mobility`, April 2019.

2. McSwain, R., Geuther, S., Howland, G., Patterson, M., Whiteside, S., and North, D. *An Experimental Approach to a Rapid Propulsion and Aeronautics Concepts Testbed*, NASA TM-2020-220437, January 2020.

3. NASA Langley Research Center, Research Directorate, `https://researchdirectorate.larc.nasa.gov/12-foot-low-speed-tunnel-12-ft-lst/`, Accessed July 2019.

4. Jackson, E., Raney, D., Glaab, L., and Derry, S., *Piloted Simulation Assessment of a High-speed Civil Transport Configuration*, NASA TP-2002-211441, 2002.

[1] All propellers were changed to be identical in size and pitch in order to more accurately determine approximate non-dimensional coefficients for each propeller.

Appendix A

Airframe Performance and Stability Plots

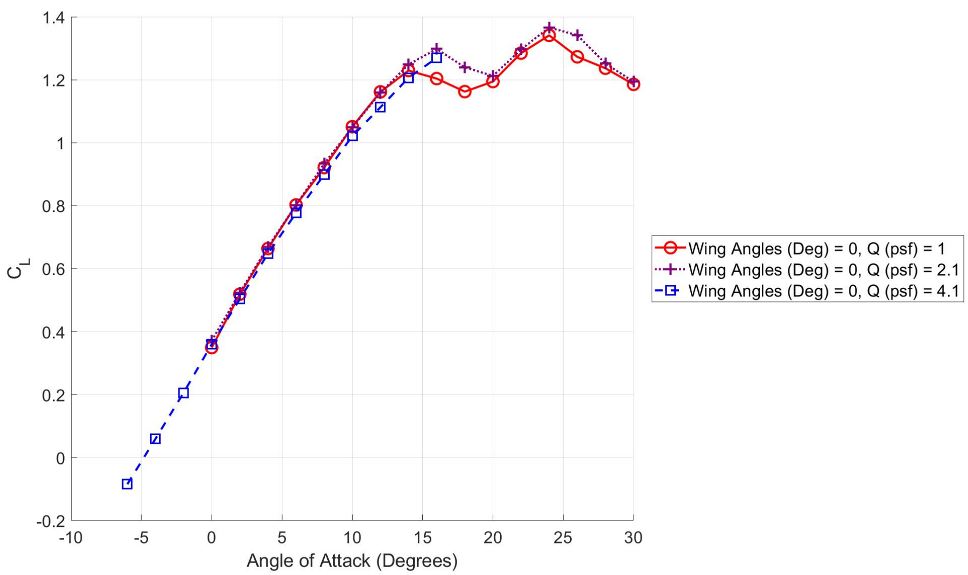

Figure 62. Propellers off C_L vs angle of attack.

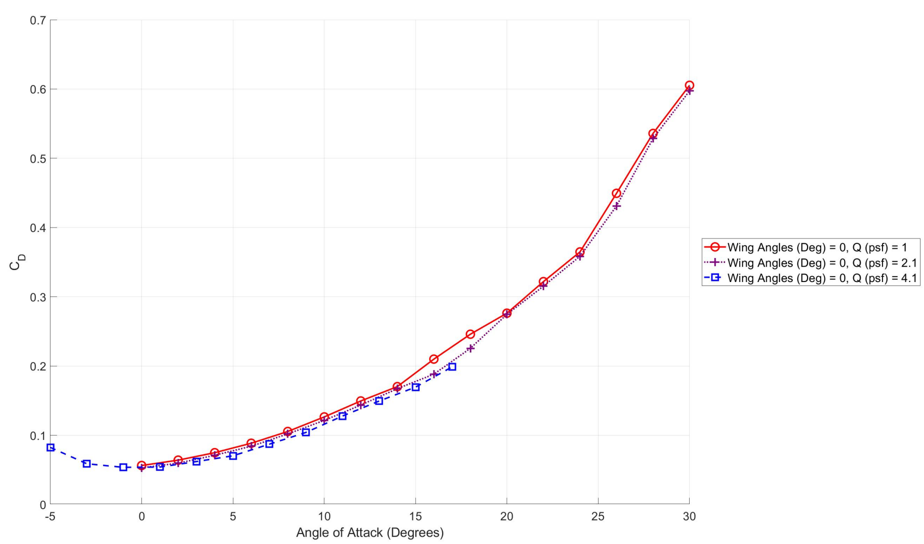

Figure 63. Propellers off C_D vs angle of attack.

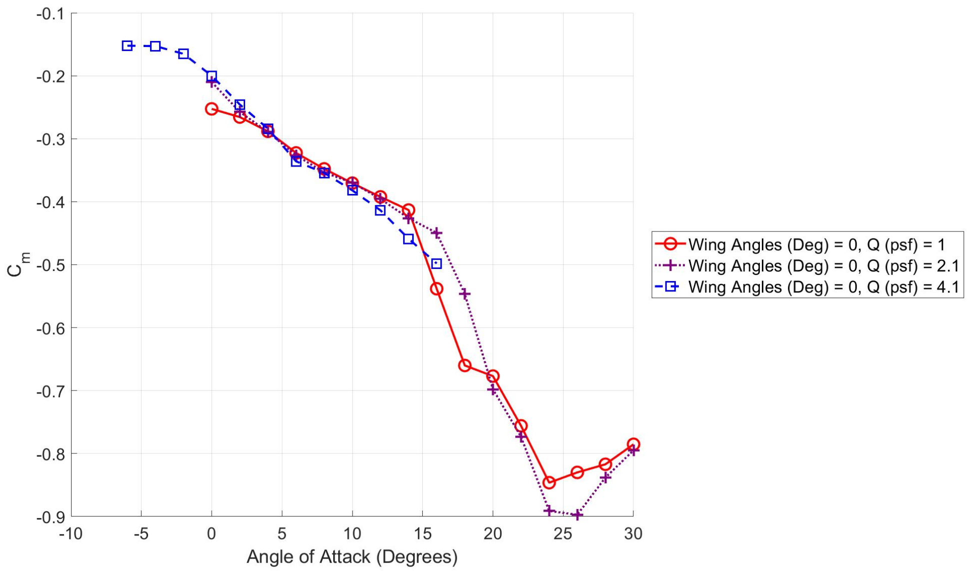

Figure 64. Propellers off C_m vs angle of attack.

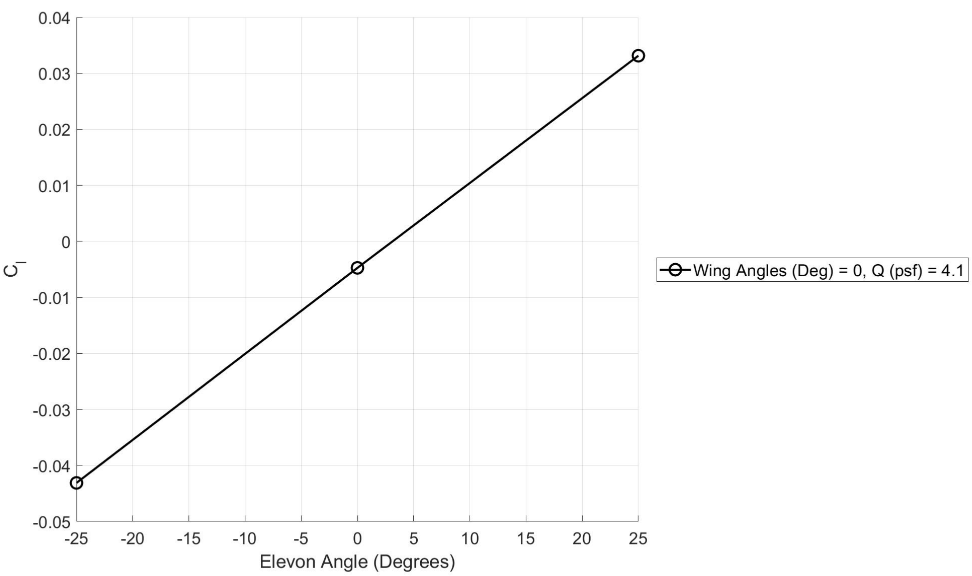

Figure 65. Propellers off C_l vs elevon deflection angle.

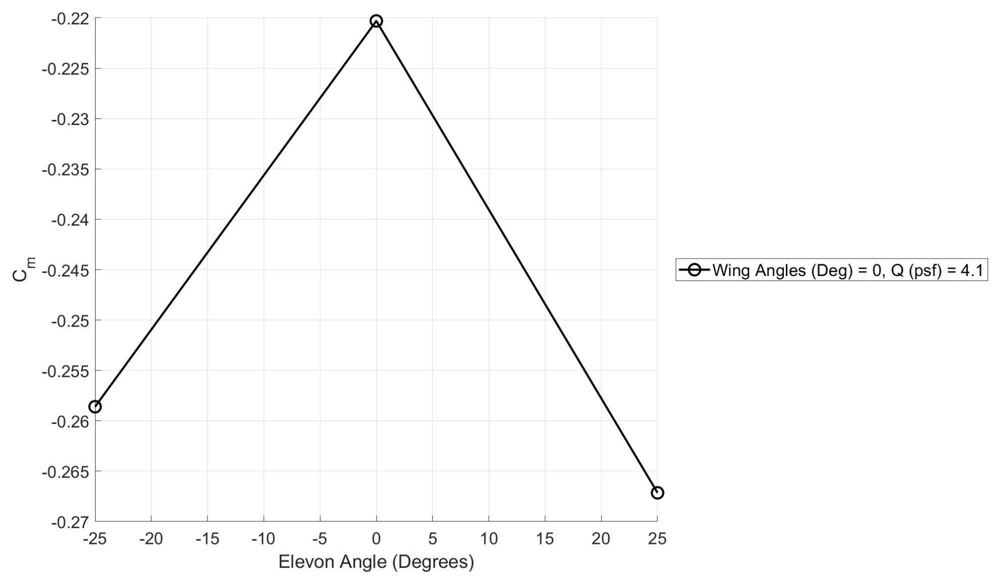

Figure 66. Propellers off C_m vs elevon deflection angle.

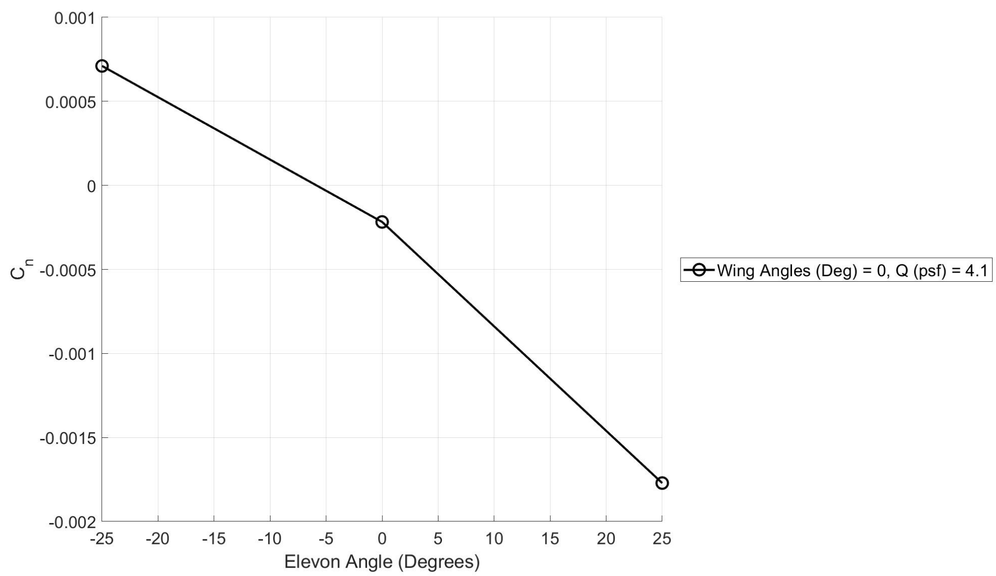

Figure 67. Propellers off C_n vs elevon deflection angle.

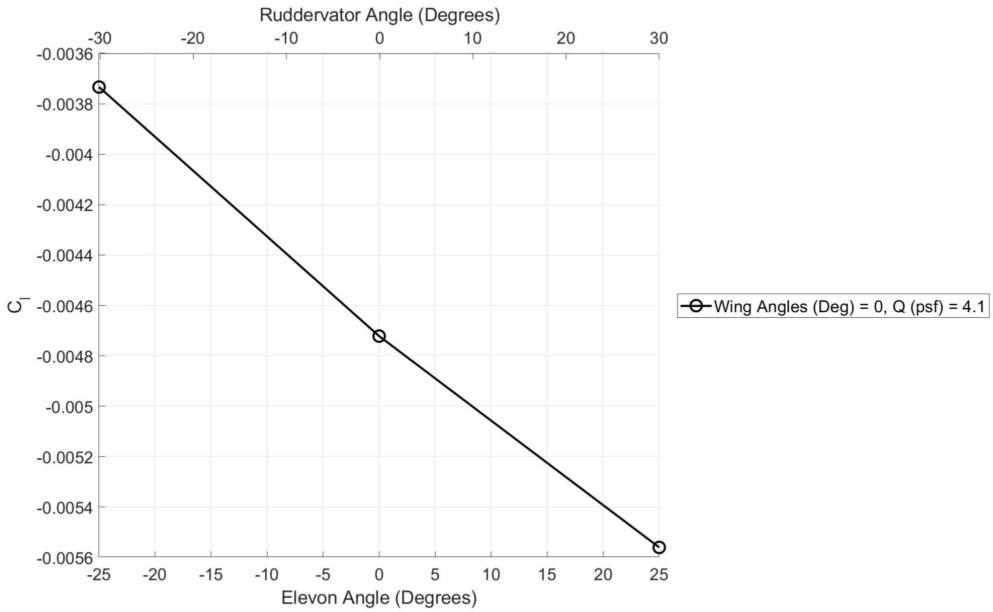

Figure 68. Propellers off C_l vs elevon and ruddervator deflection angles.

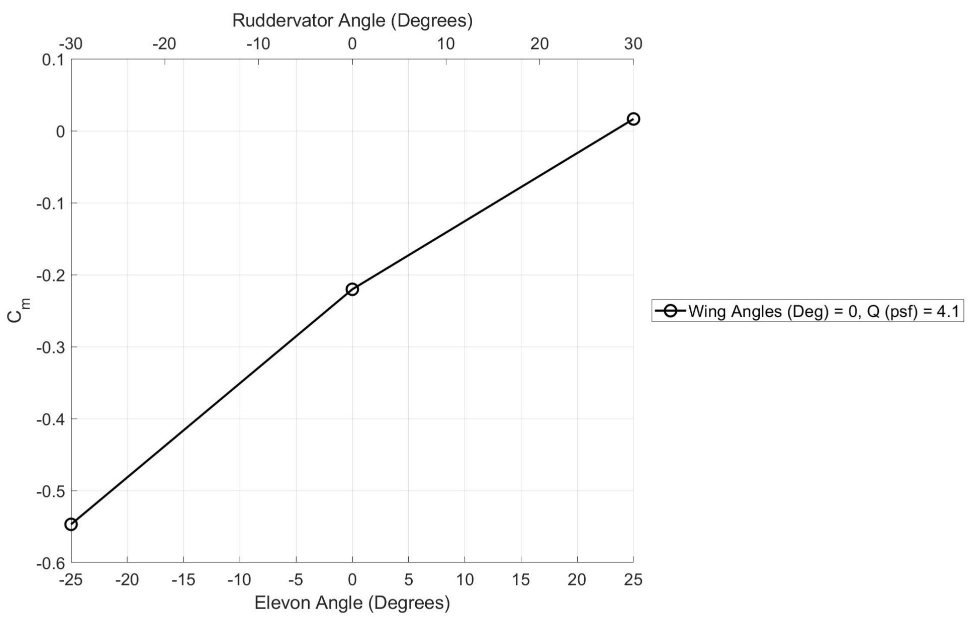

Figure 69. Propellers off C_m vs elevon and ruddervator deflection angles.

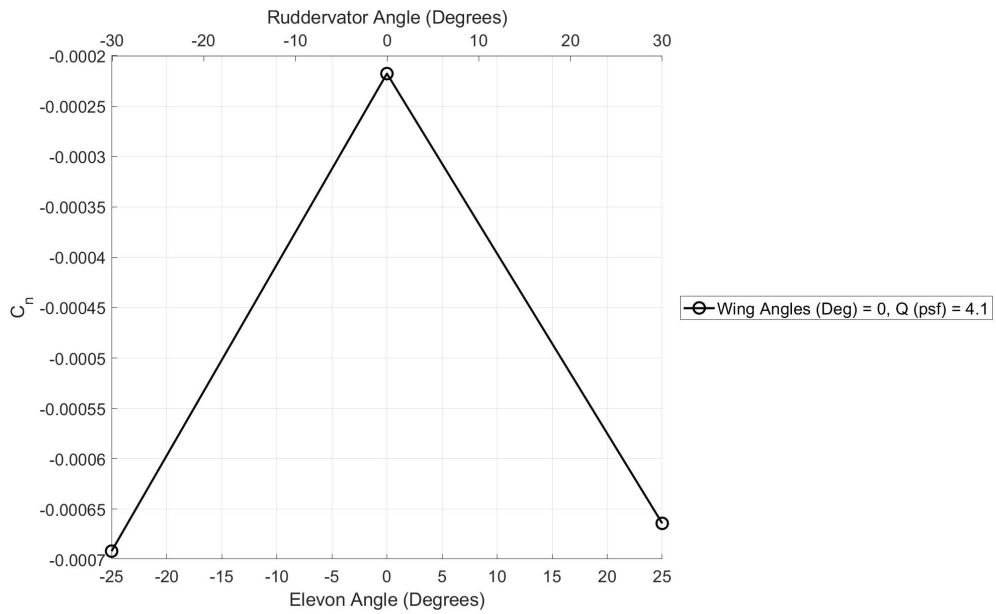

Figure 70. Propellers off C_n vs elevon and ruddervator deflection angles.

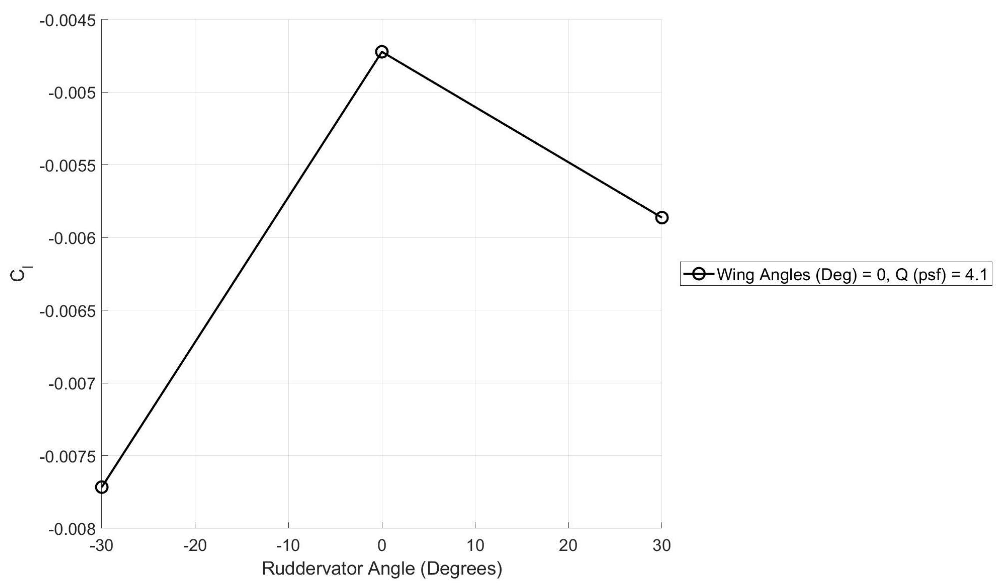

Figure 71. Propellers off C_l vs ruddervator deflection angle.

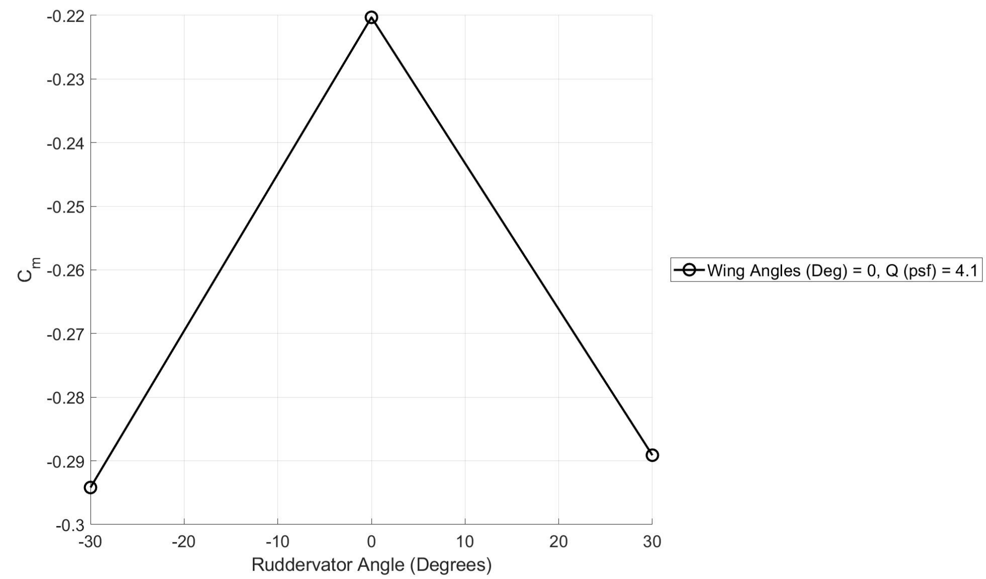

Figure 72. Propellers off C_m vs ruddervator deflection angle.

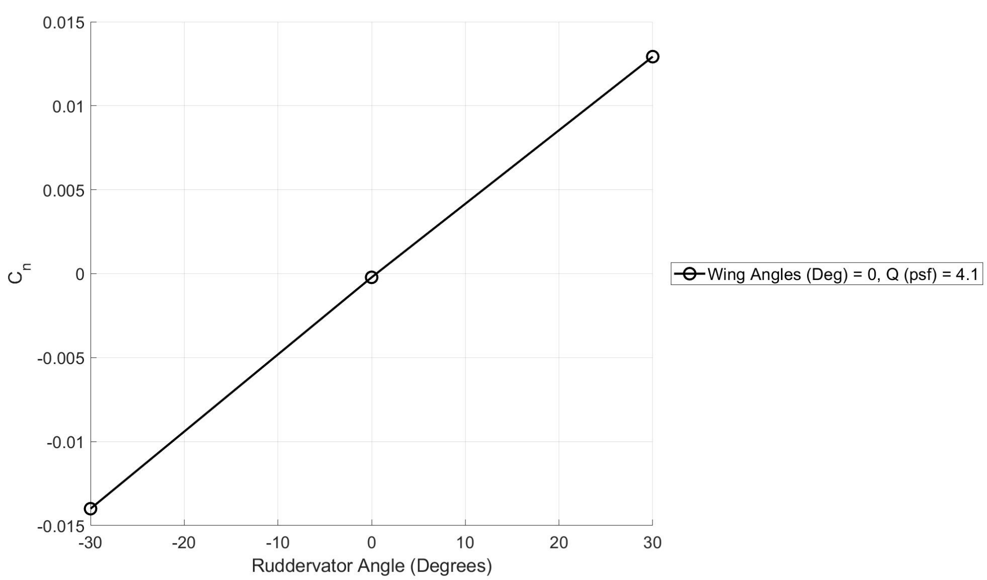

Figure 73. Propellers off C_n vs ruddervator deflection angle.

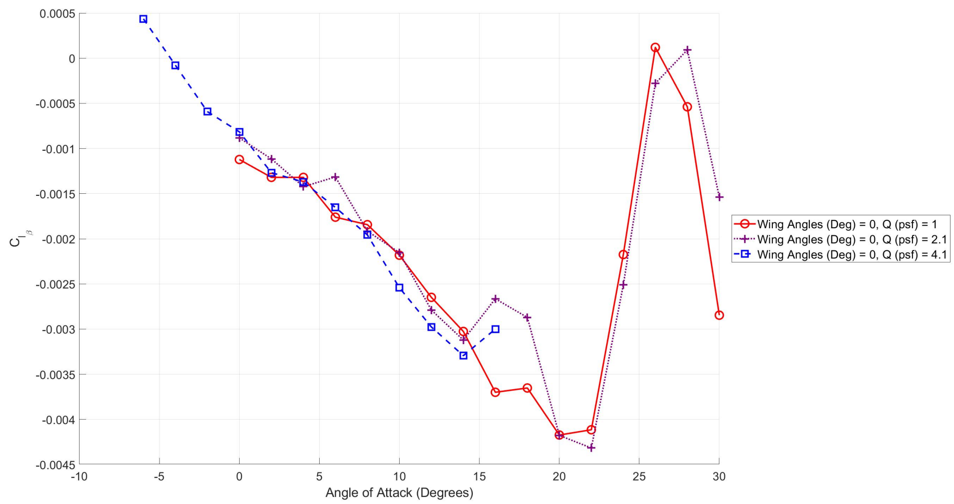

Figure 74. Propellers off C_{l_β} vs angle of attack with Q variation.

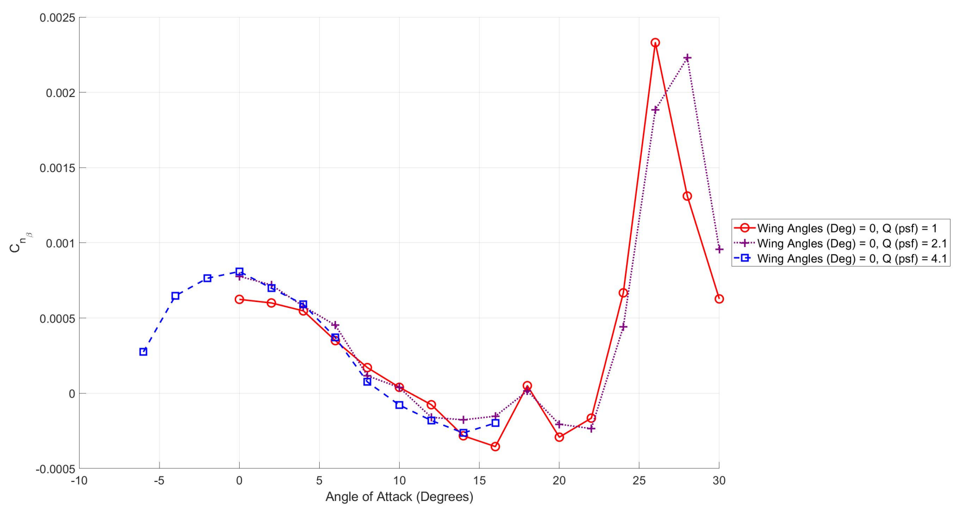

Figure 75. Propellers off C_{n_β} vs angle of attack with Q variation.

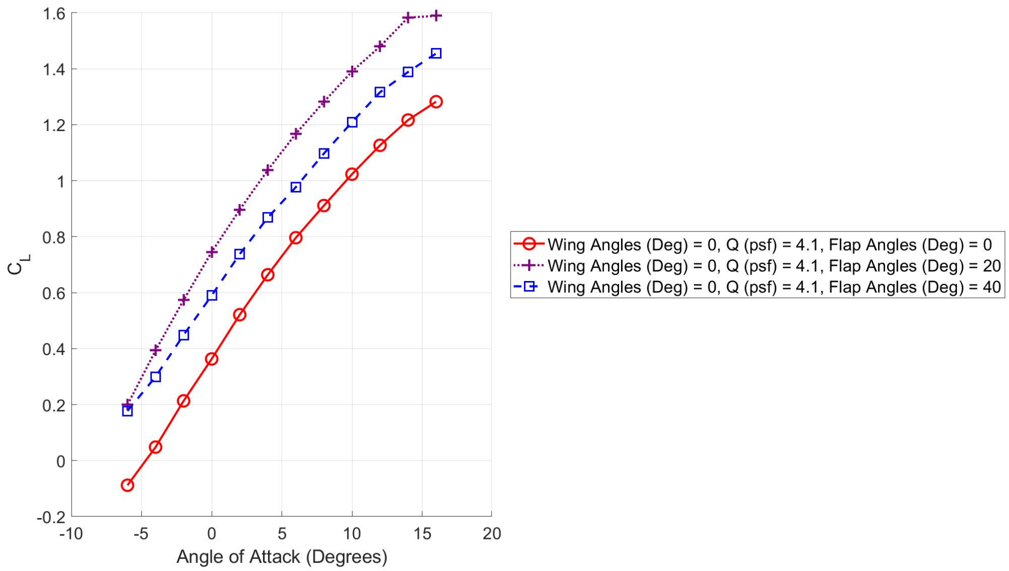

Figure 76. Propellers off C_L vs angle of attack with all flaps' deflection.

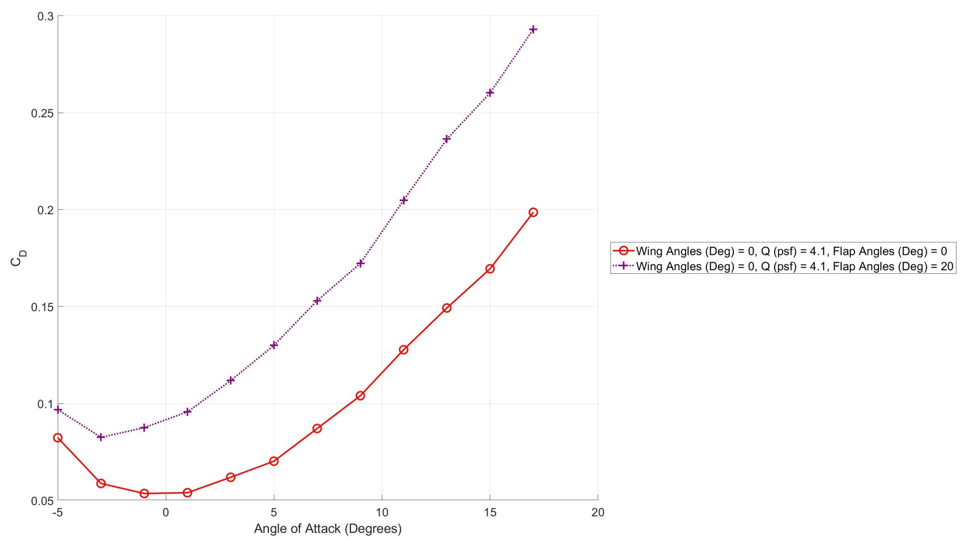

Figure 77. Propellers off C_D vs angle of attack with all flaps' deflection.

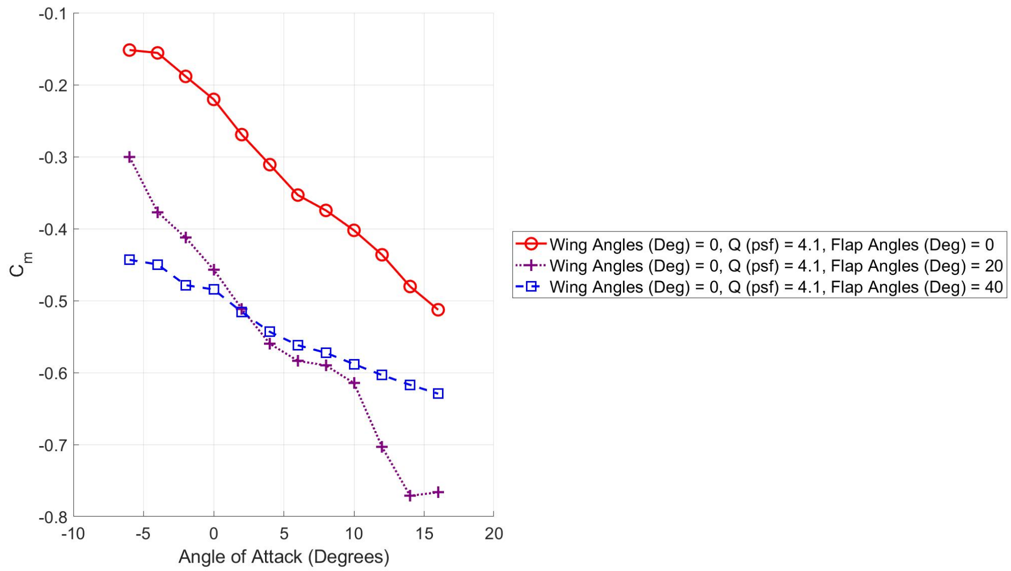

Figure 78. Propellers off C_m vs angle of attack with all flaps' deflection.

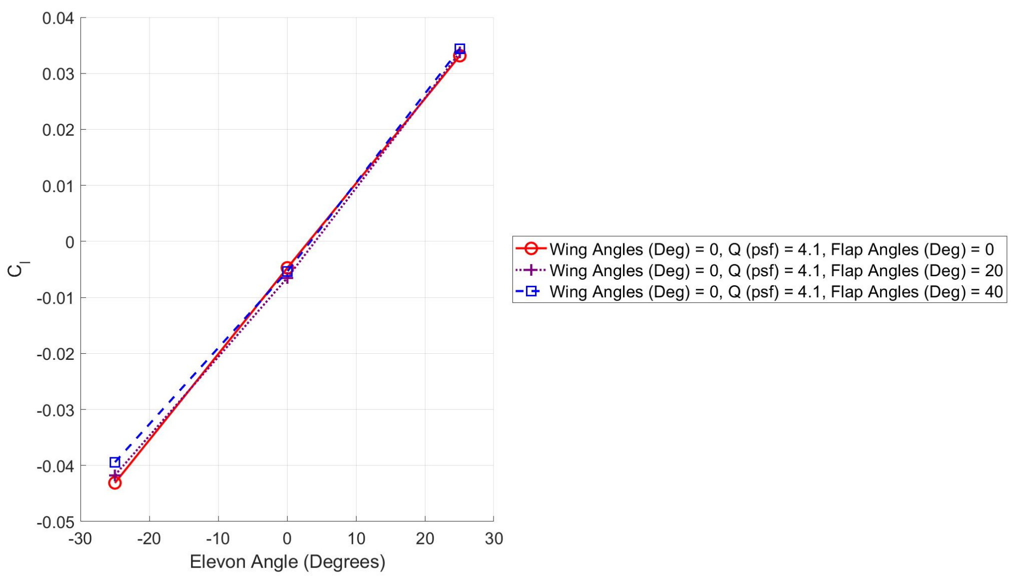

Figure 79. Propellers off C_l vs elevon deflection angle with all flaps' deflection.

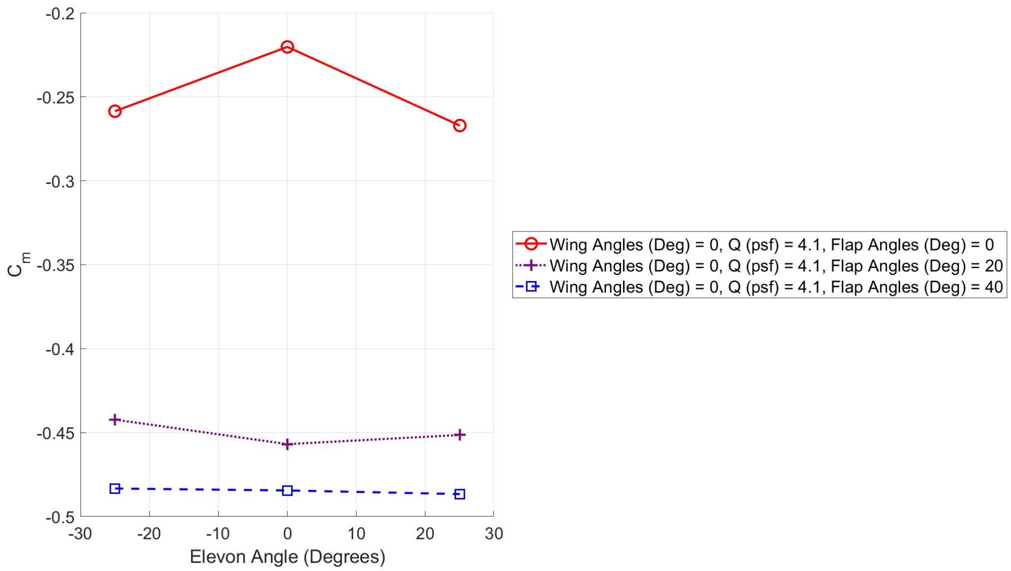

Figure 80. Propellers off C_m vs elevon deflection angle with all flaps' deflection.

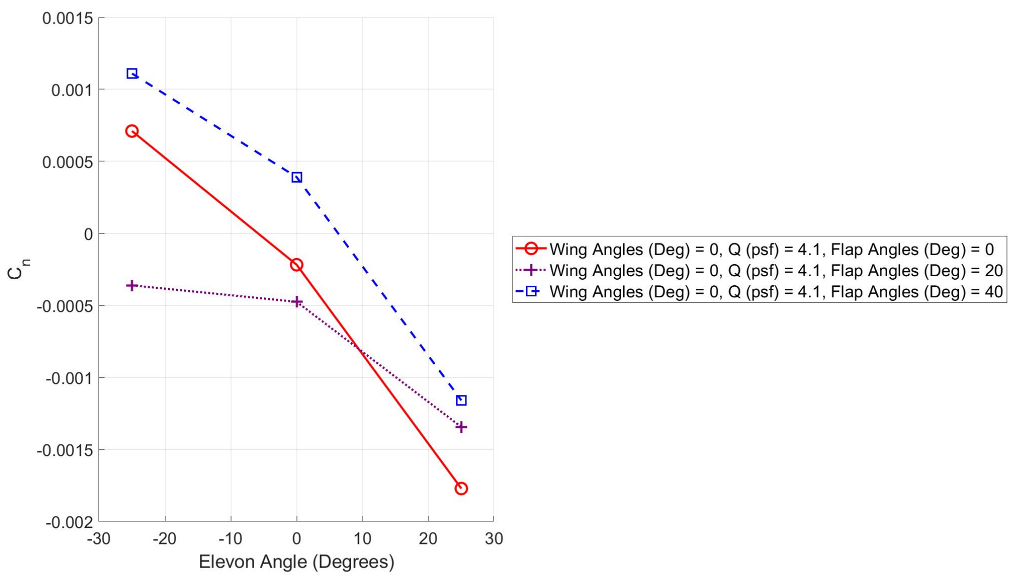

Figure 81. Propellers off C_n vs elevon deflection angle with all flaps' deflection.

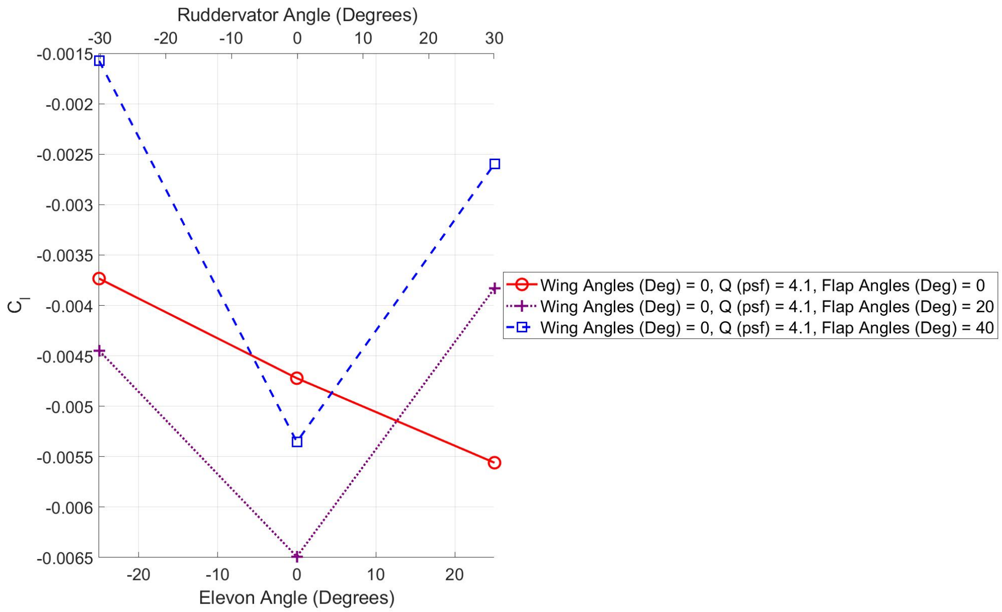

Figure 82. Propellers off C_l vs elevon and ruddervator deflection angles with all flaps' deflection.

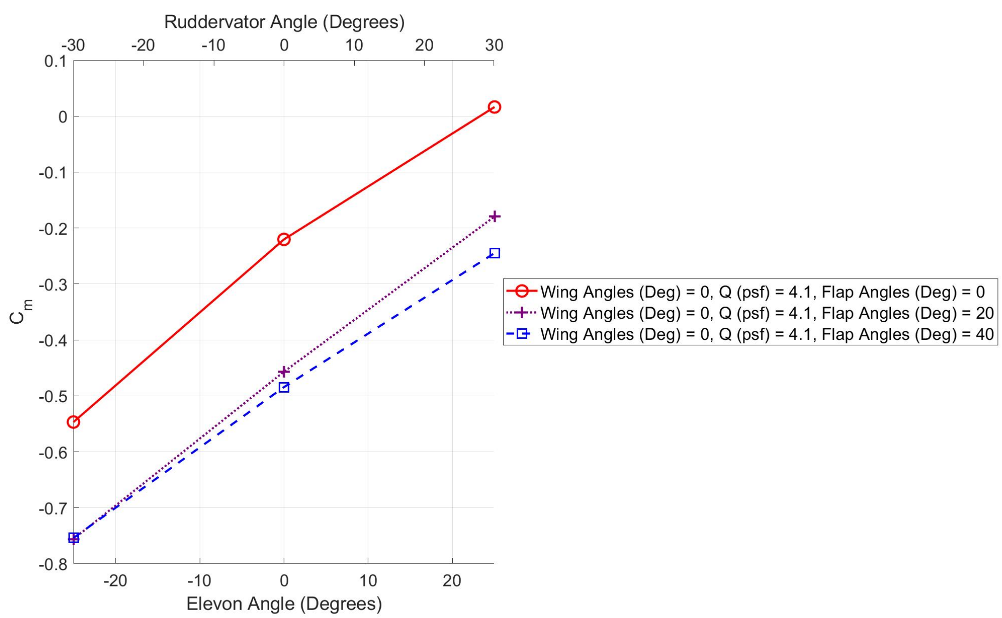

Figure 83. Propellers off C_m vs elevon and ruddervator deflection angles with all flaps' deflection.

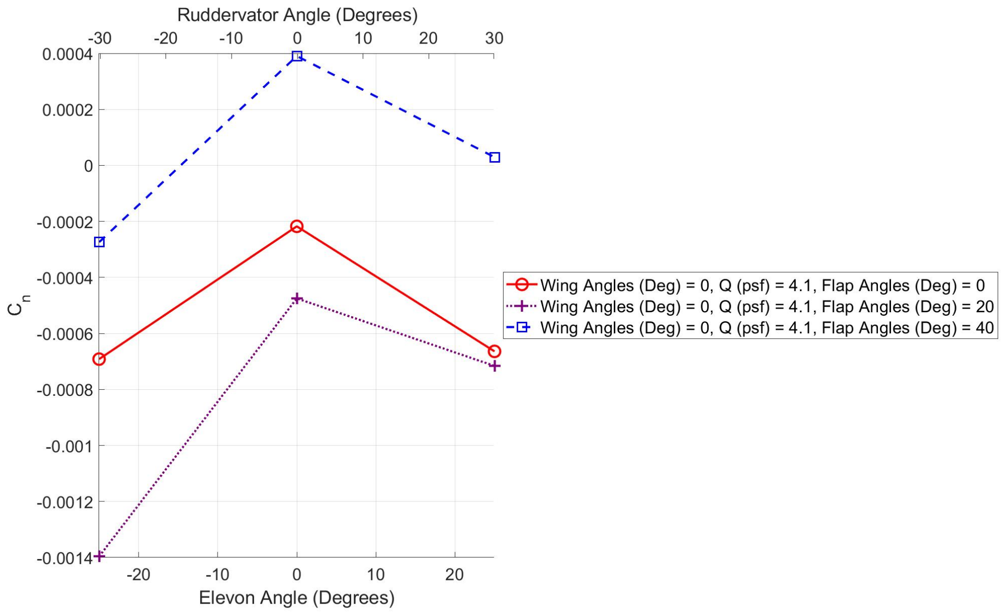

Figure 84. Propellers off C_n vs elevon and ruddervator deflection angles with all flaps' deflection.

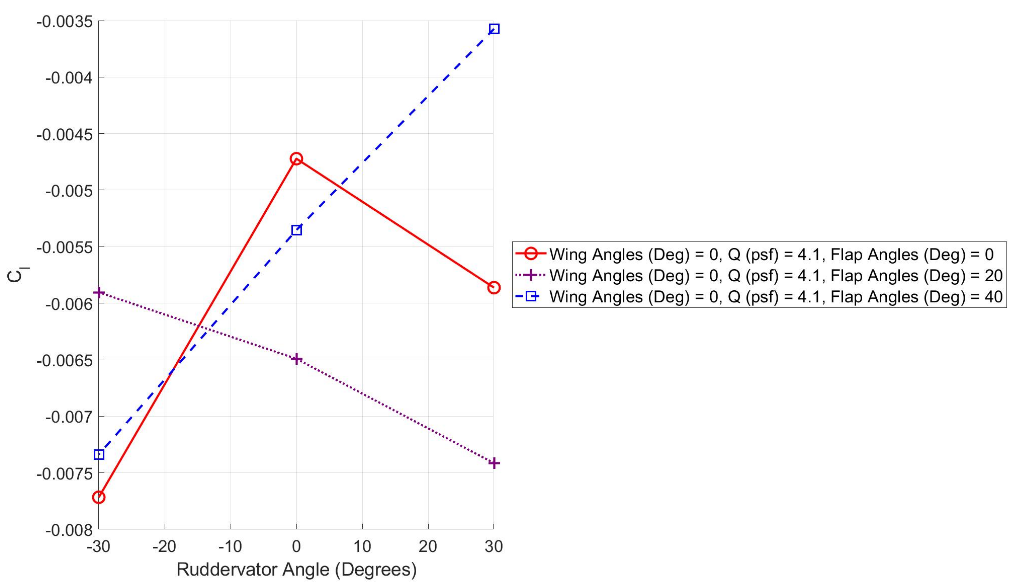

Figure 85. Propellers off C_l vs ruddervator deflection angle with all flaps' deflection.

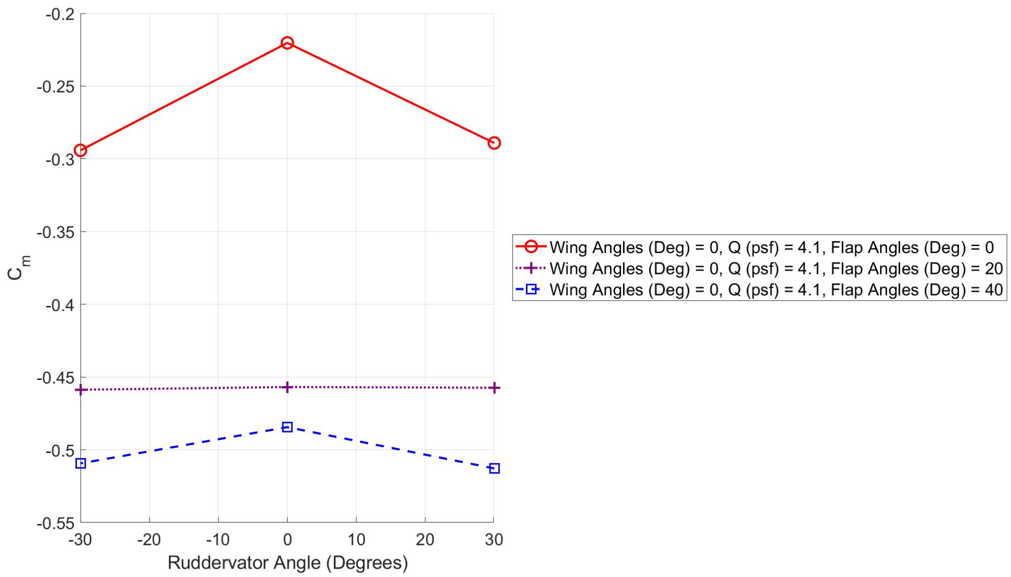

Figure 86. Propellers off C_m vs ruddervator deflection angle with all flaps' deflection.

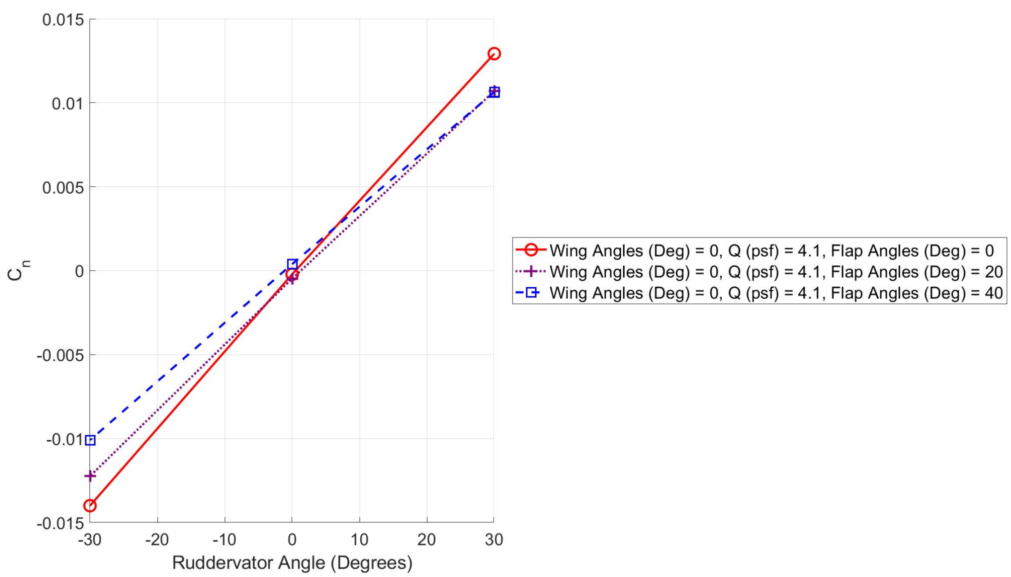

Figure 87. Propellers off C_n vs ruddervator deflection angle with all flaps' deflection.

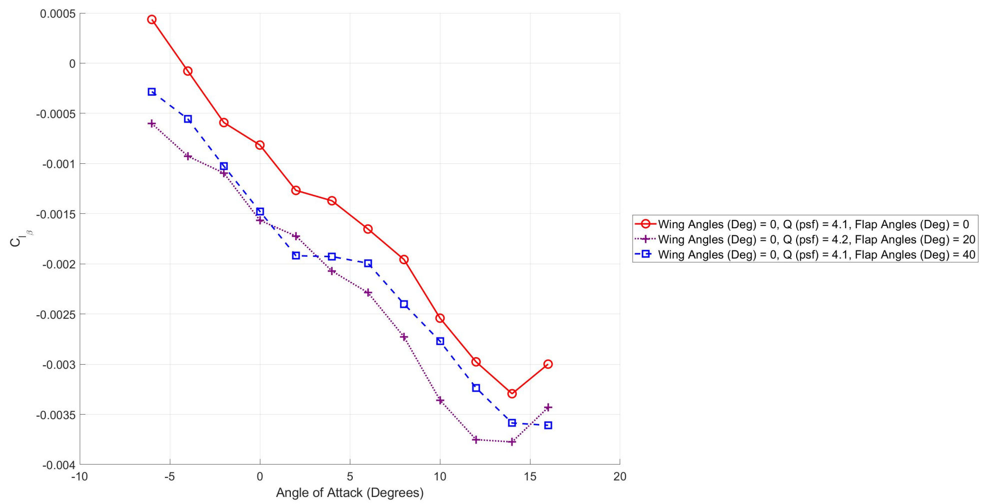

Figure 88. Propellers off C_{l_β} vs angle of attack with all flaps' deflection.

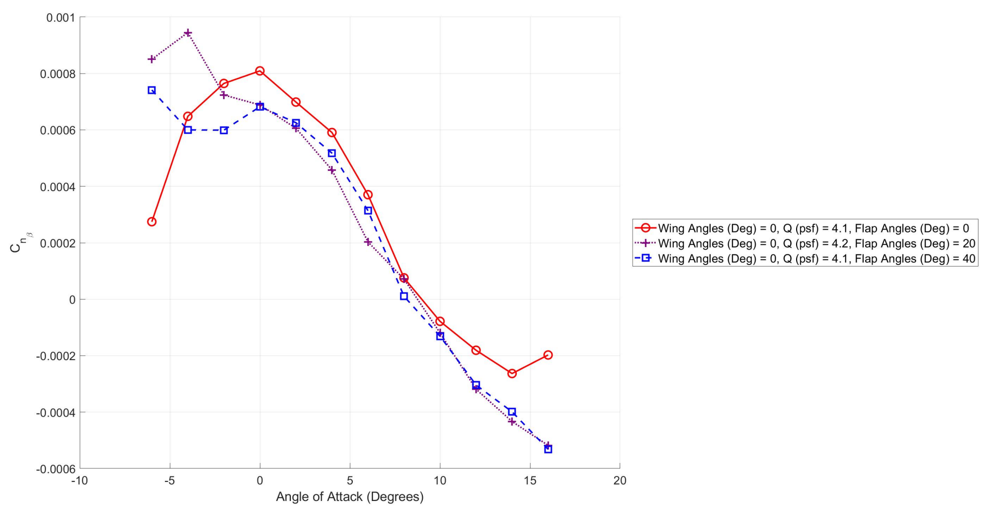

Figure 89. Propellers off C_{n_β} vs angle of attack with all flaps' deflection.

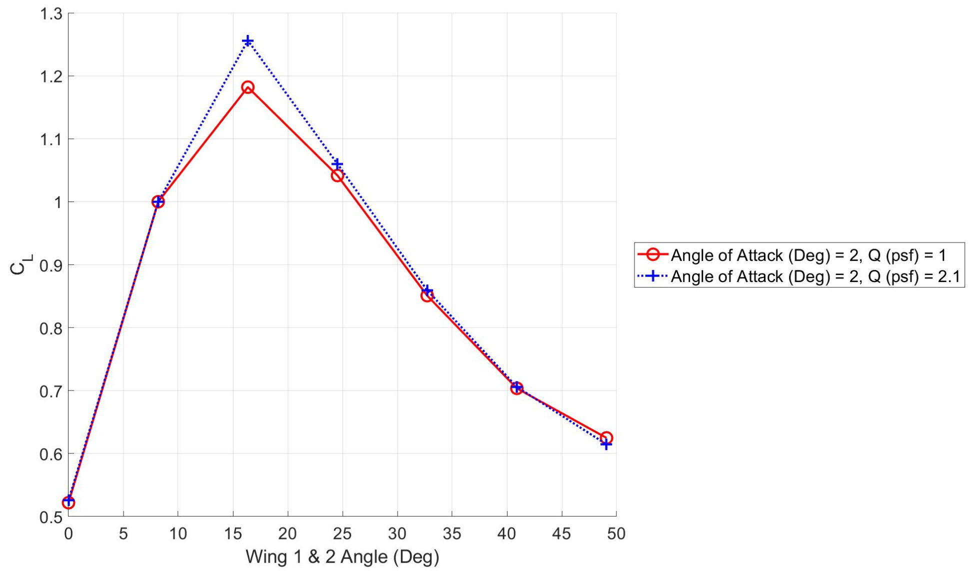

Figure 90. Propellers off C_L vs wing angle variation.

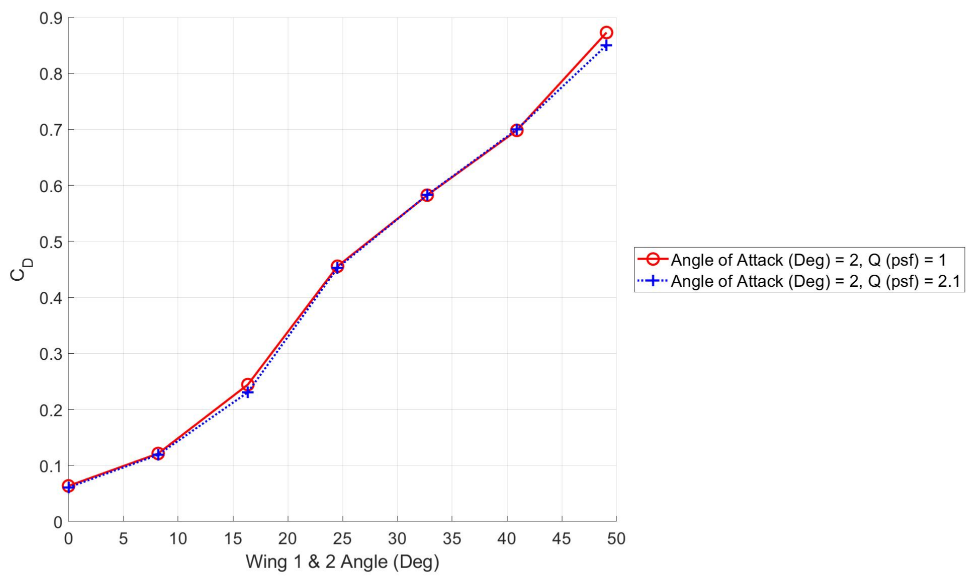

Figure 91. Propellers off C_D vs wing angle variation.

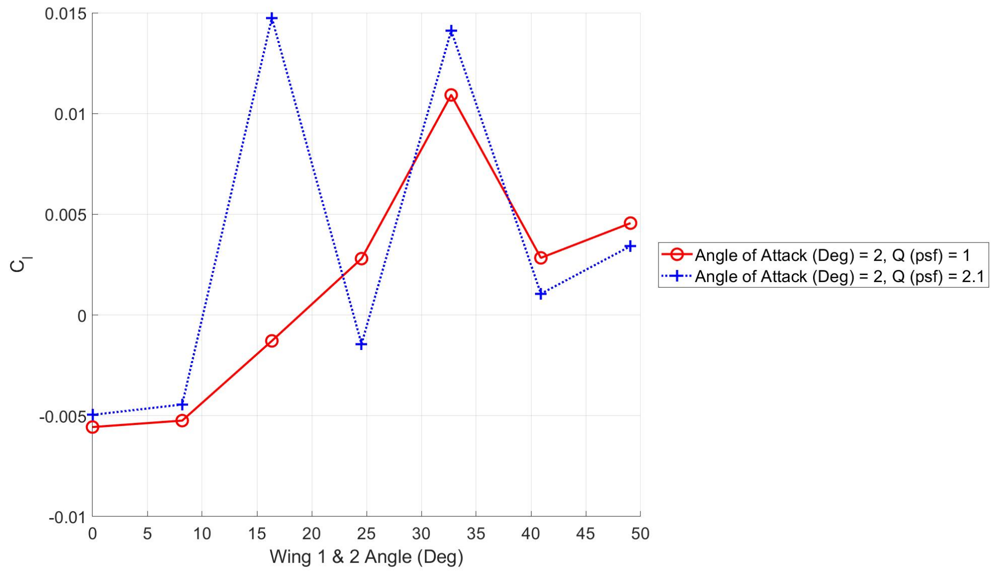

Figure 92. Propellers off C_l vs wing angle variation.

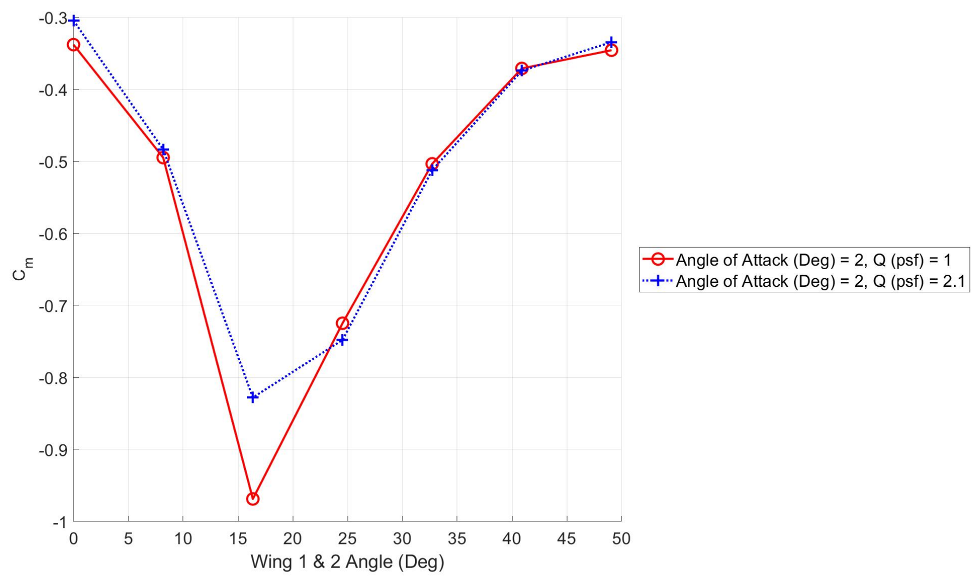

Figure 93. Propellers off C_m vs wing angle variation.

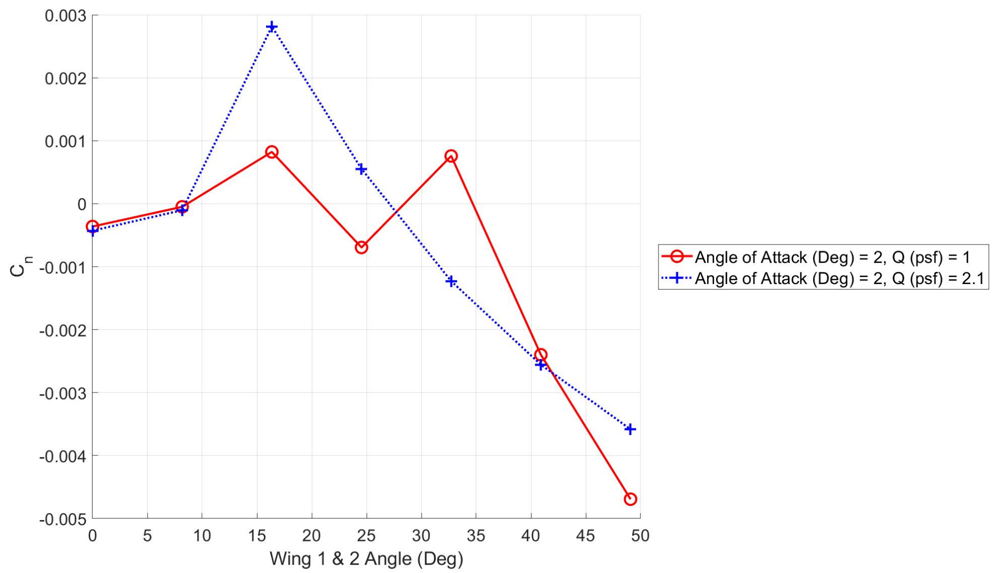

Figure 94. Propellers off C_n vs wing angle variation.

Appendix B

Hover Performance and Stability Plots

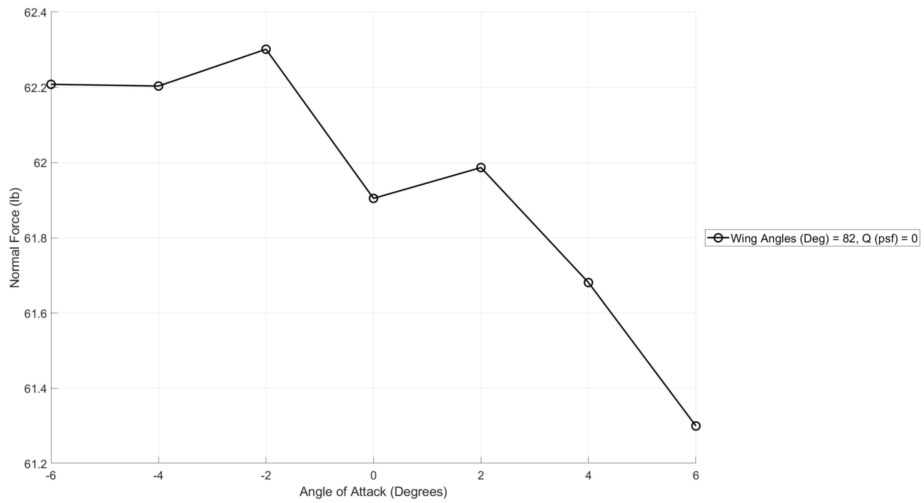

Figure 95. Hover trim point normal force vs angle of attack.

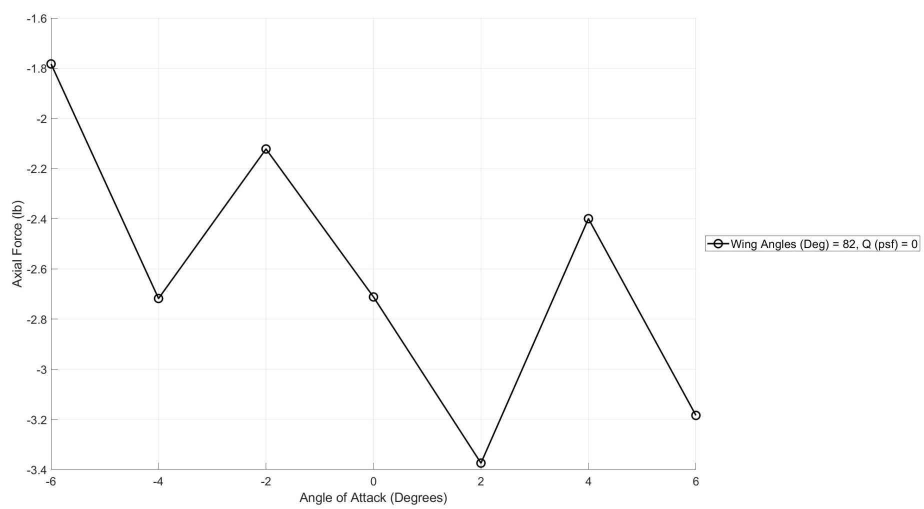

Figure 96. Hover trim point axial force vs angle of attack.

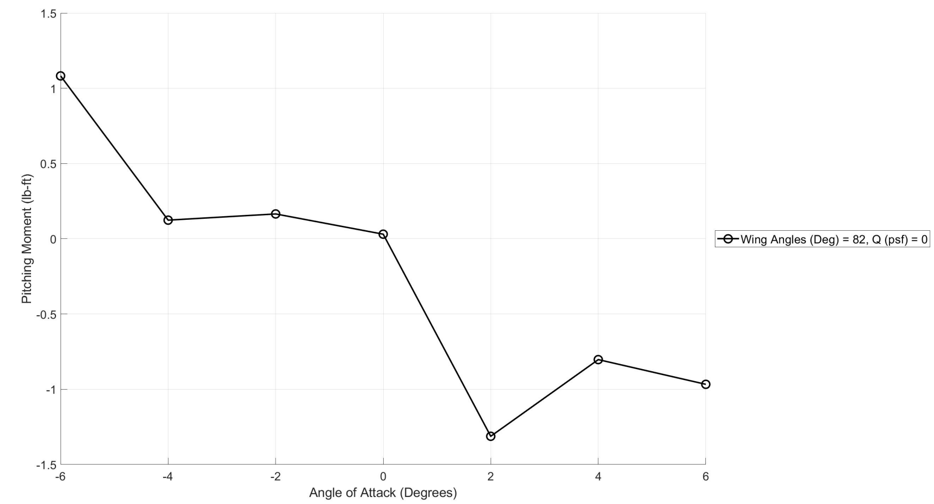

Figure 97. Hover trim point pitching moment vs angle of attack.

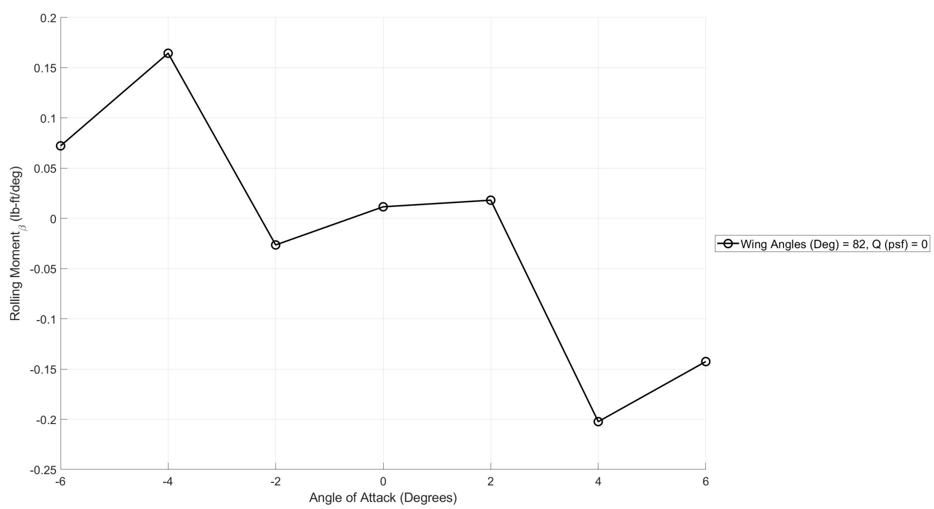

Figure 98. Hover trim point rolling moment$_\beta$ vs angle of attack.

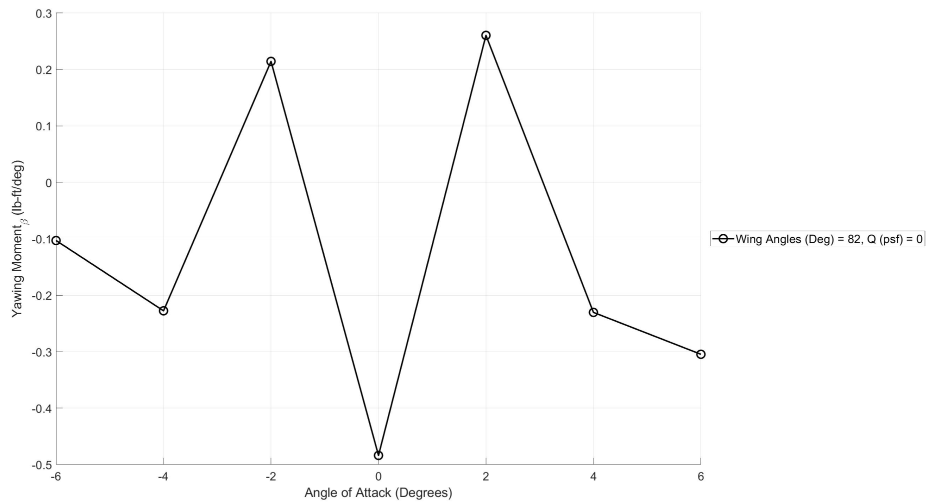

Figure 99. Hover trim point yawing moment$_\beta$ vs angle of attack.

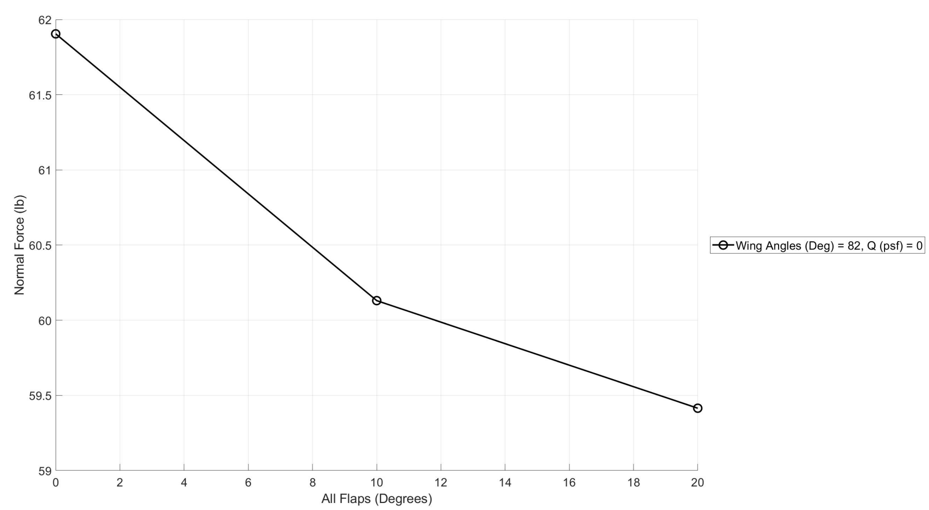

Figure 100. Hover trim point normal force vs all flap deflection angle.

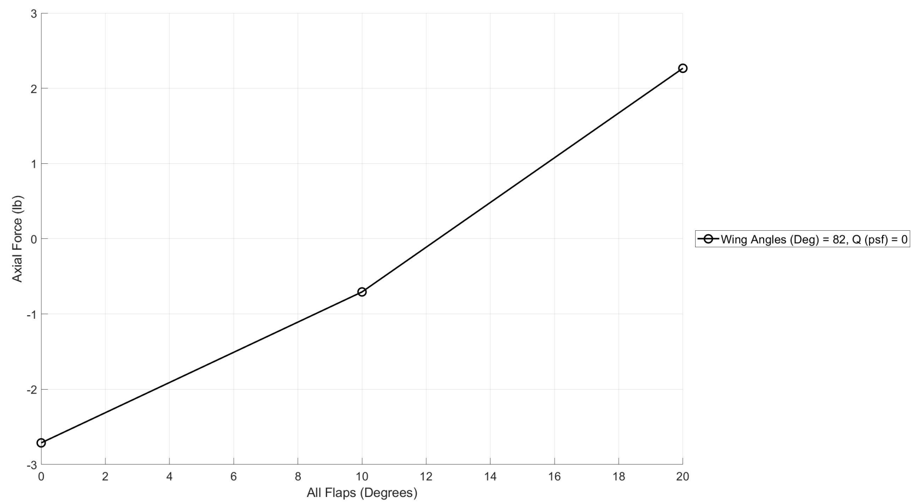

Figure 101. Hover trim point axial force vs all flap deflection angle.

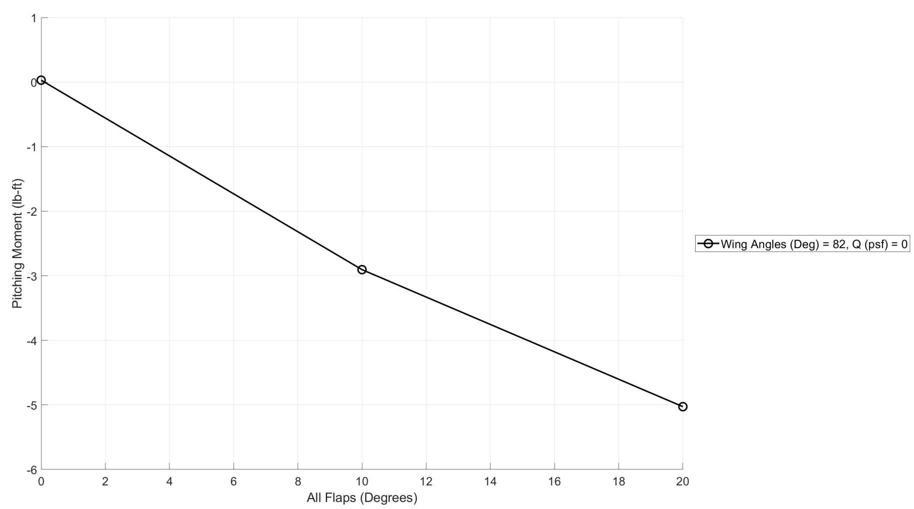

Figure 102. Hover trim point pitching moment vs all flap deflection angle.

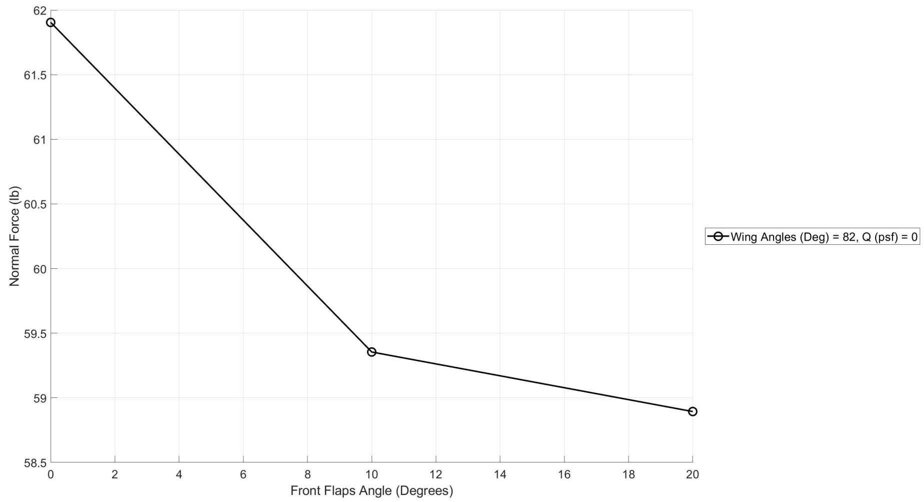

Figure 103. Hover trim point normal force vs front flap deflection angle.

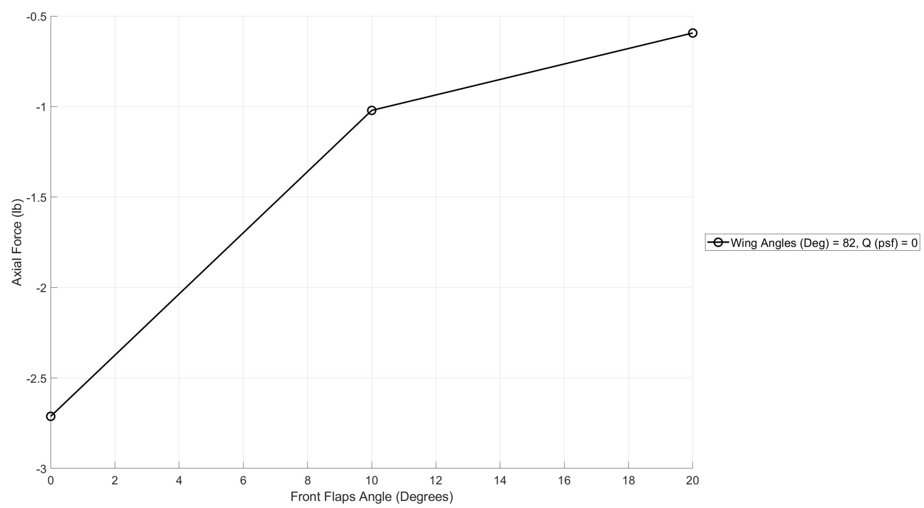

Figure 104. Hover trim point axial force vs front flap deflection angle.

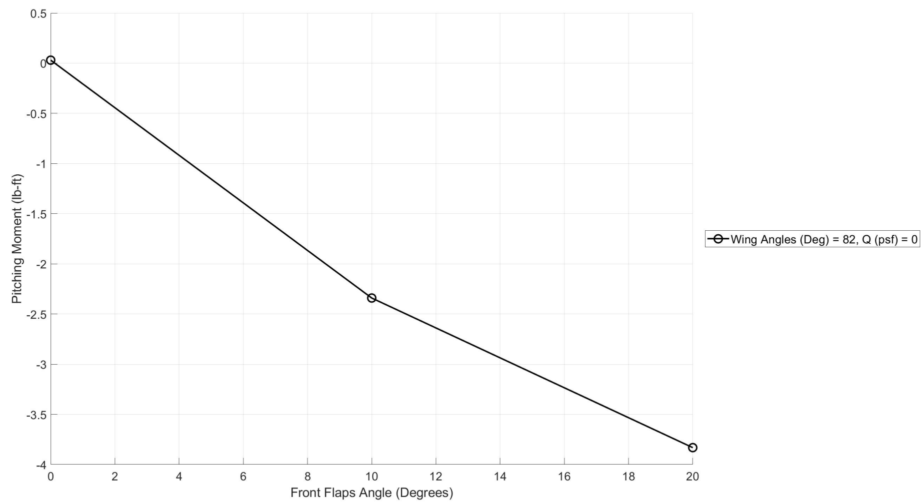

Figure 105. Hover trim point pitching moment vs front flap deflection angle.

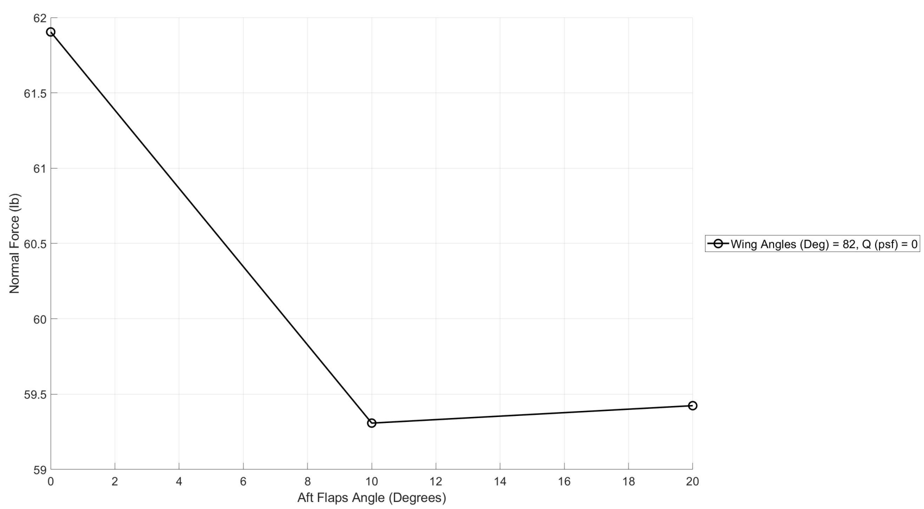

Figure 106. Hover trim point normal force vs aft flap deflection angle.

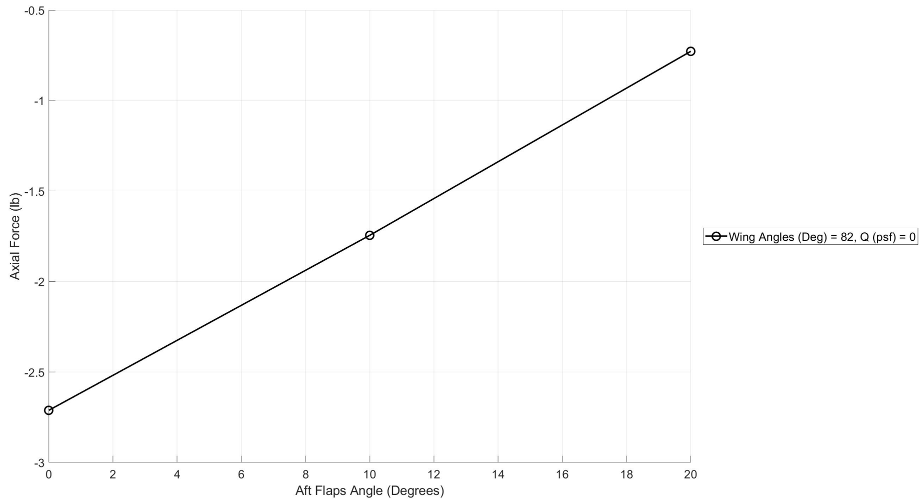

Figure 107. Hover trim point axial force vs aft flap deflection angle.

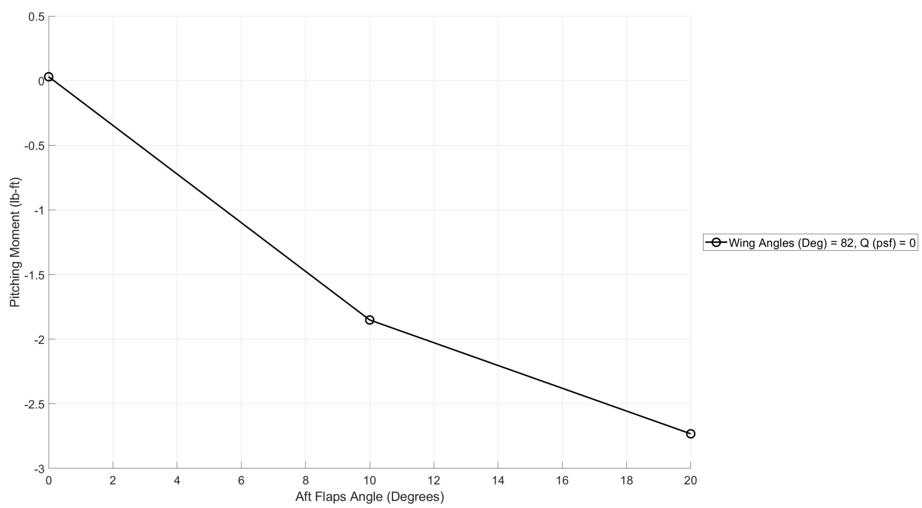

Figure 108. Hover trim point pitching moment vs aft flap deflection angle.

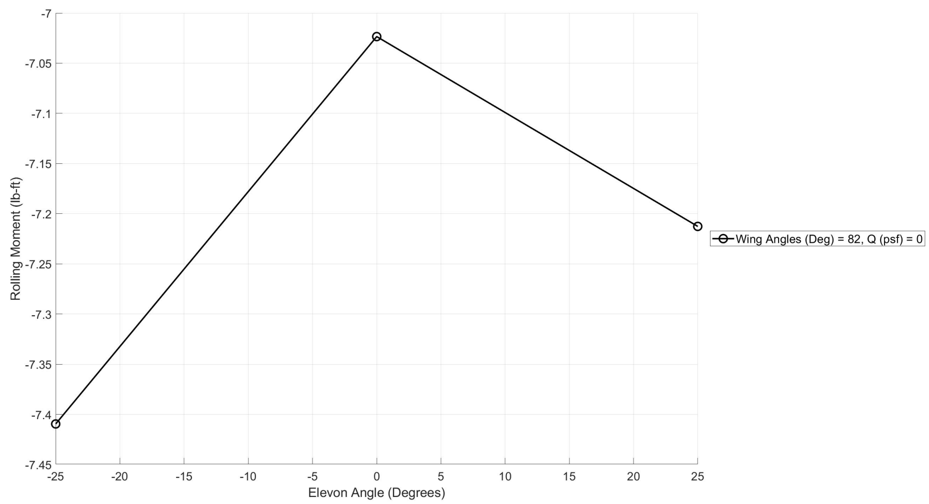

Figure 109. Hover trim point rolling moment vs elevon deflection angle.

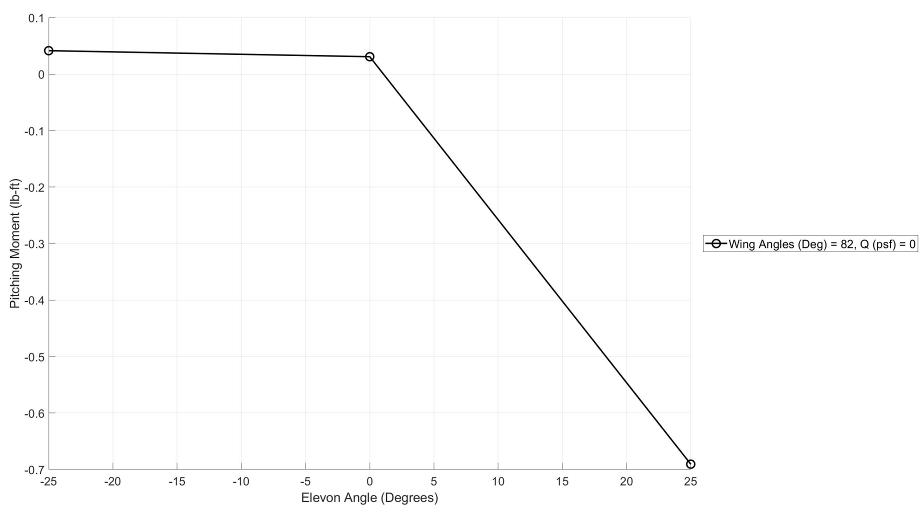

Figure 110. Hover trim point pitching moment vs elevon deflection angle.

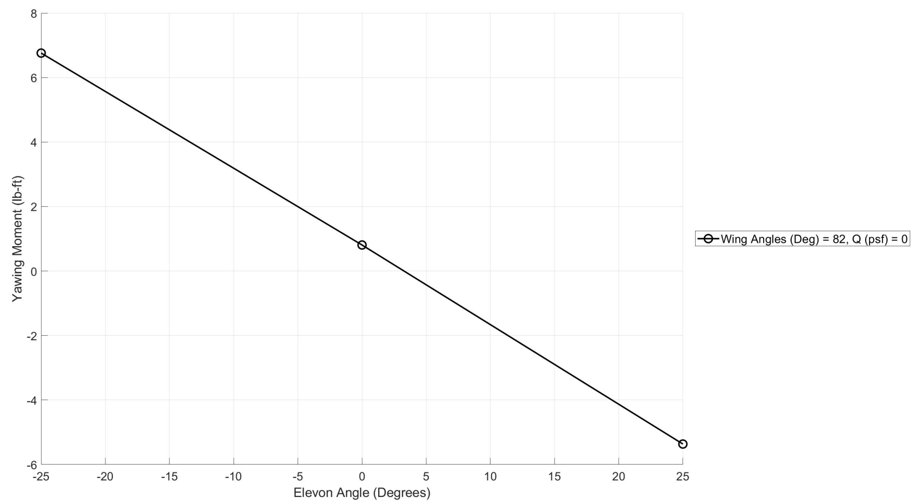

Figure 111. Hover trim point yawing moment vs elevon deflection angle.

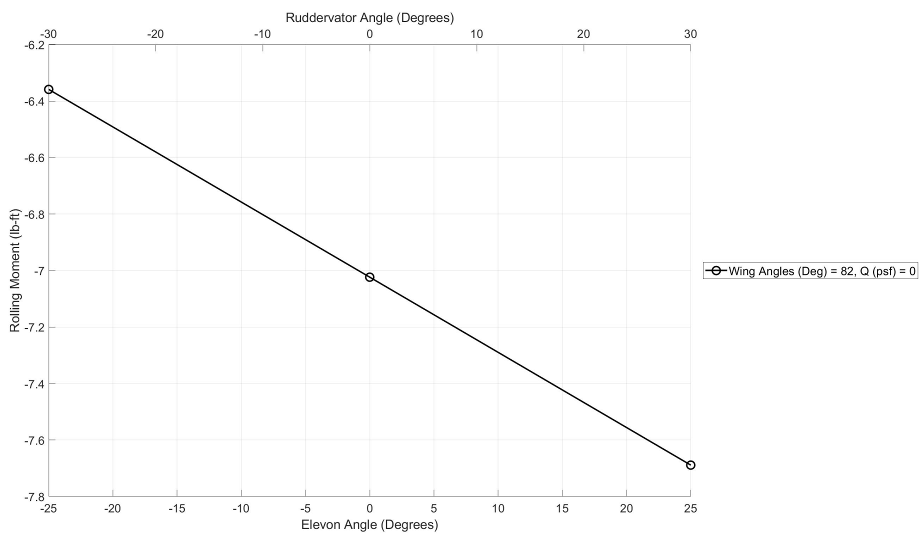

Figure 112. Hover trim point rolling moment vs elevon and ruddervator deflection angles.

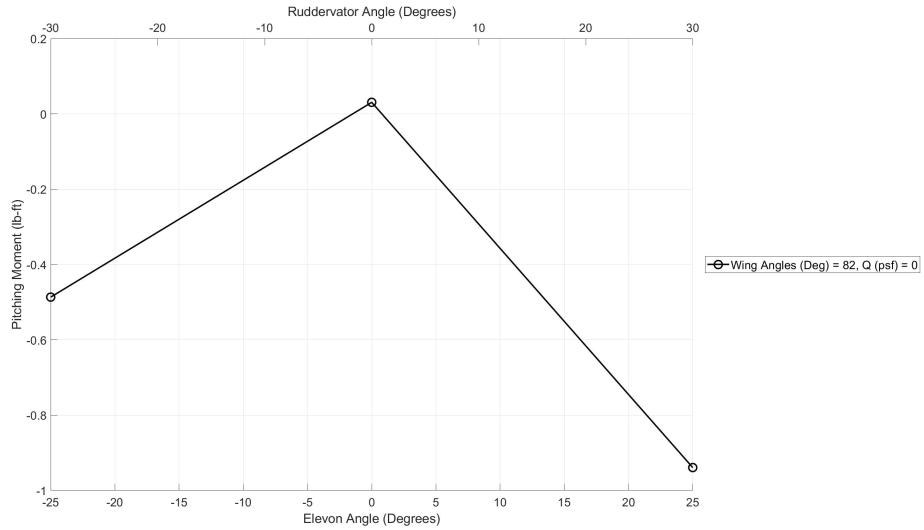

Figure 113. Hover trim point pitching moment vs elevon and ruddervator deflection angles.

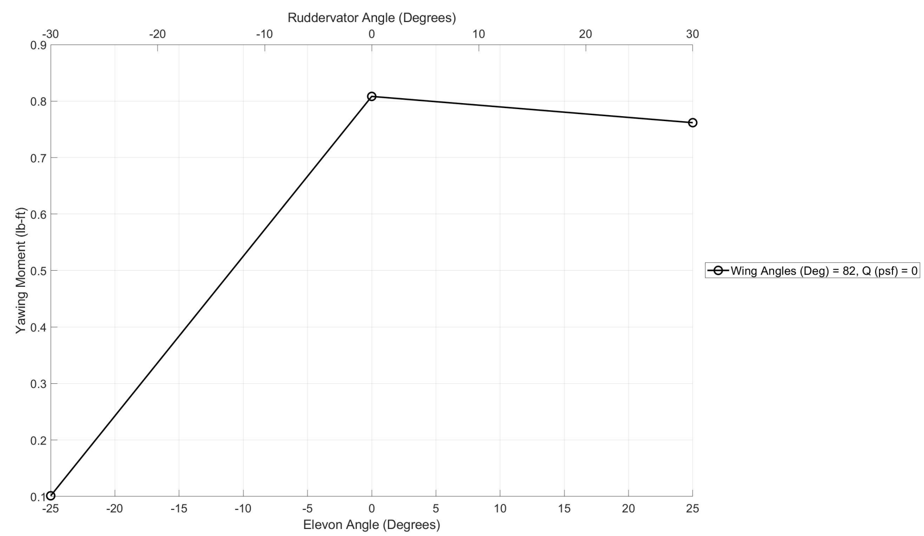

Figure 114. Hover trim point yawing moment vs elevon and ruddervator deflection angles.

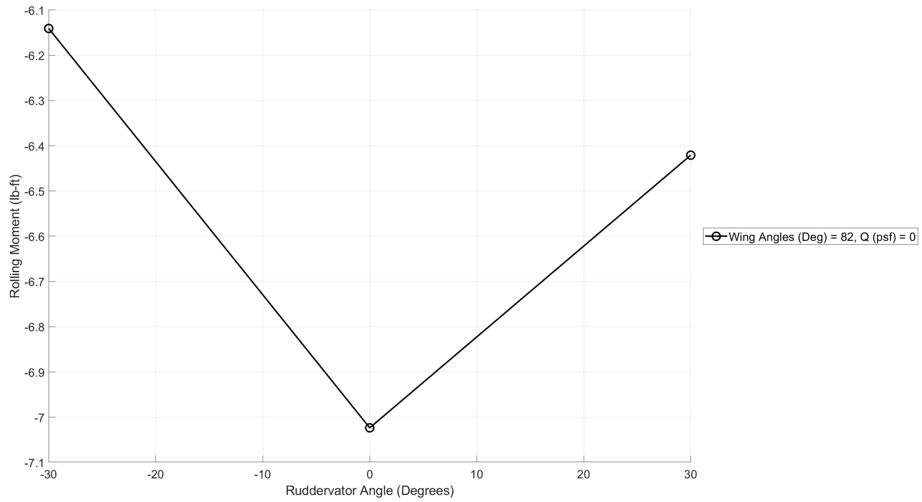

Figure 115. Hover trim point rolling moment vs ruddervator deflection angle.

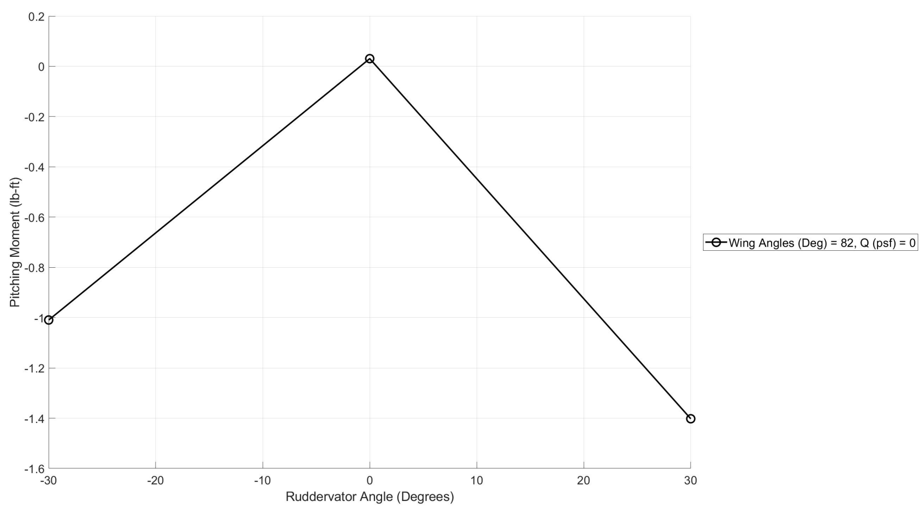

Figure 116. Hover trim point pitching moment vs ruddervator deflection angle.

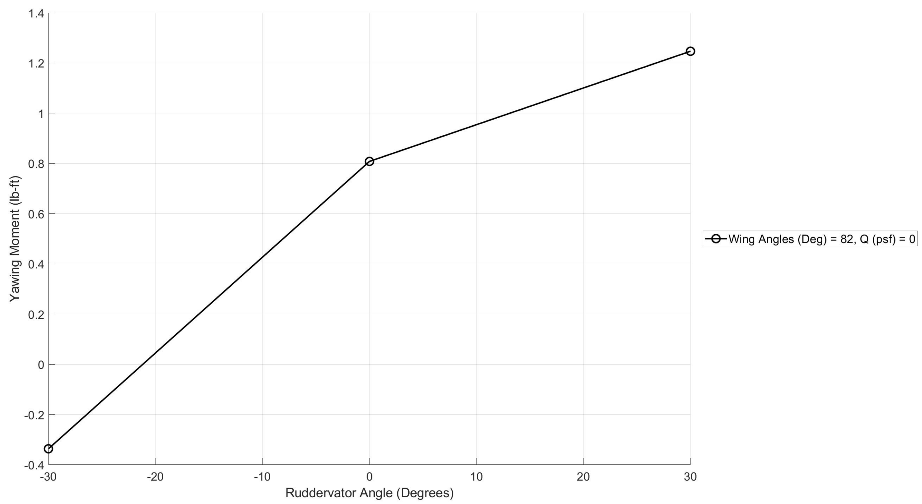

Figure 117. Hover trim point yawing moment vs ruddervator deflection angle.

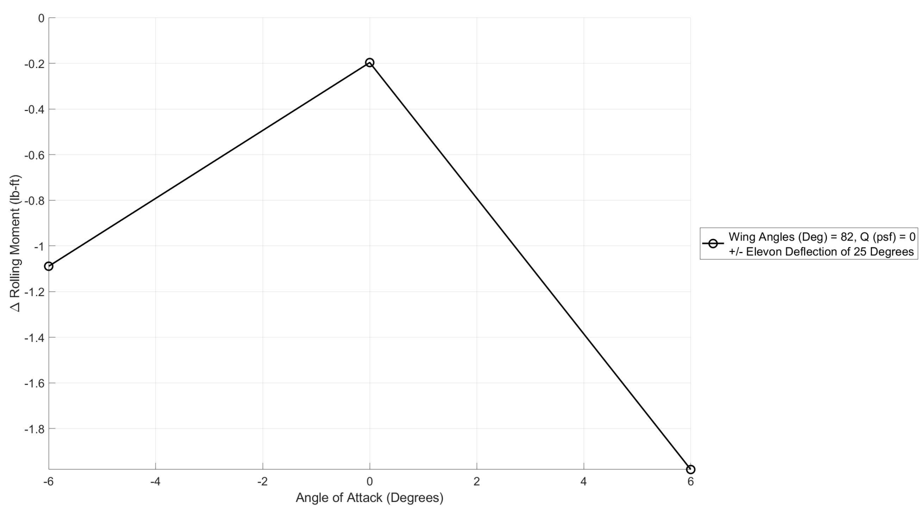

Figure 118. Hover trim point Δ rolling moment vs angle of attack for elevon deflection.

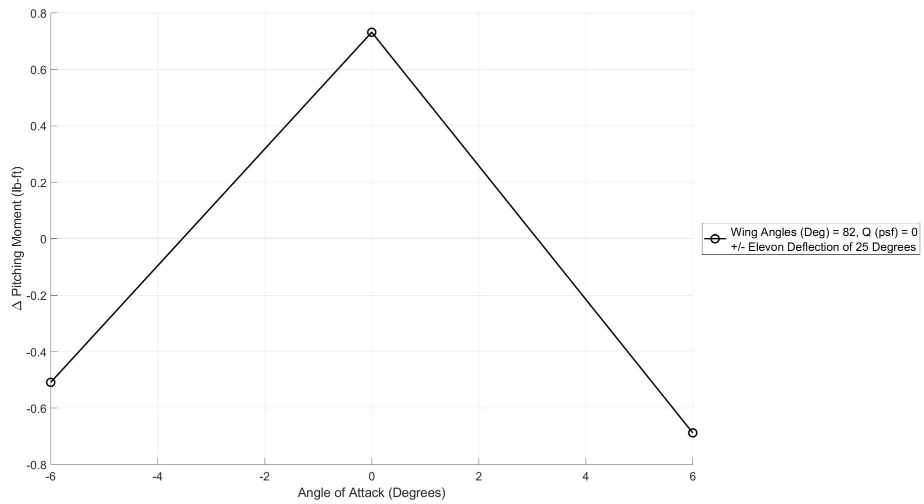

Figure 119. Hover trim point Δ pitching moment vs angle of attack for elevon deflection.

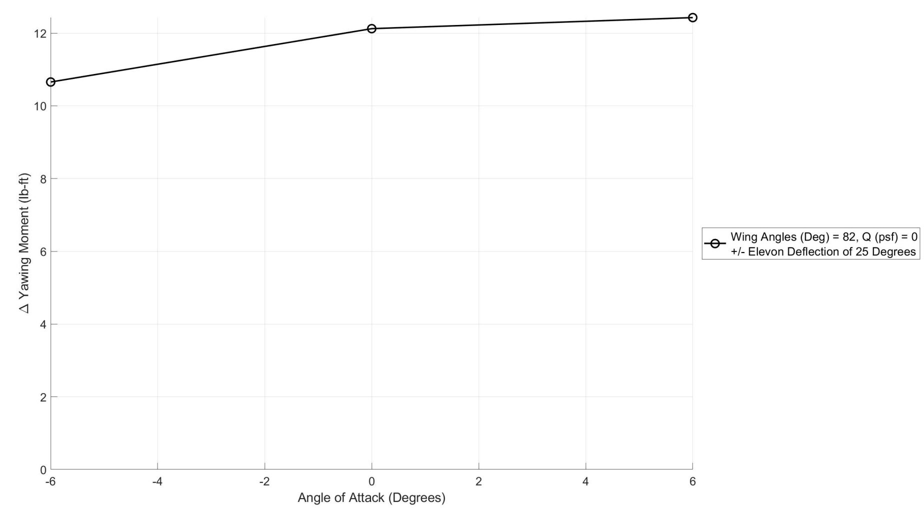

Figure 120. Hover trim point Δ yawing moment vs angle of attack for elevon deflection.

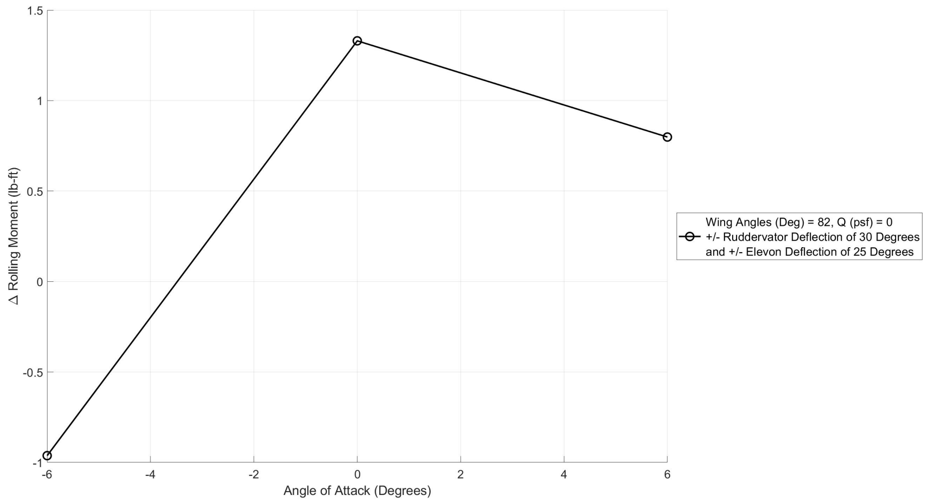

Figure 121. Hover trim point Δ rolling moment vs angle of attack for elevon and ruddervator deflection.

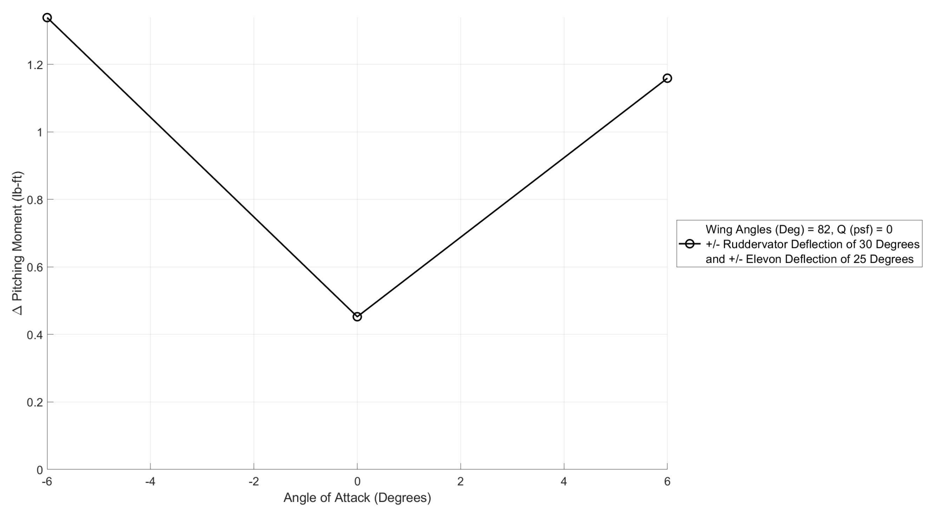

Figure 122. Hover trim point Δ pitching moment vs angle of attack for elevon and ruddervator deflection.

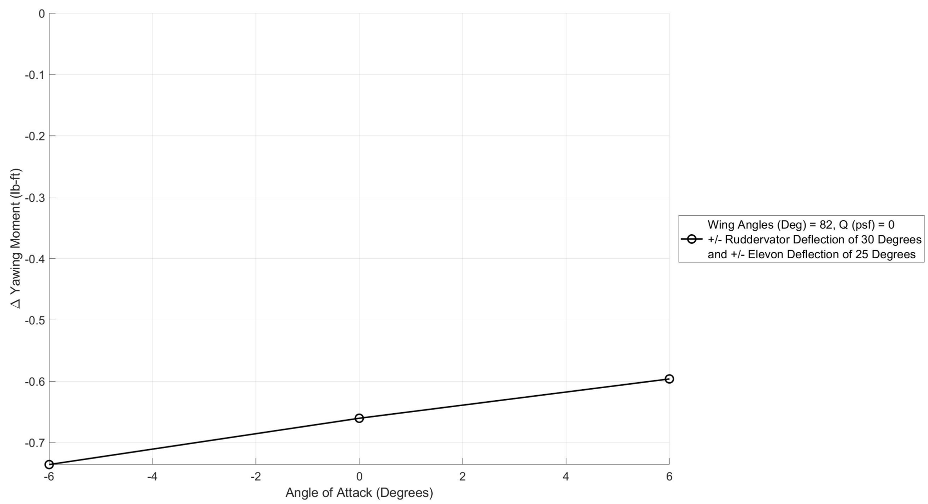

Figure 123. Hover trim point Δ yawing moment vs angle of attack for elevon and ruddervator deflection.

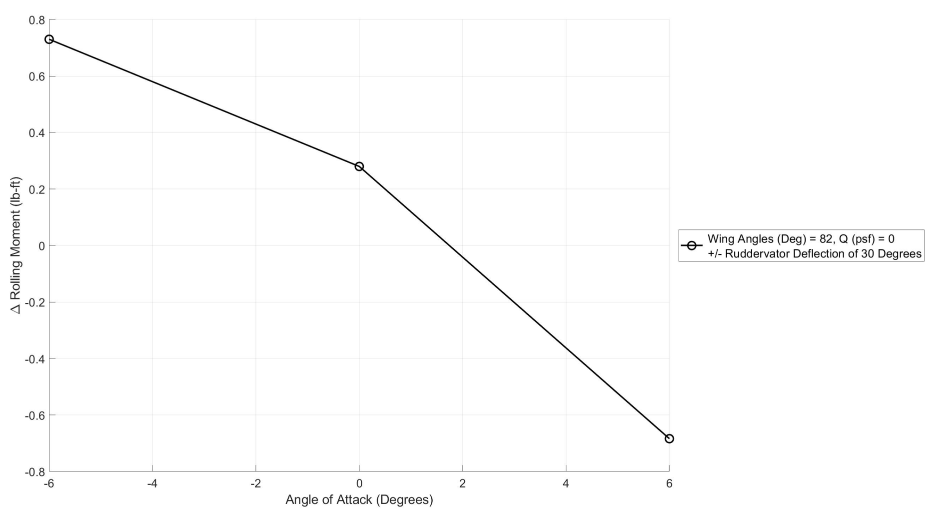

Figure 124. Hover trim point Δ rolling moment vs angle of attack for ruddervator deflection.

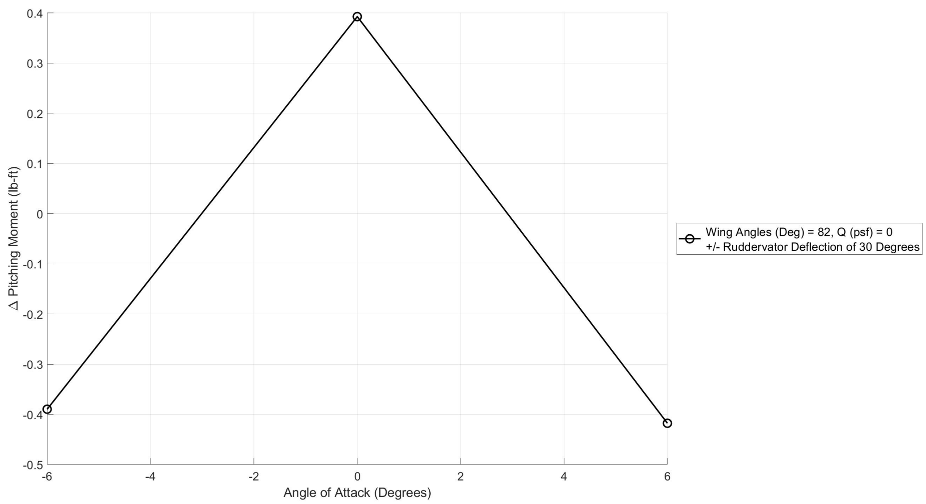

Figure 125. Hover trim point Δ pitching moment vs angle of attack for ruddervator deflection.

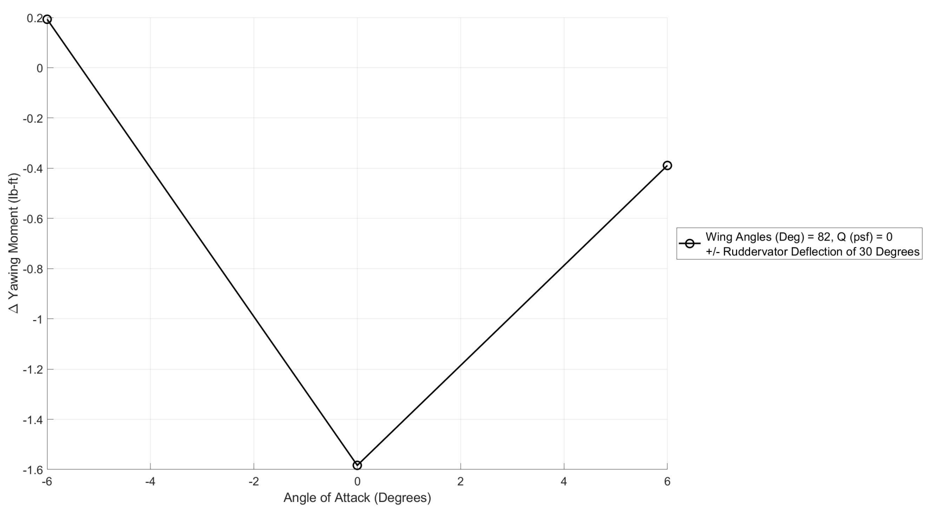

Figure 126. Hover trim point Δ yawing moment vs angle of attack for ruddervator deflection.

Appendix C

Transition Performance and Stability Plots

C.1 Transition Wing Angles 56 Degrees Performance and Stability Plots

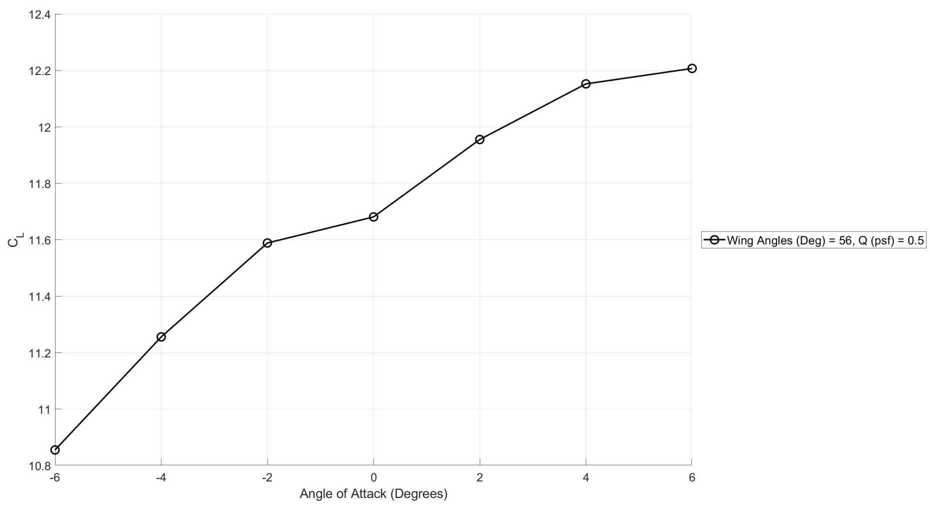

Figure 127. Wing angles 56 degrees trim point C_L vs angle of attack.

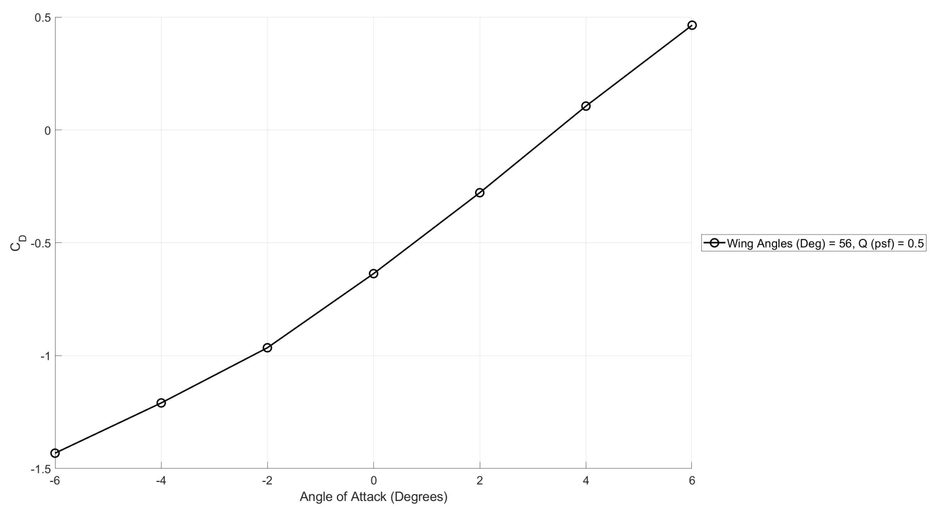

Figure 128. Wing angles 56 degrees trim point C_D vs angle of attack.

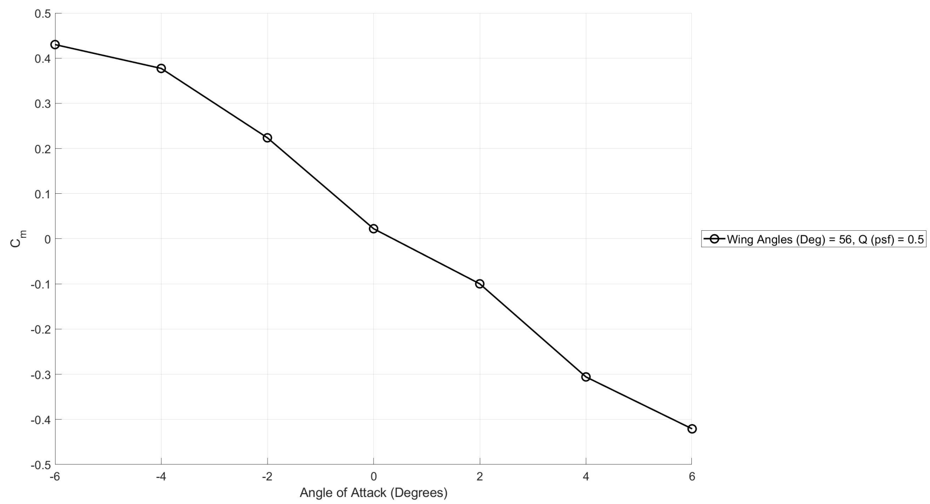

Figure 129. Wing angles 56 degrees trim point C_m vs angle of attack.

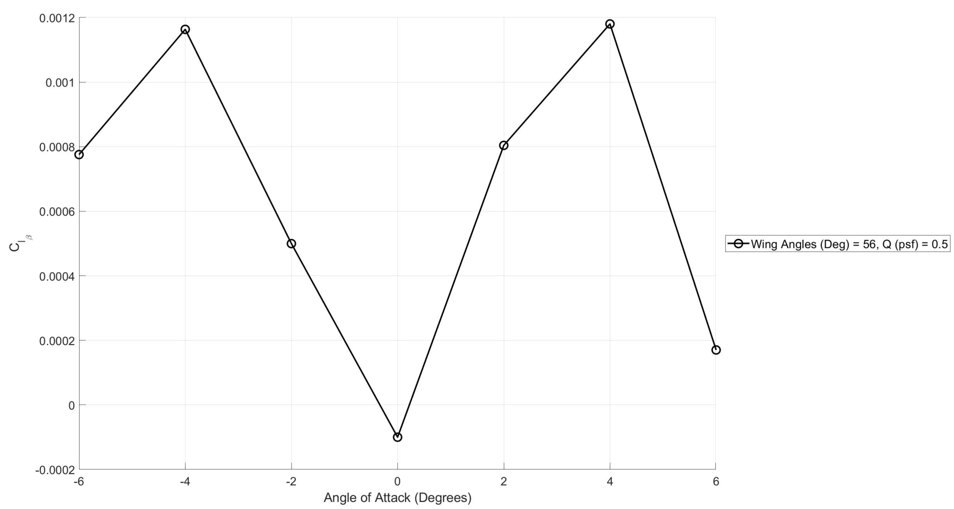

Figure 130. Wing angles 56 degrees trim point C_{l_β} vs angle of attack.

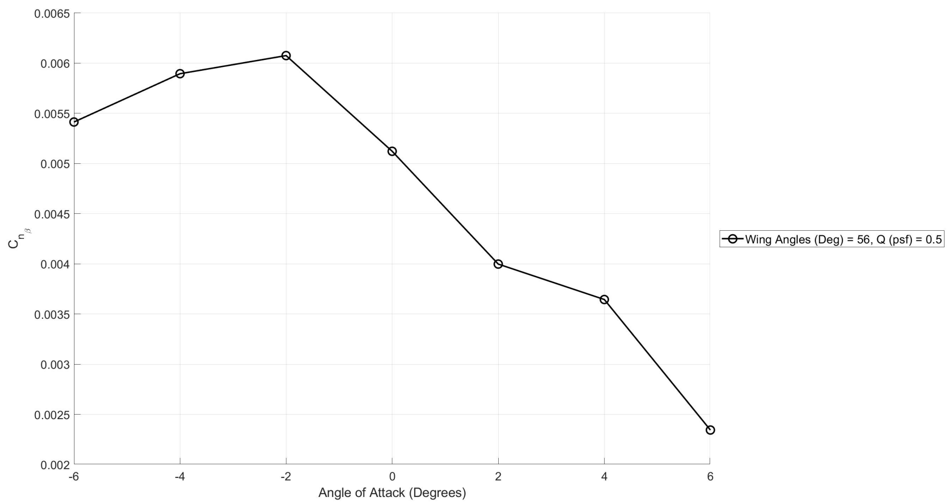

Figure 131. Wing angles 56 degrees trim point C_{n_β} vs angle of attack.

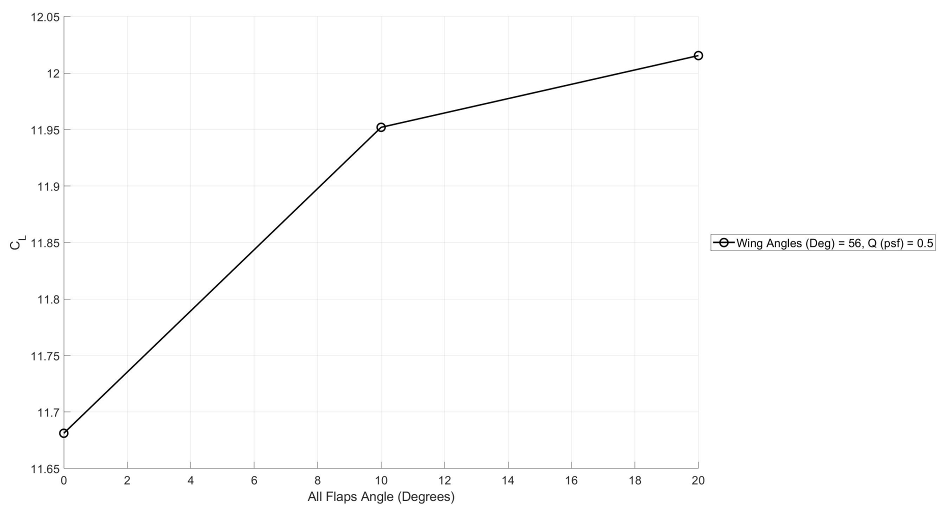

Figure 132. Wing angles 56 degrees trim point C_L vs all flap deflection angle.

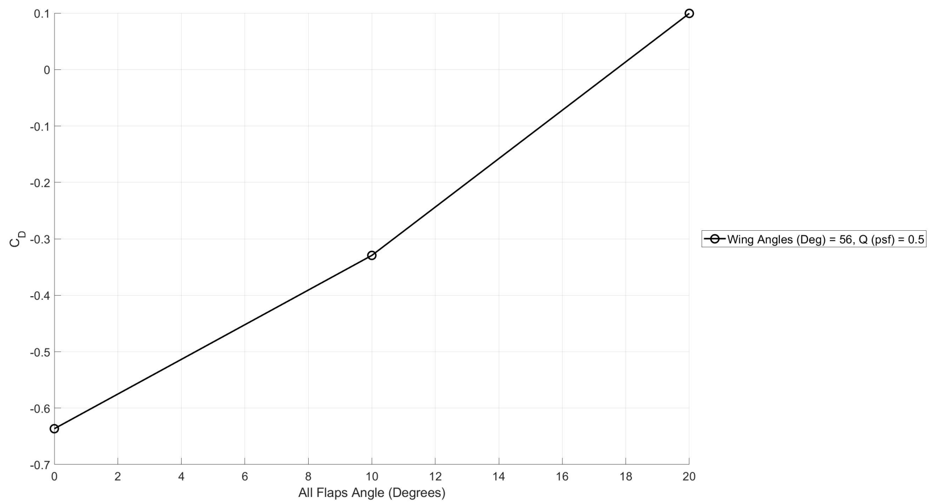

Figure 133. Wing angles 56 degrees trim point C_D vs all flap deflection angle.

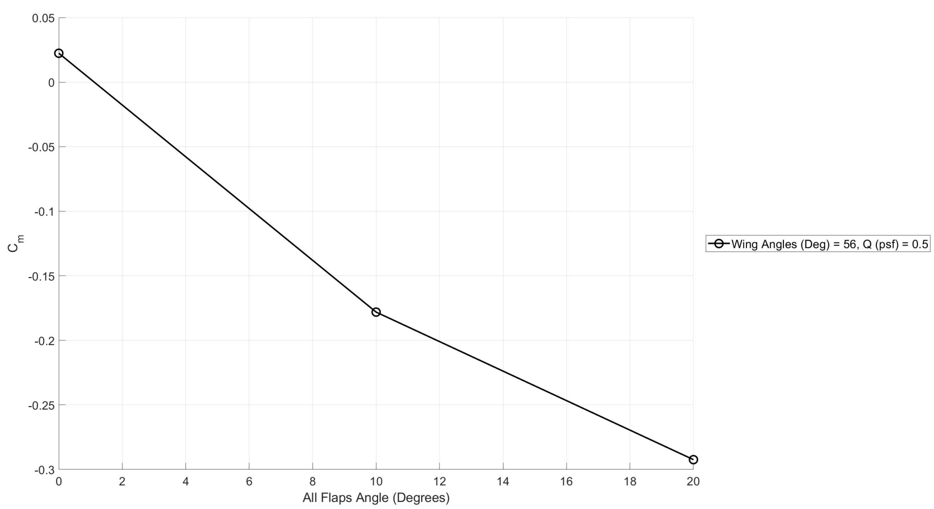

Figure 134. Wing angles 56 degrees trim point C_m vs all flap deflection angle.

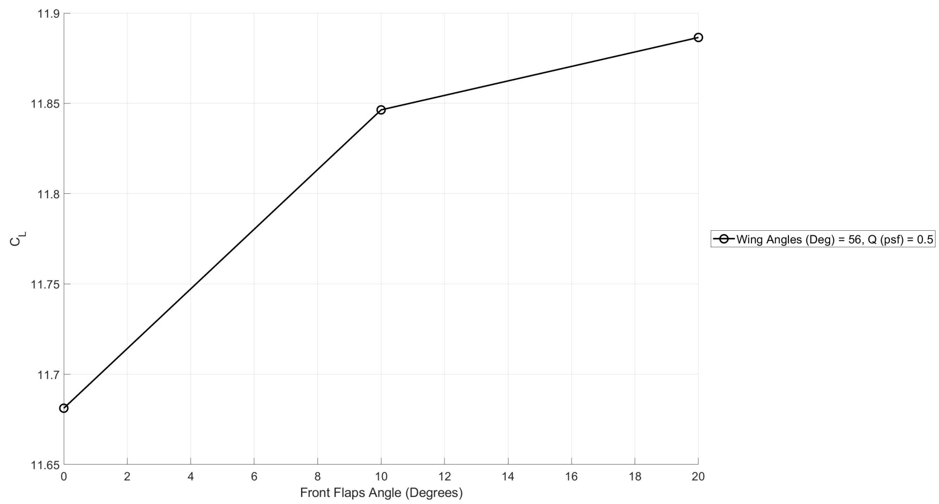

Figure 135. Wing angles 56 degrees trim point C_L vs front flap deflection angle.

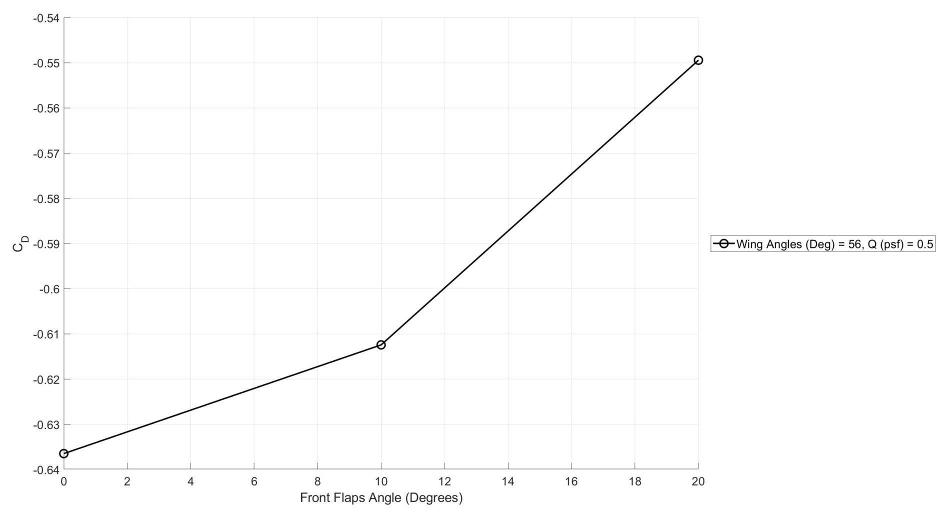

Figure 136. Wing angles 56 degrees trim point C_D vs front flap deflection angle.

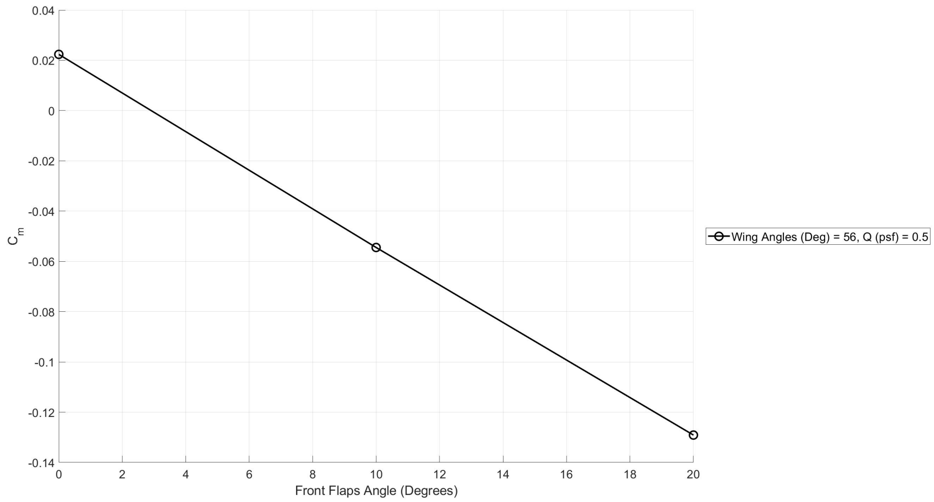

Figure 137. Wing angles 56 degrees trim point C_m vs front flap deflection angle.

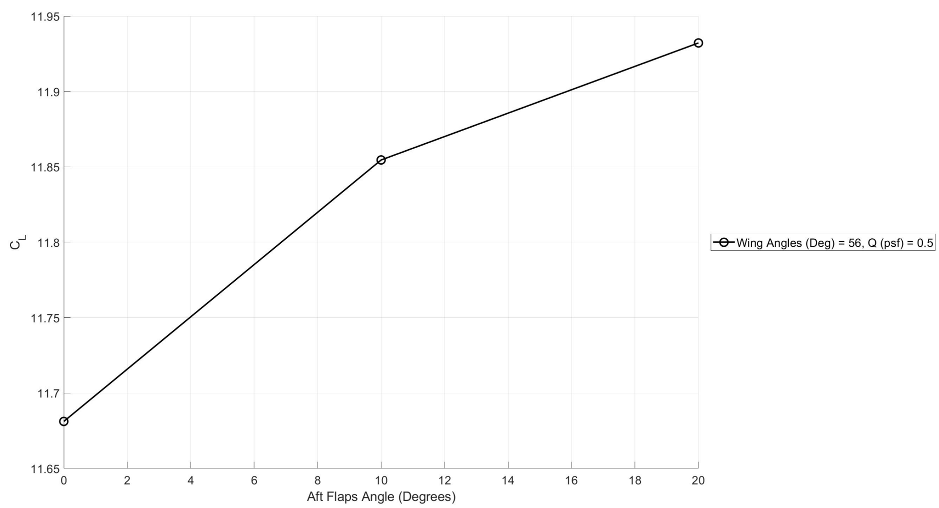

Figure 138. Wing angles 56 degrees trim point C_L vs aft flap deflection angle.

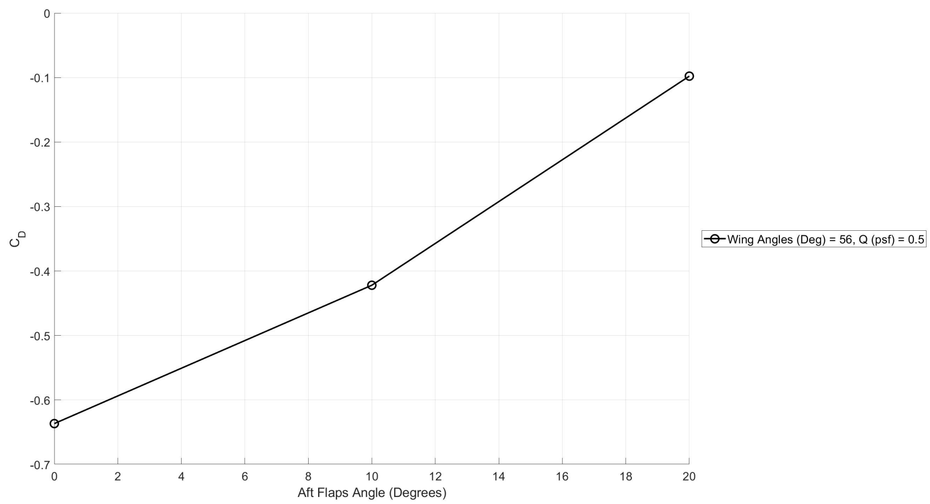

Figure 139. Wing angles 56 degrees trim point C_D vs aft flap deflection angle.

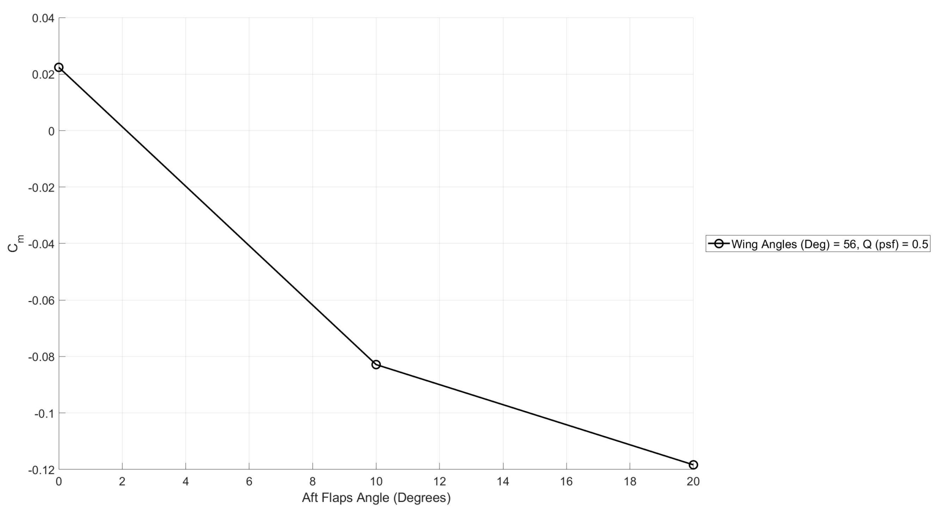

Figure 140. Wing angles 56 degrees trim point C_m vs aft flap deflection angle.

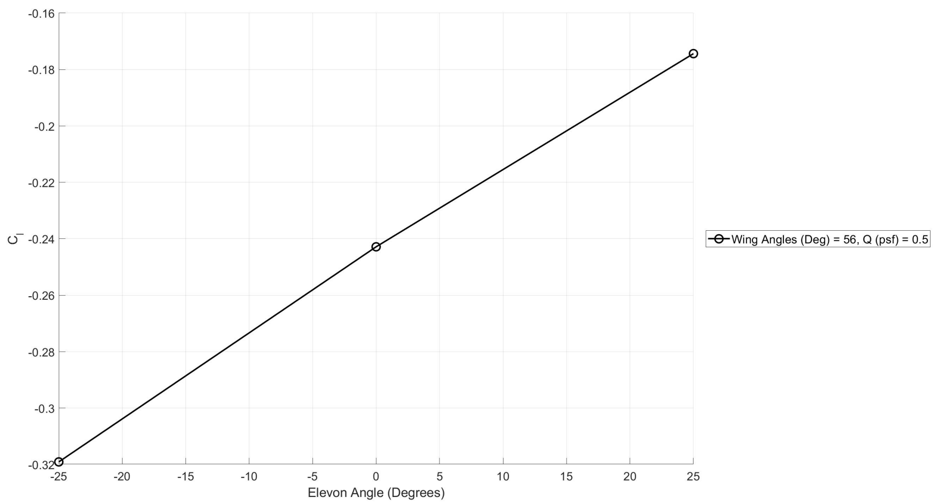

Figure 141. Wing angles 56 degrees trim point C_l vs elevon deflection angle.

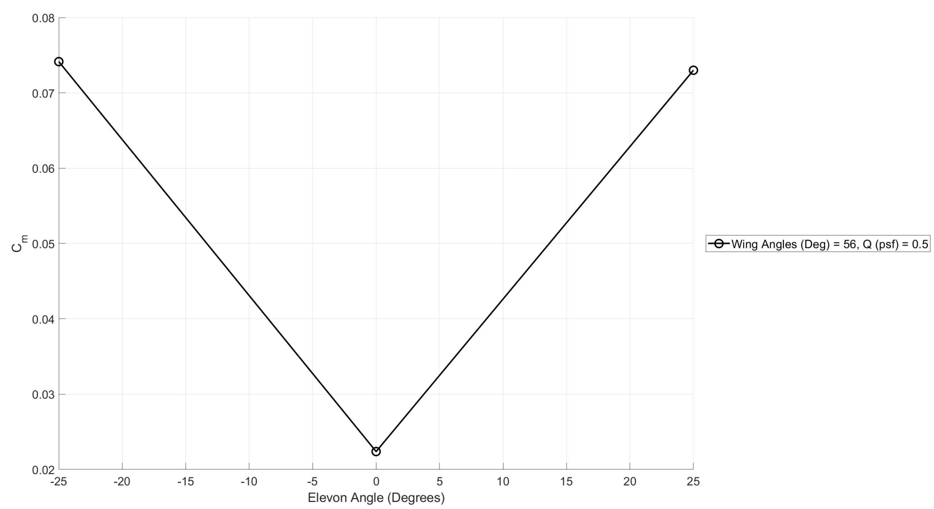

Figure 142. Wing angles 56 degrees trim point C_m vs elevon deflection angle.

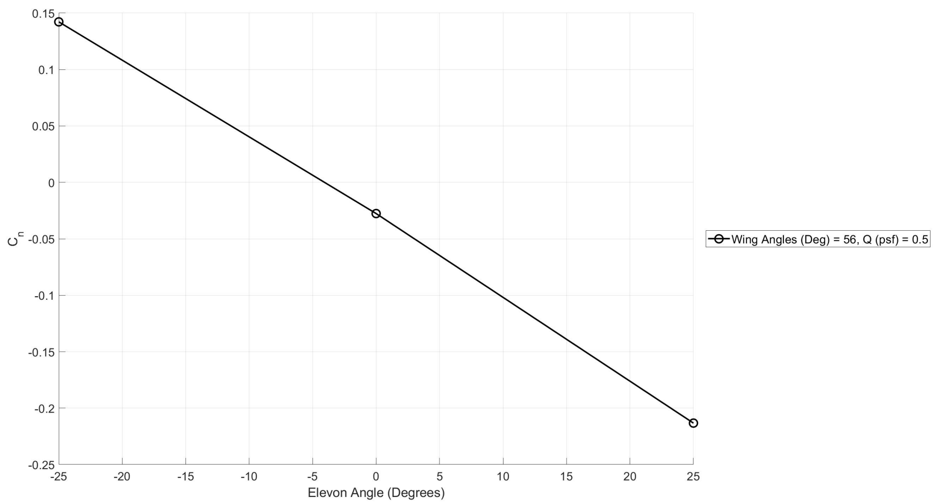

Figure 143. Wing angles 56 degrees trim point C_n vs elevon deflection angle.

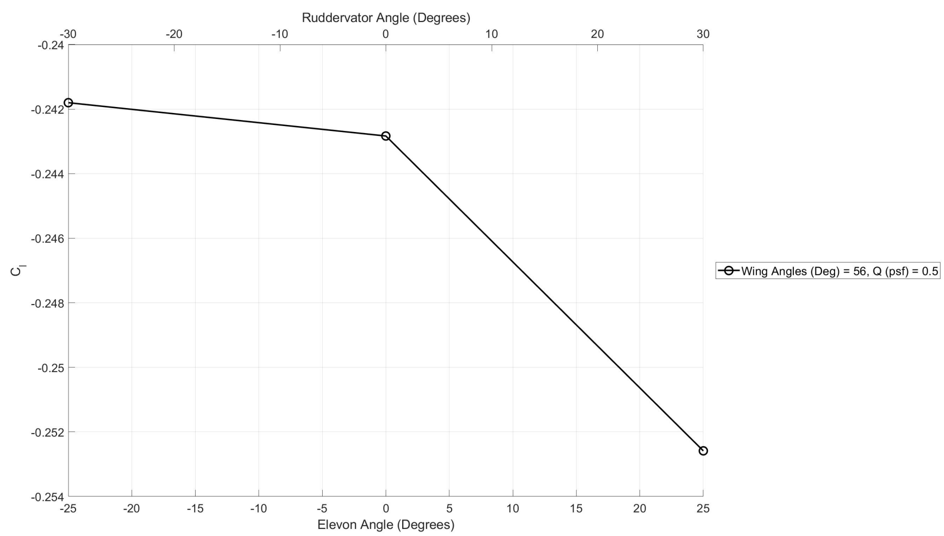

Figure 144. Wing angles 56 degrees trim point C_l vs elevon and ruddervator deflection angles.

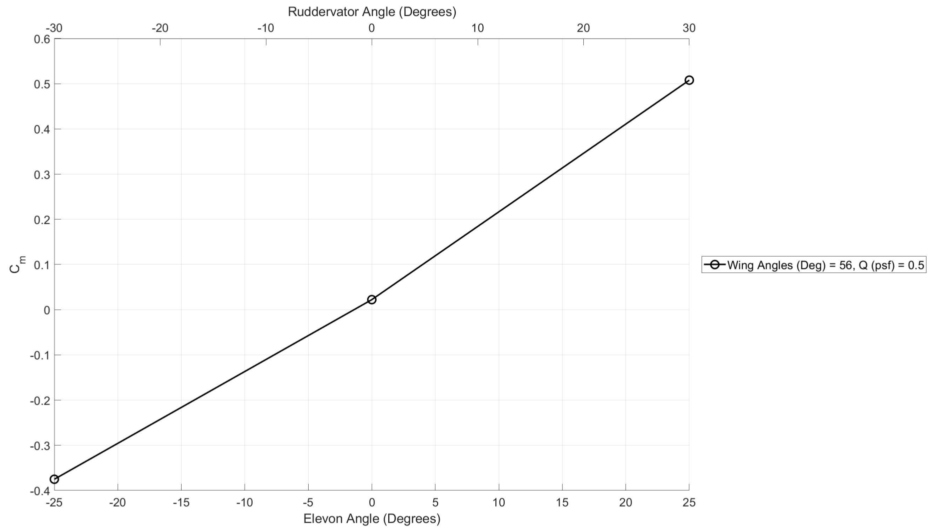

Figure 145. Wing angles 56 degrees trim point C_m vs elevon and ruddervator deflection angles.

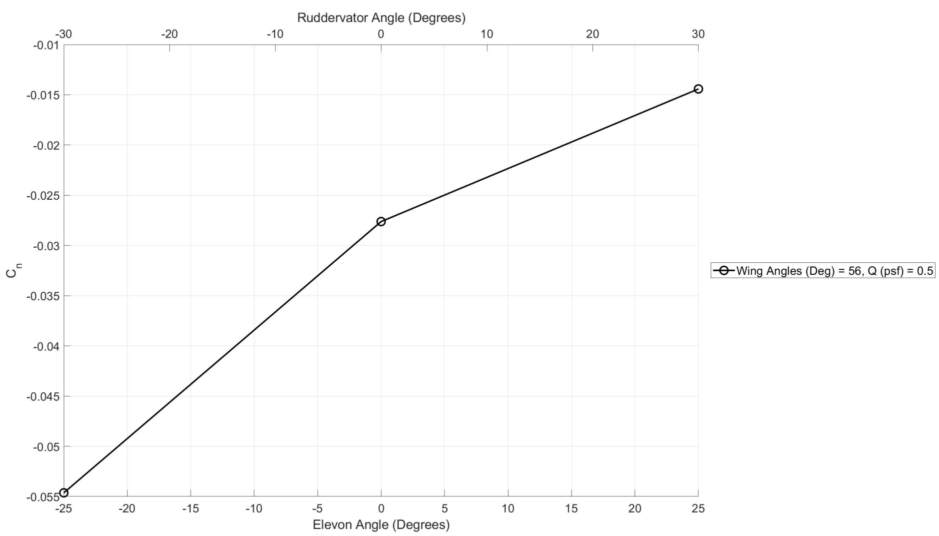

Figure 146. Wing angles 56 degrees trim point C_n vs elevon and ruddervator deflection angles.

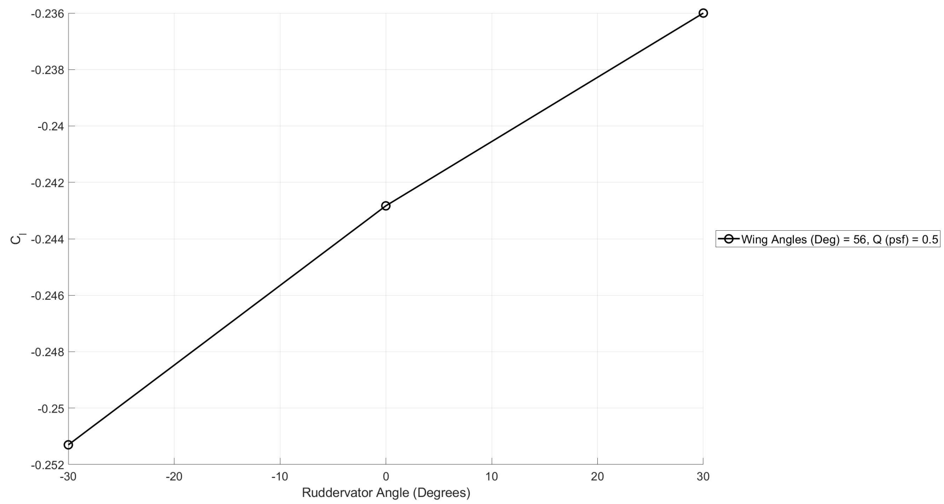

Figure 147. Wing angles 56 degrees trim point C_l vs ruddervator deflection angle.

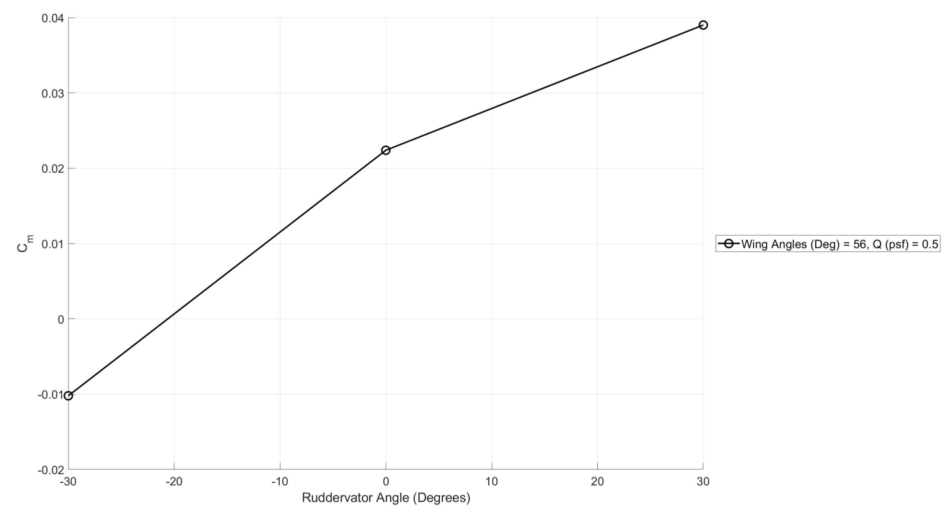

Figure 148. Wing angles 56 degrees trim point C_m vs ruddervator deflection angle.

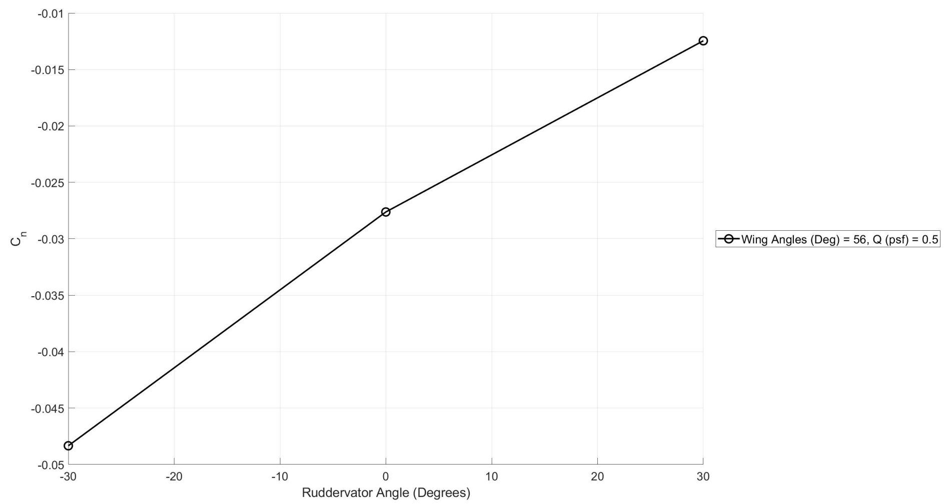

Figure 149. Wing angles 56 degrees trim point C_n vs ruddervator deflection angle.

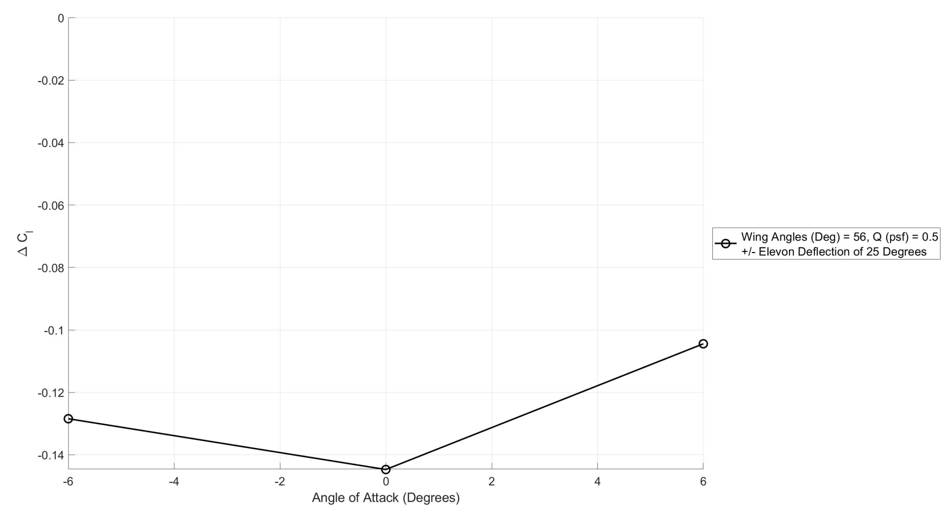

Figure 150. Wing angles 56 degrees trim point Δ C_l vs angle of attack for elevon deflection.

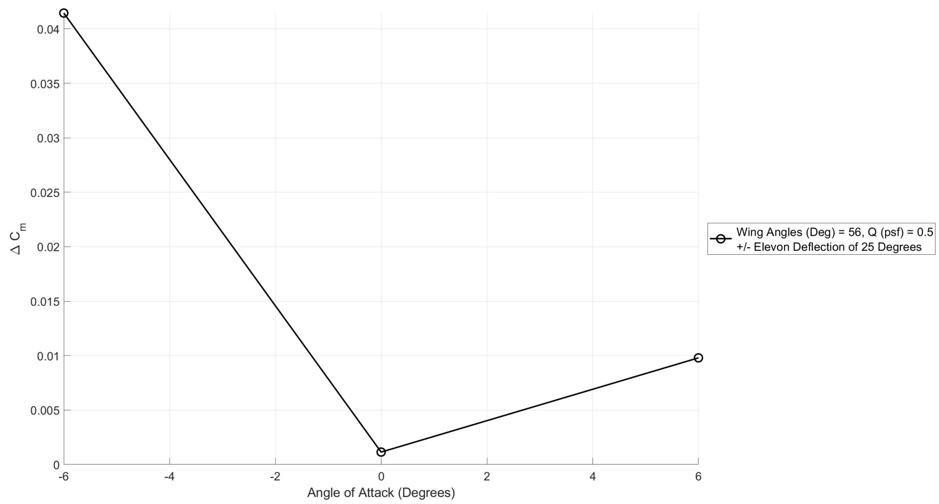

Figure 151. Wing angles 56 degrees trim point Δ C_m vs angle of attack for elevon deflection.

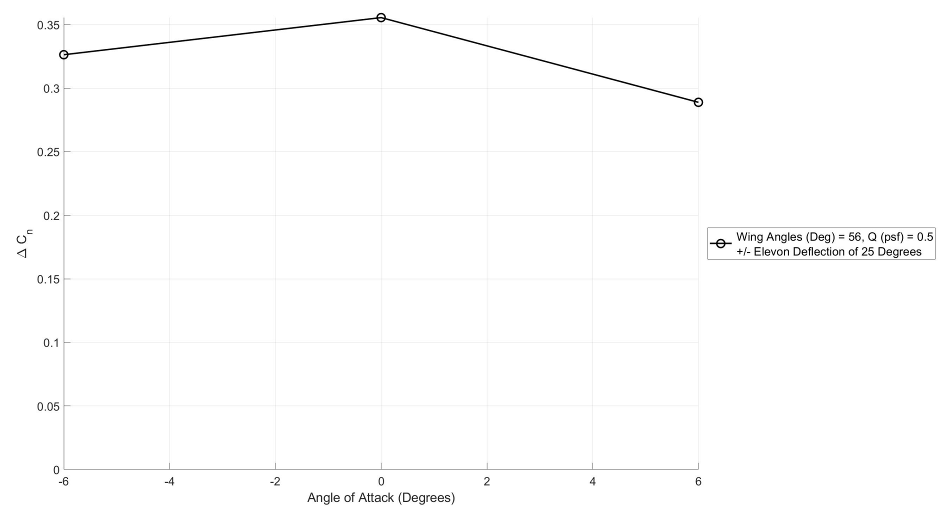

Figure 152. Wing angles 56 degrees trim point Δ C_n vs angle of attack for elevon deflection.

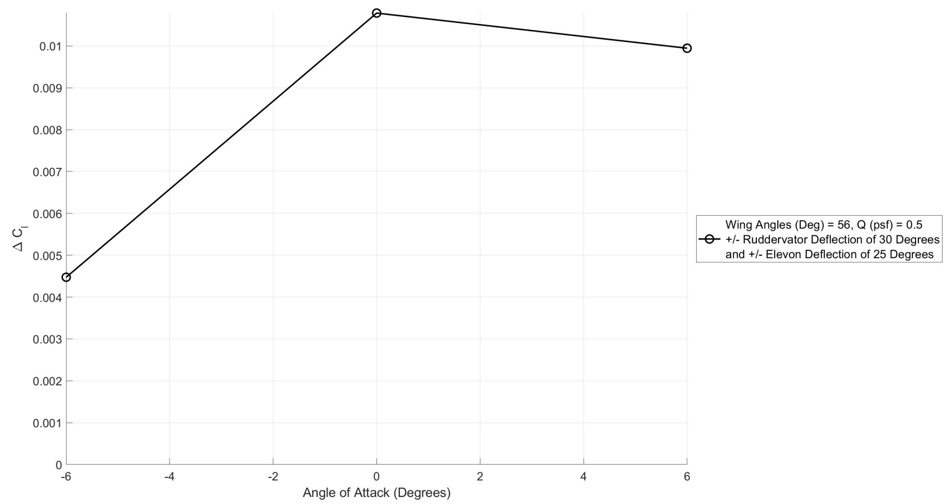

Figure 153. Wing angles 56 degrees trim point Δ C_l vs angle of attack for elevon and ruddervator deflection.

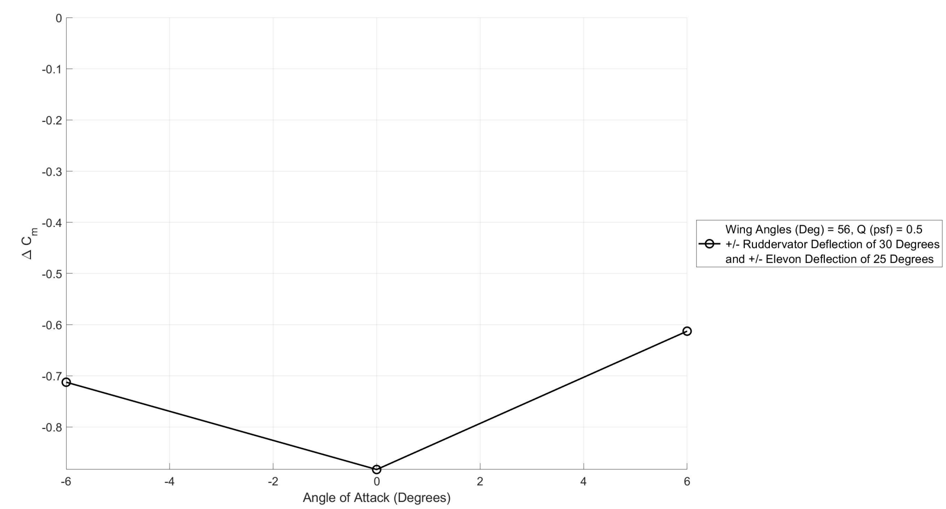

Figure 154. Wing angles 56 degrees trim point Δ C_m vs angle of attack for elevon and ruddervator deflection.

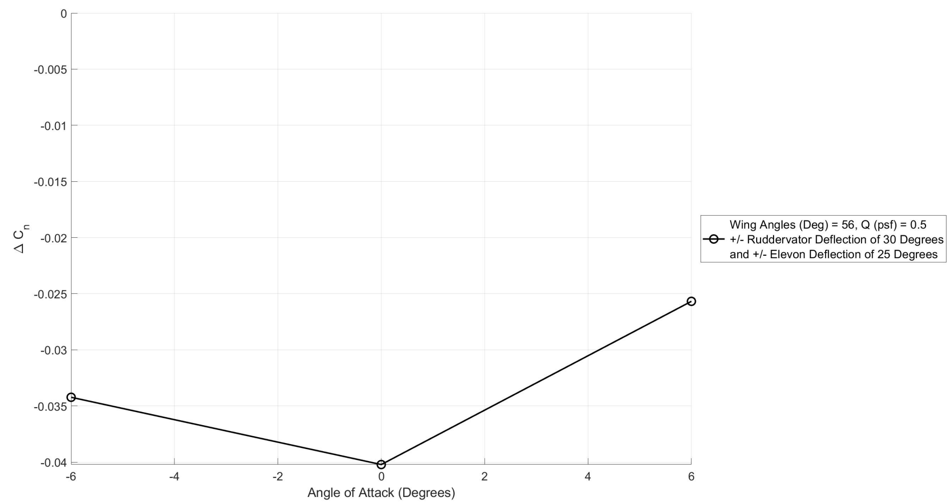

Figure 155. Wing angles 56 degrees trim point Δ C_n vs angle of attack for elevon and ruddervator deflection.

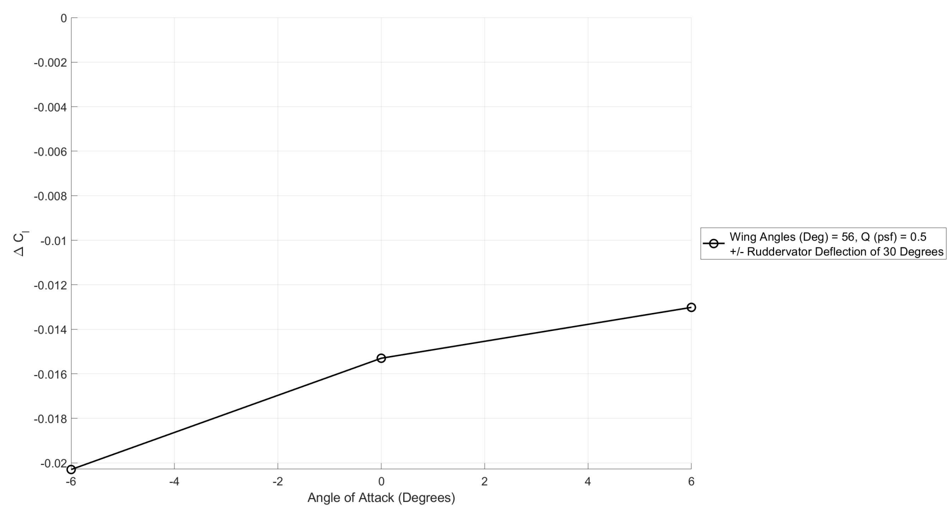

Figure 156. Wing angles 56 degrees trim point Δ C_l vs angle of attack for ruddervator deflection.

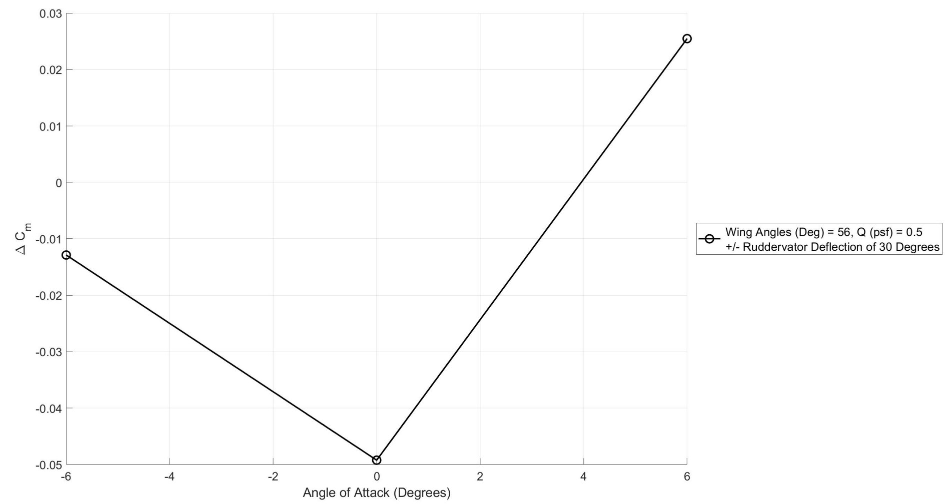

Figure 157. Wing angles 56 degrees trim point Δ C_m vs angle of attack for ruddervator deflection.

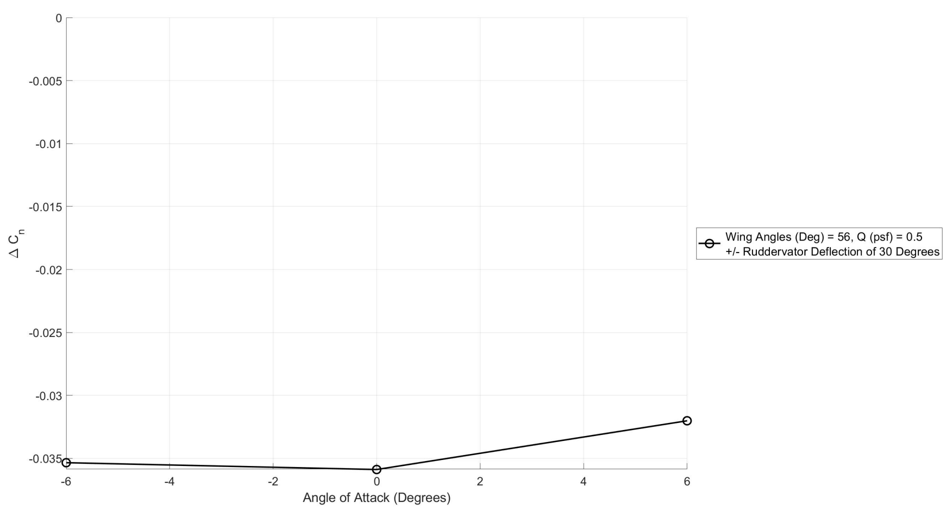

Figure 158. Wing angles 56 degrees trim point Δ C_n vs angle of attack for ruddervator deflection.

C.2 Transition Wing Angles 51 Degrees Performance and Stability Plots

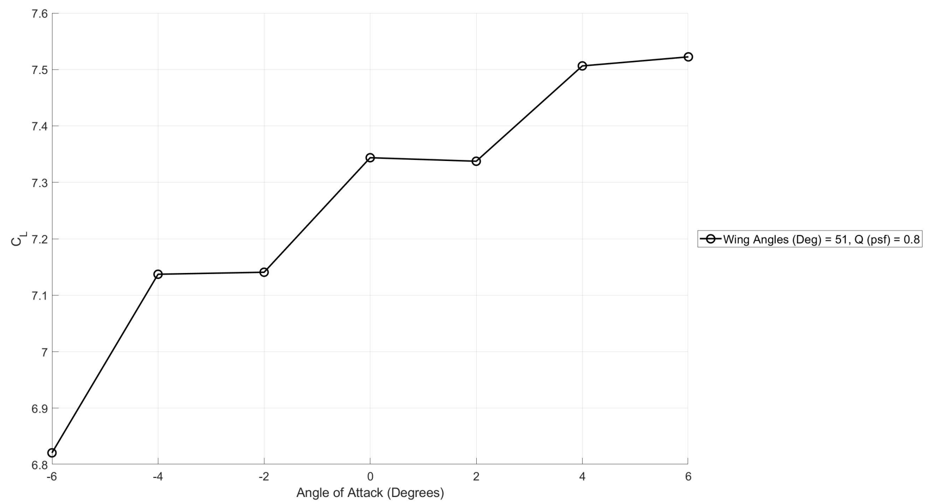

Figure 159. Wing angles 51 degrees trim point C_L vs angle of attack.

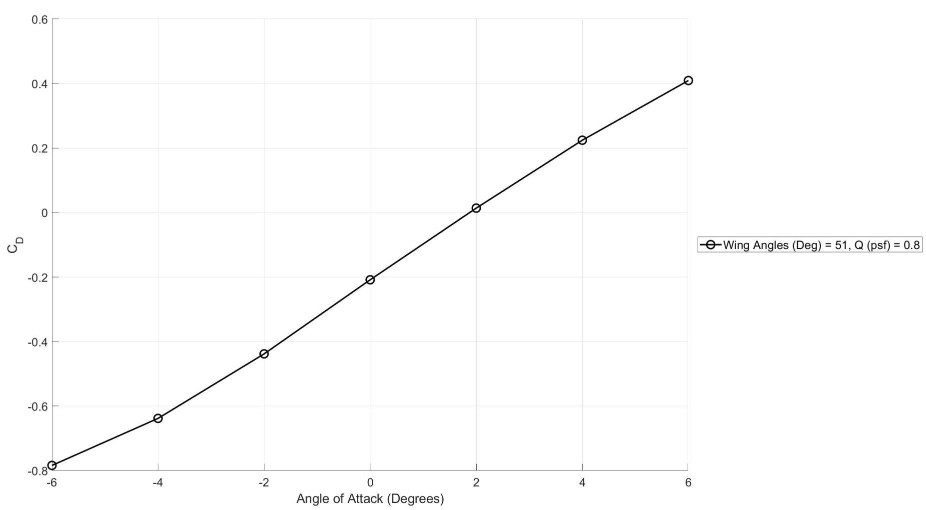

Figure 160. Wing angles 51 degrees trim point C_D vs angle of attack.

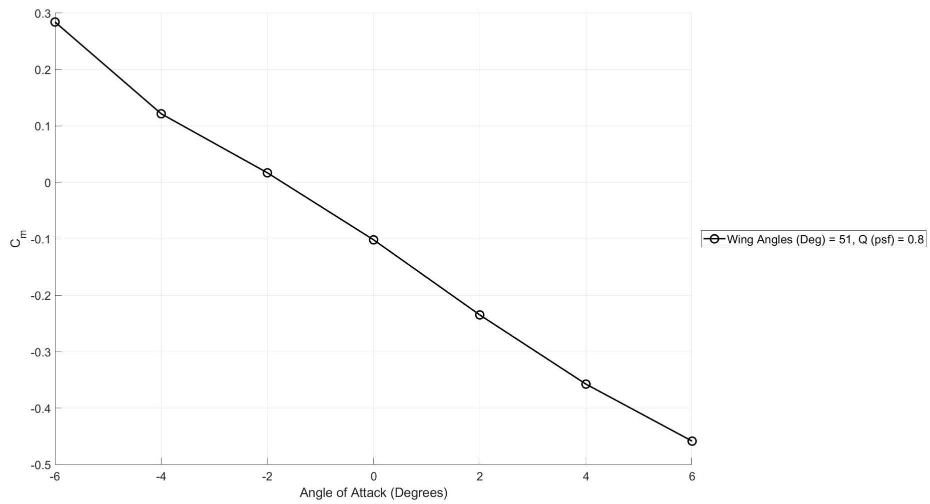

Figure 161. Wing angles 51 degrees trim point C_m vs angle of attack.

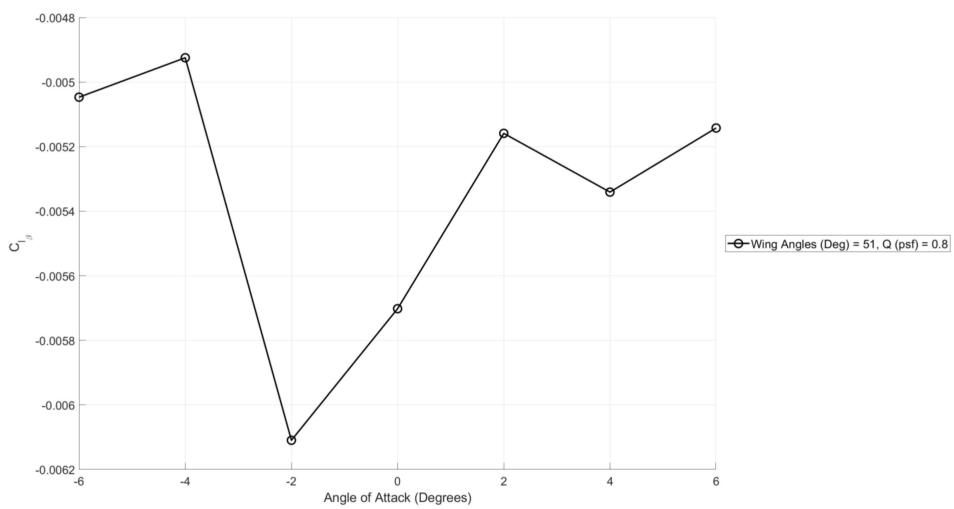

Figure 162. Wing angles 51 degrees trim point C_{l_β} vs angle of attack.

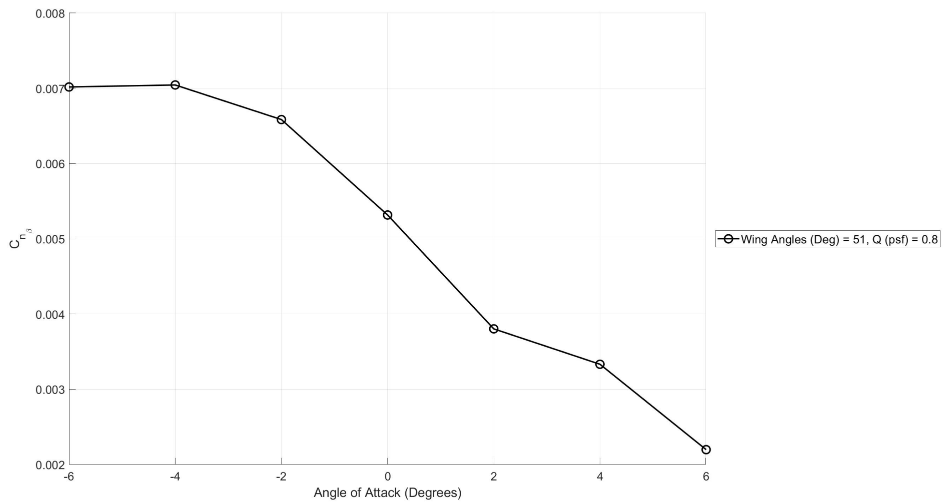

Figure 163. Wing angles 51 degrees trim point C_{n_β} vs angle of attack.

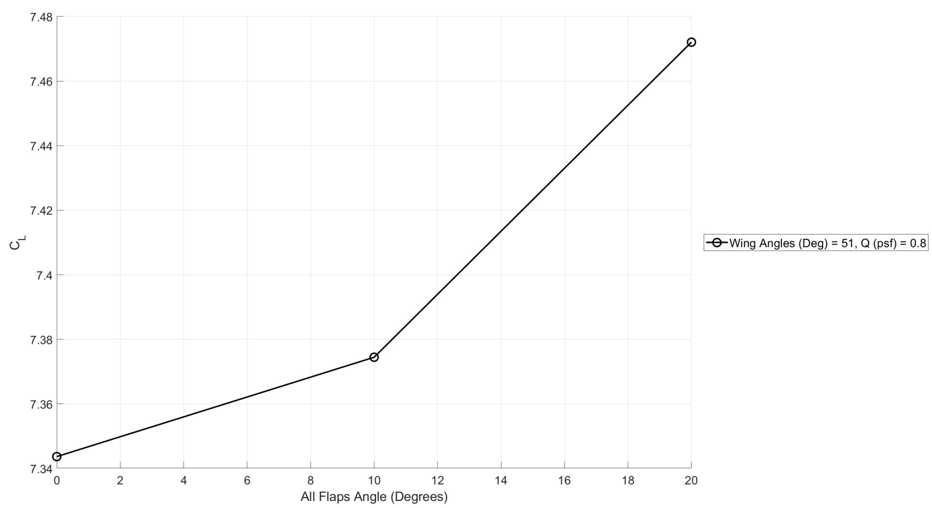

Figure 164. Wing angles 51 degrees trim point C_L vs all flap deflection angle.

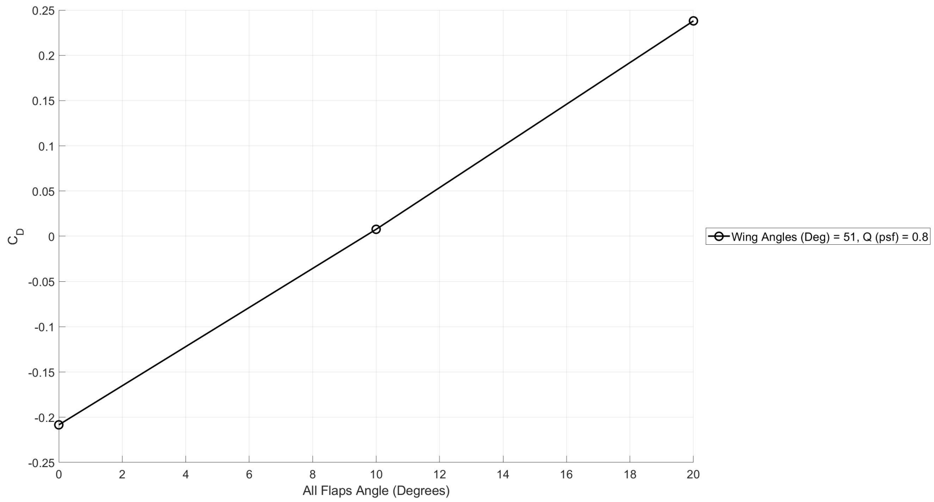

Figure 165. Wing angles 51 degrees trim point C_D vs all flap deflection angle.

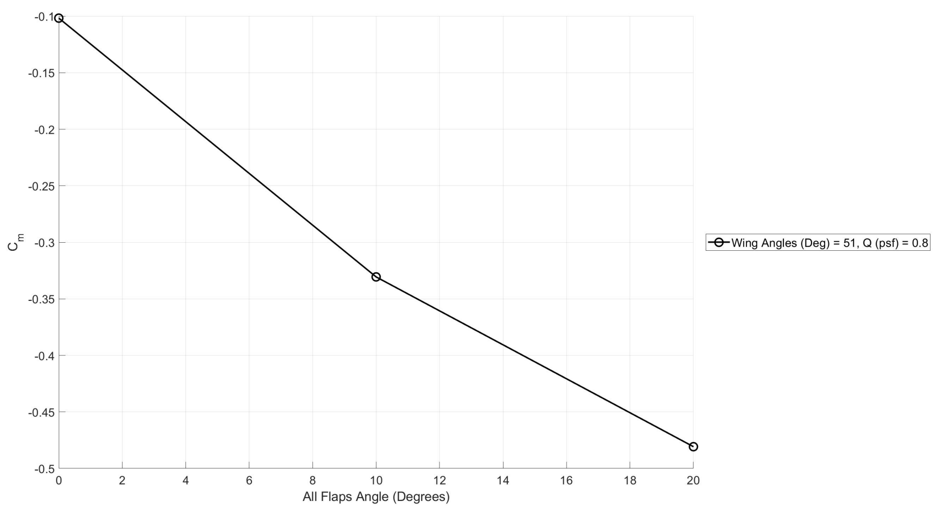

Figure 166. Wing angles 51 degrees trim point C_m vs all flap deflection angle.

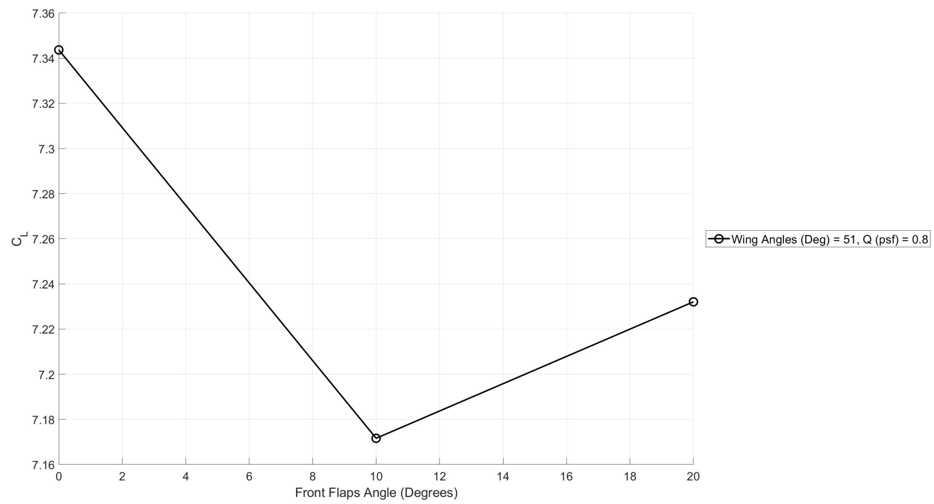

Figure 167. Wing angles 51 degrees trim point C_L vs front flap deflection angle.

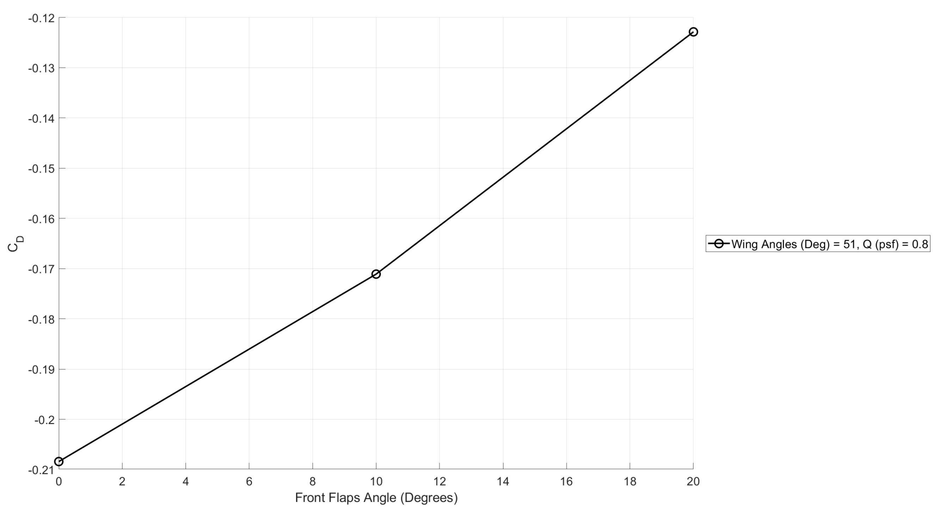

Figure 168. Wing angles 51 degrees trim point C_D vs front flap deflection angle.

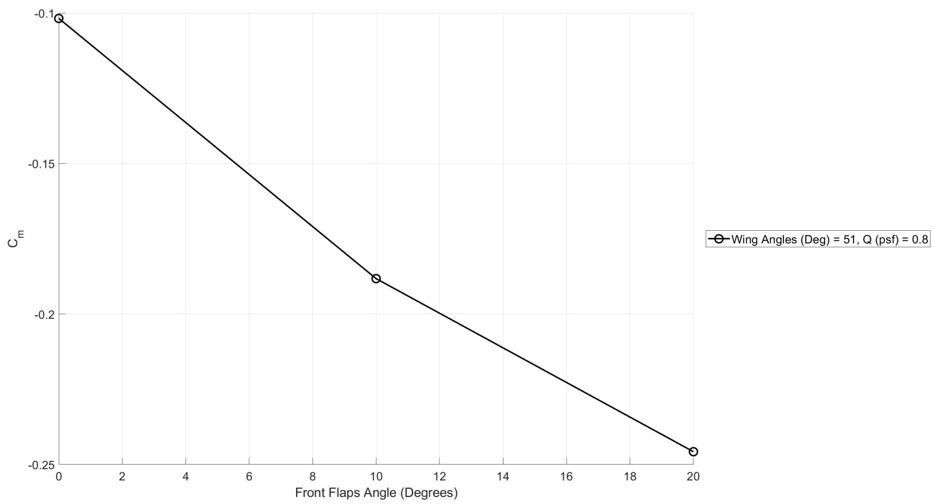

Figure 169. Wing angles 51 degrees trim point C_m vs front flap deflection angle.

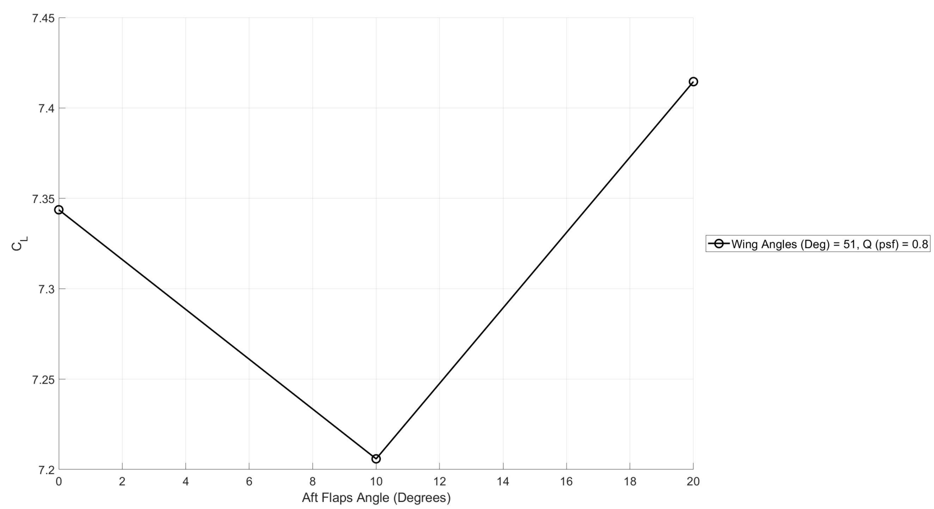

Figure 170. Wing angles 51 degrees trim point C_L vs aft flap deflection angle.

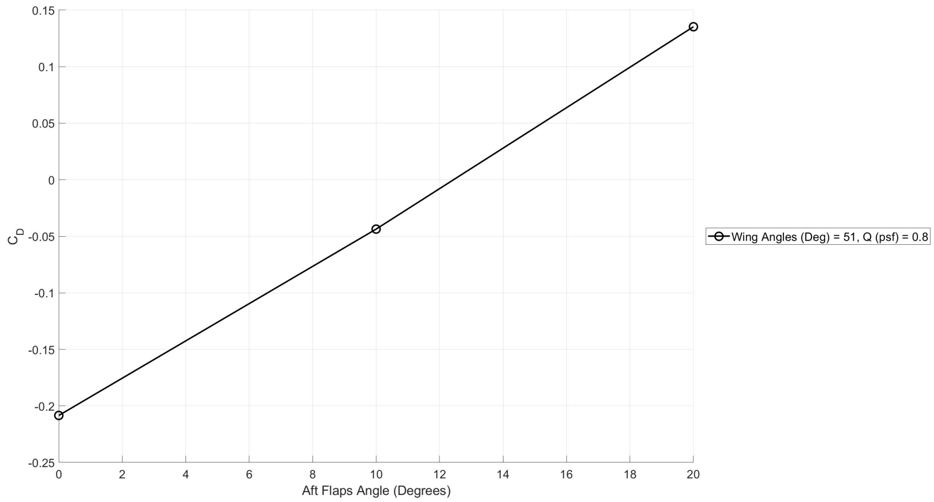

Figure 171. Wing angles 51 degrees trim point C_D vs aft flap deflection angle.

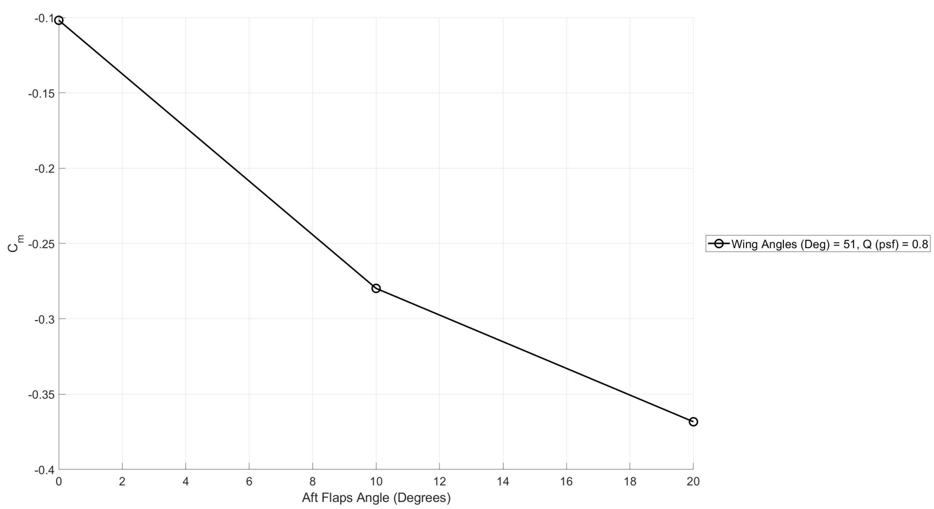

Figure 172. Wing angles 51 degrees trim point C_m vs aft flap deflection angle.

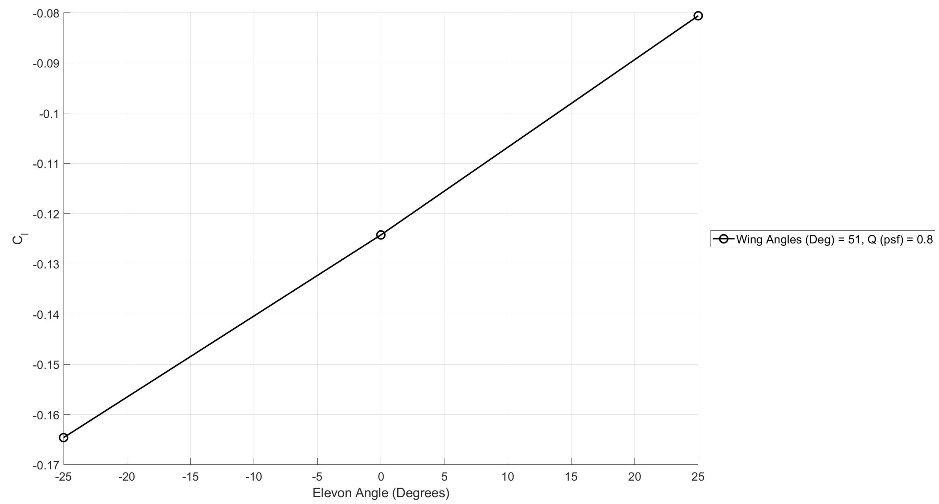

Figure 173. Wing angles 51 degrees trim point C_l vs elevon deflection angle.

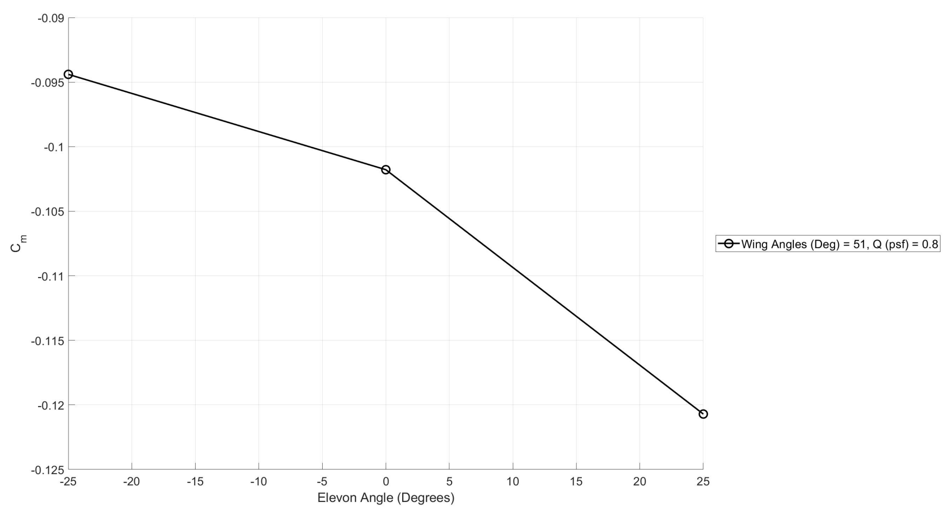

Figure 174. Wing angles 51 degrees trim point C_m vs elevon deflection angle.

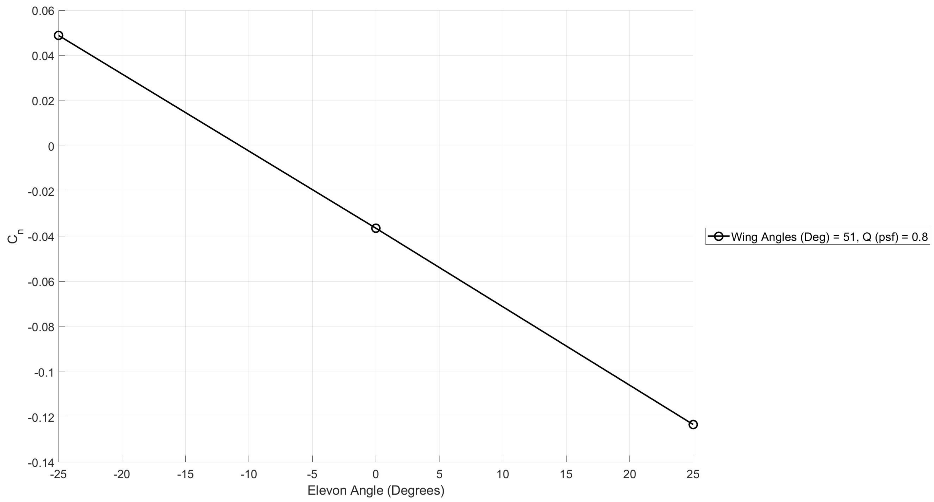

Figure 175. Wing angles 51 degrees trim point C_n vs elevon deflection angle.

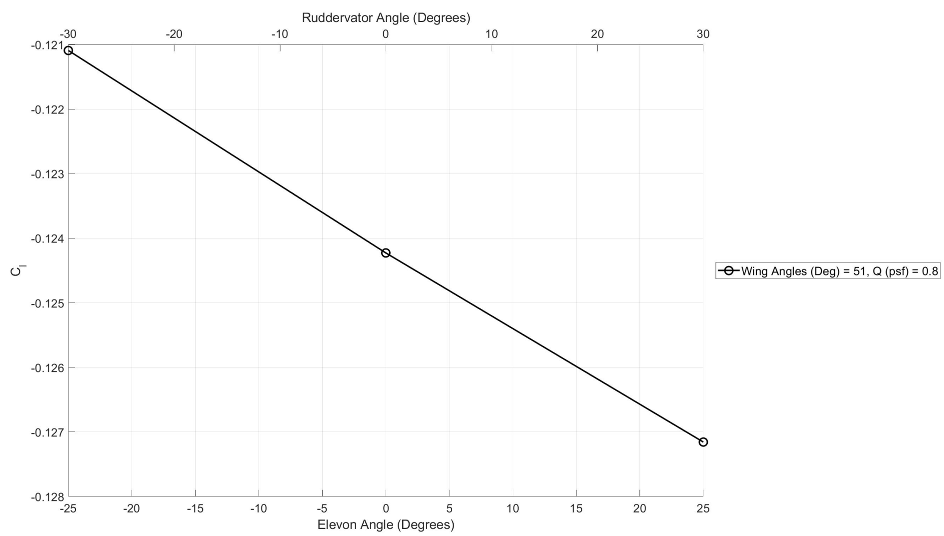

Figure 176. Wing angles 51 degrees trim point C_l vs elevon and ruddervator deflection angles.

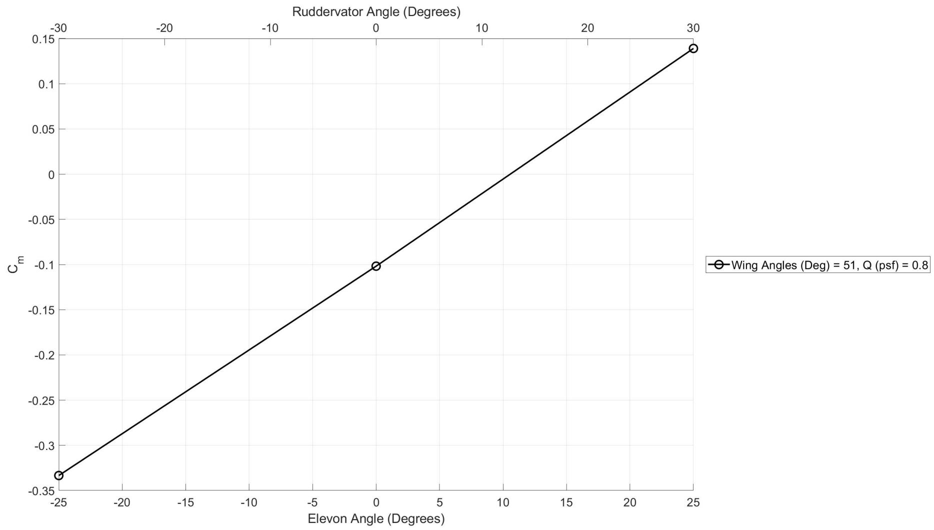

Figure 177. Wing angles 51 degrees trim point C_m vs elevon and ruddervator deflection angles.

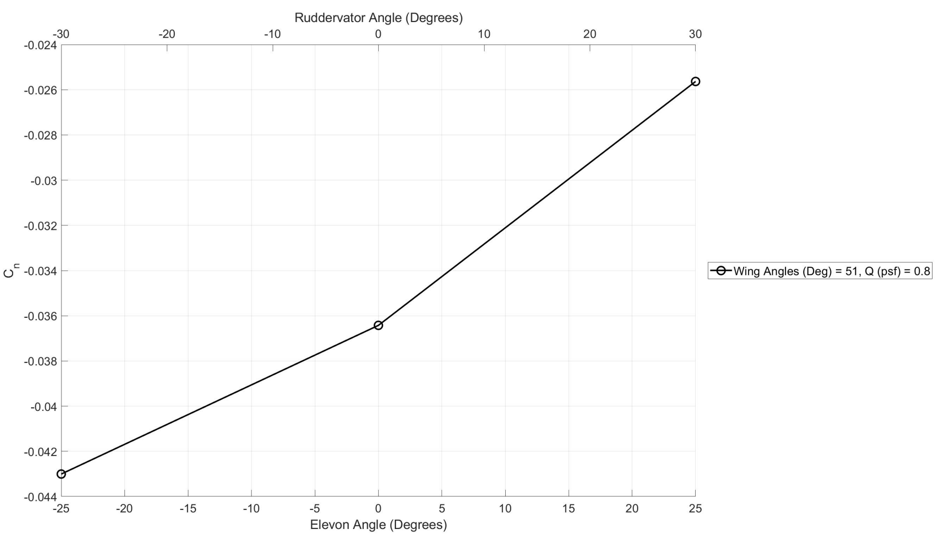

Figure 178. Wing angles 51 degrees trim point C_n vs elevon and ruddervator deflection angles.

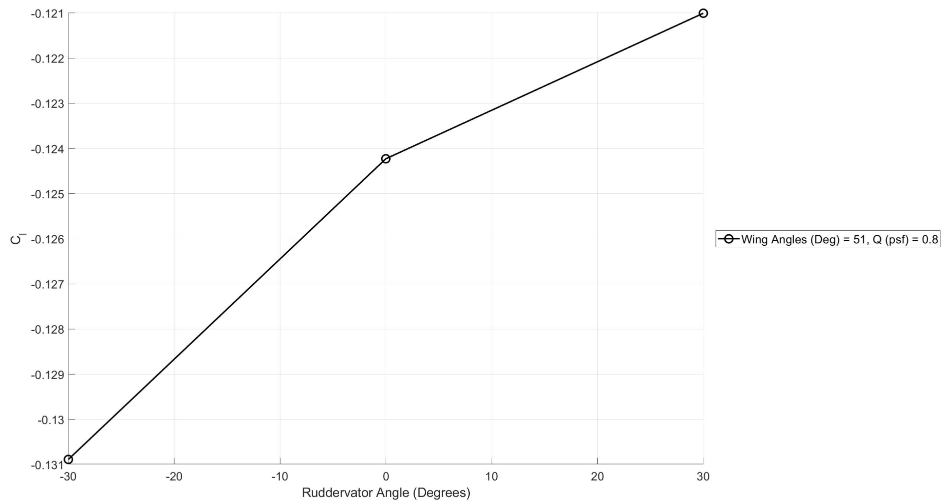

Figure 179. Wing angles 51 degrees trim point C_l vs ruddervator deflection angle.

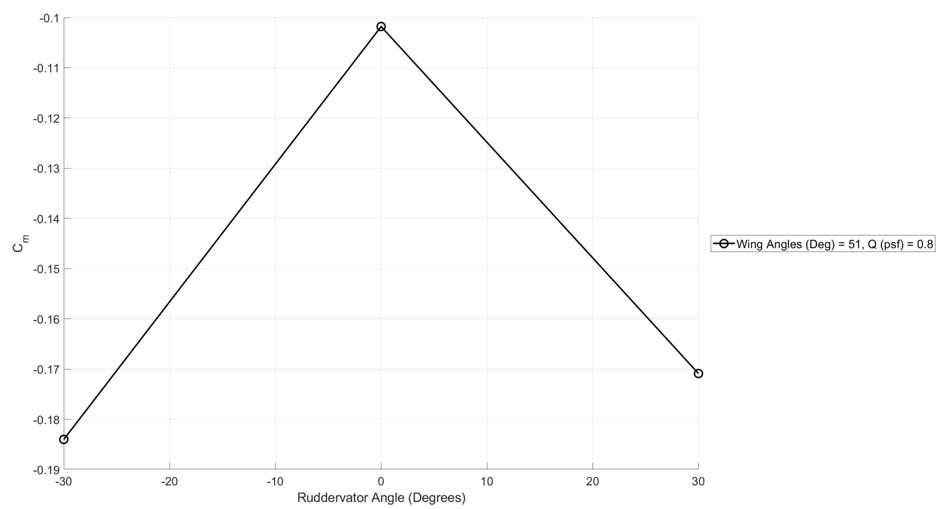

Figure 180. Wing angles 51 degrees trim point C_m vs ruddervator deflection angle.

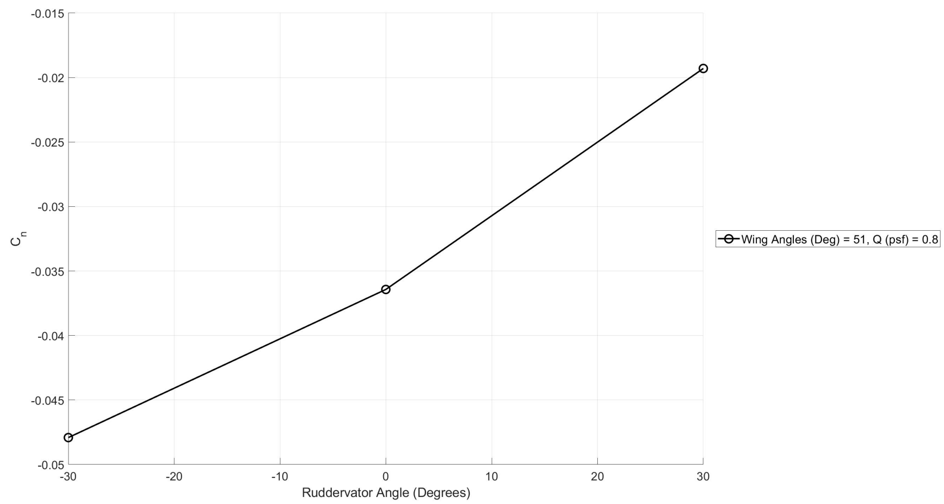

Figure 181. Wing angles 51 degrees trim point C_n vs ruddervator deflection angle.

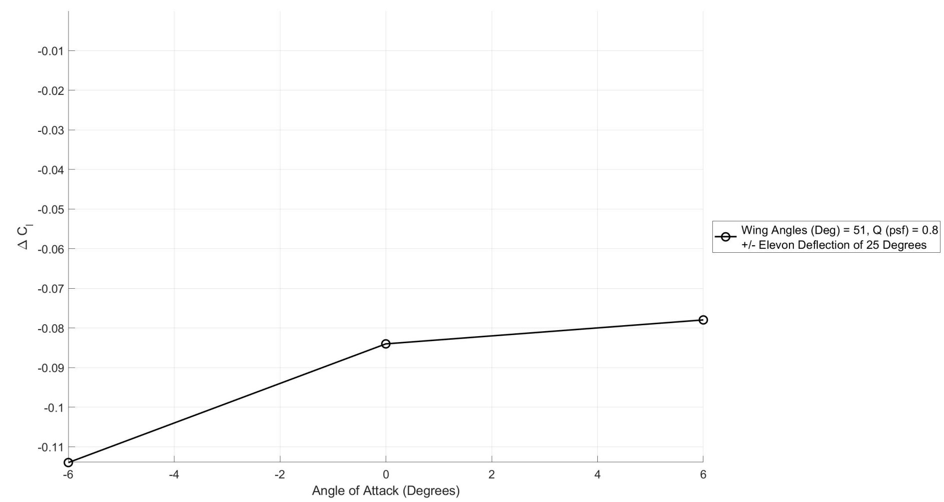

Figure 182. Wing angles 51 degrees trim point Δ C_l vs angle of attack for elevon deflection.

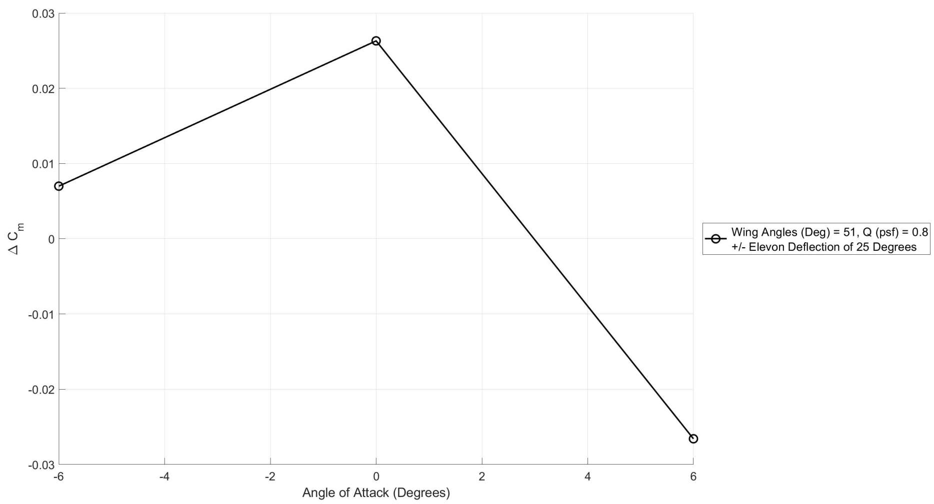

Figure 183. Wing angles 51 degrees trim point Δ C$_m$ vs angle of attack for elevon deflection.

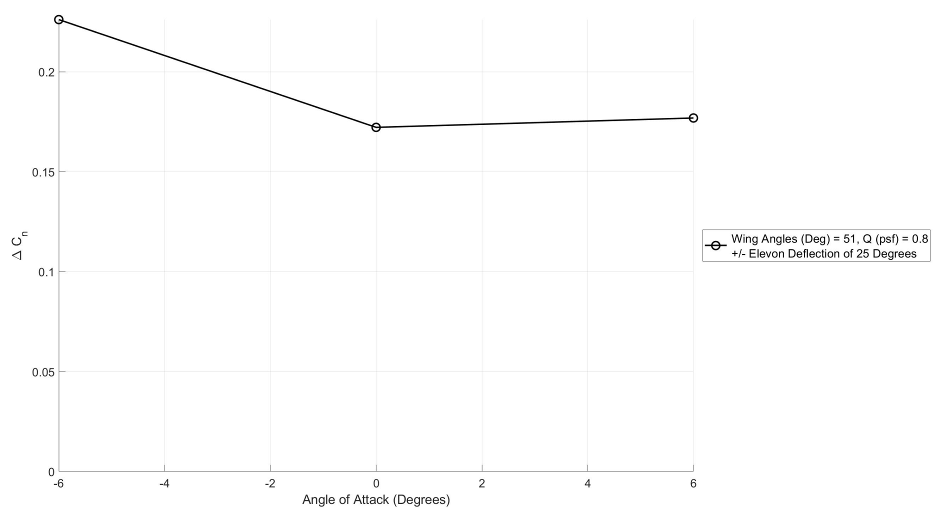

Figure 184. Wing angles 51 degrees trim point Δ C$_n$ vs angle of attack for elevon deflection.

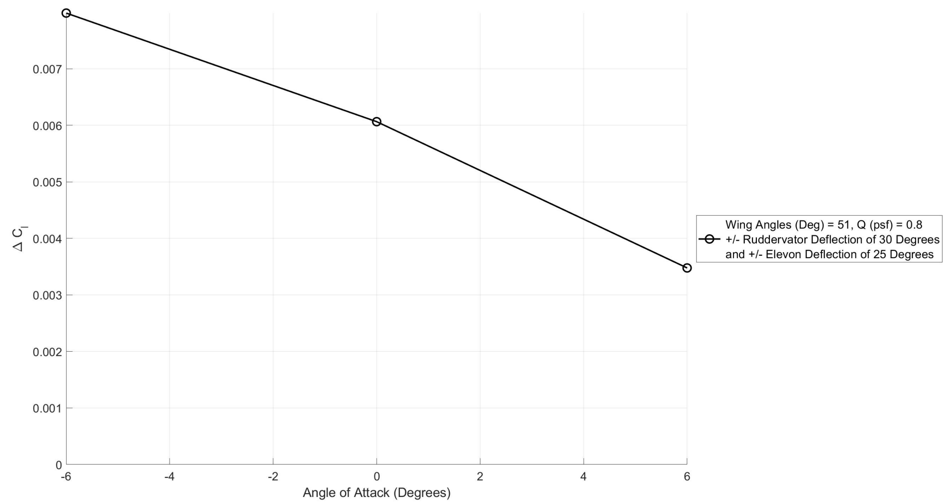

Figure 185. Wing angles 51 degrees trim point Δ C_l vs angle of attack for elevon and ruddervator deflection.

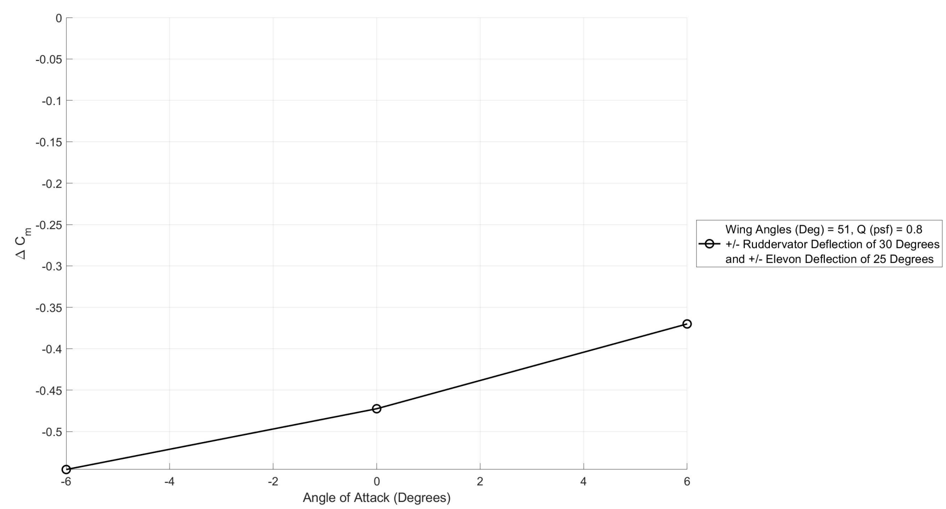

Figure 186. Wing angles 51 degrees trim point Δ C_m vs angle of attack for elevon and ruddervator deflection.

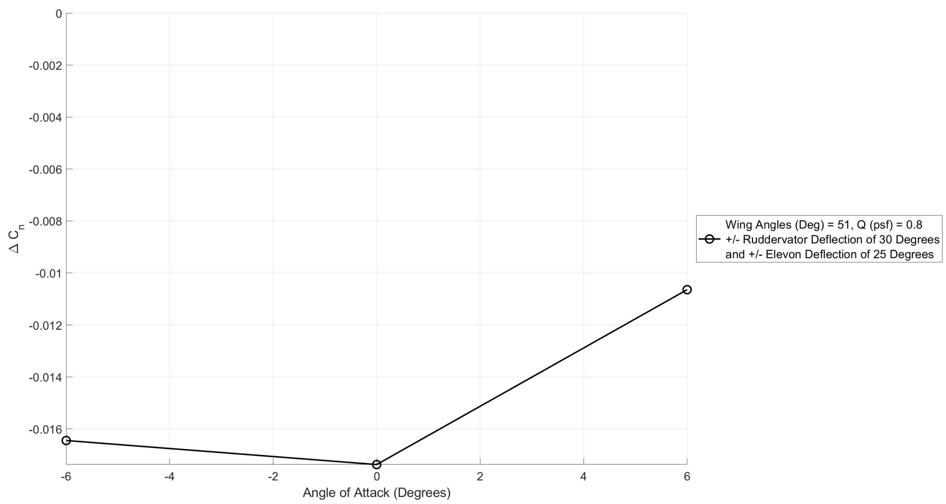

Figure 187. Wing angles 51 degrees trim point Δ C_n vs angle of attack for elevon and ruddervator deflection.

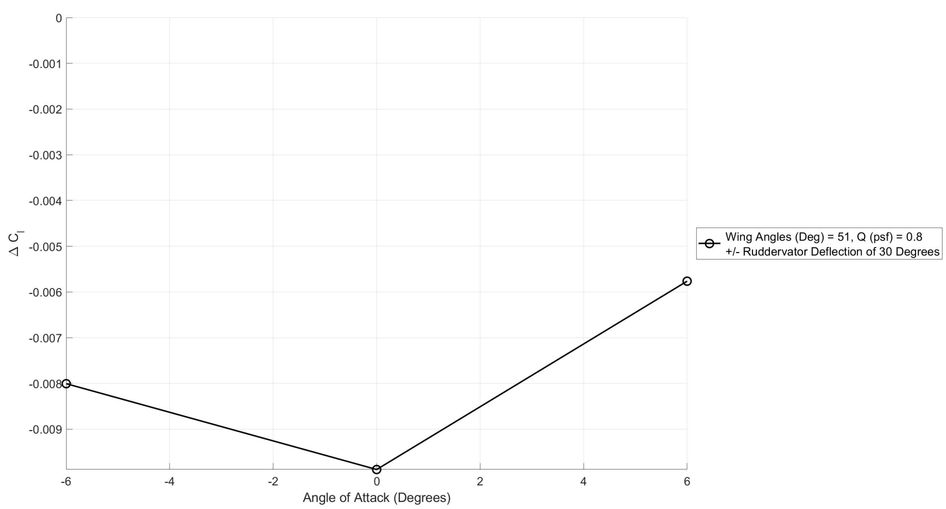

Figure 188. Wing angles 51 degrees trim point Δ C_l vs angle of attack for ruddervator deflection.

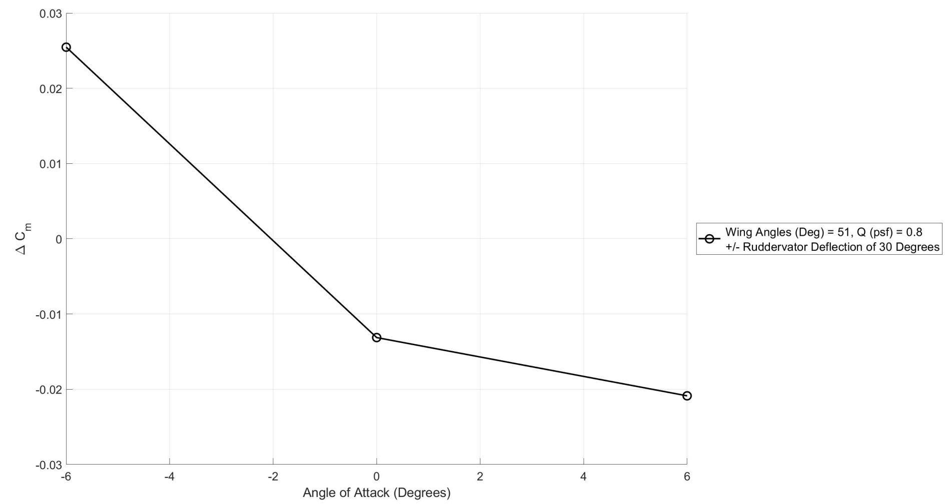

Figure 189. Wing angles 51 degrees trim point Δ C_m vs angle of attack for ruddervator deflection.

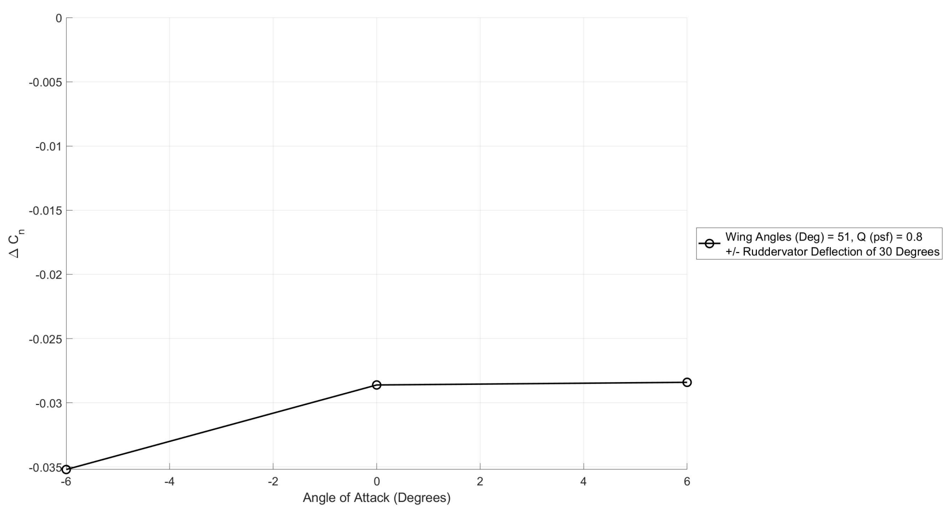

Figure 190. Wing angles 51 degrees trim point Δ C_n vs angle of attack for ruddervator deflection.

C.3 Transition Wing Angles 47 Degrees Performance and Stability Plots

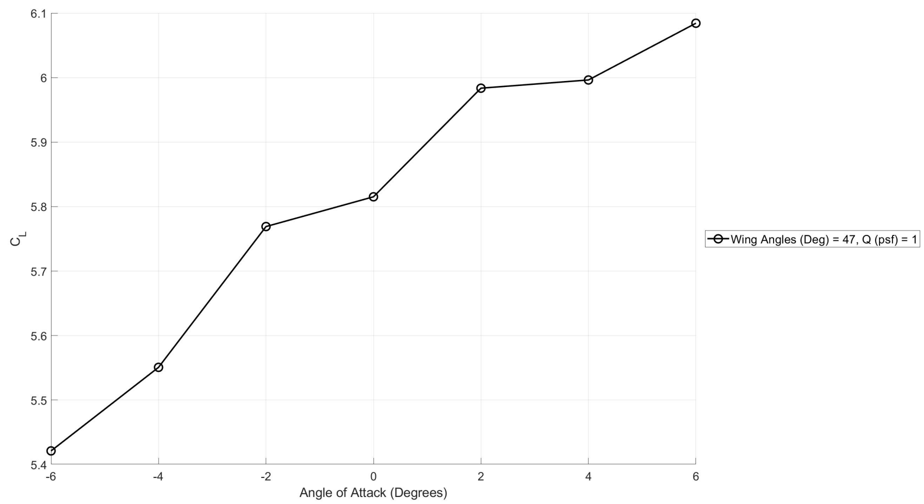

Figure 191. Wing angles 47 degrees trim point C_L vs angle of attack.

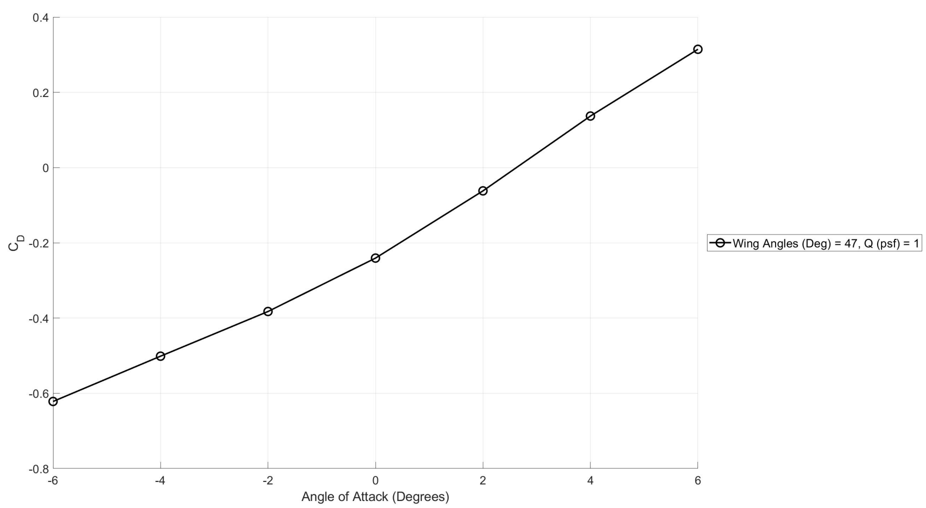

Figure 192. Wing angles 47 degrees trim point C_D vs angle of attack.

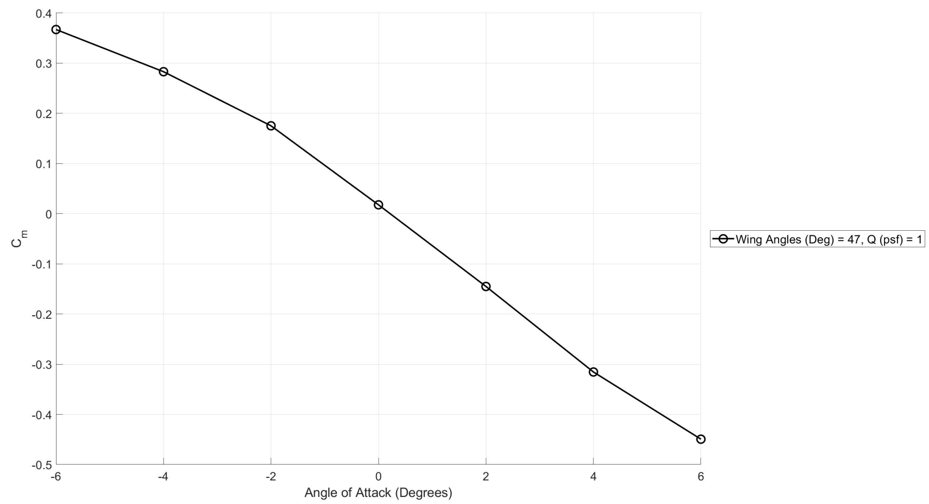

Figure 193. Wing angles 47 degrees trim point C_m vs angle of attack.

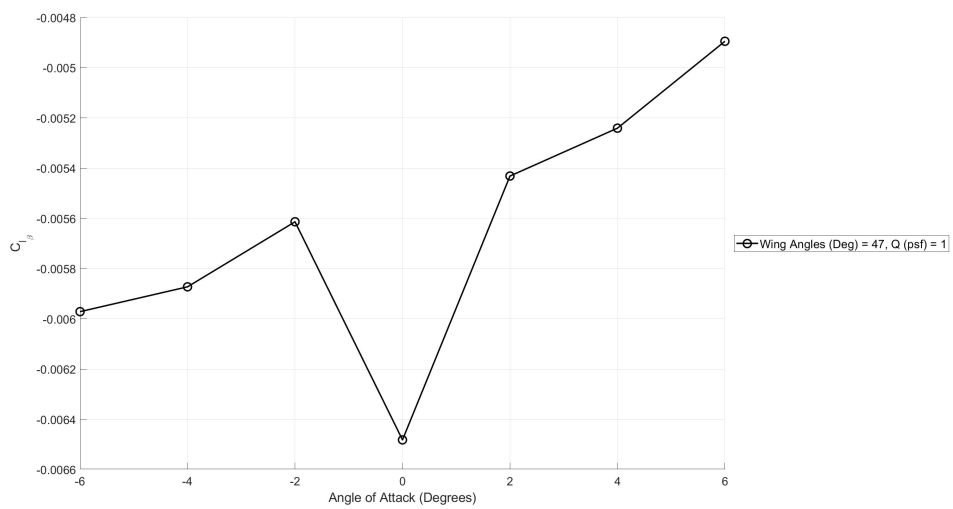

Figure 194. Wing angles 47 degrees trim point C_{l_β} vs angle of attack.

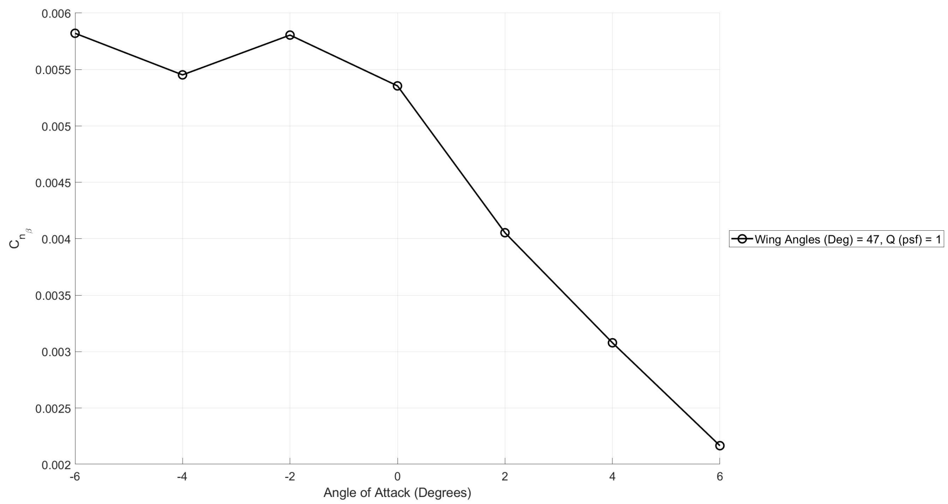

Figure 195. Wing angles 47 degrees trim point C_{n_β} vs angle of attack.

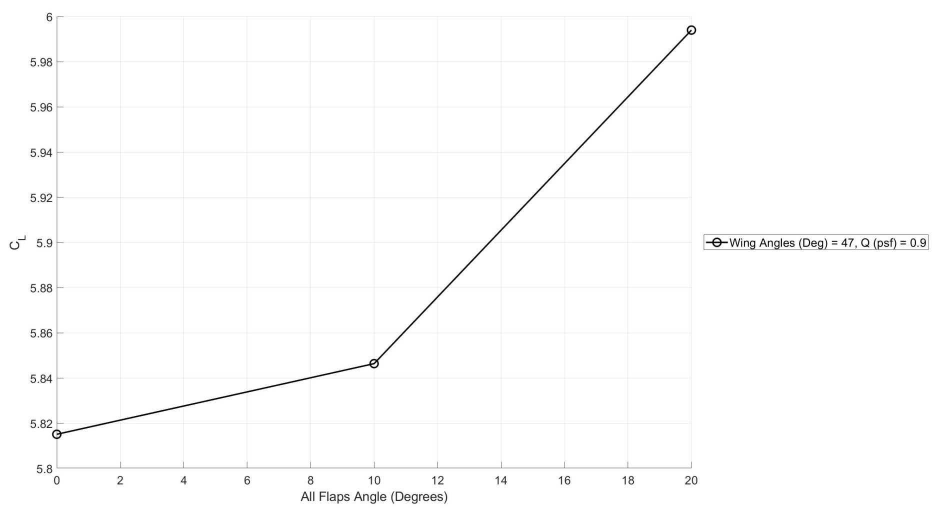

Figure 196. Wing angles 47 degrees trim point C_L vs all flap deflection angle.

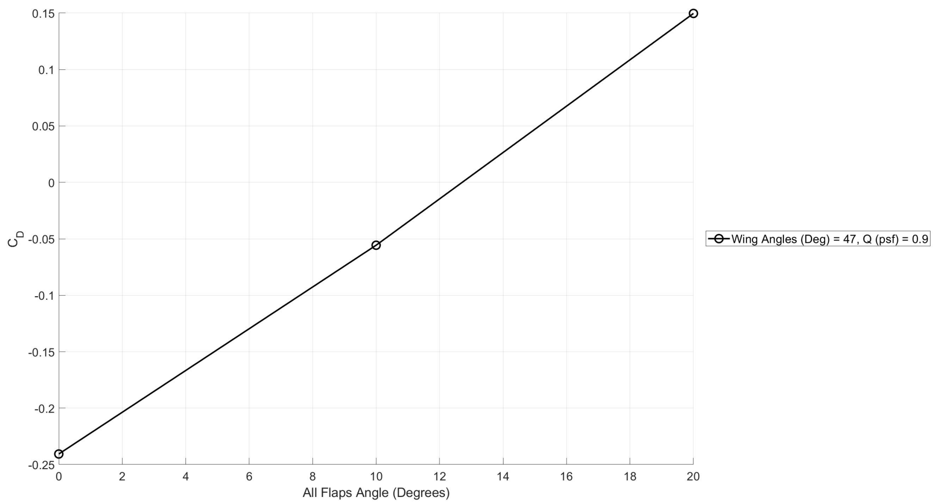

Figure 197. Wing angles 47 degrees trim point C_D vs all flap deflection angle.

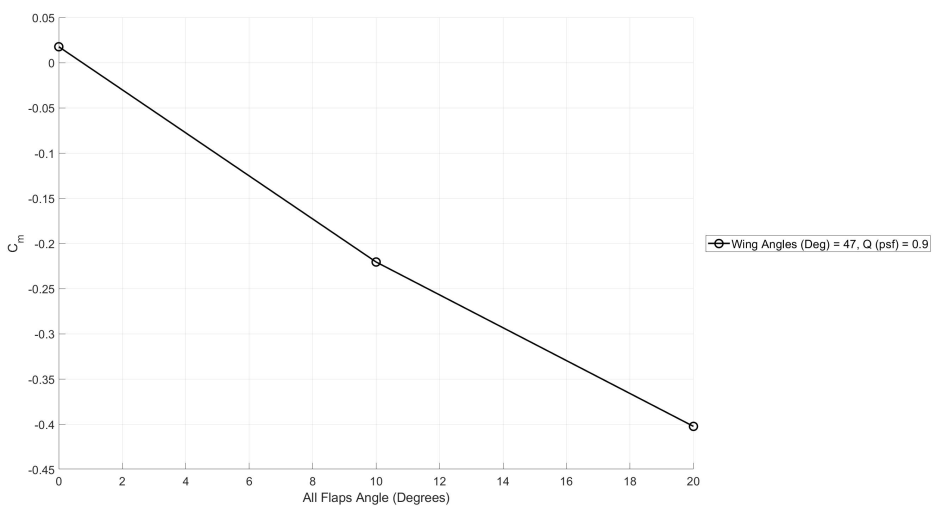

Figure 198. Wing angles 47 degrees trim point C_m vs all flap deflection angle.

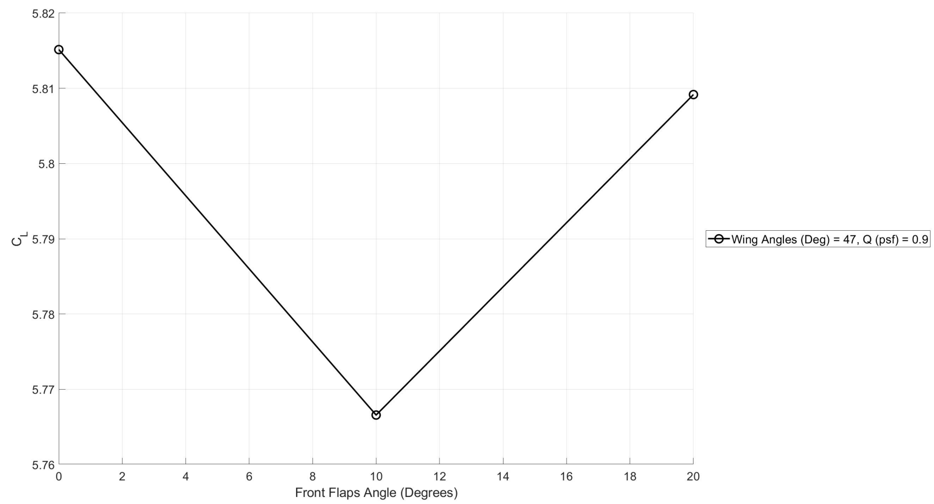

Figure 199. Wing angles 47 degrees trim point C_L vs front flap deflection angle.

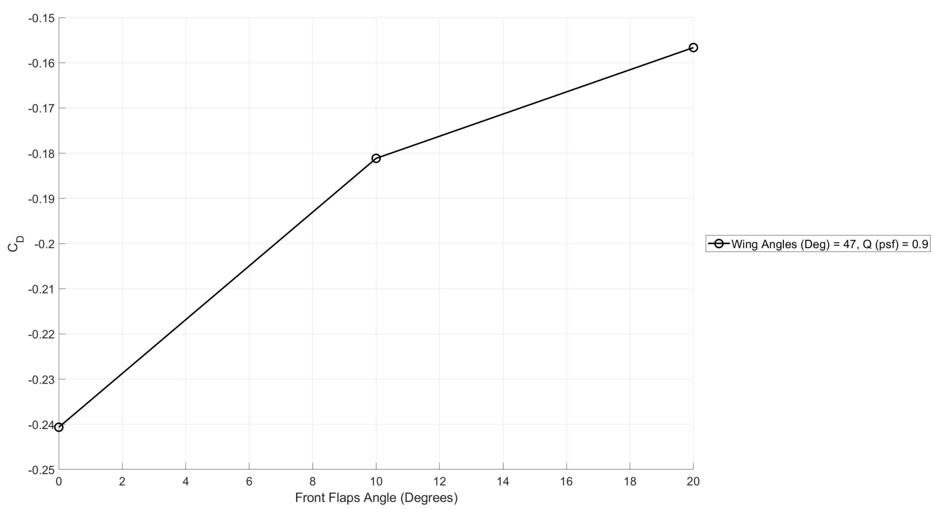

Figure 200. Wing angles 47 degrees trim point C_D vs front flap deflection angle.

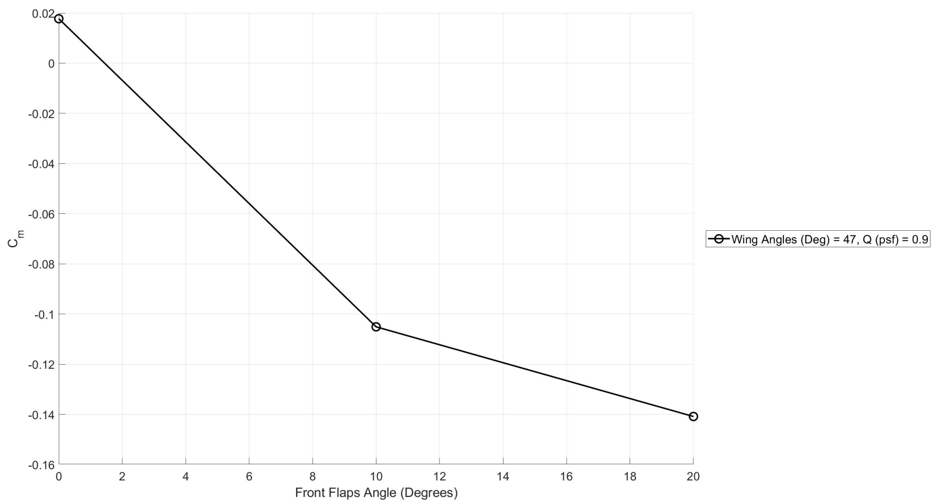

Figure 201. Wing angles 47 degrees trim point C_m vs front flap deflection angle.

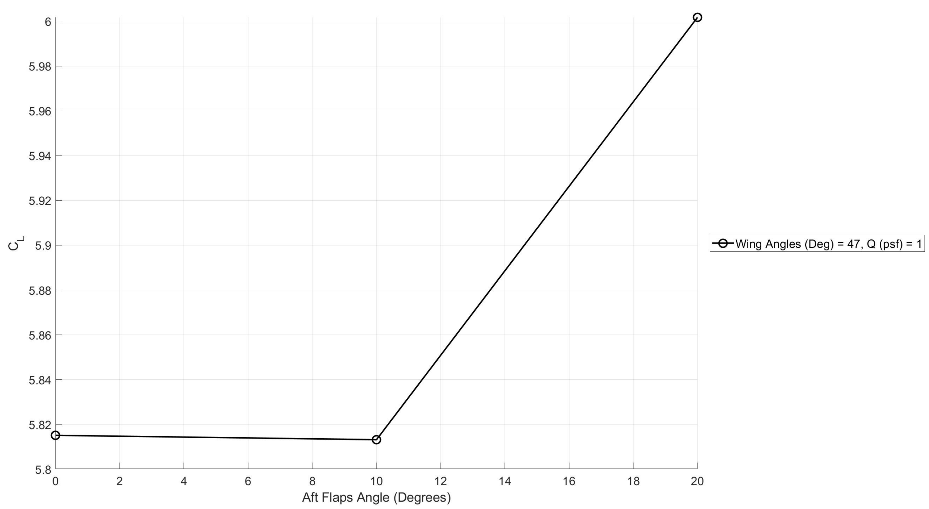

Figure 202. Wing angles 47 degrees trim point C_L vs aft flap deflection angle.

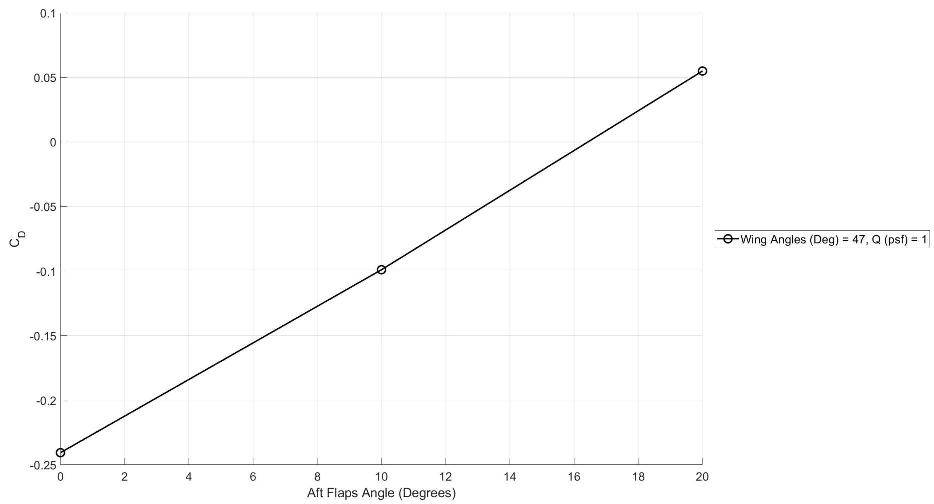

Figure 203. Wing angles 47 degrees trim point C_D vs aft flap deflection angle.

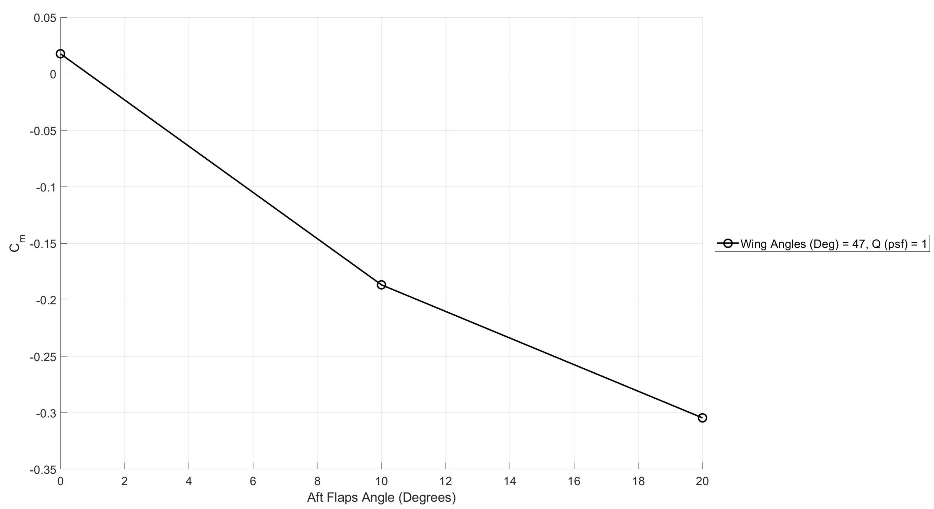

Figure 204. Wing angles 47 degrees trim point C_m vs aft flap deflection angle.

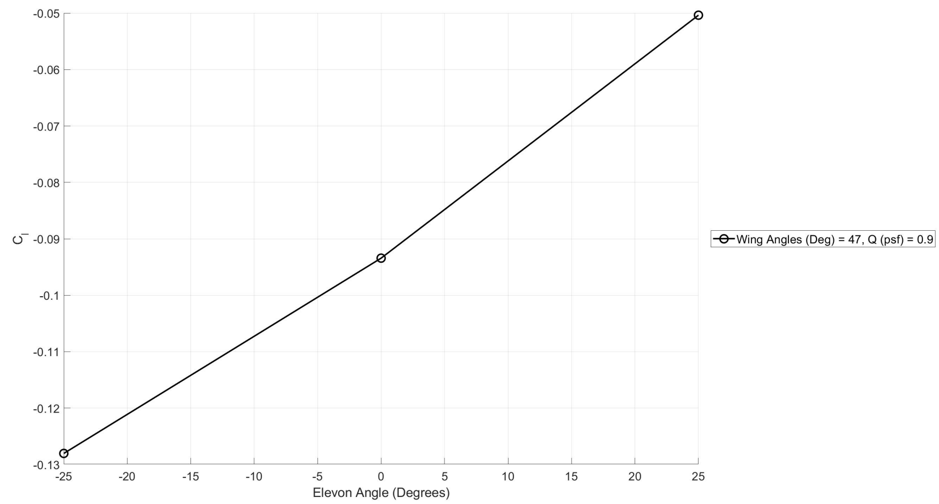

Figure 205. Wing angles 47 degrees trim point C_l vs elevon deflection angle.

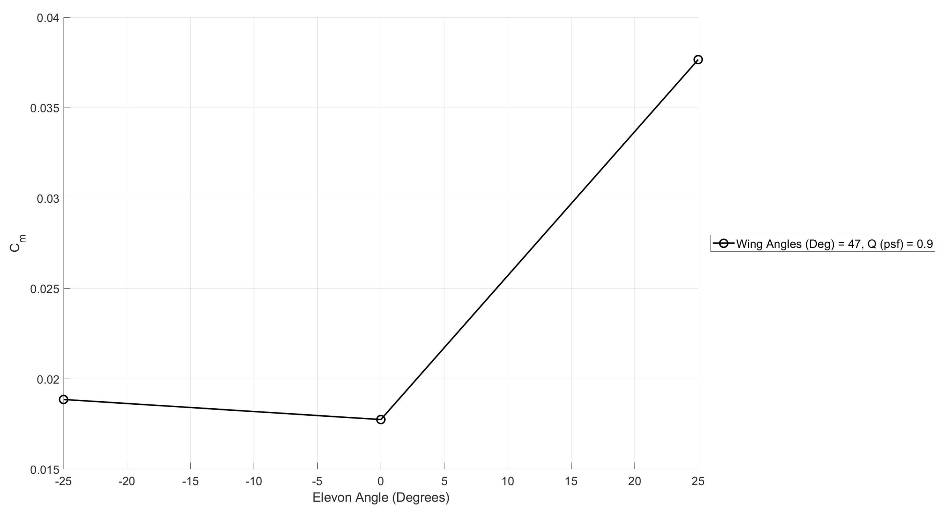

Figure 206. Wing angles 47 degrees trim point C_m vs elevon deflection angle.

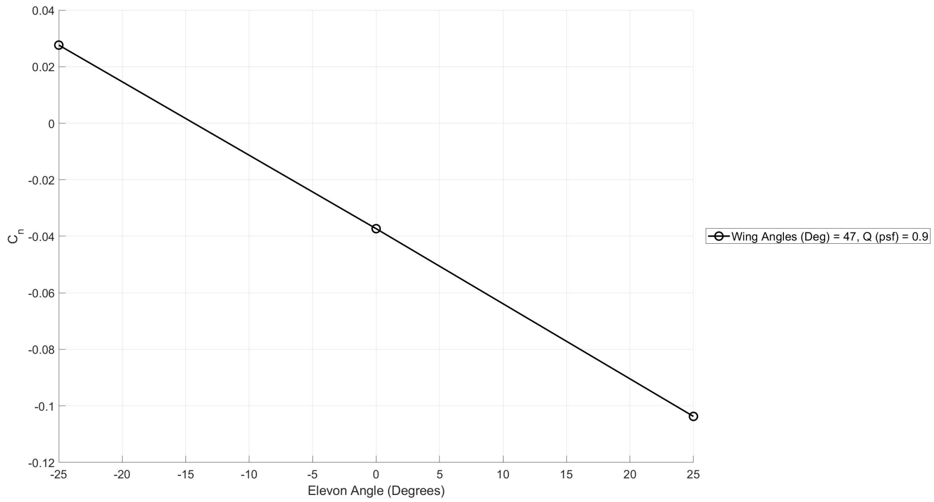

Figure 207. Wing angles 47 degrees trim point C_n vs elevon deflection angle.

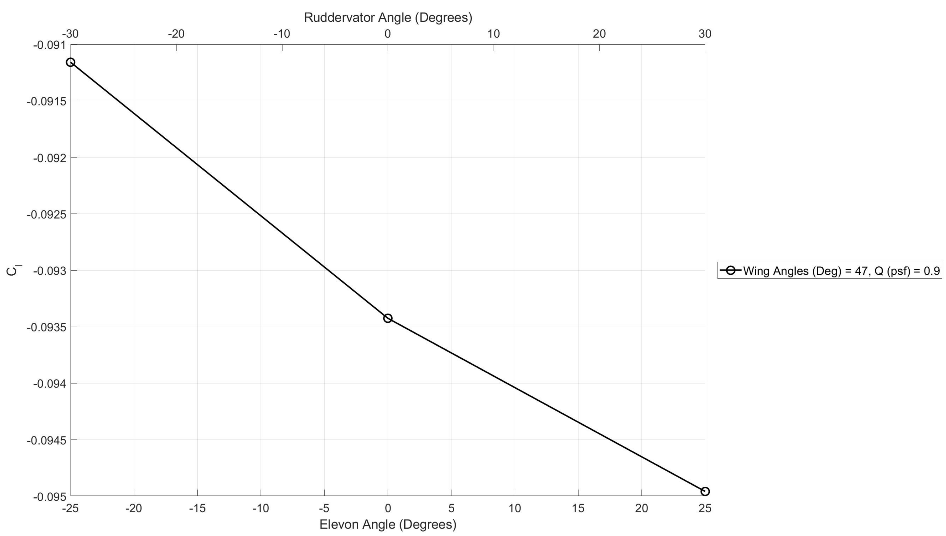

Figure 208. Wing angles 47 degrees trim point C_l vs elevon and ruddervator deflection angles.

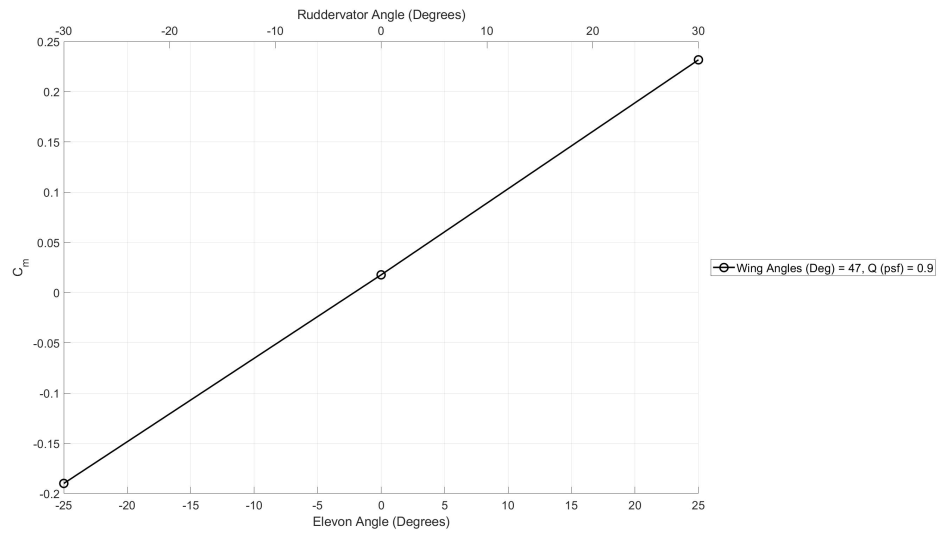

Figure 209. Wing angles 47 degrees trim point C_m vs elevon and ruddervator deflection angles.

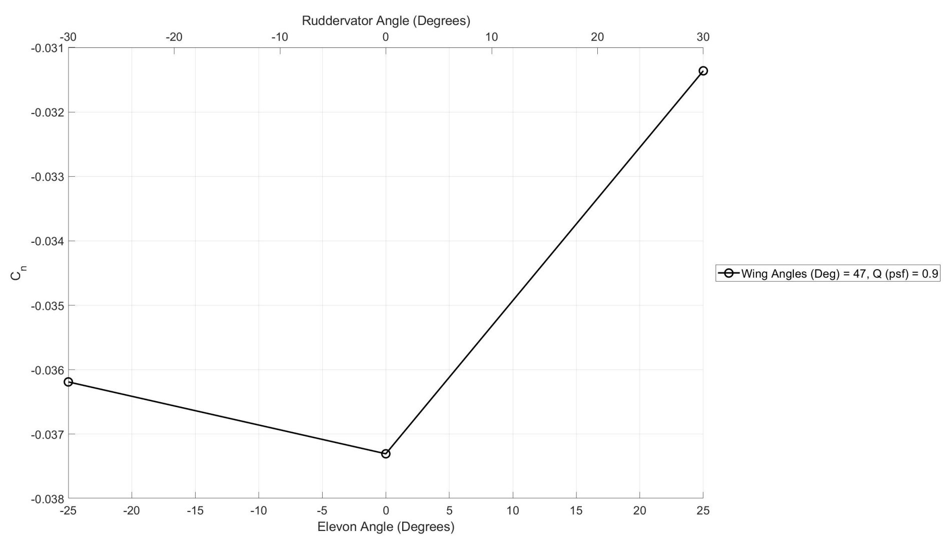

Figure 210. Wing angles 47 degrees trim point C_n vs elevon and ruddervator deflection angles.

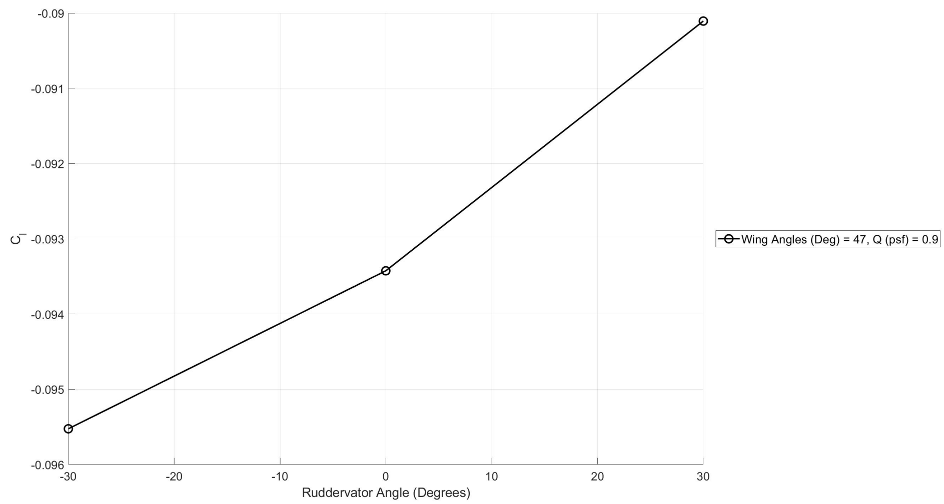

Figure 211. Wing angles 47 degrees trim point C_l vs ruddervator deflection angle.

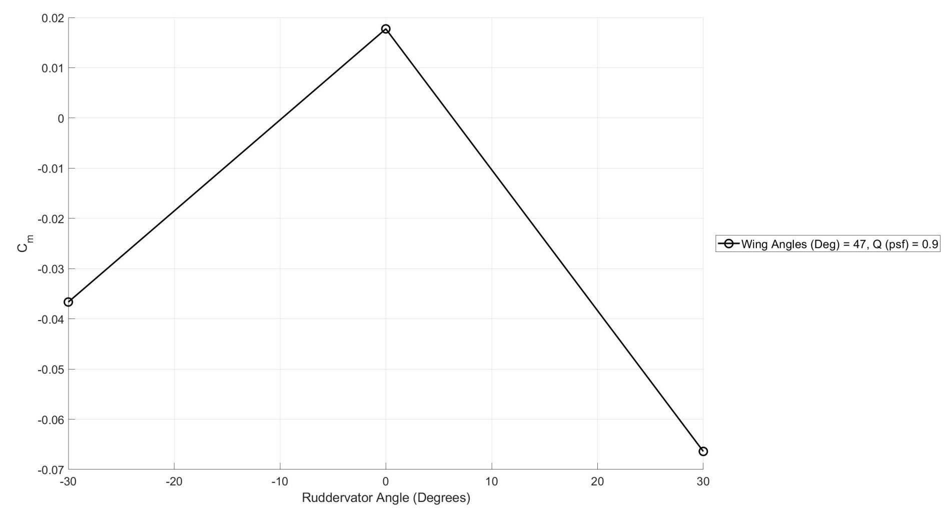

Figure 212. Wing angles 47 degrees trim point C_m vs ruddervator deflection angle.

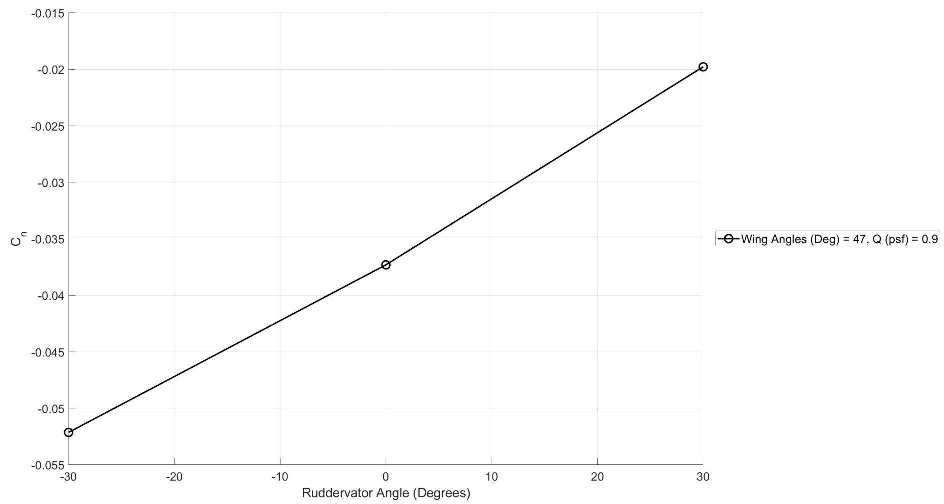

Figure 213. Wing angles 47 degrees trim point C_n vs ruddervator deflection angle.

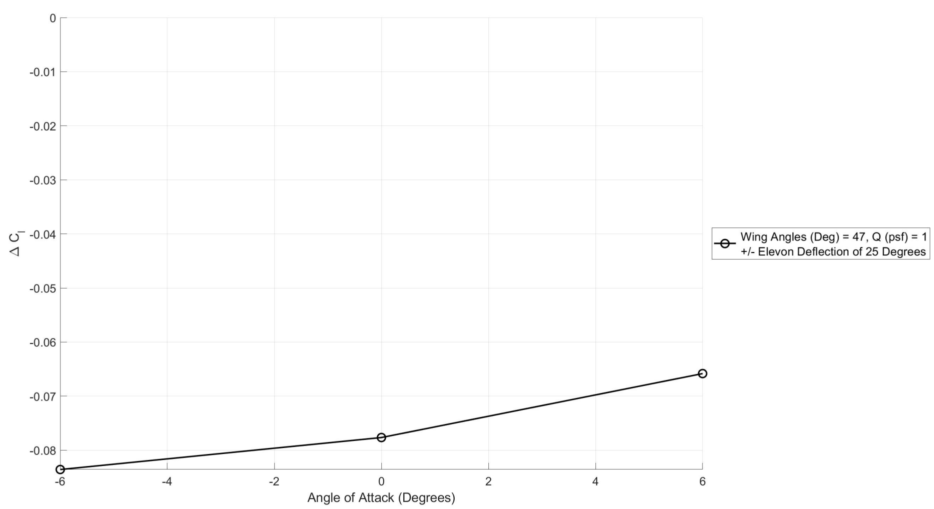

Figure 214. Wing angles 47 degrees trim point Δ C_l vs angle of attack for elevon deflection.

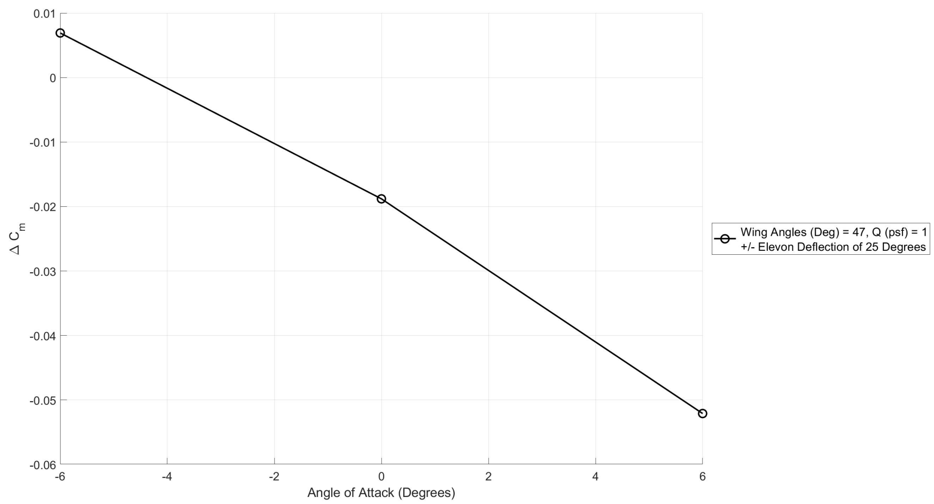

Figure 215. Wing angles 47 degrees trim point Δ C_m vs angle of attack for elevon deflection.

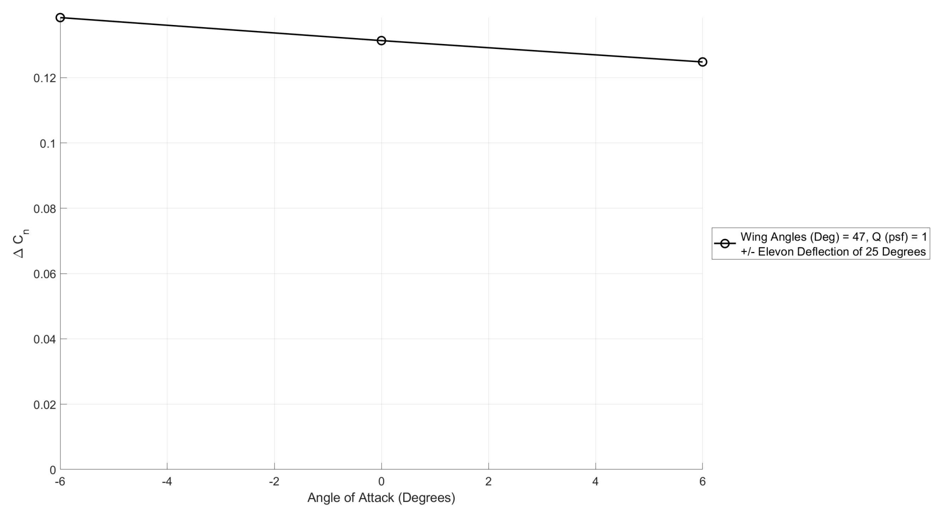

Figure 216. Wing angles 47 degrees trim point Δ C_n vs angle of attack for elevon deflection.

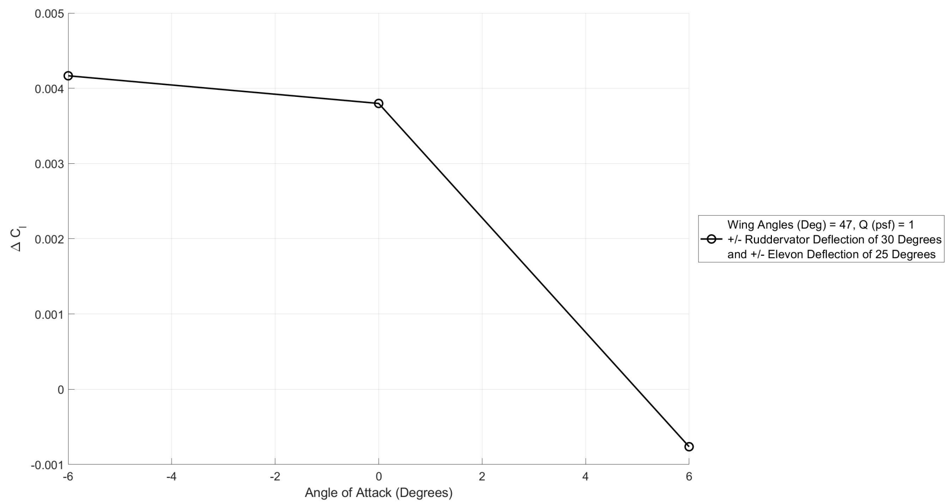

Figure 217. Wing angles 47 degrees trim point Δ C_l vs angle of attack for elevon and ruddervator deflection.

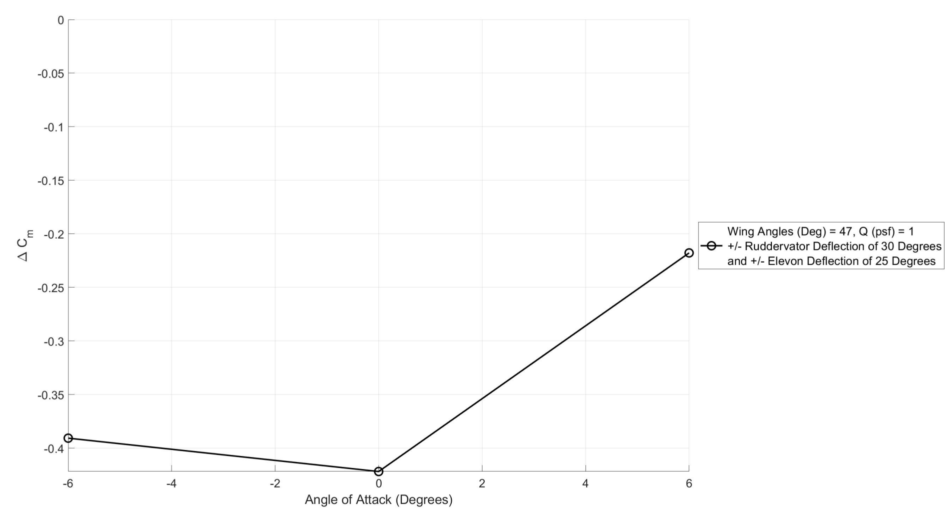

Figure 218. Wing angles 47 degrees trim point Δ C_m vs angle of attack for elevon and ruddervator deflection.

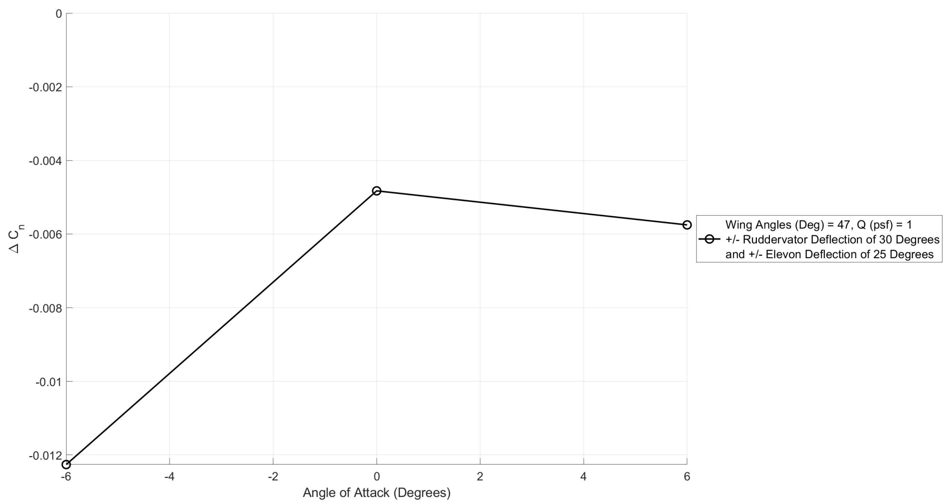

Figure 219. Wing angles 47 degrees trim point Δ C_n vs angle of attack for elevon and ruddervator deflection.

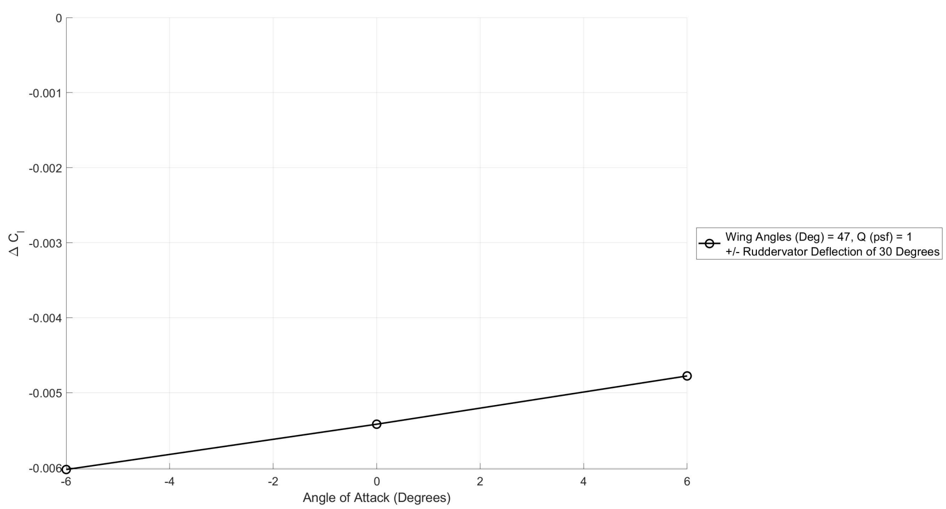

Figure 220. Wing angles 47 degrees trim point Δ C_l vs angle of attack for ruddervator deflection.

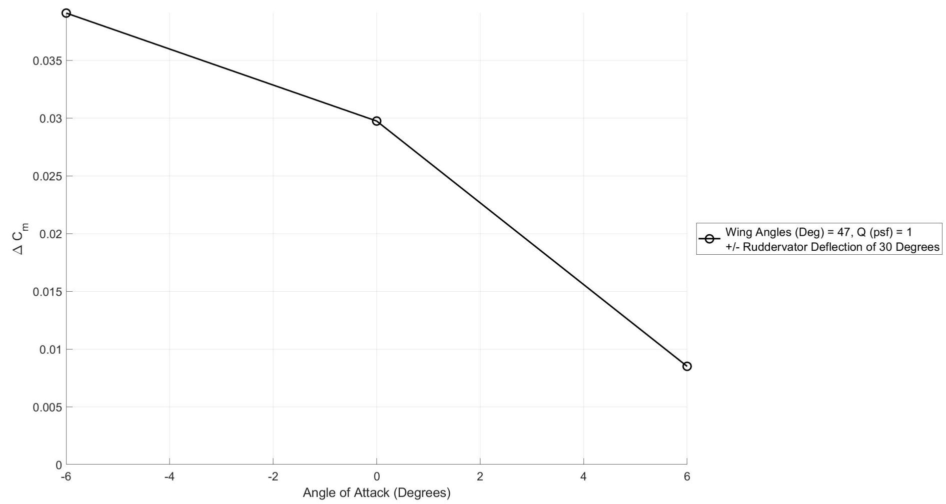

Figure 221. Wing angles 47 degrees trim point Δ C_m vs angle of attack for ruddervator deflection.

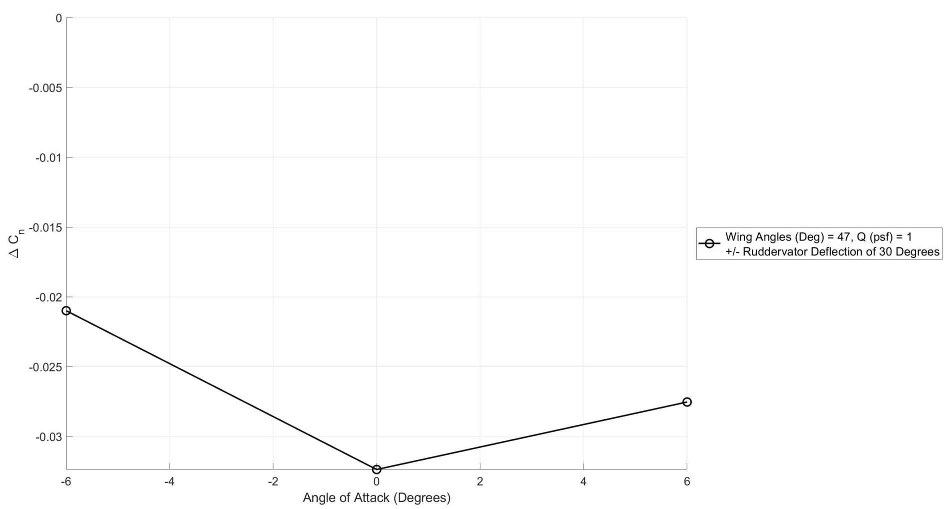

Figure 222. Wing angles 47 degrees trim point Δ C_n vs angle of attack for ruddervator deflection.

C.4 Transition Wing Angles 43 Degrees Performance and Stability Plots

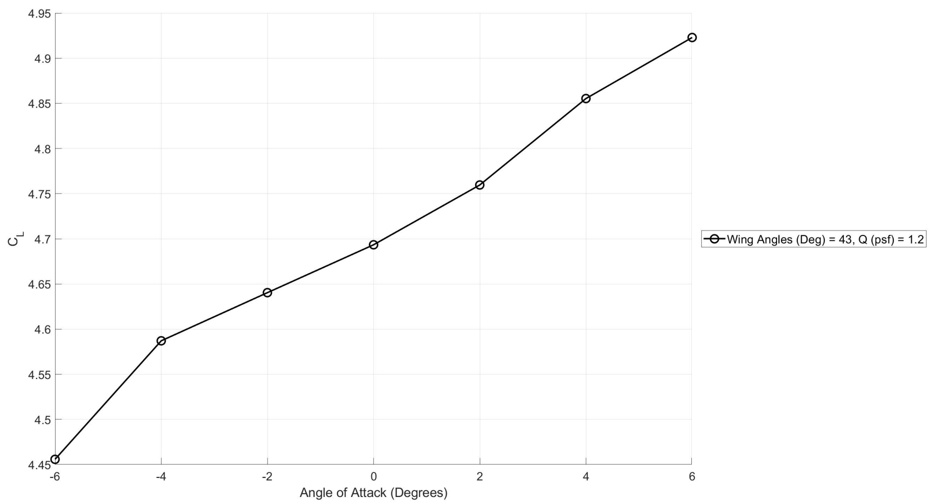

Figure 223. Wing angles 43 degrees trim point C_L vs angle of attack.

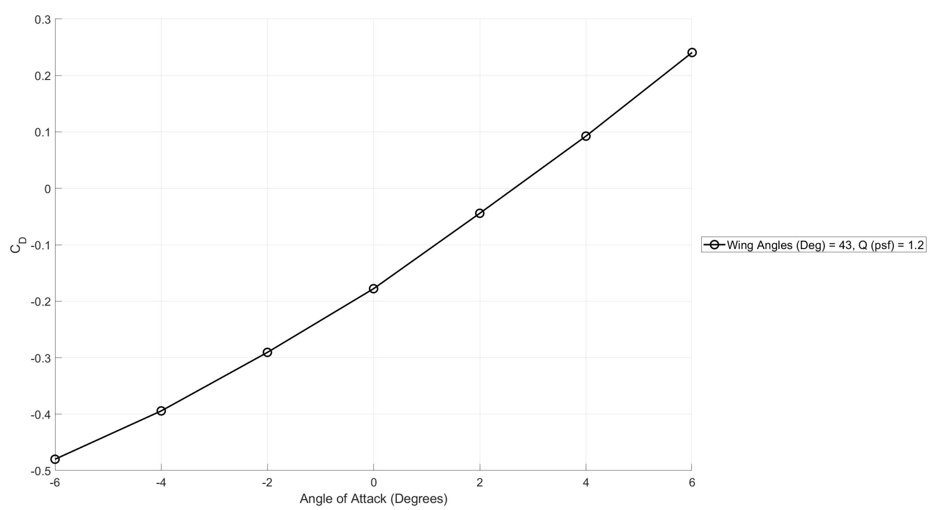

Figure 224. Wing angles 43 degrees trim point C_D vs angle of attack.

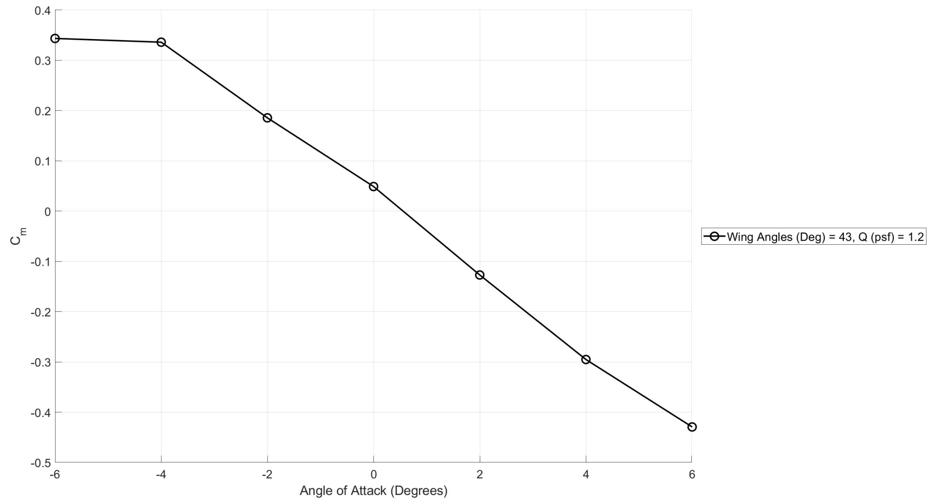

Figure 225. Wing angles 43 degrees trim point C_m vs angle of attack.

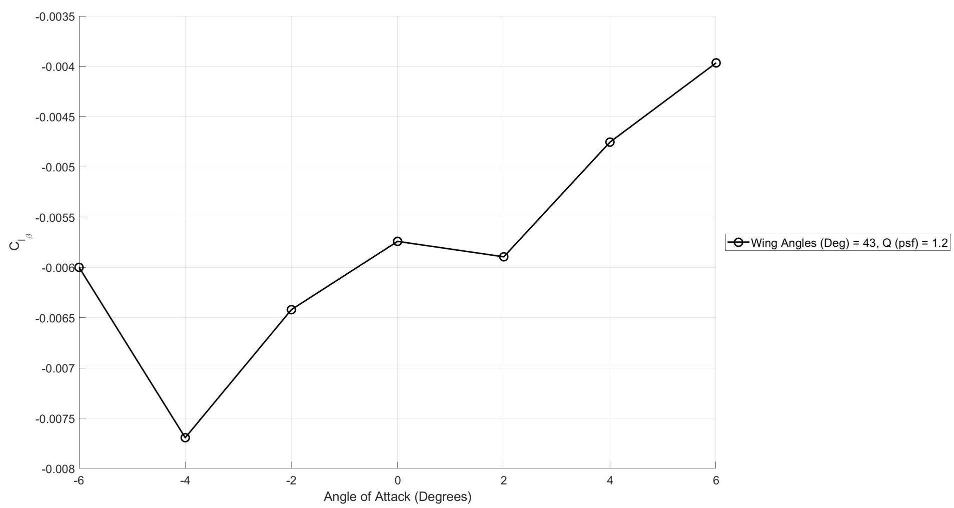

Figure 226. Wing angles 43 degrees trim point C_{l_β} vs angle of attack.

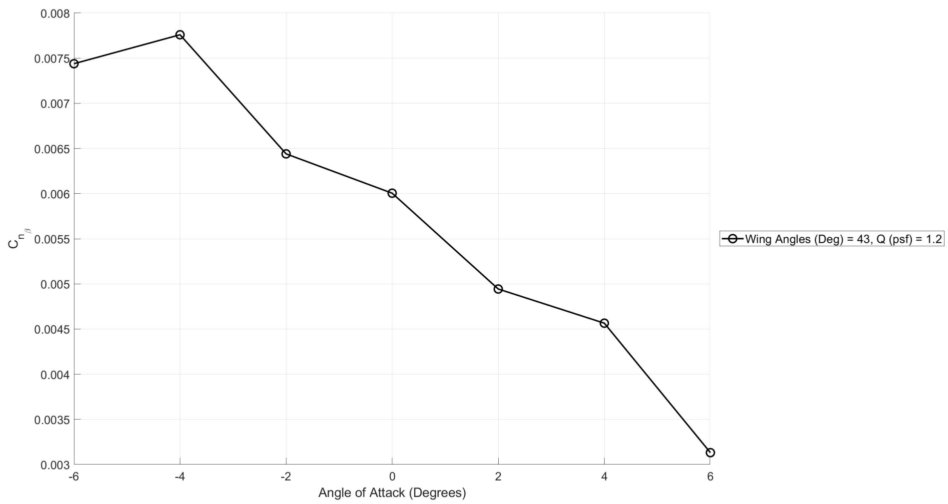

Figure 227. Wing angles 43 degrees trim point C_{n_β} vs angle of attack.

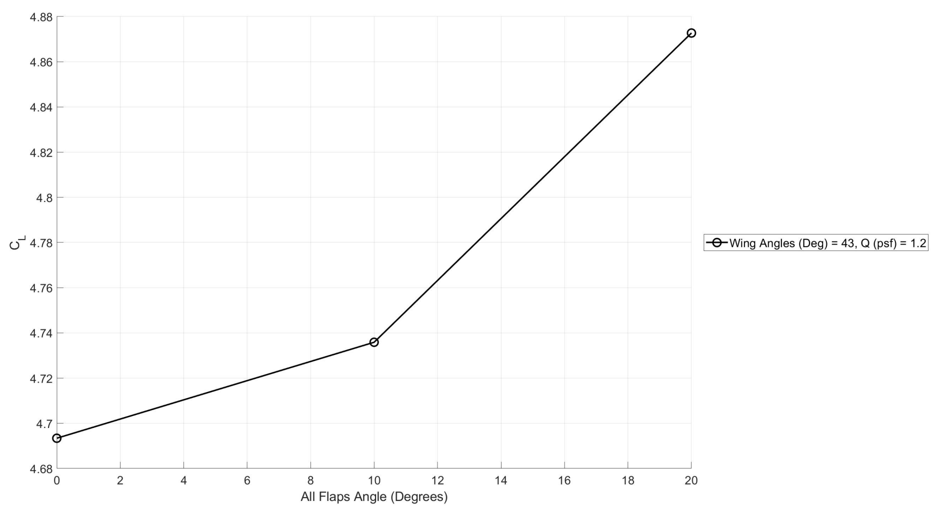

Figure 228. Wing angles 43 degrees trim point C_L vs all flap deflection angle.

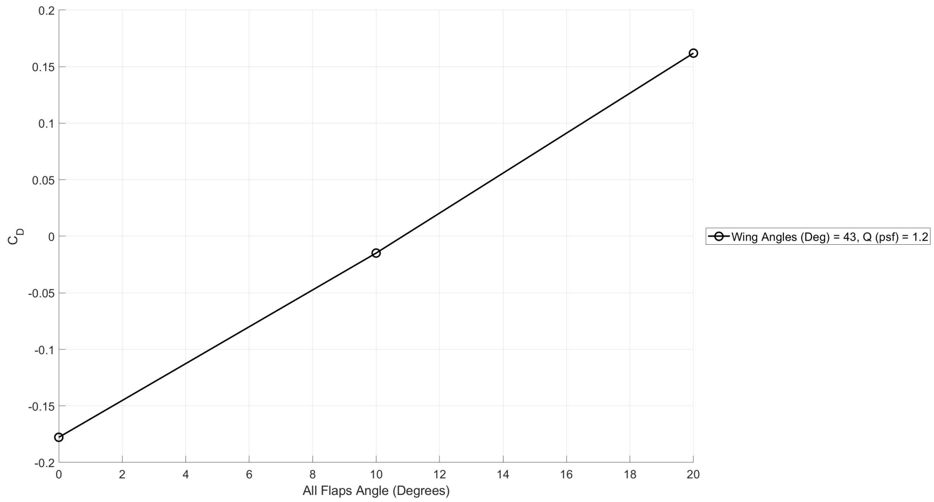

Figure 229. Wing angles 43 degrees trim point C_D vs all flap deflection angle.

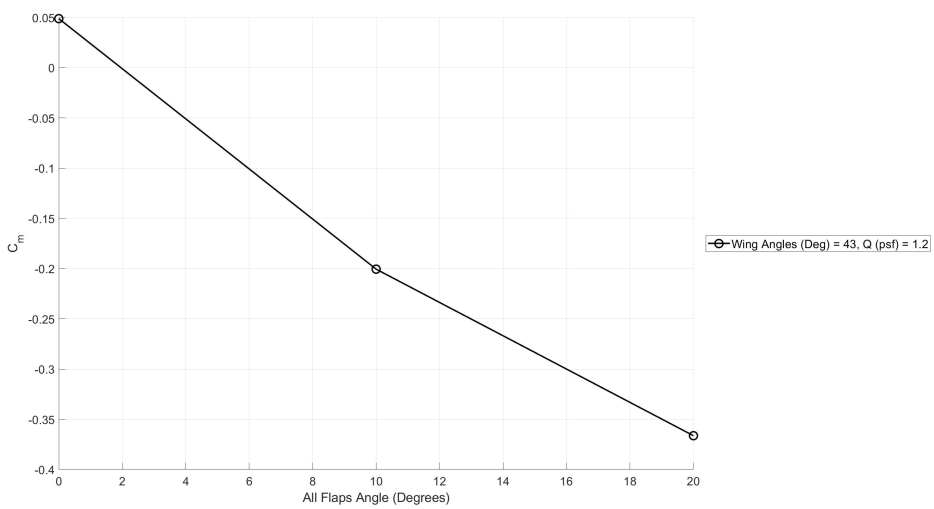

Figure 230. Wing angles 43 degrees trim point C_m vs all flap deflection angle.

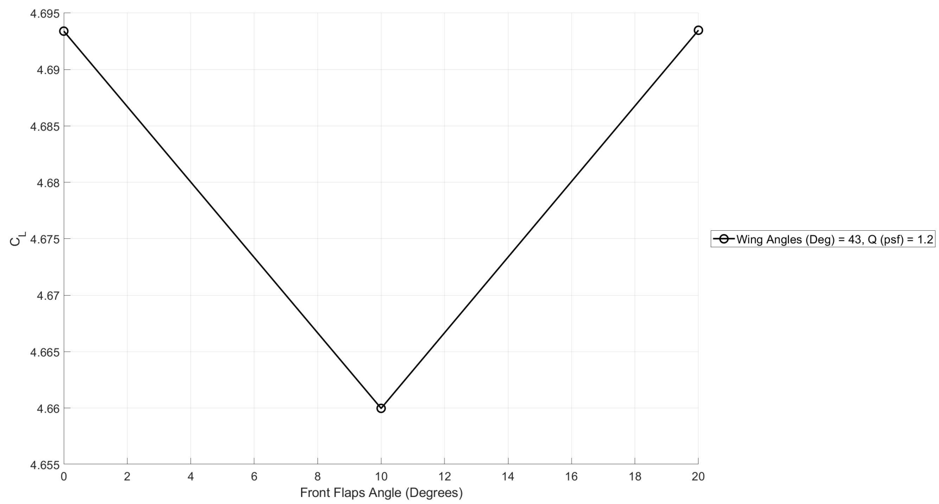

Figure 231. Wing angles 43 degrees trim point C_L vs front flap deflection angle.

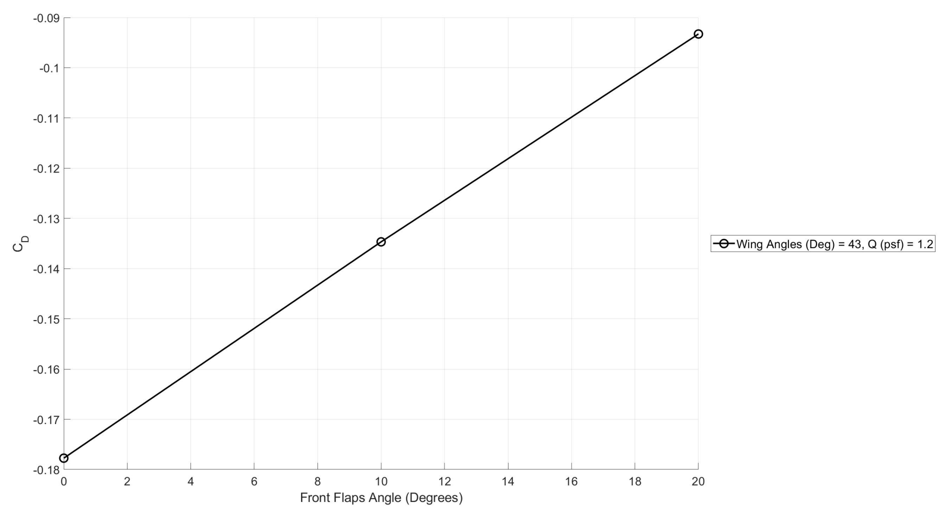

Figure 232. Wing angles 43 degrees trim point C_D vs front flap deflection angle.

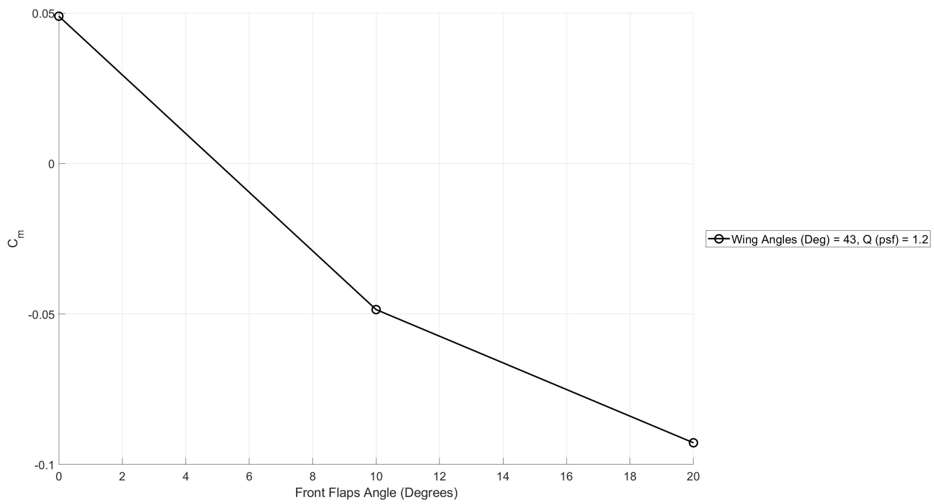

Figure 233. Wing angles 43 degrees trim point C_m vs front flap deflection angle.

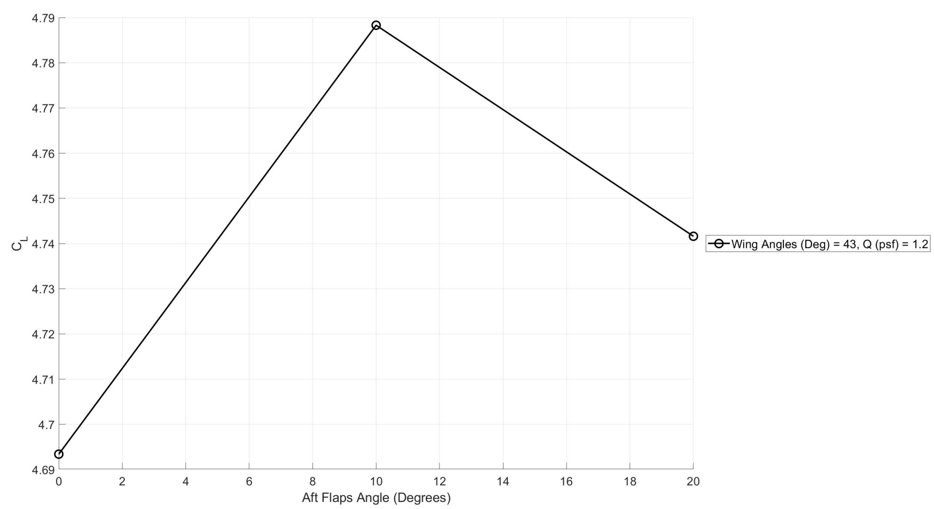

Figure 234. Wing angles 43 degrees trim point C_L vs aft flap deflection angle.

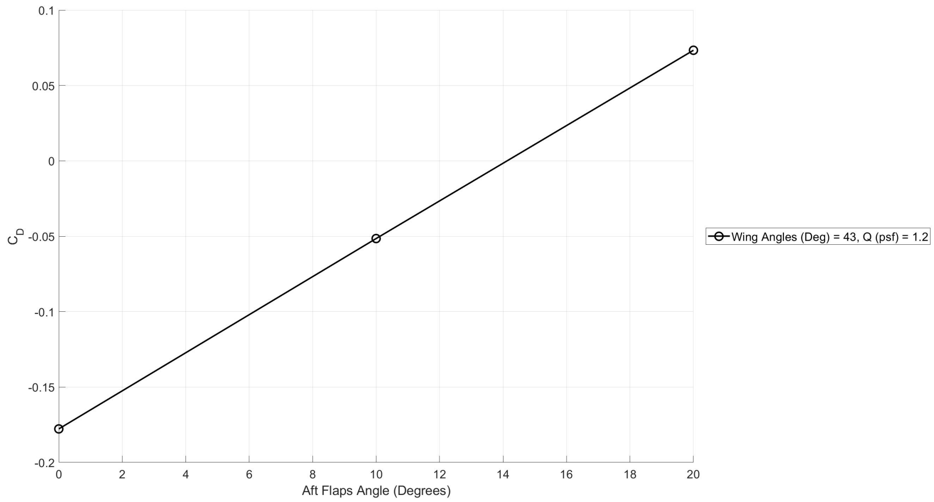

Figure 235. Wing angles 43 degrees trim point C_D vs aft flap deflection angle.

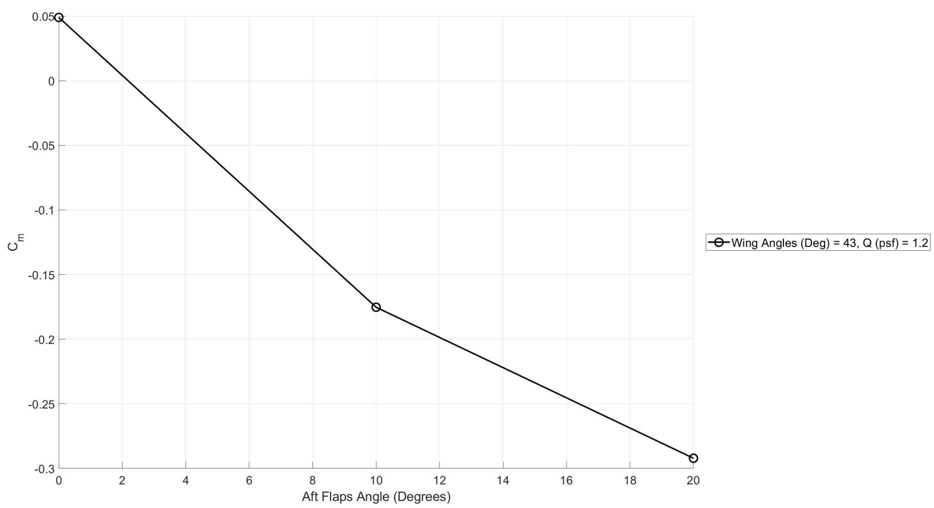

Figure 236. Wing angles 43 degrees trim point C_m vs aft flap deflection angle.

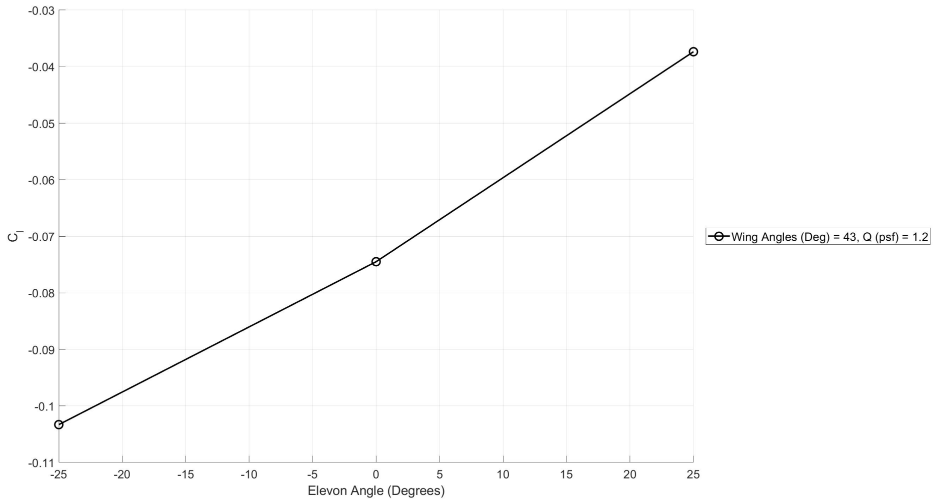

Figure 237. Wing angles 43 degrees trim point C_l vs elevon deflection angle.

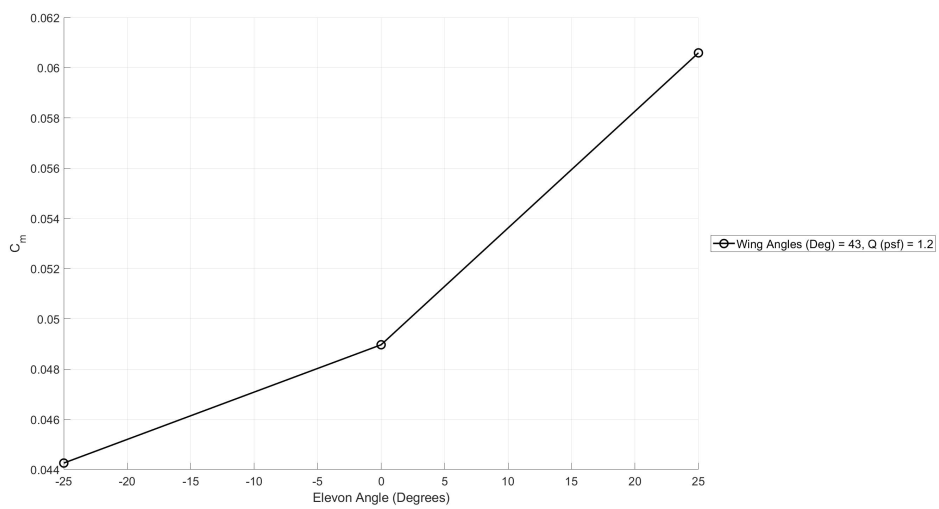

Figure 238. Wing angles 43 degrees trim point C_m vs elevon deflection angle.

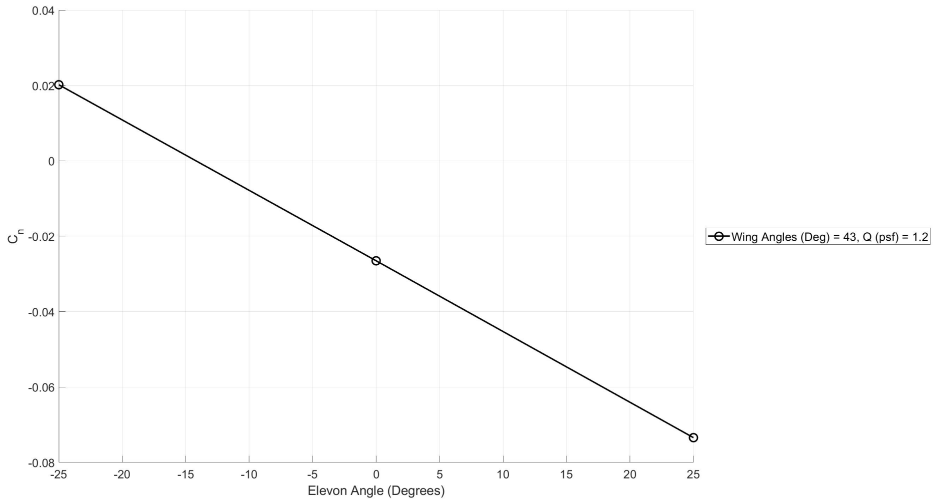

Figure 239. Wing angles 43 degrees trim point C_n vs elevon deflection angle.

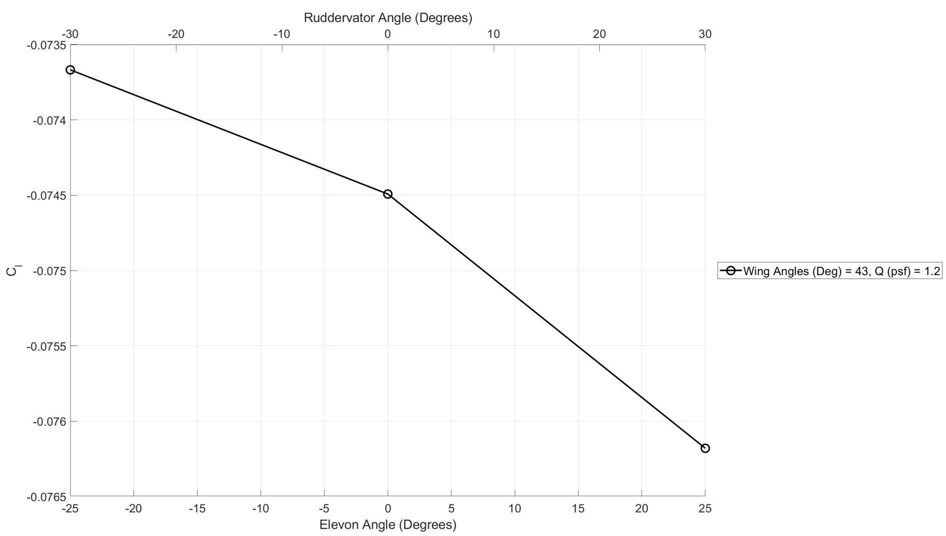

Figure 240. Wing angles 43 degrees trim point C_l vs elevon and ruddervator deflection angles.

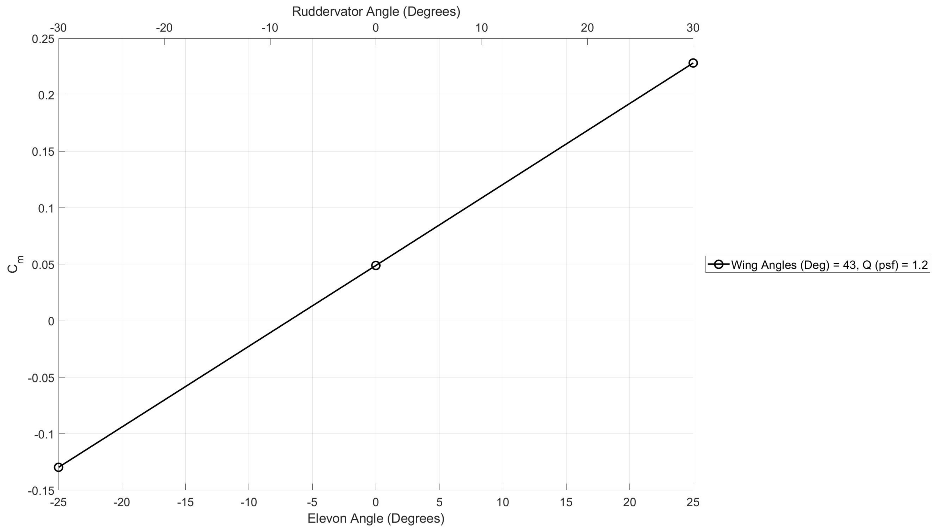

Figure 241. Wing angles 43 degrees trim point C_m vs elevon and ruddervator deflection angles.

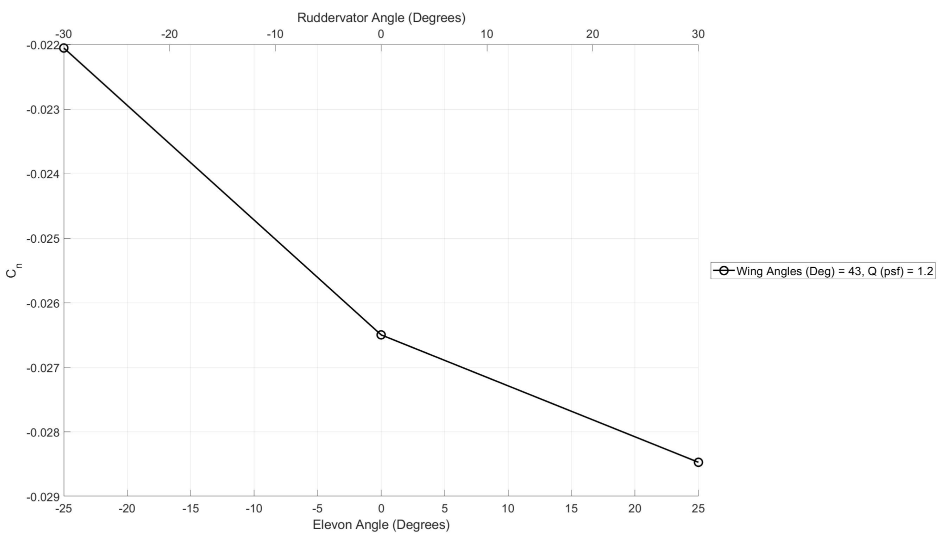

Figure 242. Wing angles 43 degrees trim point C_n vs elevon and ruddervator deflection angles.

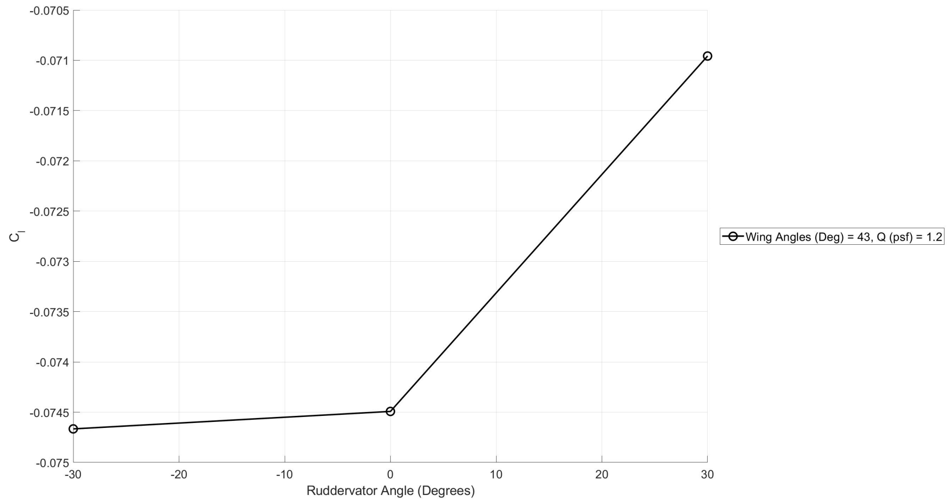

Figure 243. Wing angles 43 degrees trim point C_l vs ruddervator deflection angle.

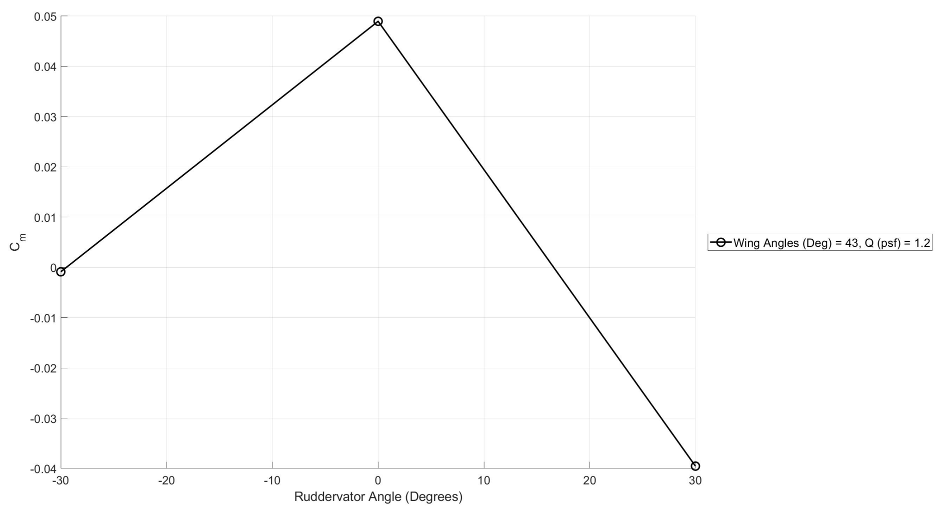

Figure 244. Wing angles 43 degrees trim point C_m vs ruddervator deflection angle.

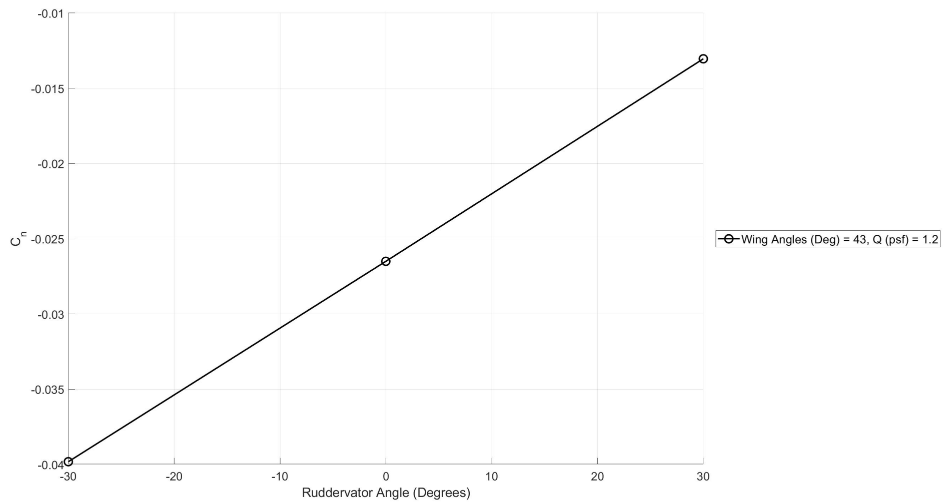

Figure 245. Wing angles 43 degrees trim point C_n vs ruddervator deflection angle.

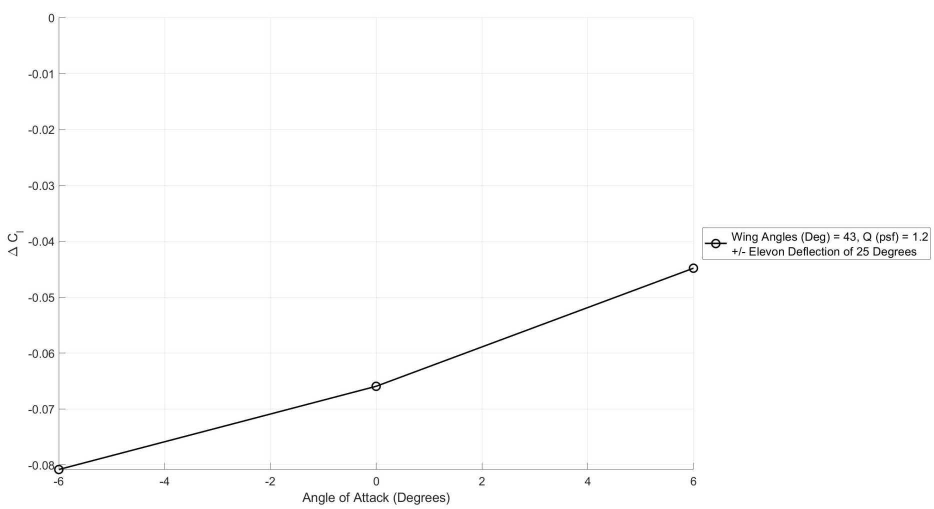

Figure 246. Wing angles 43 degrees trim point Δ C_l vs angle of attack for elevon deflection.

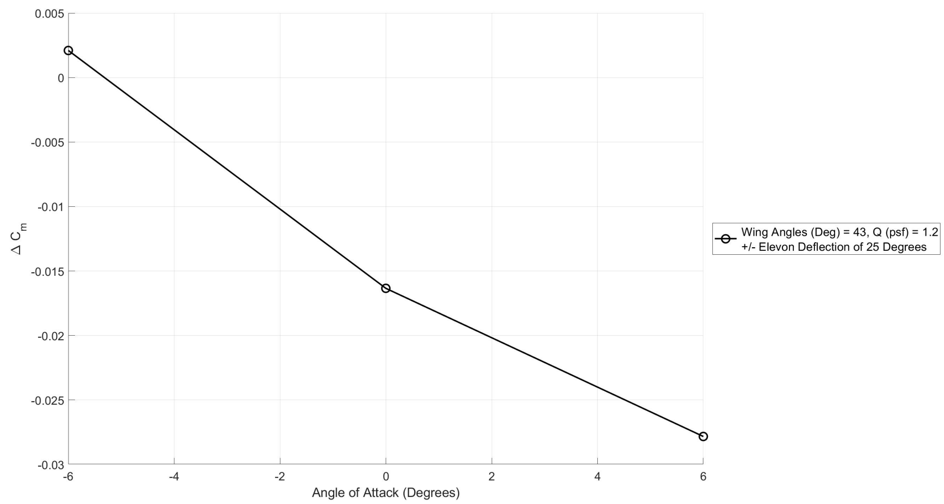

Figure 247. Wing angles 43 degrees trim point Δ C_m vs angle of attack for elevon deflection.

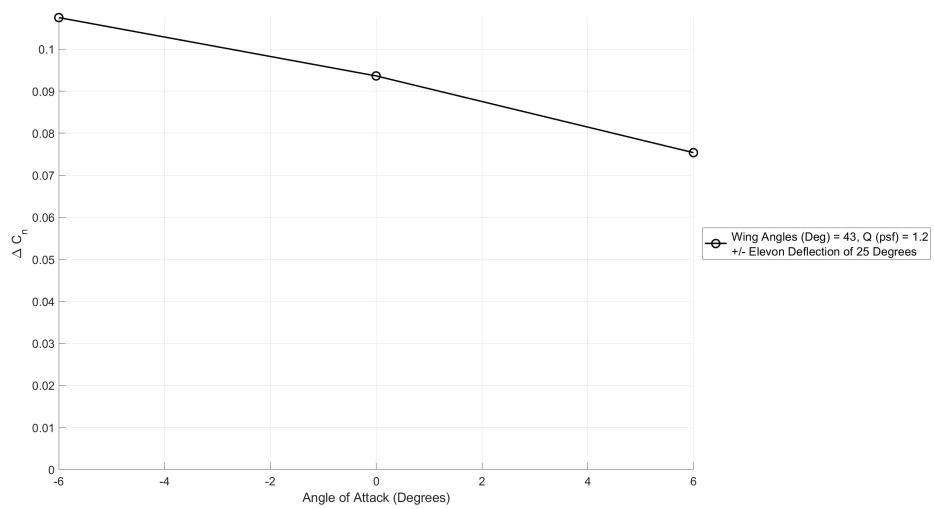

Figure 248. Wing angles 43 degrees trim point Δ C_n vs angle of attack for elevon deflection.

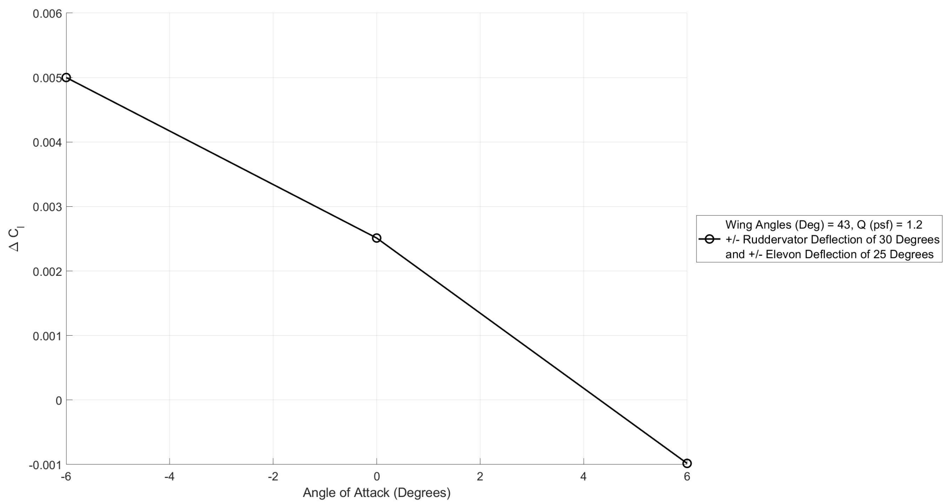

Figure 249. Wing angles 43 degrees trim point Δ C_l vs angle of attack for elevon and ruddervator deflection.

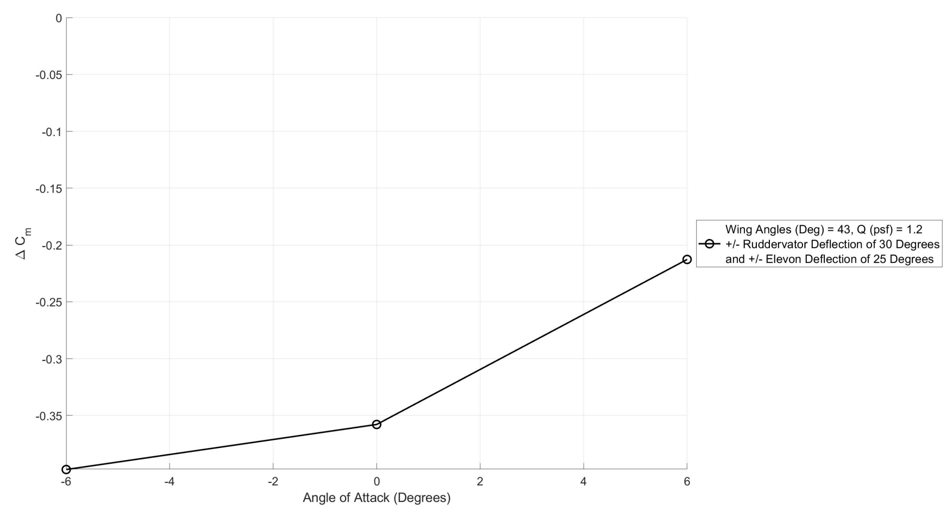

Figure 250. Wing angles 43 degrees trim point Δ C_m vs angle of attack for elevon and ruddervator deflection.

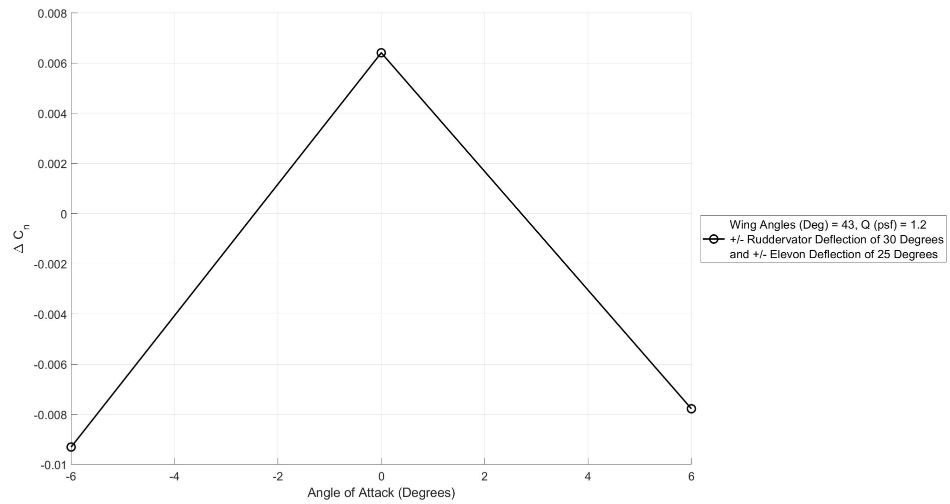

Figure 251. Wing angles 43 degrees trim point Δ C_n vs angle of attack for elevon and ruddervator deflection.

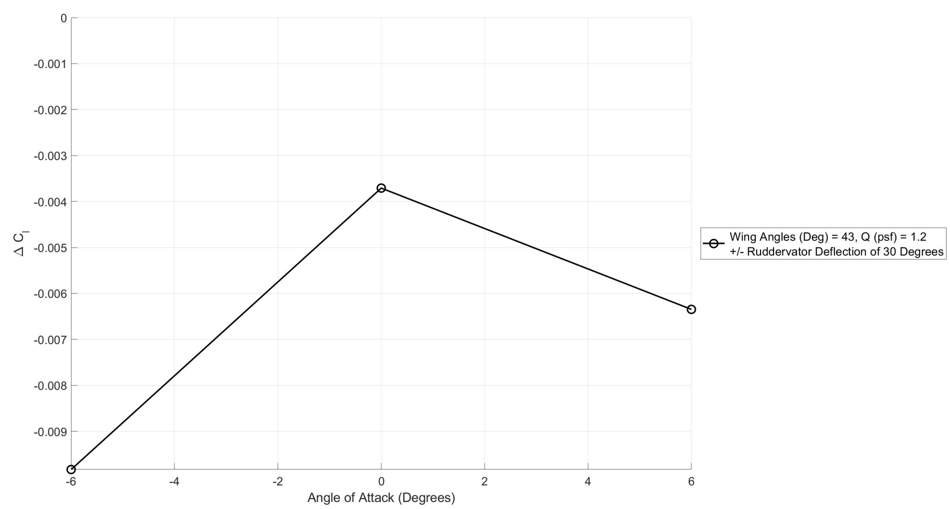

Figure 252. Wing angles 43 degrees trim point Δ C_l vs angle of attack for ruddervator deflection.

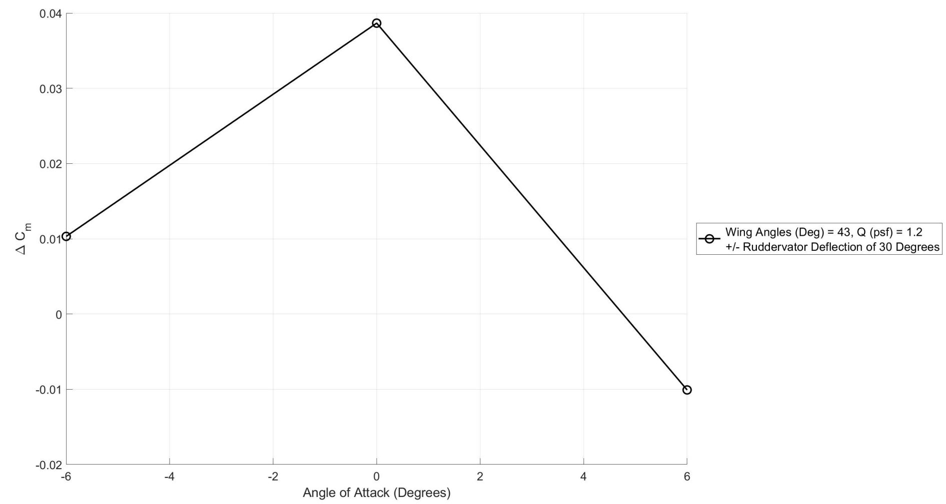

Figure 253. Wing angles 43 degrees trim point Δ C_m vs angle of attack for ruddervator deflection.

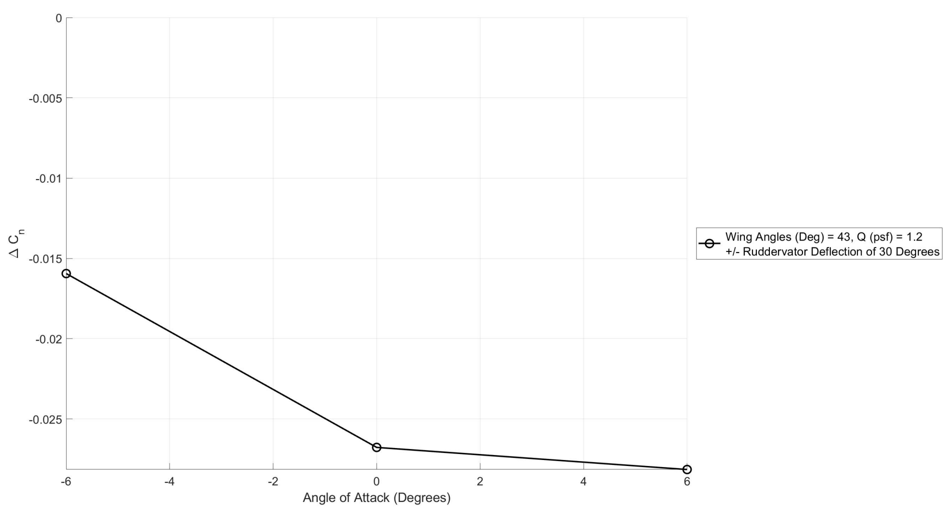

Figure 254. Wing angles 43 degrees trim point Δ C_n vs angle of attack for ruddervator deflection.

C.5 Transition Wing Angles 38 Degrees Performance and Stability Plots

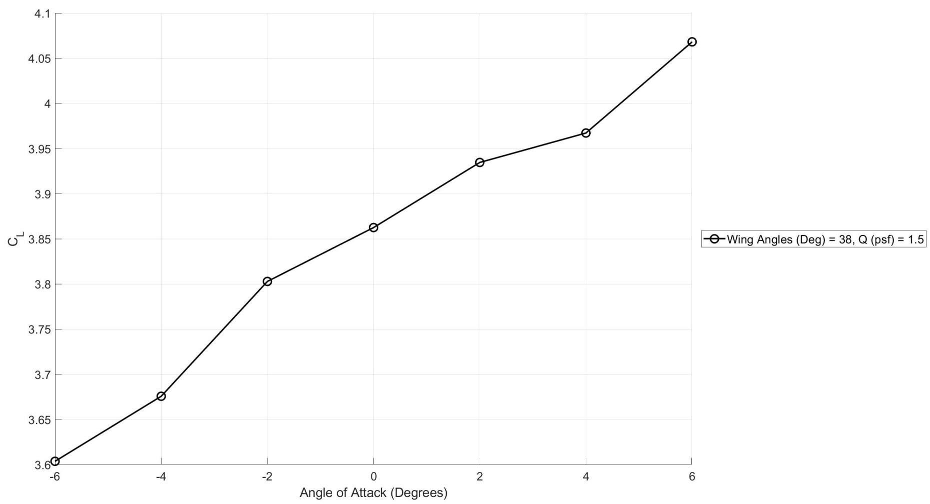

Figure 255. Wing angles 38 degrees trim point C_L vs angle of attack.

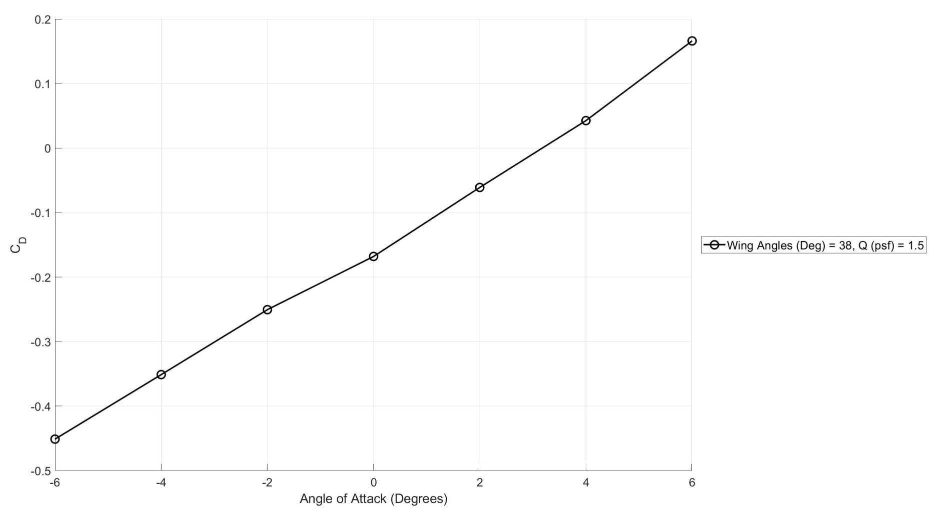

Figure 256. Wing angles 38 degrees trim point C_D vs angle of attack.

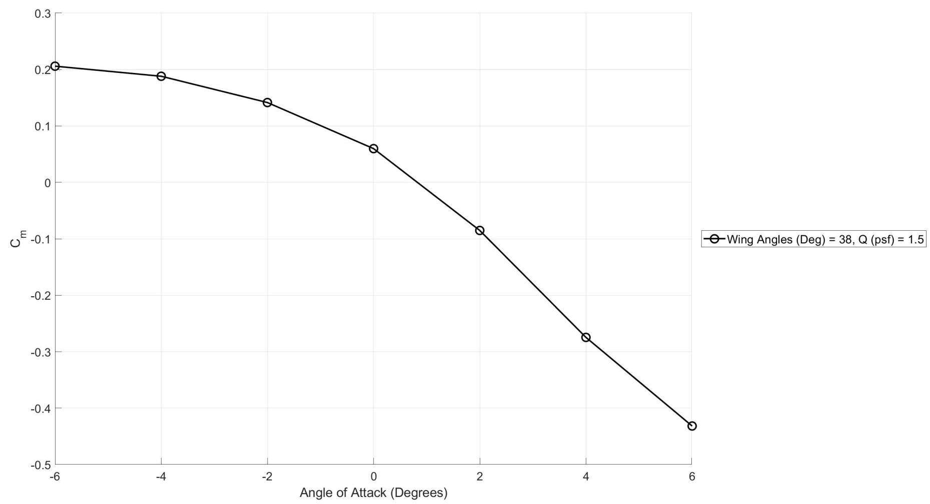

Figure 257. Wing angles 38 degrees trim point C_m vs angle of attack.

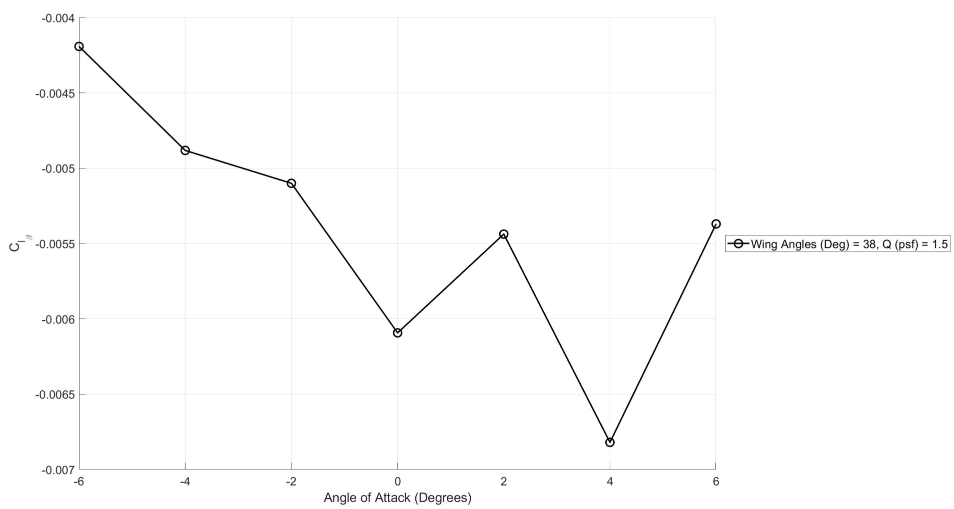

Figure 258. Wing angles 38 degrees trim point C_{l_β} vs angle of attack.

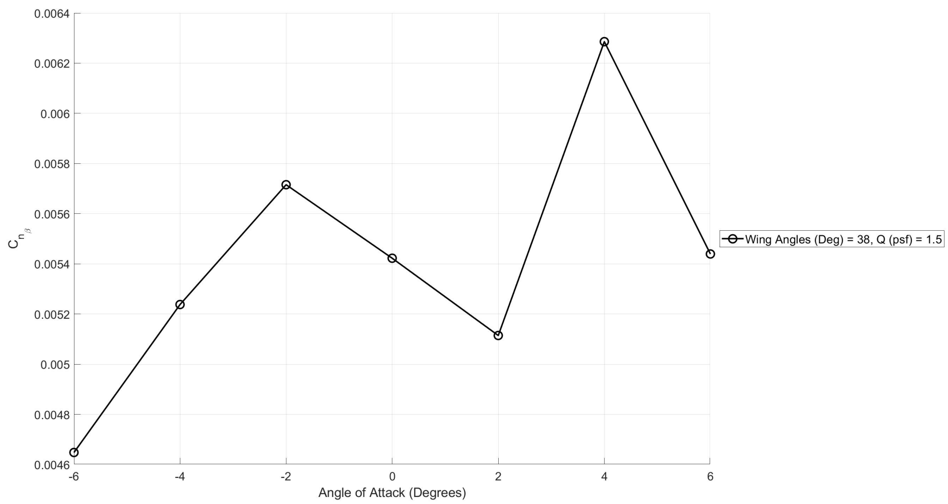

Figure 259. Wing angles 38 degrees trim point C_{n_β} vs angle of attack.

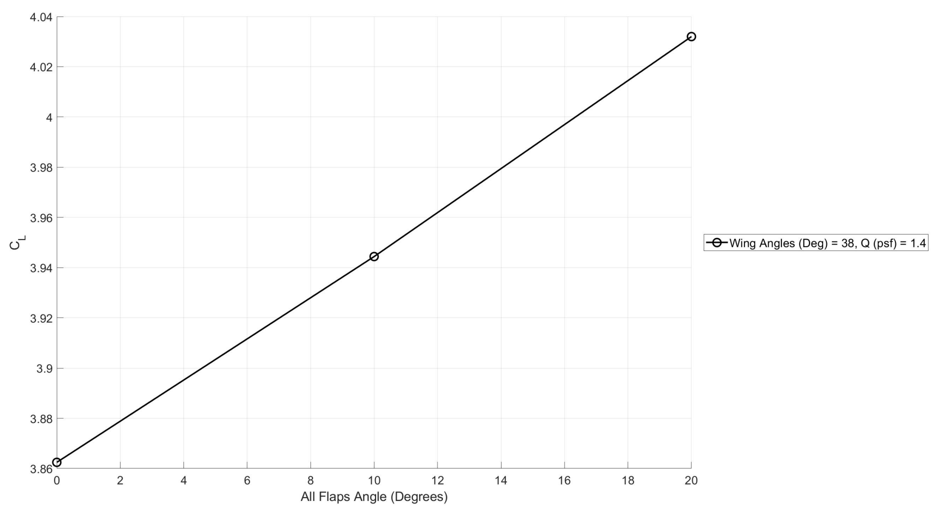

Figure 260. Wing angles 38 degrees trim point C_L vs all flap deflection angle.

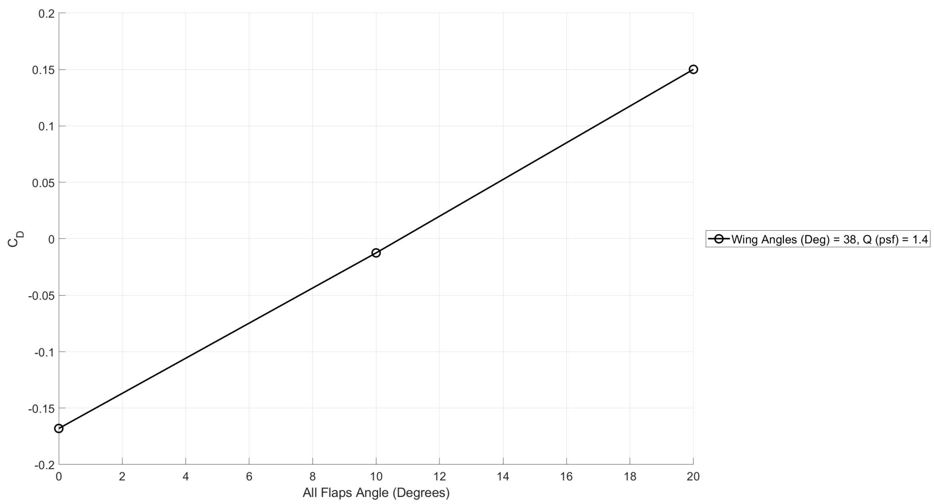

Figure 261. Wing angles 38 degrees trim point C_D vs all flap deflection angle.

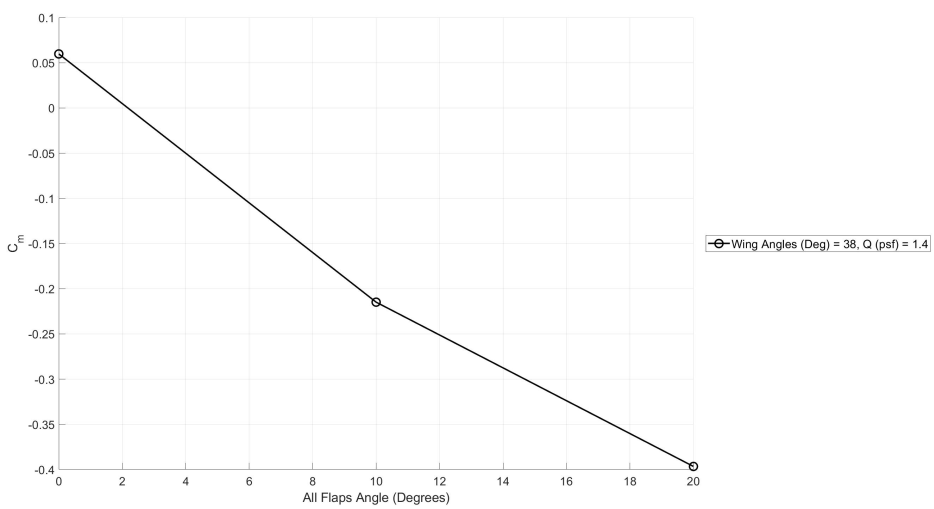

Figure 262. Wing angles 38 degrees trim point C_m vs all flap deflection angle.

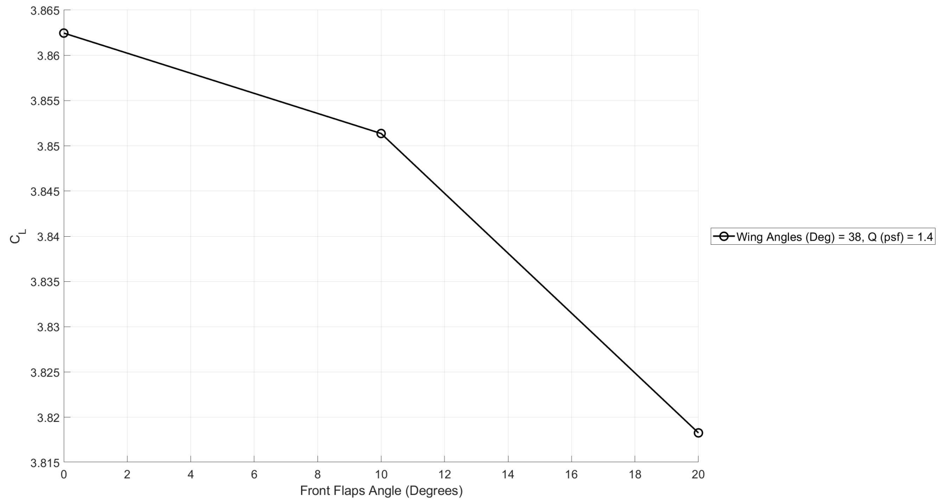

Figure 263. Wing angles 38 degrees trim point C_L vs front flap deflection angle.

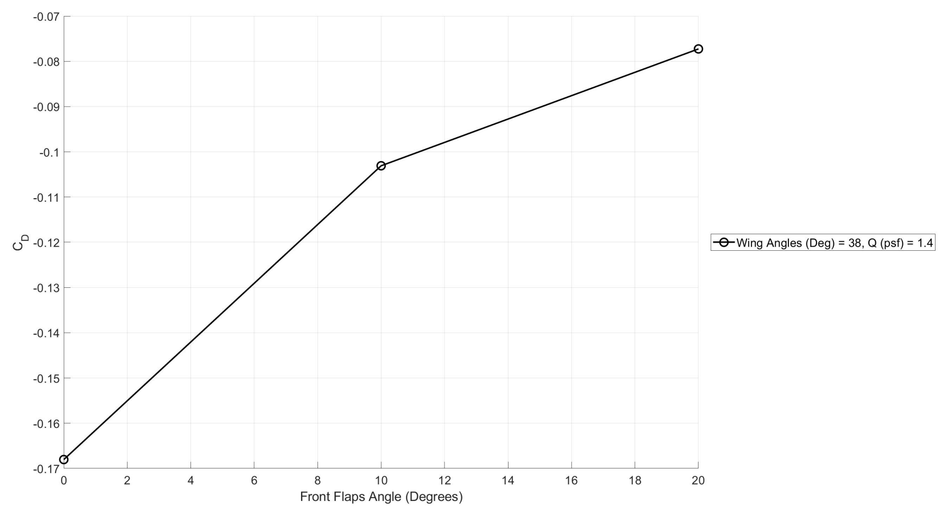

Figure 264. Wing angles 38 degrees trim point C_D vs front flap deflection angle.

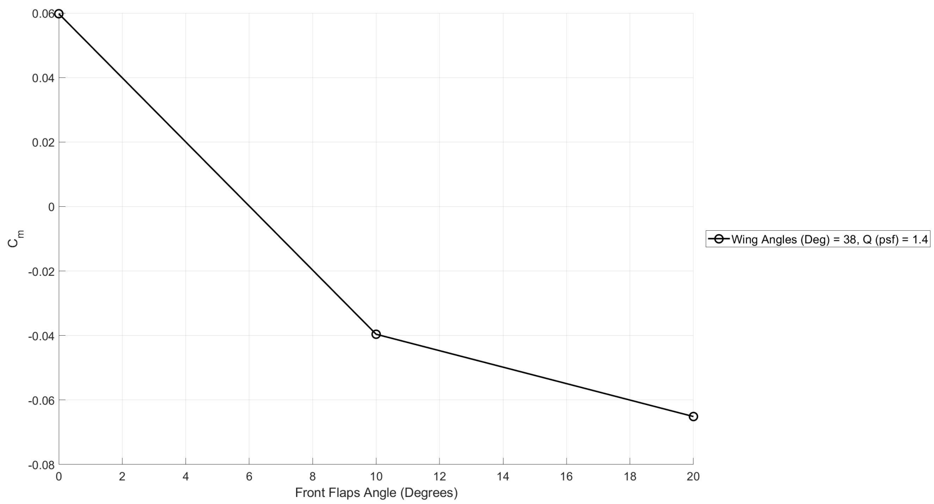

Figure 265. Wing angles 38 degrees trim point C_m vs front flap deflection angle.

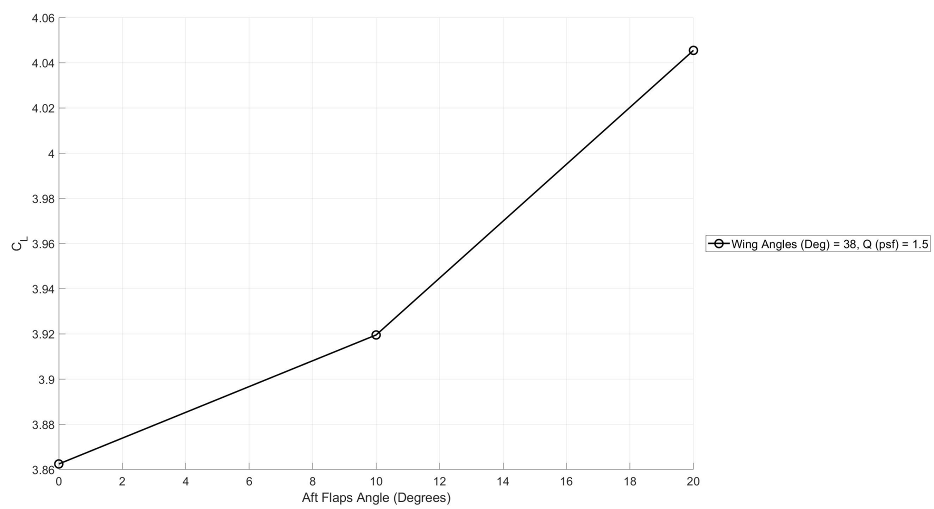

Figure 266. Wing angles 38 degrees trim point C_L vs aft flap deflection angle.

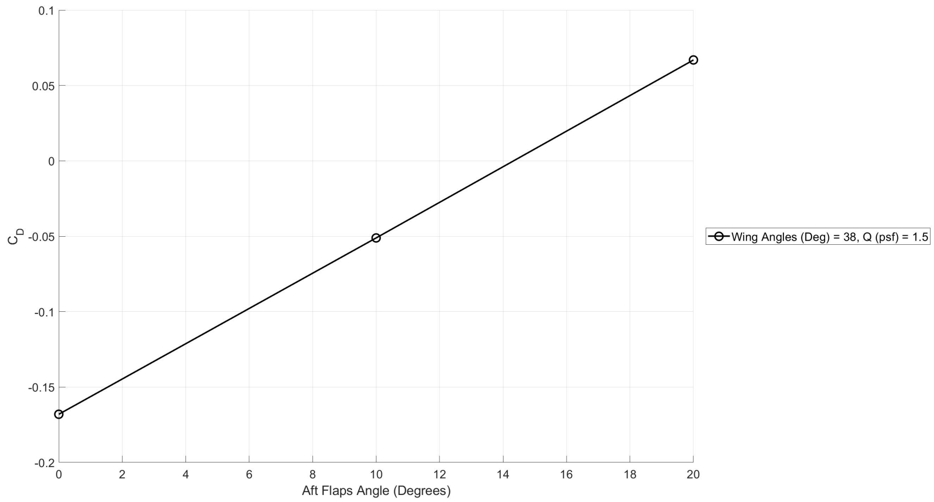

Figure 267. Wing angles 38 degrees trim point C_D vs aft flap deflection angle.

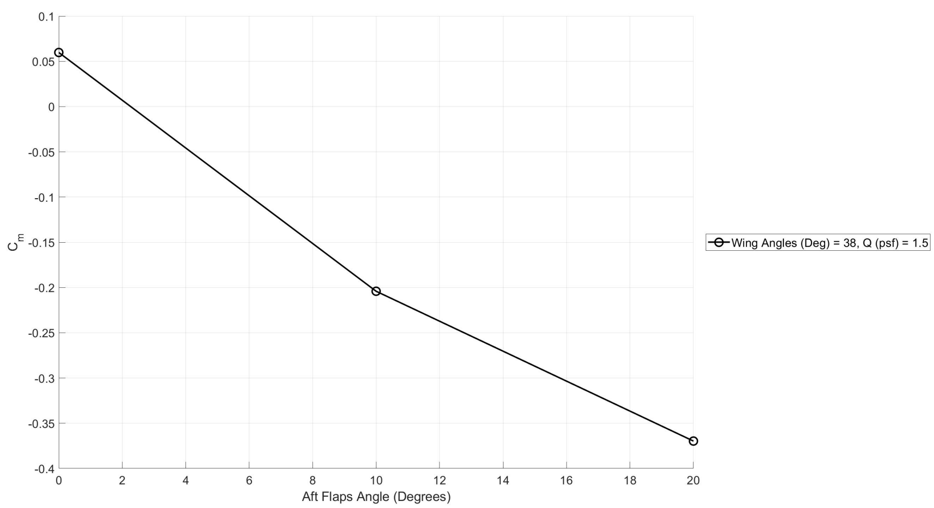

Figure 268. Wing angles 38 degrees trim point C_m vs aft flap deflection angle.

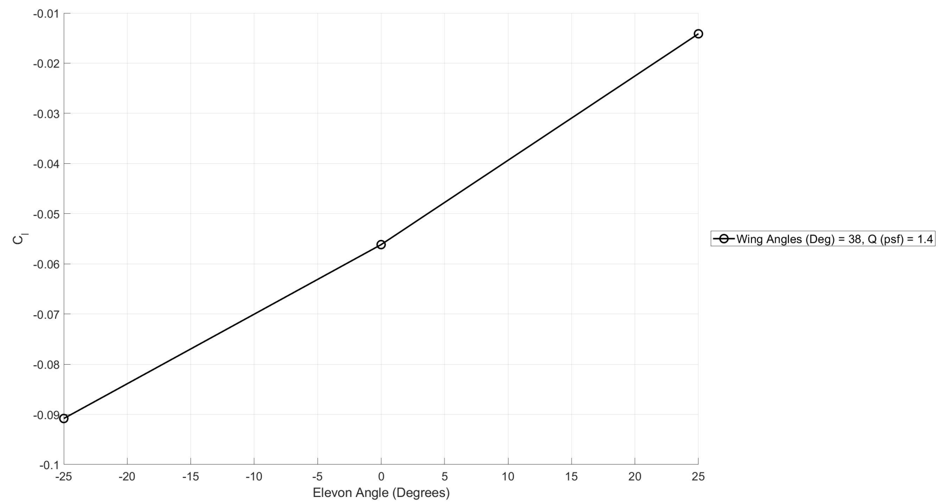

Figure 269. Wing angles 38 degrees trim point C_l vs elevon deflection angle.

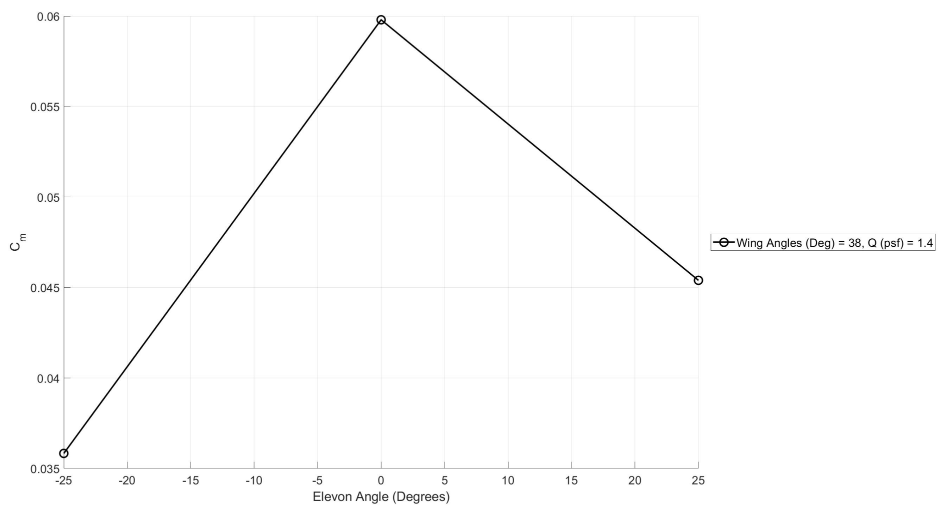

Figure 270. Wing angles 38 degrees trim point C_m vs elevon deflection angle.

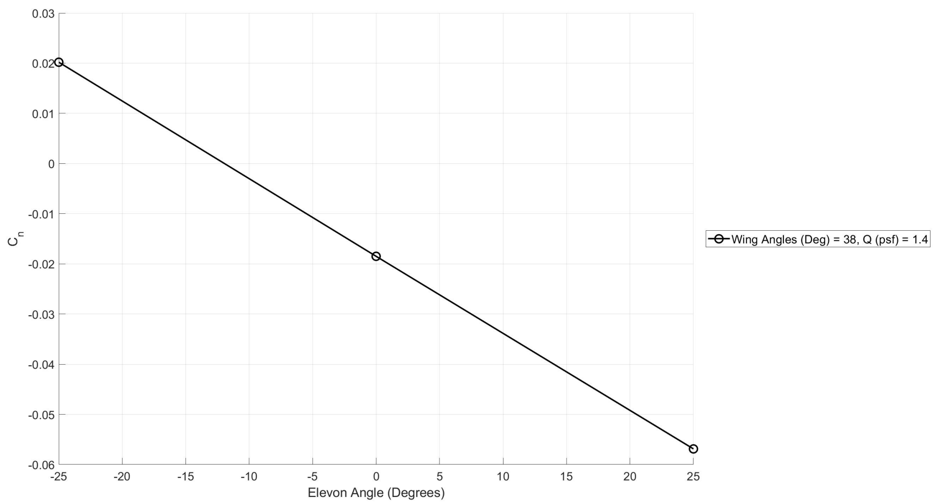

Figure 271. Wing angles 38 degrees trim point C_n vs elevon deflection angle.

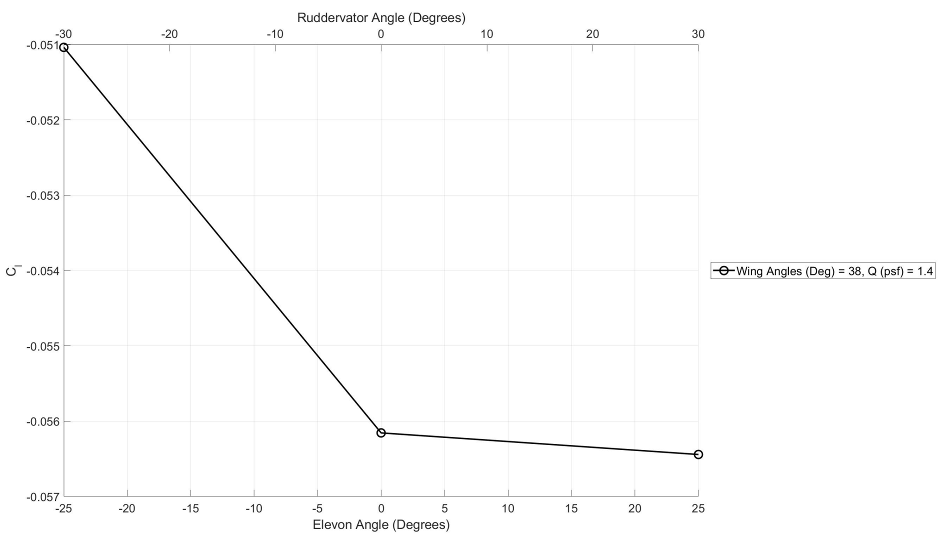

Figure 272. Wing angles 38 degrees trim point C_l vs elevon and ruddervator deflection angles.

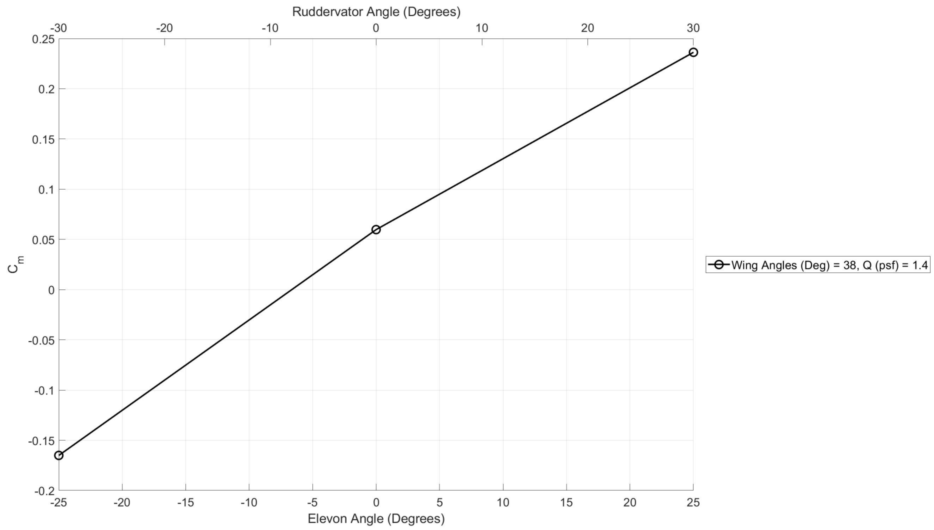

Figure 273. Wing angles 38 degrees trim point C_m vs elevon and ruddervator deflection angles.

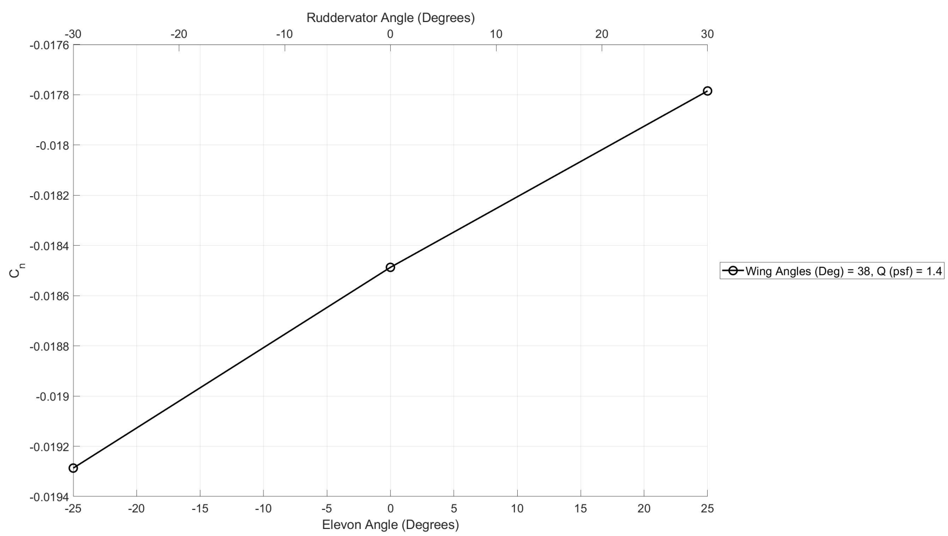

Figure 274. Wing angles 38 degrees trim point C_n vs elevon and ruddervator deflection angles.

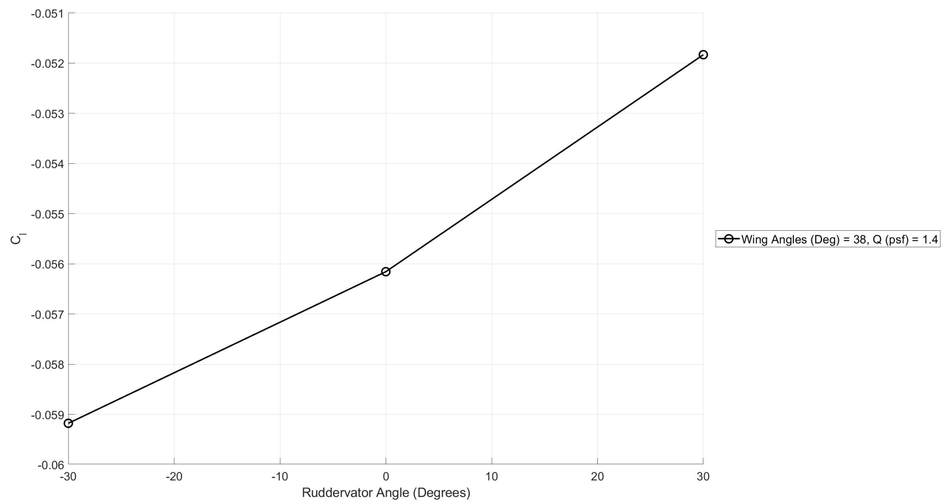

Figure 275. Wing angles 38 degrees trim point C_l vs ruddervator deflection angle.

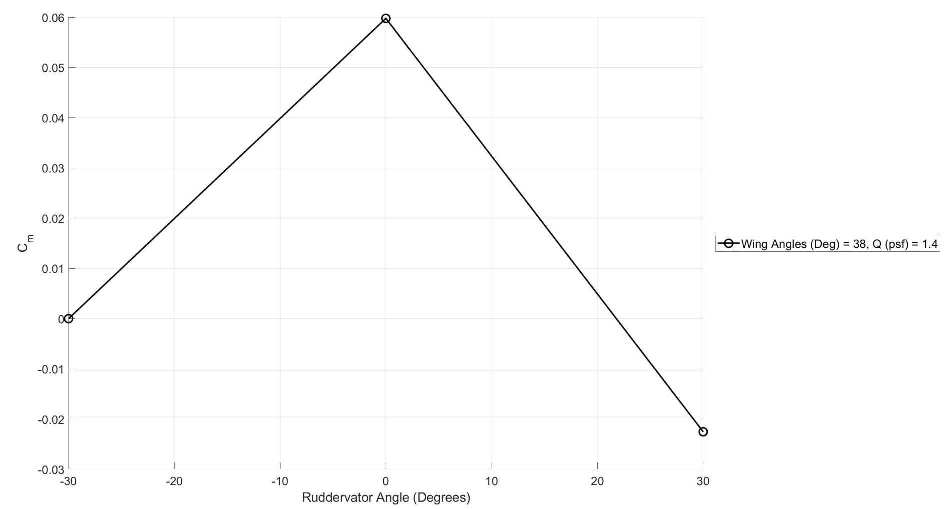

Figure 276. Wing angles 38 degrees trim point C_m vs ruddervator deflection angle.

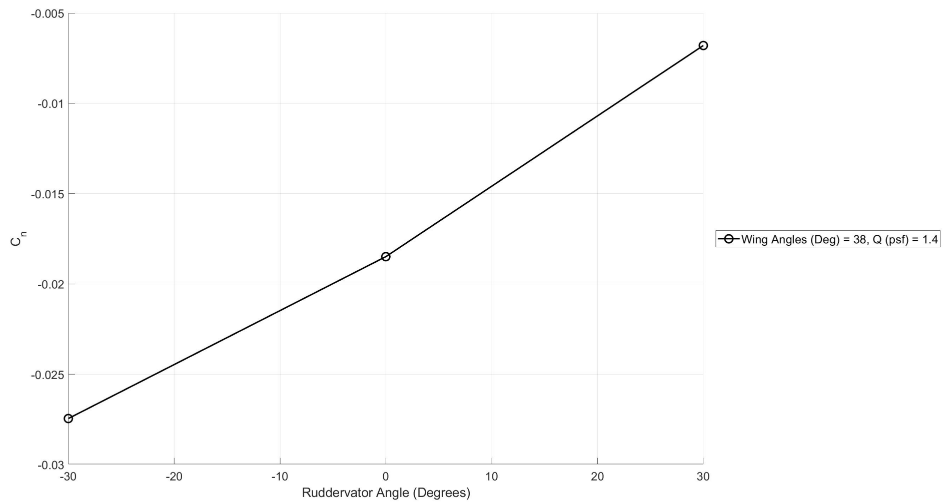

Figure 277. Wing angles 38 degrees trim point C_n vs ruddervator deflection angle.

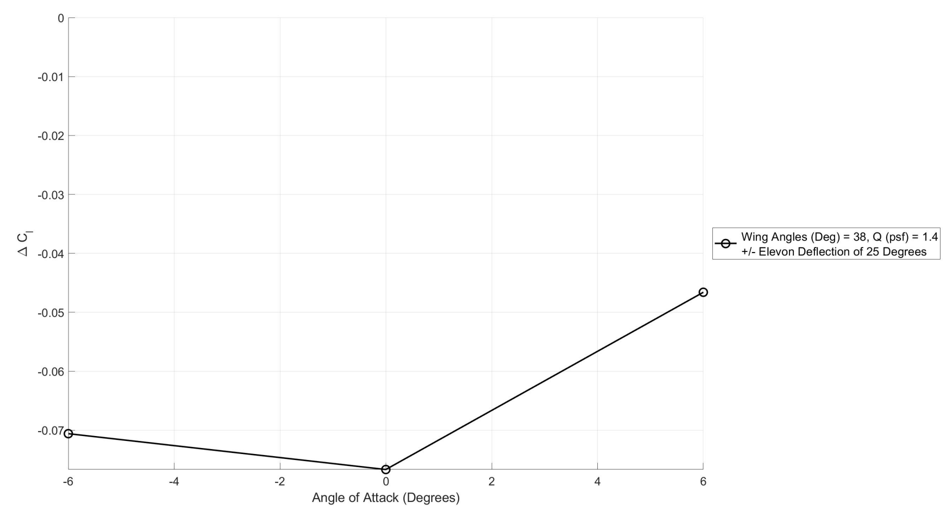

Figure 278. Wing angles 38 degrees trim point Δ C_l vs angle of attack for elevon deflection.

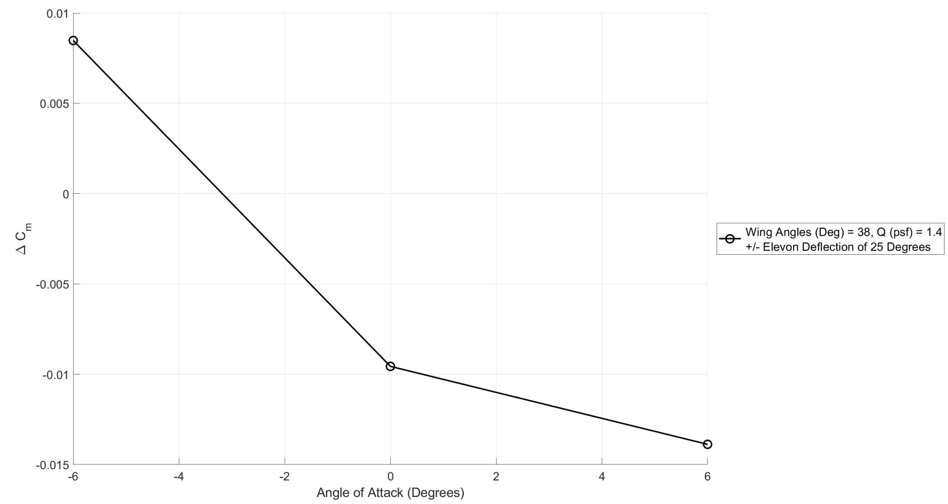

Figure 279. Wing angles 38 degrees trim point Δ C_m vs angle of attack for elevon deflection.

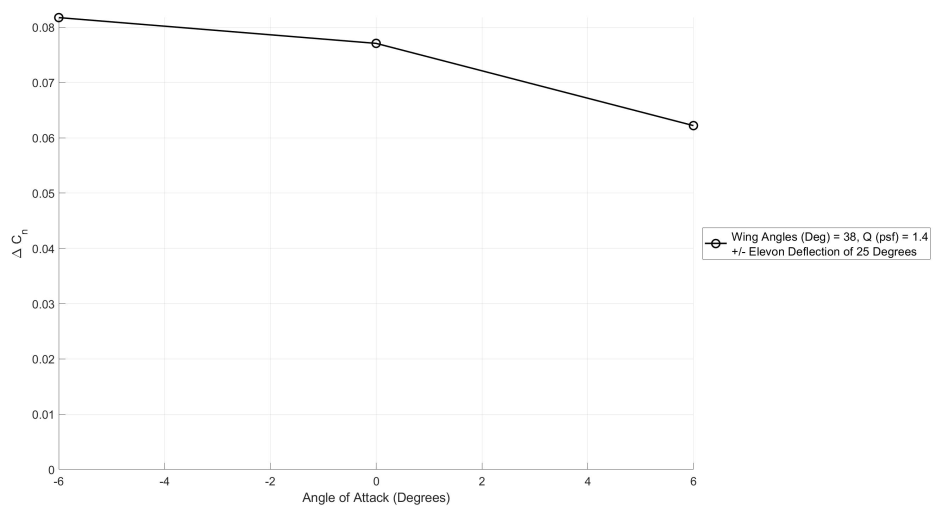

Figure 280. Wing angles 38 degrees trim point Δ C_n vs angle of attack for elevon deflection.

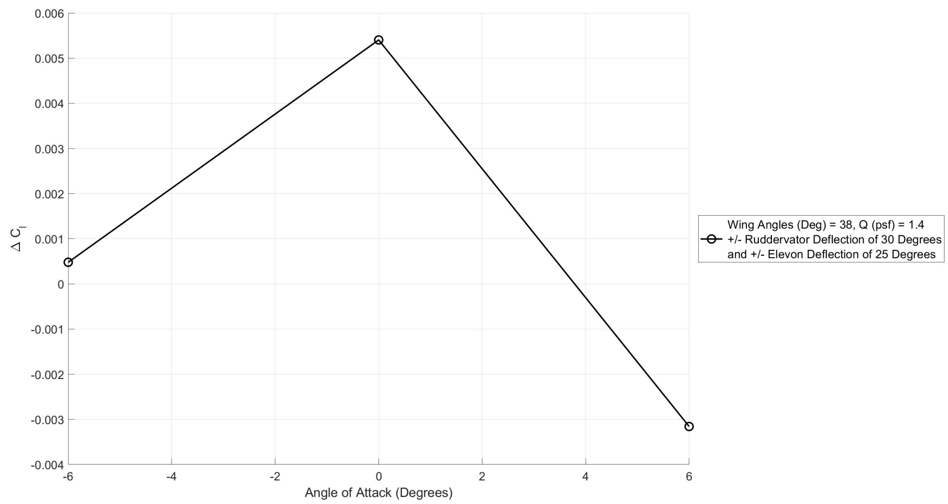

Figure 281. Wing angles 38 degrees trim point Δ C_l vs angle of attack for elevon and ruddervator deflection.

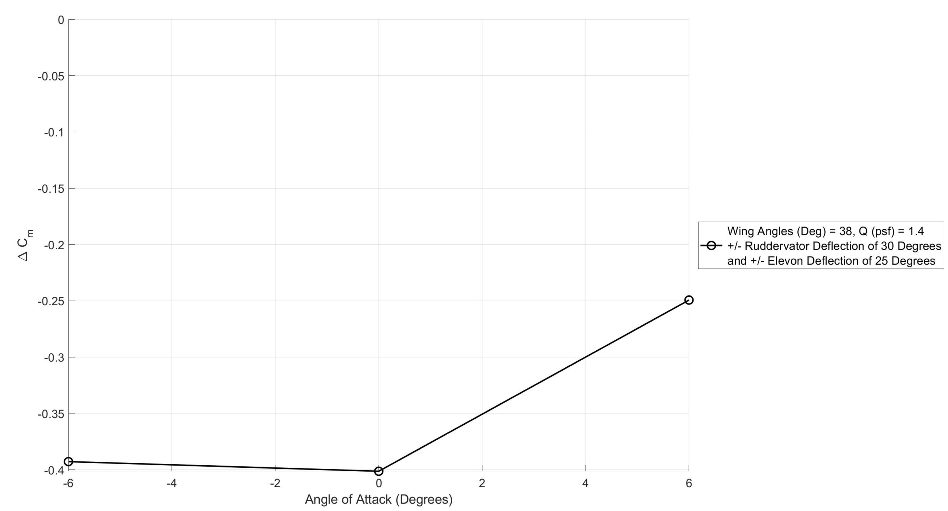

Figure 282. Wing angles 38 degrees trim point Δ C_m vs angle of attack for elevon and ruddervator deflection.

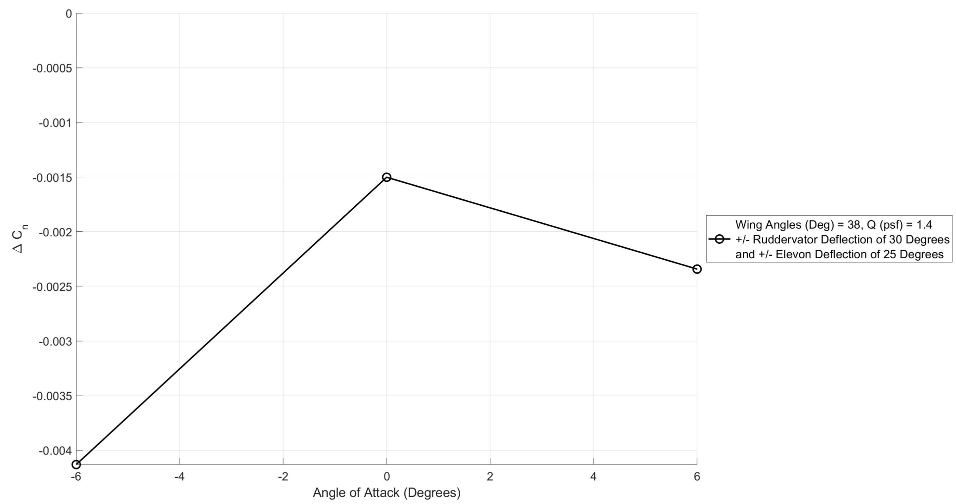

Figure 283. Wing angles 38 degrees trim point Δ C_n vs angle of attack for elevon and ruddervator deflection.

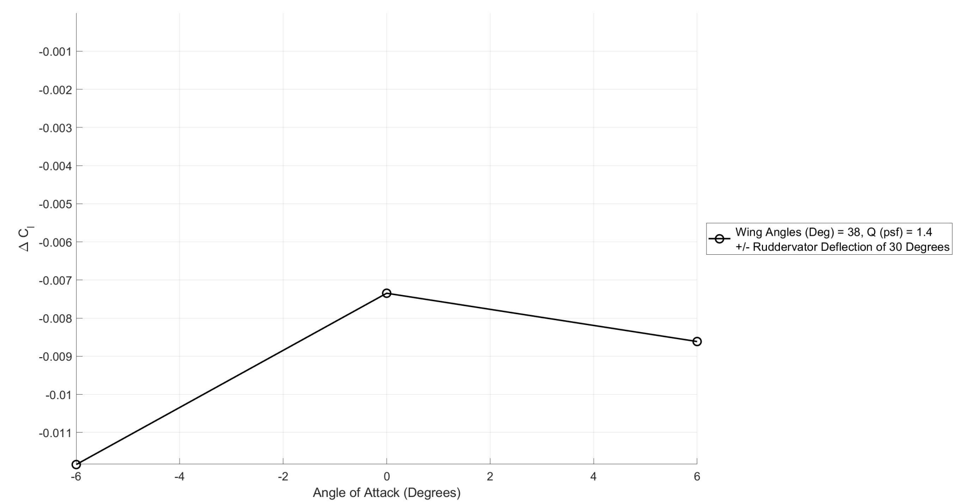

Figure 284. Wing angles 38 degrees trim point Δ C_l vs angle of attack for ruddervator deflection.

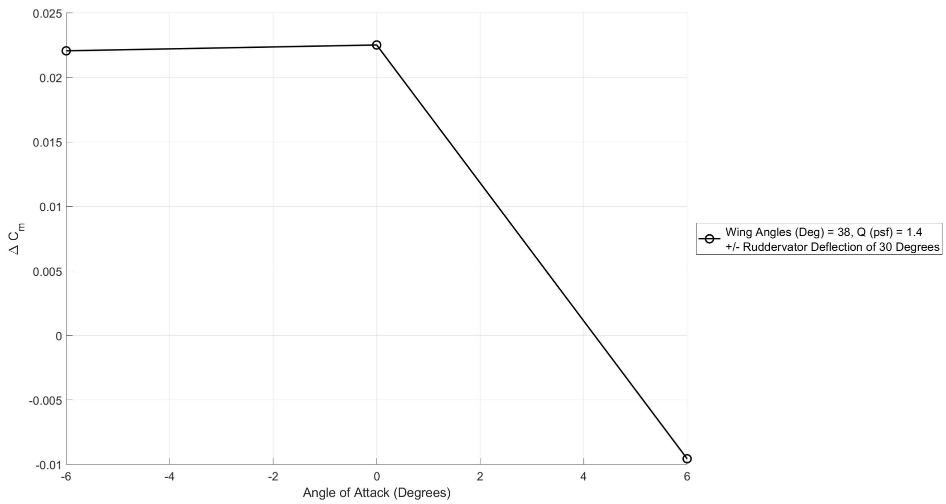

Figure 285. Wing angles 38 degrees trim point Δ C_m vs angle of attack for ruddervator deflection.

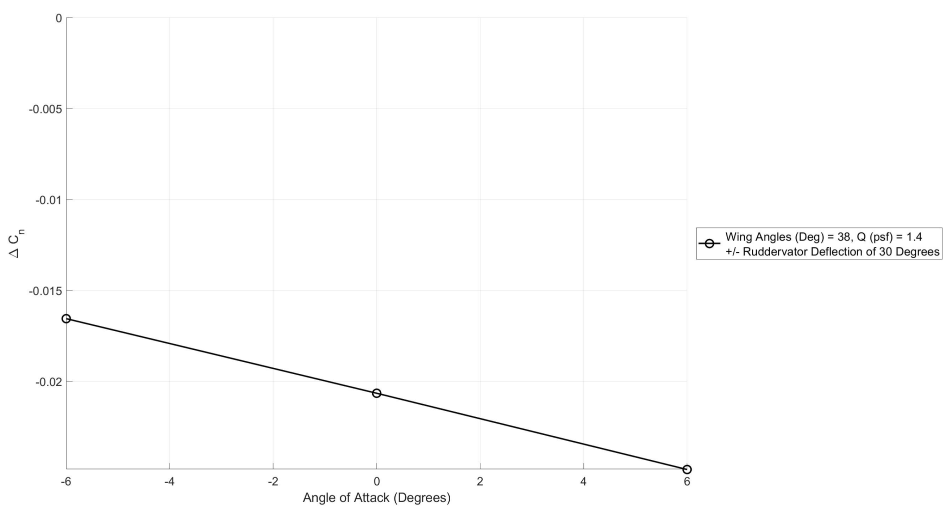

Figure 286. Wing angles 38 degrees trim point Δ C_n vs angle of attack for ruddervator deflection.

C.6 Transition Wing Angles 35 Degrees Performance and Stability Plots

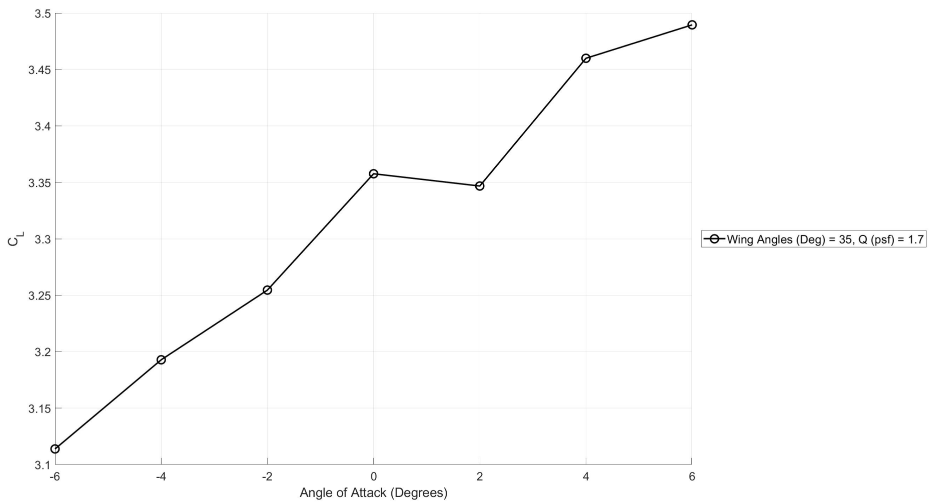

Figure 287. Wing angles 35 degrees trim point C_L vs angle of attack.

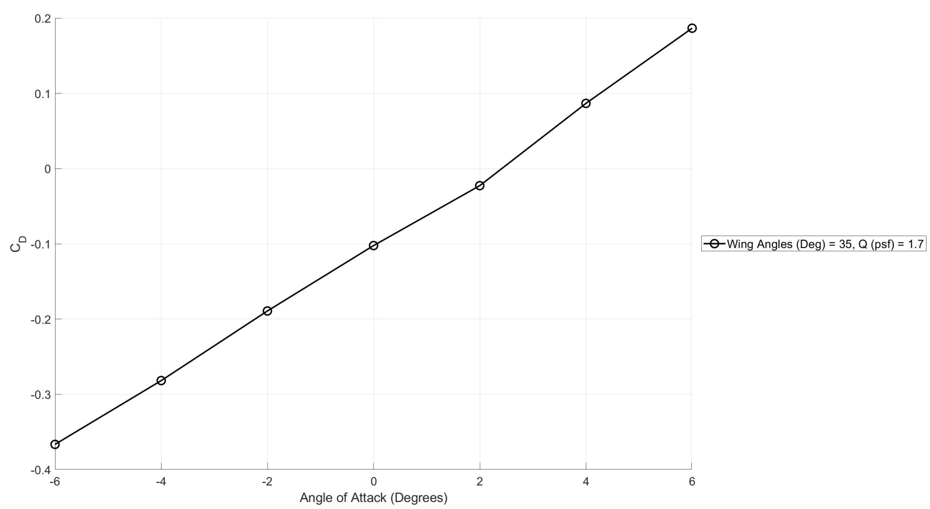

Figure 288. Wing angles 35 degrees trim point C_D vs angle of attack.

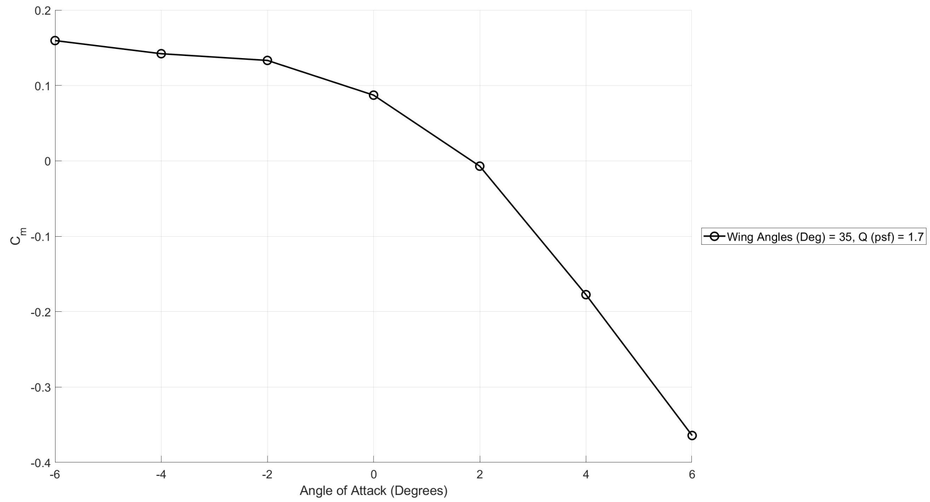

Figure 289. Wing angles 35 degrees trim point C_m vs angle of attack.

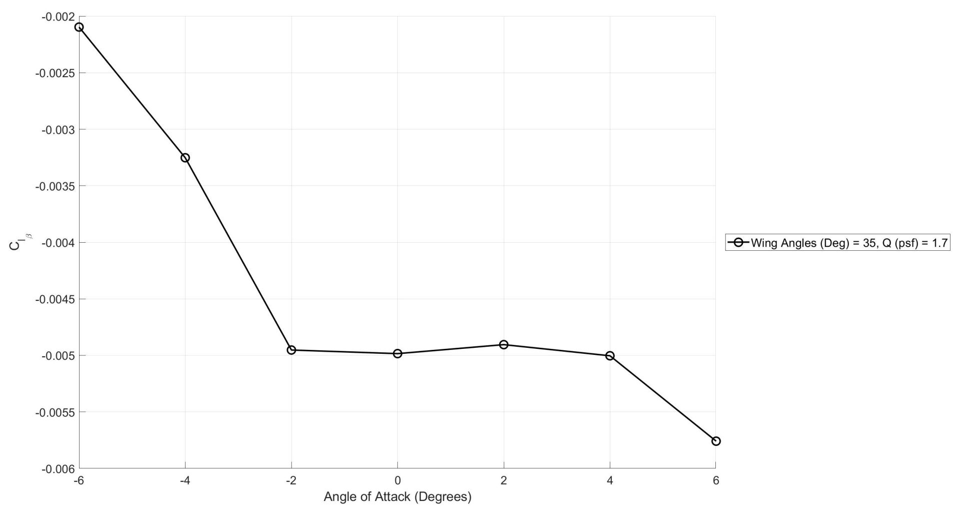

Figure 290. Wing angles 35 degrees trim point C_{l_β} vs angle of attack.

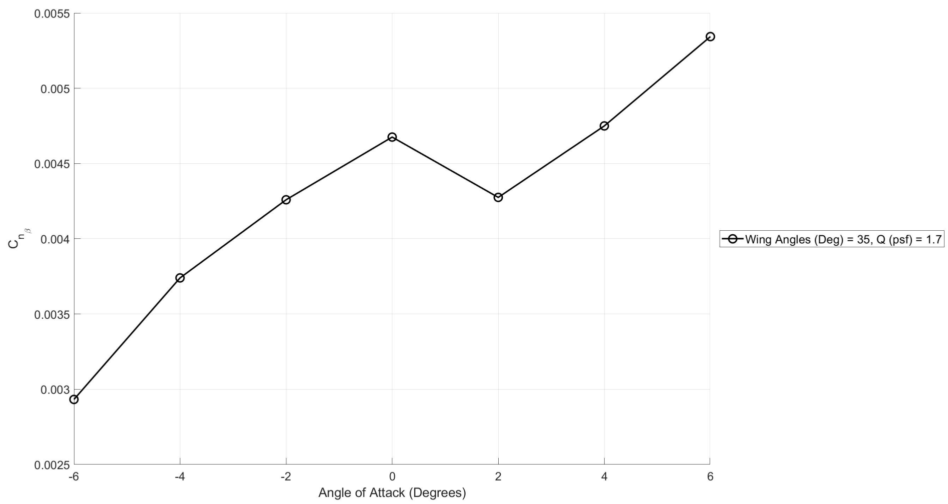

Figure 291. Wing angles 35 degrees trim point C_{n_β} vs angle of attack.

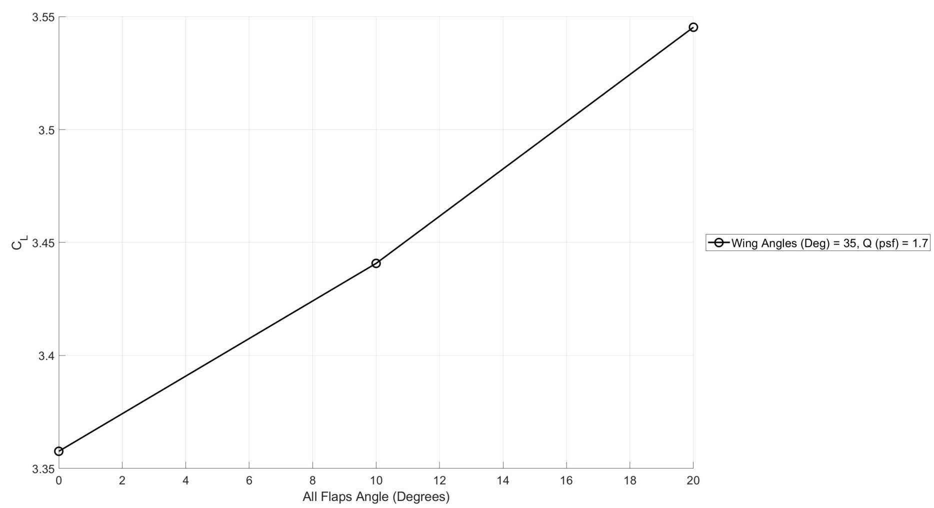

Figure 292. Wing angles 35 degrees trim point C_L vs all flap deflection angle.

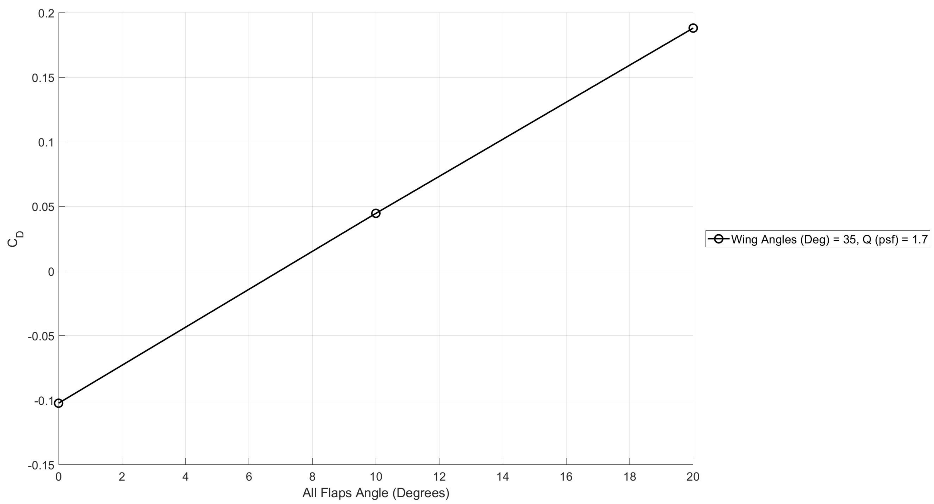

Figure 293. Wing angles 35 degrees trim point C_D vs all flap deflection angle.

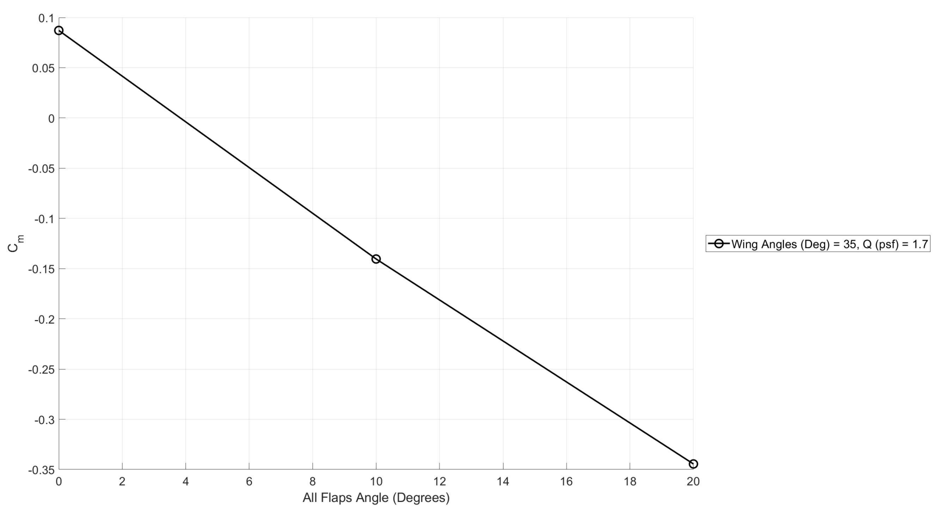

Figure 294. Wing angles 35 degrees trim point C_m vs all flap deflection angle.

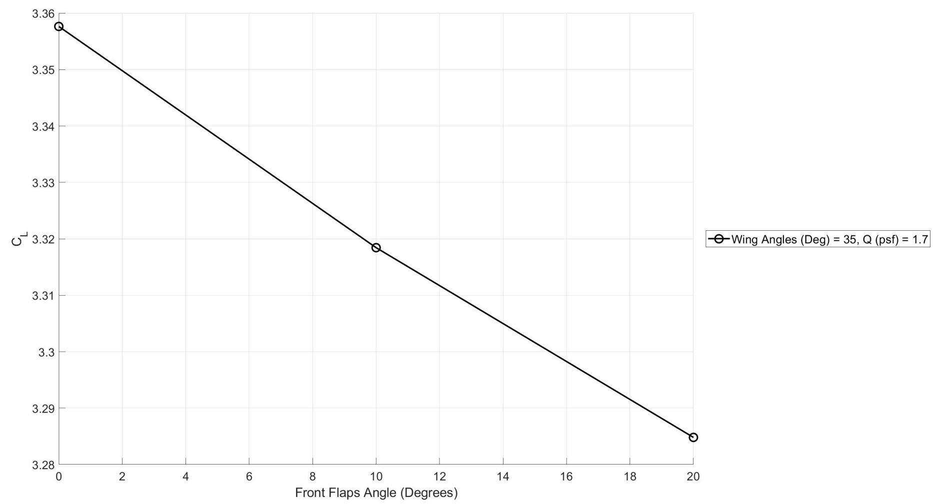

Figure 295. Wing angles 35 degrees trim point C_L vs front flap deflection angle.

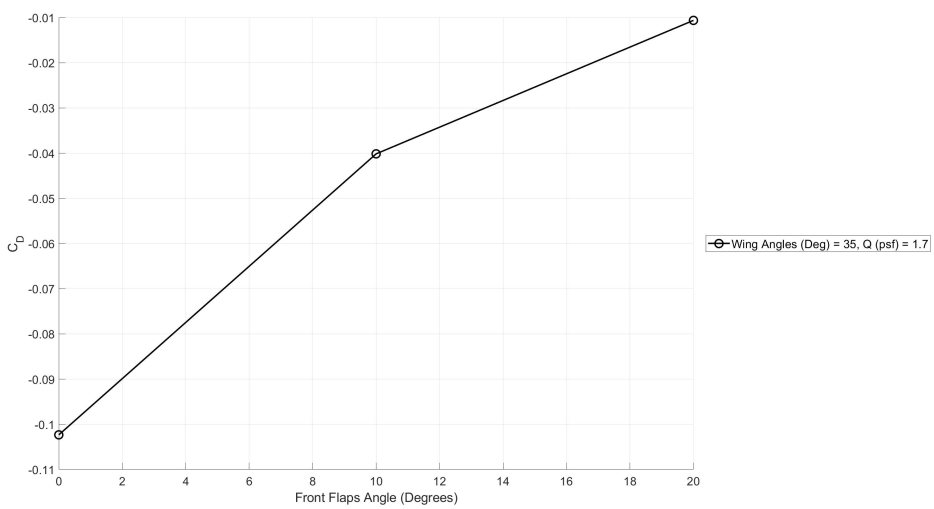

Figure 296. Wing angles 35 degrees trim point C_D vs front flap deflection angle.

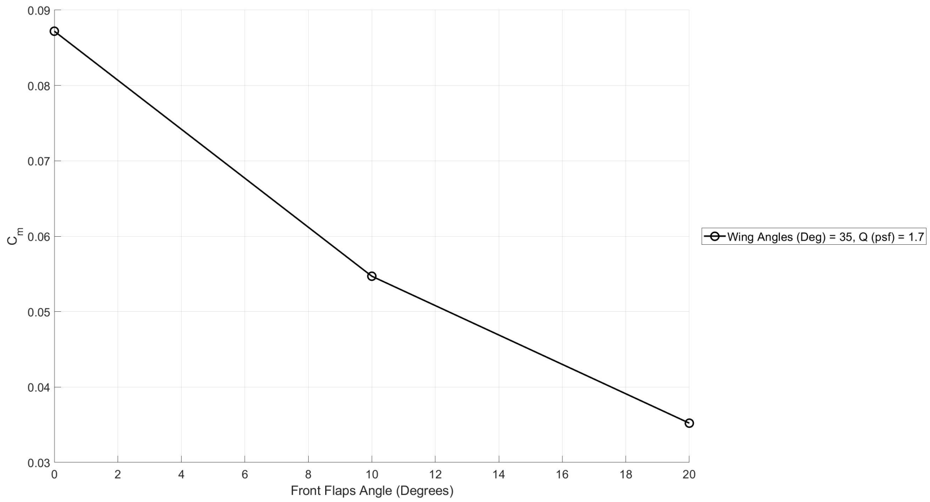

Figure 297. Wing angles 35 degrees trim point C_m vs front flap deflection angle.

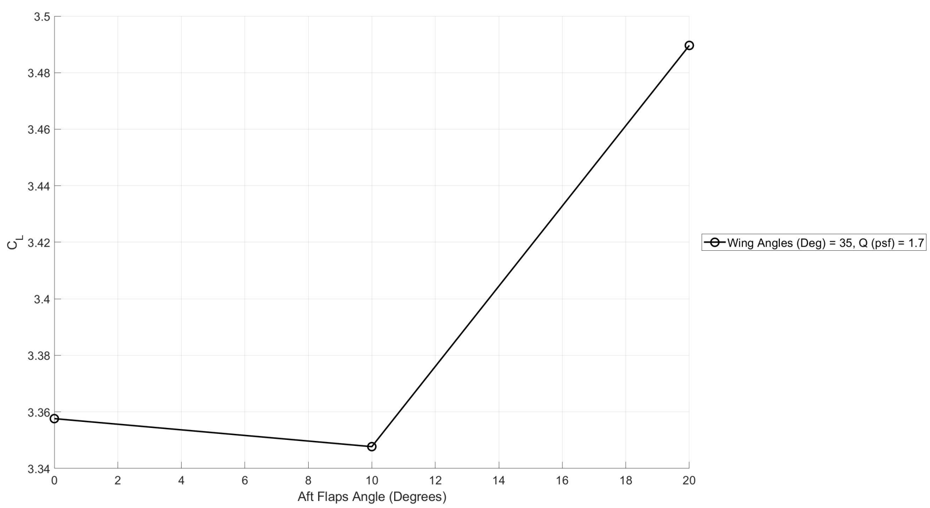

Figure 298. Wing angles 35 degrees trim point C_L vs aft flap deflection angle.

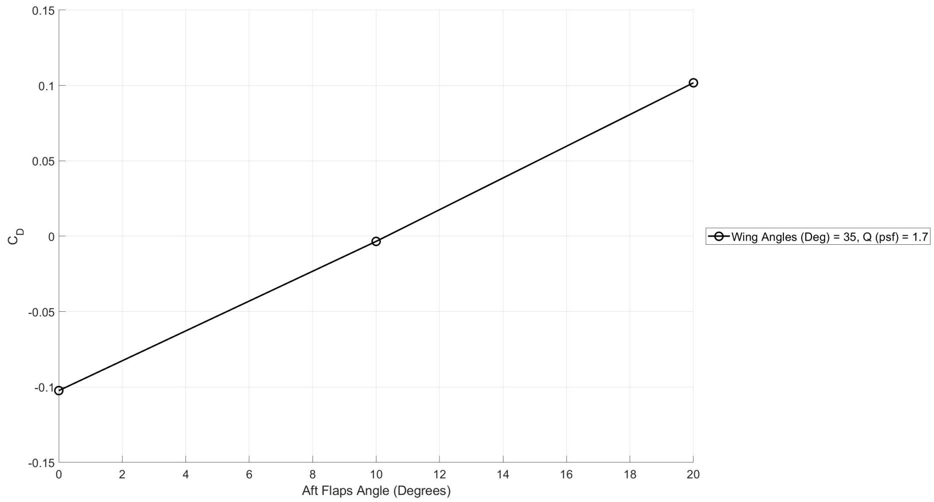

Figure 299. Wing angles 35 degrees trim point C_D vs aft flap deflection angle.

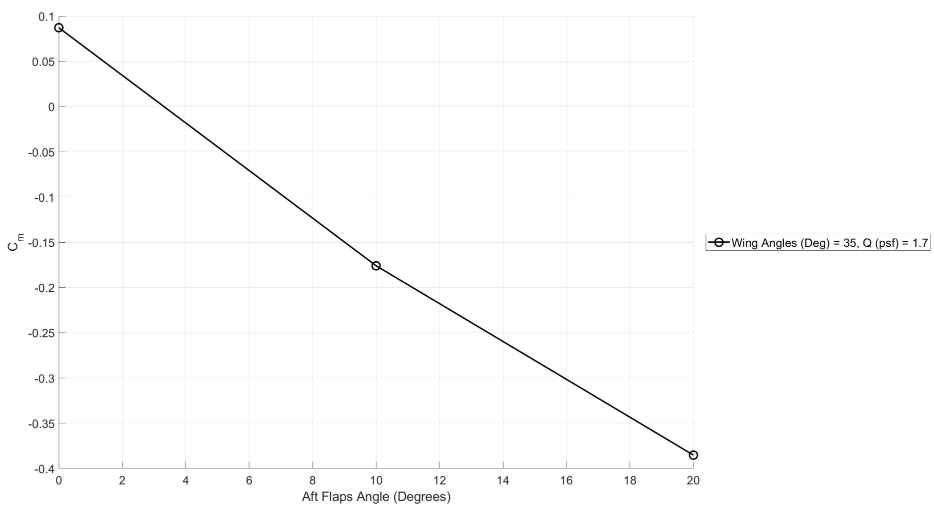

Figure 300. Wing angles 35 degrees trim point C_m vs aft flap deflection angle.

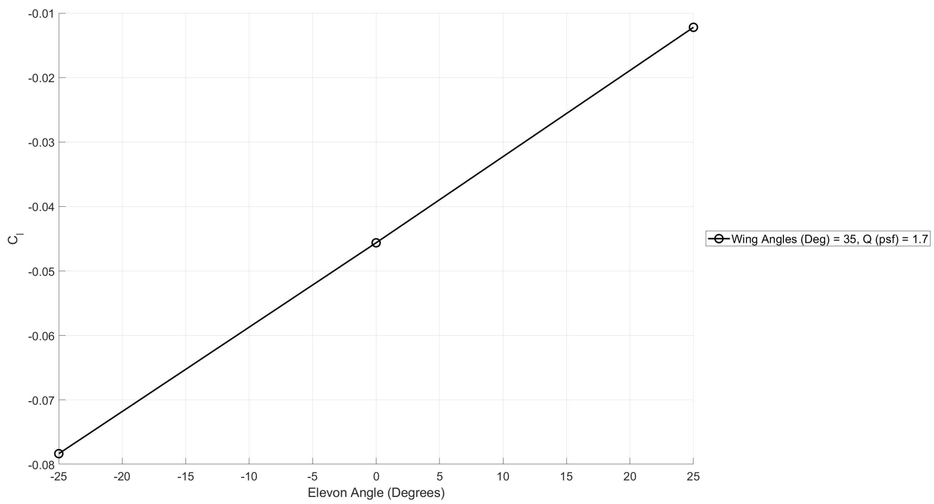

Figure 301. Wing angles 35 degrees trim point C_l vs elevon deflection angle.

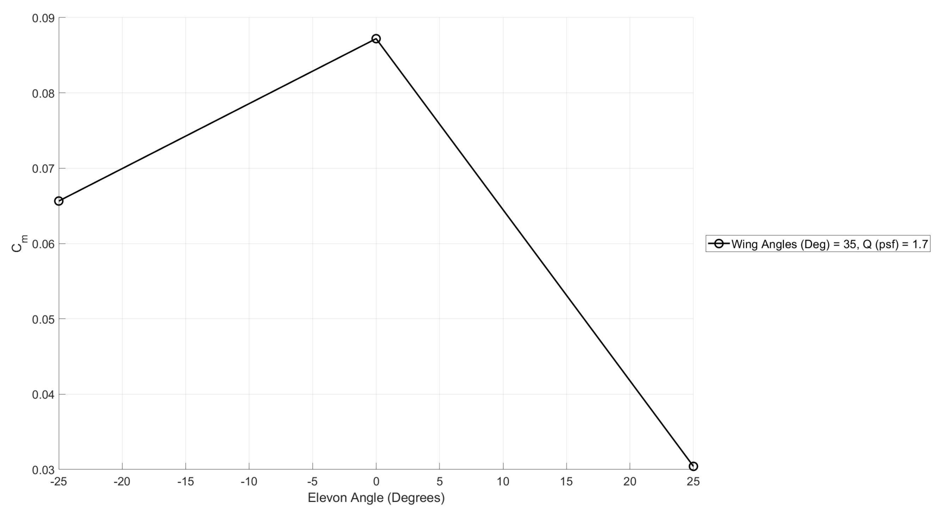

Figure 302. Wing angles 35 degrees trim point C_m vs elevon deflection angle.

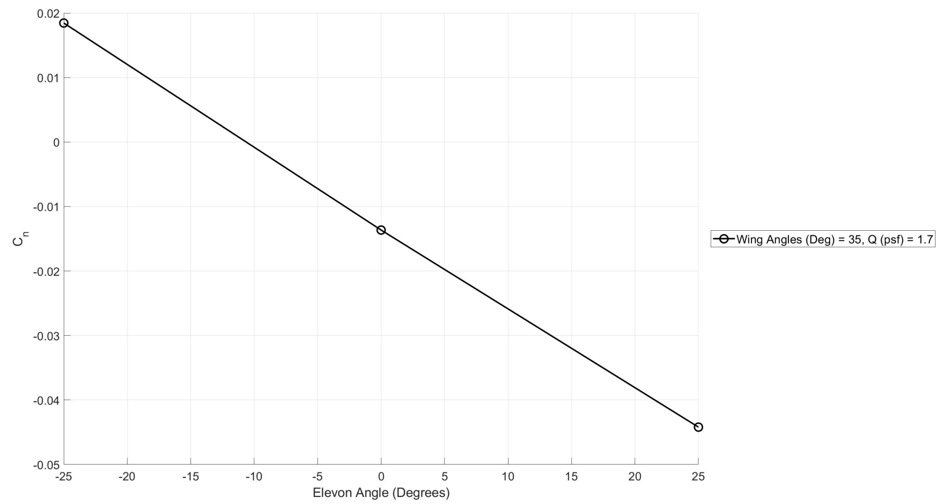

Figure 303. Wing angles 35 degrees trim point C_n vs elevon deflection angle.

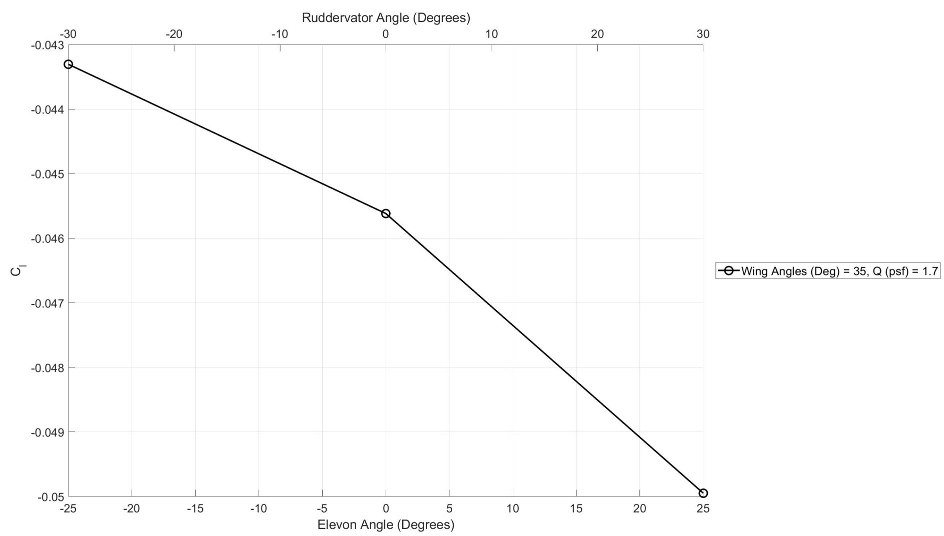

Figure 304. Wing angles 35 degrees trim point C_l vs elevon and ruddervator deflection angles.

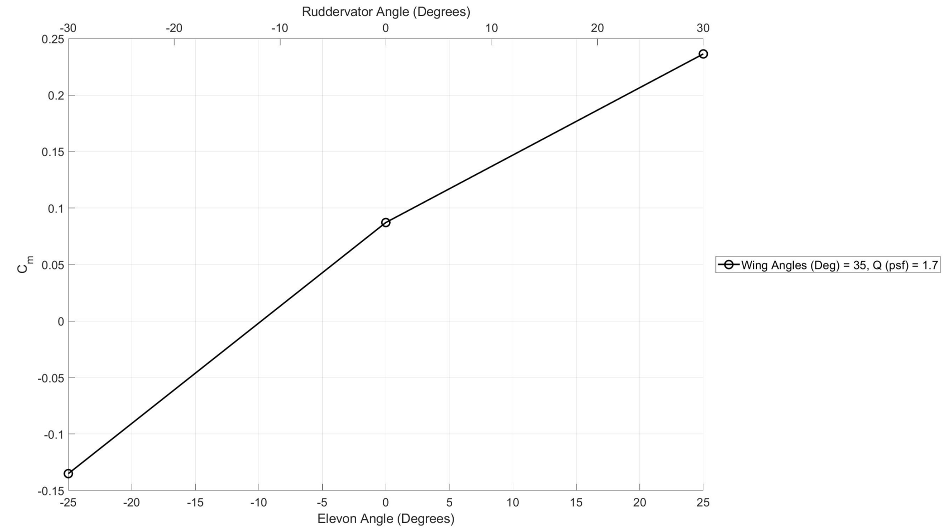

Figure 305. Wing angles 35 degrees trim point C_m vs elevon and ruddervator deflection angles.

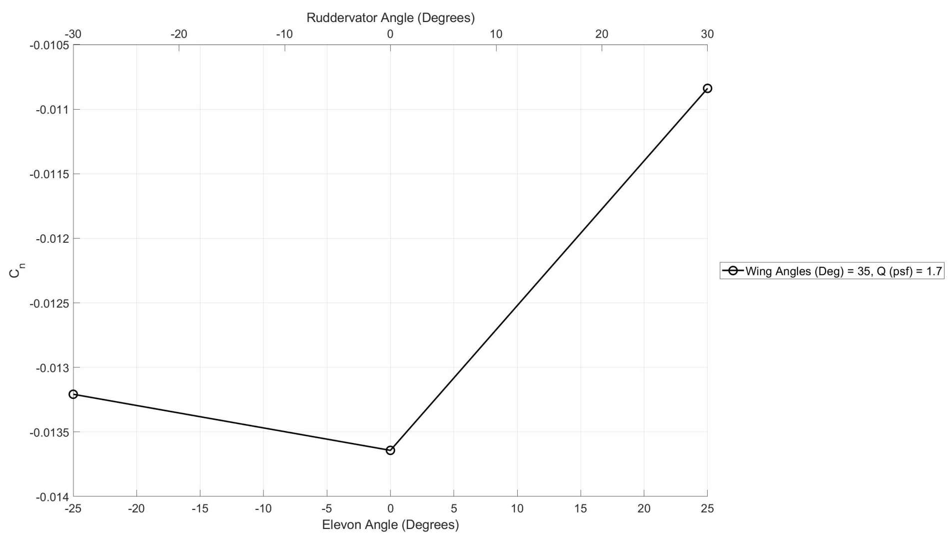

Figure 306. Wing angles 35 degrees trim point C_n vs elevon and ruddervator deflection angles.

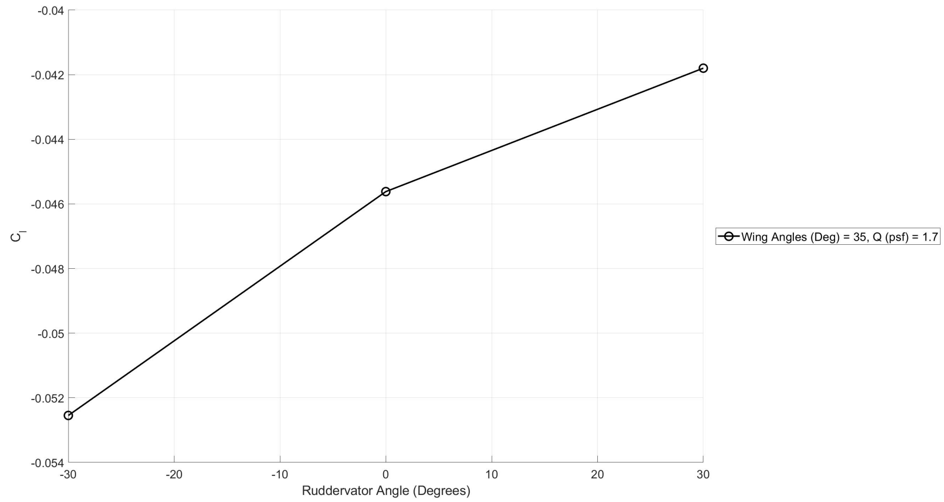

Figure 307. Wing angles 35 degrees trim point C_l vs ruddervator deflection angle.

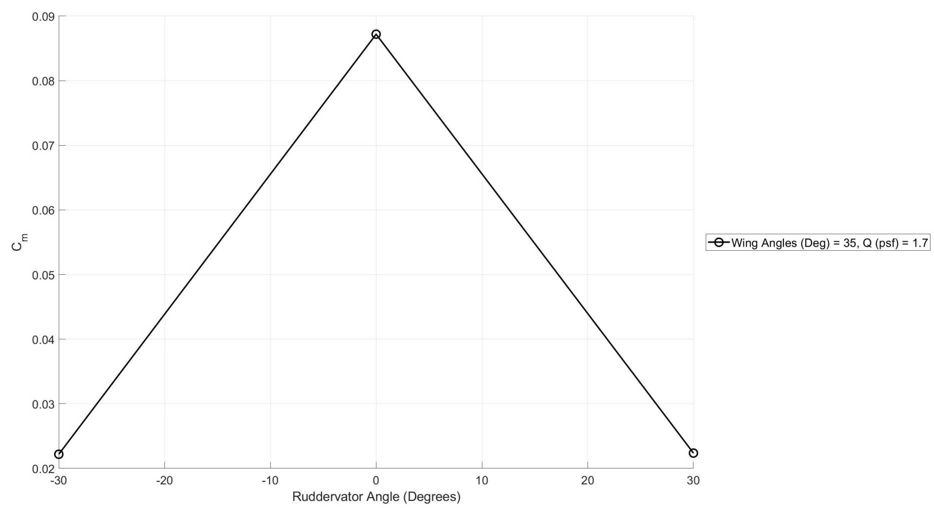

Figure 308. Wing angles 35 degrees trim point C_m vs ruddervator deflection angle.

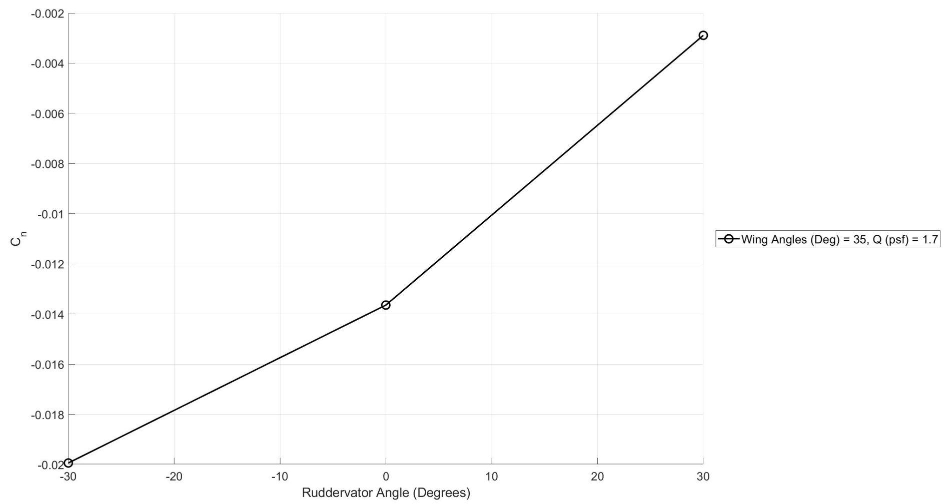

Figure 309. Wing angles 35 degrees trim point C_n vs ruddervator deflection angle.

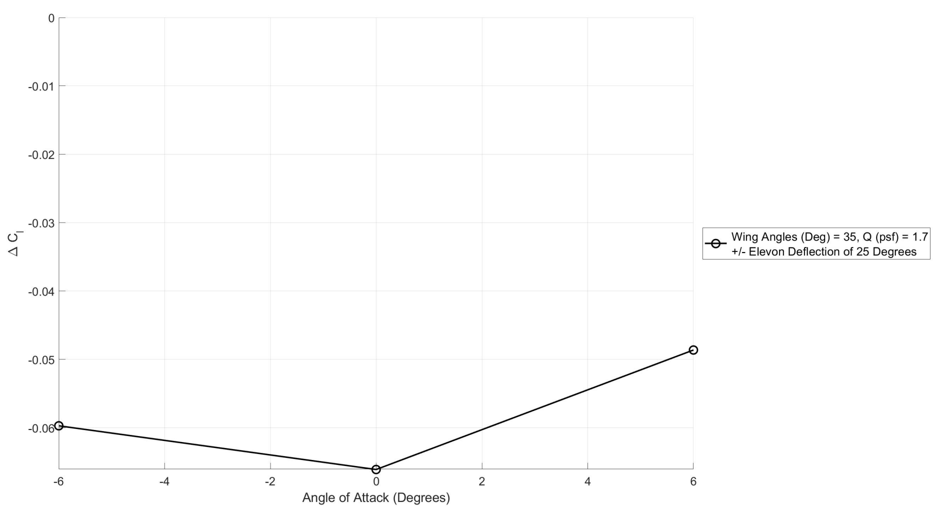

Figure 310. Wing angles 35 degrees trim point Δ C_l vs angle of attack for elevon deflection.

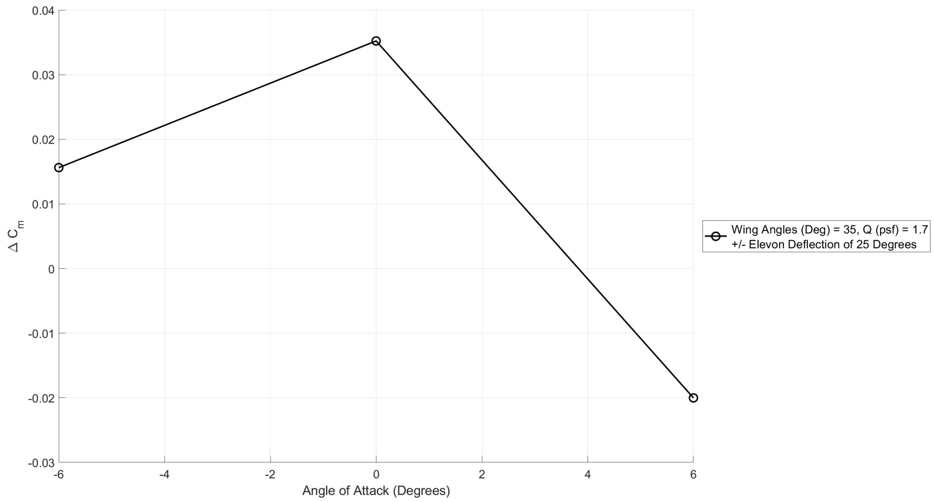

Figure 311. Wing angles 35 degrees trim point Δ C_m vs angle of attack for elevon deflection.

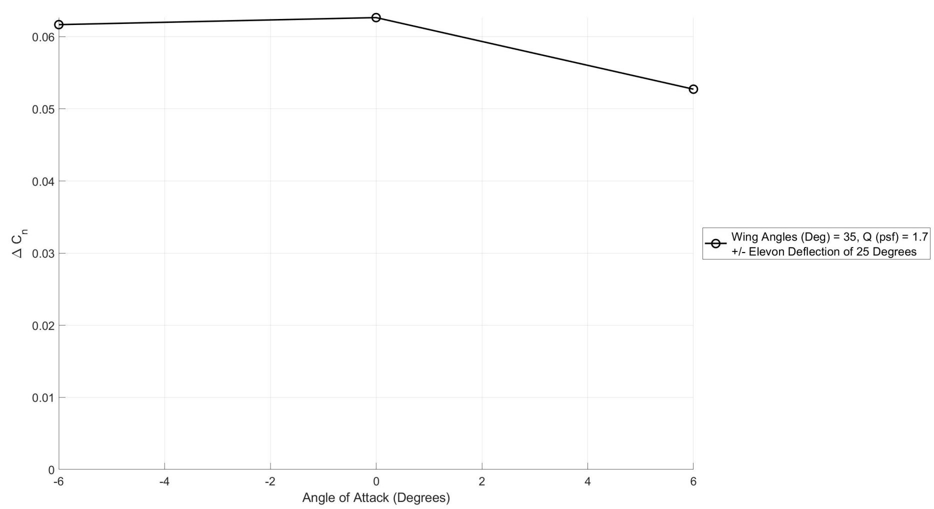

Figure 312. Wing angles 35 degrees trim point Δ C_n vs angle of attack for elevon deflection.

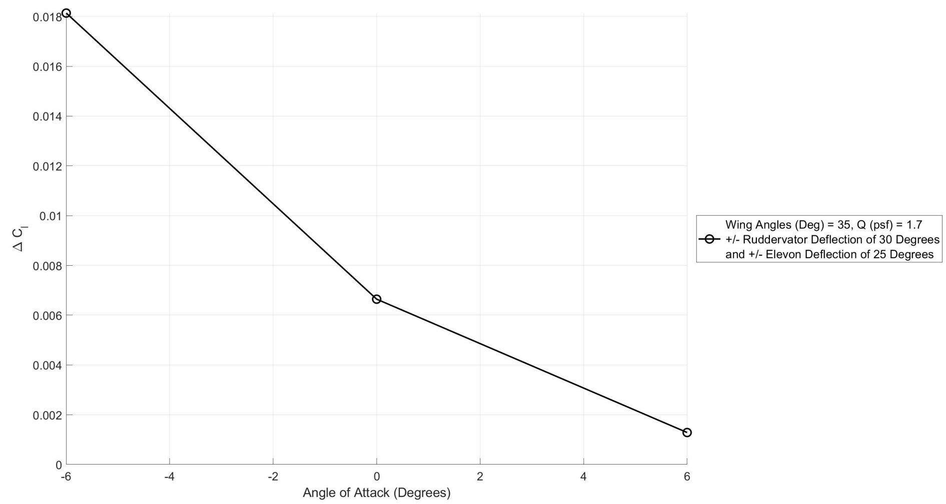

Figure 313. Wing angles 35 degrees trim point Δ C_l vs angle of attack for elevon and ruddervator deflection.

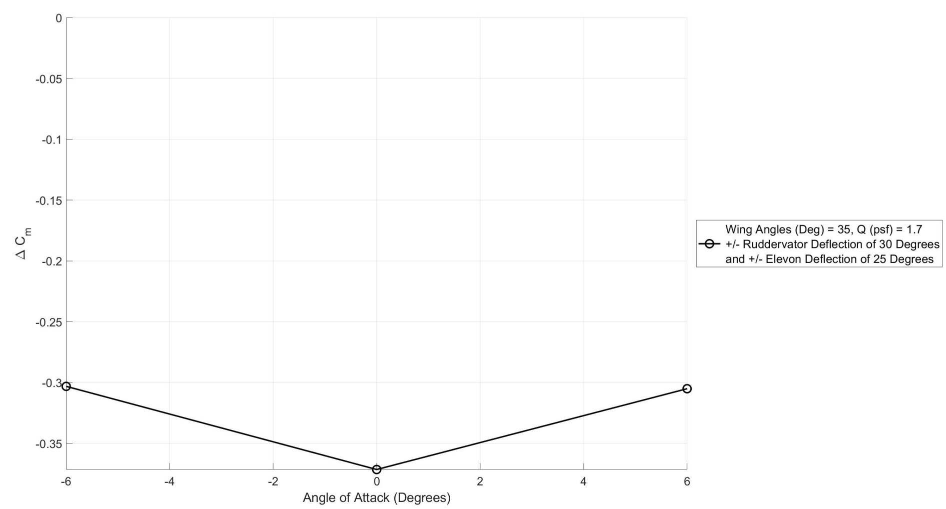

Figure 314. Wing angles 35 degrees trim point Δ C_m vs angle of attack for elevon and ruddervator deflection.

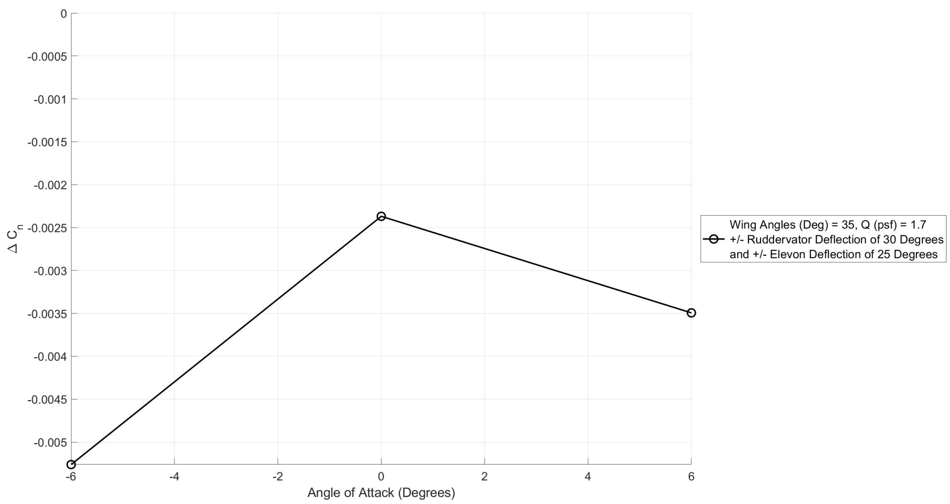

Figure 315. Wing angles 35 degrees trim point Δ C_n vs angle of attack for elevon and ruddervator deflection.

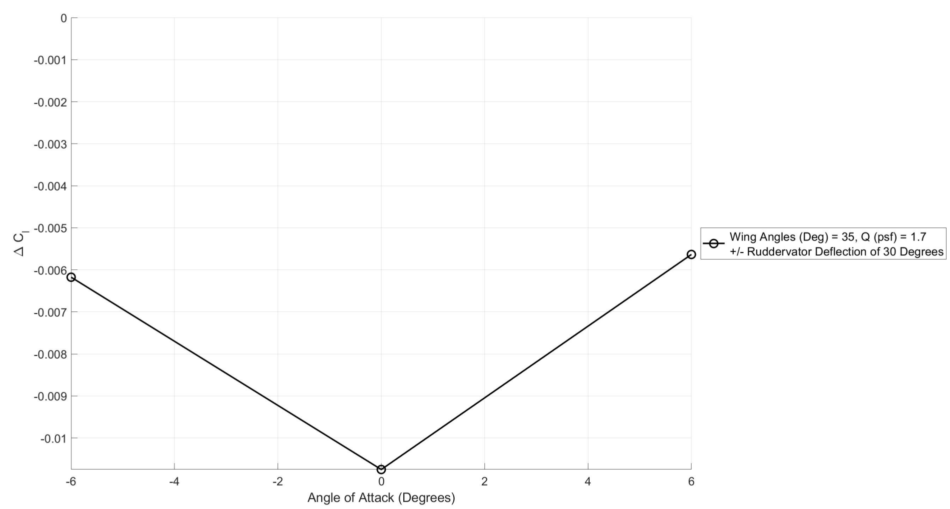

Figure 316. Wing angles 35 degrees trim point Δ C_l vs angle of attack for ruddervator deflection.

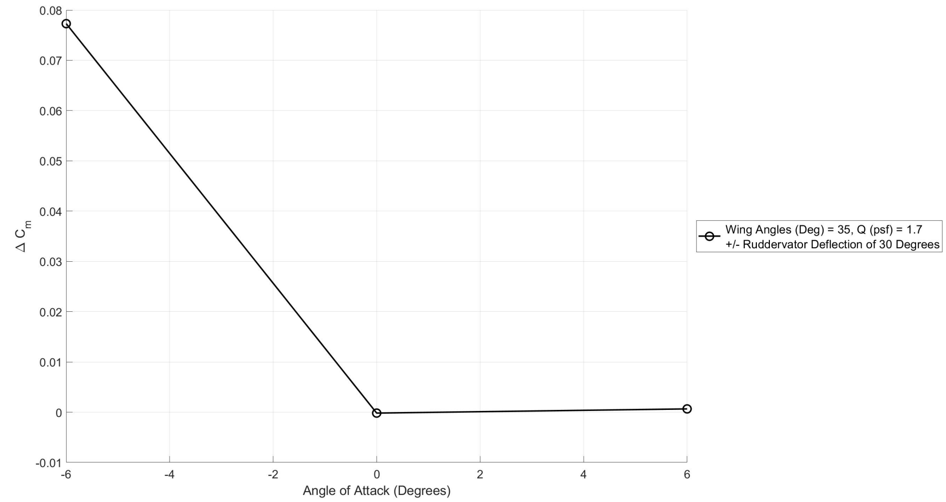

Figure 317. Wing angles 35 degrees trim point Δ C$_m$ vs angle of attack for ruddervator deflection.

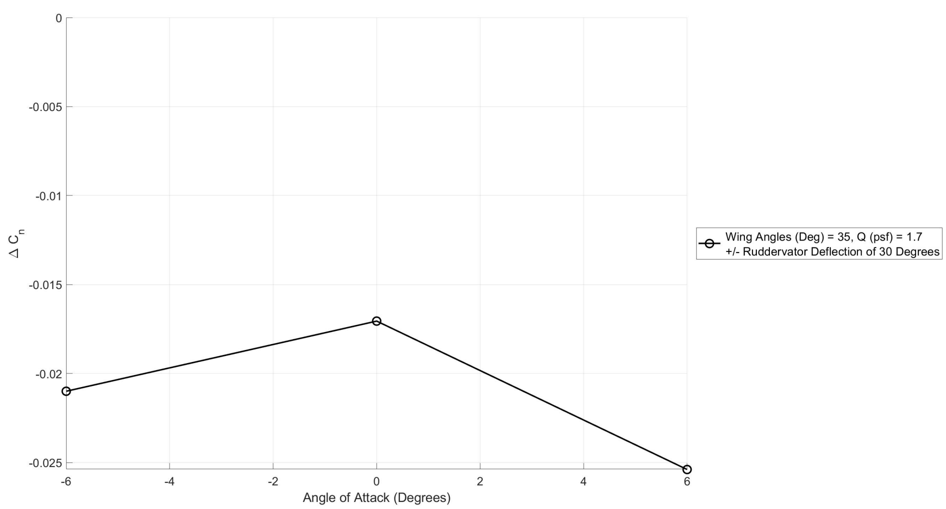

Figure 318. Wing angles 35 degrees trim point Δ C$_n$ vs angle of attack for ruddervator deflection.

C.7 Transition Wing Angles 32 Degrees Performance and Stability Plots

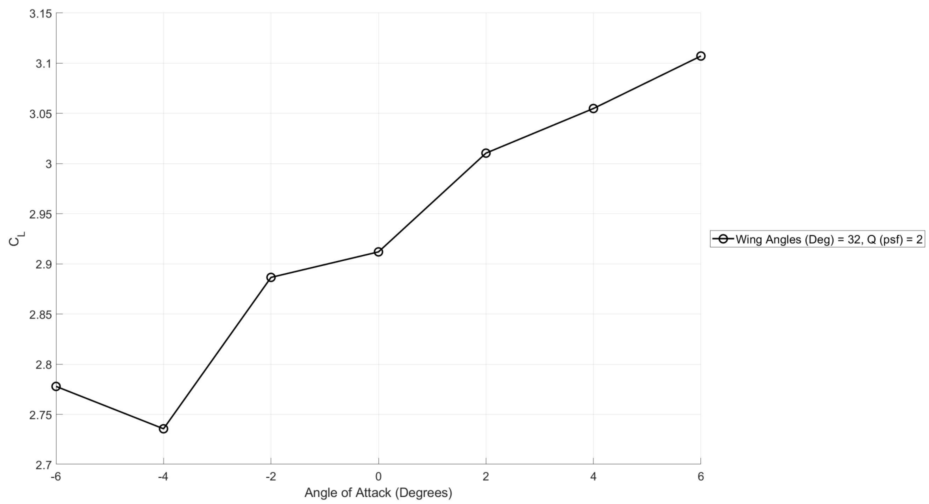

Figure 319. Wing angles 32 degrees trim point C_L vs angle of attack.

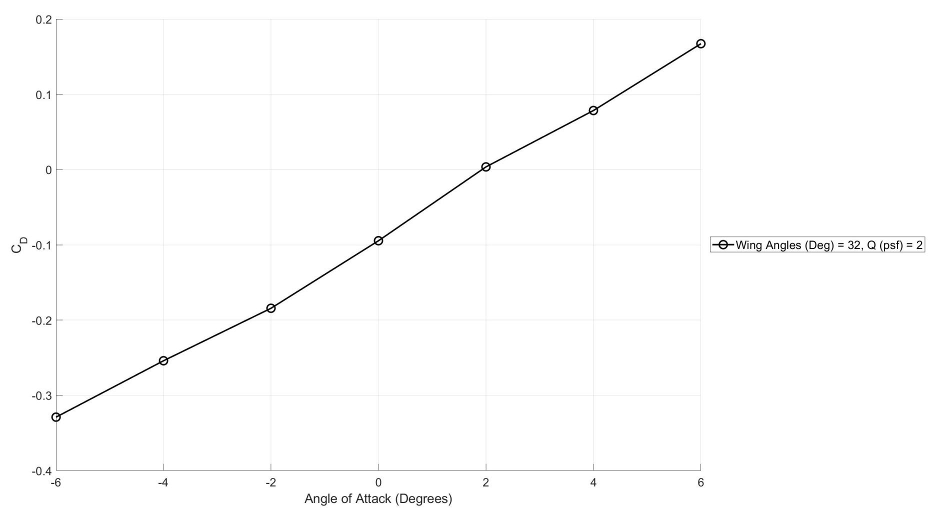

Figure 320. Wing angles 32 degrees trim point C_D vs angle of attack.

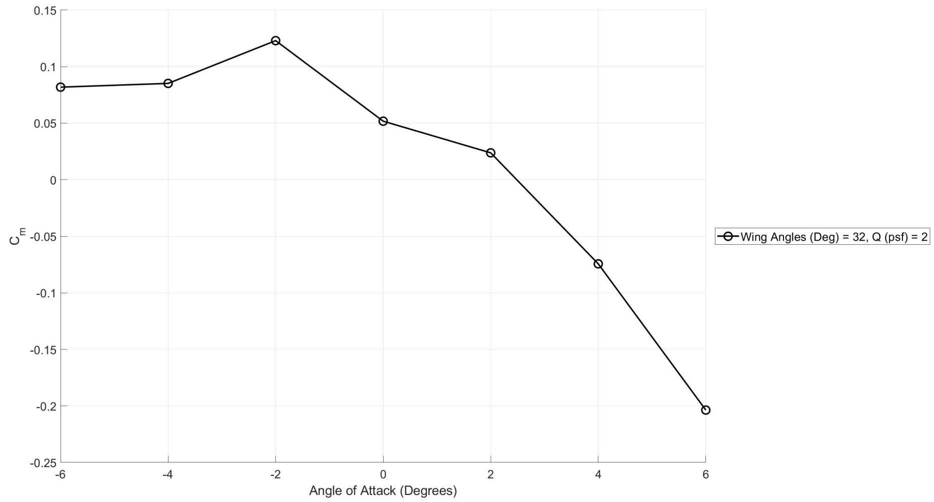

Figure 321. Wing angles 32 degrees trim point C_m vs angle of attack.

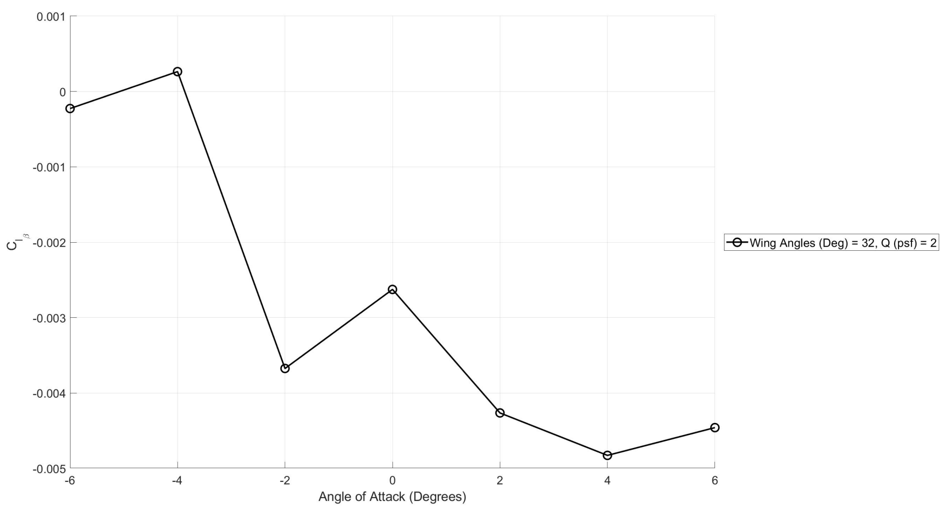

Figure 322. Wing angles 32 degrees trim point C_{l_β} vs angle of attack.

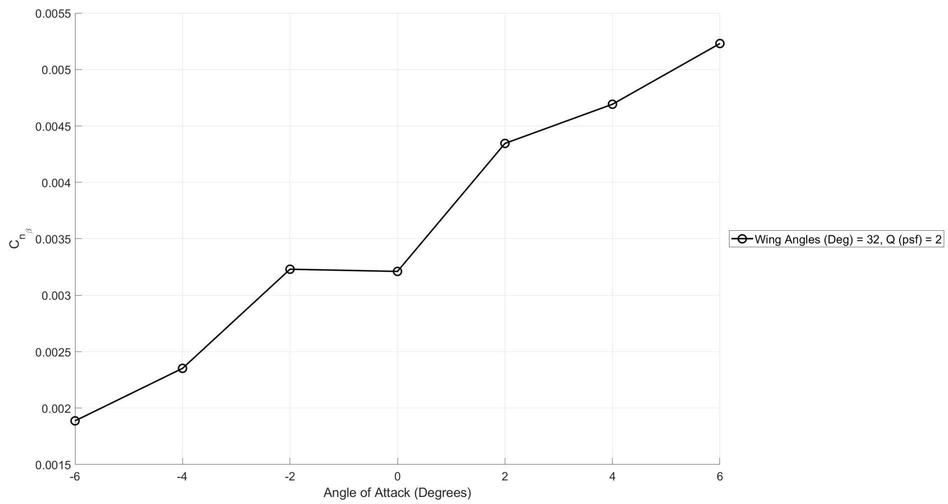

Figure 323. Wing angles 32 degrees trim point C_{n_β} vs angle of attack.

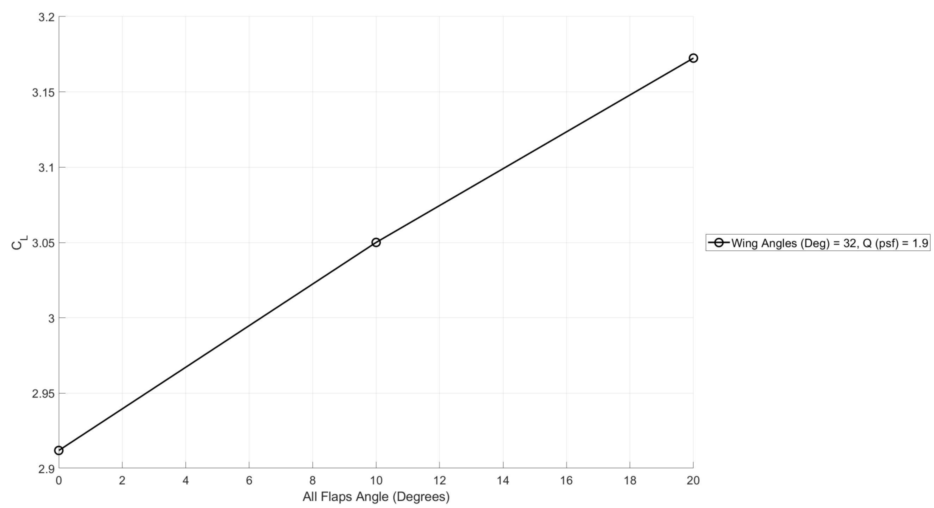

Figure 324. Wing angles 32 degrees trim point C_L vs all flap deflection angle.

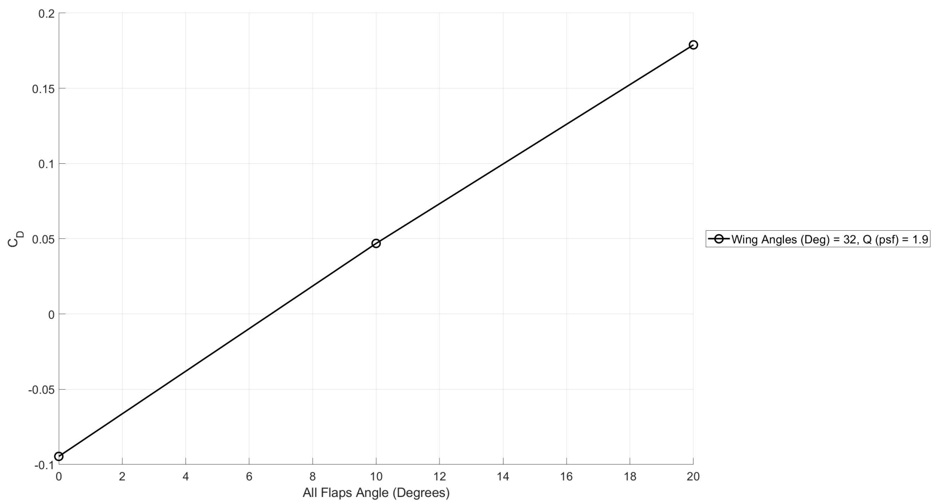

Figure 325. Wing angles 32 degrees trim point C_D vs all flap deflection angle.

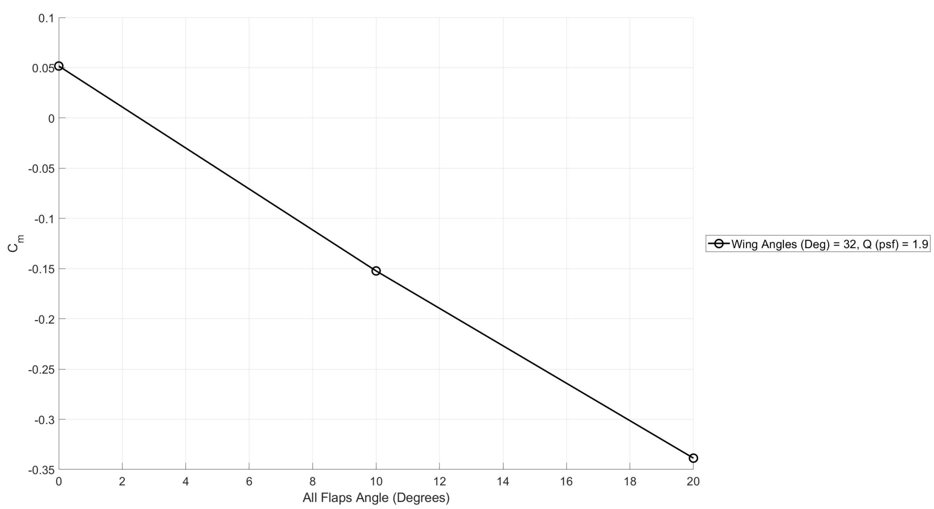

Figure 326. Wing angles 32 degrees trim point C_m vs all flap deflection angle.

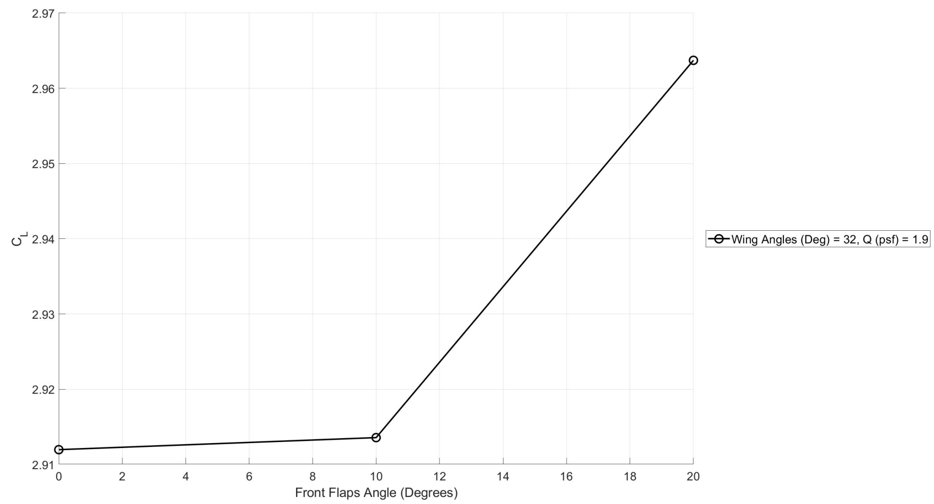

Figure 327. Wing angles 32 degrees trim point C_L vs front flap deflection angle.

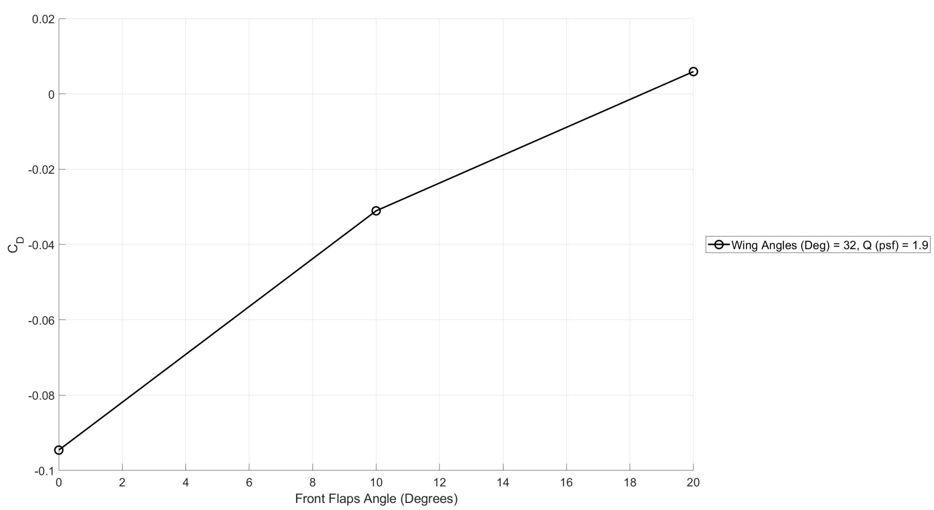

Figure 328. Wing angles 32 degrees trim point C_D vs front flap deflection angle.

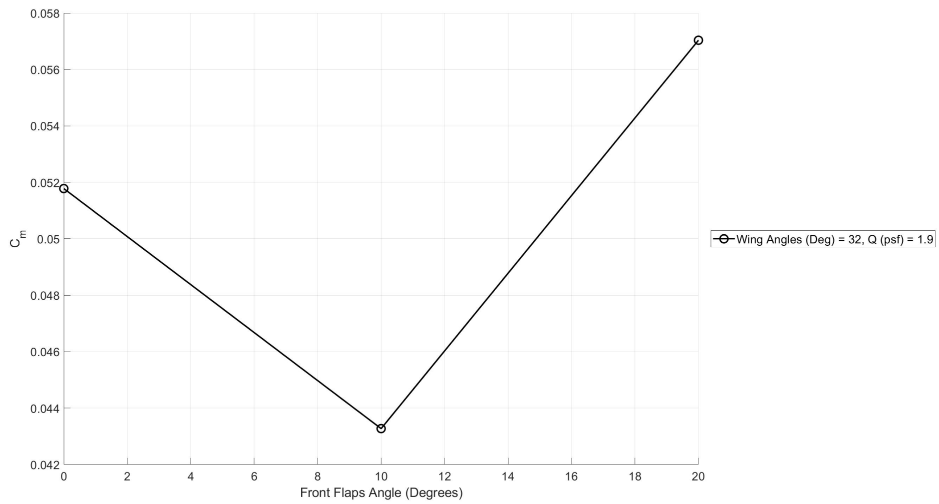

Figure 329. Wing angles 32 degrees trim point C_m vs front flap deflection angle.

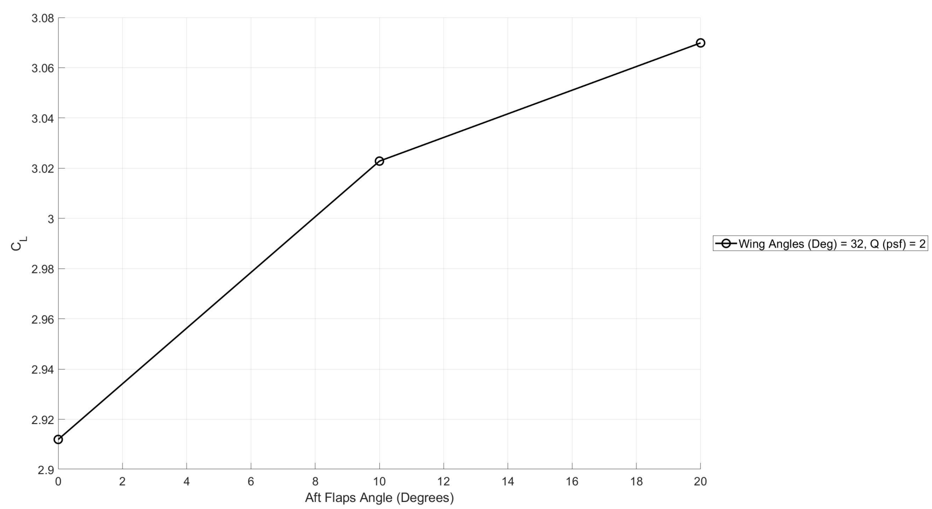

Figure 330. Wing angles 32 degrees trim point C_L vs aft flap deflection angle.

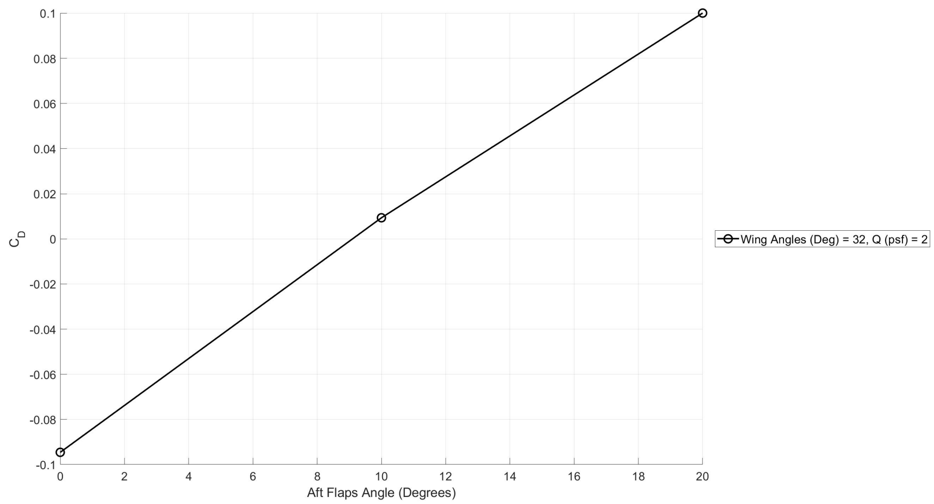

Figure 331. Wing angles 32 degrees trim point C_D vs aft flap deflection angle.

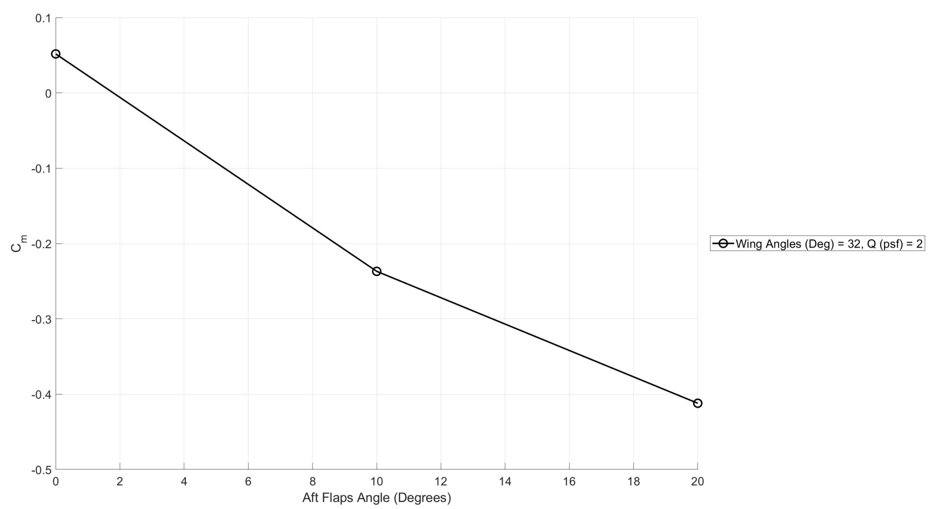

Figure 332. Wing angles 32 degrees trim point C_m vs aft flap deflection angle.

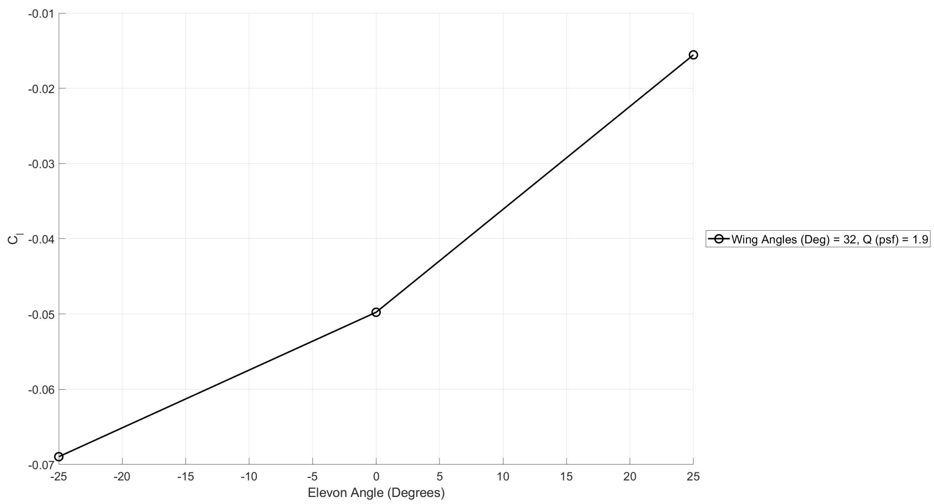

Figure 333. Wing angles 32 degrees trim point C_l vs elevon deflection angle.

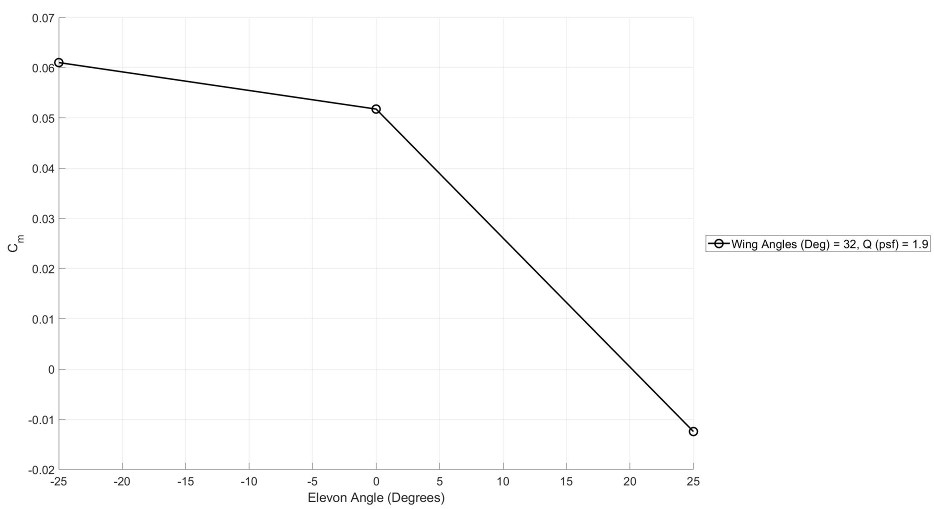

Figure 334. Wing angles 32 degrees trim point C_m vs elevon deflection angle.

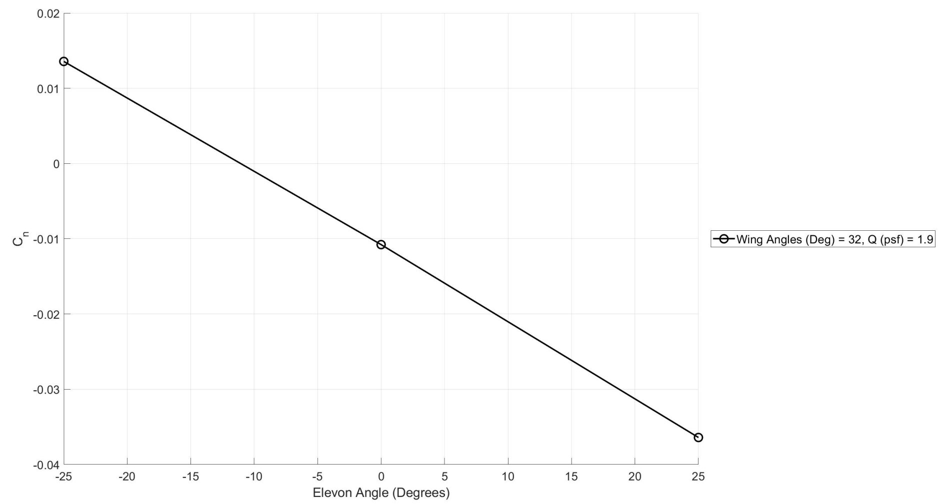

Figure 335. Wing angles 32 degrees trim point C_n vs elevon deflection angle.

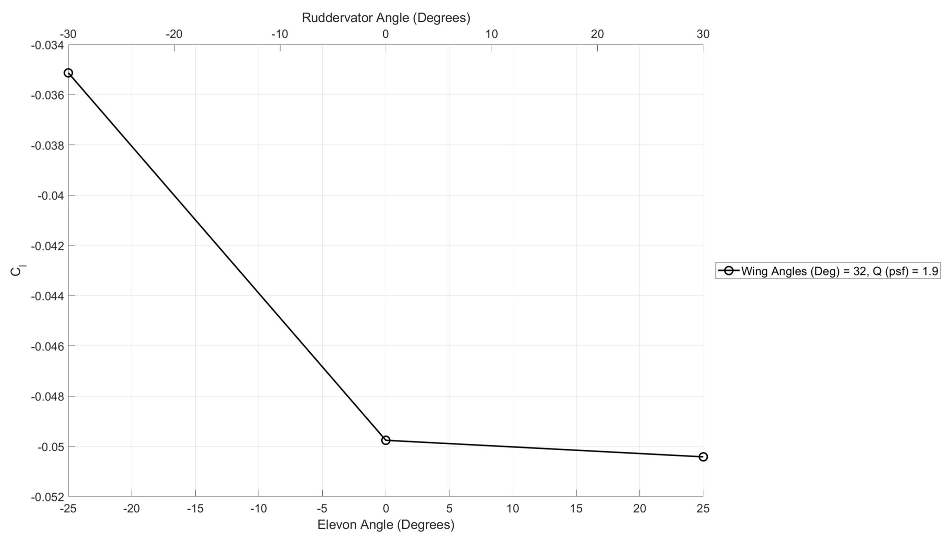

Figure 336. Wing angles 32 degrees trim point C_l vs elevon and ruddervator deflection angles.

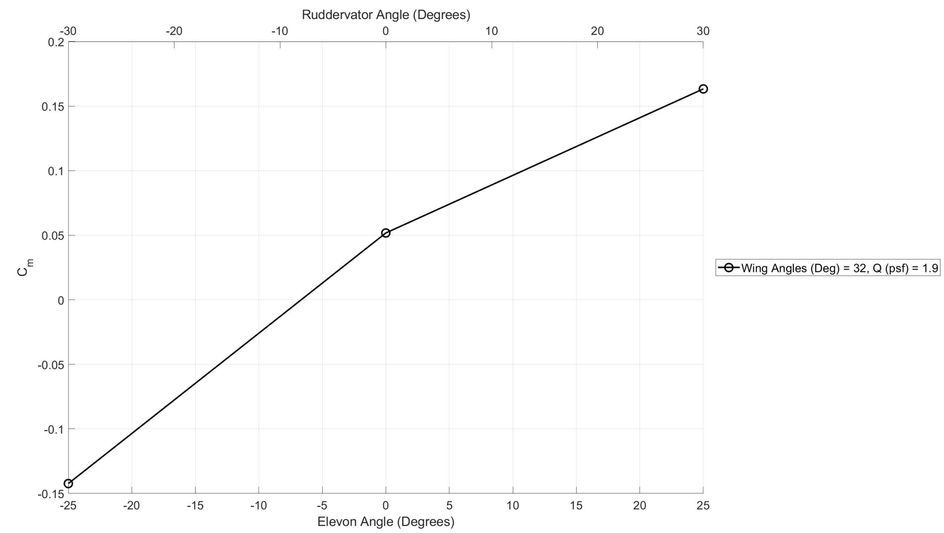

Figure 337. Wing angles 32 degrees trim point C_m vs elevon and ruddervator deflection angles.

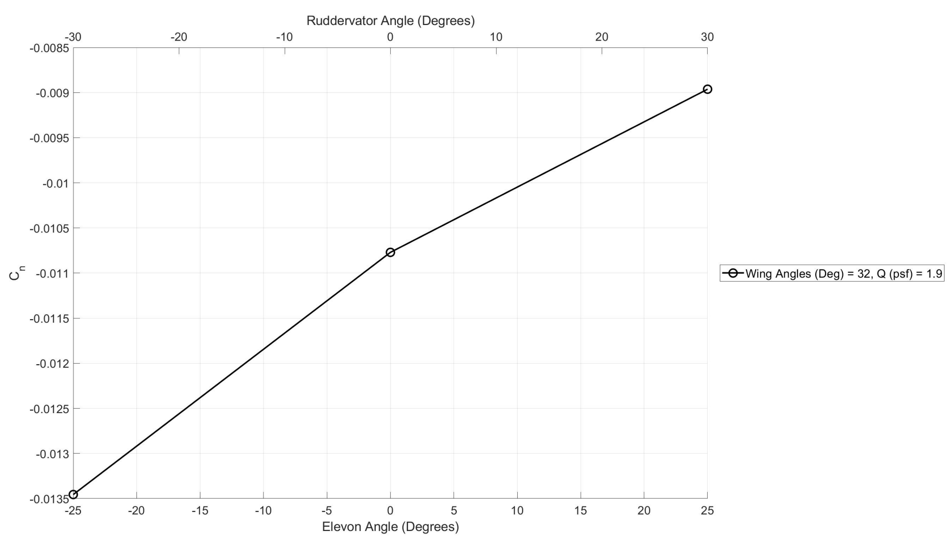

Figure 338. Wing angles 32 degrees trim point C_n vs elevon and ruddervator deflection angles.

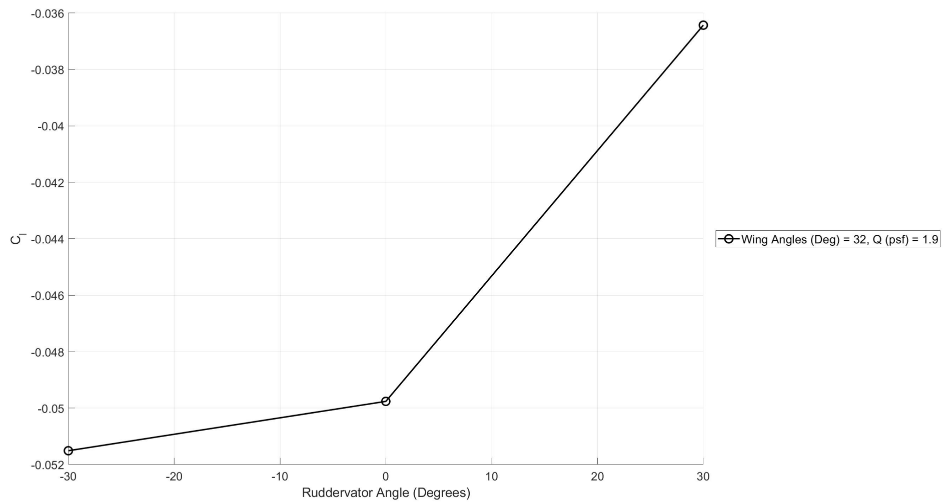

Figure 339. Wing angles 32 degrees trim point C_l vs ruddervator deflection angle.

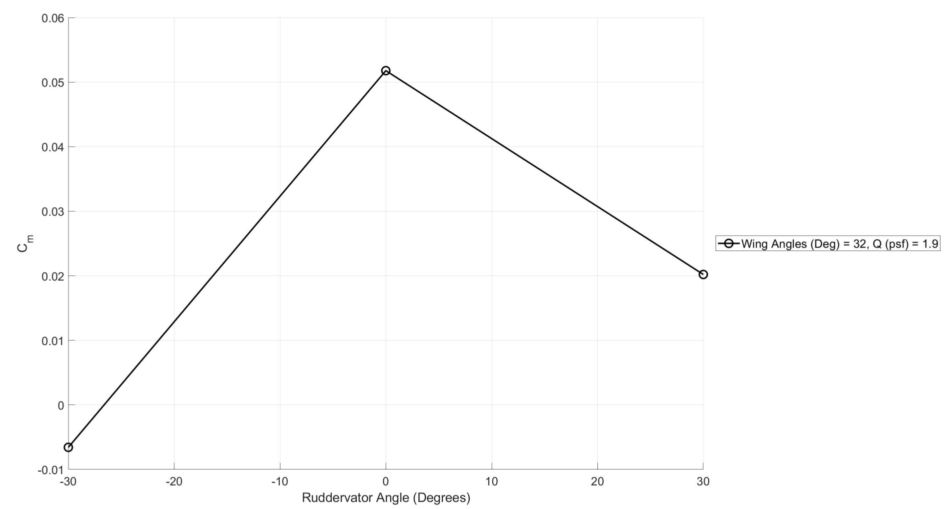

Figure 340. Wing angles 32 degrees trim point C_m vs ruddervator deflection angle.

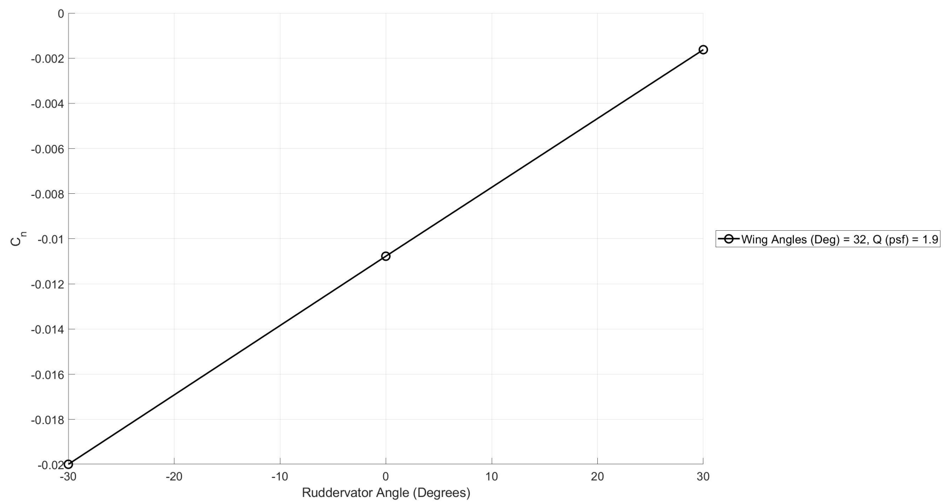

Figure 341. Wing angles 32 degrees trim point C_n vs ruddervator deflection angle.

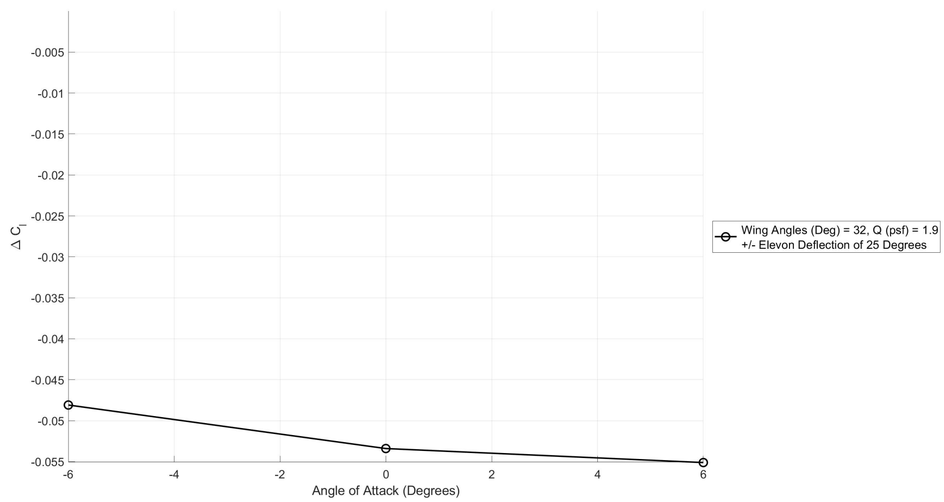

Figure 342. Wing angles 32 degrees trim point Δ C_l vs angle of attack for elevon deflection.

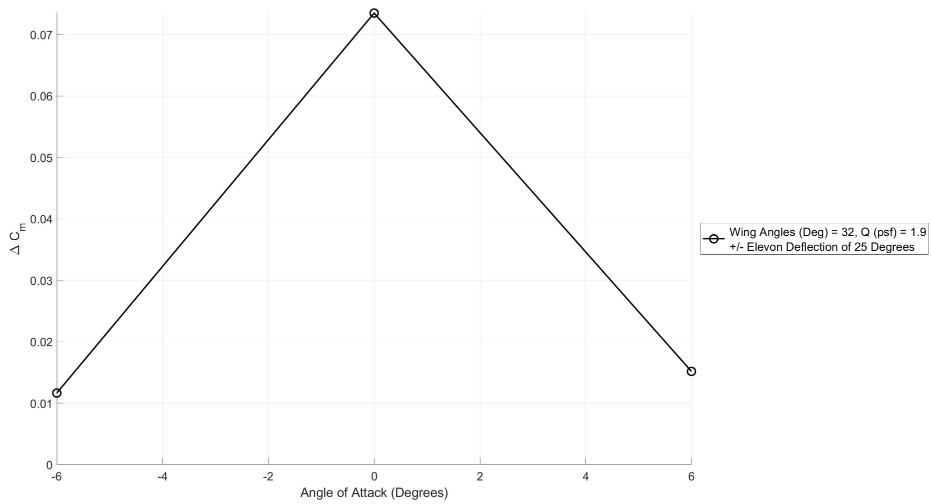

Figure 343. Wing angles 32 degrees trim point Δ C_m vs angle of attack for elevon deflection.

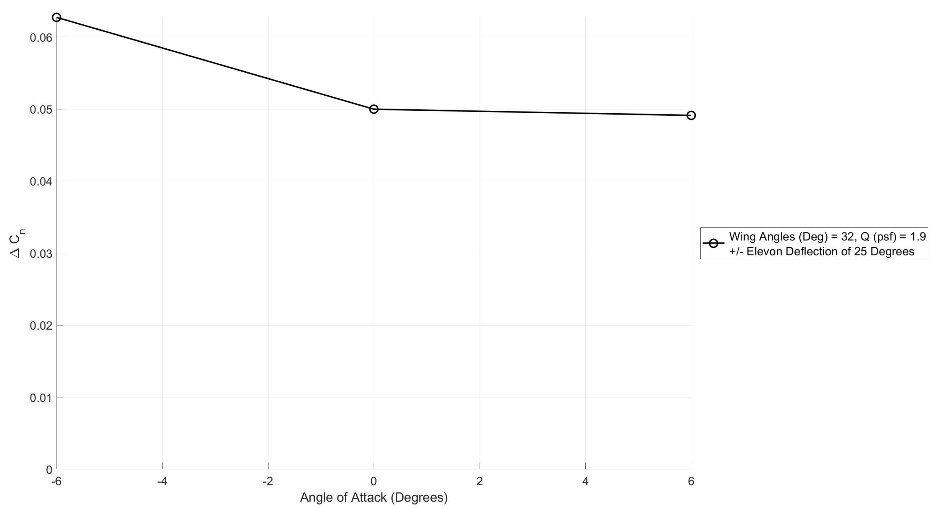

Figure 344. Wing angles 32 degrees trim point Δ C_n vs angle of attack for elevon deflection.

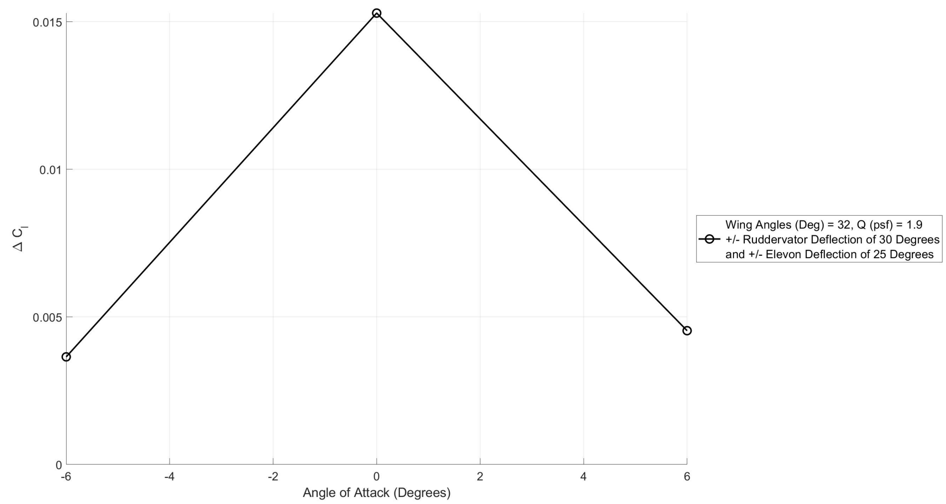

Figure 345. Wing angles 32 degrees trim point Δ C$_l$ vs angle of attack for elevon and ruddervator deflection.

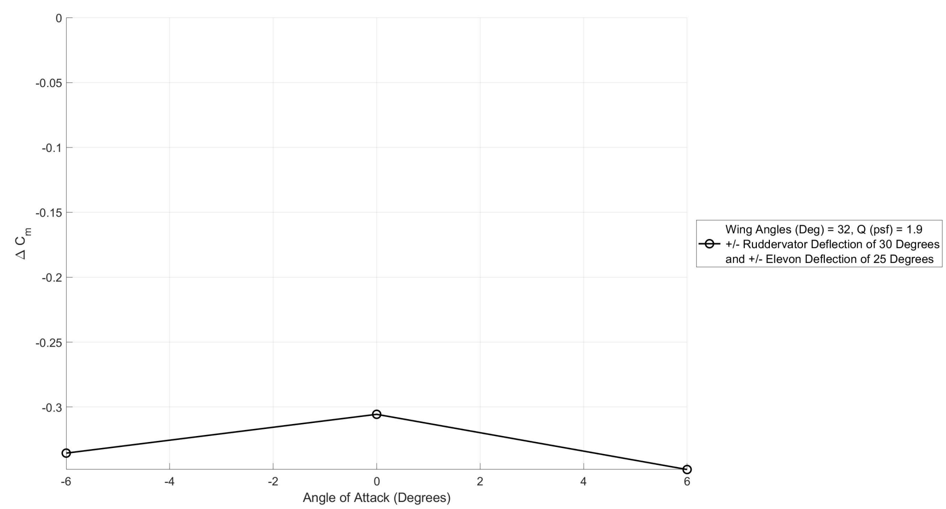

Figure 346. Wing angles 32 degrees trim point Δ C$_m$ vs angle of attack for elevon and ruddervator deflection.

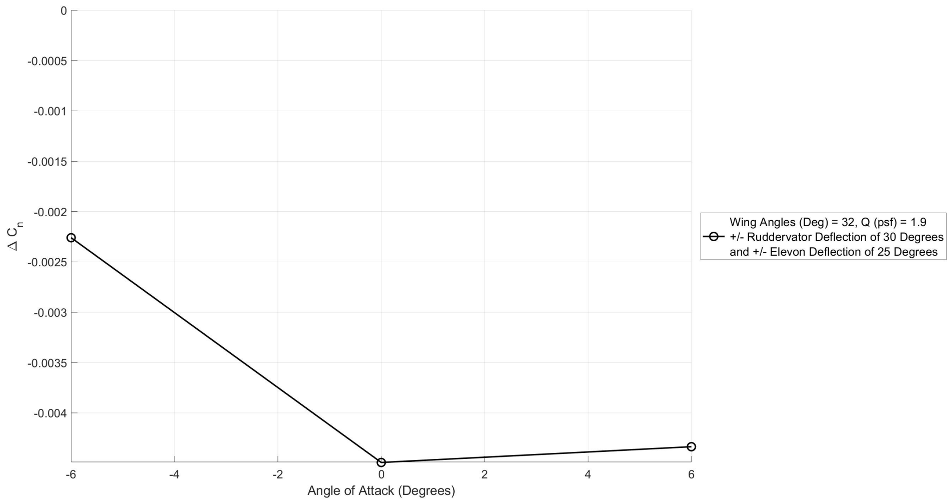

Figure 347. Wing angles 32 degrees trim point Δ C_n vs angle of attack for elevon and ruddervator deflection.

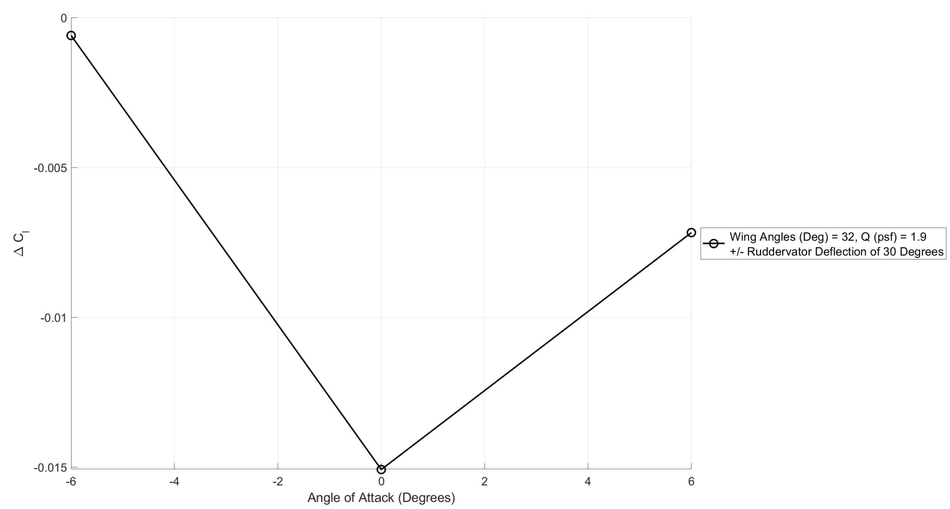

Figure 348. Wing angles 32 degrees trim point Δ C_l vs angle of attack for ruddervator deflection.

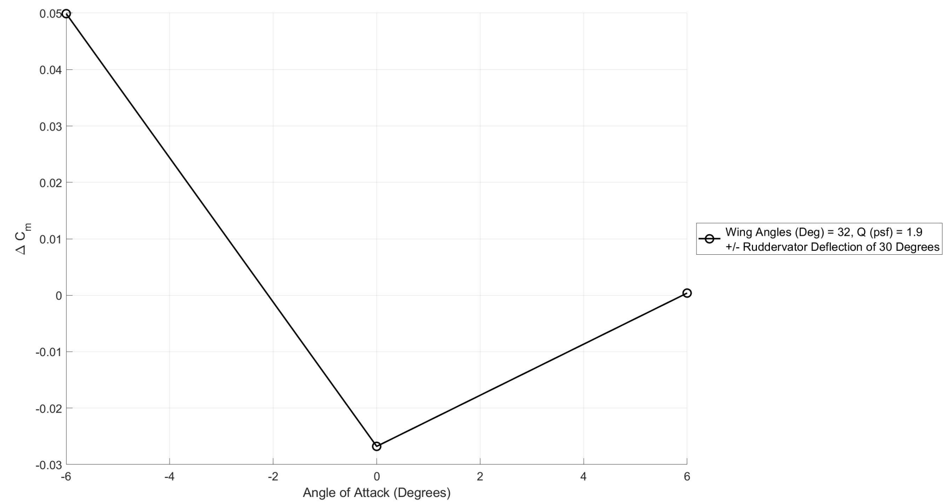

Figure 349. Wing angles 32 degrees trim point Δ C_m vs angle of attack for ruddervator deflection.

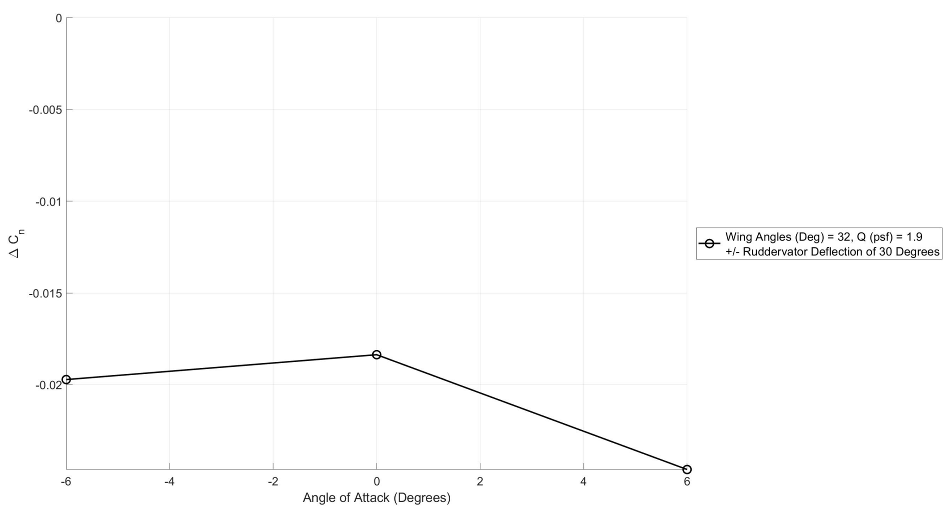

Figure 350. Wing angles 32 degrees trim point Δ C_n vs angle of attack for ruddervator deflection.

C.8 Transition Wing Angles 30 Degrees Performance and Stability Plots

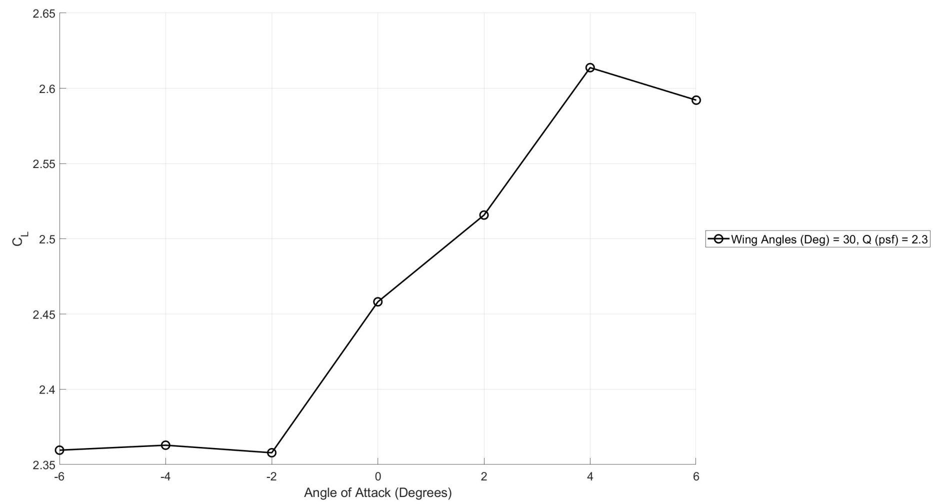

Figure 351. Wing angles 30 degrees trim point C_L vs angle of attack.

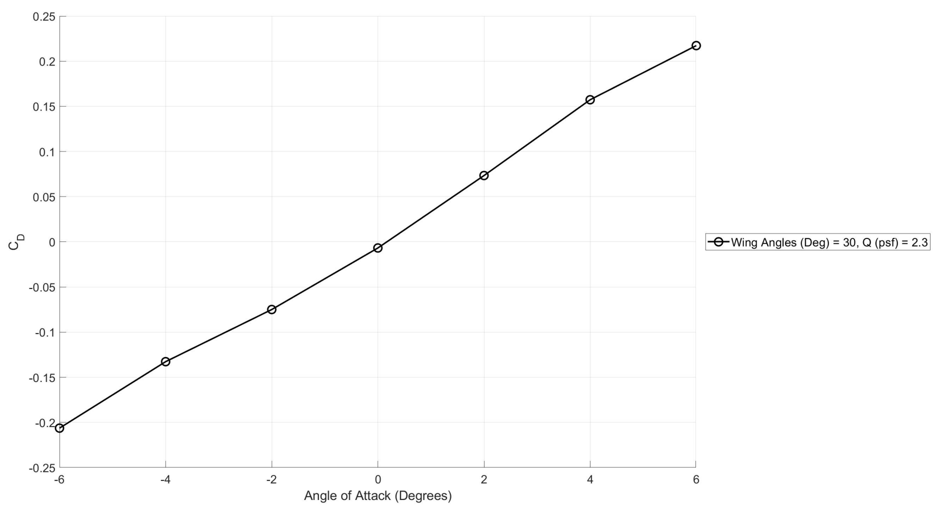

Figure 352. Wing angles 30 degrees trim point C_D vs angle of attack.

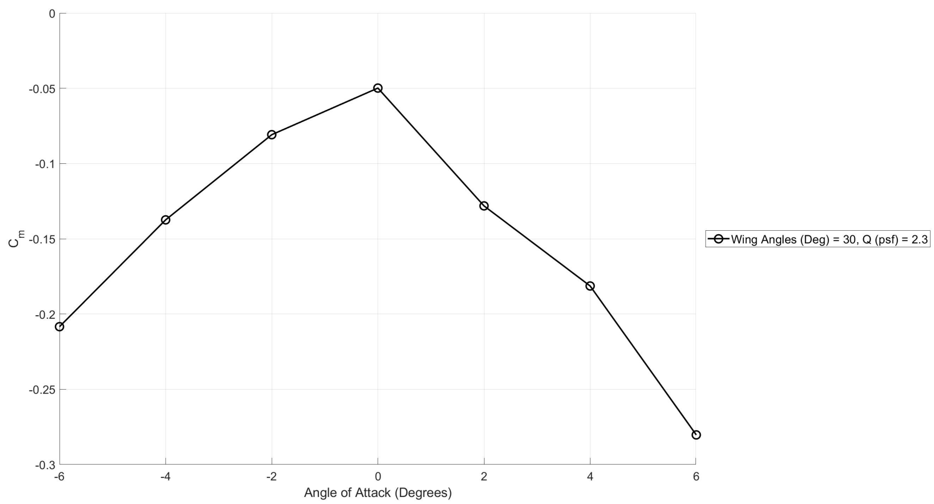

Figure 353. Wing angles 30 degrees trim point C_m vs angle of attack.

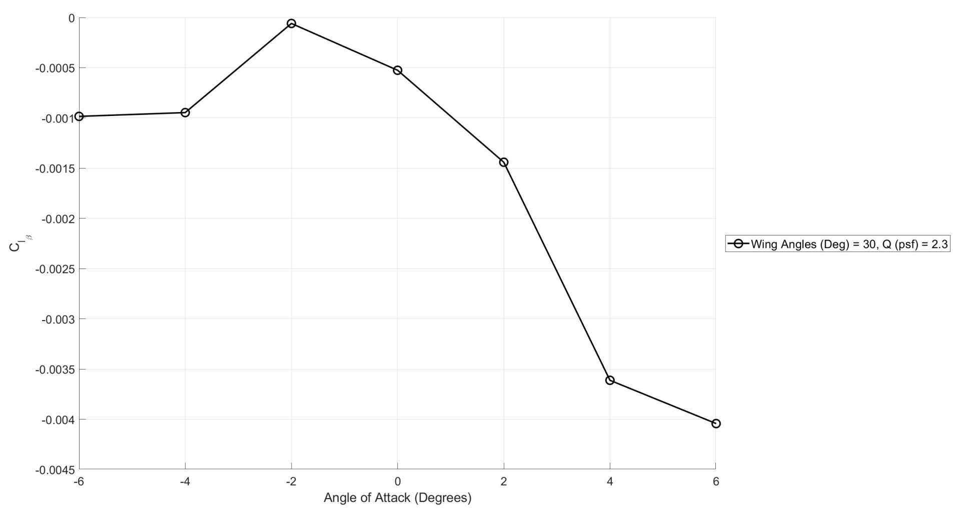

Figure 354. Wing angles 30 degrees trim point C_{l_β} vs angle of attack.

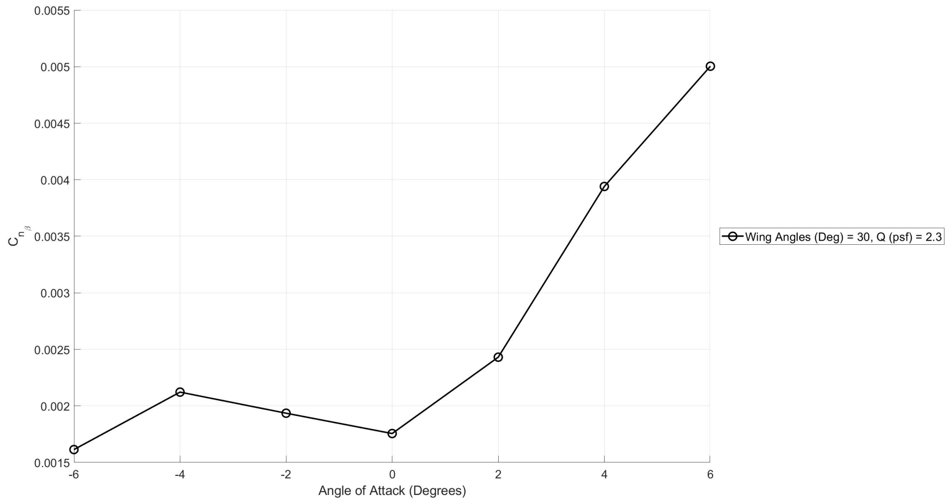

Figure 355. Wing angles 30 degrees trim point C_{n_β} vs angle of attack.

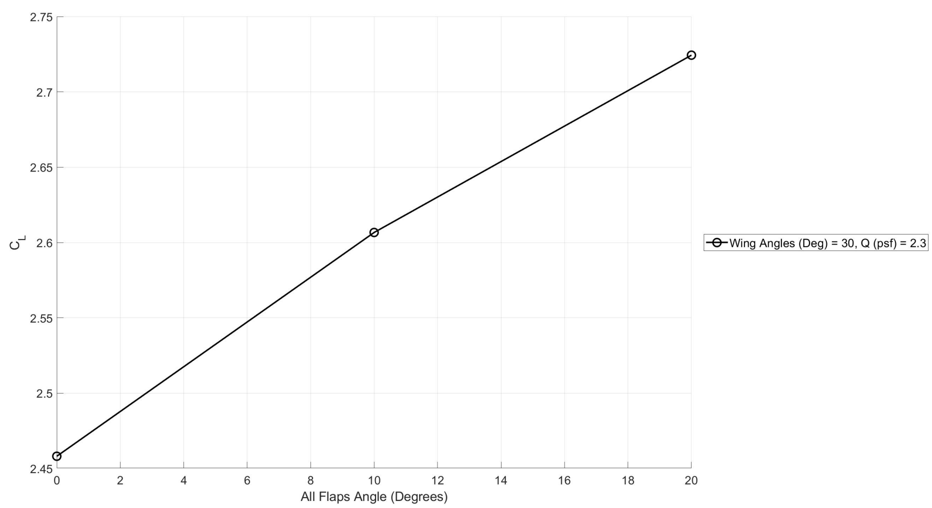

Figure 356. Wing angles 30 degrees trim point C_L vs all flap deflection angle.

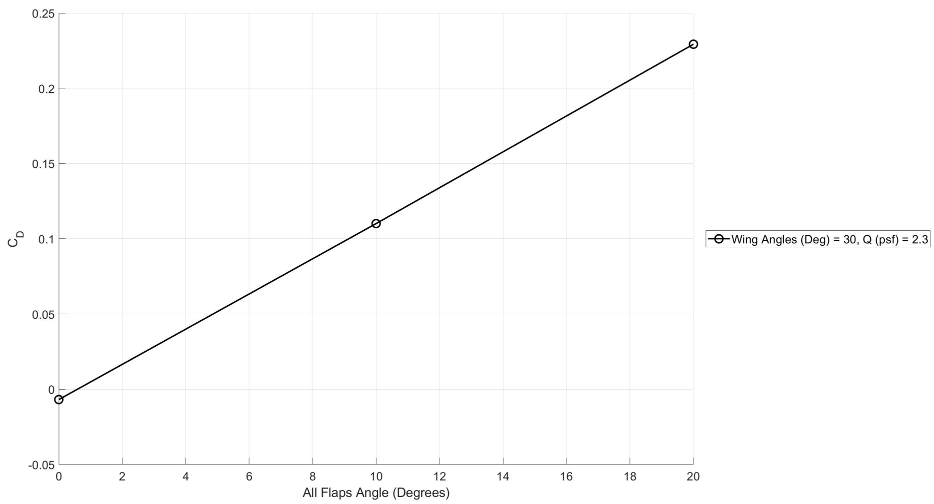

Figure 357. Wing angles 30 degrees trim point C_D vs all flap deflection angle.

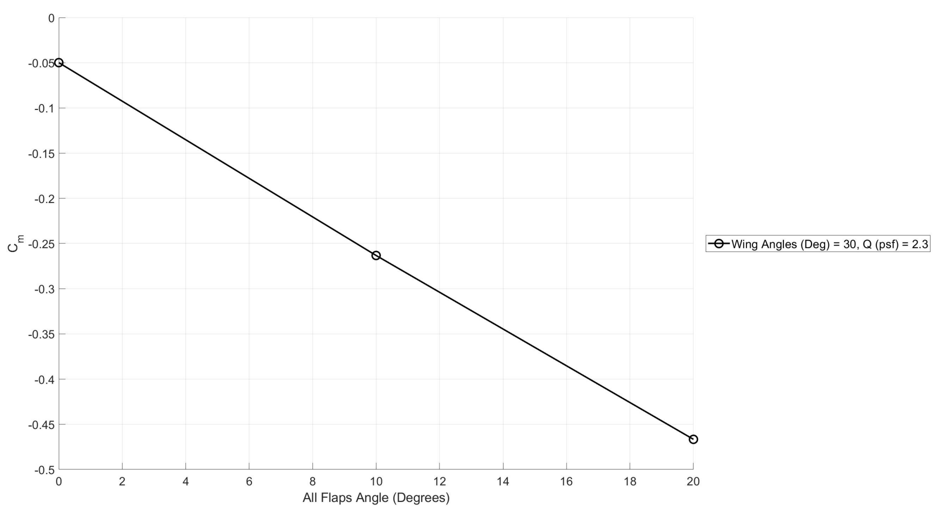

Figure 358. Wing angles 30 degrees trim point C_m vs all flap deflection angle.

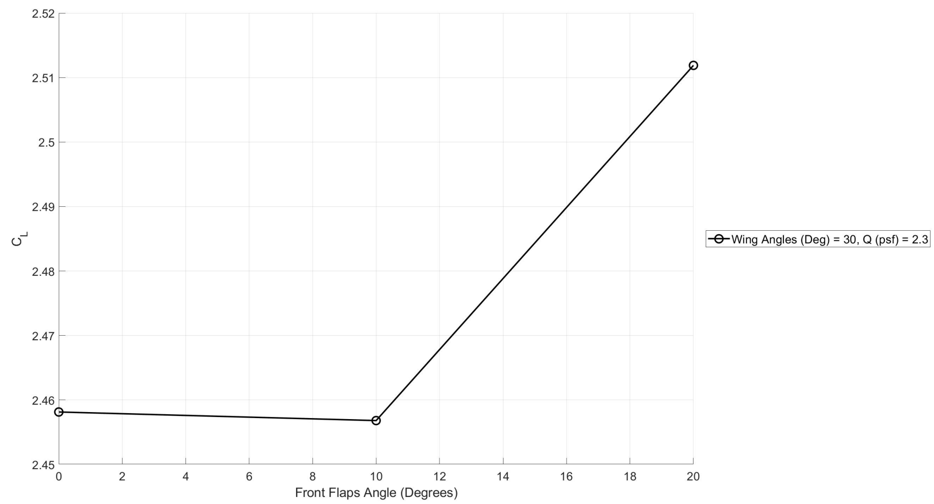

Figure 359. Wing angles 30 degrees trim point C_L vs front flap deflection angle.

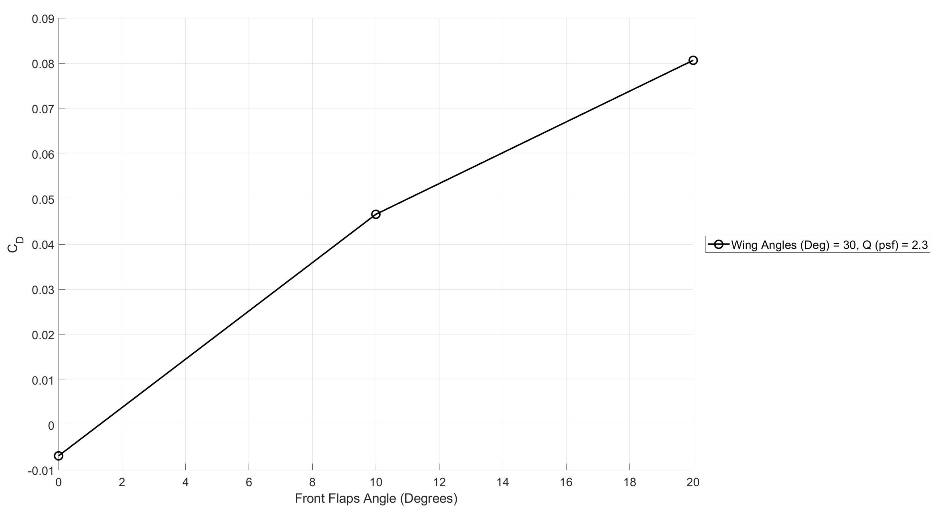

Figure 360. Wing angles 30 degrees trim point C_D vs front flap deflection angle.

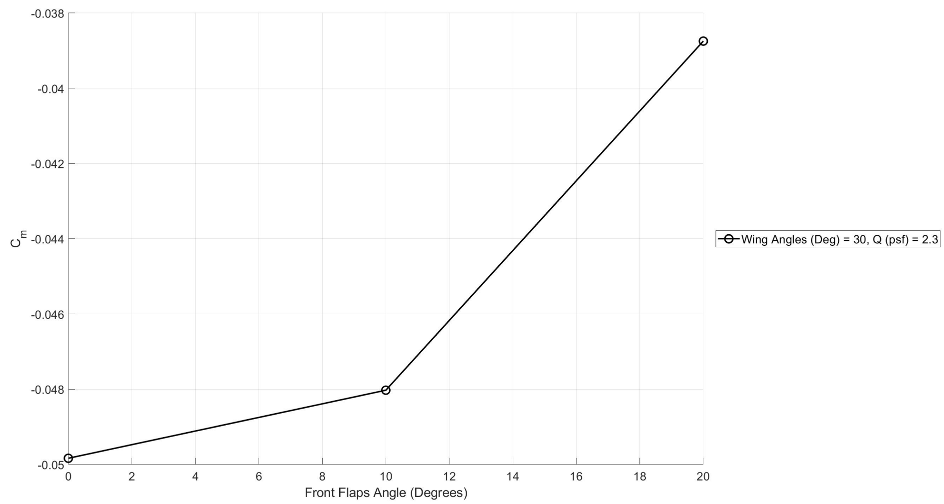

Figure 361. Wing angles 30 degrees trim point C_m vs front flap deflection angle.

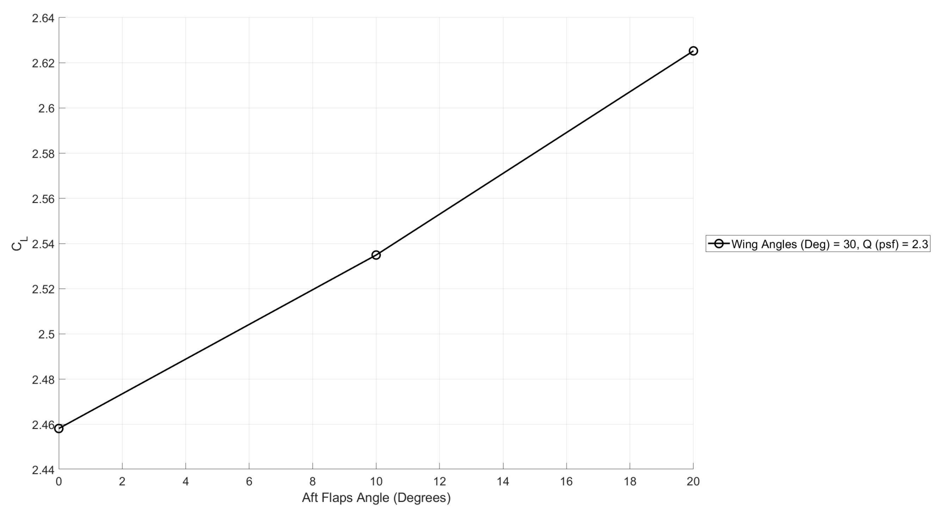

Figure 362. Wing angles 30 degrees trim point C_L vs aft flap deflection angle.

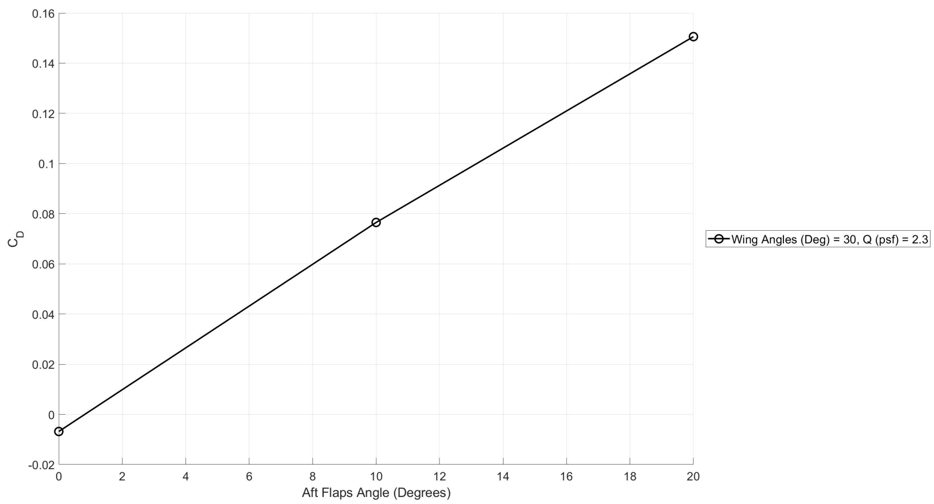

Figure 363. Wing angles 30 degrees trim point C_D vs aft flap deflection angle.

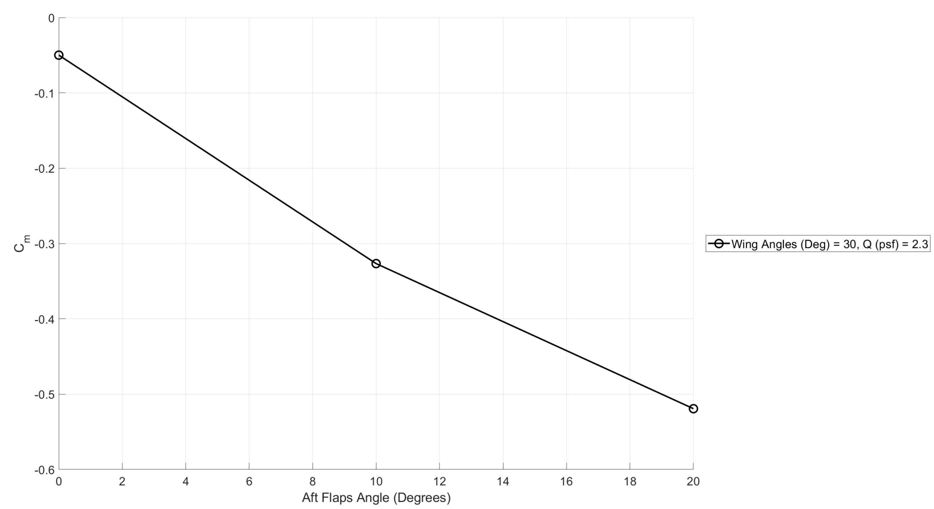

Figure 364. Wing angles 30 degrees trim point C_m vs aft flap deflection angle.

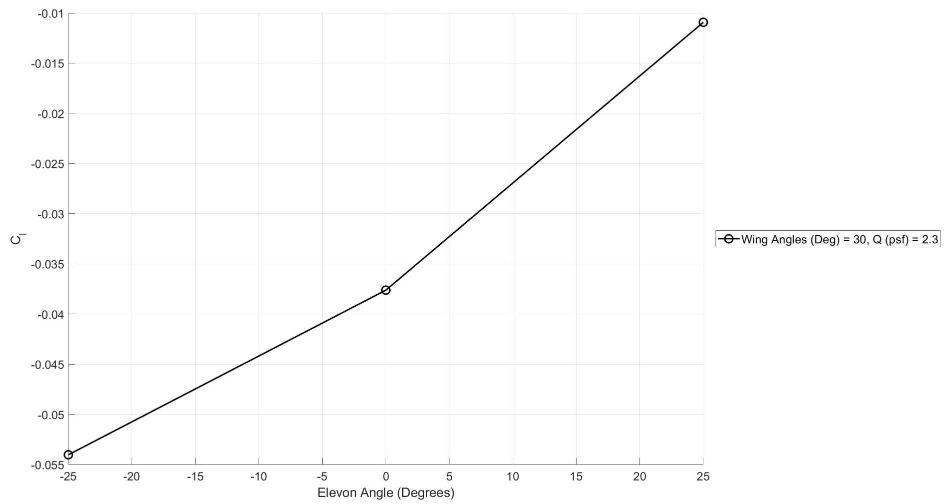

Figure 365. Wing angles 30 degrees trim point C_l vs elevon deflection angle.

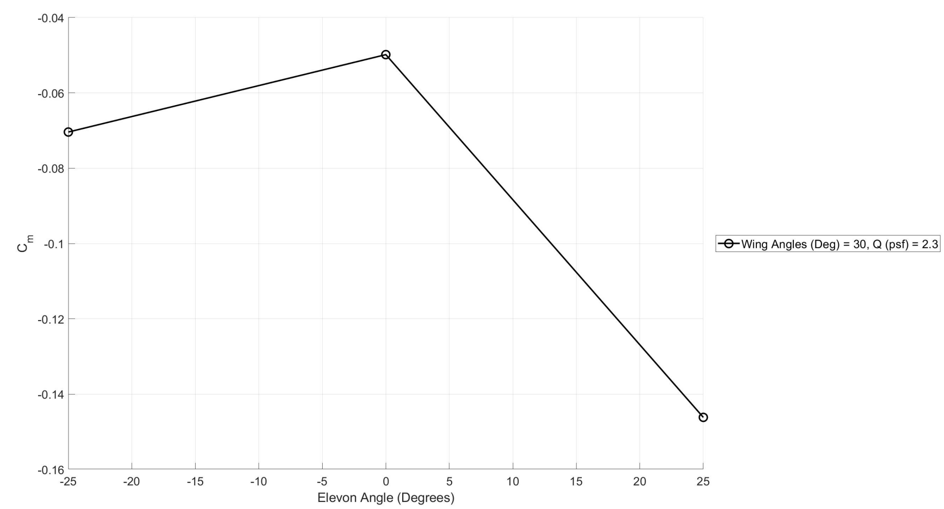

Figure 366. Wing angles 30 degrees trim point C_m vs elevon deflection angle.

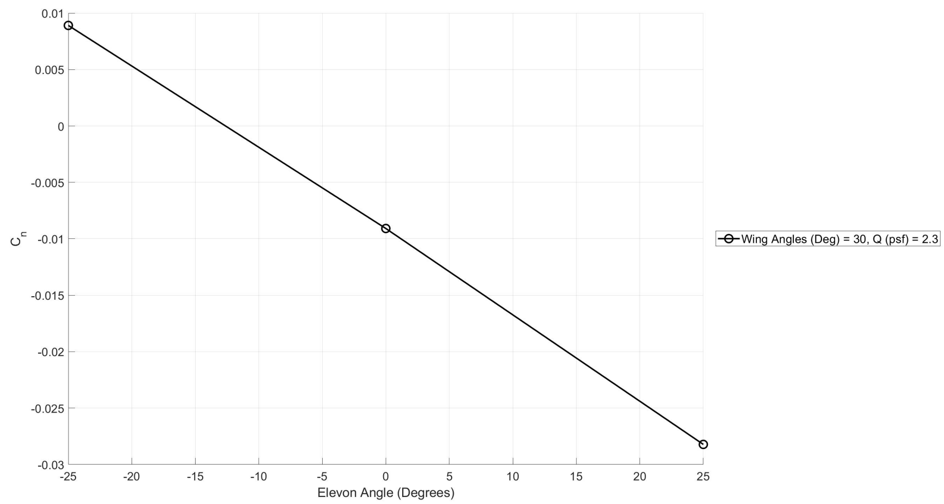

Figure 367. Wing angles 30 degrees trim point C_n vs elevon deflection angle.

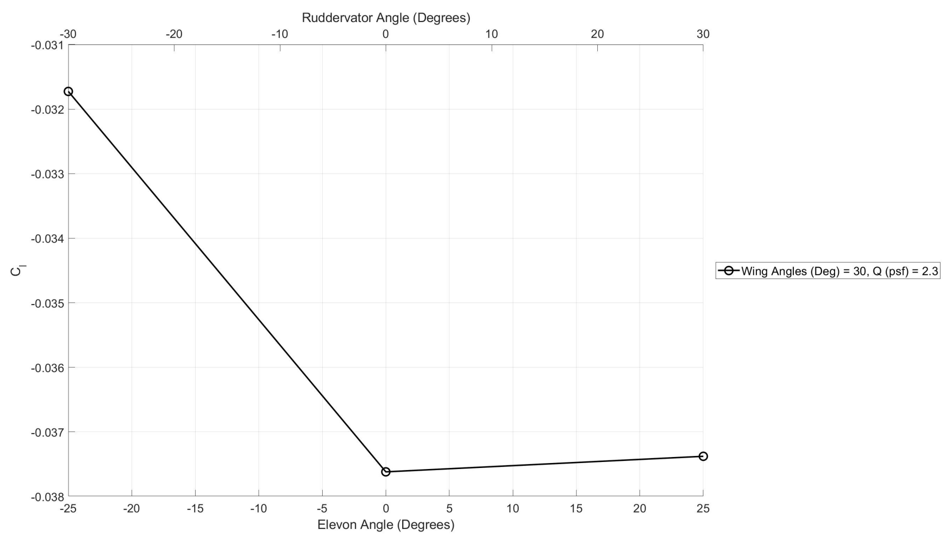

Figure 368. Wing angles 30 degrees trim point C_l vs elevon and ruddervator deflection angles.

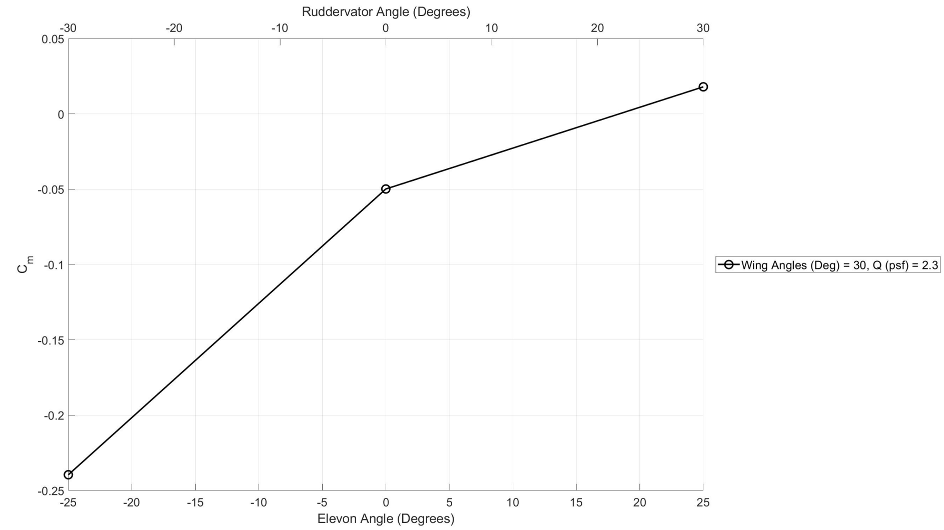

Figure 369. Wing angles 30 degrees trim point C_m vs elevon and ruddervator deflection angles.

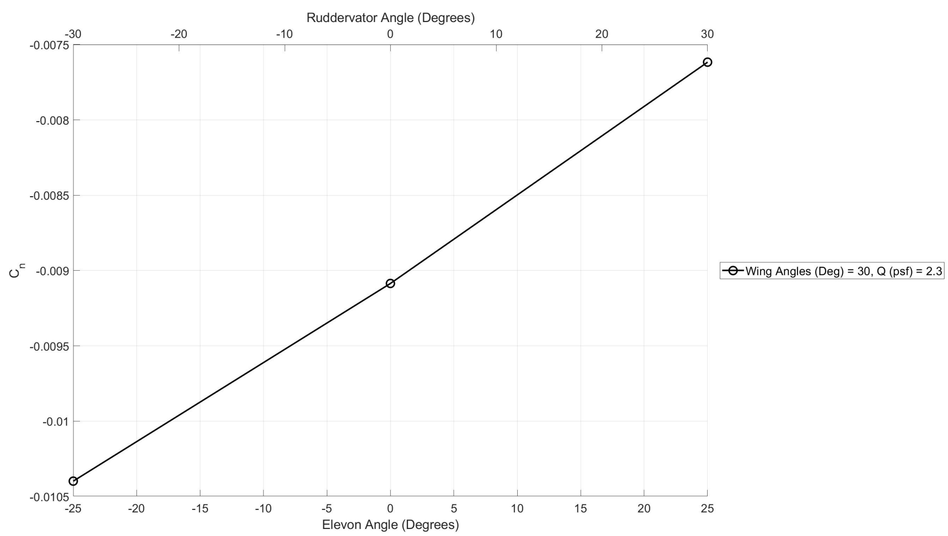

Figure 370. Wing angles 30 degrees trim point C_n vs elevon and ruddervator deflection angles.

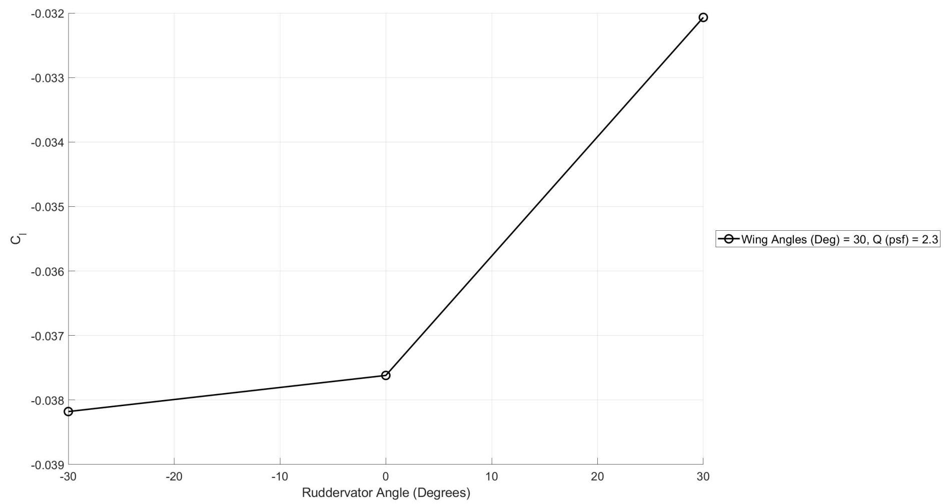

Figure 371. Wing angles 30 degrees trim point C_l vs ruddervator deflection angle.

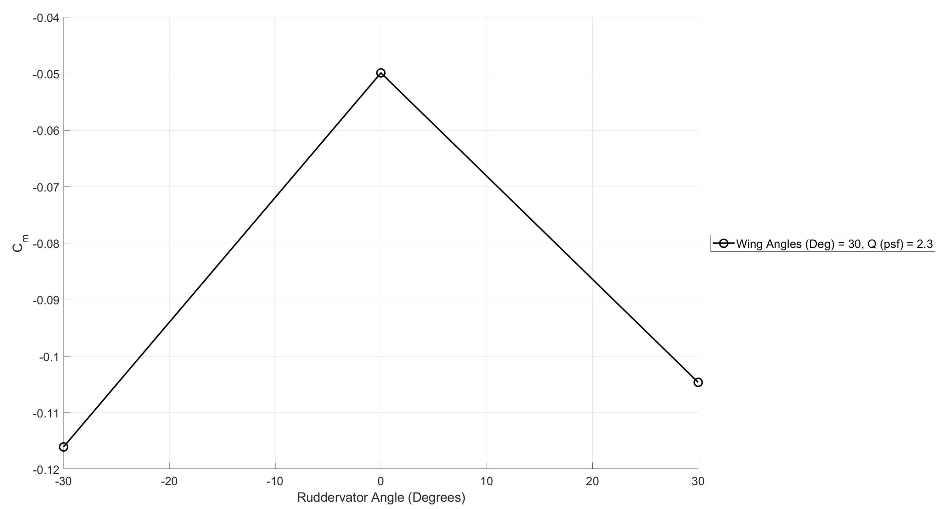

Figure 372. Wing angles 30 degrees trim point C_m vs ruddervator deflection angle.

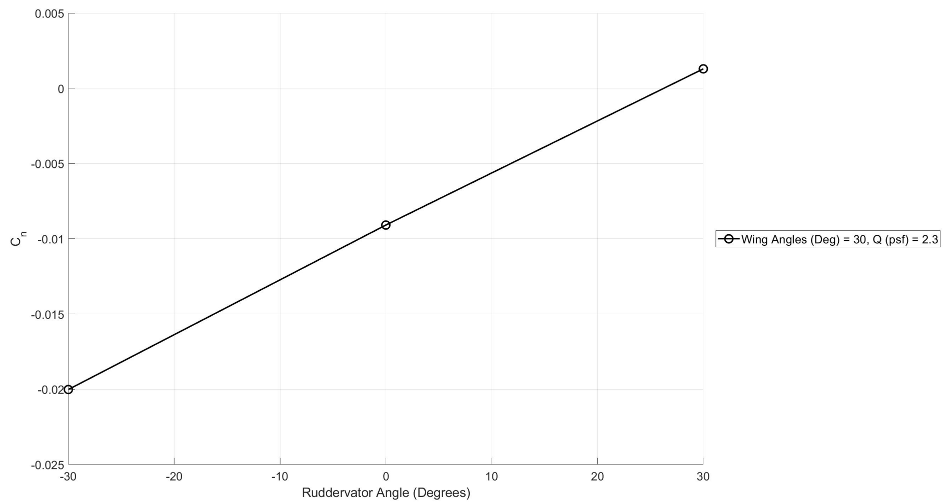

Figure 373. Wing angles 30 degrees trim point C_n vs ruddervator deflection angle.

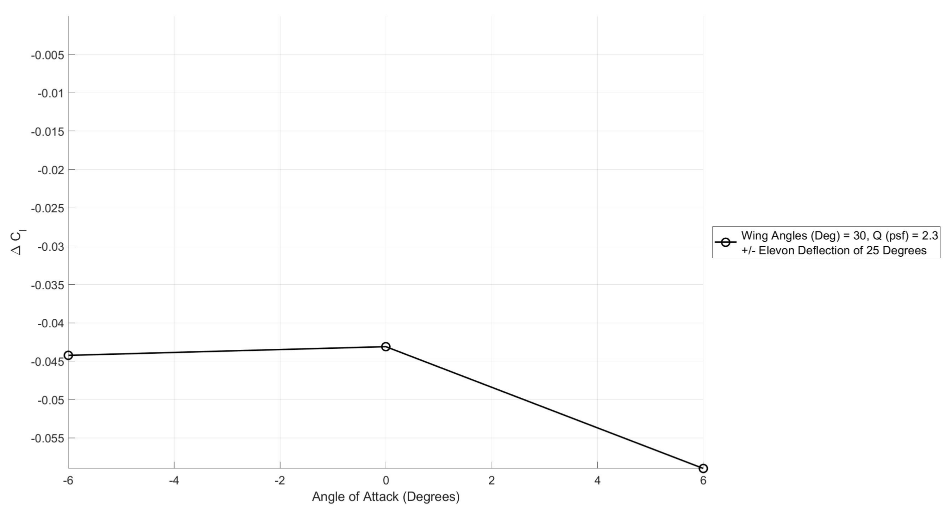

Figure 374. Wing angles 30 degrees trim point Δ C_l vs angle of attack for elevon deflection.

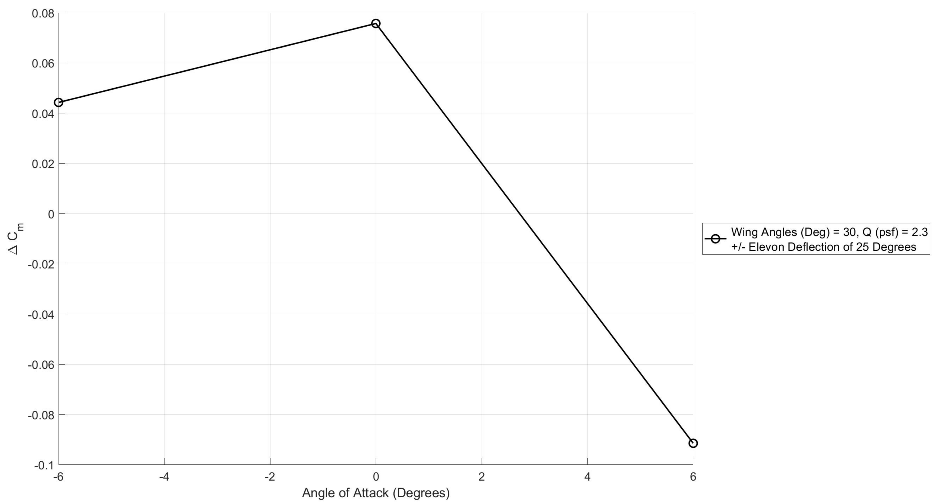

Figure 375. Wing angles 30 degrees trim point Δ C_m vs angle of attack for elevon deflection.

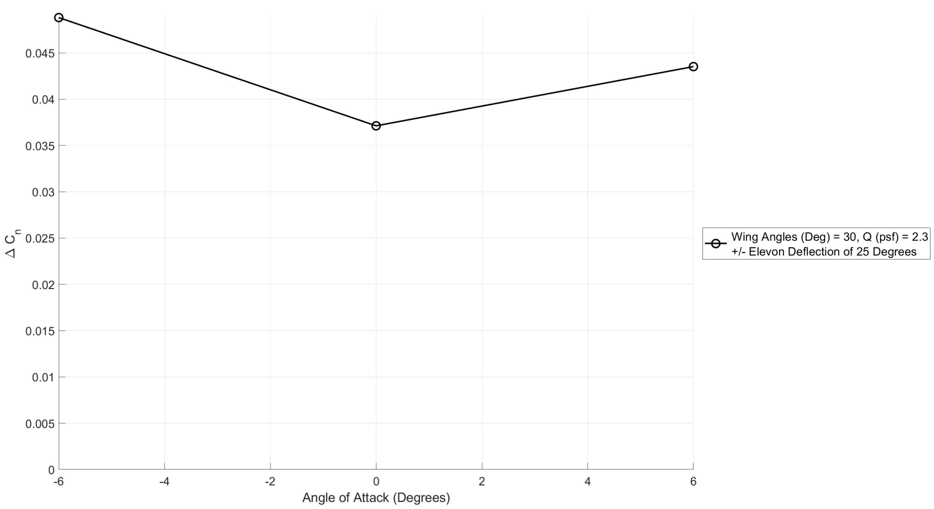

Figure 376. Wing angles 30 degrees trim point Δ C_n vs angle of attack for elevon deflection.

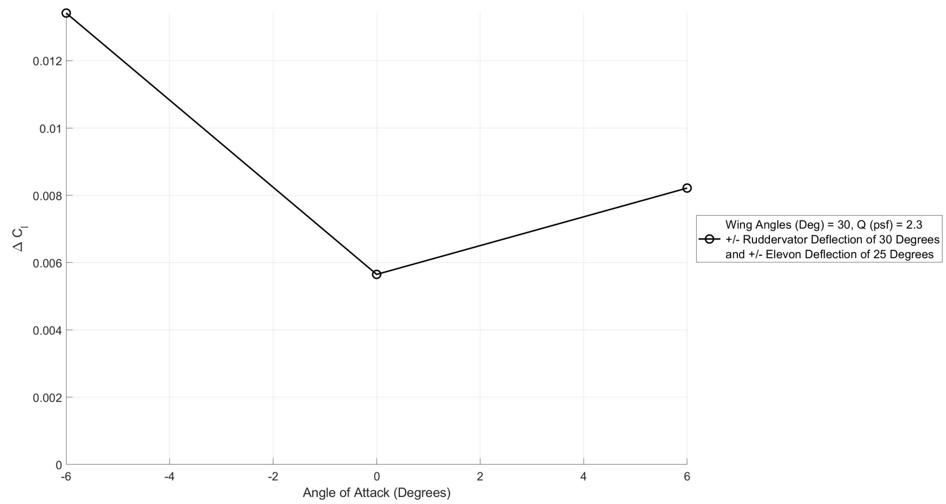

Figure 377. Wing angles 30 degrees trim point Δ C_l vs angle of attack for elevon and ruddervator deflection.

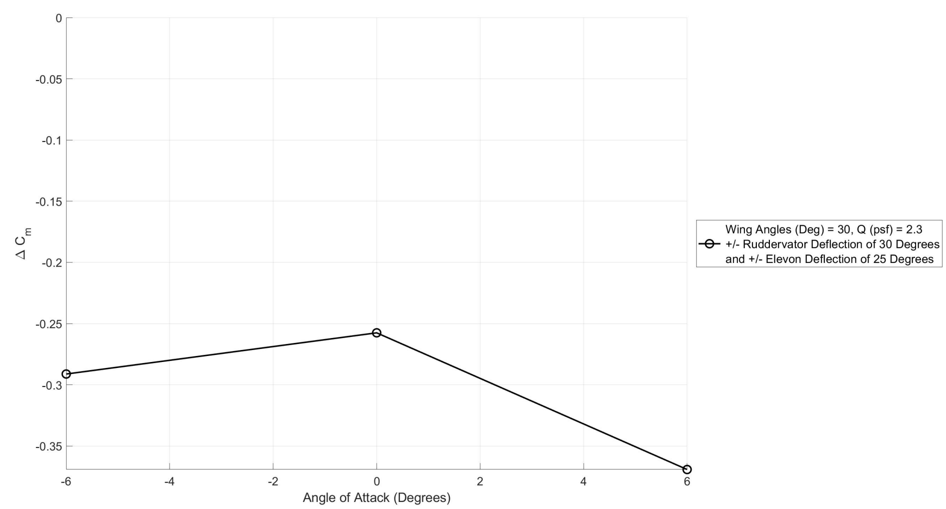

Figure 378. Wing angles 30 degrees trim point Δ C_m vs angle of attack for elevon and ruddervator deflection.

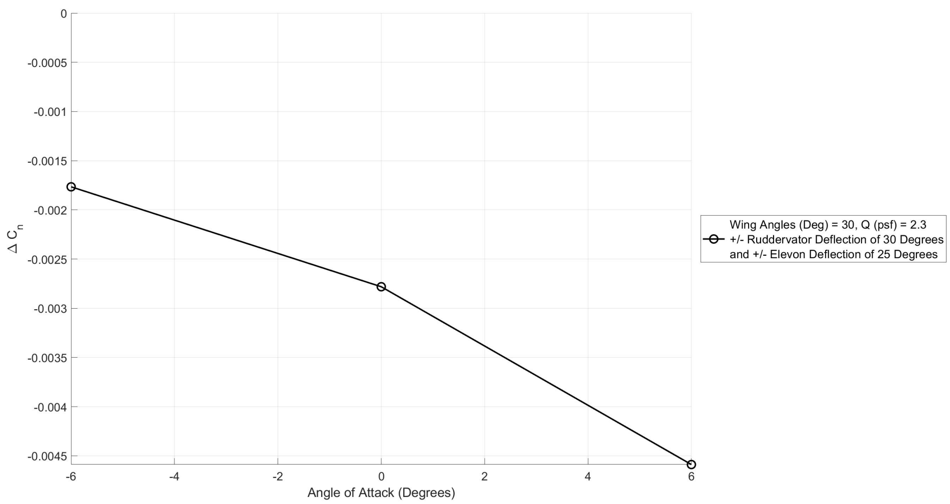

Figure 379. Wing angles 30 degrees trim point Δ C_n vs angle of attack for elevon and ruddervator deflection.

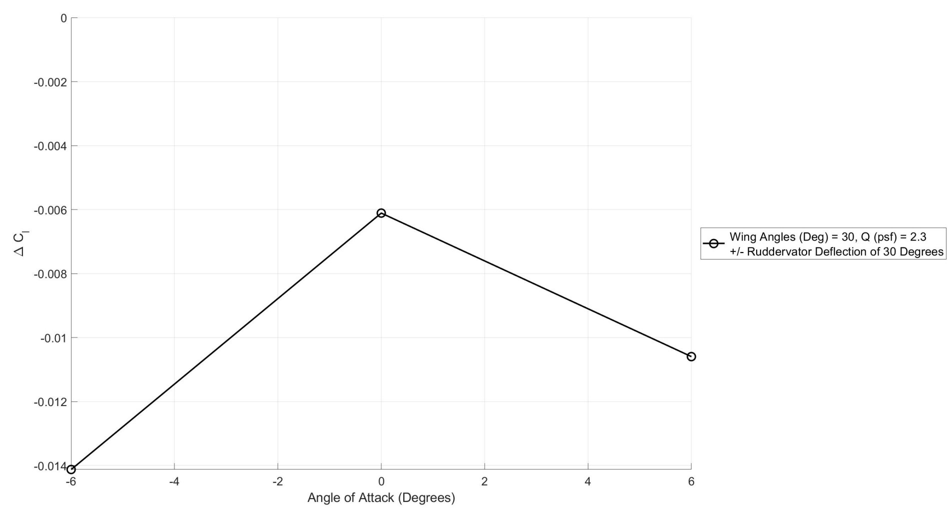

Figure 380. Wing angles 30 degrees trim point Δ C_l vs angle of attack for ruddervator deflection.

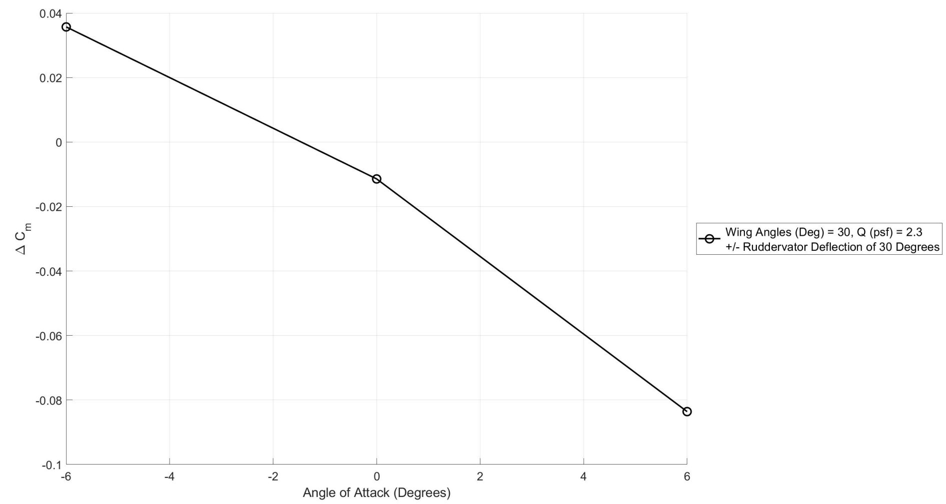

Figure 381. Wing angles 30 degrees trim point Δ C_m vs angle of attack for ruddervator deflection.

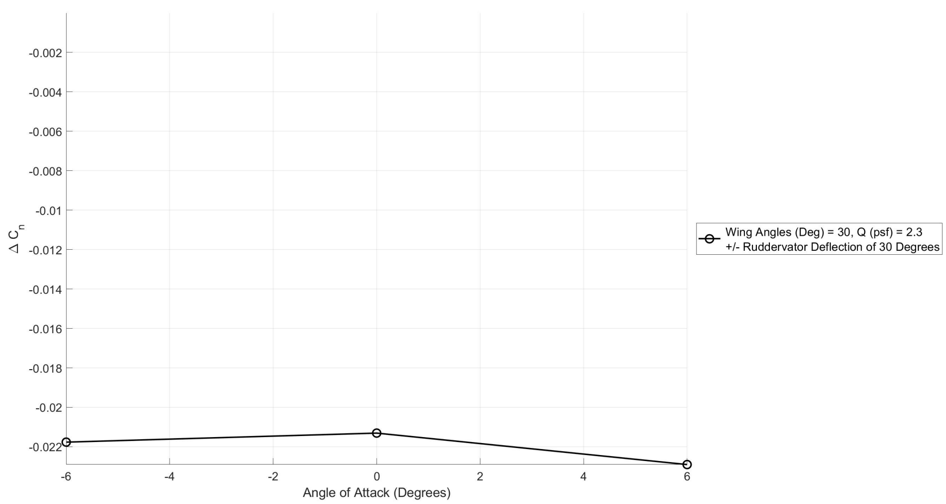

Figure 382. Wing angles 30 degrees trim point Δ C_n vs angle of attack for ruddervator deflection.

C.9 Transition Wing Angles 27 Degrees Performance and Stability Plots

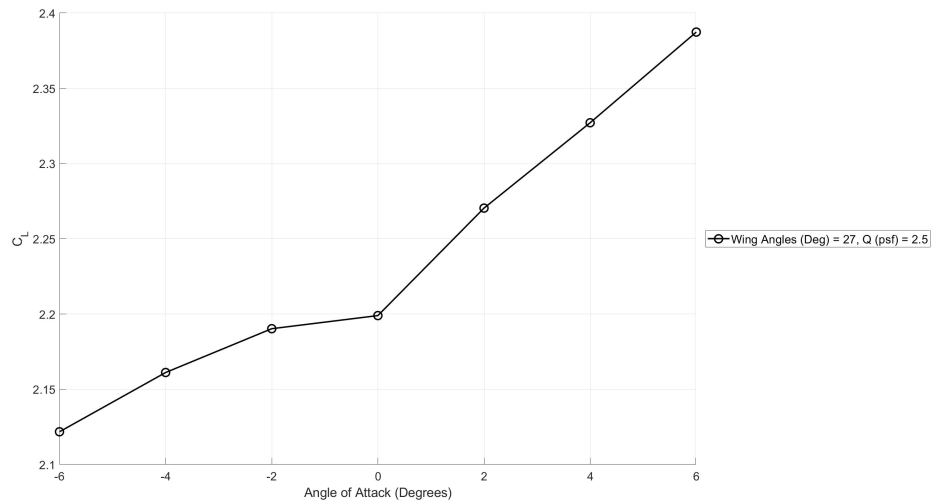

Figure 383. Wing angles 27 degrees trim point C_L vs angle of attack.

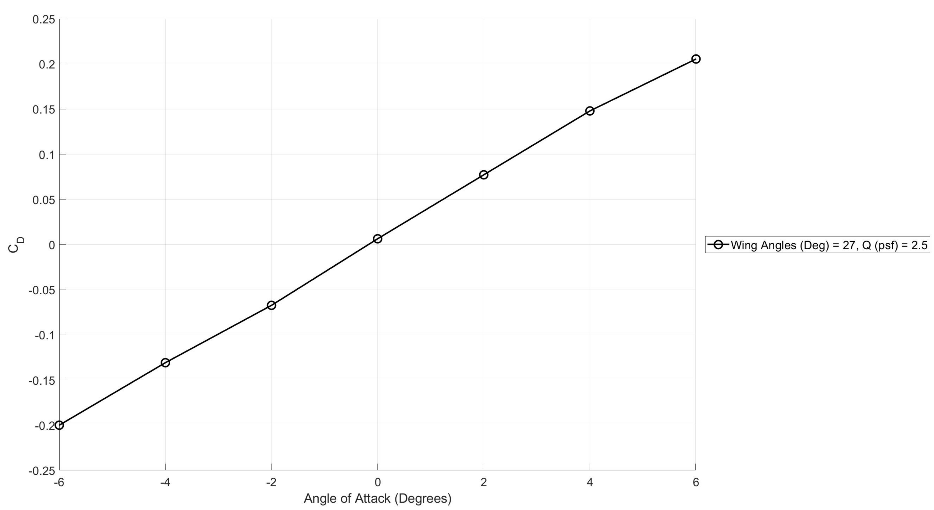

Figure 384. Wing angles 27 degrees trim point C_D vs angle of attack.

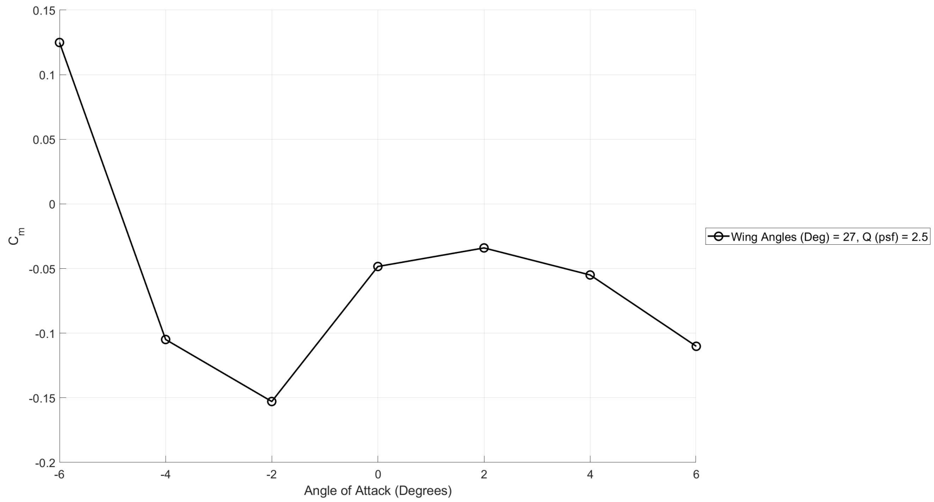

Figure 385. Wing angles 27 degrees trim point C_m vs angle of attack.

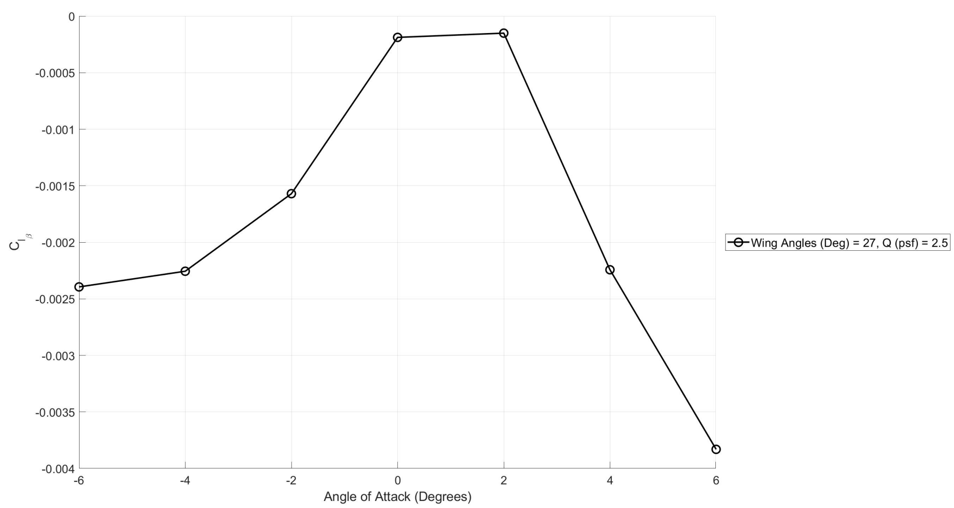

Figure 386. Wing angles 27 degrees trim point C_{l_β} vs angle of attack.

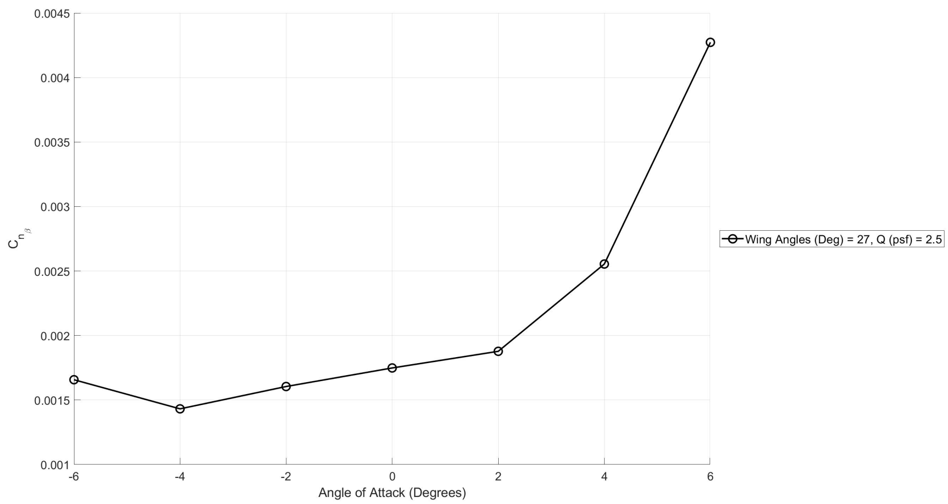

Figure 387. Wing angles 27 degrees trim point C_{n_β} vs angle of attack.

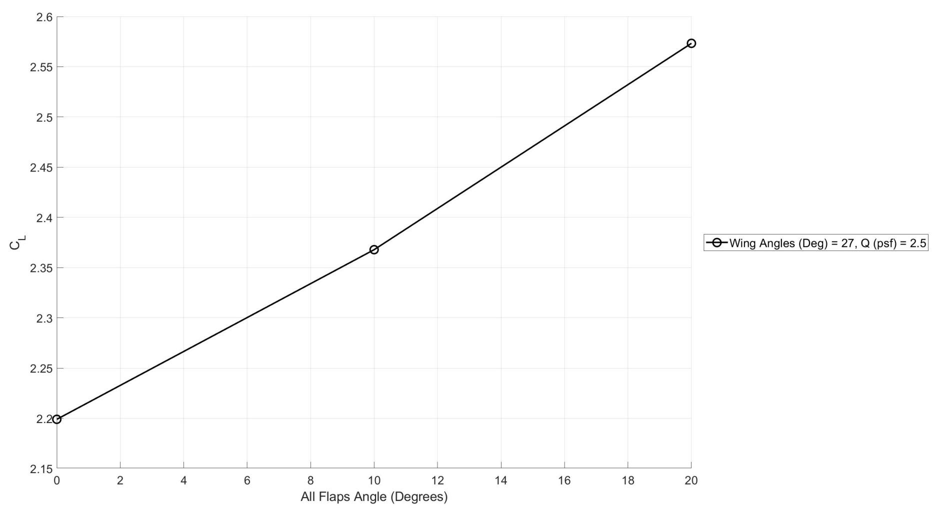

Figure 388. Wing angles 27 degrees trim point C_L vs all flap deflection angle.

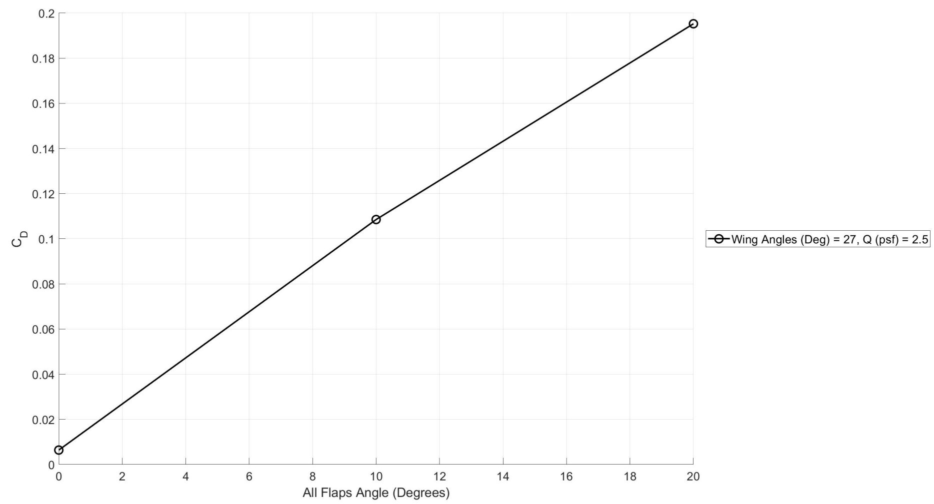

Figure 389. Wing angles 27 degrees trim point C_D vs all flap deflection angle.

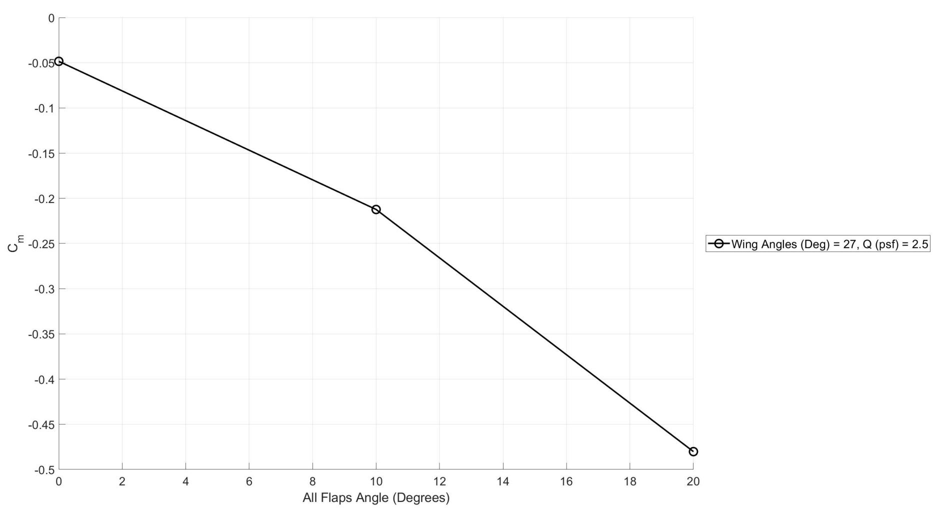

Figure 390. Wing angles 27 degrees trim point C_m vs all flap deflection angle.

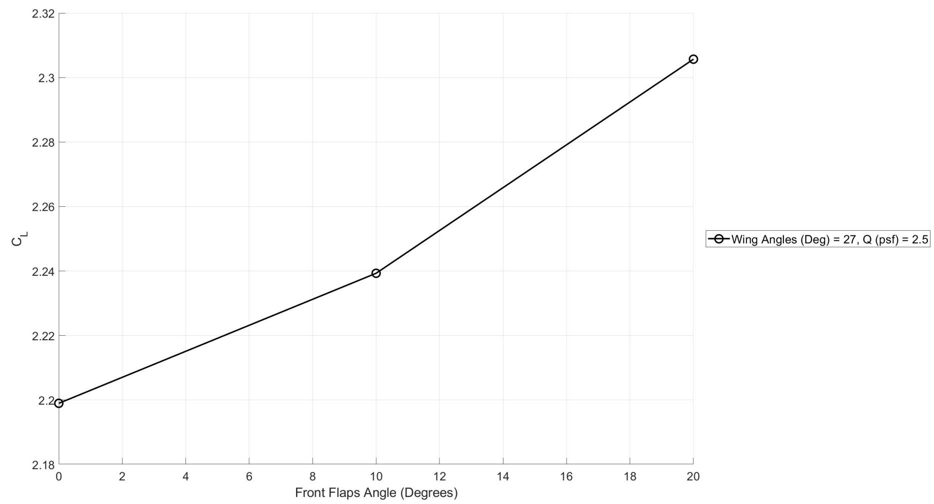

Figure 391. Wing angles 27 degrees trim point C_L vs front flap deflection angle.

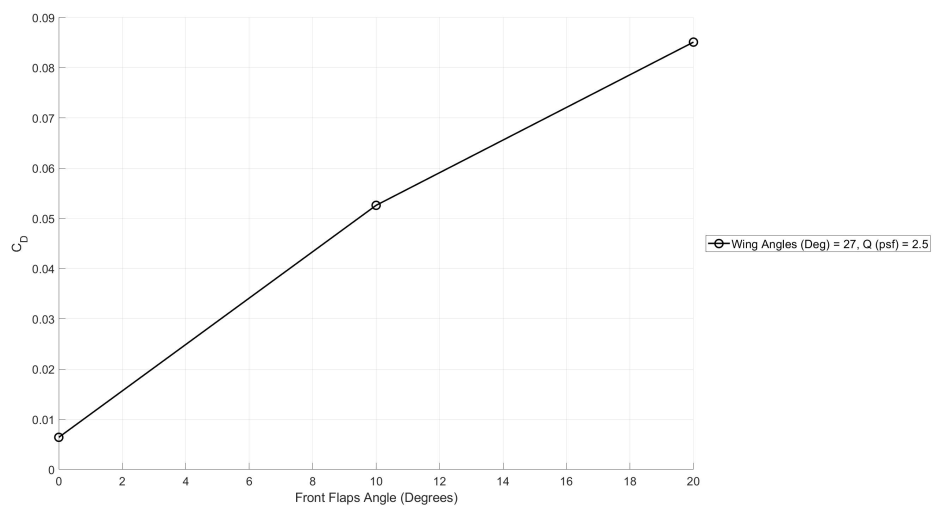

Figure 392. Wing angles 27 degrees trim point C_D vs front flap deflection angle.

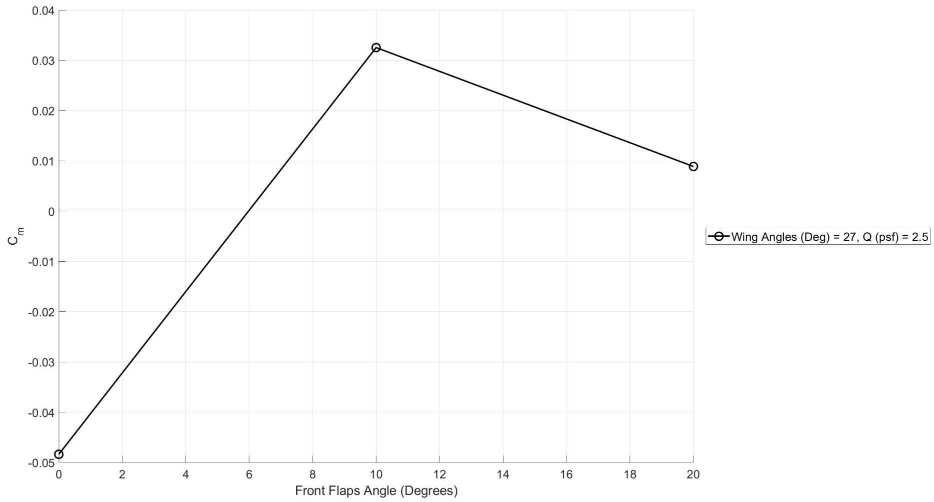

Figure 393. Wing angles 27 degrees trim point C_m vs front flap deflection angle.

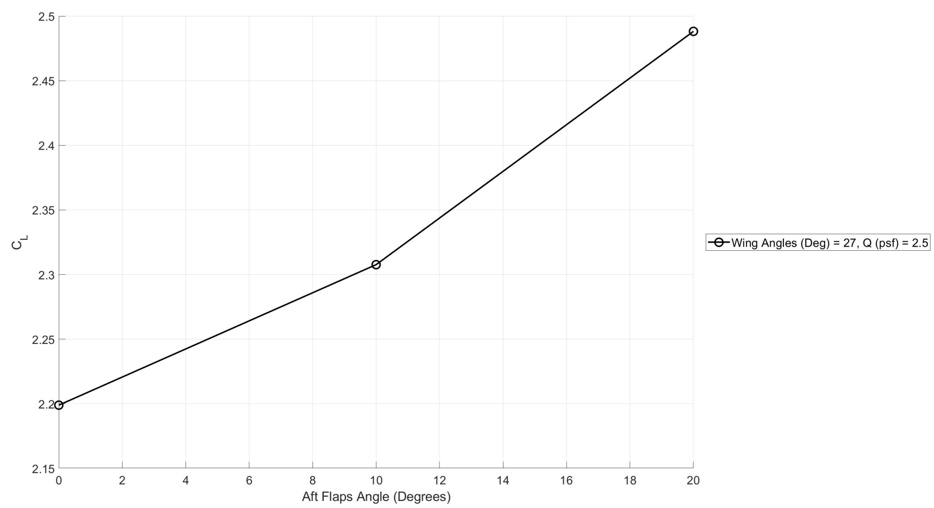

Figure 394. Wing angles 27 degrees trim point C_L vs aft flap deflection angle.

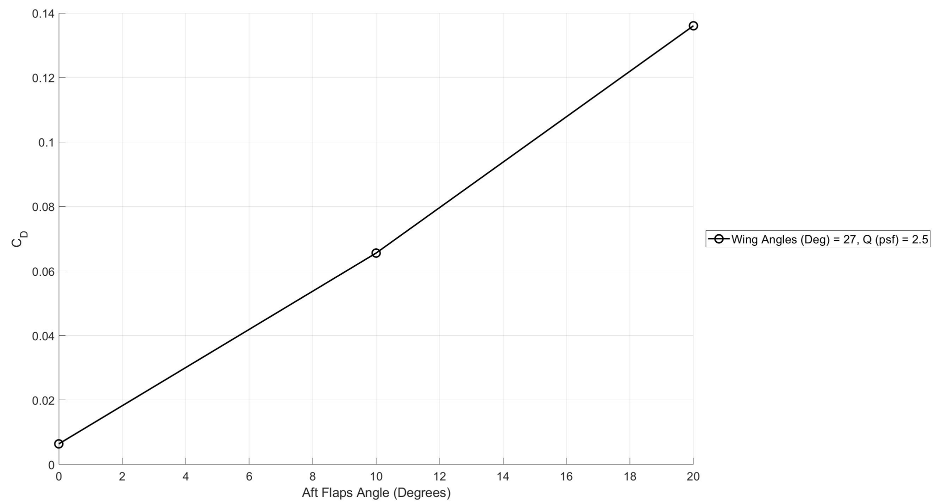

Figure 395. Wing angles 27 degrees trim point C_D vs aft flap deflection angle.

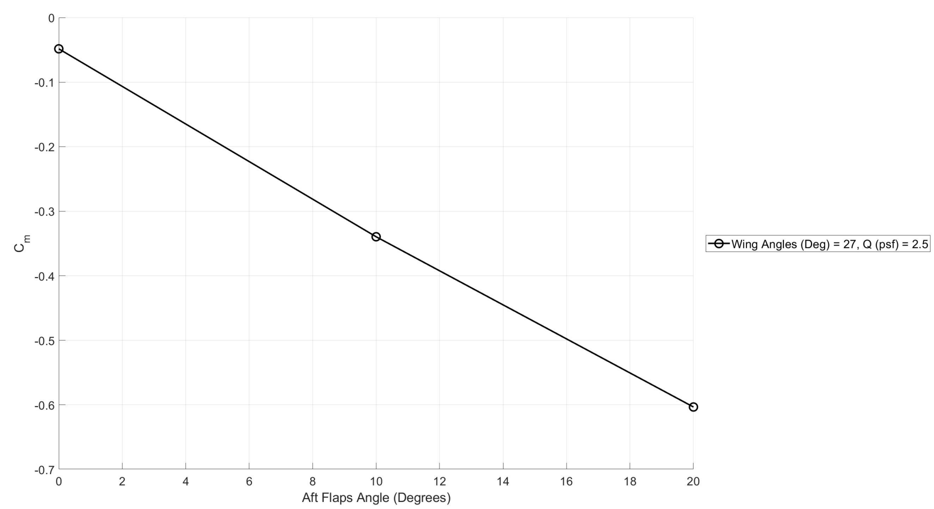

Figure 396. Wing angles 27 degrees trim point C_m vs aft flap deflection angle.

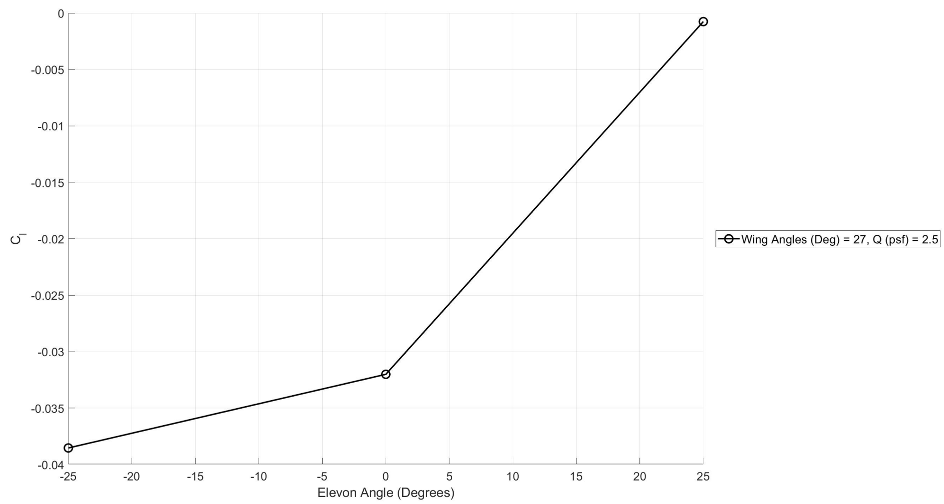

Figure 397. Wing angles 27 degrees trim point C_l vs elevon deflection angle.

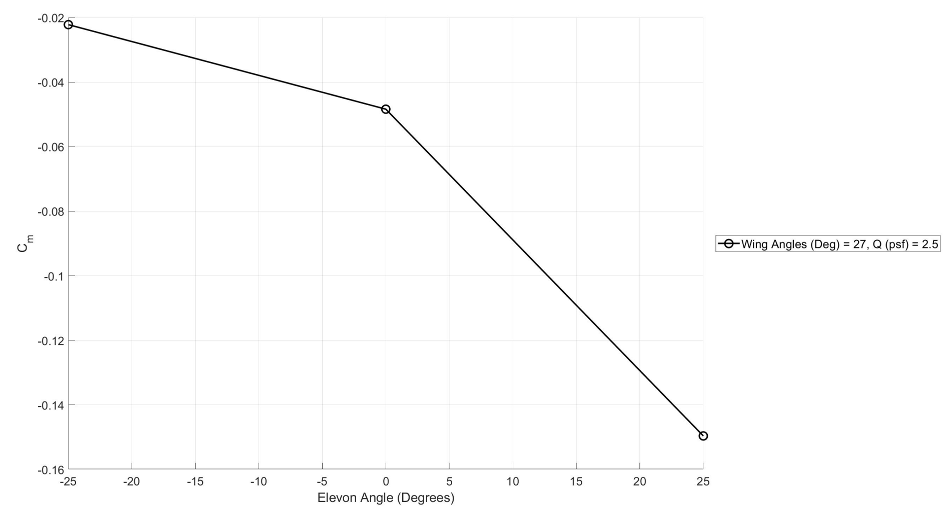

Figure 398. Wing angles 27 degrees trim point C_m vs elevon deflection angle.

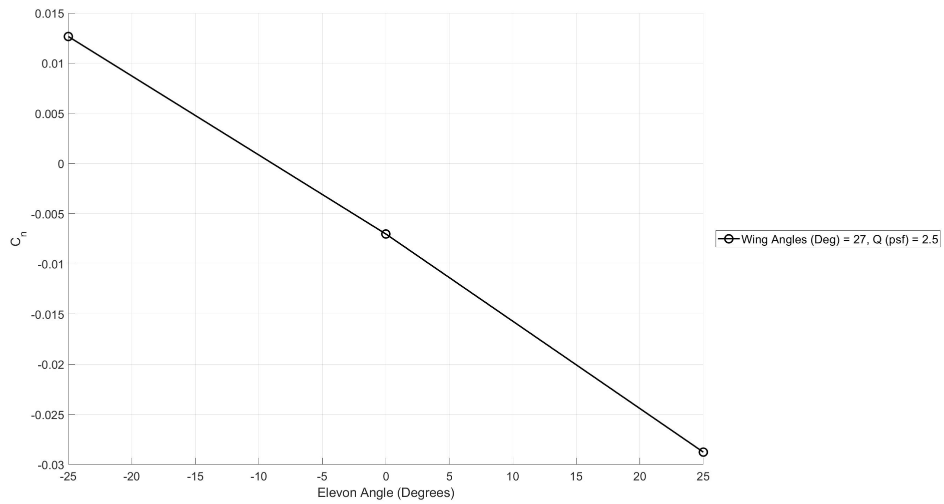

Figure 399. Wing angles 27 degrees trim point C_n vs elevon deflection angle.

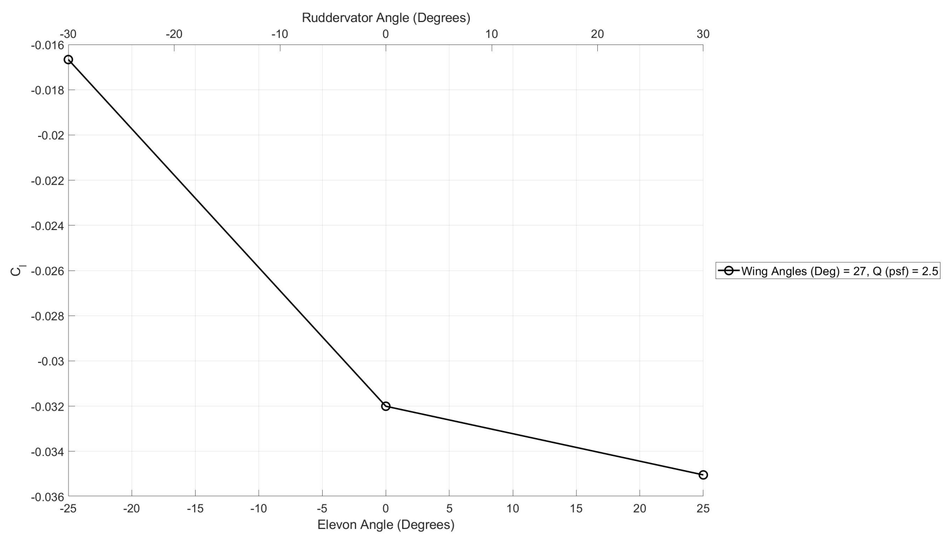

Figure 400. Wing angles 27 degrees trim point C_l vs elevon and ruddervator deflection angles.

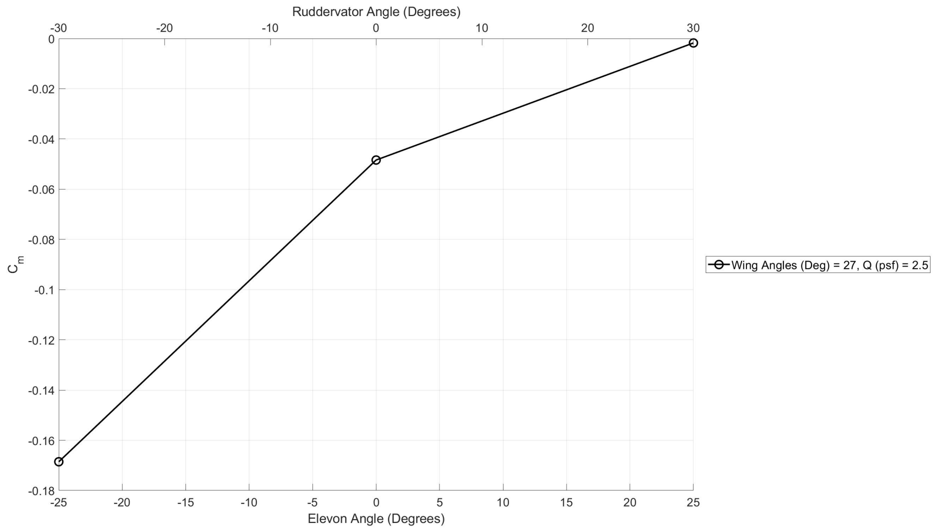

Figure 401. Wing angles 27 degrees trim point C_m vs elevon and ruddervator deflection angles.

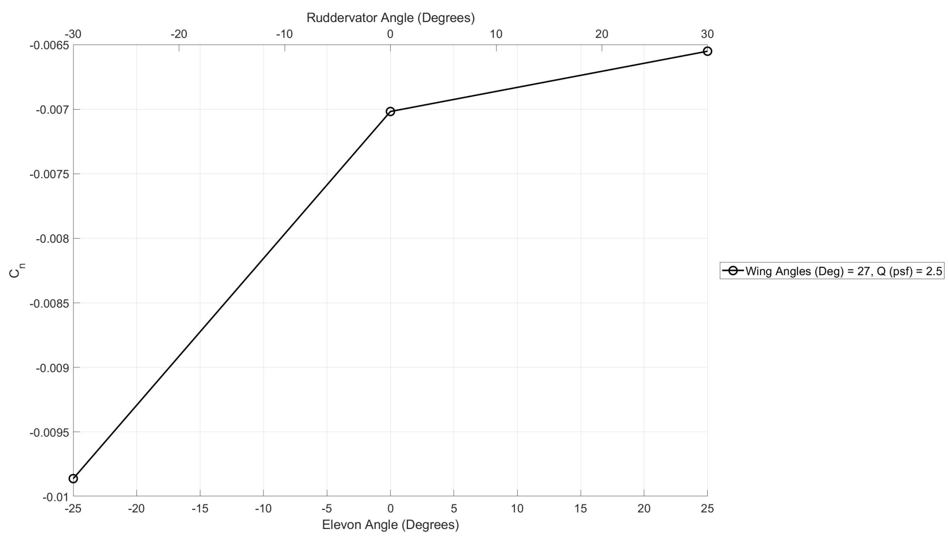

Figure 402. Wing angles 27 degrees trim point C_n vs elevon and ruddervator deflection angles.

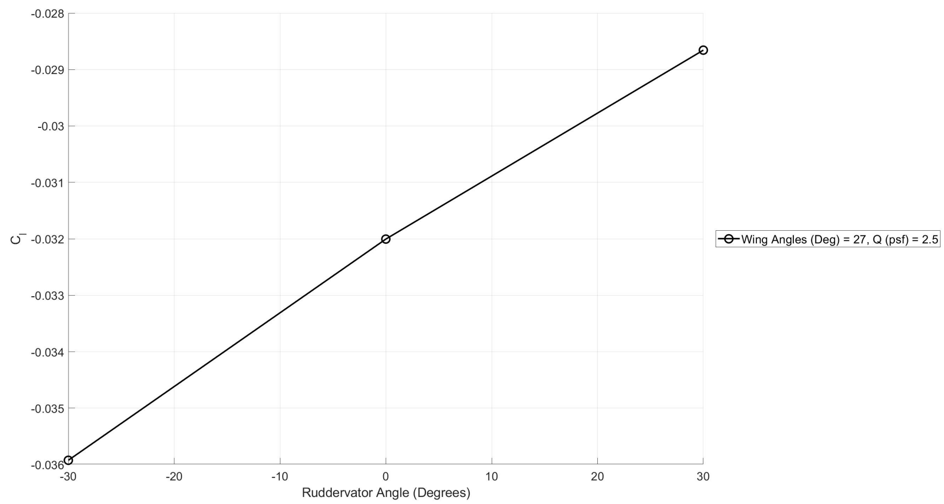

Figure 403. Wing angles 27 degrees trim point C_l vs ruddervator deflection angle.

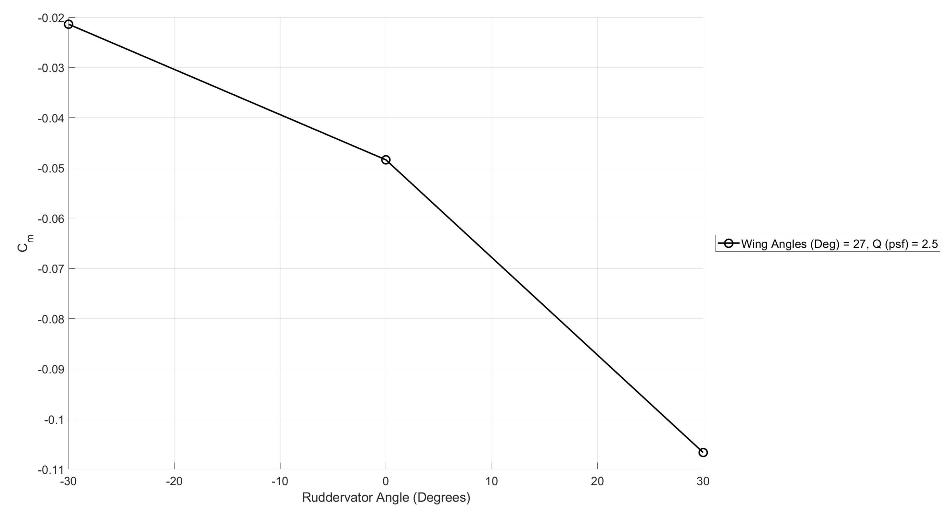

Figure 404. Wing angles 27 degrees trim point C_m vs ruddervator deflection angle.

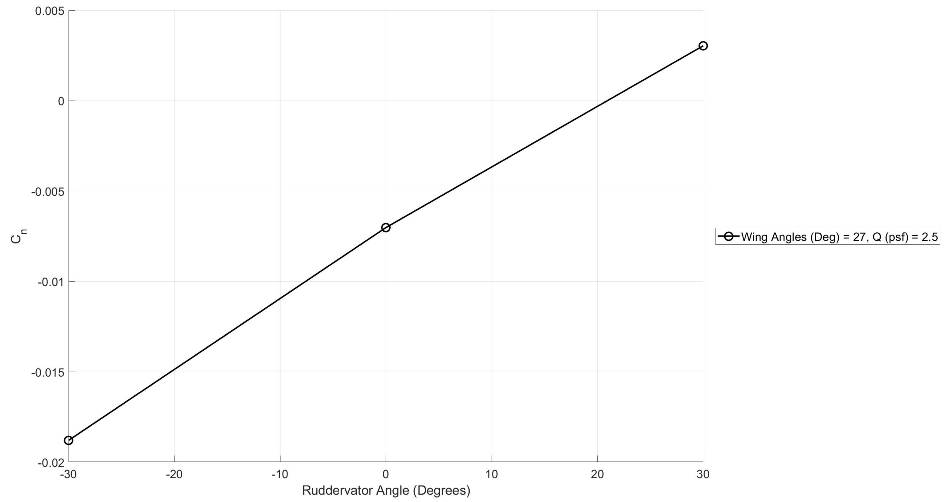

Figure 405. Wing angles 27 degrees trim point C_n vs ruddervator deflection angle.

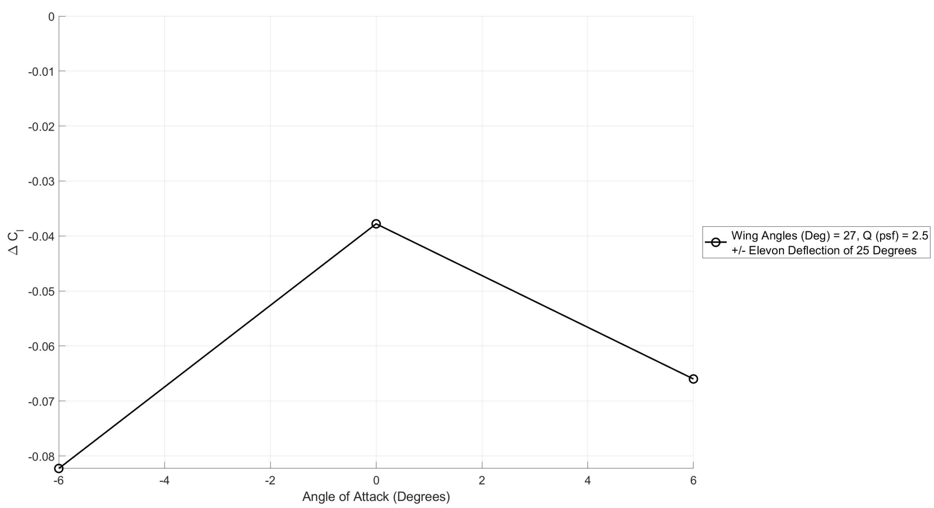

Figure 406. Wing angles 27 degrees trim point Δ C_l vs angle of attack for elevon deflection.

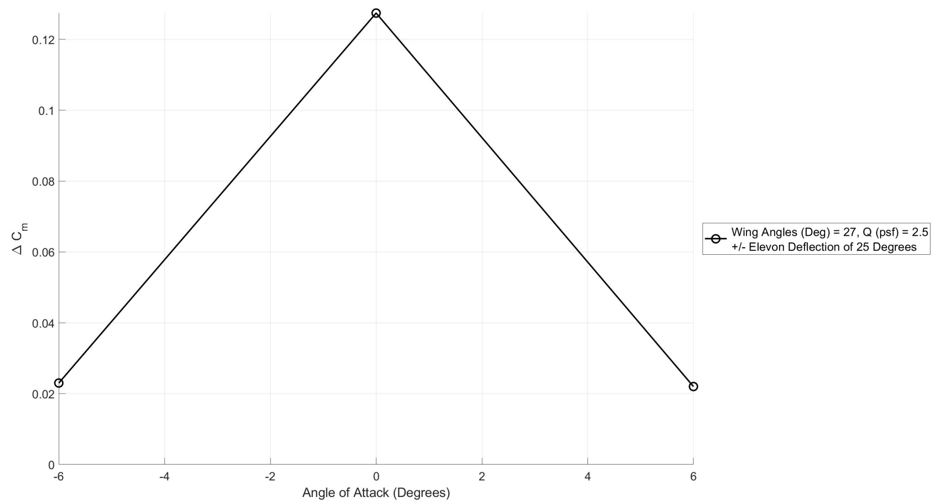

Figure 407. Wing angles 27 degrees trim point Δ C_m vs angle of attack for elevon deflection.

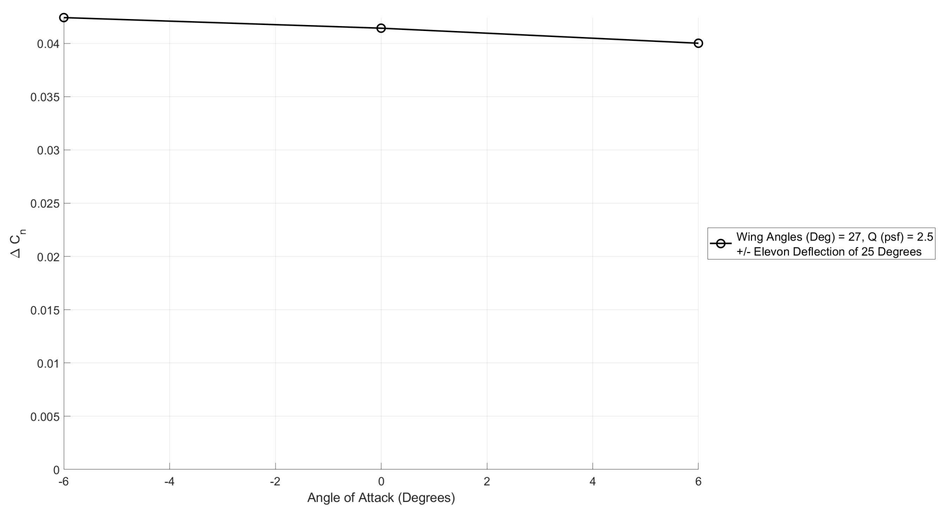

Figure 408. Wing angles 27 degrees trim point Δ C_n vs angle of attack for elevon deflection.

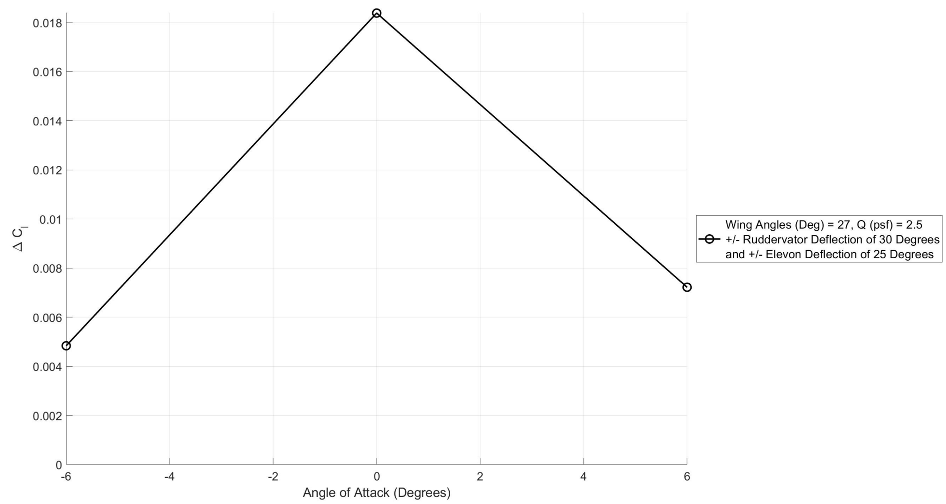

Figure 409. Wing angles 27 degrees trim point Δ C_l vs angle of attack for elevon and ruddervator deflection.

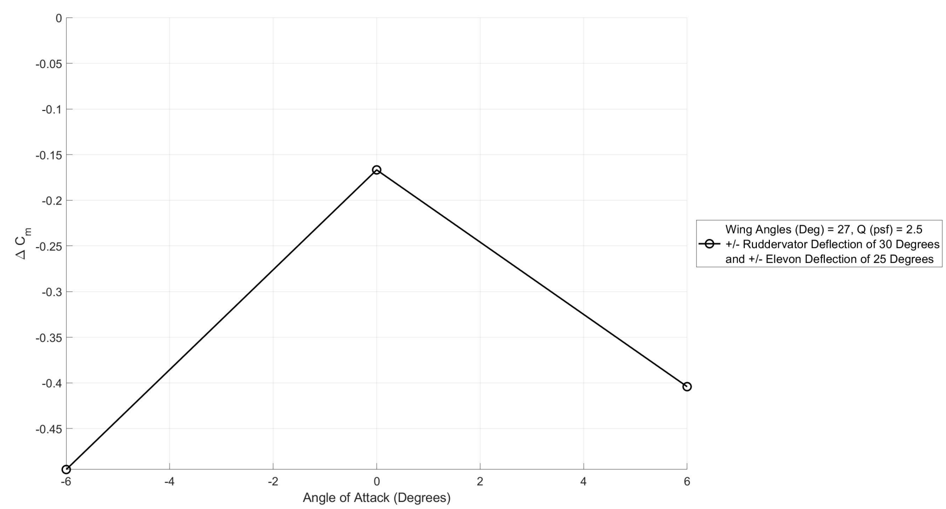

Figure 410. Wing angles 27 degrees trim point Δ C_m vs angle of attack for elevon and ruddervator deflection.

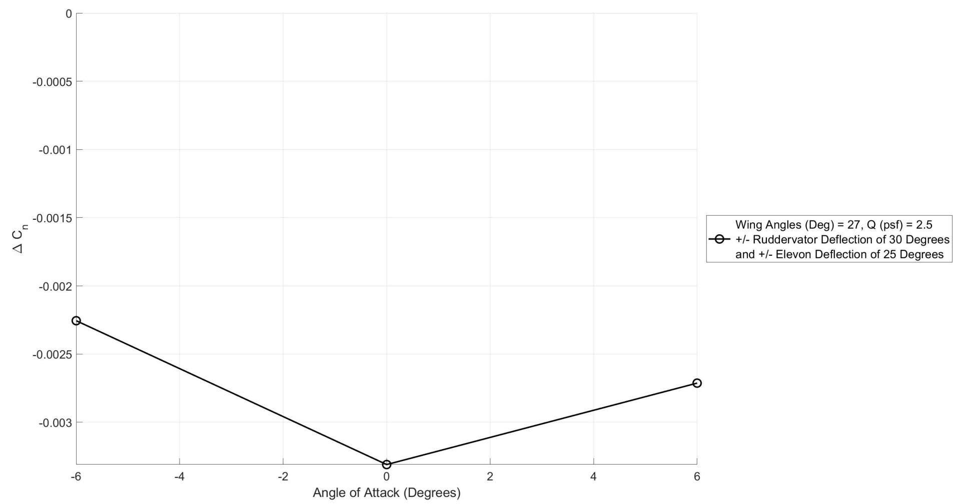

Figure 411. Wing angles 27 degrees trim point Δ C_n vs angle of attack for elevon and ruddervator deflection.

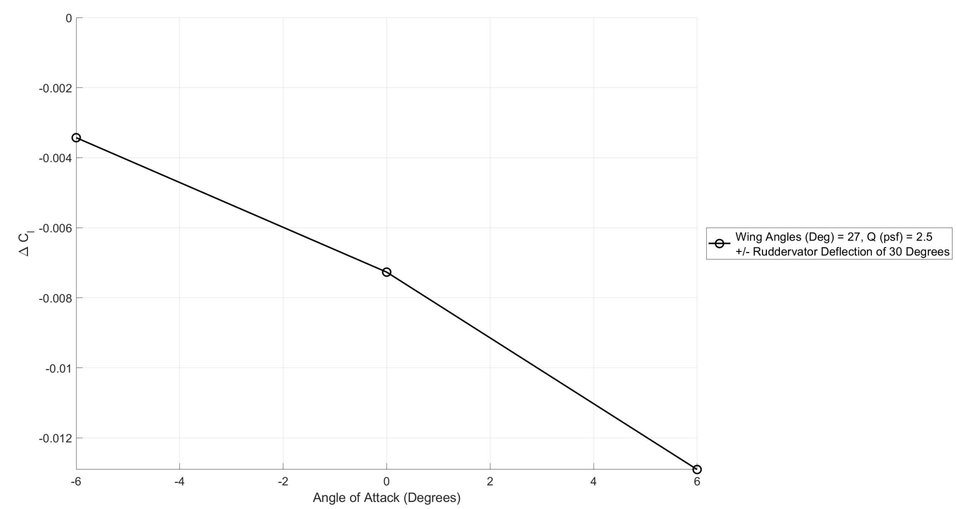

Figure 412. Wing angles 27 degrees trim point Δ C_l vs angle of attack for ruddervator deflection.

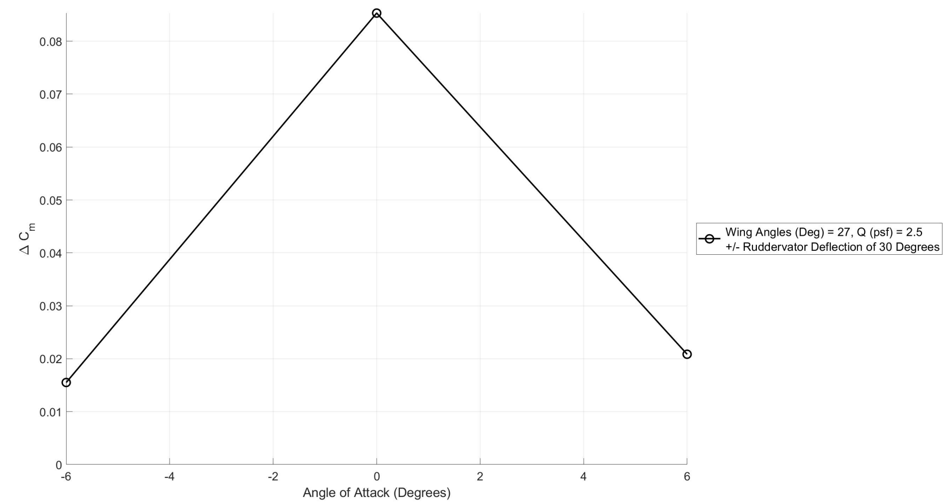

Figure 413. Wing angles 27 degrees trim point Δ C_m vs angle of attack for ruddervator deflection.

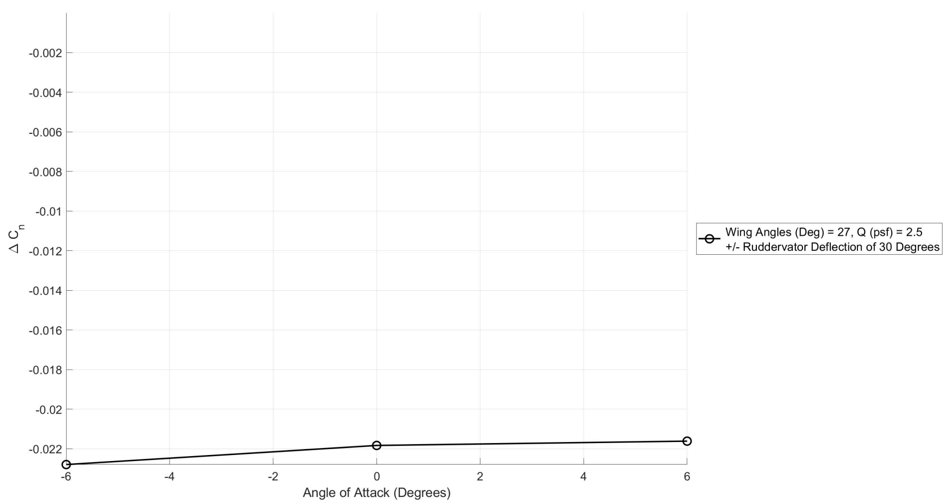

Figure 414. Wing angles 27 degrees trim point Δ C_n vs angle of attack for ruddervator deflection.

C.10 Transition Wing Angles 23 Degrees Performance and Stability Plots

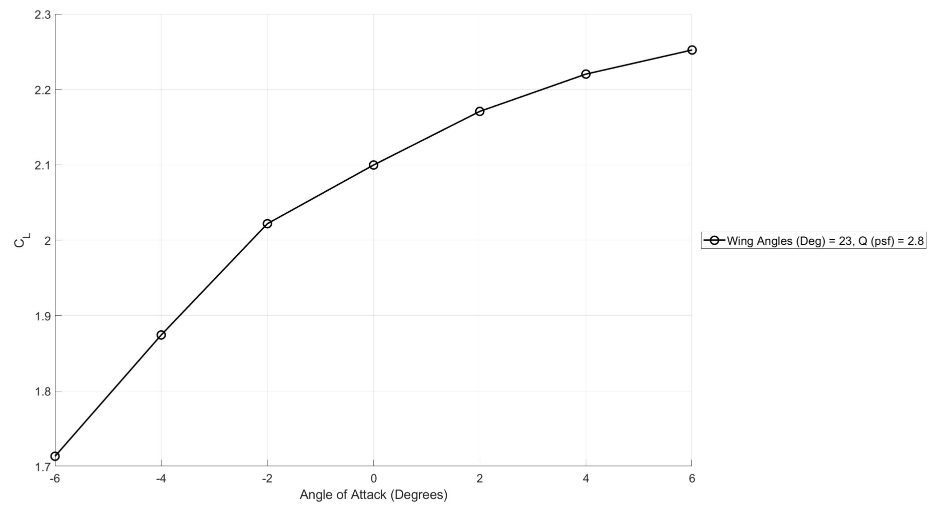

Figure 415. Wing angles 23 degrees trim point C_L vs angle of attack.

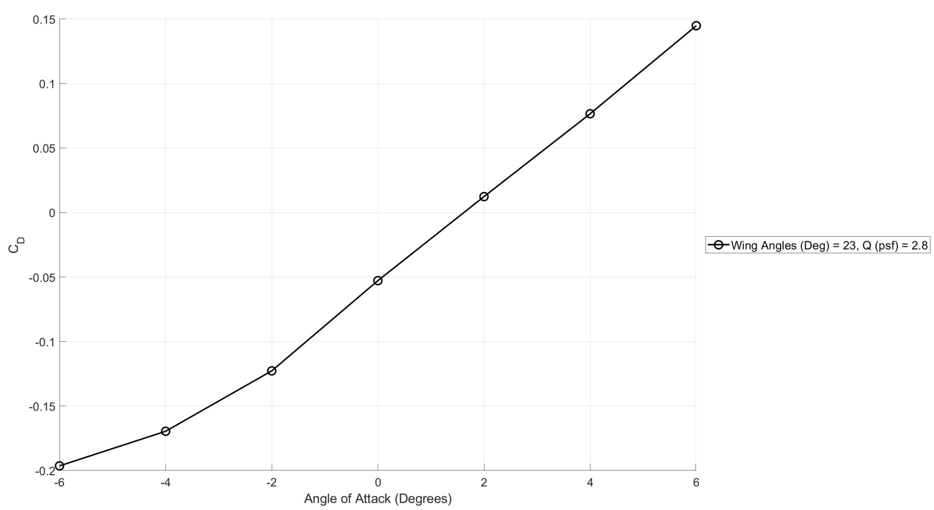

Figure 416. Wing angles 23 degrees trim point C_D vs angle of attack.

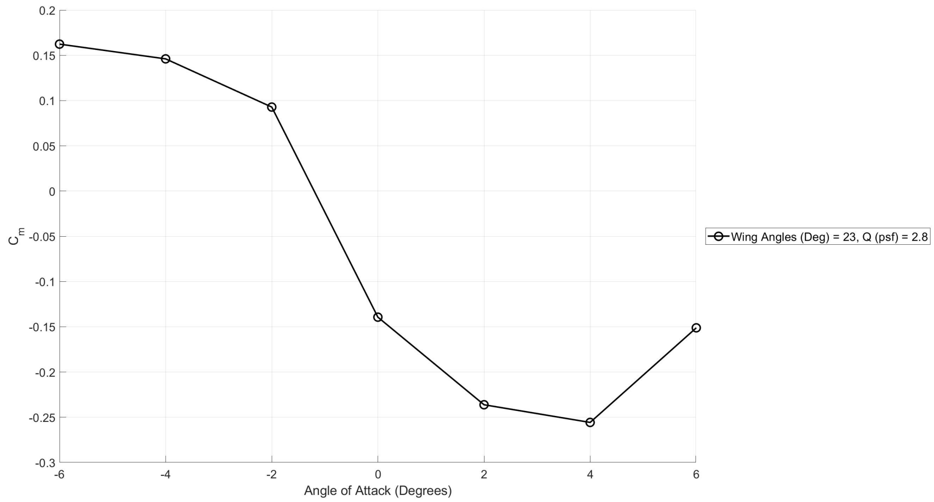

Figure 417. Wing angles 23 degrees trim point C_m vs angle of attack.

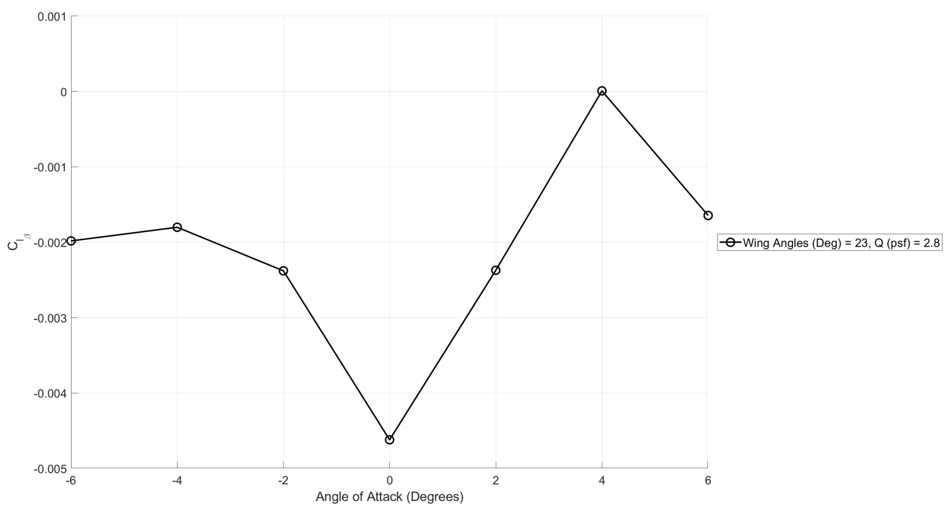

Figure 418. Wing angles 23 degrees trim point C_{l_β} vs angle of attack.

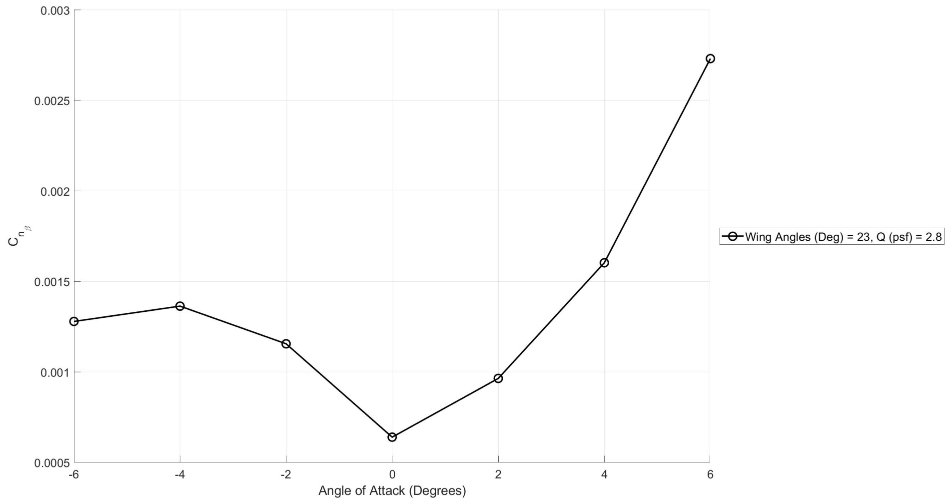

Figure 419. Wing angles 23 degrees trim point C_{n_β} vs angle of attack.

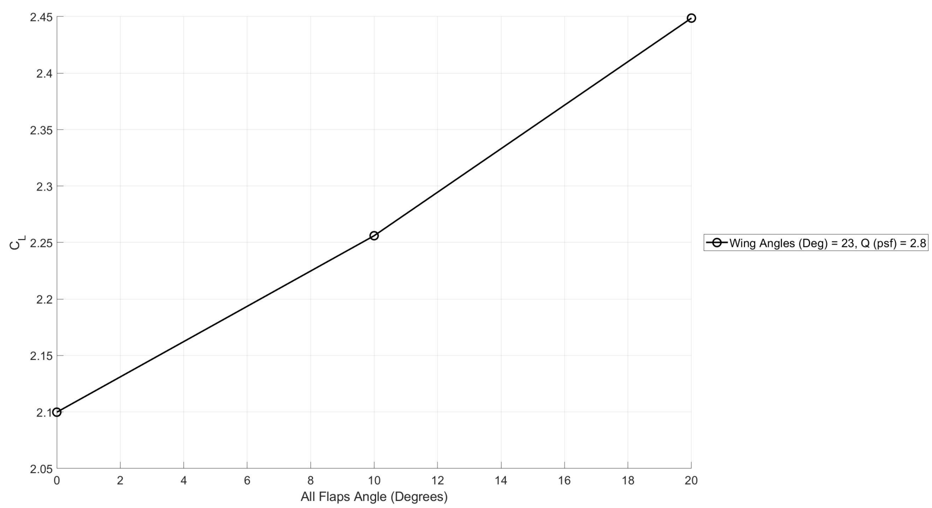

Figure 420. Wing angles 23 degrees trim point C_L vs all flap deflection angle.

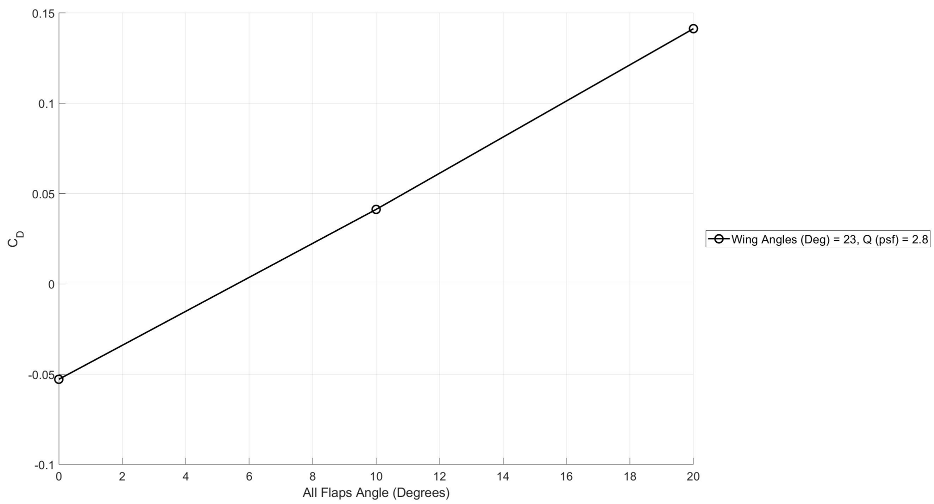

Figure 421. Wing angles 23 degrees trim point C_D vs all flap deflection angle.

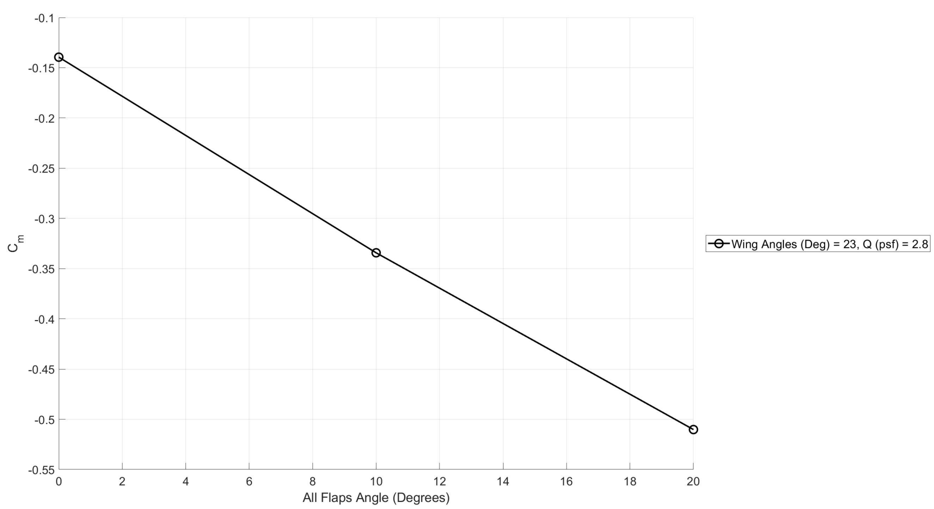

Figure 422. Wing angles 23 degrees trim point C_m vs all flap deflection angle.

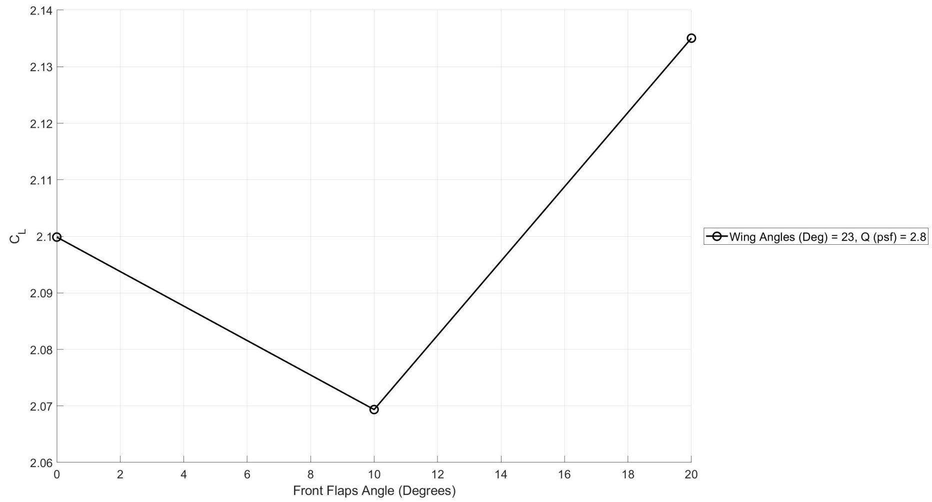

Figure 423. Wing angles 23 degrees trim point C_L vs front flap deflection angle.

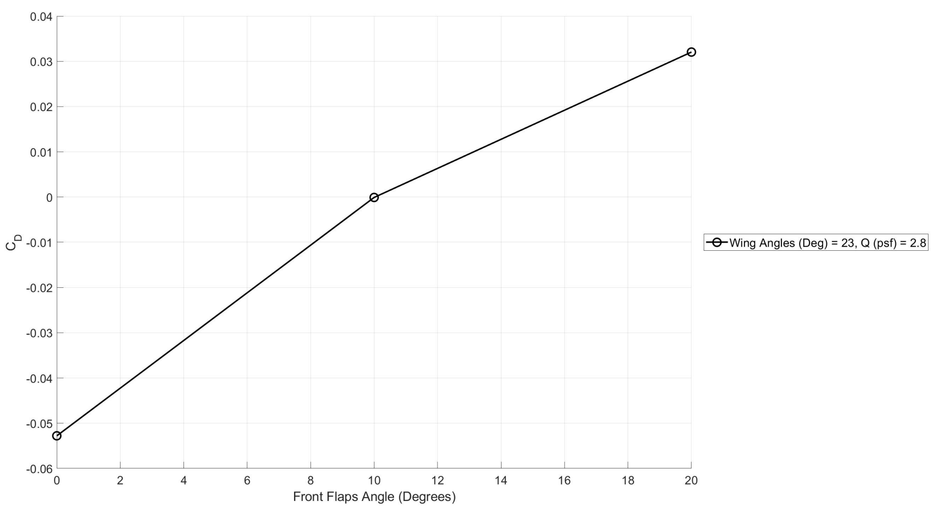

Figure 424. Wing angles 23 degrees trim point C_D vs front flap deflection angle.

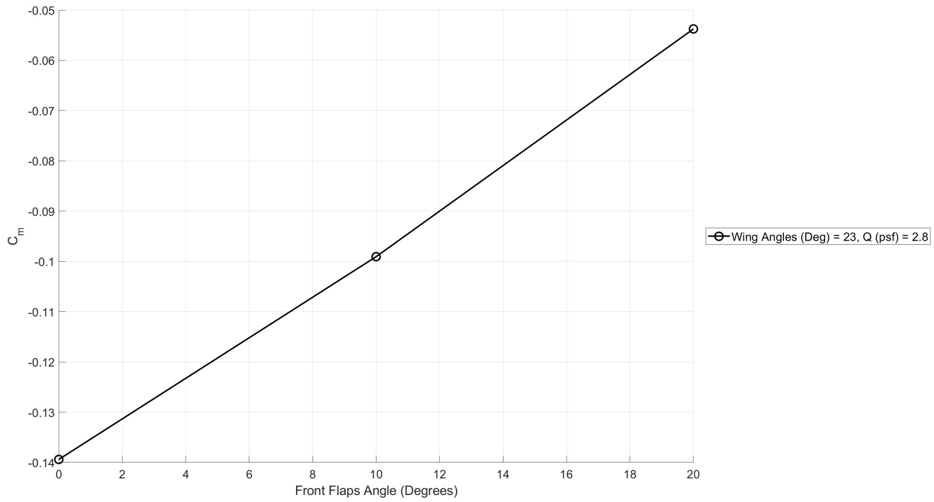

Figure 425. Wing angles 23 degrees trim point C_m vs front flap deflection angle.

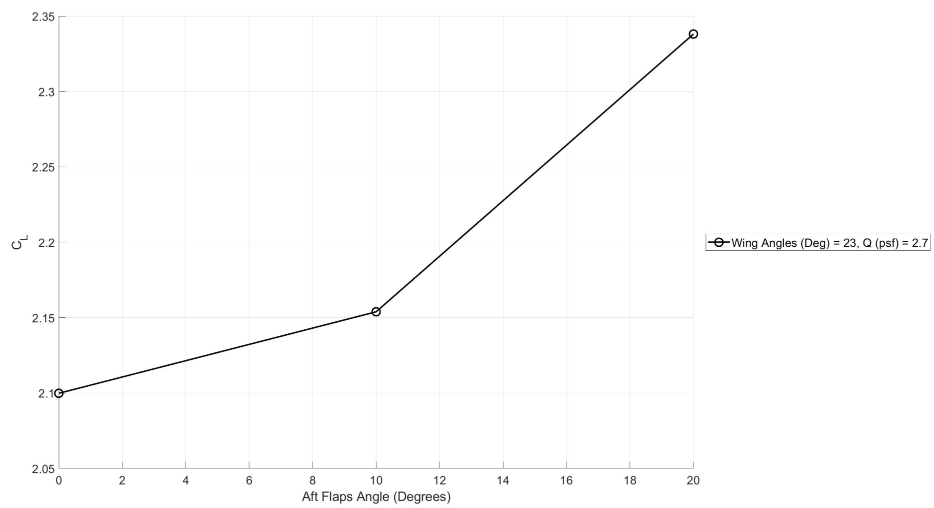

Figure 426. Wing angles 23 degrees trim point C_L vs aft flap deflection angle.

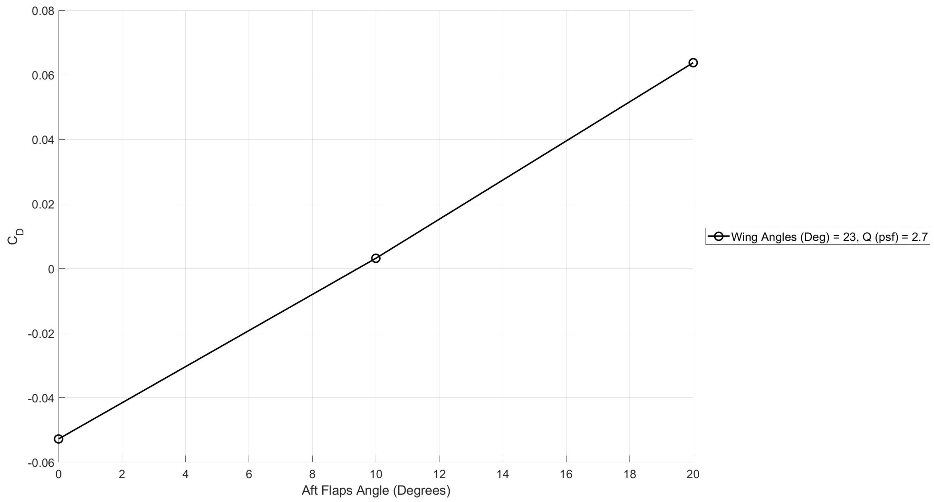

Figure 427. Wing angles 23 degrees trim point C_D vs aft flap deflection angle.

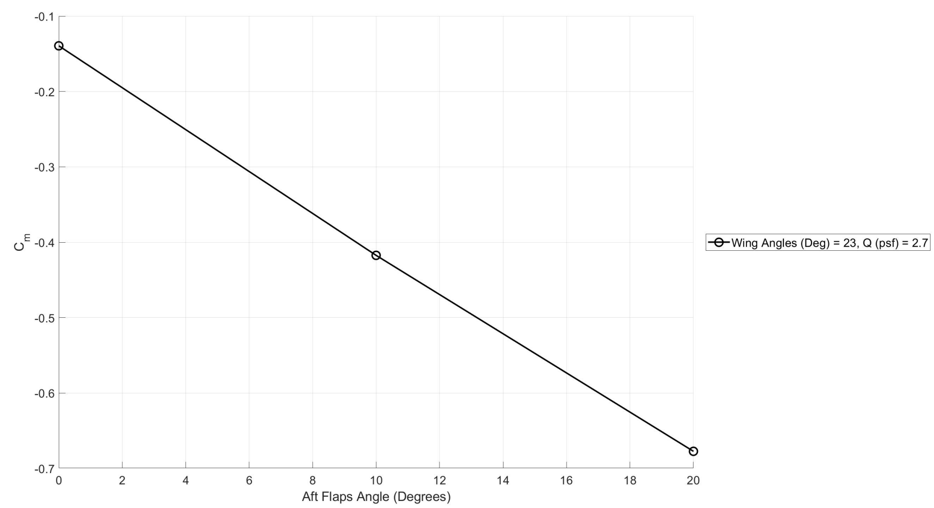

Figure 428. Wing angles 23 degrees trim point C_m vs aft flap deflection angle.

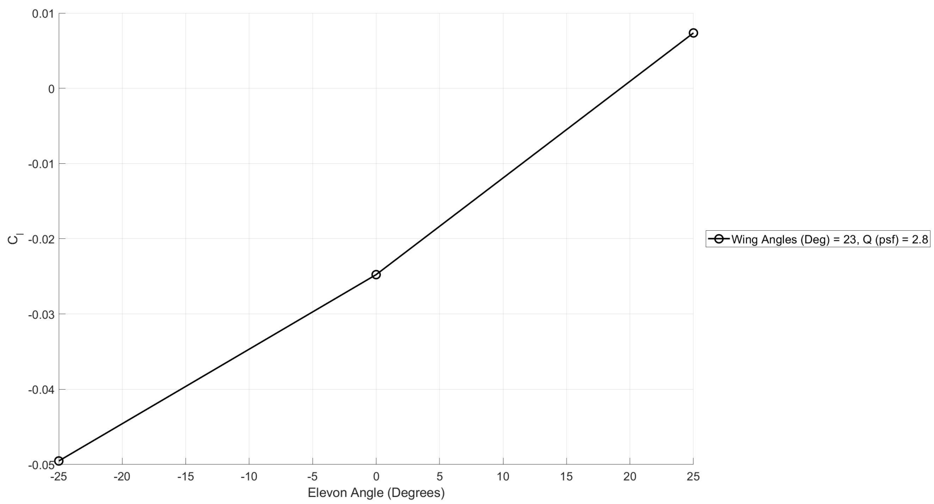

Figure 429. Wing angles 23 degrees trim point C_l vs elevon deflection angle.

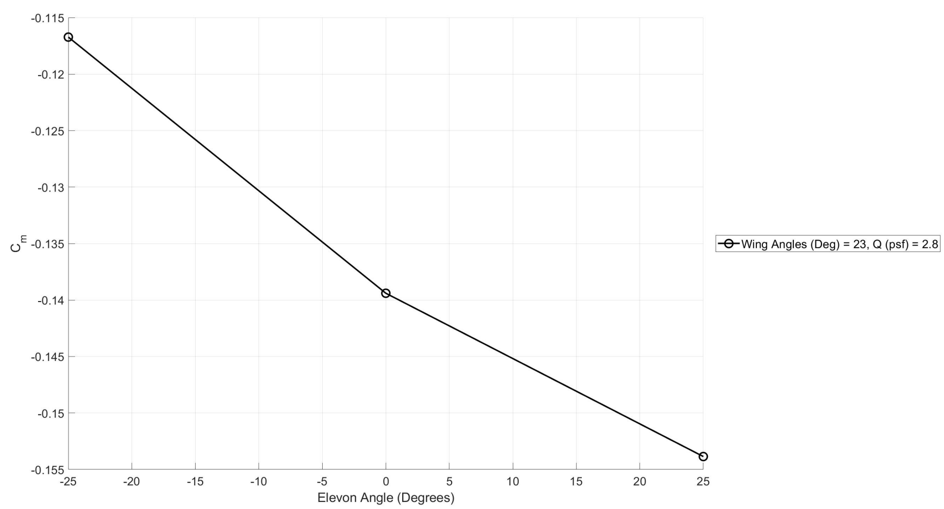

Figure 430. Wing angles 23 degrees trim point C_m vs elevon deflection angle.

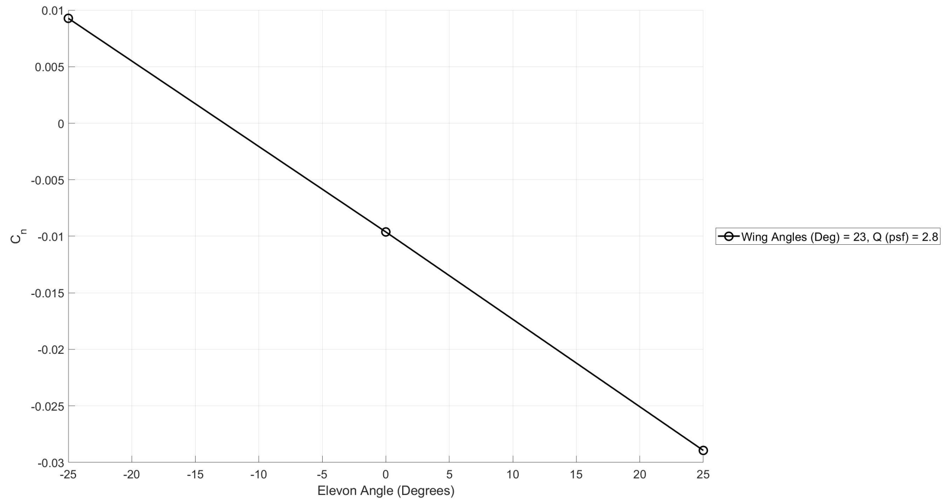

Figure 431. Wing angles 23 degrees trim point C_n vs elevon deflection angle.

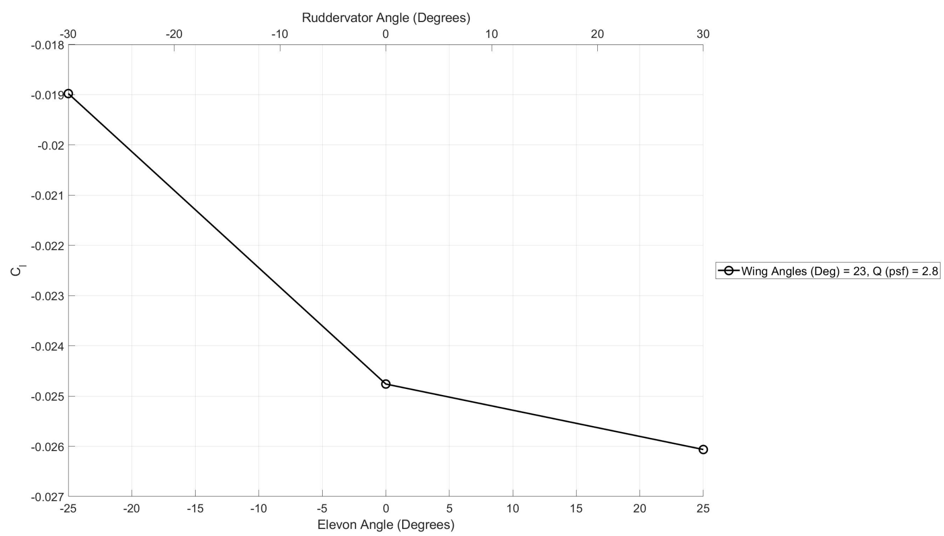

Figure 432. Wing angles 23 degrees trim point C_l vs elevon and ruddervator deflection angles.

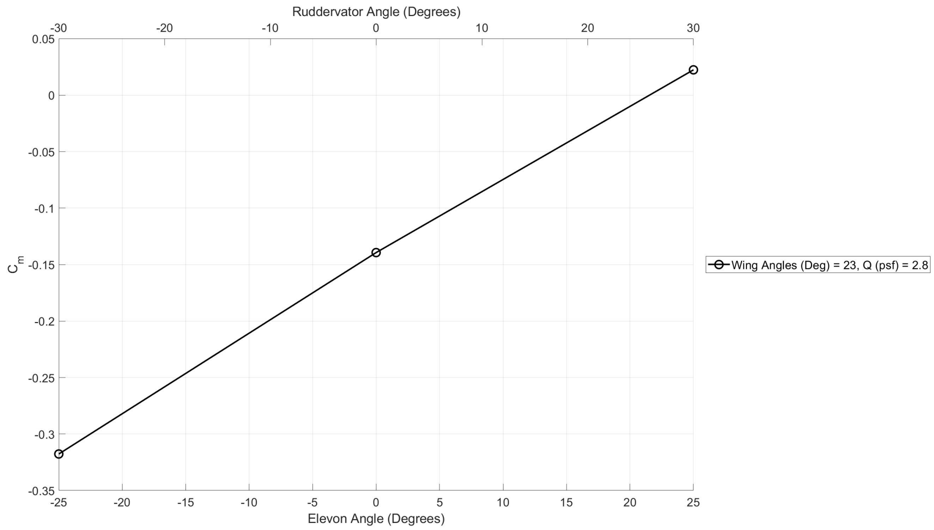

Figure 433. Wing angles 23 degrees trim point C_m vs elevon and ruddervator deflection angles.

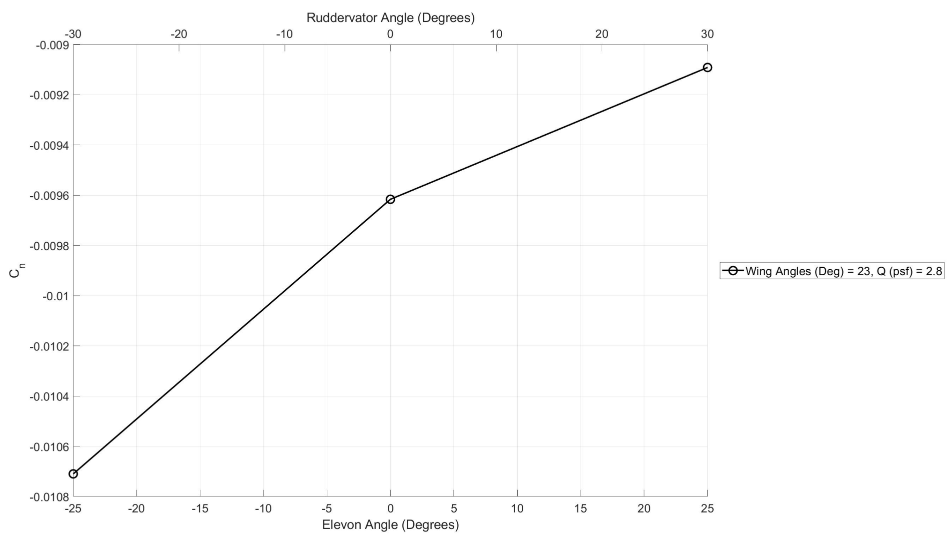

Figure 434. Wing angles 23 degrees trim point C_n vs elevon and ruddervator deflection angles.

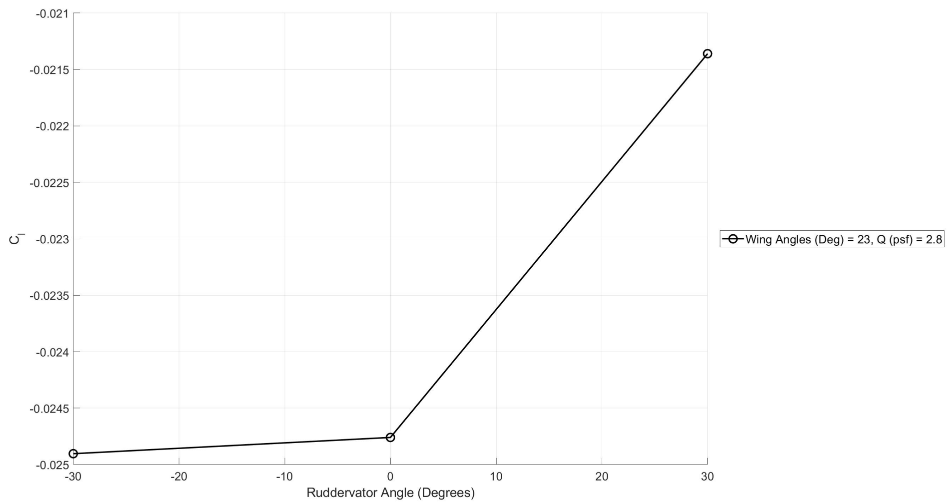

Figure 435. Wing angles 23 degrees trim point C_l vs ruddervator deflection angle.

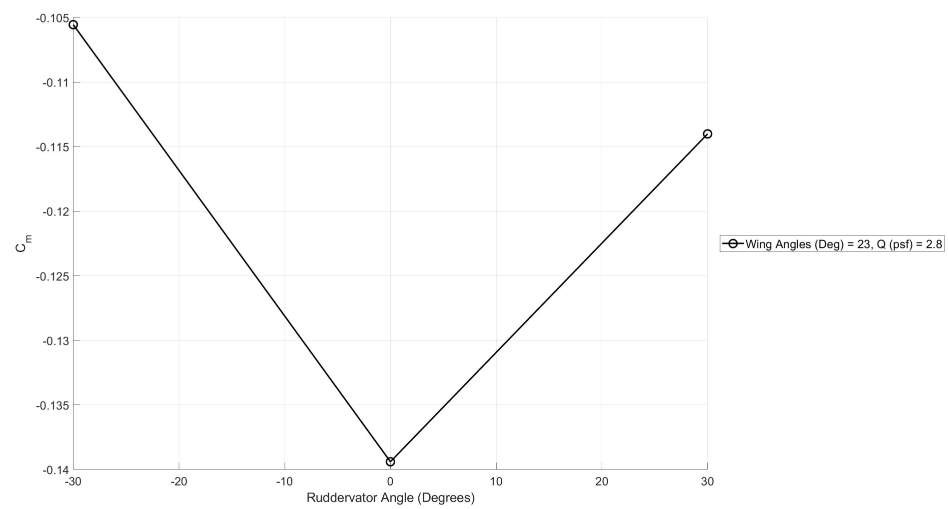

Figure 436. Wing angles 23 degrees trim point C_m vs ruddervator deflection angle.

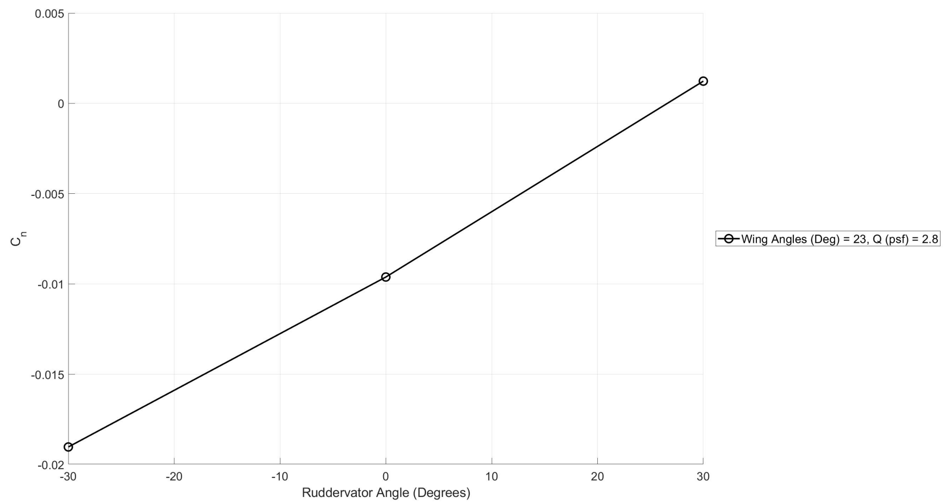

Figure 437. Wing angles 23 degrees trim point C_n vs ruddervator deflection angle.

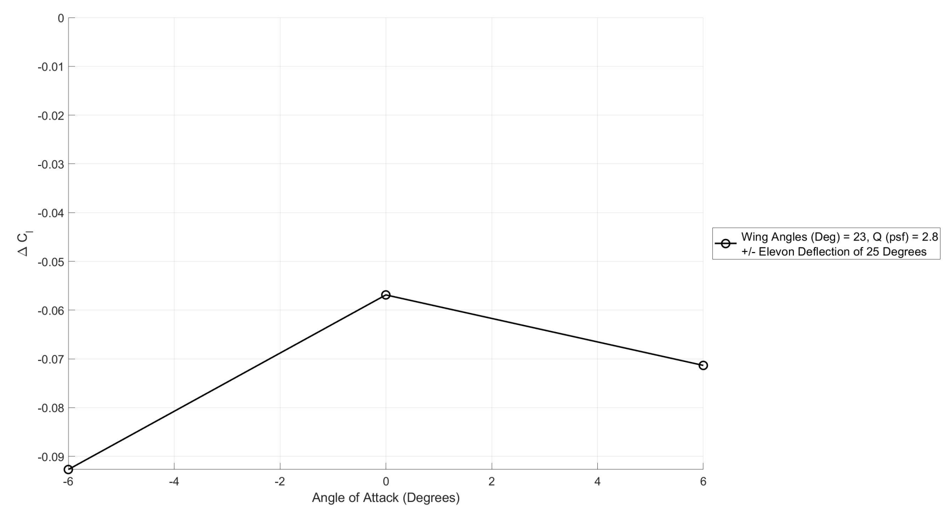

Figure 438. Wing angles 23 degrees trim point Δ C_l vs angle of attack for elevon deflection.

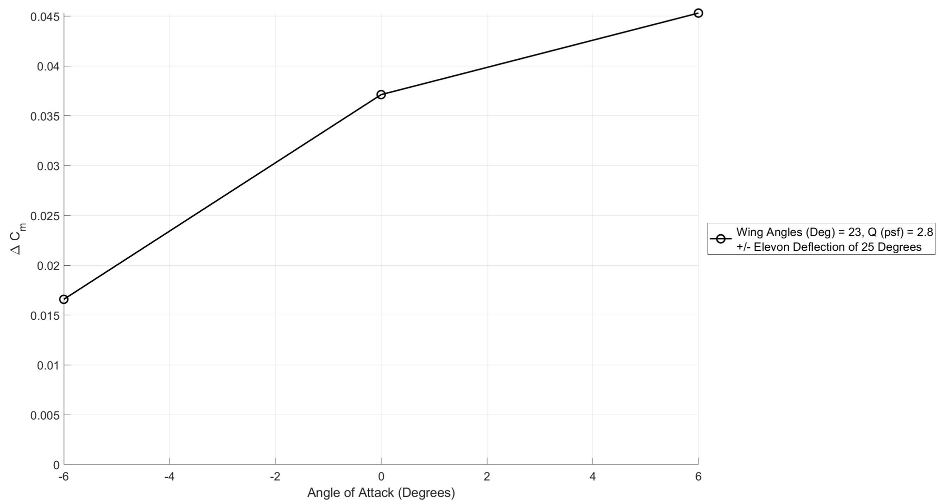

Figure 439. Wing angles 23 degrees trim point Δ C_m vs angle of attack for elevon deflection.

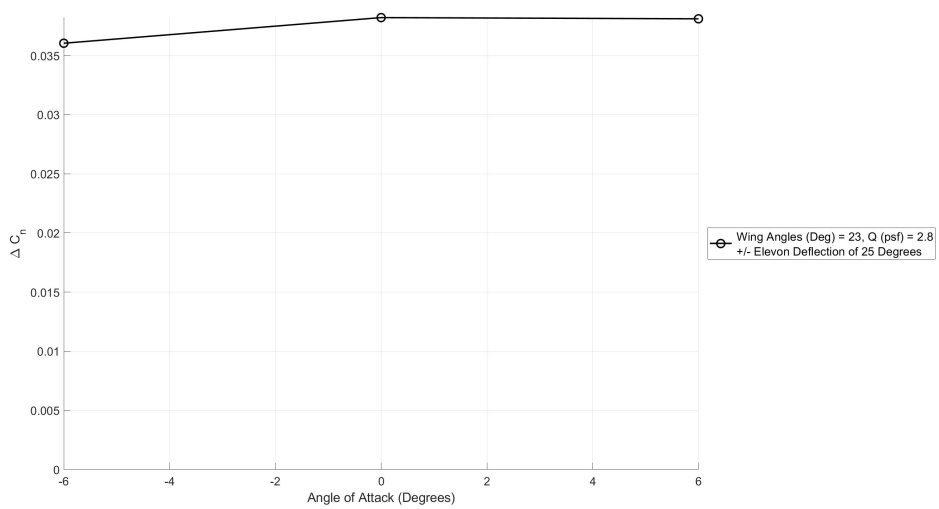

Figure 440. Wing angles 23 degrees trim point Δ C_n vs angle of attack for elevon deflection.

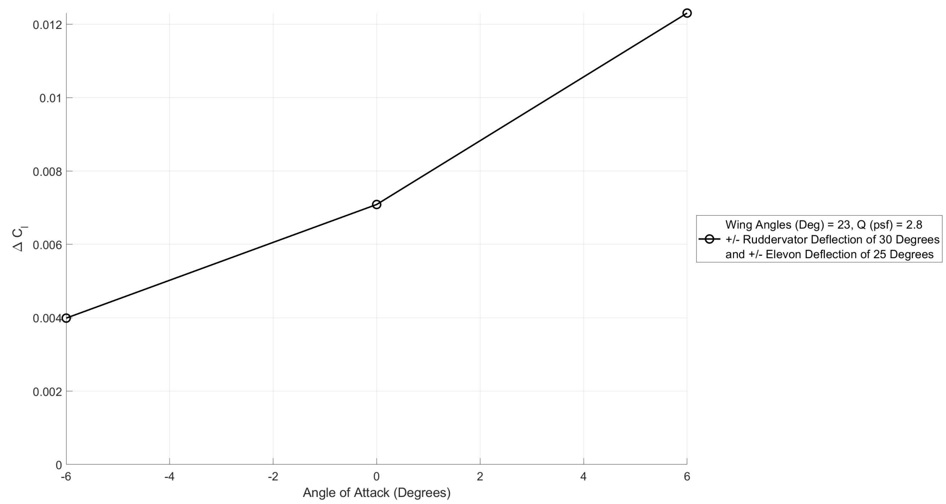

Figure 441. Wing angles 23 degrees trim point Δ C_l vs angle of attack for elevon and ruddervator deflection.

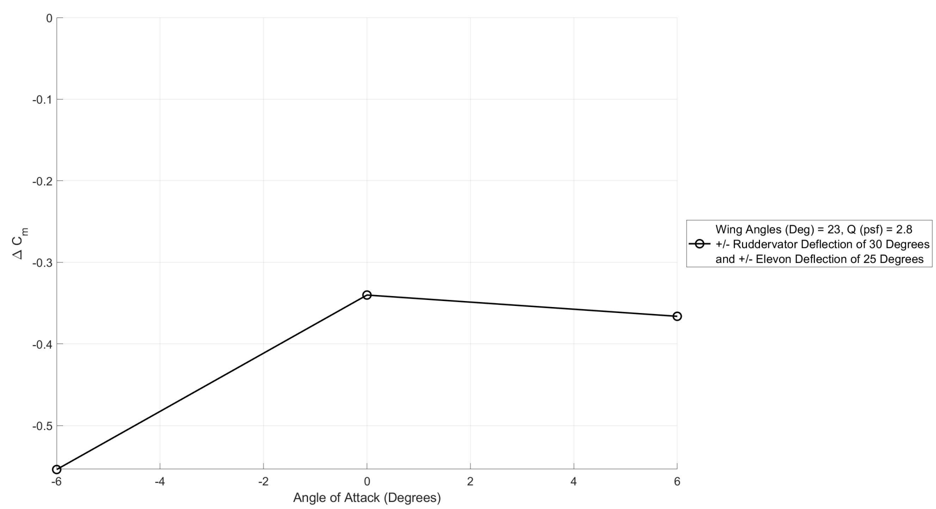

Figure 442. Wing angles 23 degrees trim point Δ C_m vs angle of attack for elevon and ruddervator deflection.

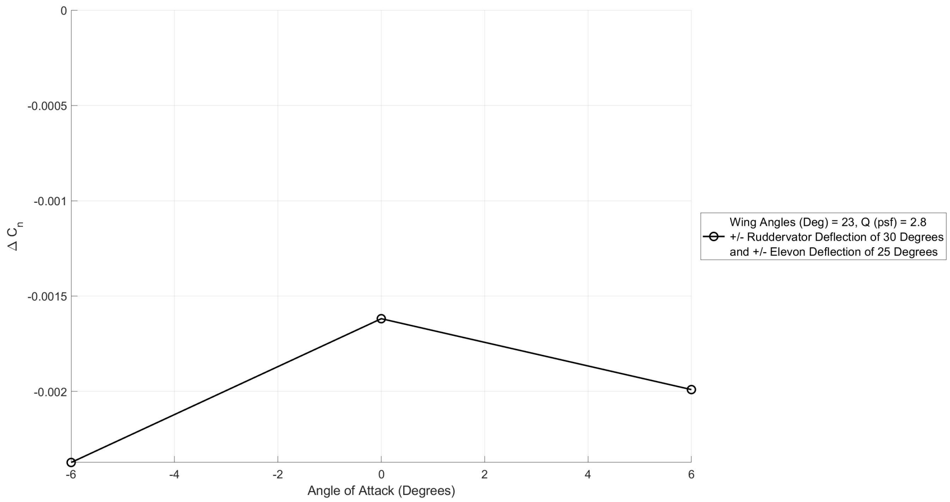

Figure 443. Wing angles 23 degrees trim point Δ C_n vs angle of attack for elevon and ruddervator deflection.

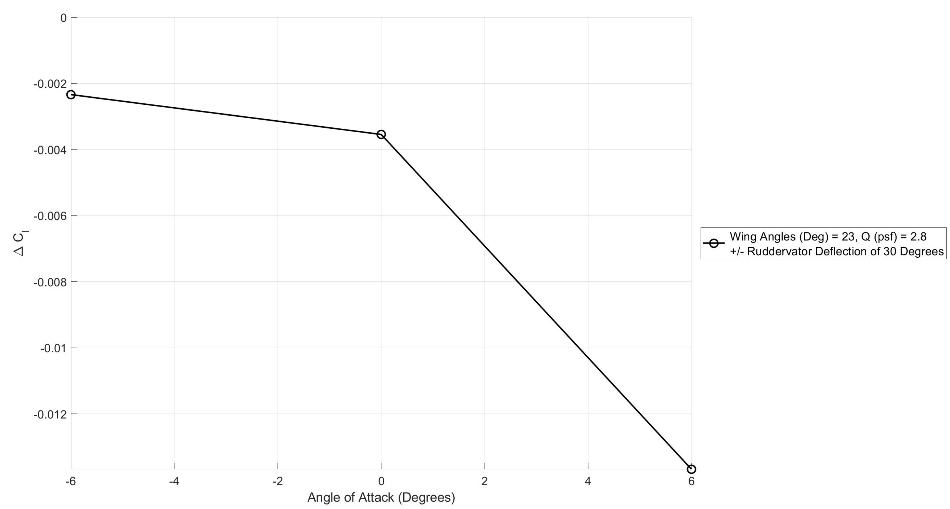

Figure 444. Wing angles 23 degrees trim point Δ C_l vs angle of attack for ruddervator deflection.

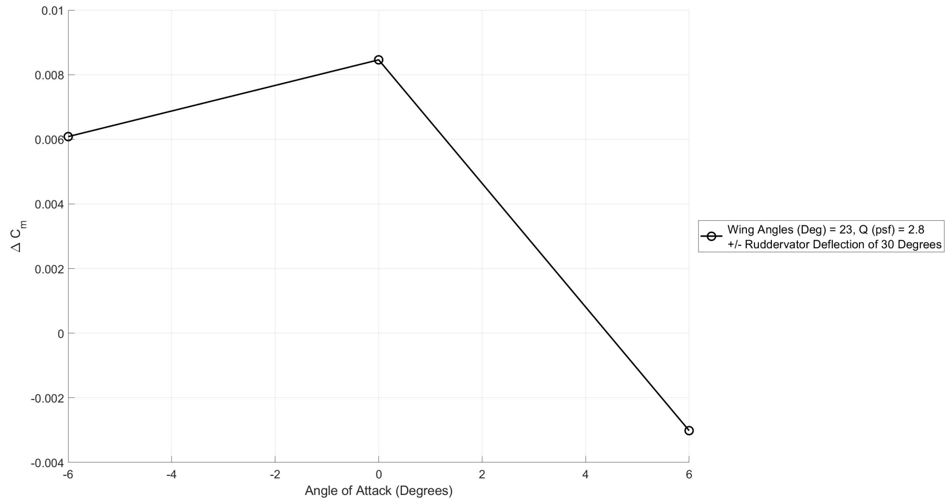

Figure 445. Wing angles 23 degrees trim point Δ C_m vs angle of attack for ruddervator deflection.

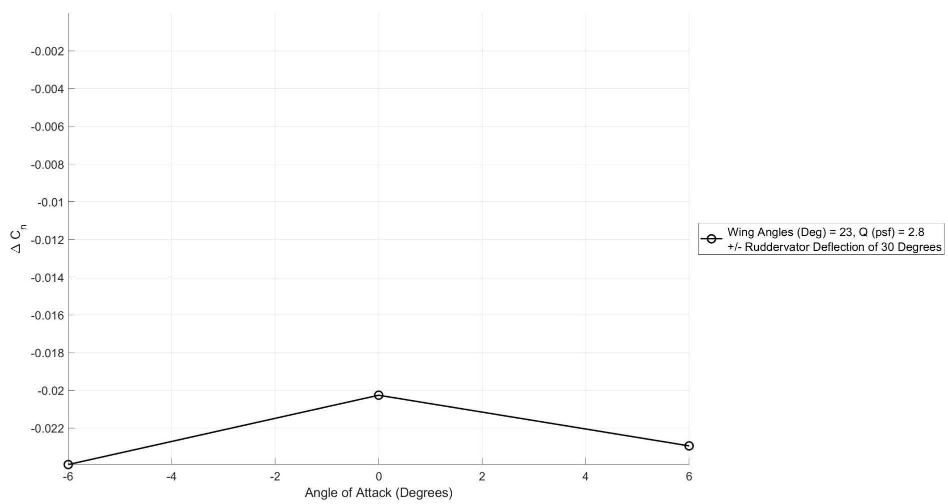

Figure 446. Wing angles 23 degrees trim point Δ C_n vs angle of attack for ruddervator deflection.

C.11 Transition Wing Angles 21 Degrees Performance and Stability Plots

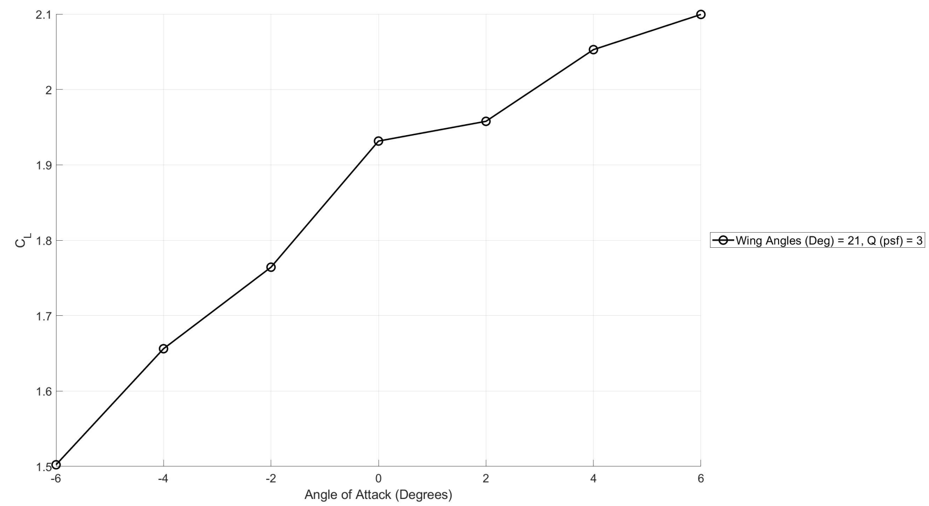

Figure 447. Wing angles 21 degrees trim point C_L vs angle of attack.

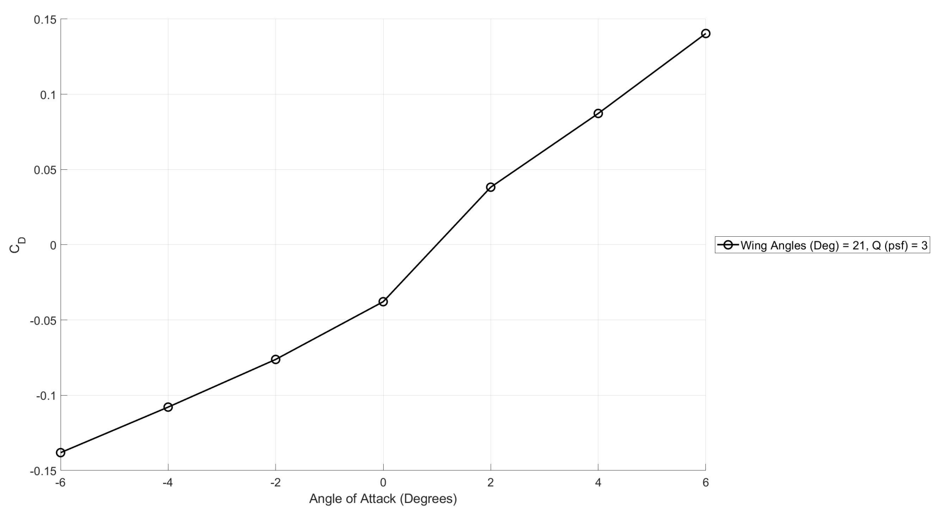

Figure 448. Wing angles 21 degrees trim point C_D vs angle of attack.

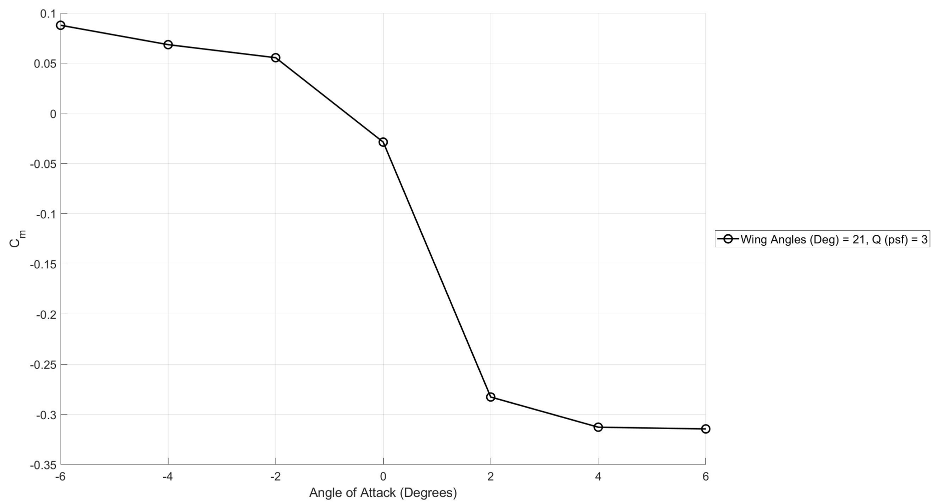

Figure 449. Wing angles 21 degrees trim point C_m vs angle of attack.

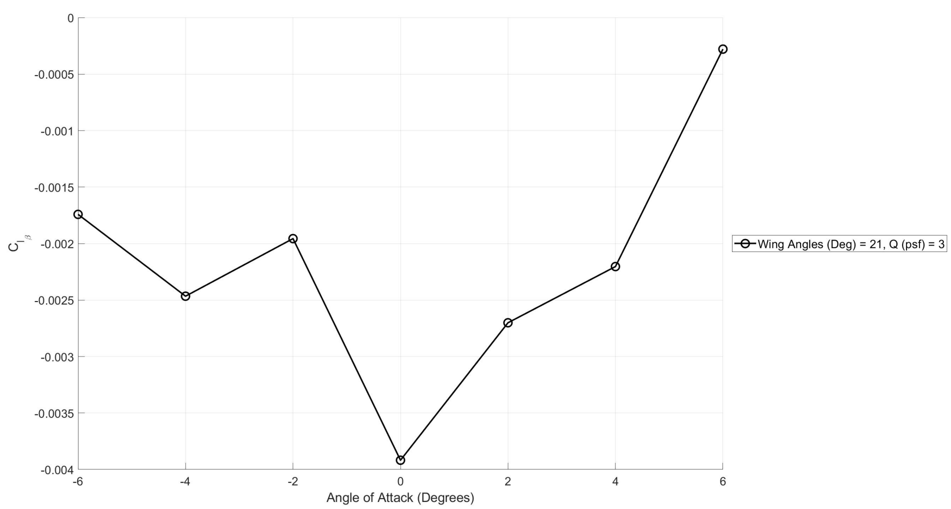

Figure 450. Wing angles 21 degrees trim point C_{l_β} vs angle of attack.

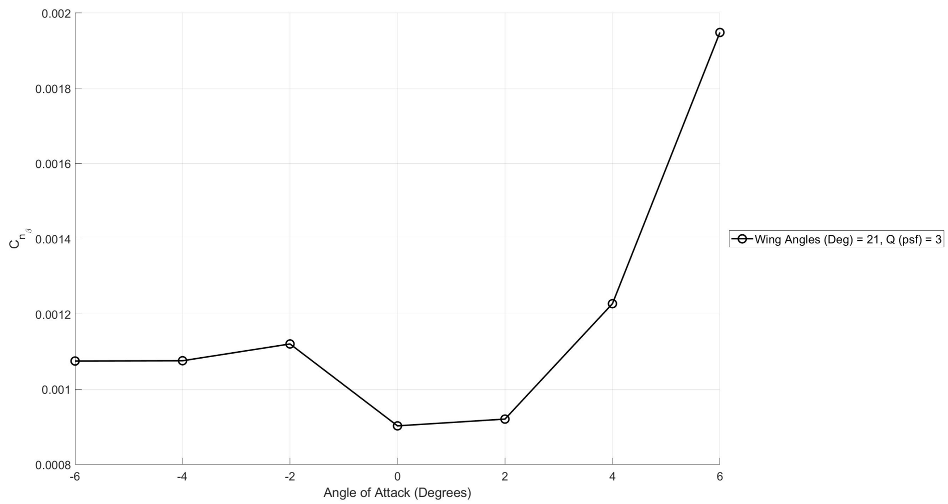

Figure 451. Wing angles 21 degrees trim point C_{n_β} vs angle of attack.

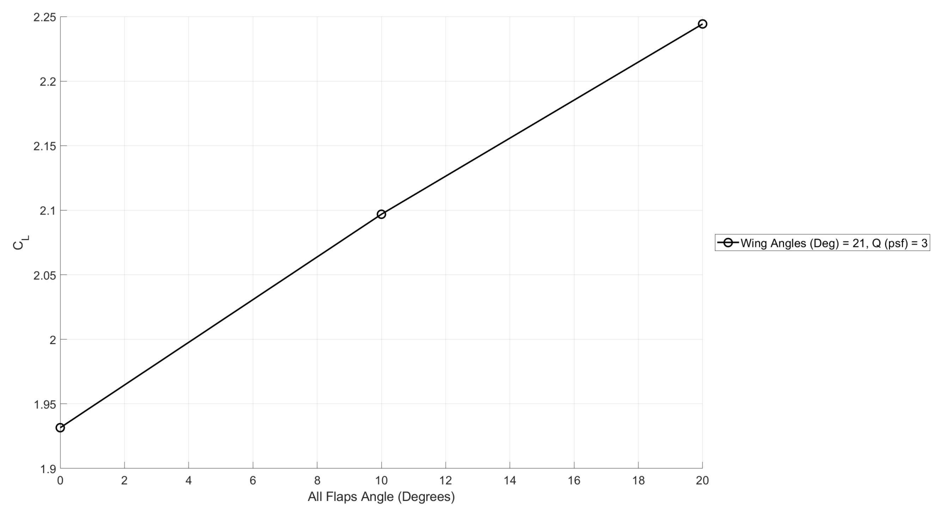

Figure 452. Wing angles 21 degrees trim point C_L vs all flap deflection angle.

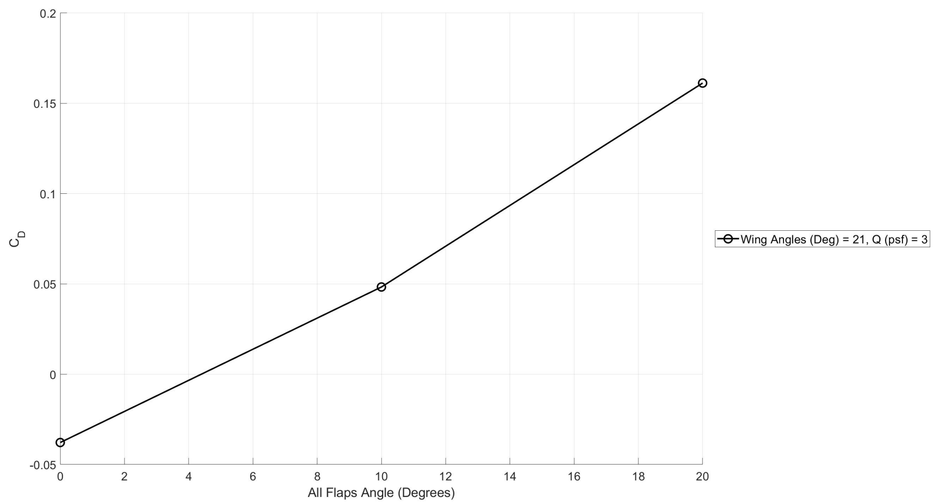

Figure 453. Wing angles 21 degrees trim point C_D vs all flap deflection angle.

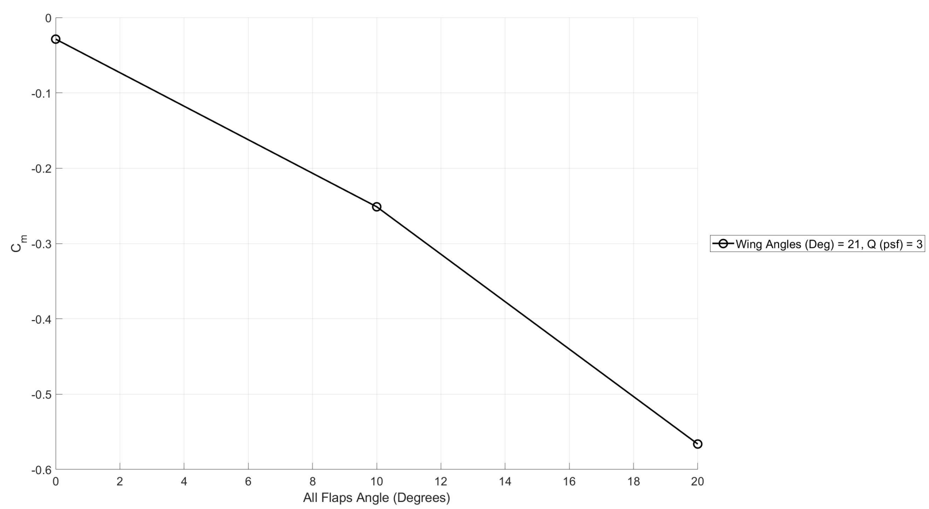

Figure 454. Wing angles 21 degrees trim point C_m vs all flap deflection angle.

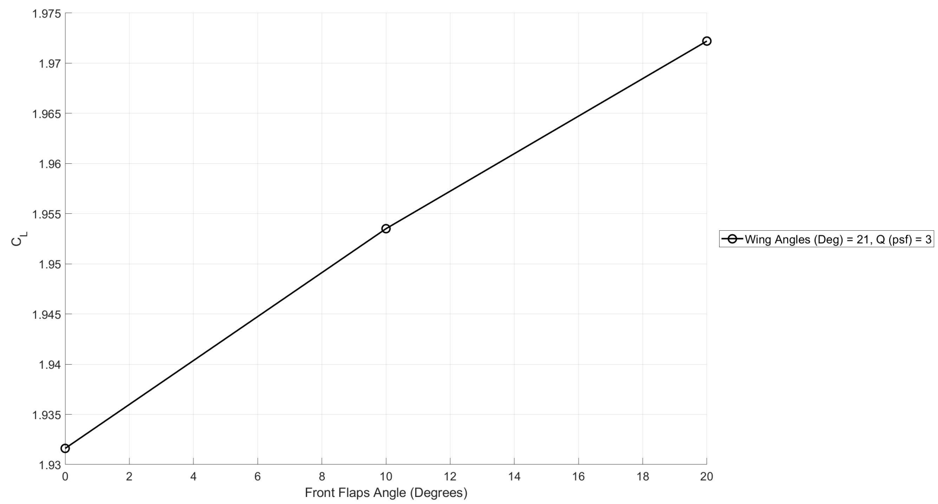

Figure 455. Wing angles 21 degrees trim point C_L vs front flap deflection angle.

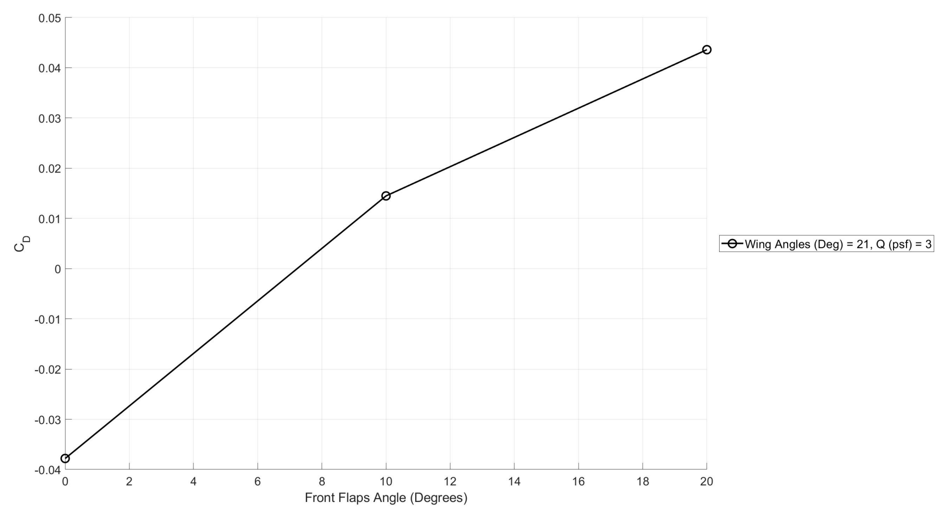

Figure 456. Wing angles 21 degrees trim point C_D vs front flap deflection angle.

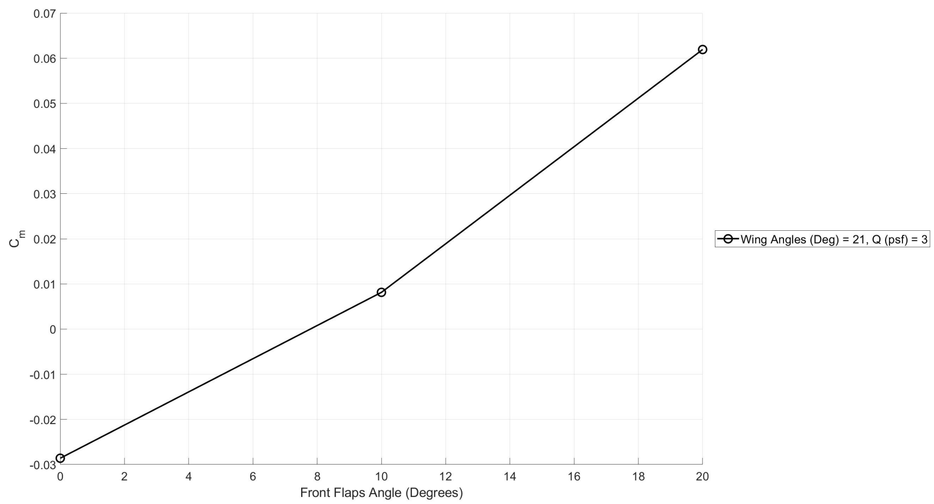

Figure 457. Wing angles 21 degrees trim point C_m vs front flap deflection angle.

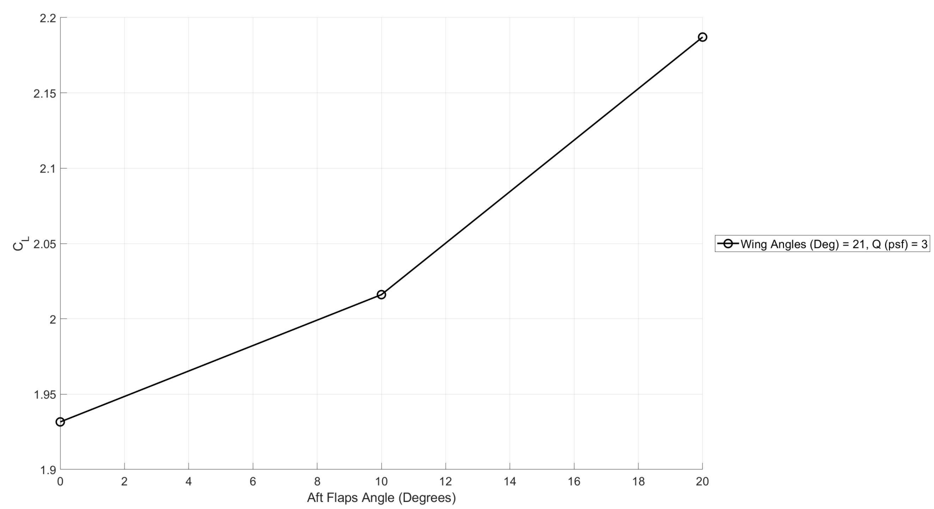

Figure 458. Wing angles 21 degrees trim point C_L vs aft flap deflection angle.

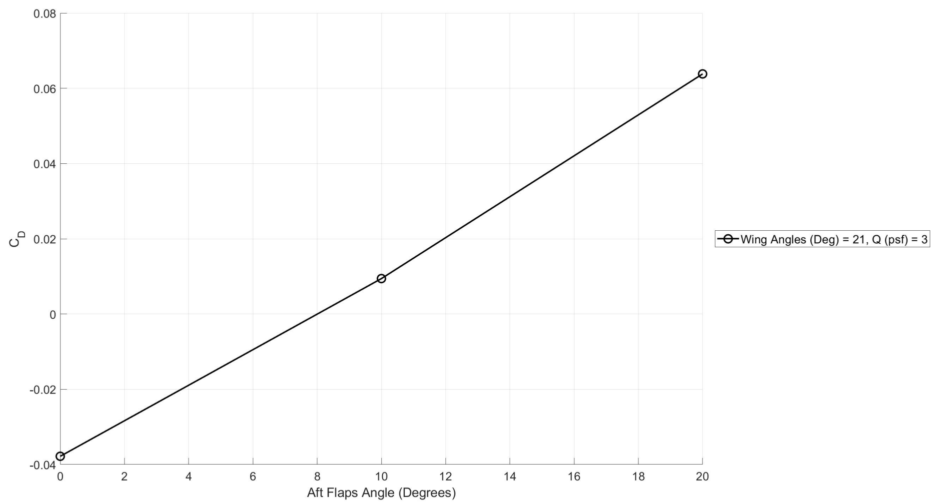

Figure 459. Wing angles 21 degrees trim point C_D vs aft flap deflection angle.

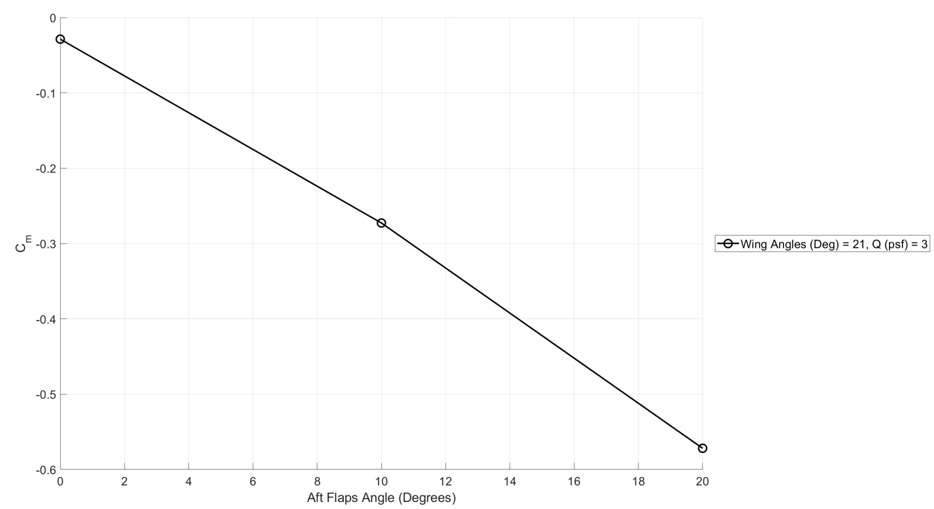

Figure 460. Wing angles 21 degrees trim point C_m vs aft flap deflection angle.

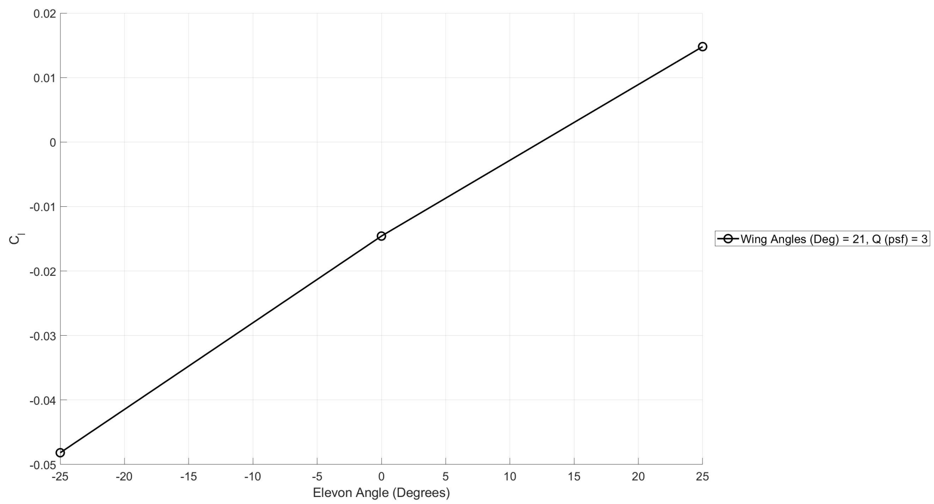

Figure 461. Wing angles 21 degrees trim point C_l vs elevon deflection angle.

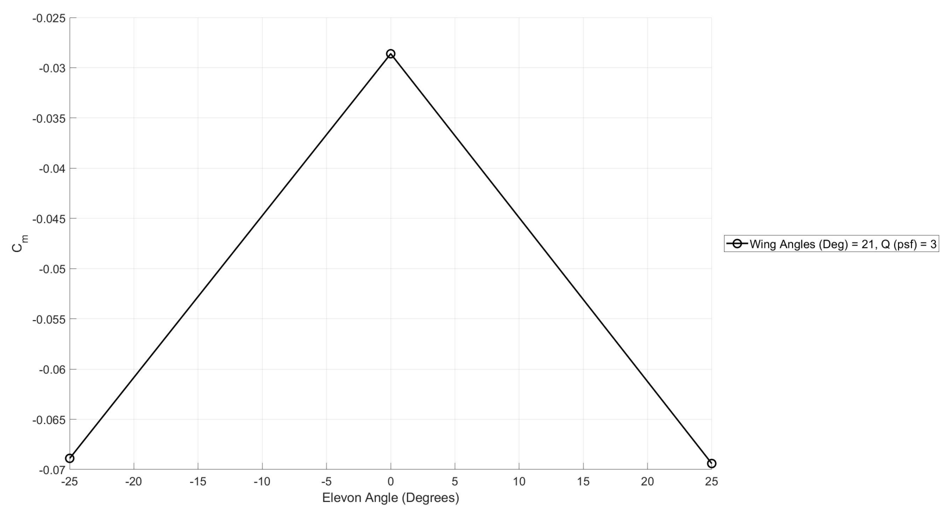

Figure 462. Wing angles 21 degrees trim point C_m vs elevon deflection angle.

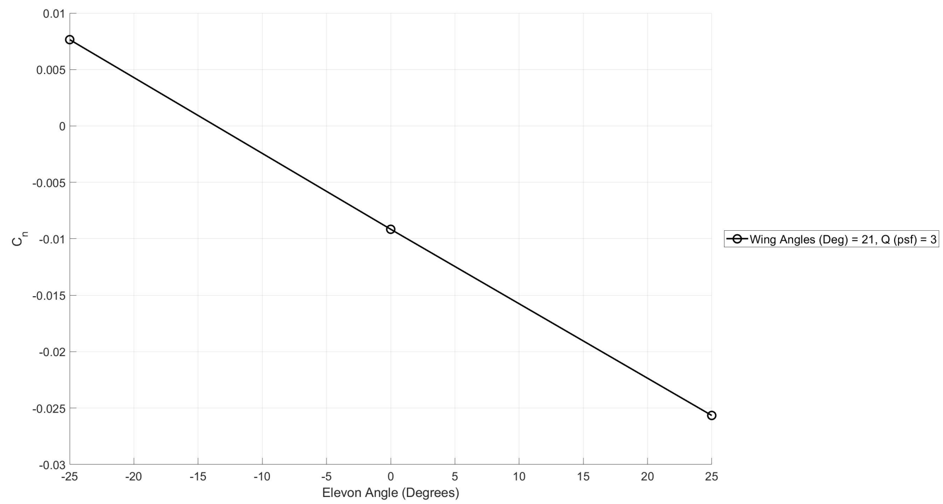

Figure 463. Wing angles 21 degrees trim point C_n vs elevon deflection angle.

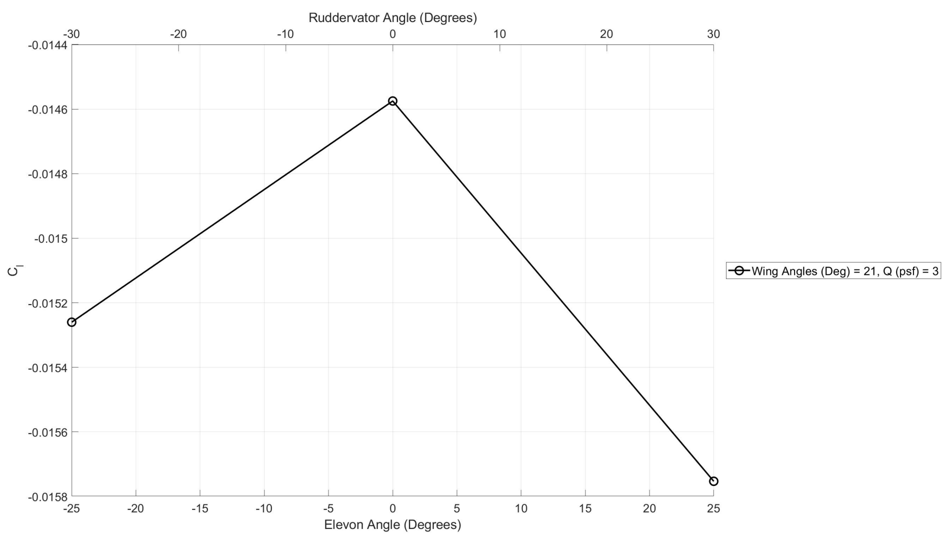

Figure 464. Wing angles 21 degrees trim point C_l vs elevon and ruddervator deflection angles.

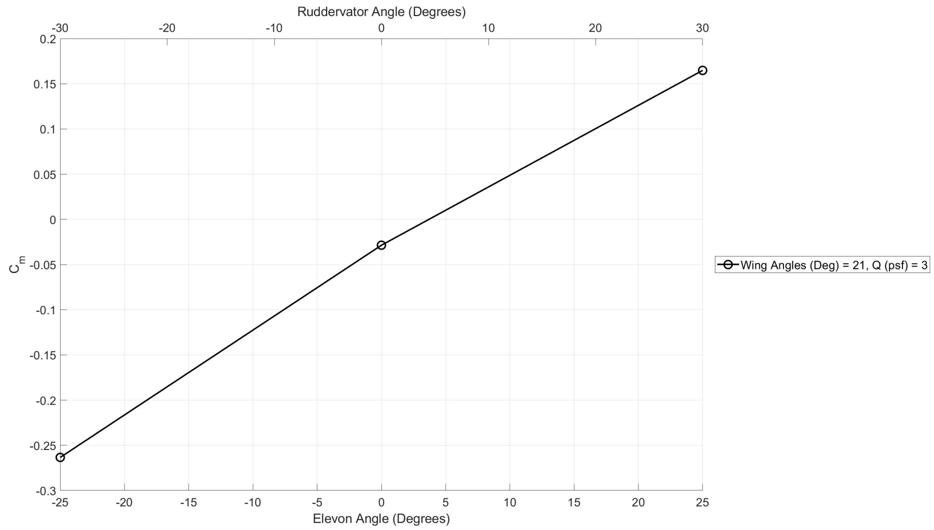

Figure 465. Wing angles 21 degrees trim point C_m vs elevon and ruddervator deflection angles.

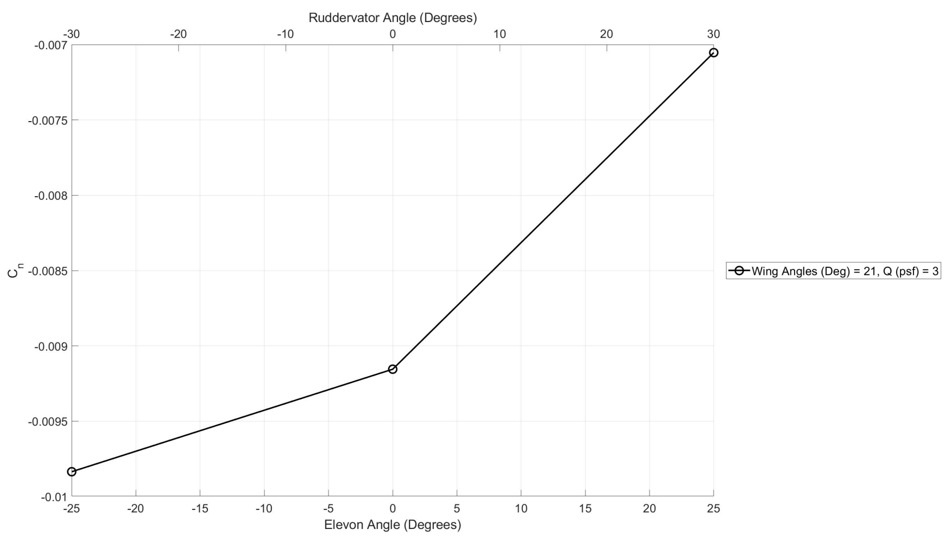

Figure 466. Wing angles 21 degrees trim point C_n vs elevon and ruddervator deflection angles.

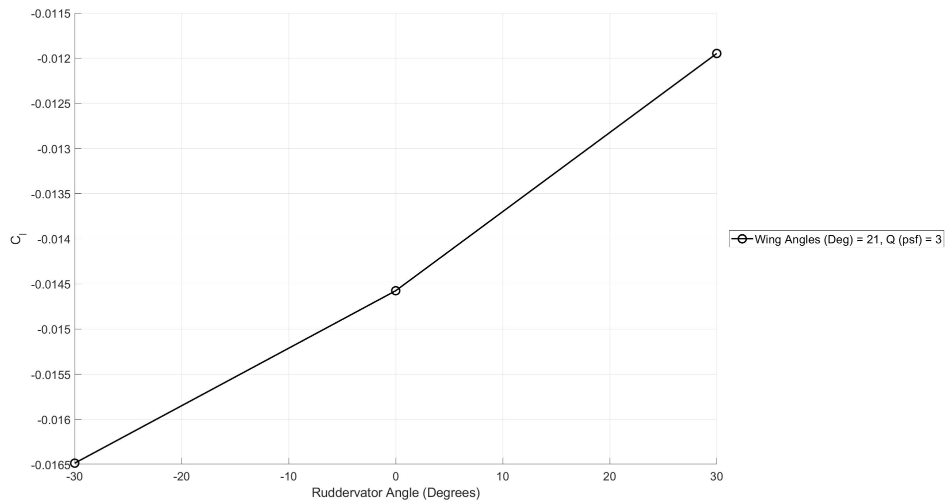

Figure 467. Wing angles 21 degrees trim point C_l vs ruddervator deflection angle.

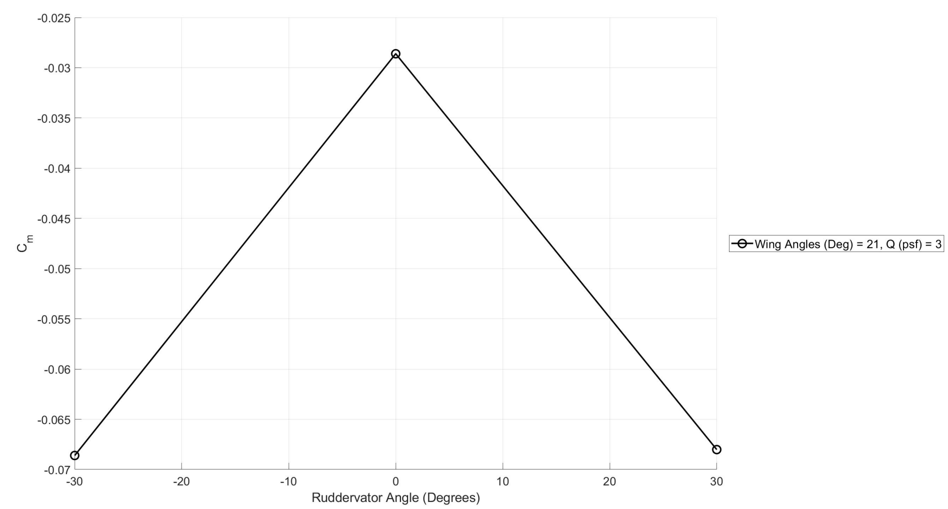

Figure 468. Wing angles 21 degrees trim point C_m vs ruddervator deflection angle.

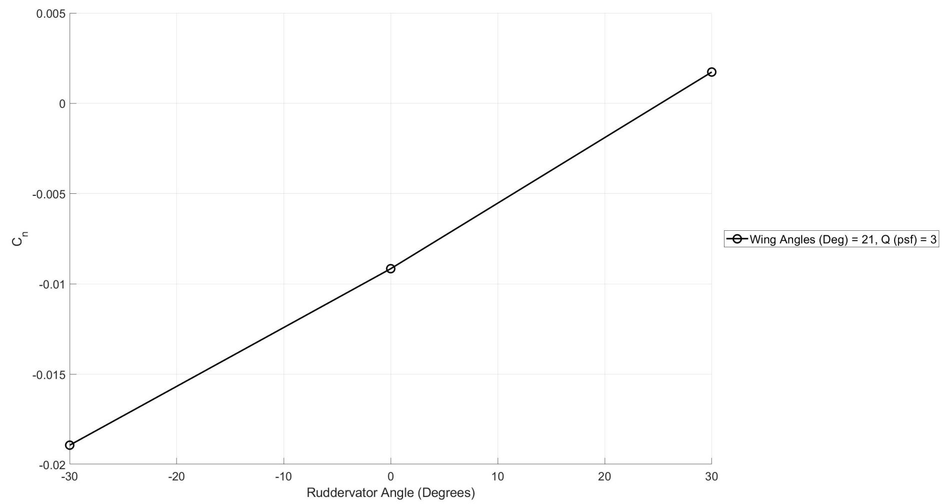

Figure 469. Wing angles 21 degrees trim point C_n vs ruddervator deflection angle.

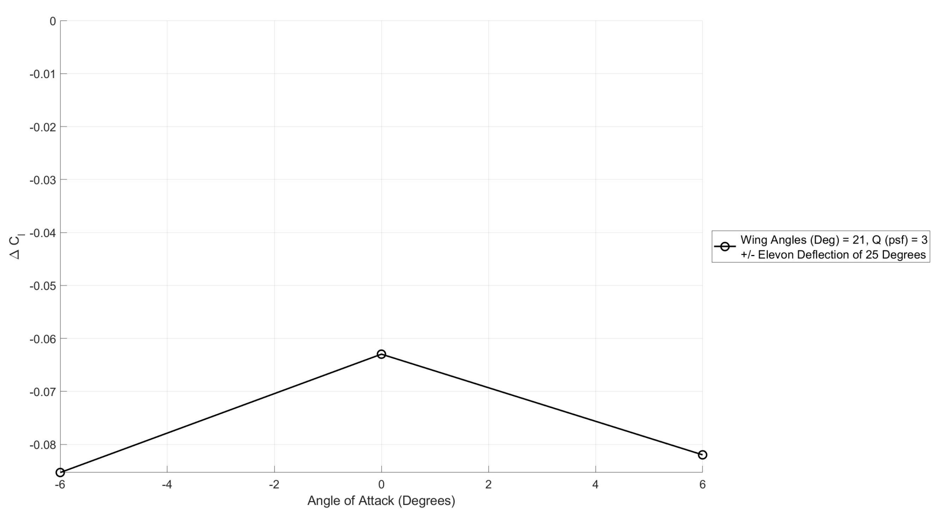

Figure 470. Wing angles 21 degrees trim point Δ C_l vs angle of attack for elevon deflection.

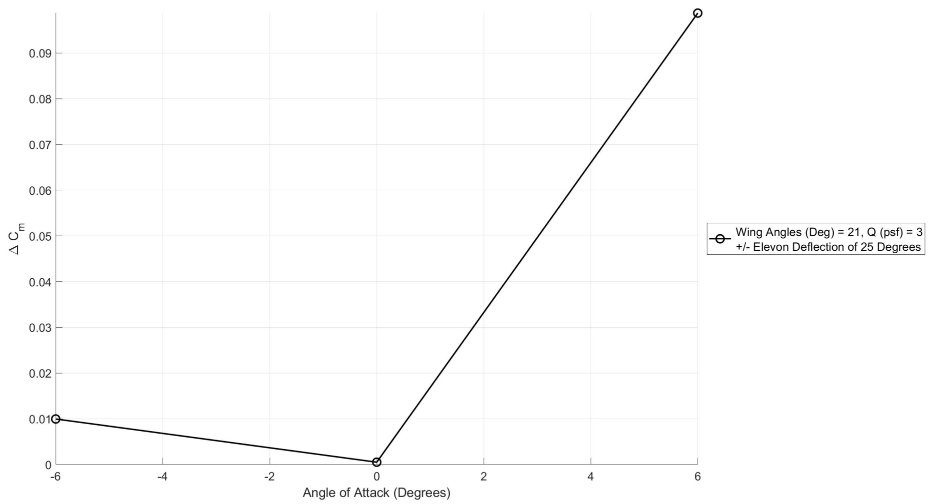

Figure 471. Wing angles 21 degrees trim point Δ C$_m$ vs angle of attack for elevon deflection.

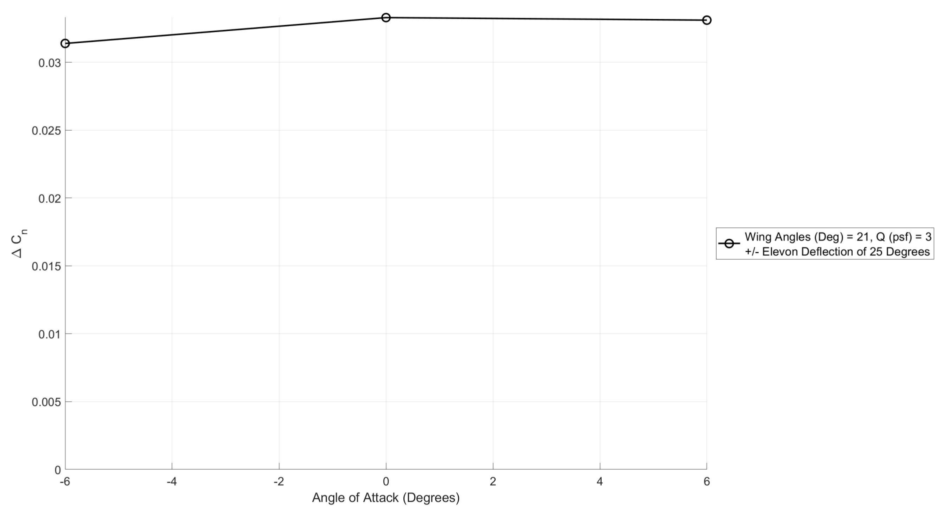

Figure 472. Wing angles 21 degrees trim point Δ C$_n$ vs angle of attack for elevon deflection.

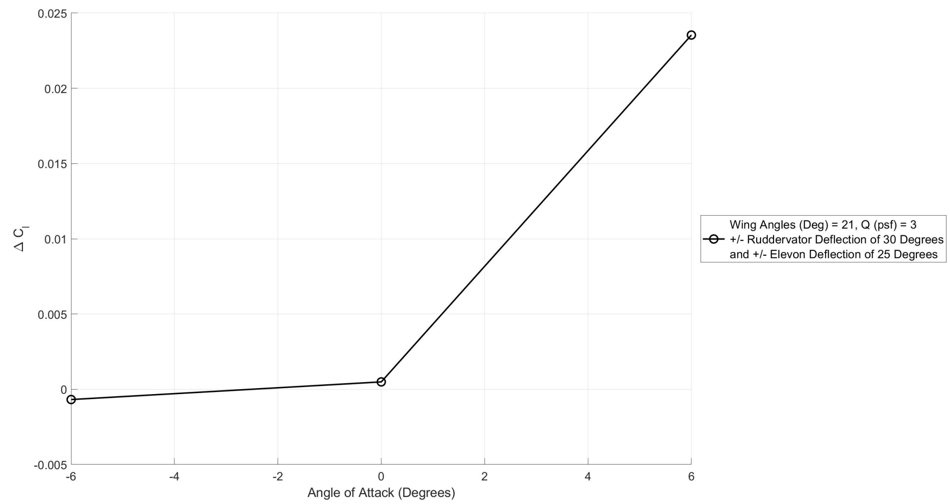

Figure 473. Wing angles 21 degrees trim point Δ C_l vs angle of attack for elevon and ruddervator deflection.

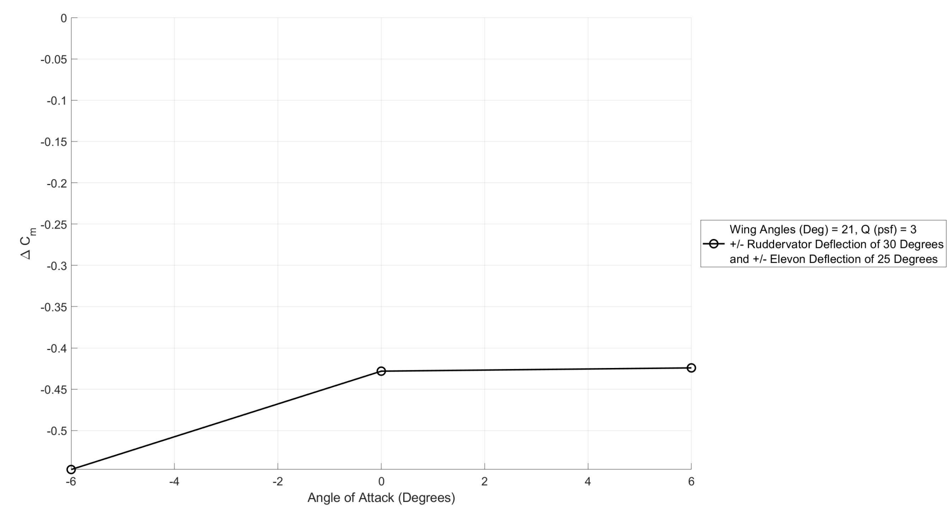

Figure 474. Wing angles 21 degrees trim point Δ C_m vs angle of attack for elevon and ruddervator deflection.

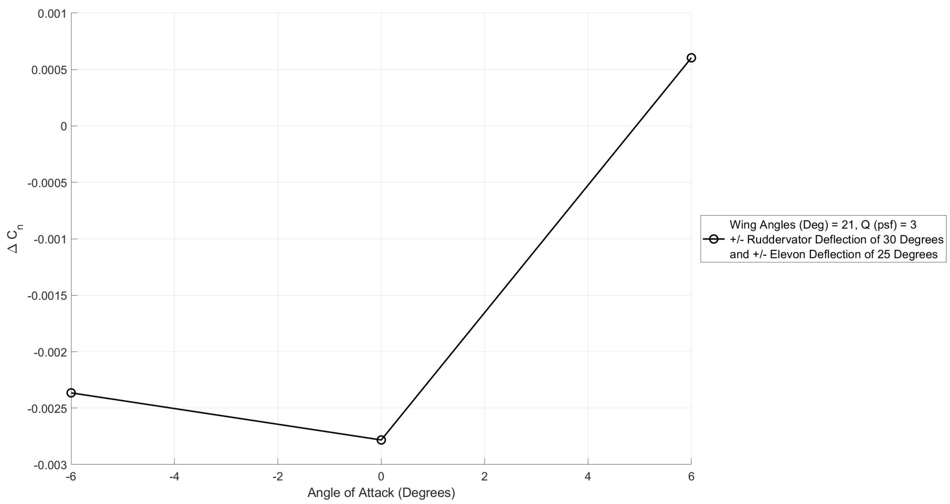

Figure 475. Wing angles 21 degrees trim point Δ C$_n$ vs angle of attack for elevon and ruddervator deflection.

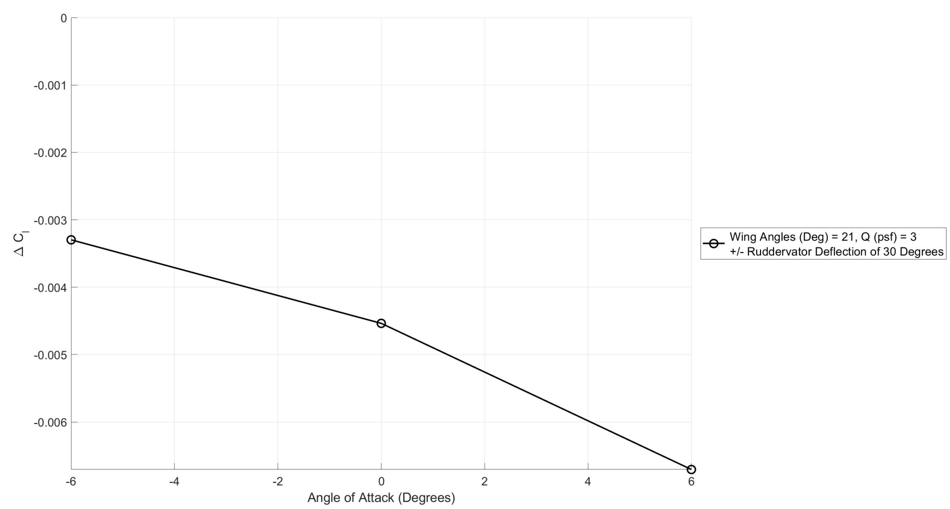

Figure 476. Wing angles 21 degrees trim point Δ C$_l$ vs angle of attack for ruddervator deflection.

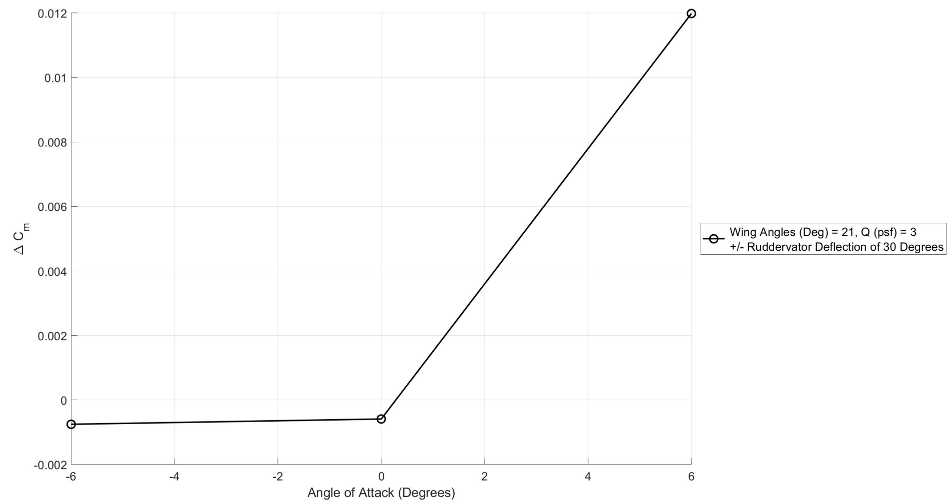

Figure 477. Wing angles 21 degrees trim point Δ C_m vs angle of attack for ruddervator deflection.

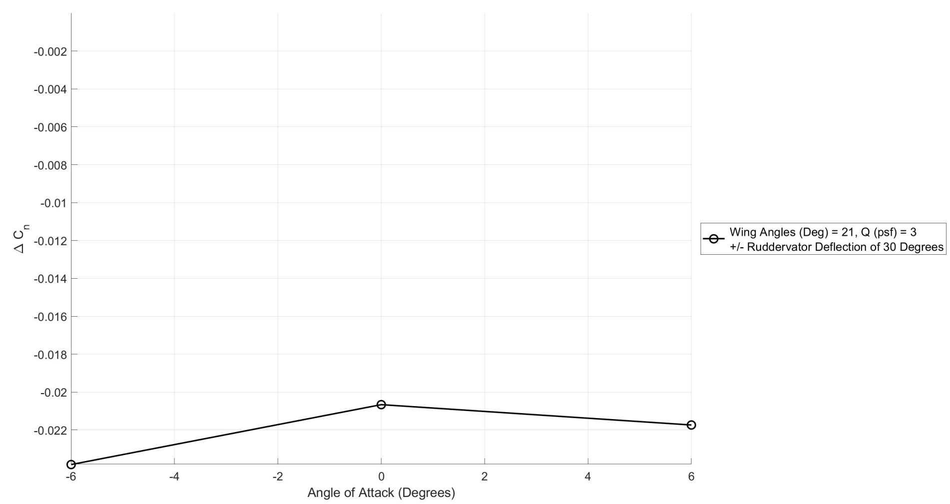

Figure 478. Wing angles 21 degrees trim point Δ C_n vs angle of attack for ruddervator deflection.

C.12 Transition Wing Angles 18 Degrees Performance and Stability Plots

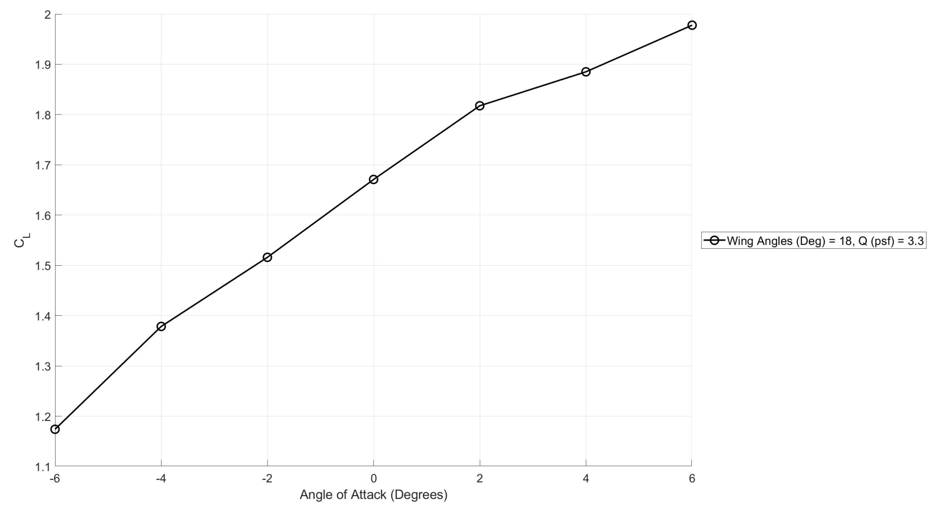

Figure 479. Wing angles 18 degrees trim point C_L vs angle of attack.

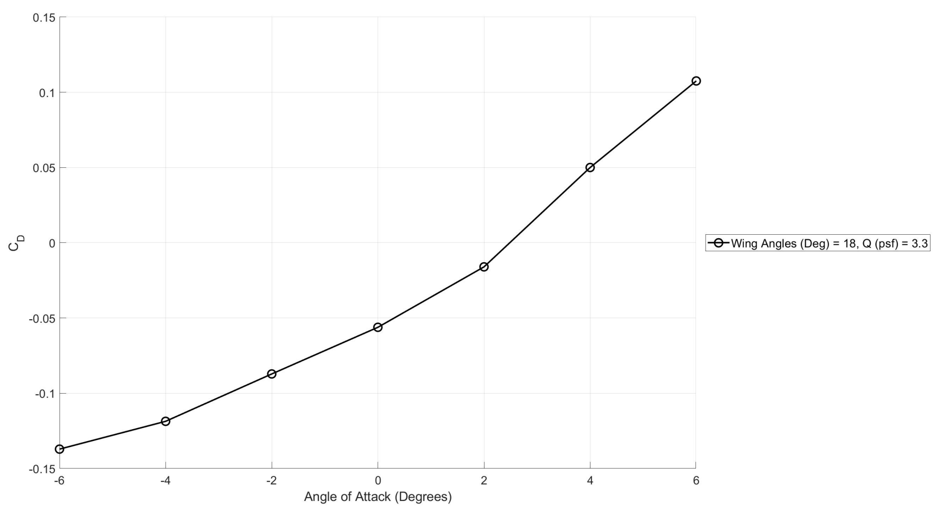

Figure 480. Wing angles 18 degrees trim point C_D vs angle of attack.

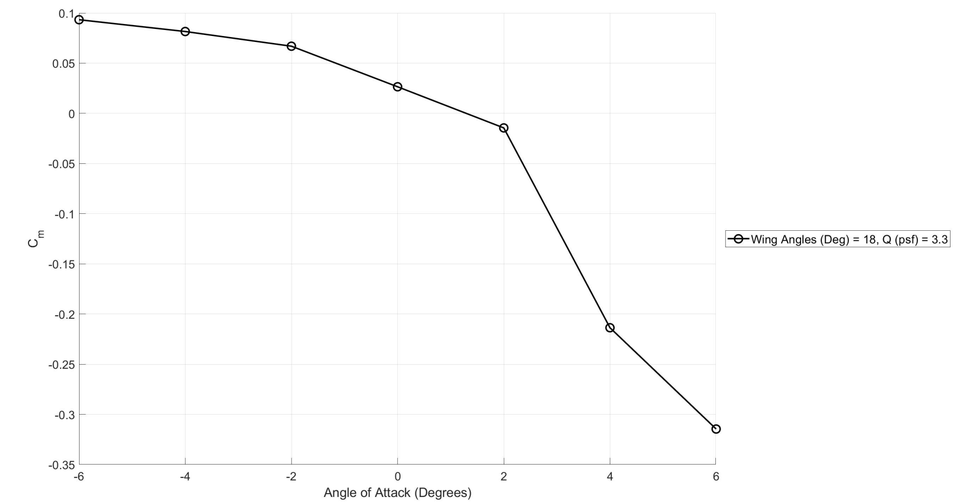

Figure 481. Wing angles 18 degrees trim point C_m vs angle of attack.

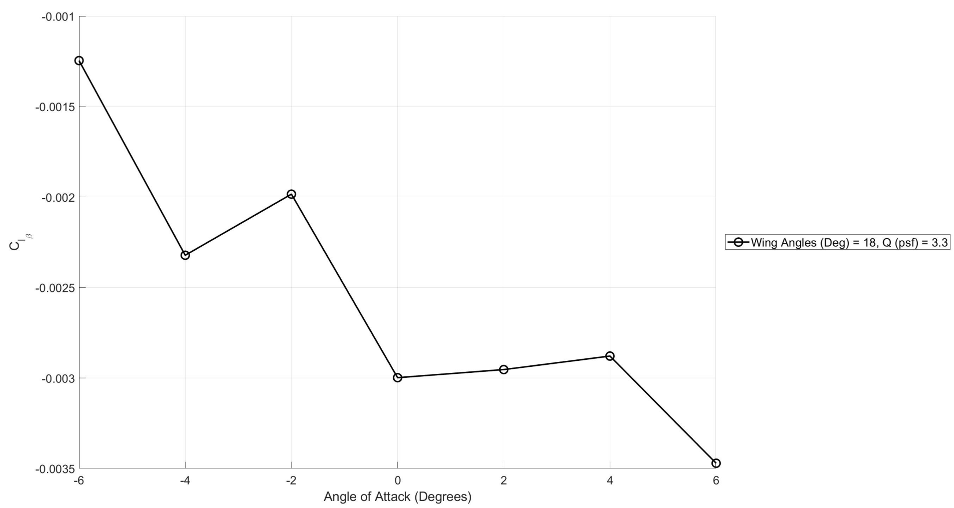

Figure 482. Wing angles 18 degrees trim point C_{l_β} vs angle of attack.

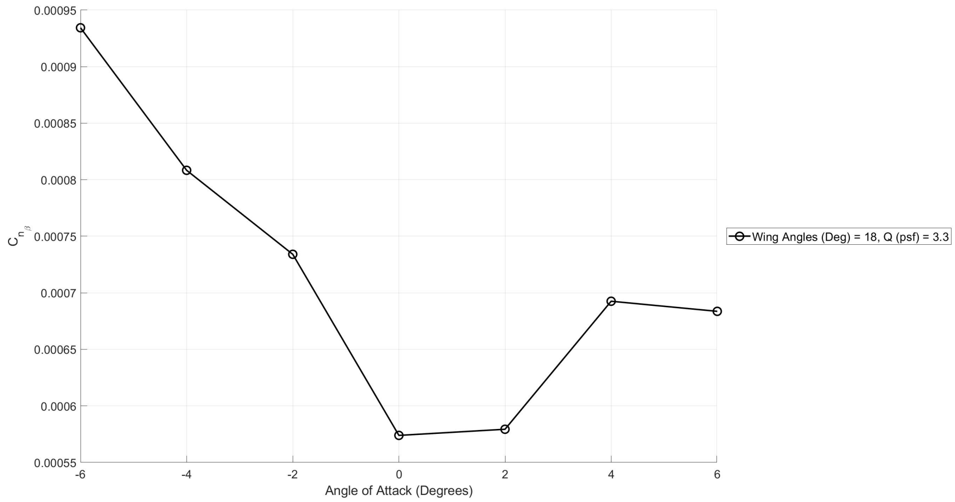

Figure 483. Wing angles 18 degrees trim point C_{n_β} vs angle of attack.

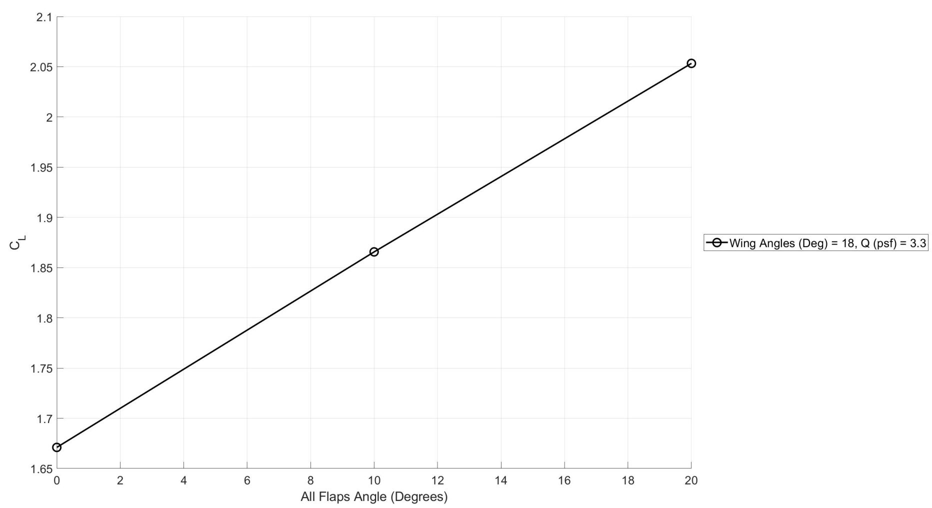

Figure 484. Wing angles 18 degrees trim point C_L vs all flap deflection angle.

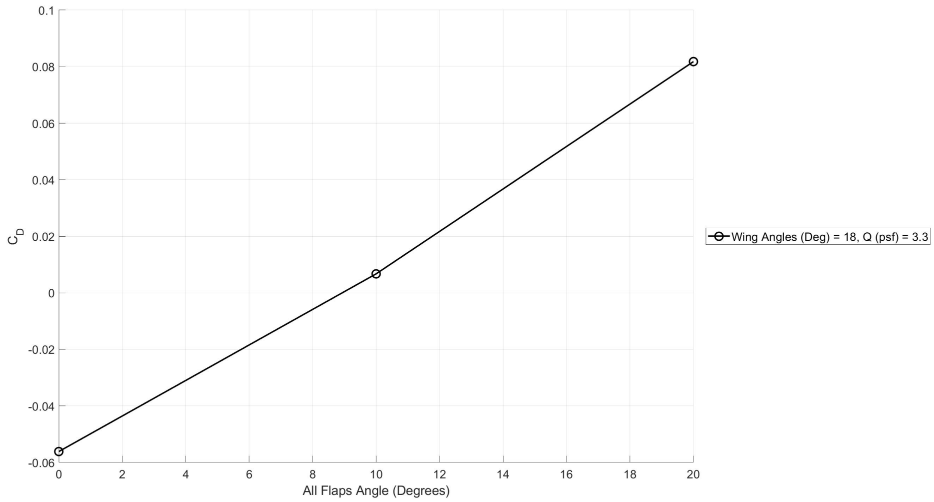

Figure 485. Wing angles 18 degrees trim point C_D vs all flap deflection angle.

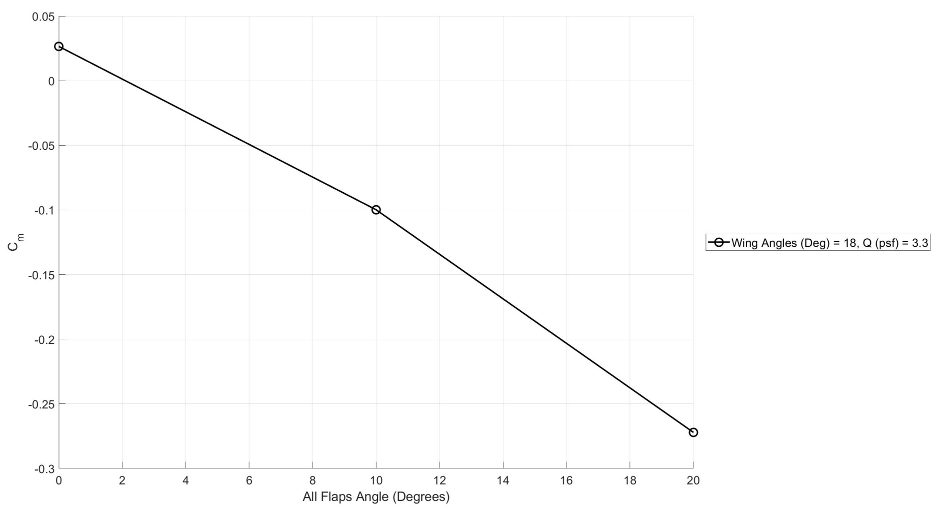

Figure 486. Wing angles 18 degrees trim point C_m vs all flap deflection angle.

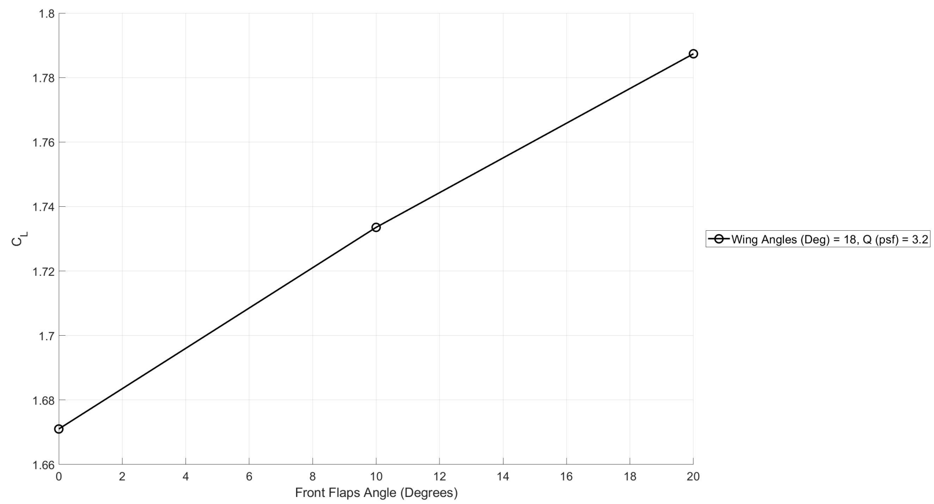

Figure 487. Wing angles 18 degrees trim point C_L vs front flap deflection angle.

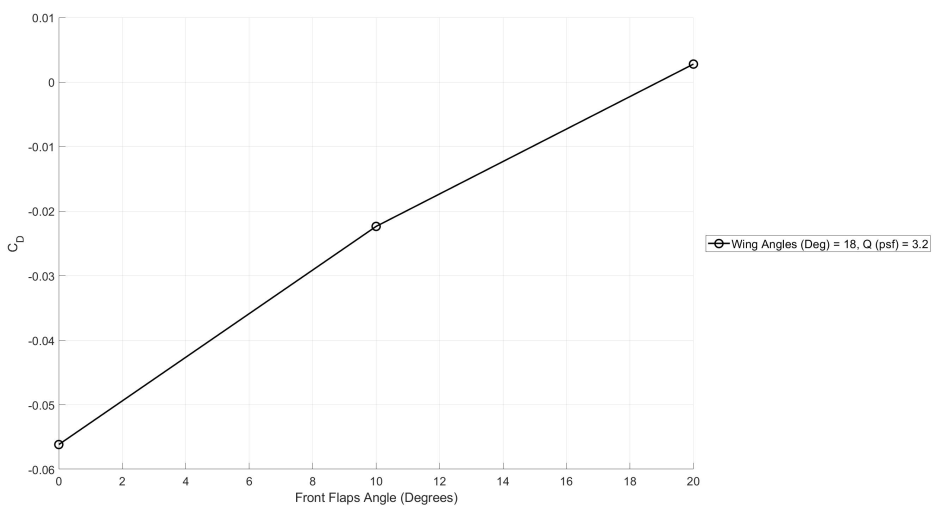

Figure 488. Wing angles 18 degrees trim point C_D vs front flap deflection angle.

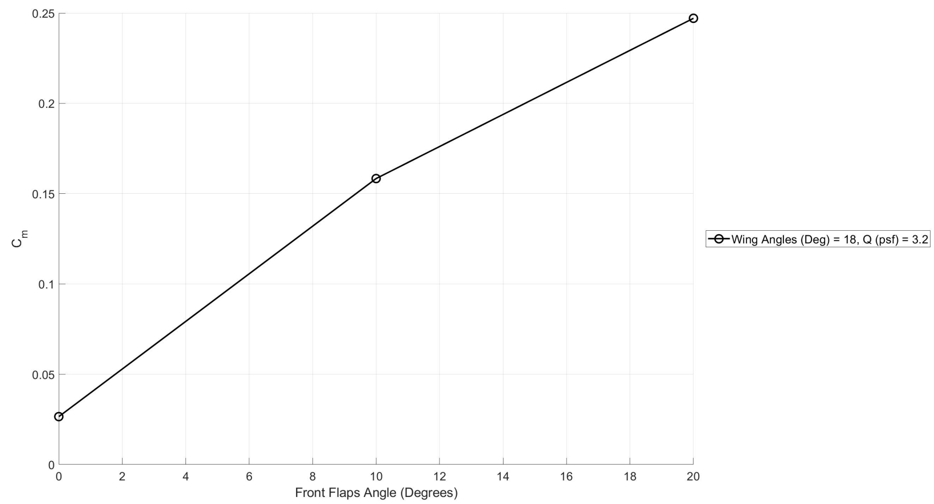

Figure 489. Wing angles 18 degrees trim point C_m vs front flap deflection angle.

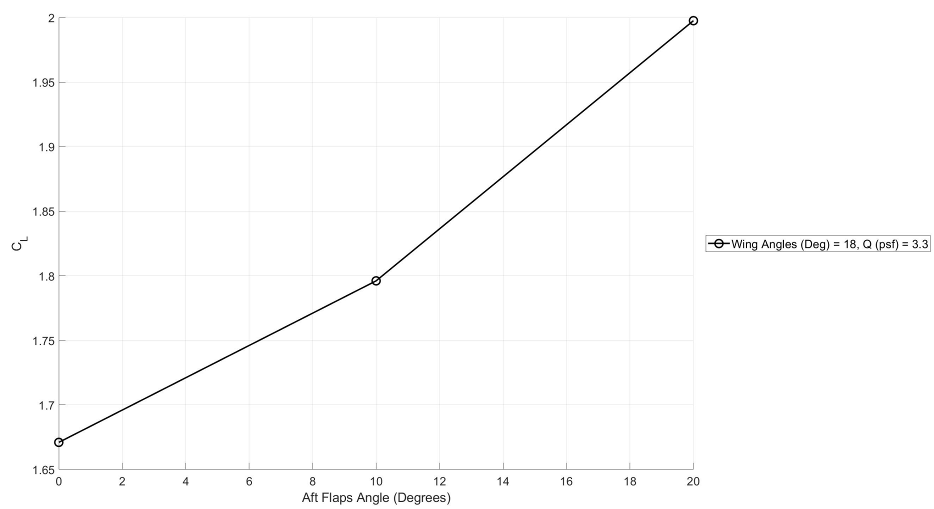

Figure 490. Wing angles 18 degrees trim point C_L vs aft flap deflection angle.

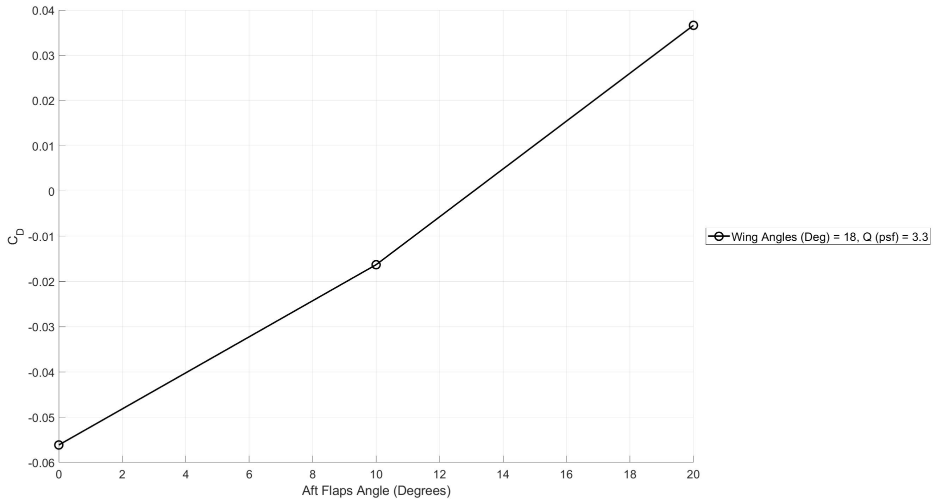

Figure 491. Wing angles 18 degrees trim point C_D vs aft flap deflection angle.

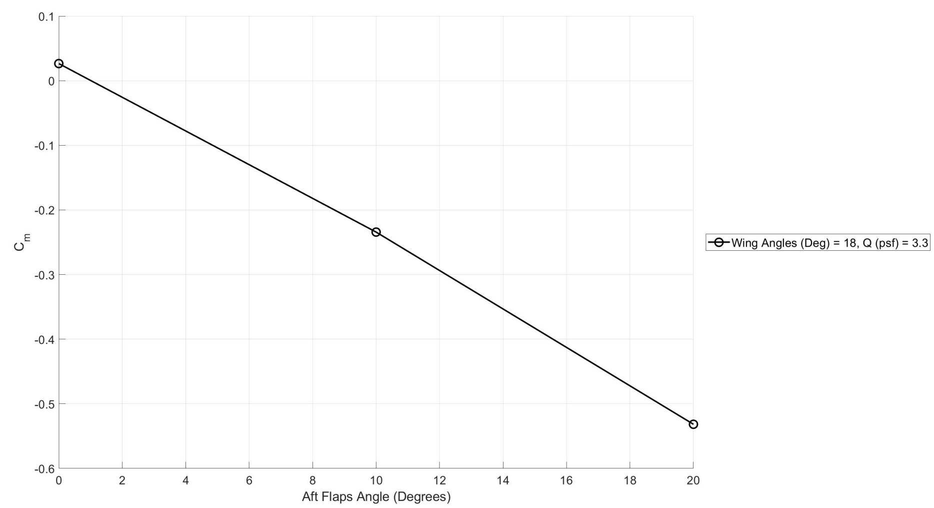

Figure 492. Wing angles 18 degrees trim point C_m vs aft flap deflection angle.

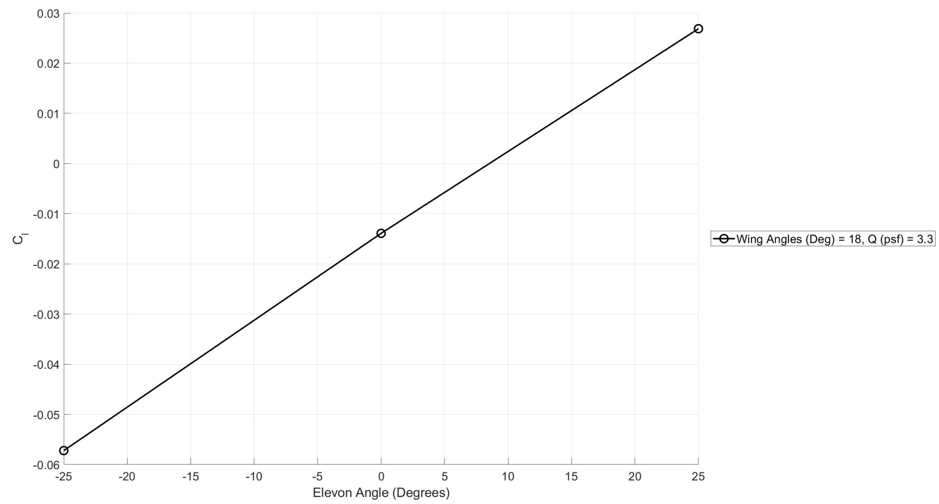

Figure 493. Wing angles 18 degrees trim point C_l vs elevon deflection angle.

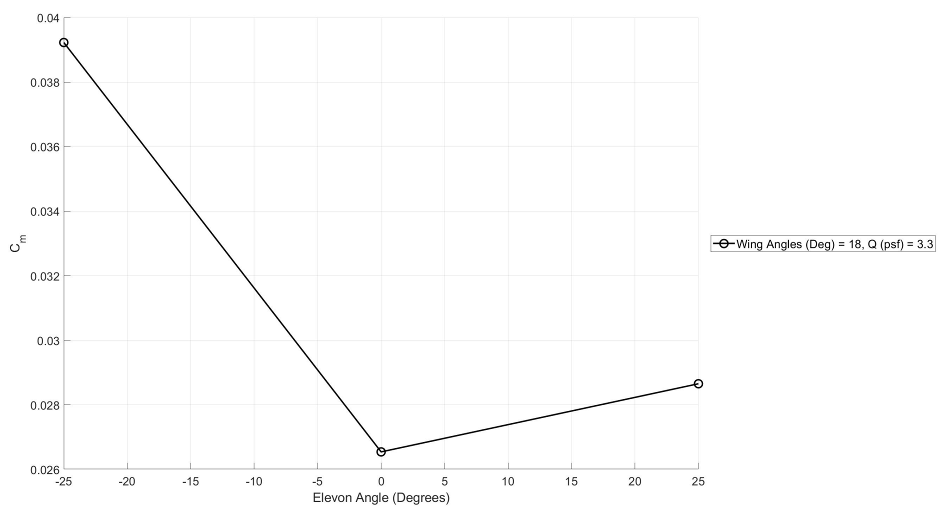

Figure 494. Wing angles 18 degrees trim point C_m vs elevon deflection angle.

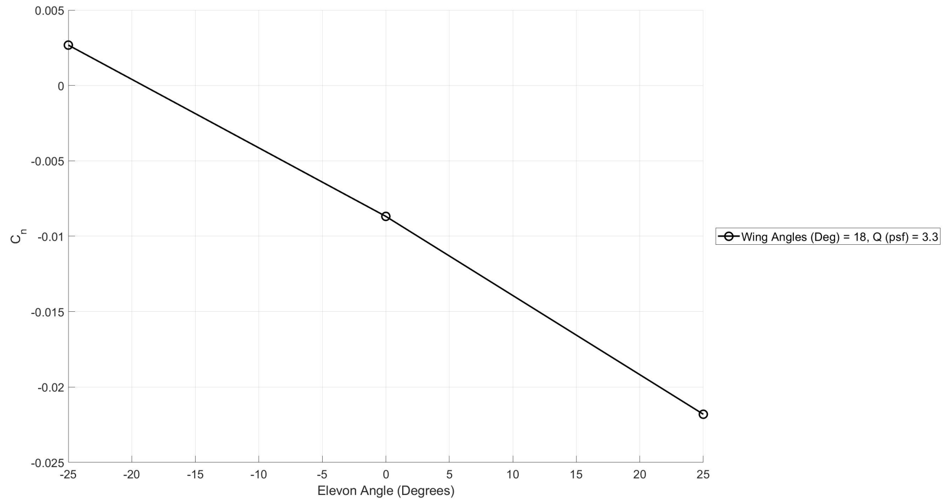

Figure 495. Wing angles 18 degrees trim point C_n vs elevon deflection angle.

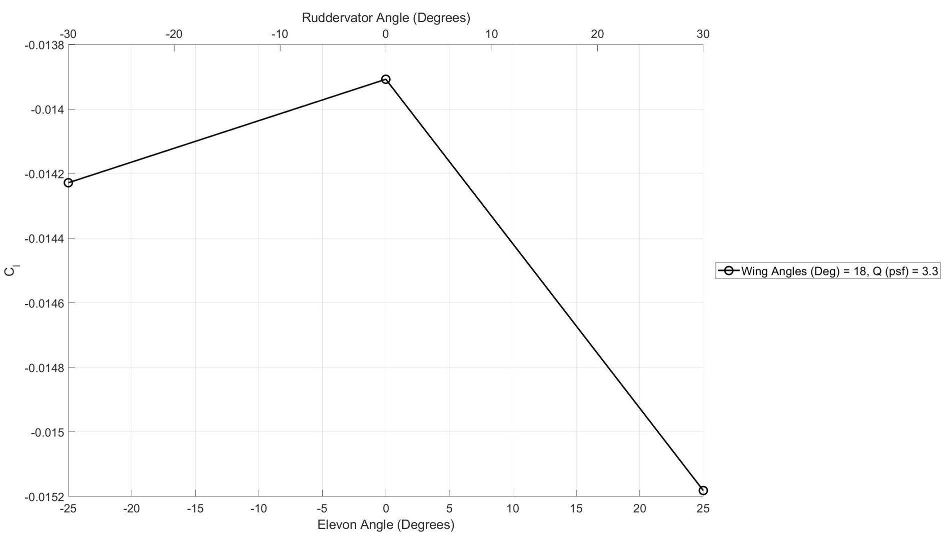

Figure 496. Wing angles 18 degrees trim point C_l vs elevon and ruddervator deflection angles.

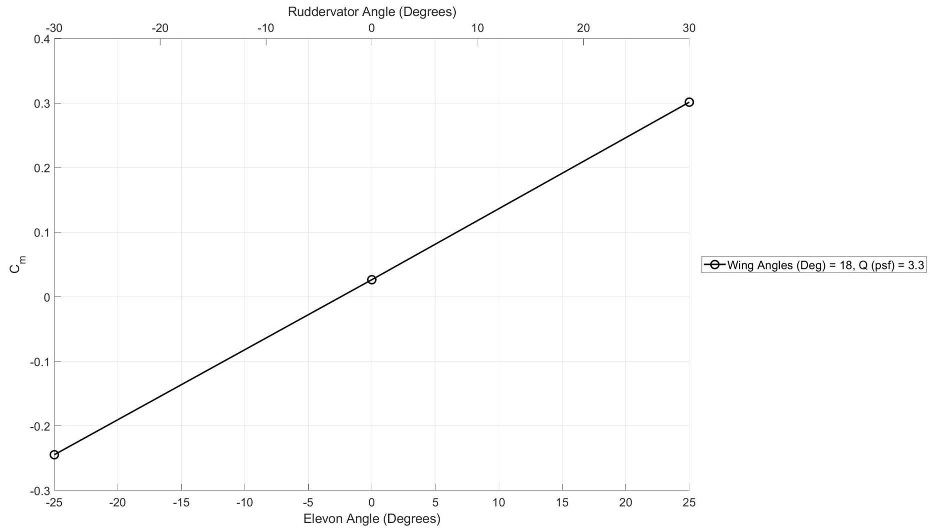

Figure 497. Wing angles 18 degrees trim point C_m vs elevon and ruddervator deflection angles.

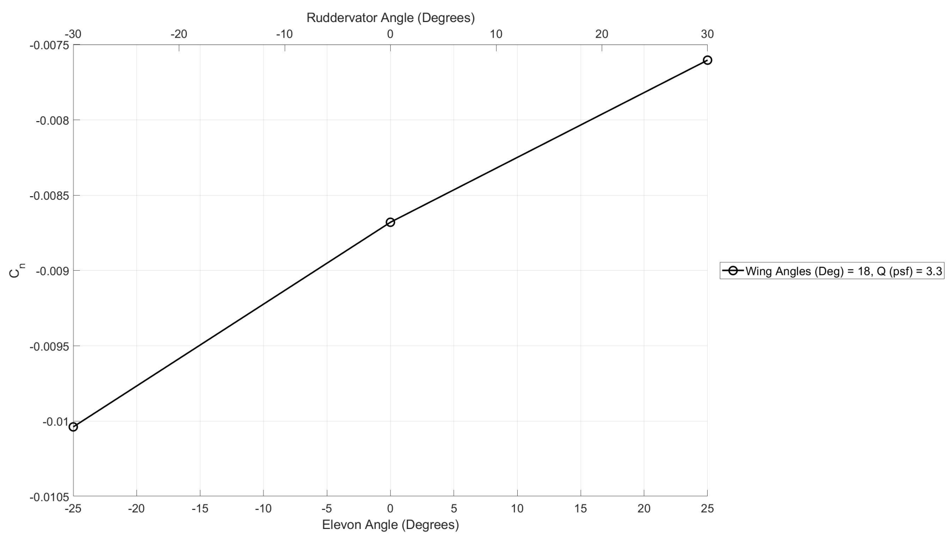

Figure 498. Wing angles 18 degrees trim point C_n vs elevon and ruddervator deflection angles.

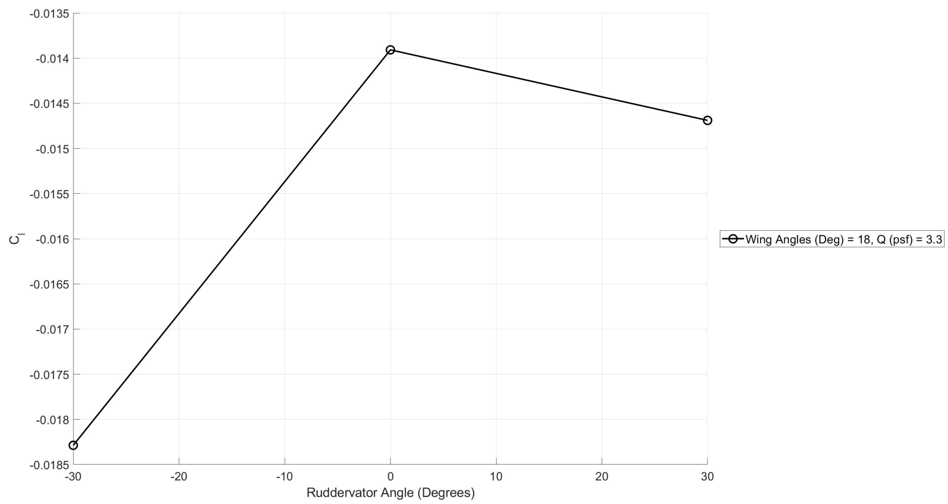

Figure 499. Wing angles 18 degrees trim point C_l vs ruddervator deflection angle.

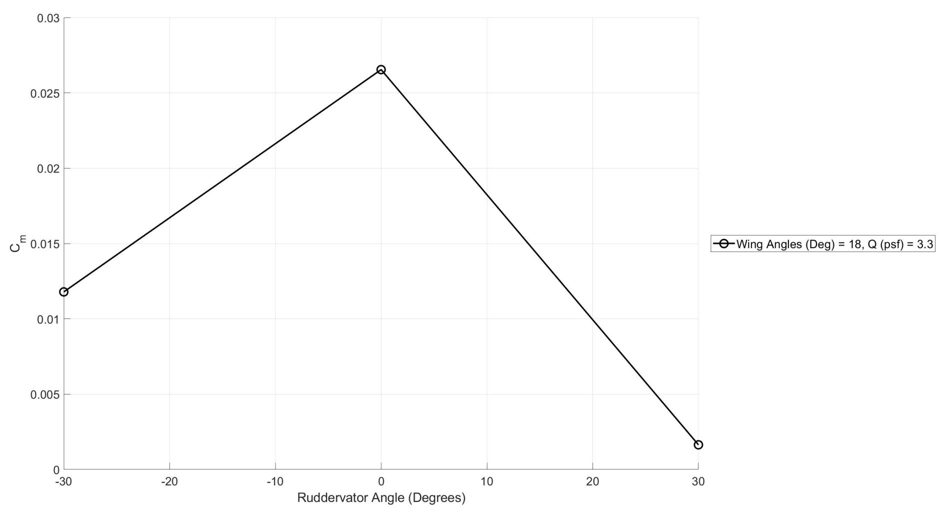

Figure 500. Wing angles 18 degrees trim point C_m vs ruddervator deflection angle.

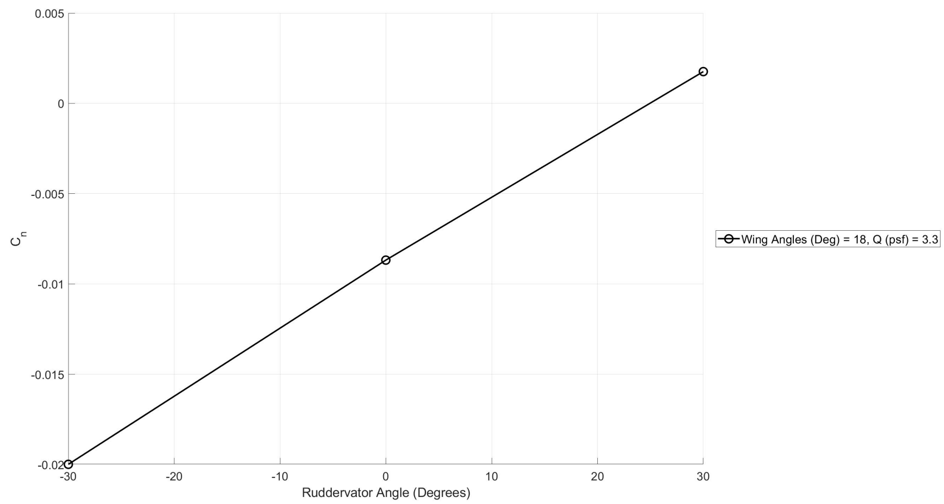

Figure 501. Wing angles 18 degrees trim point C_n vs ruddervator deflection angle.

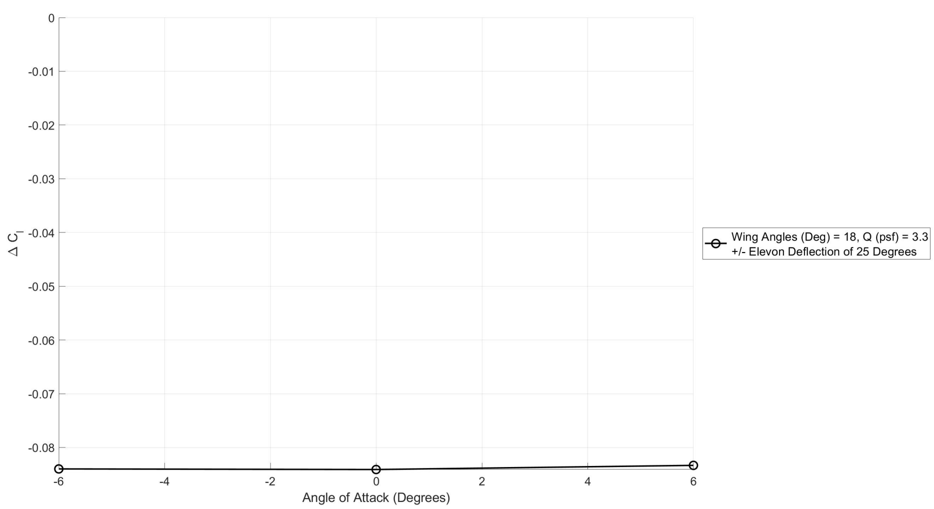

Figure 502. Wing angles 18 degrees trim point Δ C_l vs angle of attack for elevon deflection.

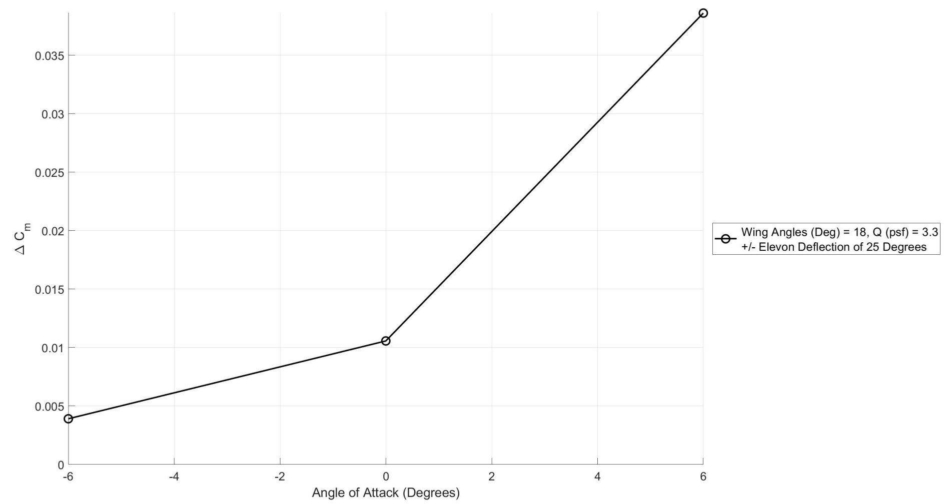

Figure 503. Wing angles 18 degrees trim point Δ C_m vs angle of attack for elevon deflection.

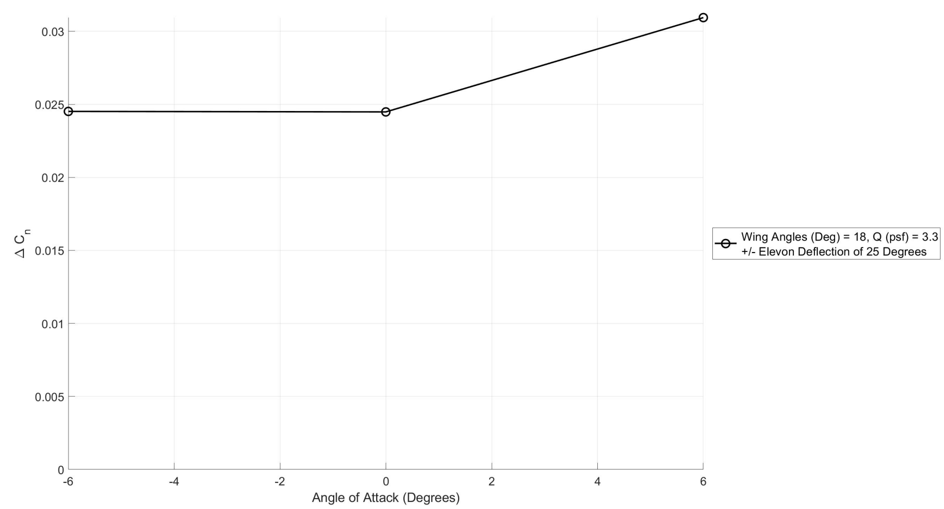

Figure 504. Wing angles 18 degrees trim point Δ C_n vs angle of attack for elevon deflection.

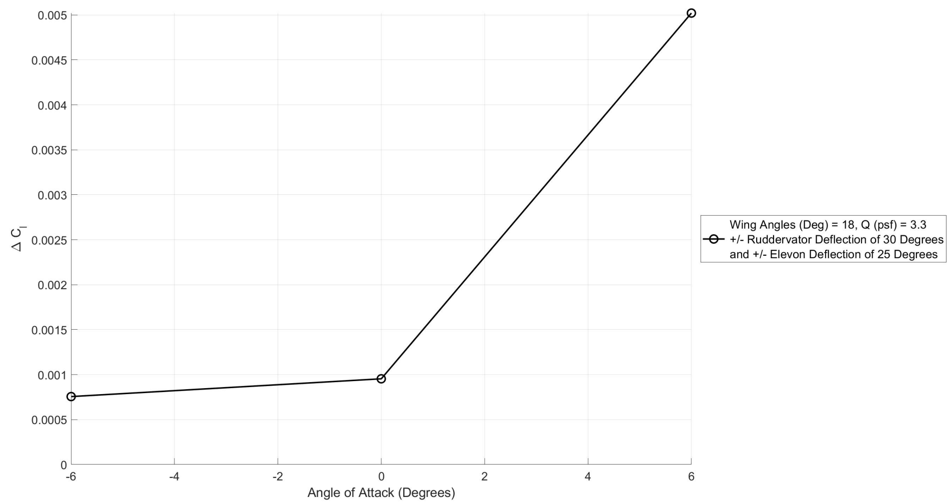

Figure 505. Wing angles 18 degrees trim point Δ C_l vs angle of attack for elevon and ruddervator deflection.

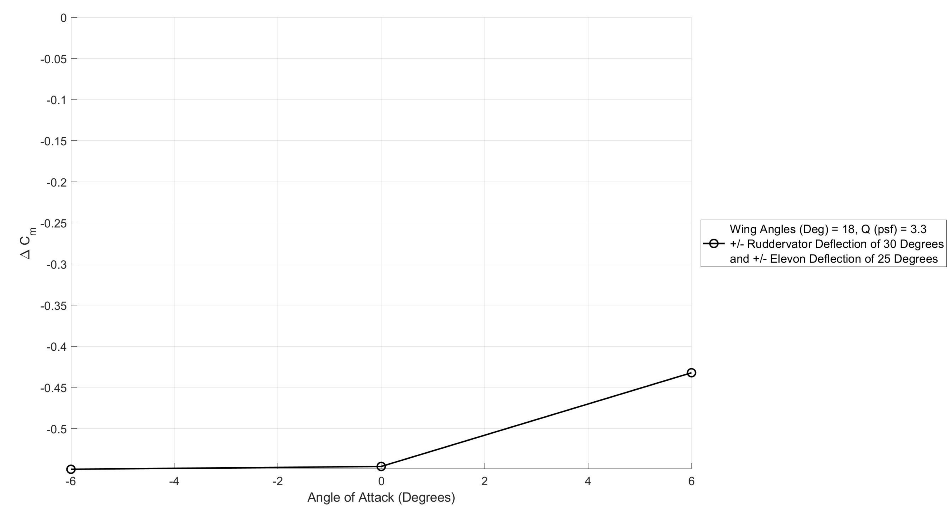

Figure 506. Wing angles 18 degrees trim point Δ C_m vs angle of attack for elevon and ruddervator deflection.

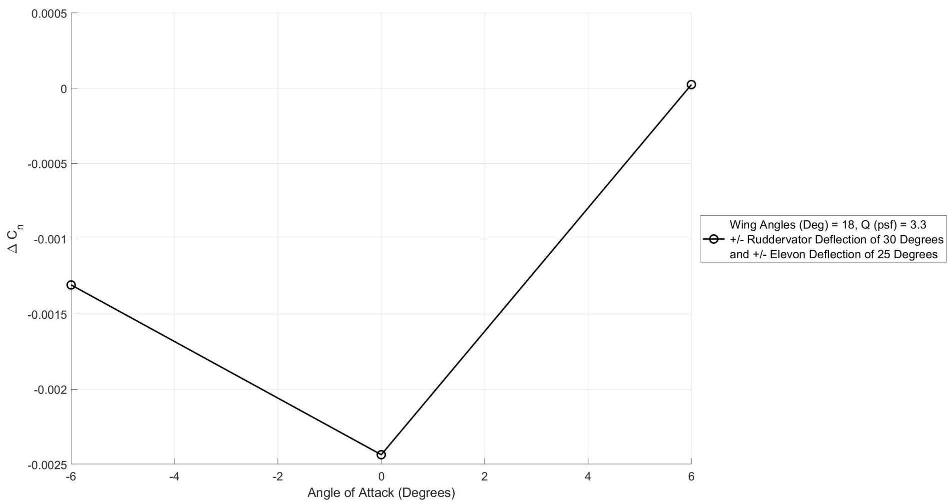

Figure 507. Wing angles 18 degrees trim point Δ C_n vs angle of attack for elevon and ruddervator deflection.

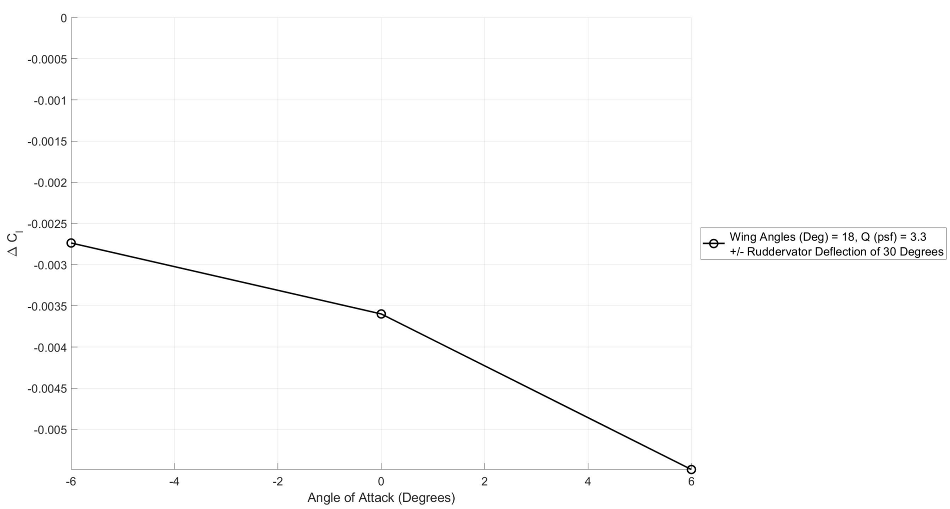

Figure 508. Wing angles 18 degrees trim point Δ C_l vs angle of attack for ruddervator deflection.

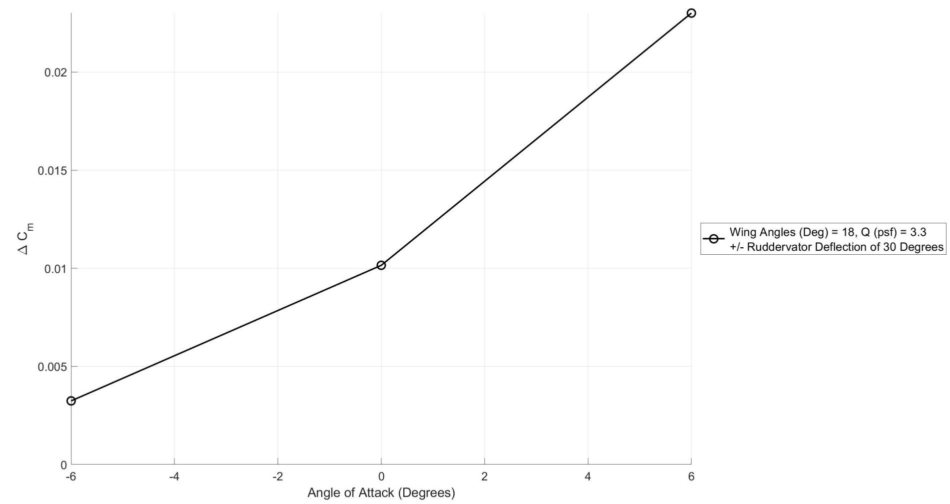

Figure 509. Wing angles 18 degrees trim point Δ C_m vs angle of attack for ruddervator deflection.

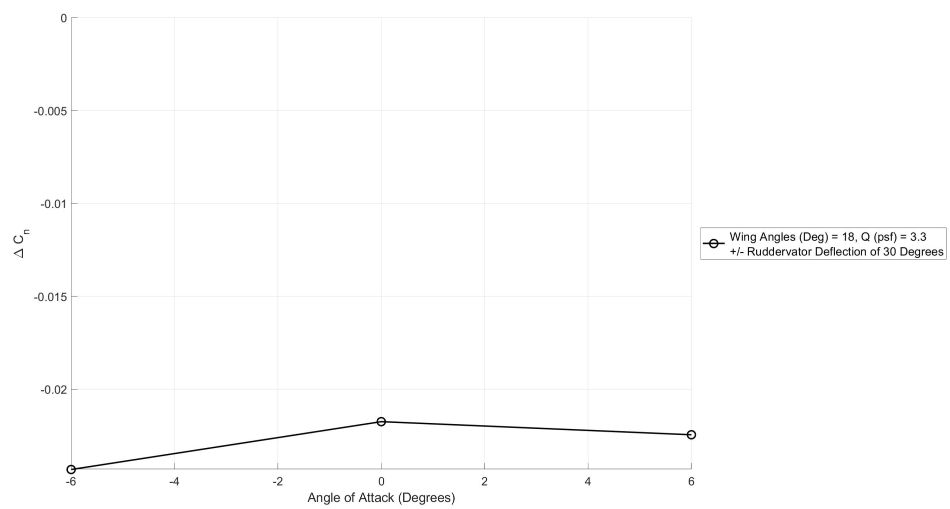

Figure 510. Wing angles 18 degrees trim point Δ C_n vs angle of attack for ruddervator deflection.

C.13 Transition Wing Angles 16 Degrees Performance and Stability Plots

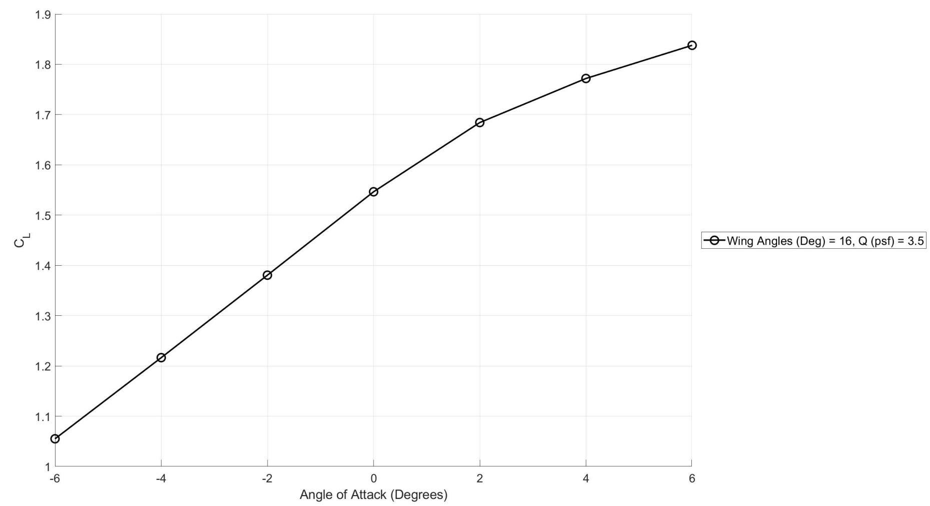

Figure 511. Wing angles 16 degrees trim point C_L vs angle of attack.

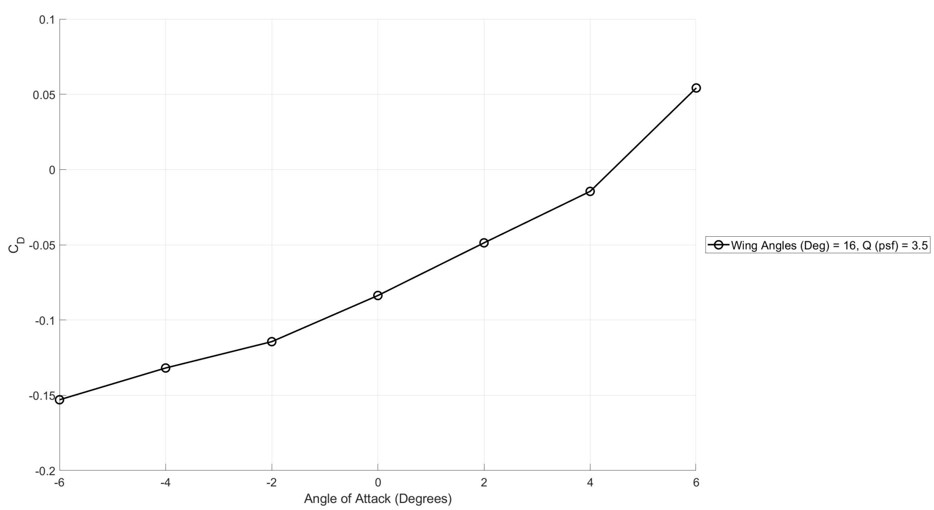

Figure 512. Wing angles 16 degrees trim point C_D vs angle of attack.

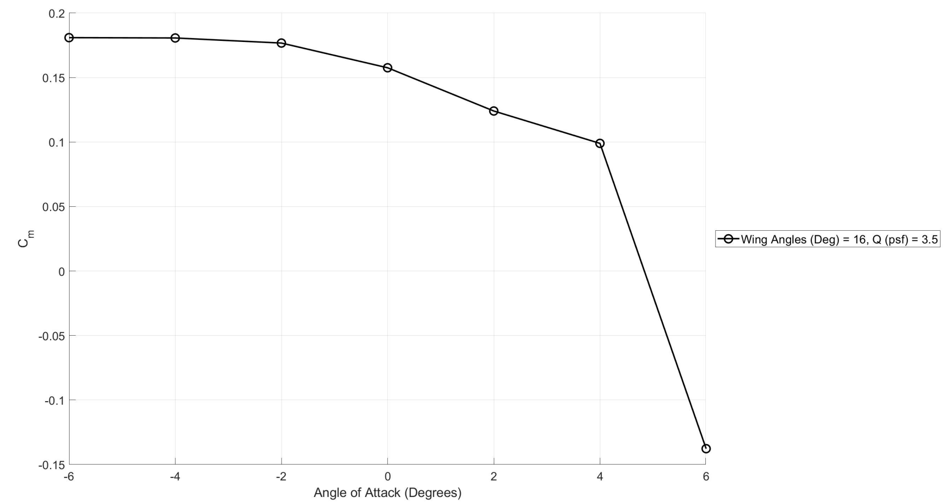

Figure 513. Wing angles 16 degrees trim point C_m vs angle of attack.

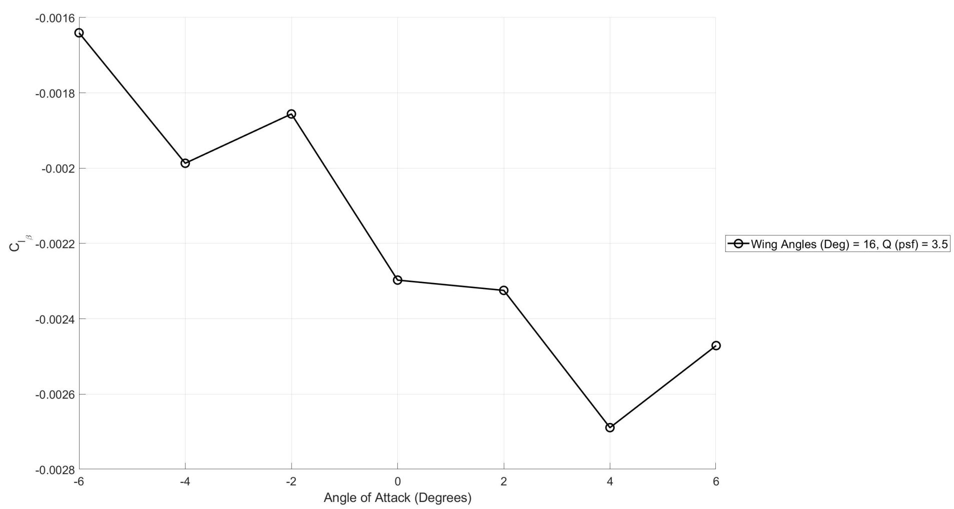

Figure 514. Wing angles 16 degrees trim point C_{l_β} vs angle of attack.

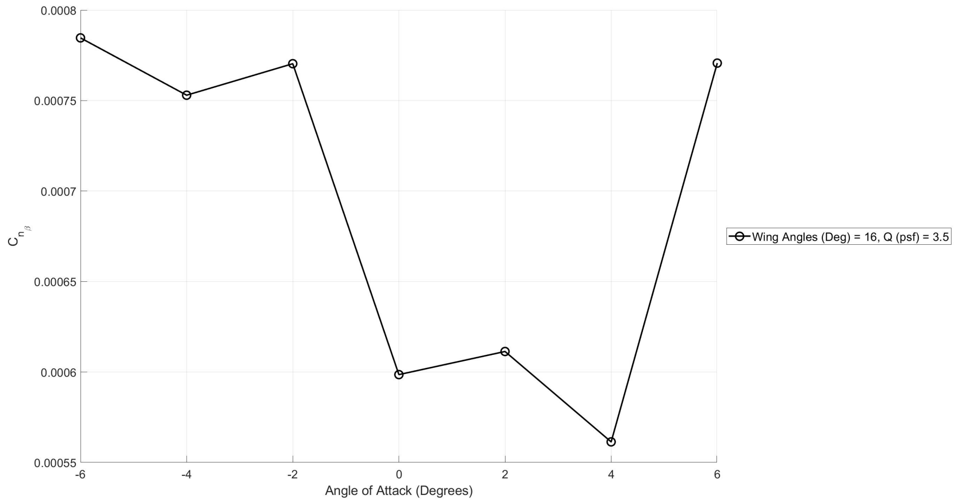

Figure 515. Wing angles 16 degrees trim point C_{n_β} vs angle of attack.

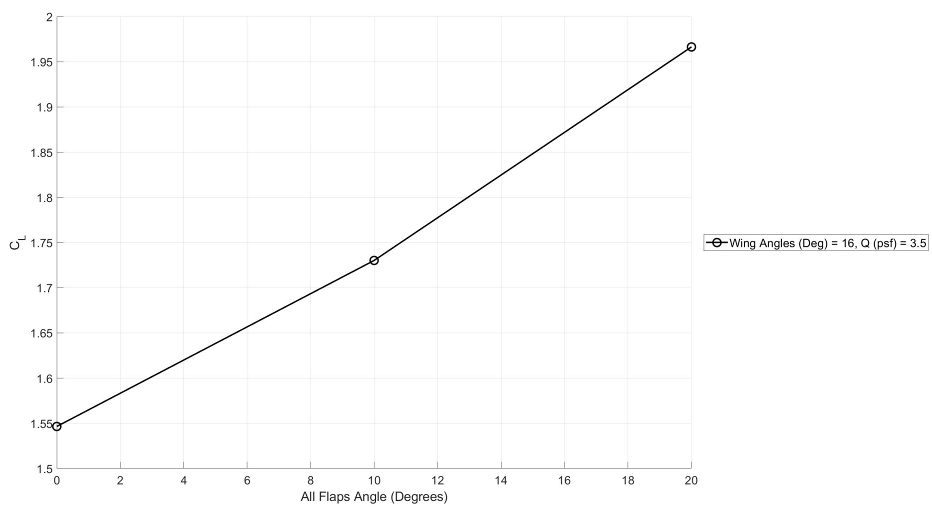

Figure 516. Wing angles 16 degrees trim point C_L vs all flap deflection angle.

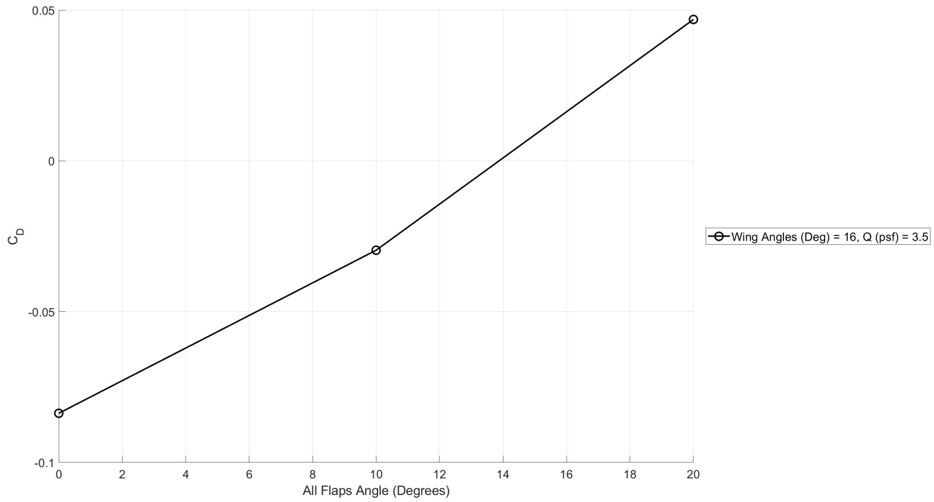

Figure 517. Wing angles 16 degrees trim point C_D vs all flap deflection angle.

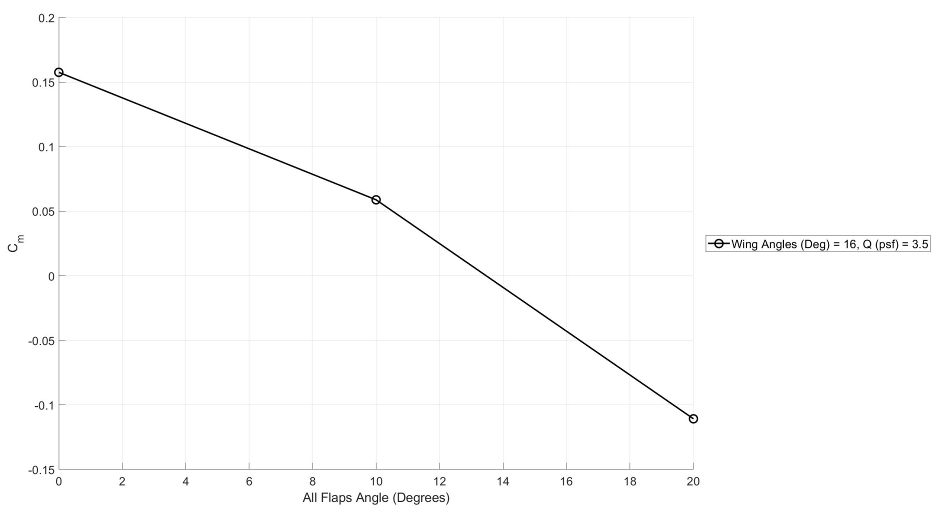

Figure 518. Wing angles 16 degrees trim point C_m vs all flap deflection angle.

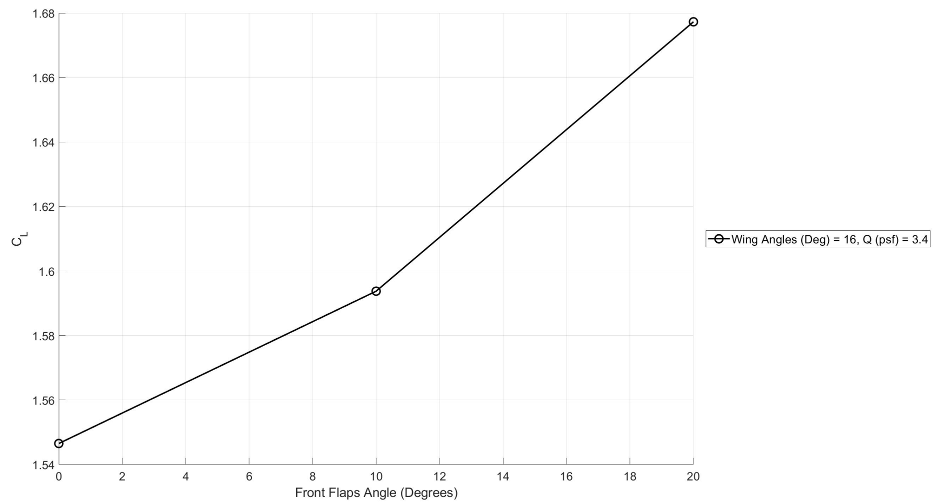

Figure 519. Wing angles 16 degrees trim point C_L vs front flap deflection angle.

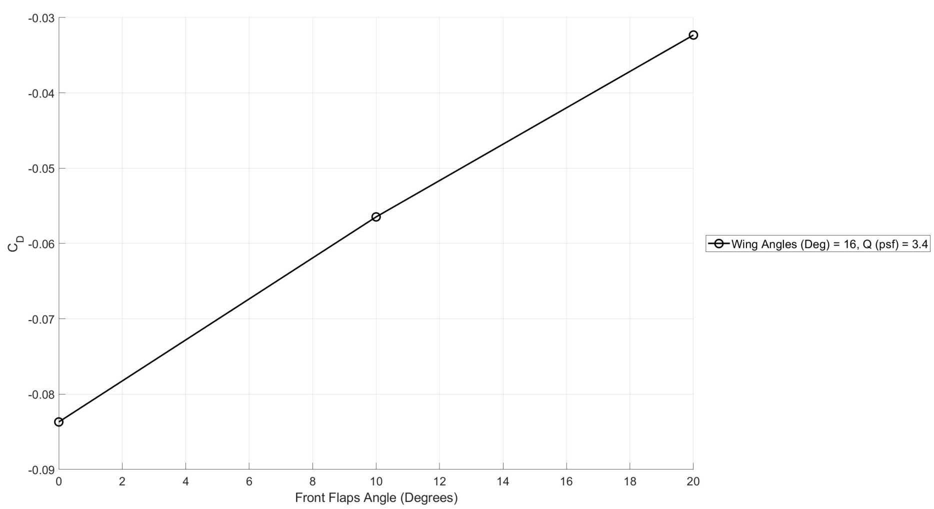

Figure 520. Wing angles 16 degrees trim point C_D vs front flap deflection angle.

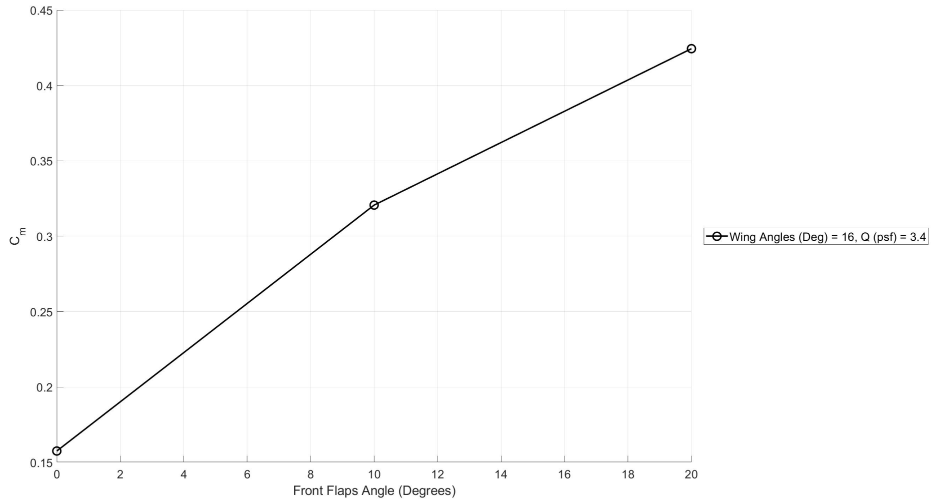

Figure 521. Wing angles 16 degrees trim point C_m vs front flap deflection angle.

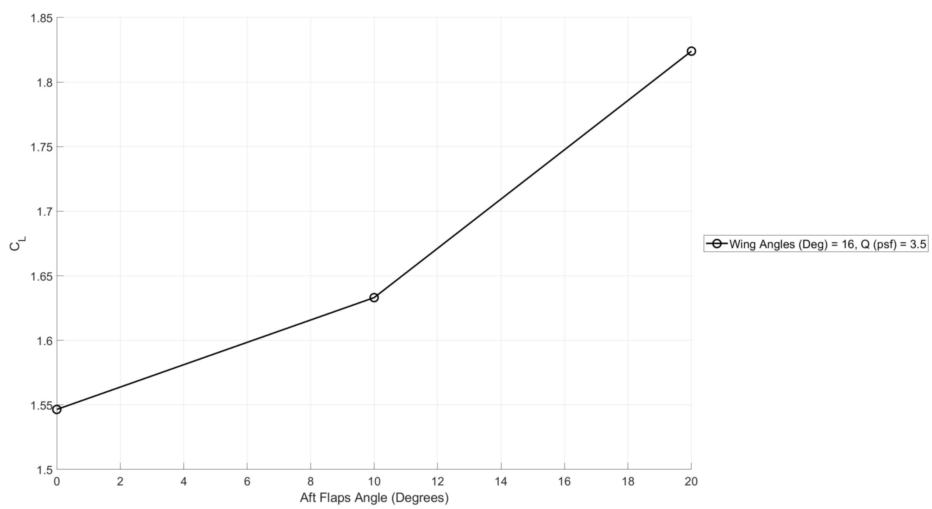

Figure 522. Wing angles 16 degrees trim point C_L vs aft flap deflection angle.

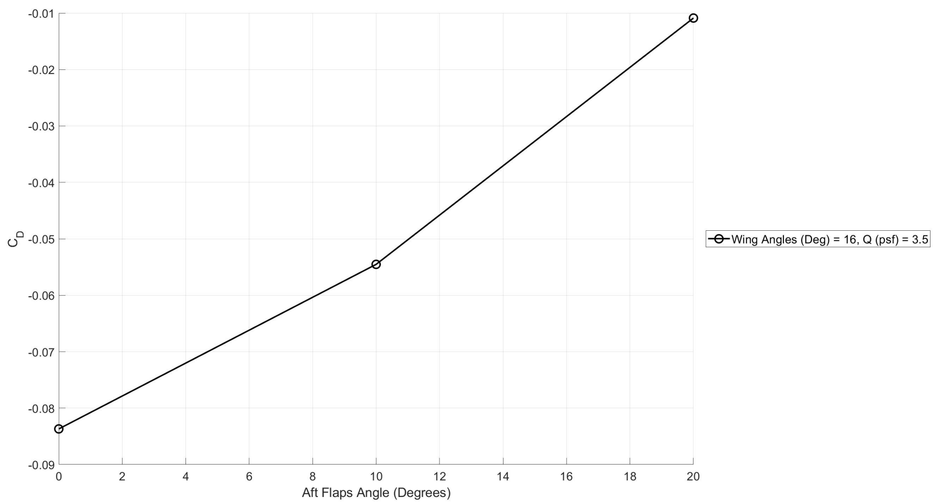

Figure 523. Wing angles 16 degrees trim point C_D vs aft flap deflection angle.

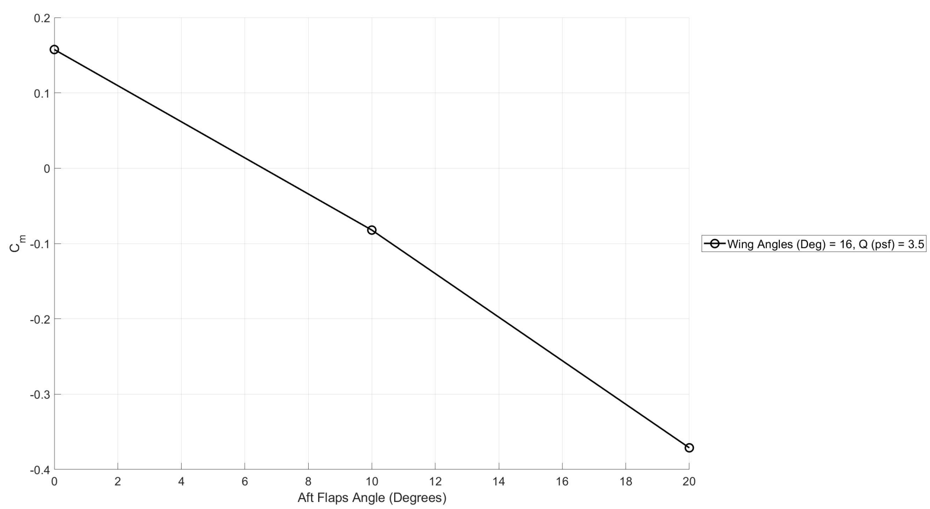

Figure 524. Wing angles 16 degrees trim point C_m vs aft flap deflection angle.

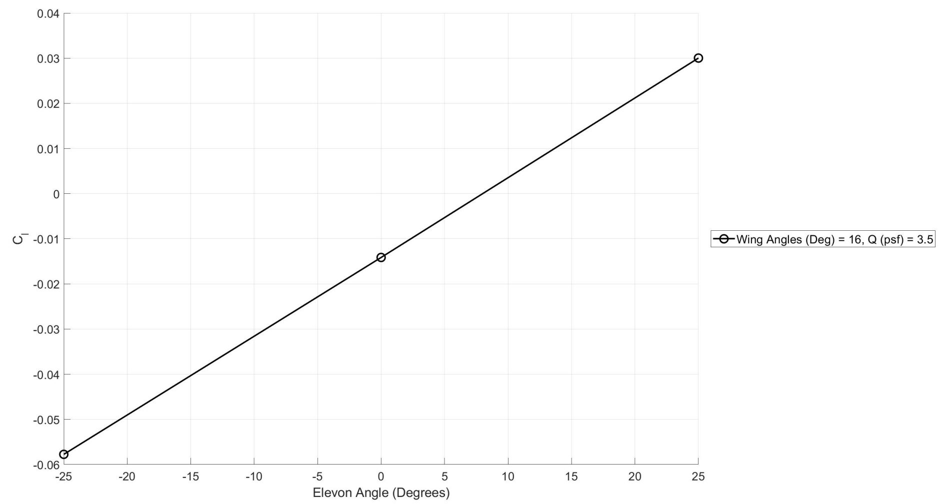

Figure 525. Wing angles 16 degrees trim point C_l vs elevon deflection angle.

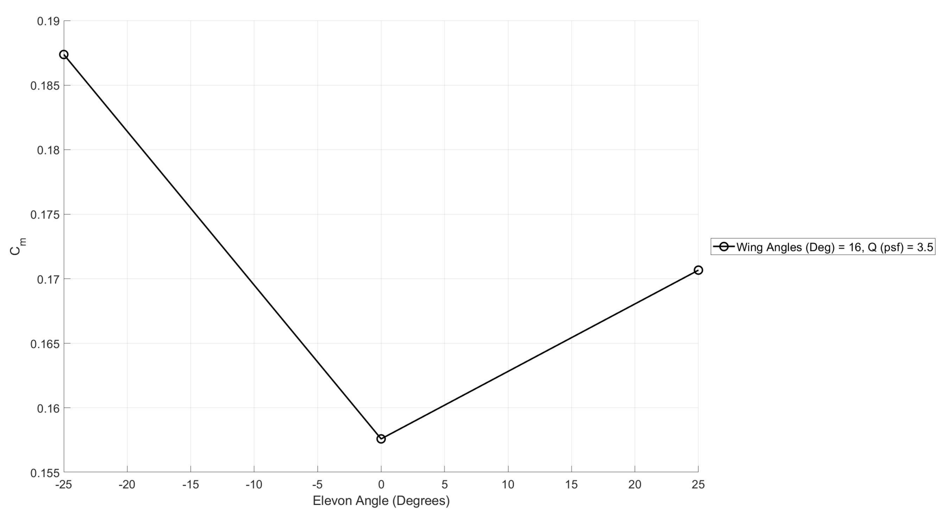

Figure 526. Wing angles 16 degrees trim point C_m vs elevon deflection angle.

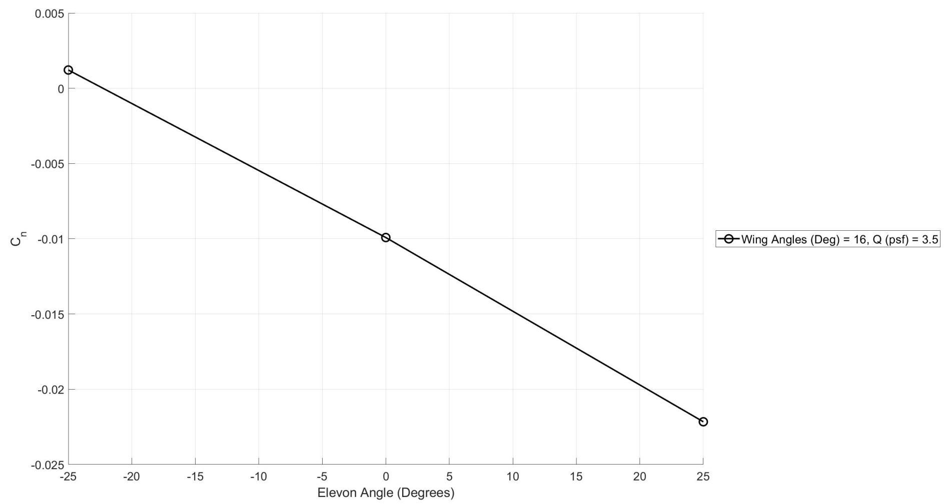

Figure 527. Wing angles 16 degrees trim point C_n vs elevon deflection angle.

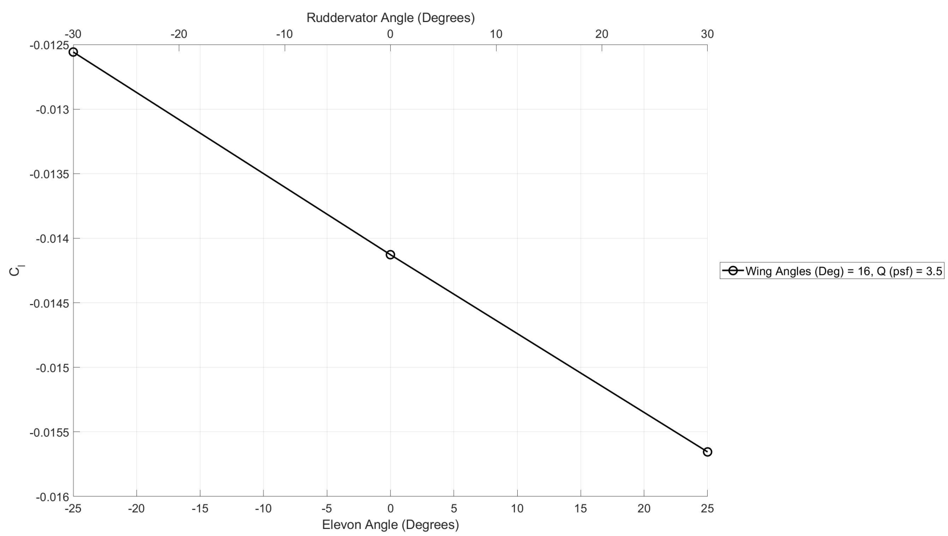

Figure 528. Wing angles 16 degrees trim point C_l vs elevon and ruddervator deflection angles.

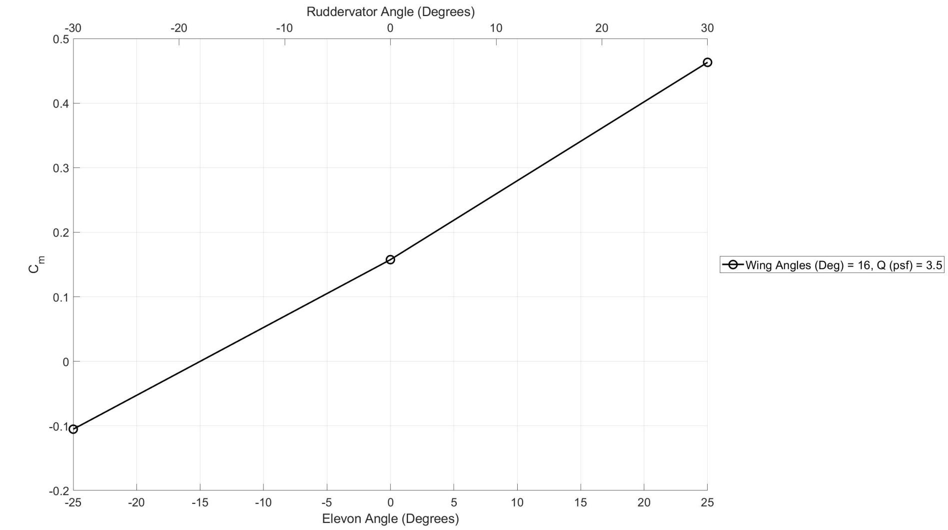

Figure 529. Wing angles 16 degrees trim point C_m vs elevon and ruddervator deflection angles.

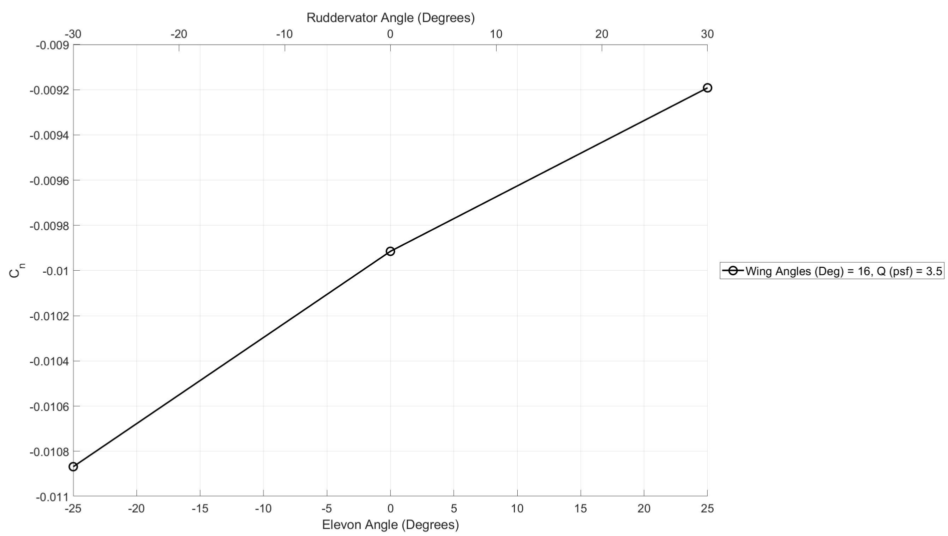

Figure 530. Wing angles 16 degrees trim point C_n vs elevon and ruddervator deflection angles.

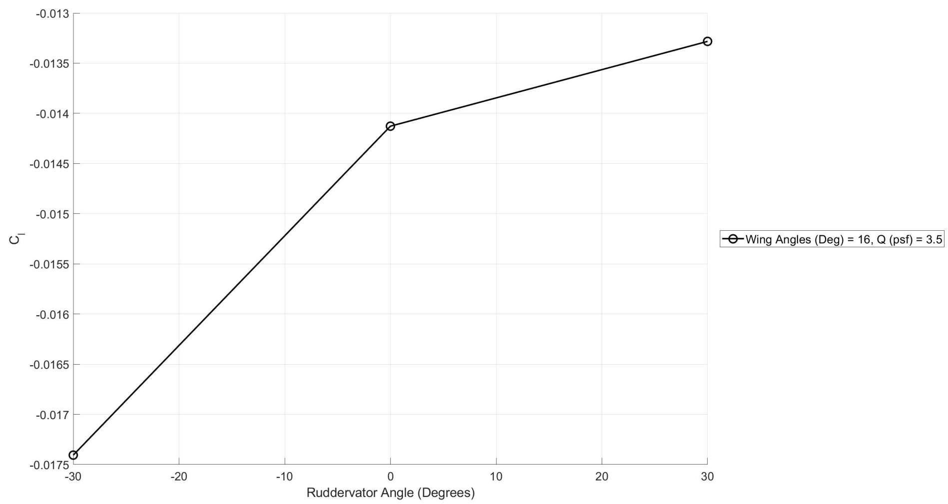

Figure 531. Wing angles 16 degrees trim point C_l vs ruddervator deflection angle.

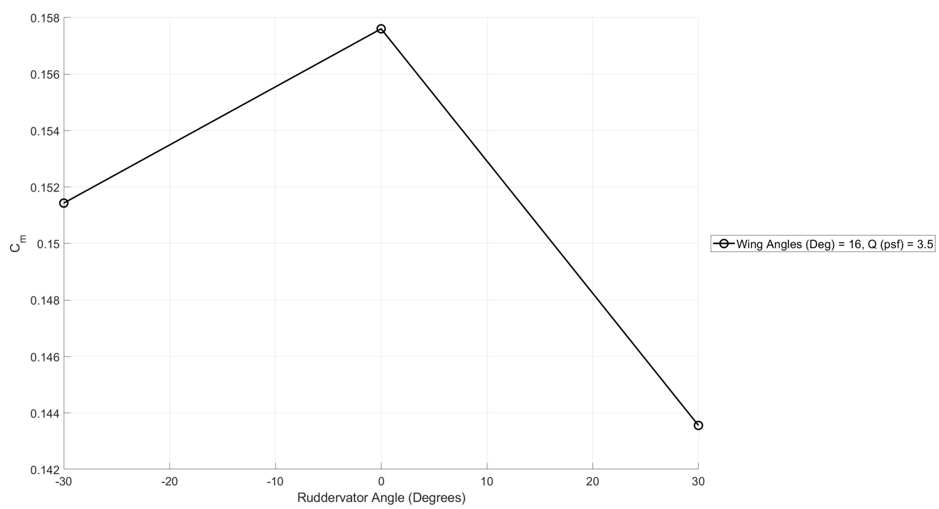

Figure 532. Wing angles 16 degrees trim point C_m vs ruddervator deflection angle.

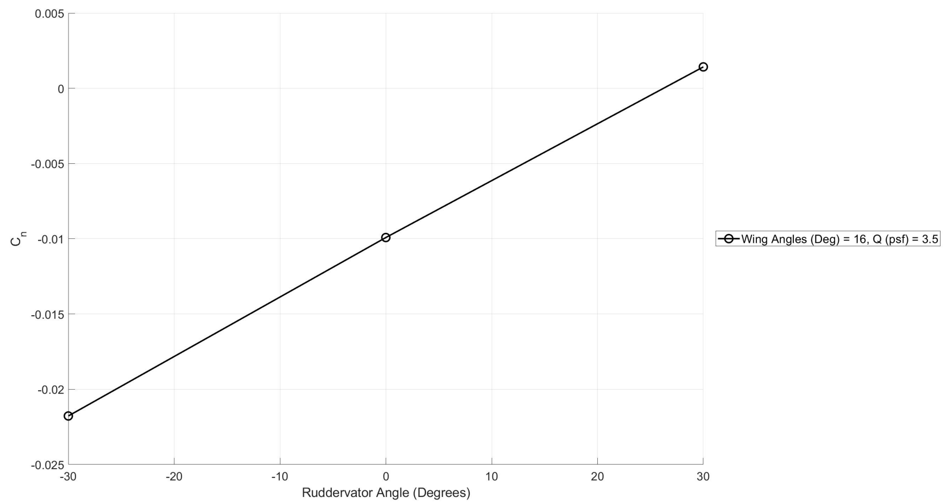

Figure 533. Wing angles 16 degrees trim point C_n vs ruddervator deflection angle.

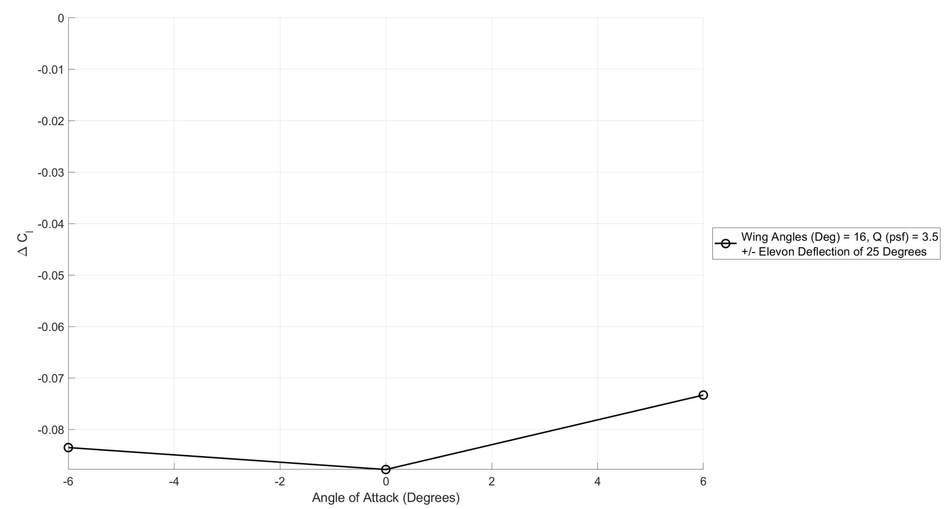

Figure 534. Wing angles 16 degrees trim point Δ C_l vs angle of attack for elevon deflection.

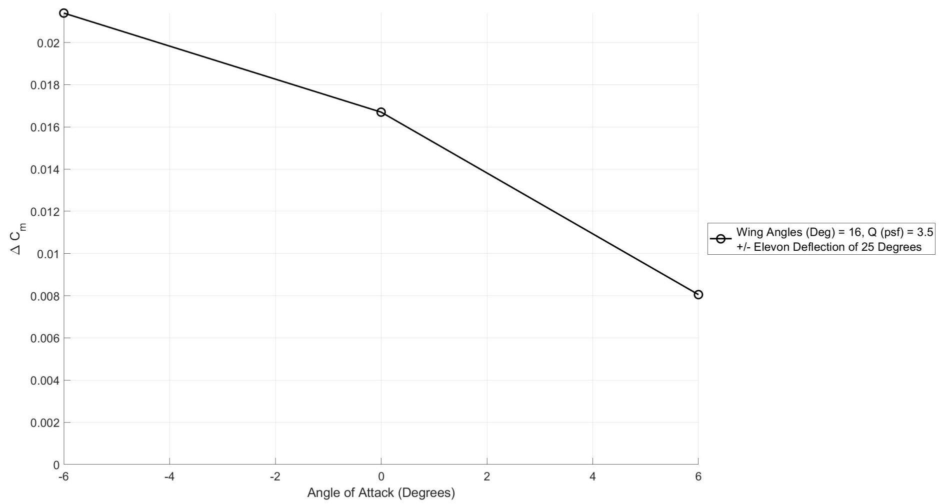

Figure 535. Wing angles 16 degrees trim point Δ C_m vs angle of attack for elevon deflection.

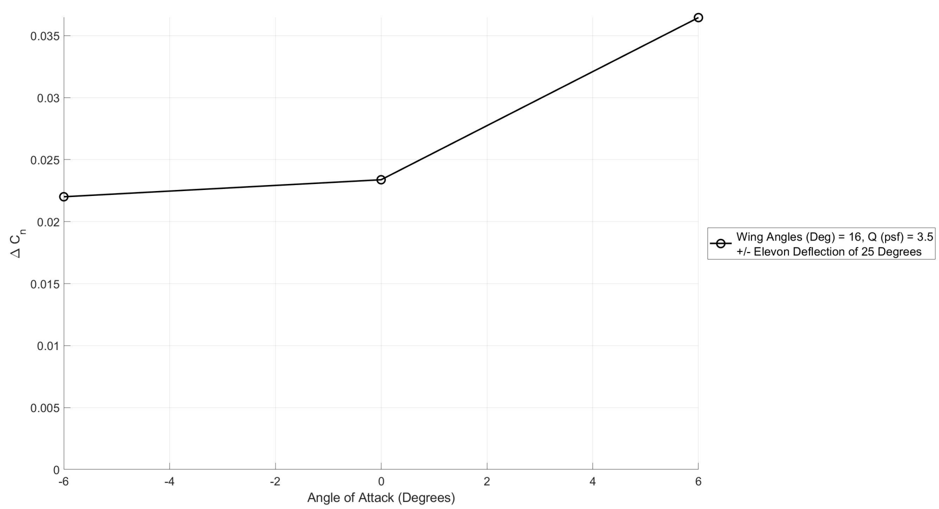

Figure 536. Wing angles 16 degrees trim point Δ C_n vs angle of attack for elevon deflection.

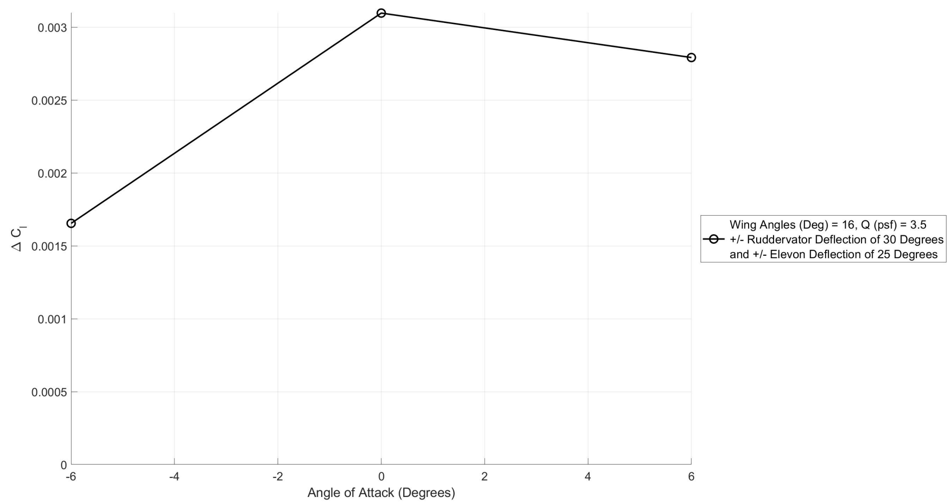

Figure 537. Wing angles 16 degrees trim point Δ C_l vs angle of attack for elevon and ruddervator deflection.

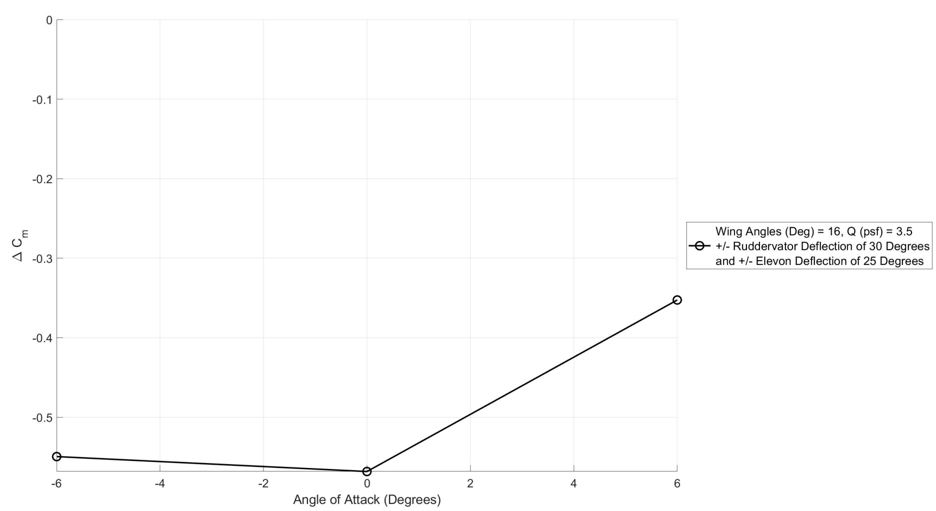

Figure 538. Wing angles 16 degrees trim point Δ C_m vs angle of attack for elevon and ruddervator deflection.

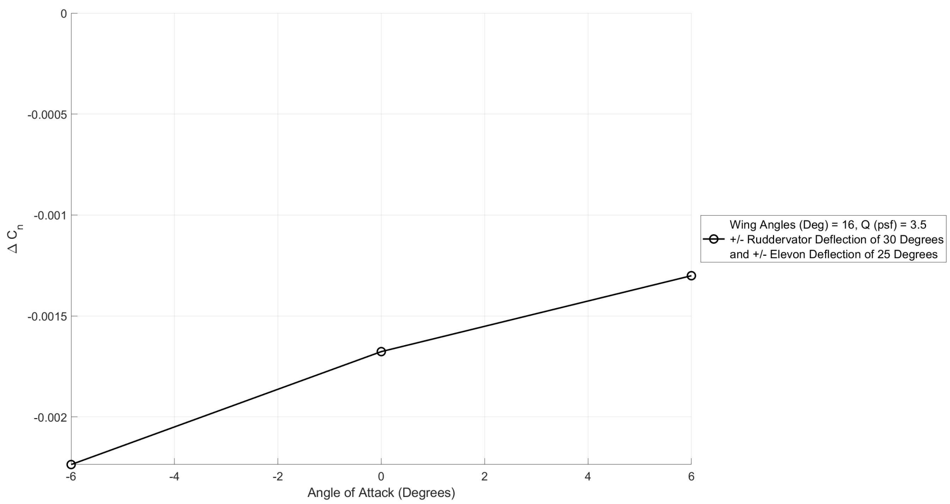

Figure 539. Wing angles 16 degrees trim point Δ C_n vs angle of attack for elevon and ruddervator deflection.

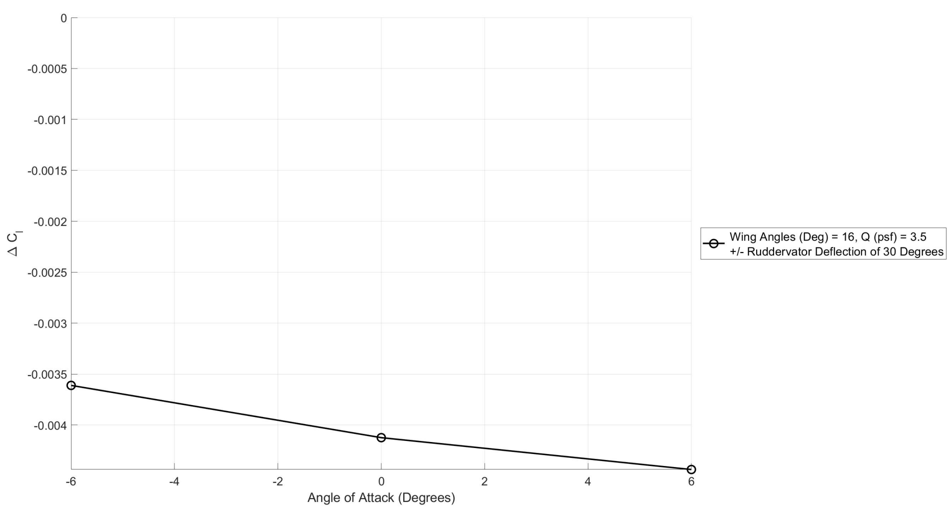

Figure 540. Wing angles 16 degrees trim point Δ C_l vs angle of attack for ruddervator deflection.

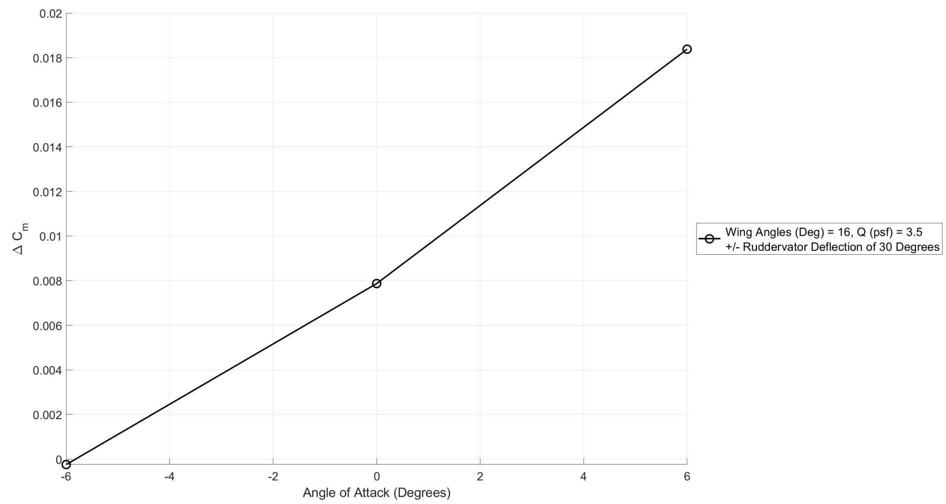

Figure 541. Wing angles 16 degrees trim point Δ C_m vs angle of attack for ruddervator deflection.

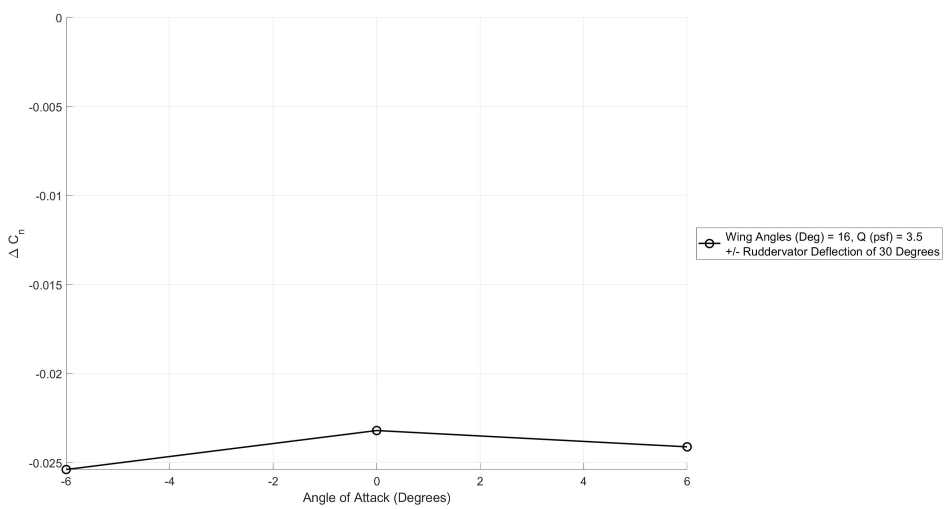

Figure 542. Wing angles 16 degrees trim point Δ C_n vs angle of attack for ruddervator deflection.

C.14 Transition Wing Angles 14 Degrees Performance and Stability Plots

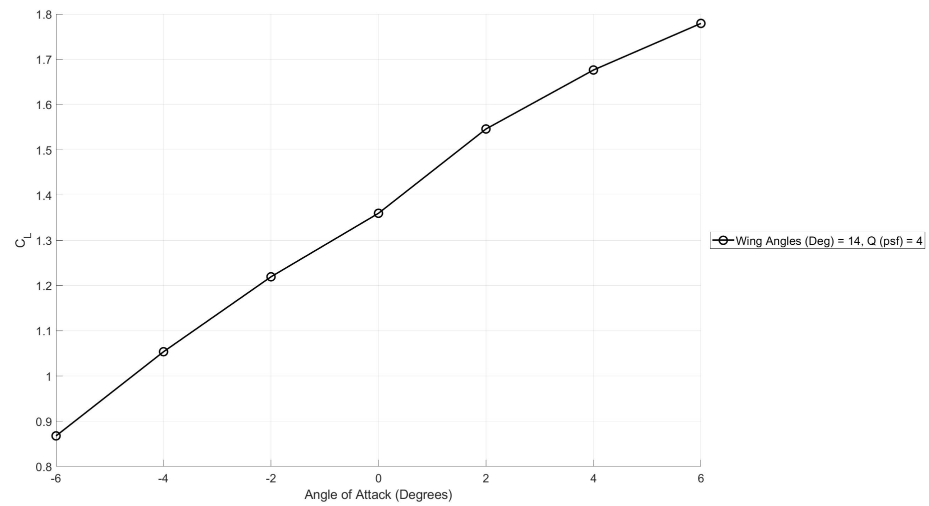

Figure 543. Wing angles 14 degrees trim point C_L vs angle of attack.

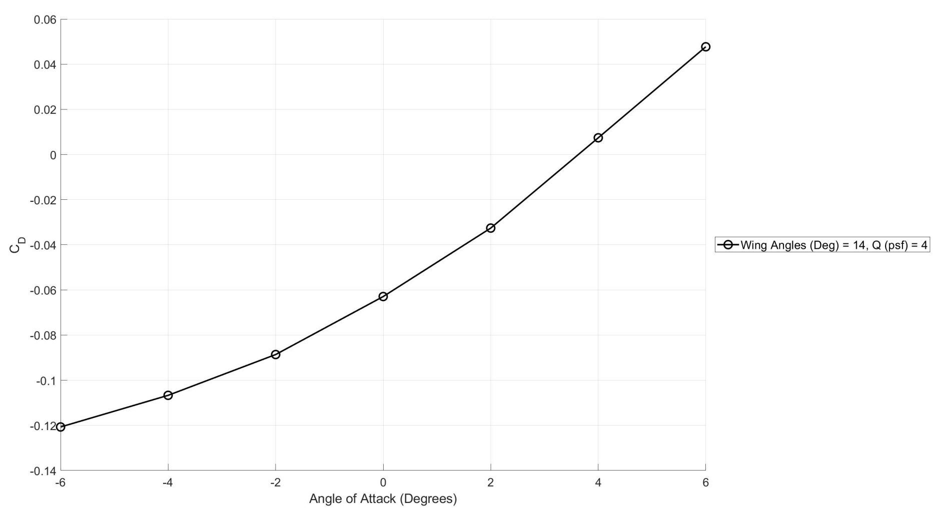

Figure 544. Wing angles 14 degrees trim point C_D vs angle of attack.

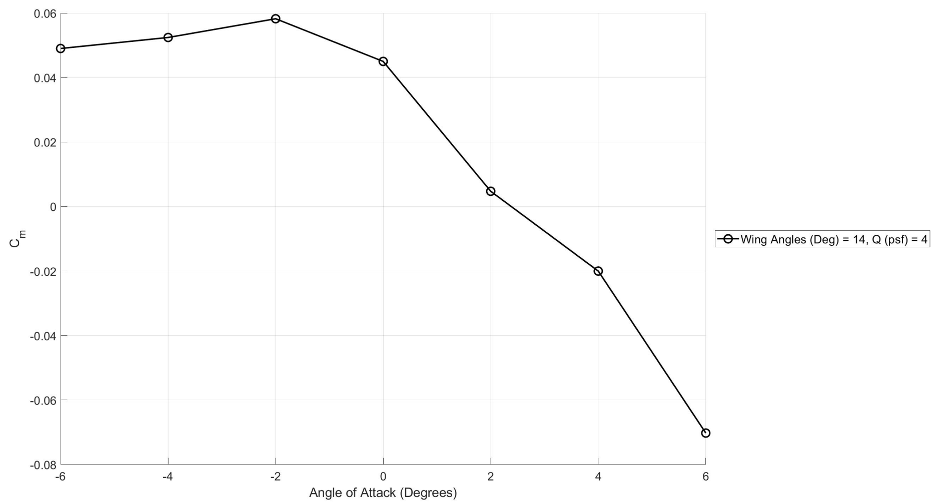

Figure 545. Wing angles 14 degrees trim point C_m vs angle of attack.

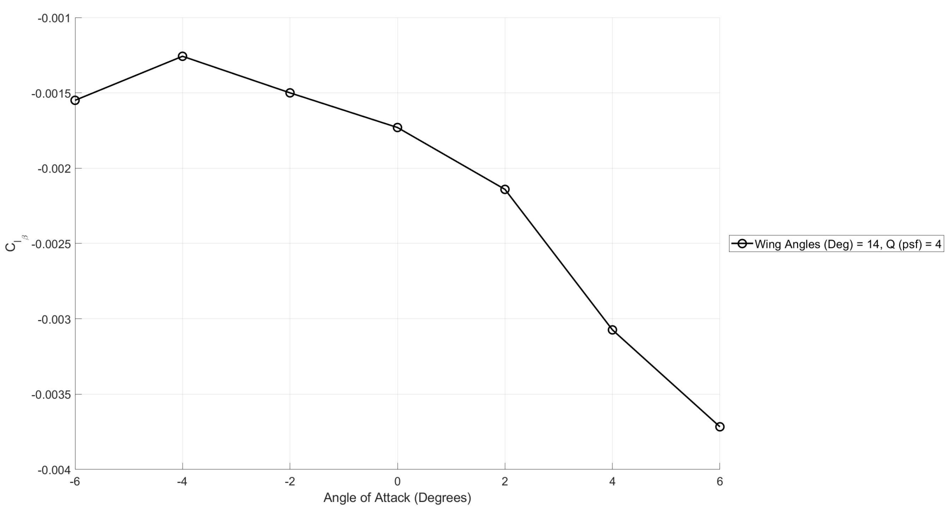

Figure 546. Wing angles 14 degrees trim point C_{l_β} vs angle of attack.

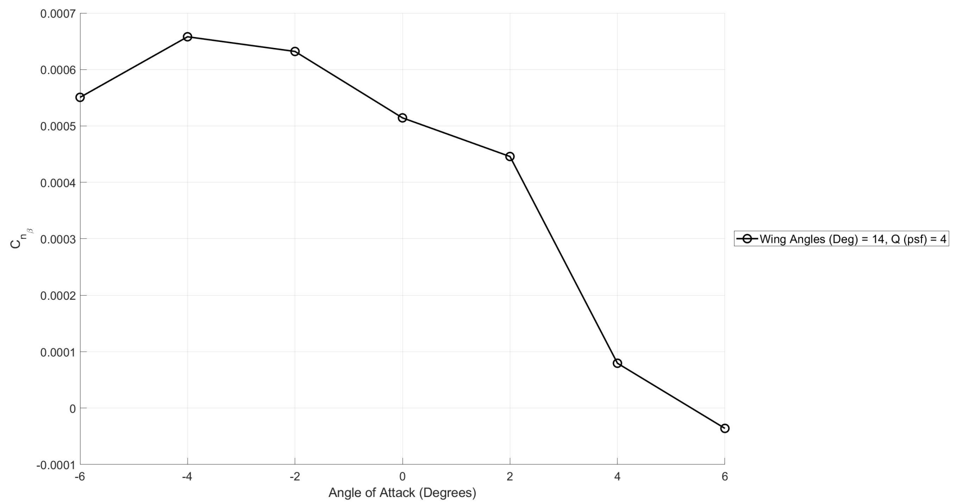

Figure 547. Wing angles 14 degrees trim point C_{n_β} vs angle of attack.

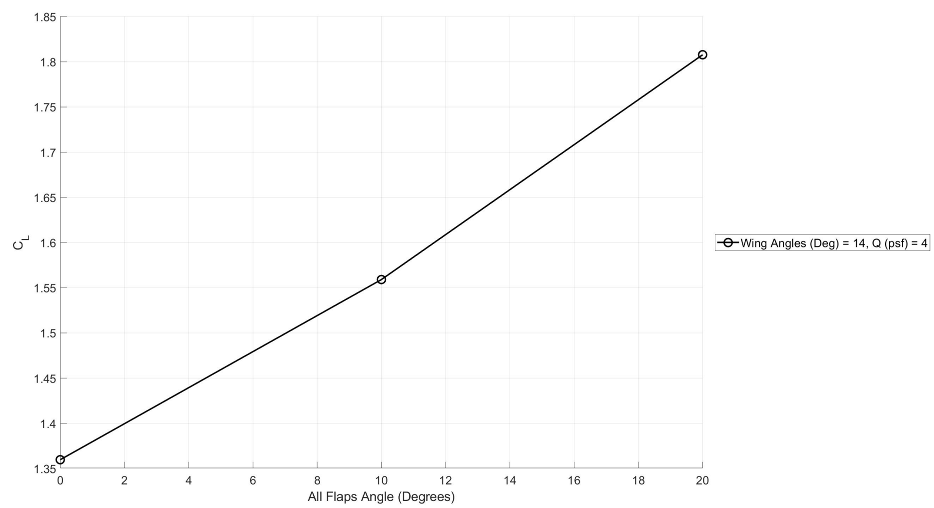

Figure 548. Wing angles 14 degrees trim point C_L vs all flap deflection angle.

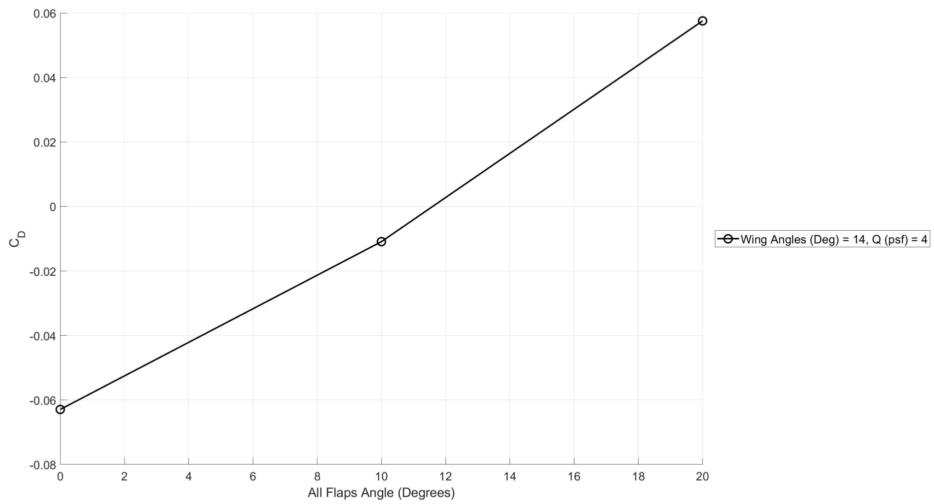

Figure 549. Wing angles 14 degrees trim point C_D vs all flap deflection angle.

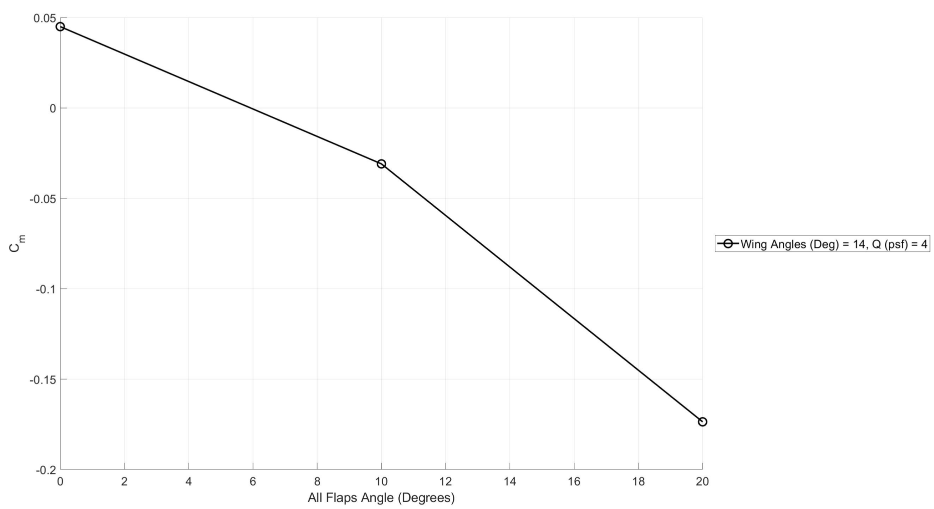

Figure 550. Wing angles 14 degrees trim point C_m vs all flap deflection angle.

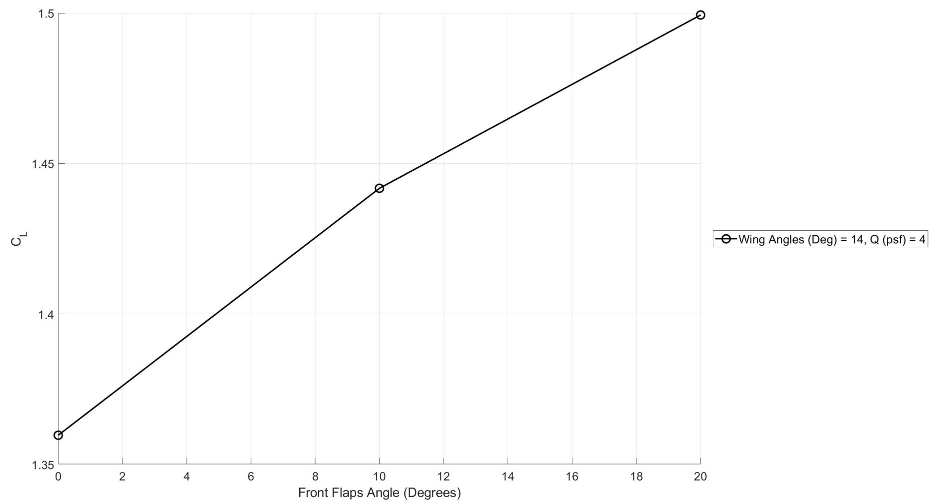

Figure 551. Wing angles 14 degrees trim point C_L vs front flap deflection angle.

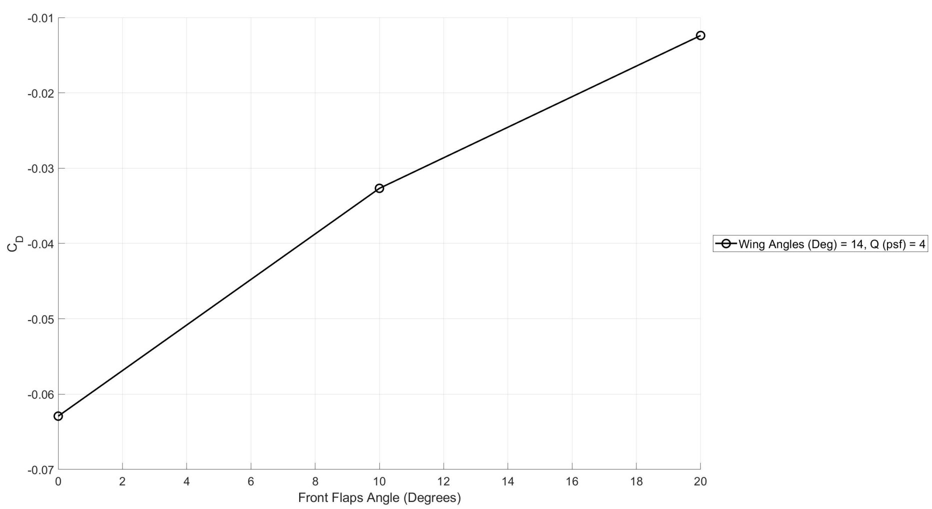

Figure 552. Wing angles 14 degrees trim point C_D vs front flap deflection angle.

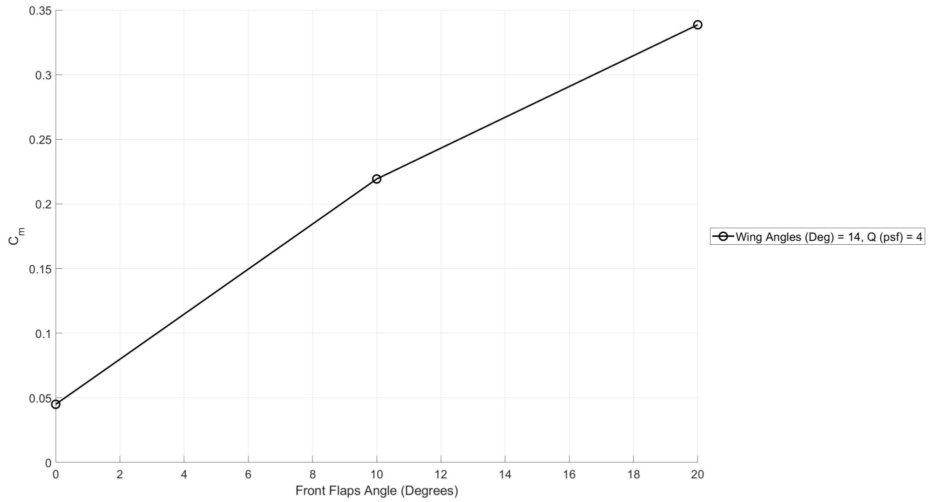

Figure 553. Wing angles 14 degrees trim point C_m vs front flap deflection angle.

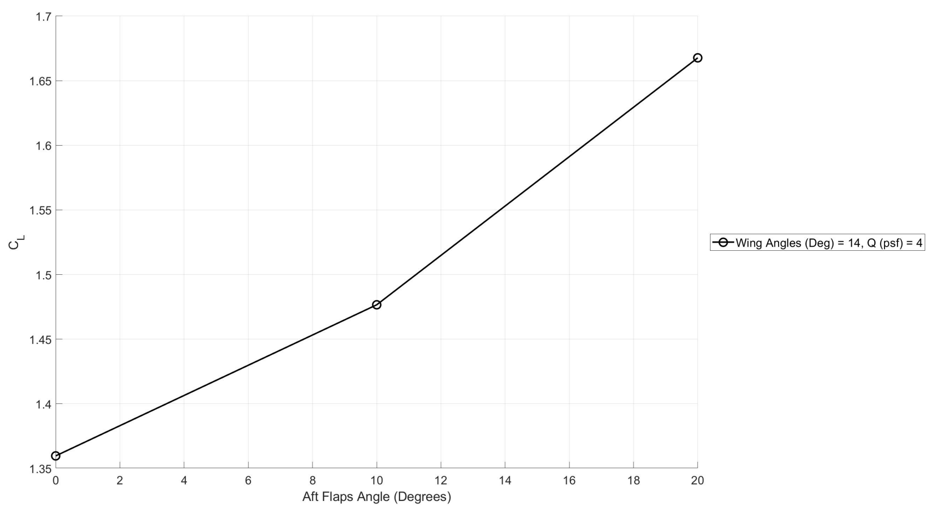

Figure 554. Wing angles 14 degrees trim point C_L vs aft flap deflection angle.

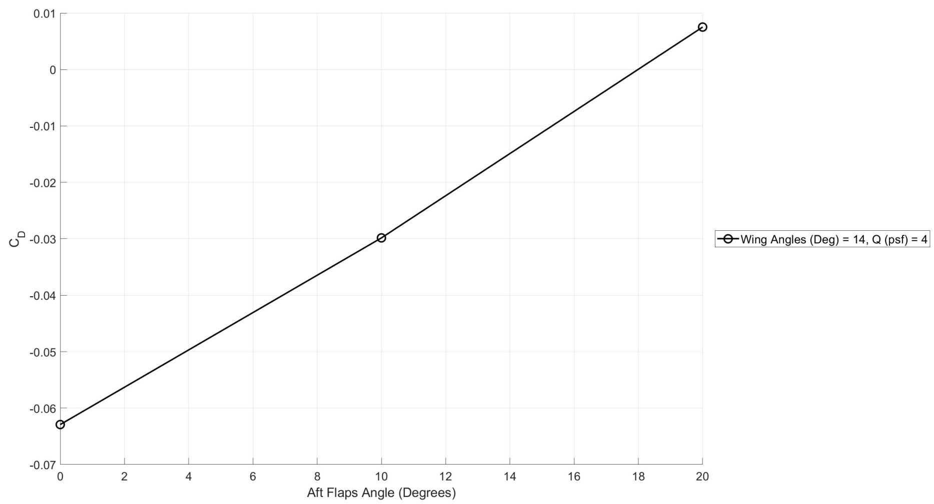

Figure 555. Wing angles 14 degrees trim point C_D vs aft flap deflection angle.

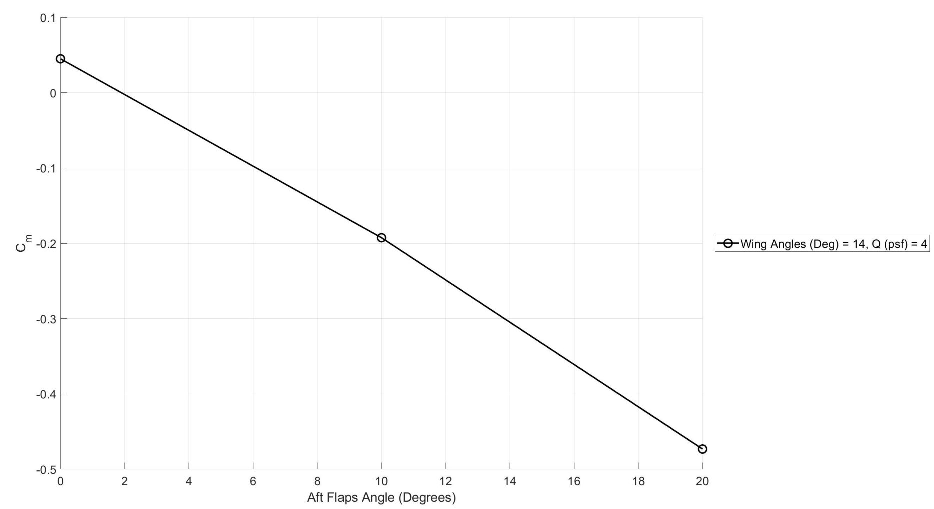

Figure 556. Wing angles 14 degrees trim point C_m vs aft flap deflection angle.

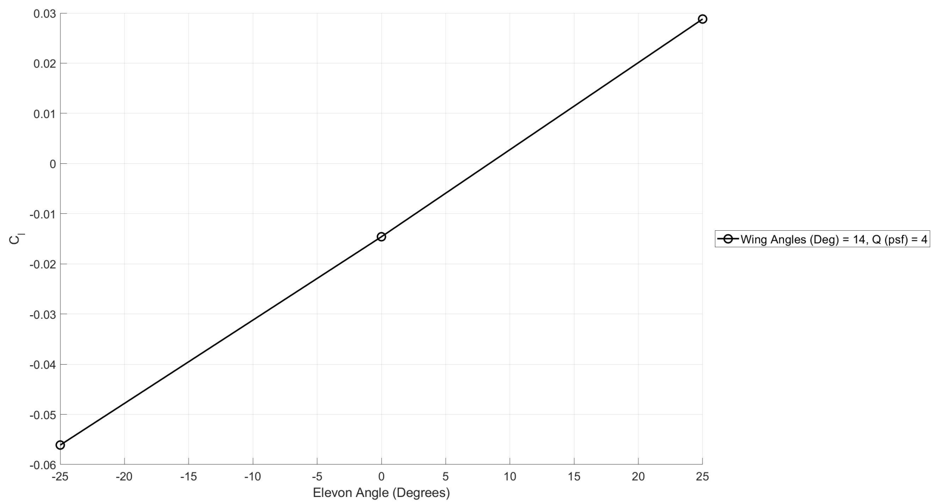

Figure 557. Wing angles 14 degrees trim point C_l vs elevon deflection angle.

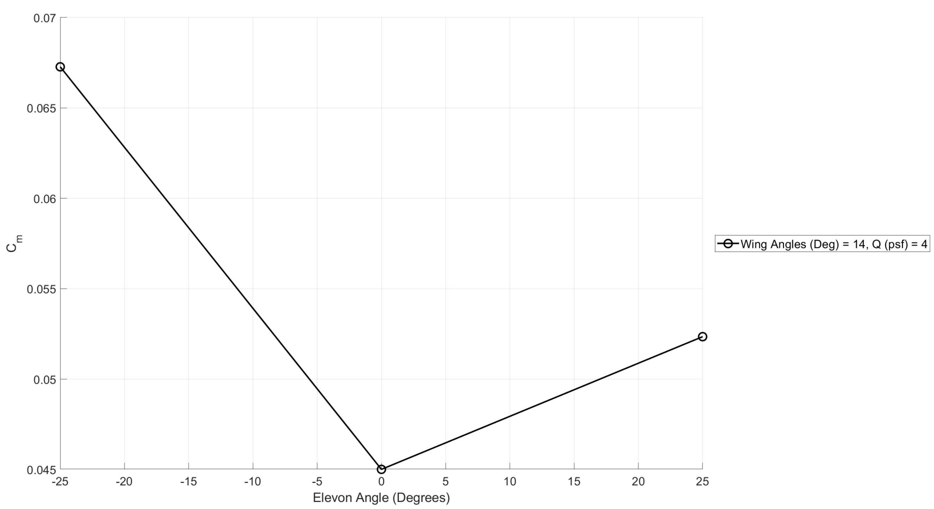

Figure 558. Wing angles 14 degrees trim point C_m vs elevon deflection angle.

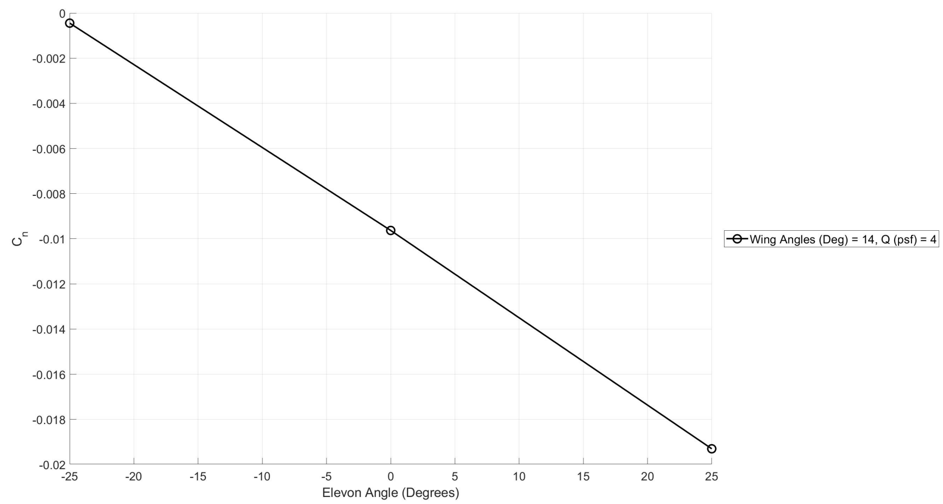

Figure 559. Wing angles 14 degrees trim point C_n vs elevon deflection angle.

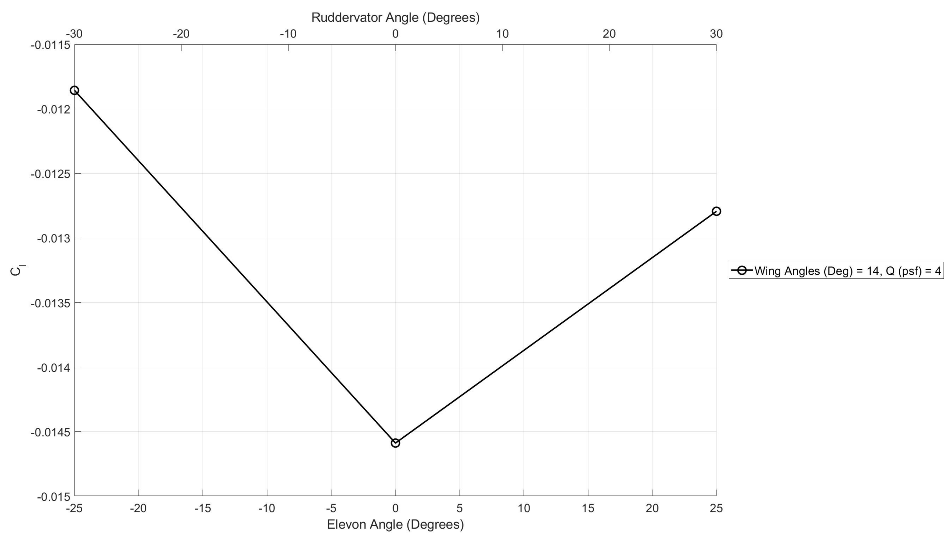

Figure 560. Wing angles 14 degrees trim point C_l vs elevon and ruddervator deflection angles.

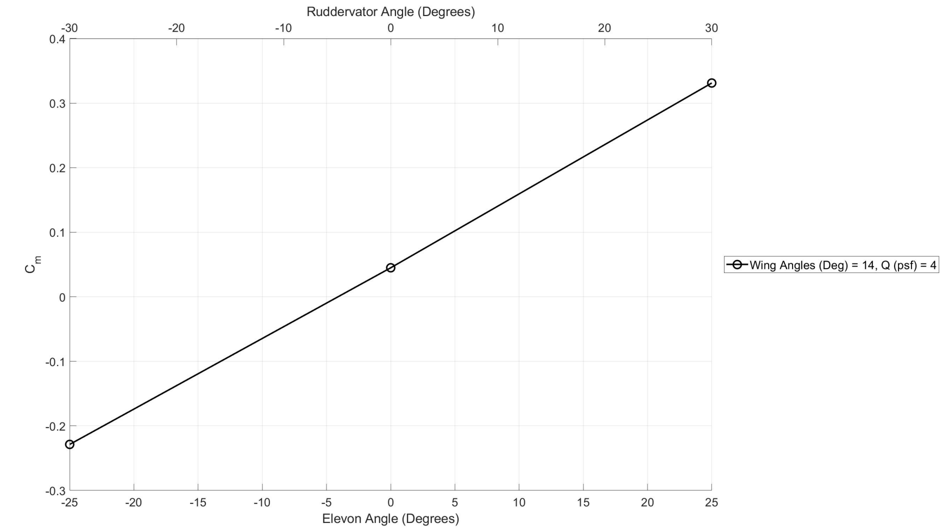

Figure 561. Wing angles 14 degrees trim point C_m vs elevon and ruddervator deflection angles.

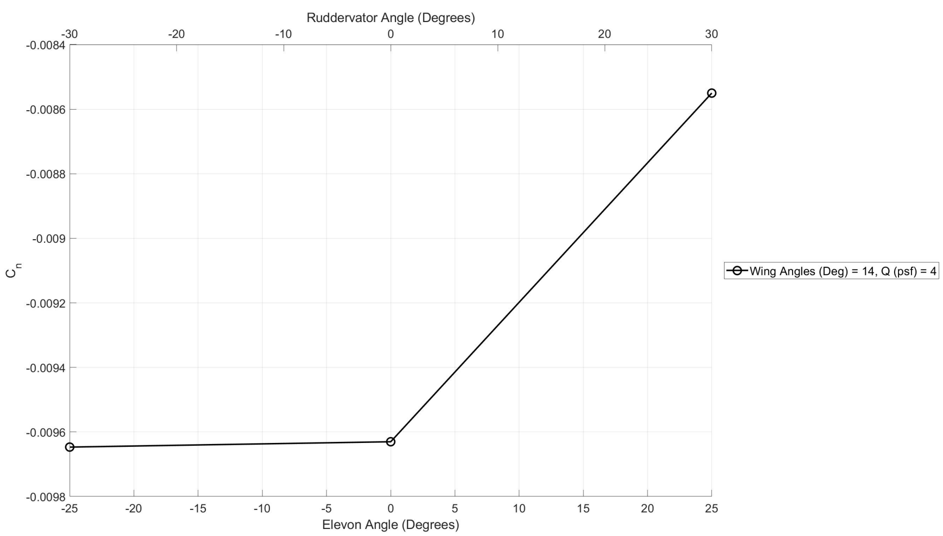

Figure 562. Wing angles 14 degrees trim point C_n vs elevon and ruddervator deflection angles.

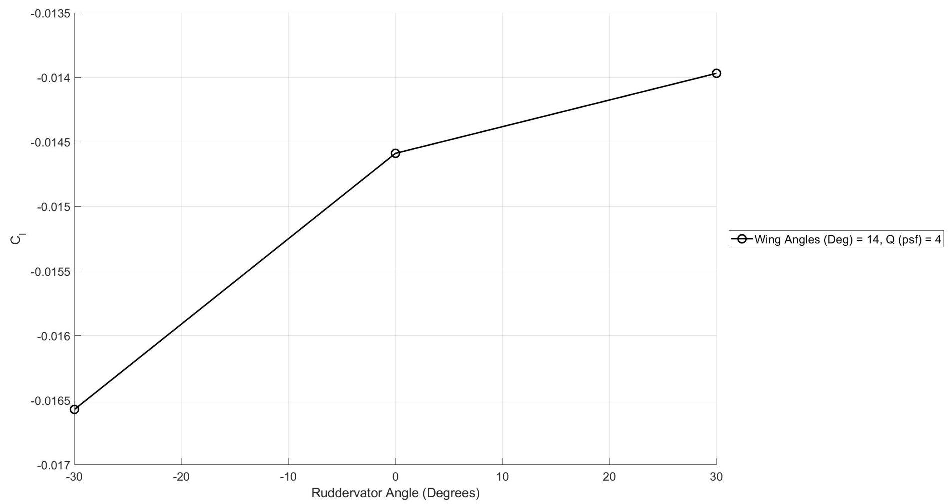

Figure 563. Wing angles 14 degrees trim point C_l vs ruddervator deflection angle.

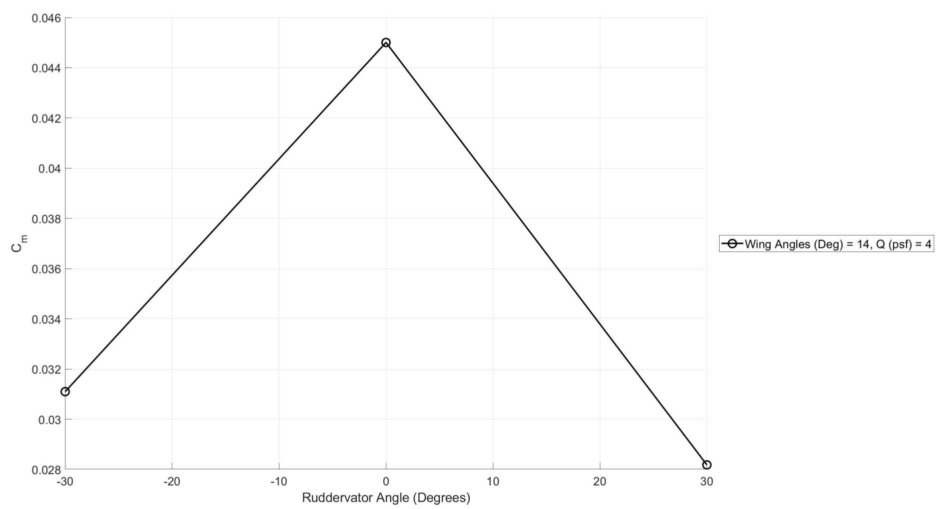

Figure 564. Wing angles 14 degrees trim point C_m vs ruddervator deflection angle.

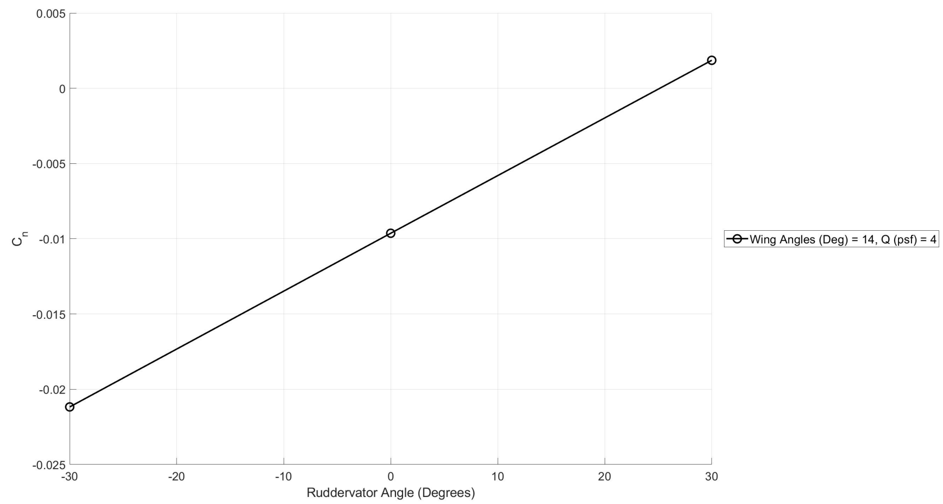

Figure 565. Wing angles 14 degrees trim point C_n vs ruddervator deflection angle.

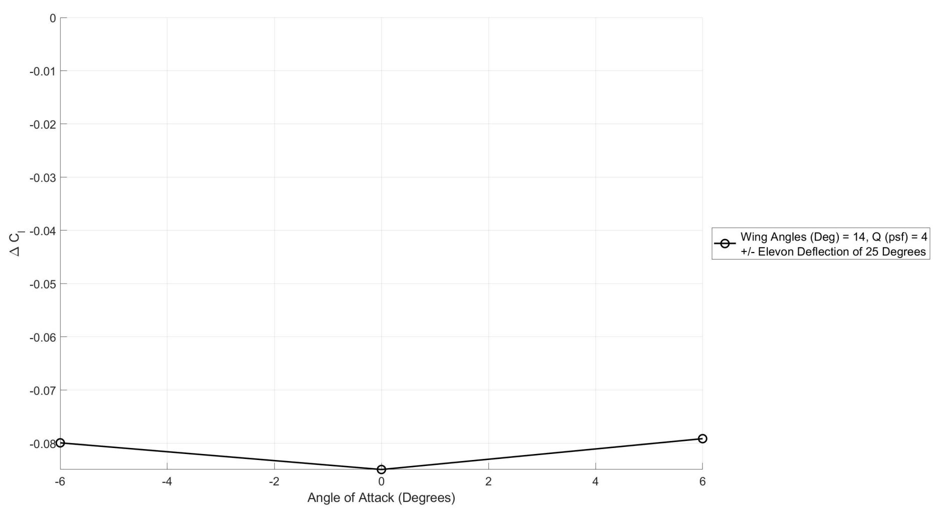

Figure 566. Wing angles 14 degrees trim point Δ C_l vs angle of attack for elevon deflection.

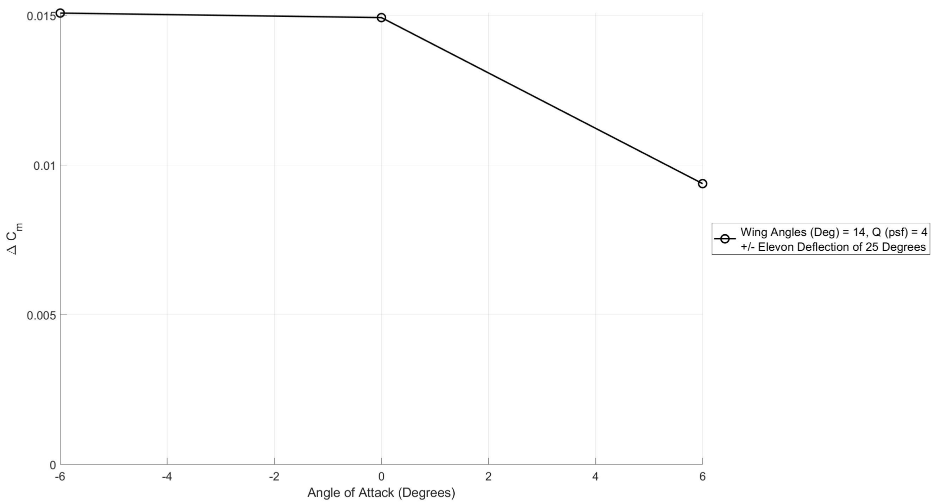

Figure 567. Wing angles 14 degrees trim point Δ C_m vs angle of attack for elevon deflection.

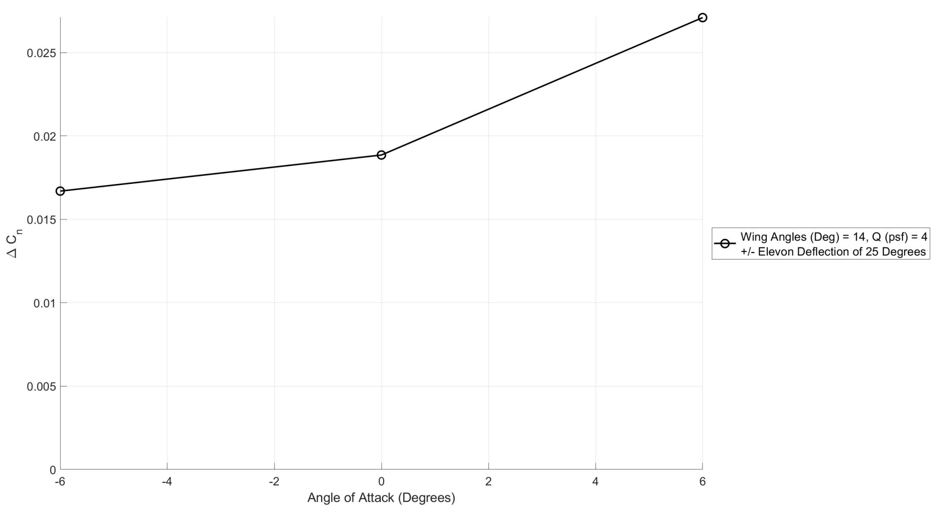

Figure 568. Wing angles 14 degrees trim point Δ C_n vs angle of attack for elevon deflection.

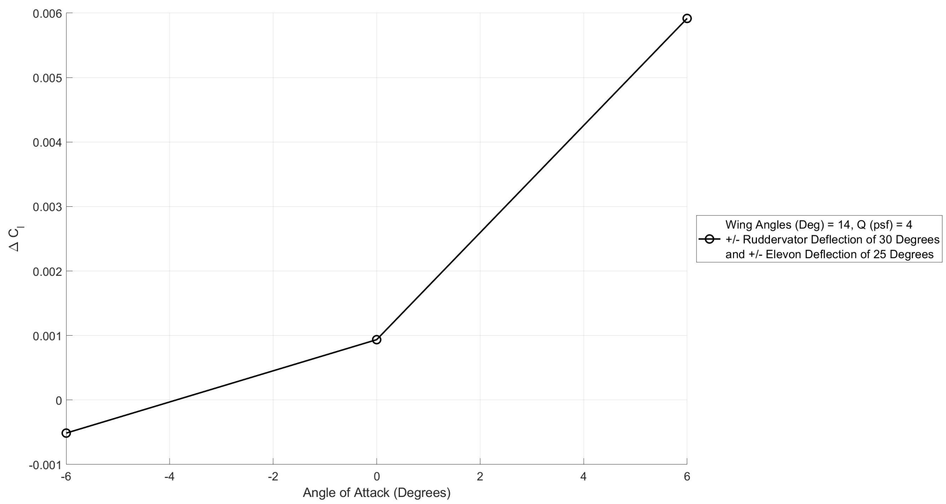

Figure 569. Wing angles 14 degrees trim point Δ C_l vs angle of attack for elevon and ruddervator deflection.

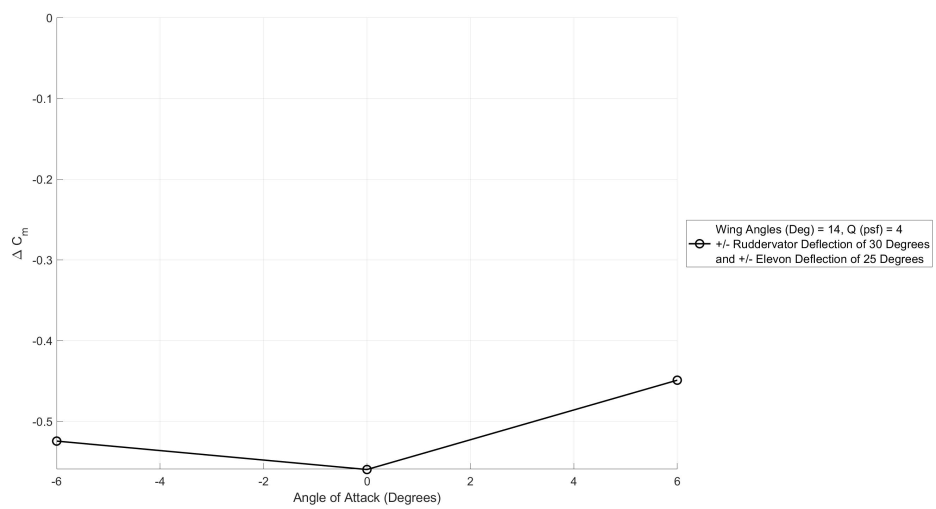

Figure 570. Wing angles 14 degrees trim point Δ C_m vs angle of attack for elevon and ruddervator deflection.

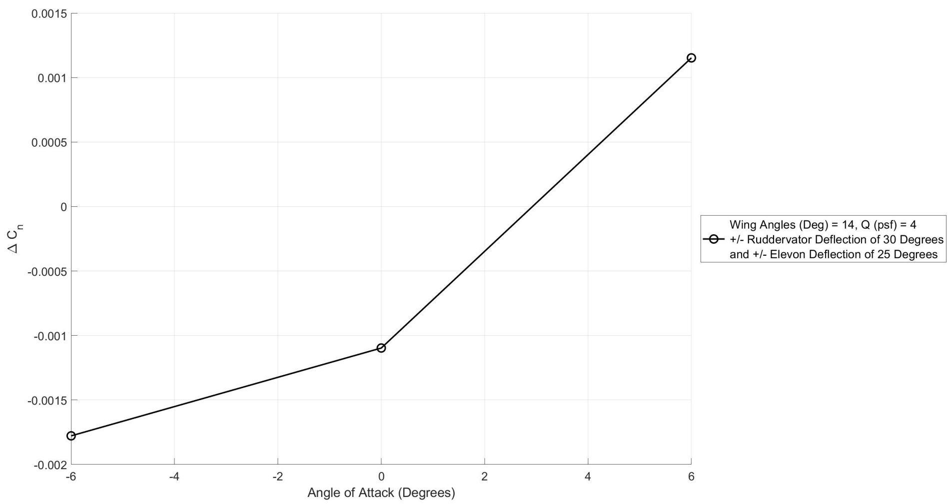

Figure 571. Wing angles 14 degrees trim point Δ C_n vs angle of attack for elevon and ruddervator deflection.

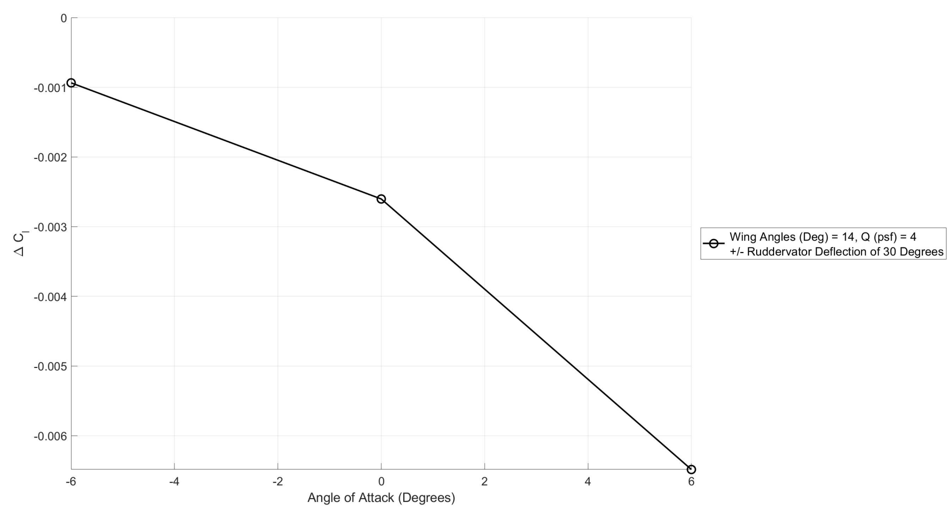

Figure 572. Wing angles 14 degrees trim point Δ C_l vs angle of attack for ruddervator deflection.

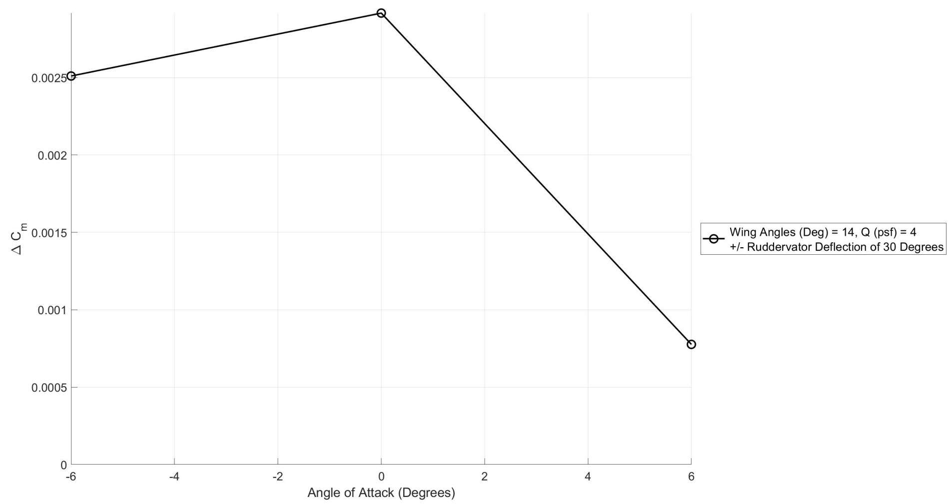

Figure 573. Wing angles 14 degrees trim point Δ C_m vs angle of attack for ruddervator deflection.

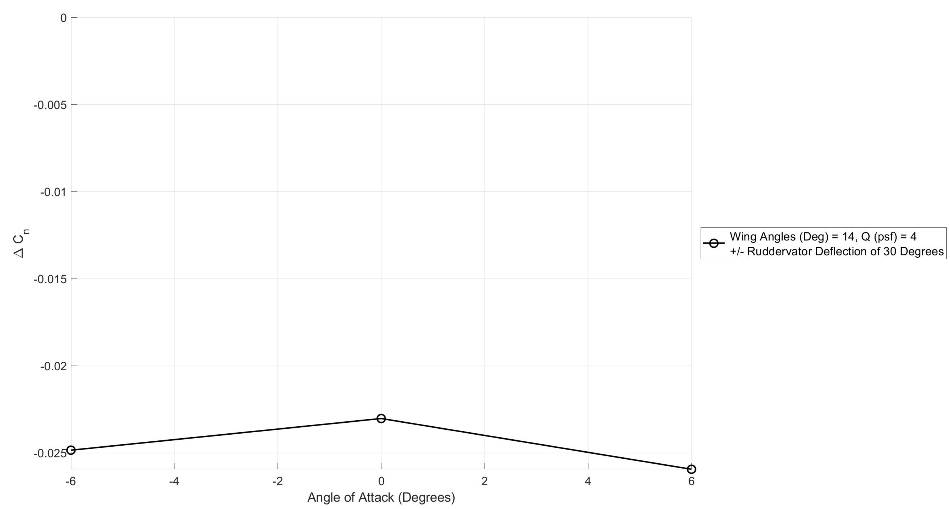

Figure 574. Wing angles 14 degrees trim point Δ C_n vs angle of attack for ruddervator deflection.

Appendix D

Forward Flight Performance and Stability Plots

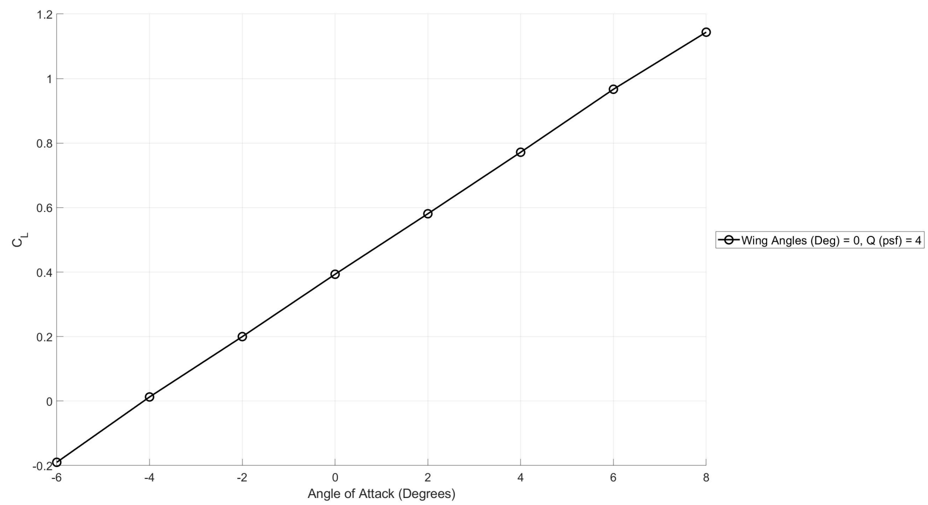

Figure 575. Forward flight trim point C_L vs angle of attack.

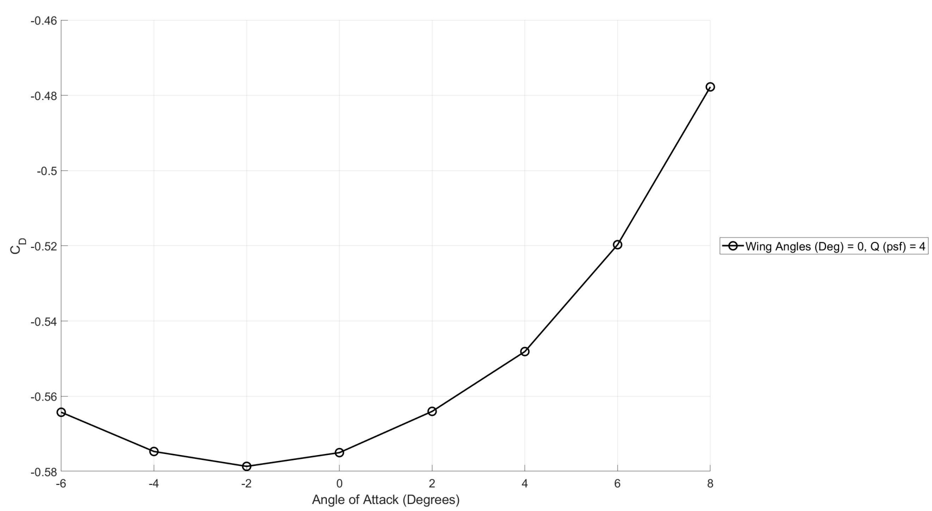

Figure 576. Forward flight trim point C_D vs angle of attack.

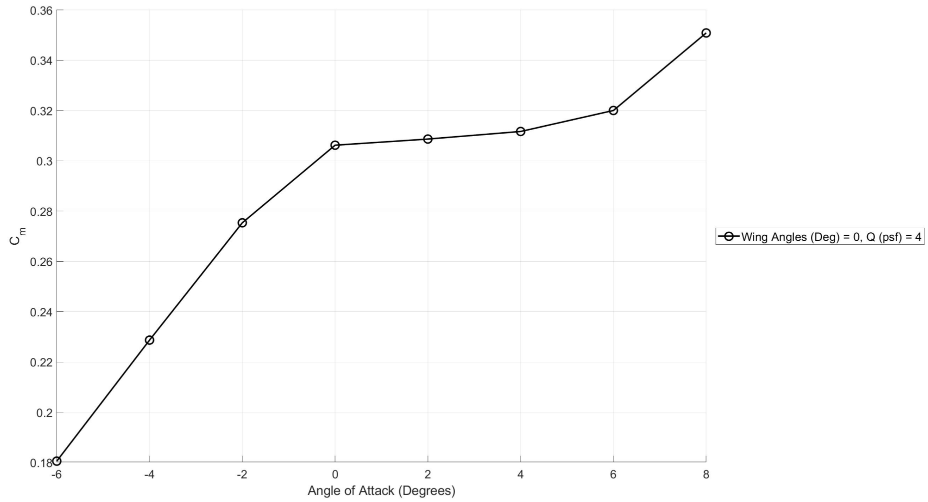

Figure 577. Forward flight trim point C_m vs angle of attack.

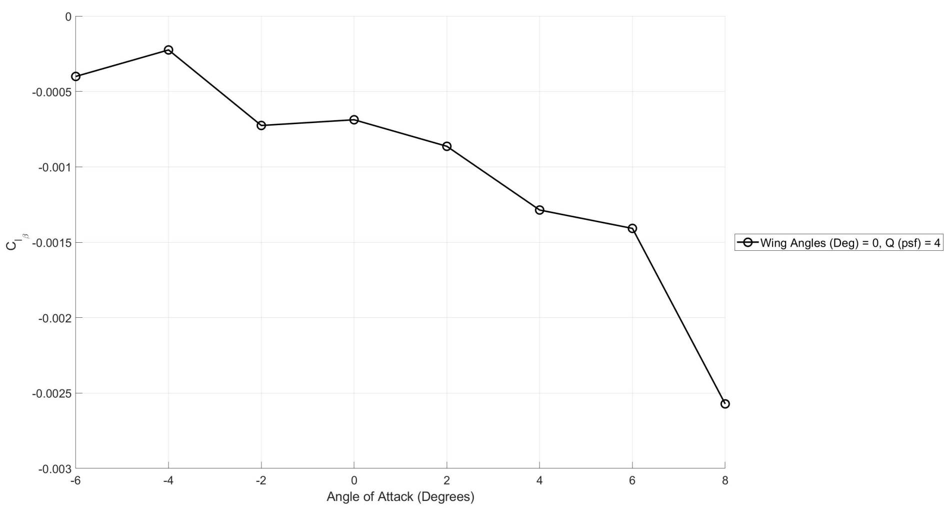

Figure 578. Forward flight trim point C_{l_β} vs angle of attack.

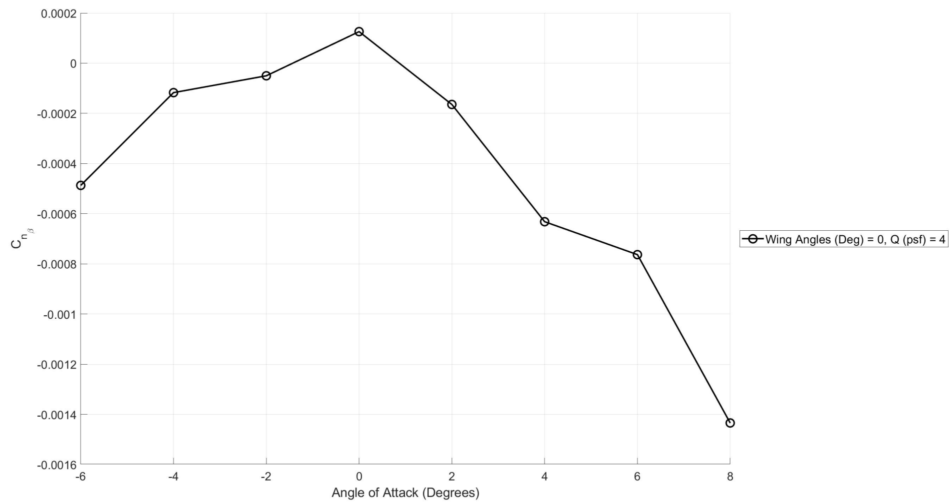

Figure 579. Forward flight trim point C_{n_β} vs angle of attack.

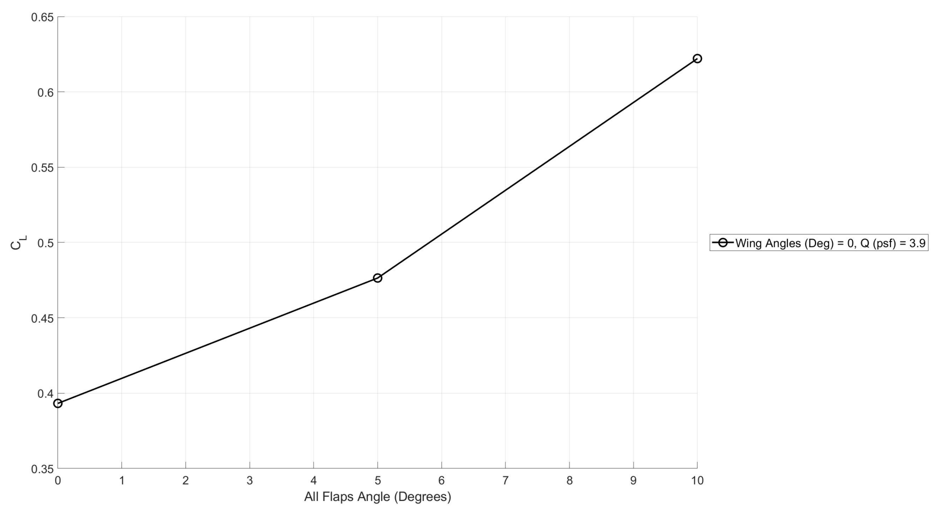

Figure 580. Forward flight trim point C_L vs all flap deflection angle.

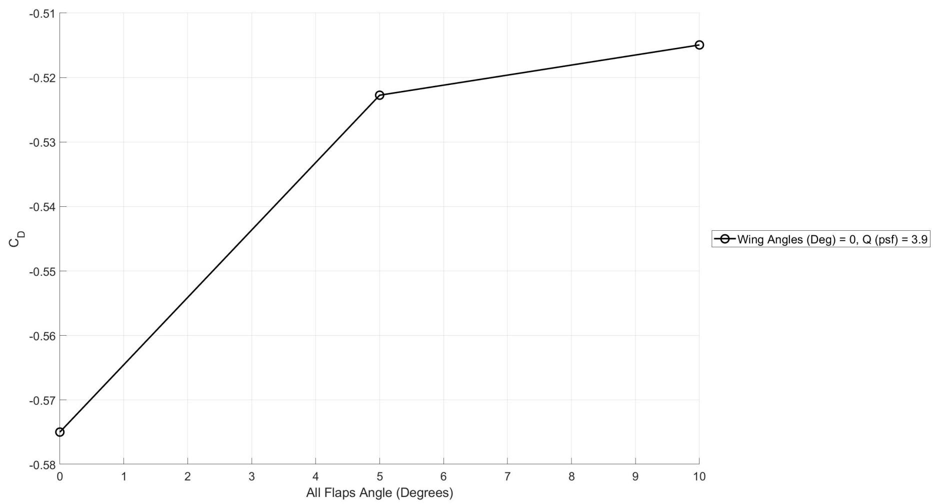

Figure 581. Forward flight trim point C_D vs all flap deflection angle.

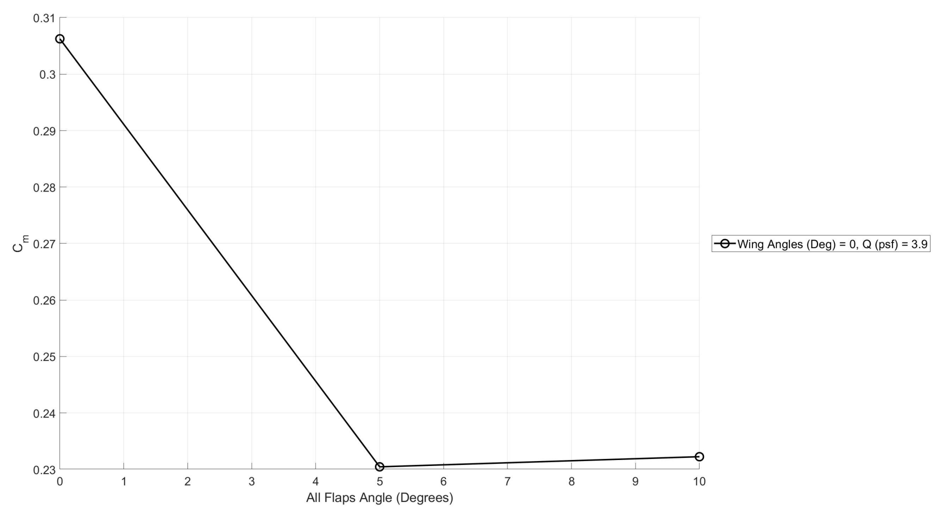

Figure 582. Forward flight trim point C_m vs all flap deflection angle.

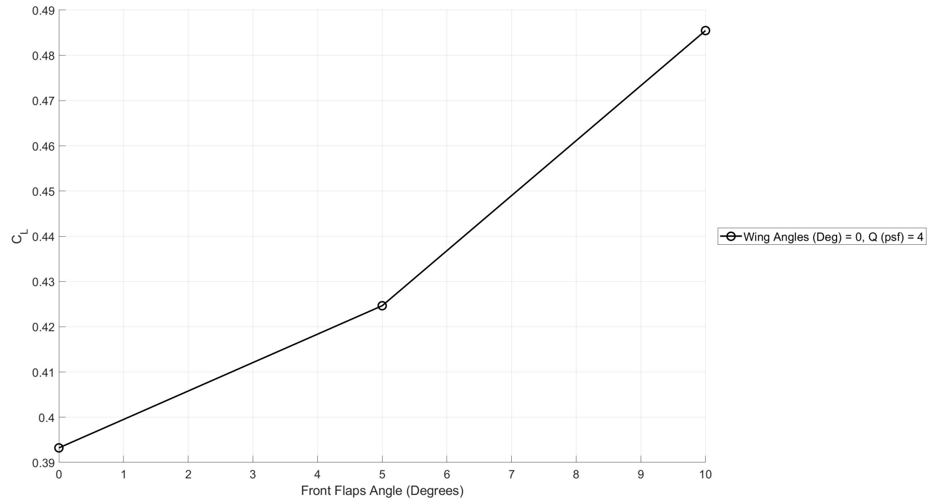

Figure 583. Forward flight trim point C_L vs front flap deflection angle.

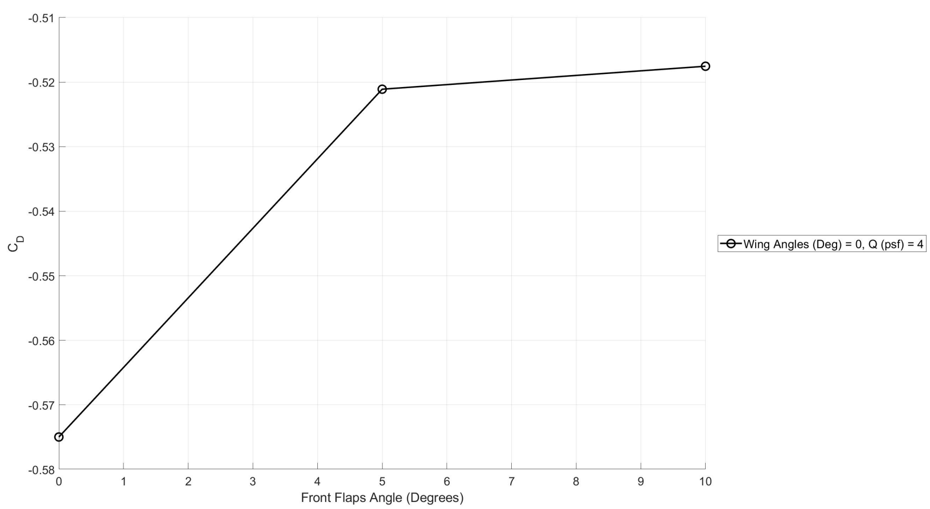

Figure 584. Forward flight trim point C_D vs front flap deflection angle.

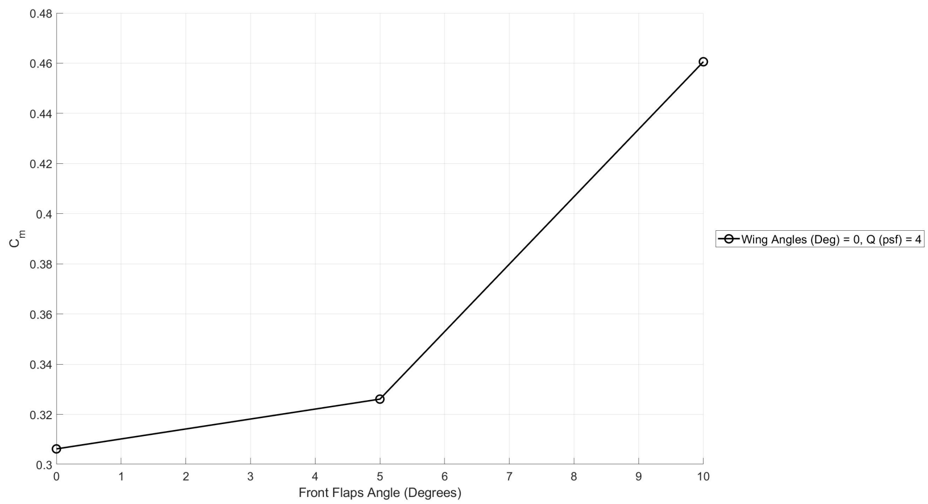

Figure 585. Forward flight trim point C_m vs front flap deflection angle.

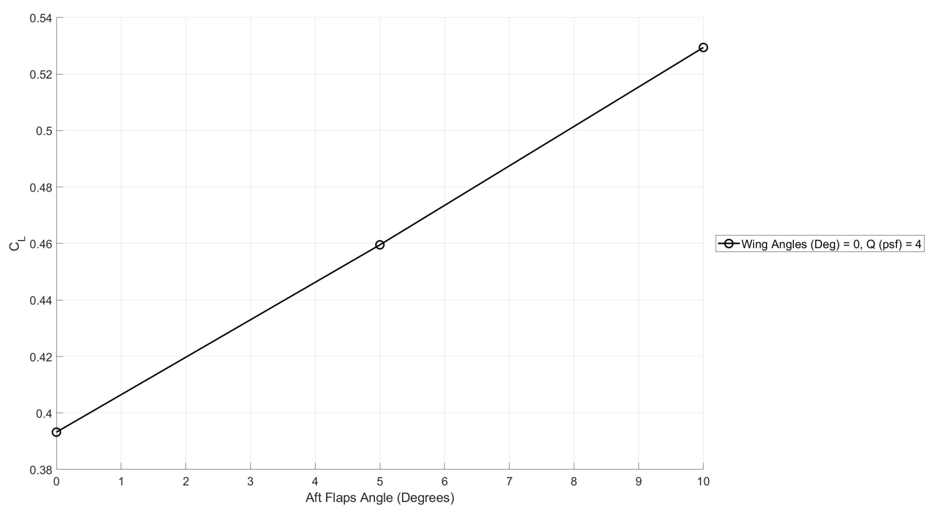

Figure 586. Forward flight trim point C_L vs aft flap deflection angle.

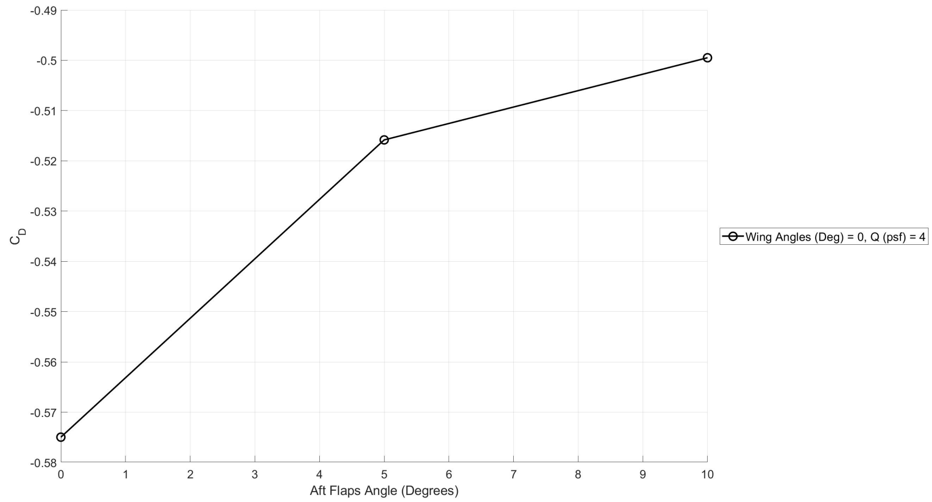

Figure 587. Forward flight trim point C_D vs aft flap deflection angle.

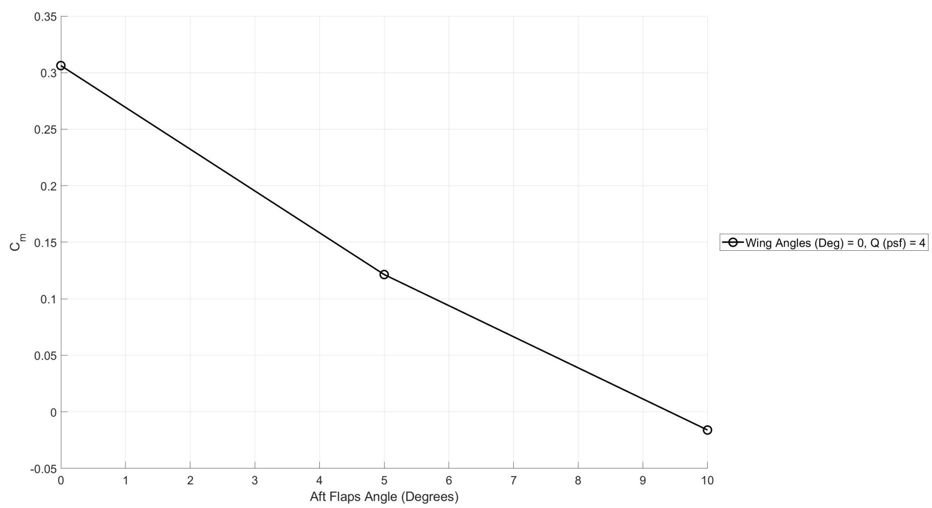

Figure 588. Forward flight trim point C_m vs aft flap deflection angle.

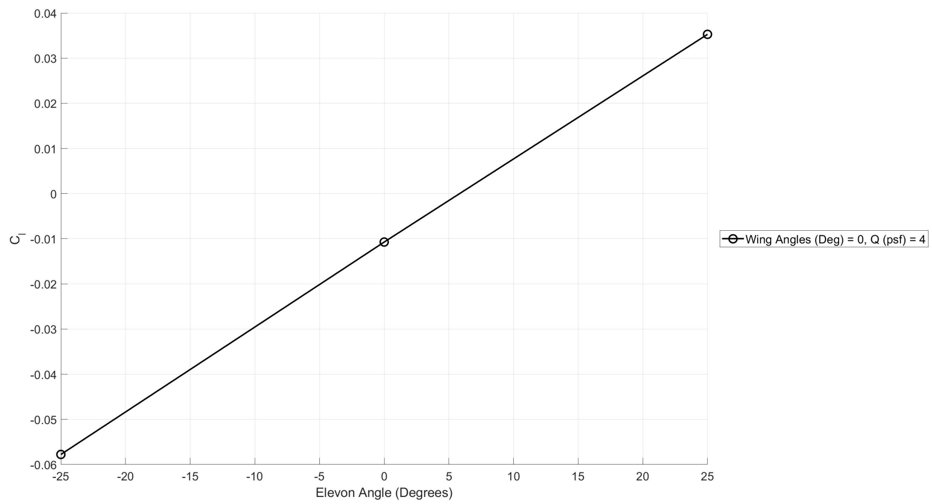

Figure 589. Forward flight trim point C_l vs elevon deflection angle.

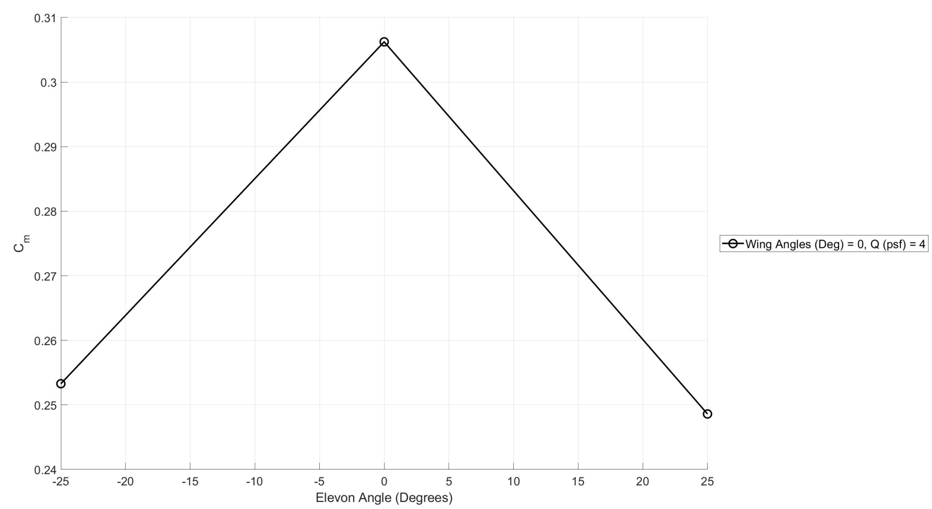

Figure 590. Forward flight trim point C_m vs elevon deflection angle.

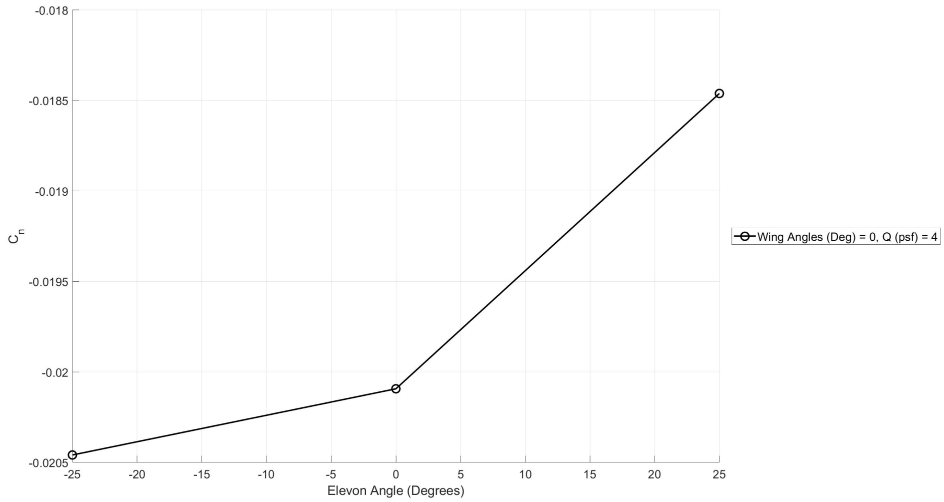

Figure 591. Forward flight trim point C_n vs elevon deflection angle.

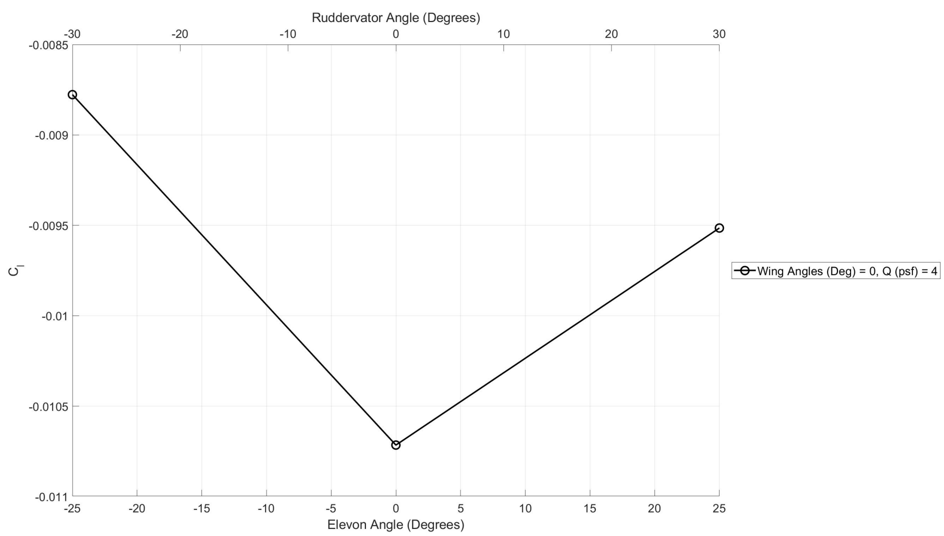

Figure 592. Forward flight trim point C_l vs elevon and ruddervator deflection angles.

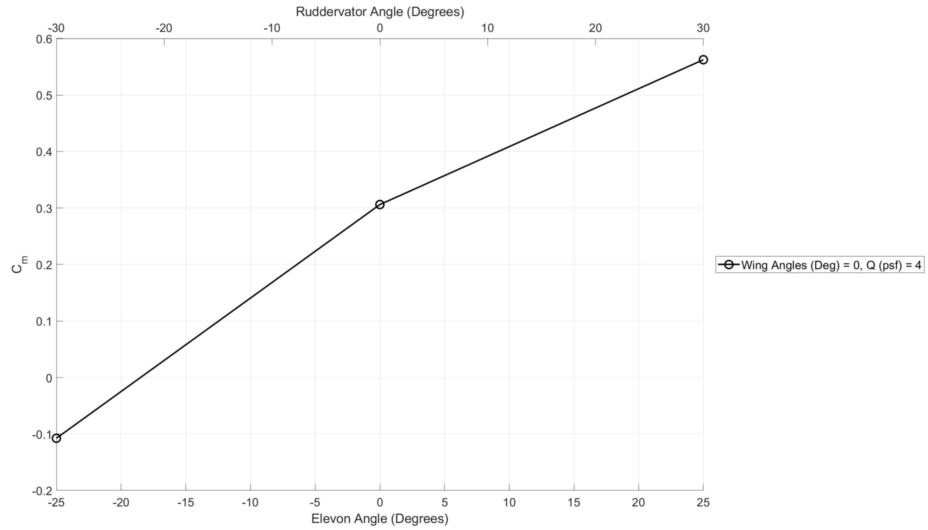

Figure 593. Forward flight trim point C_m vs elevon and ruddervator deflection angles.

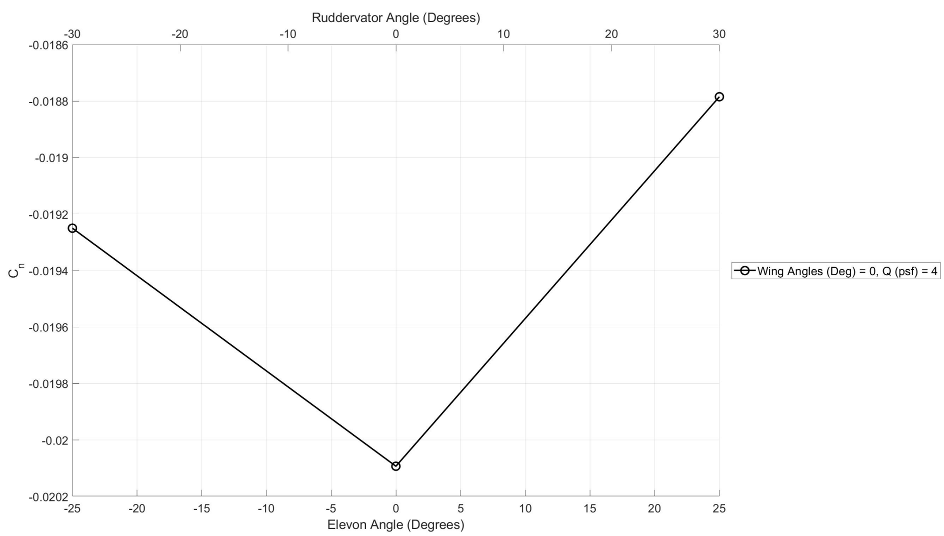

Figure 594. Forward flight trim point C_n vs elevon and ruddervator deflection angles.

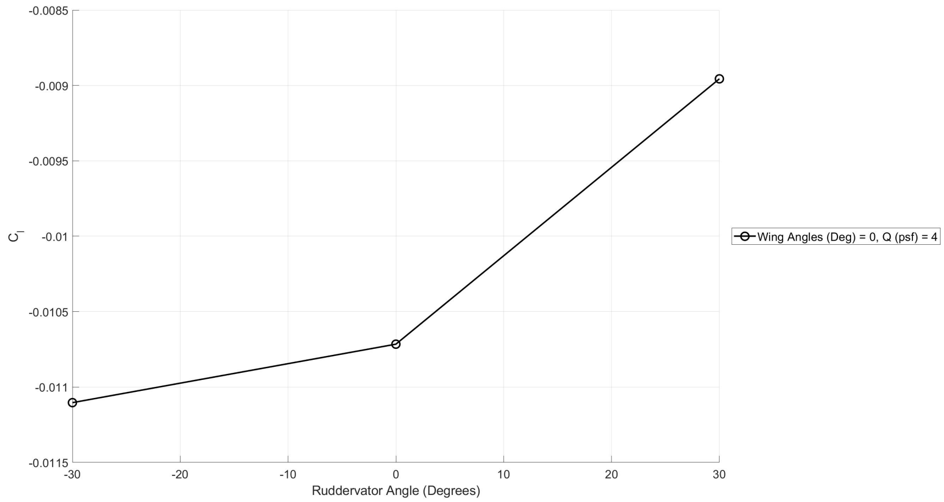

Figure 595. Forward flight trim point C_l vs ruddervator deflection angle.

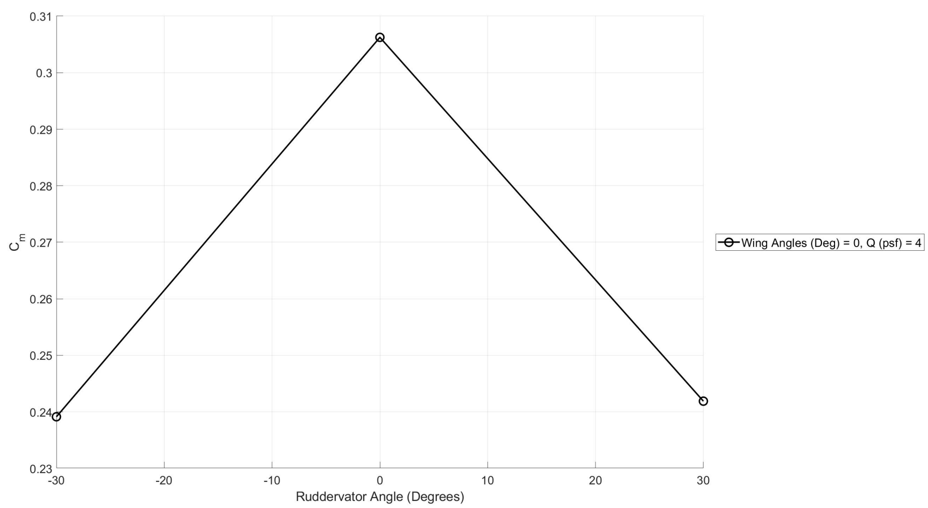

Figure 596. Forward flight trim point C_m vs ruddervator deflection angle.

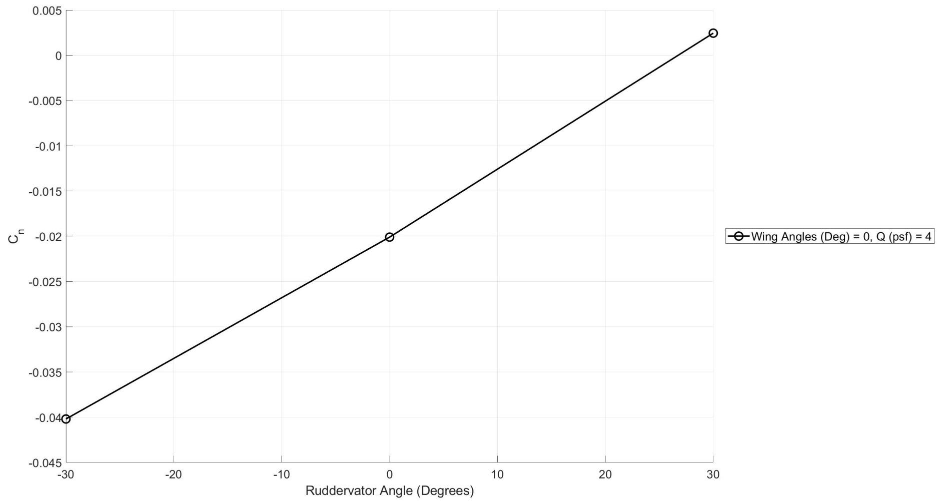

Figure 597. Forward flight trim point C_n vs ruddervator deflection angle.

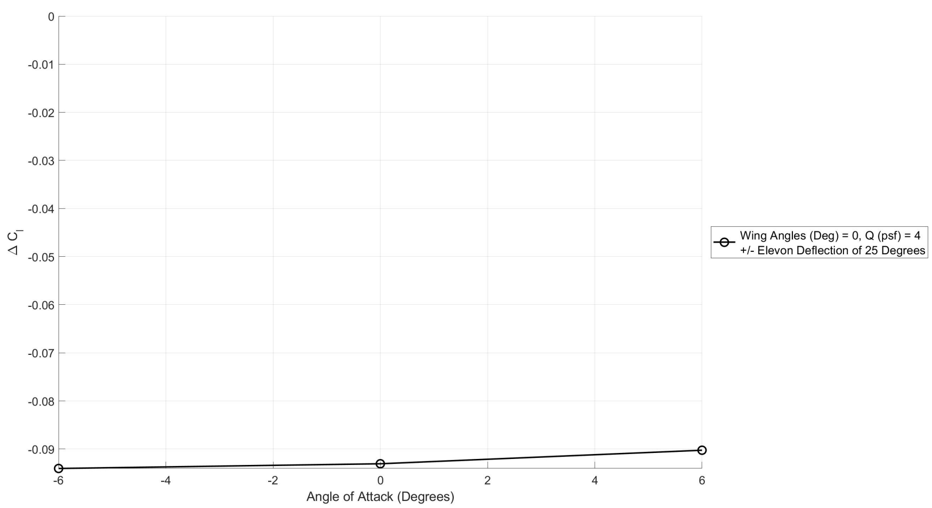

Figure 598. Forward flight trim point Δ C_l vs angle of attack for elevon deflection.

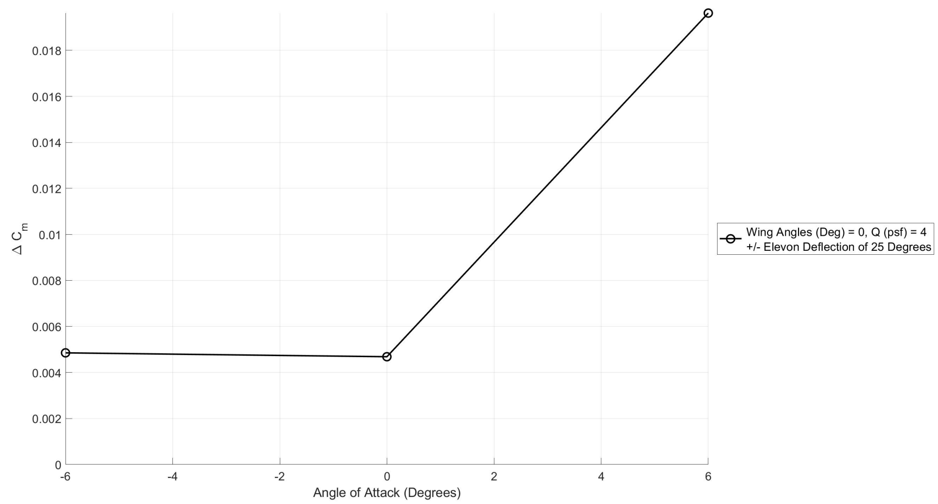

Figure 599. Forward flight trim point Δ C_m vs angle of attack for elevon deflection.

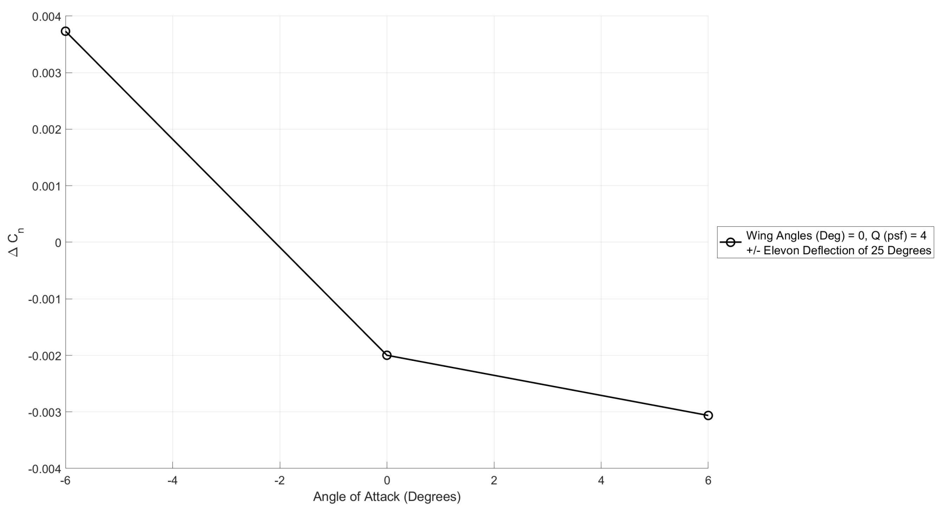

Figure 600. Forward flight trim point Δ C_n vs angle of attack for elevon deflection.

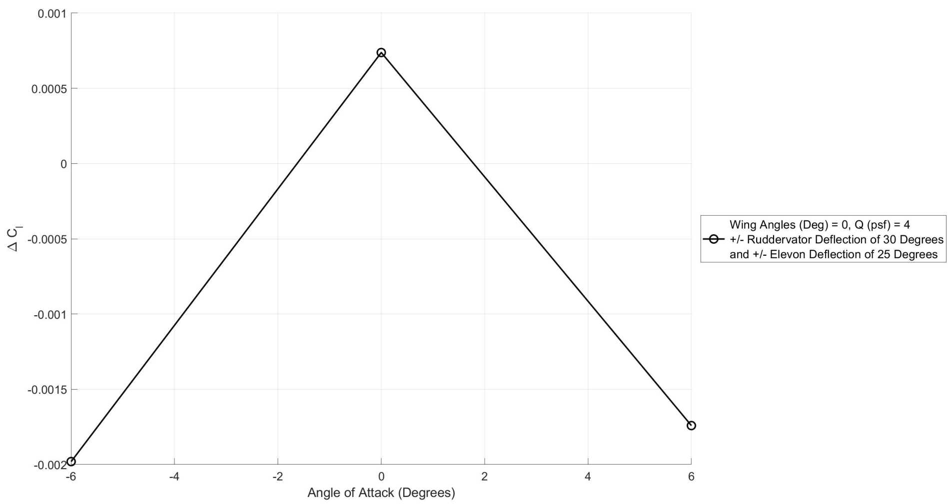

Figure 601. Forward flight trim point Δ C_l vs angle of attack for elevon and ruddervator deflection.

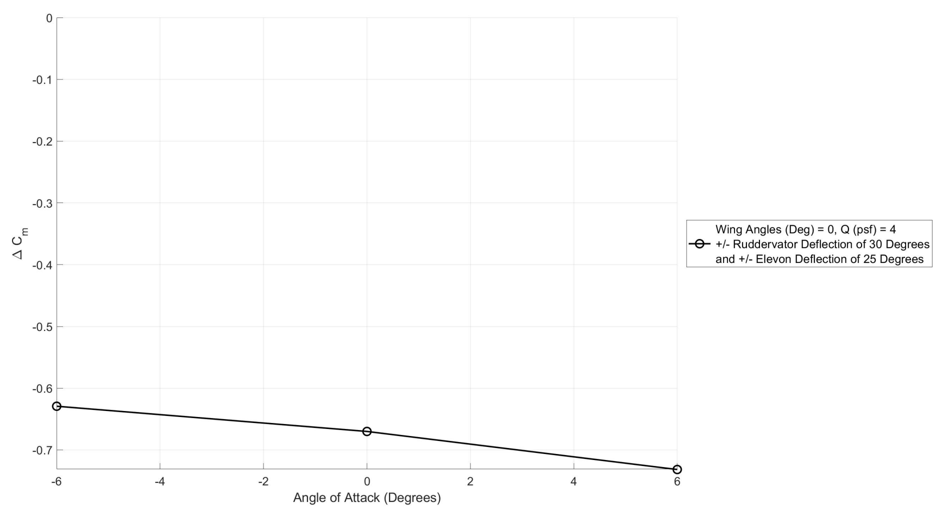

Figure 602. Forward flight trim point Δ C_m vs angle of attack for elevon and ruddervator deflection.

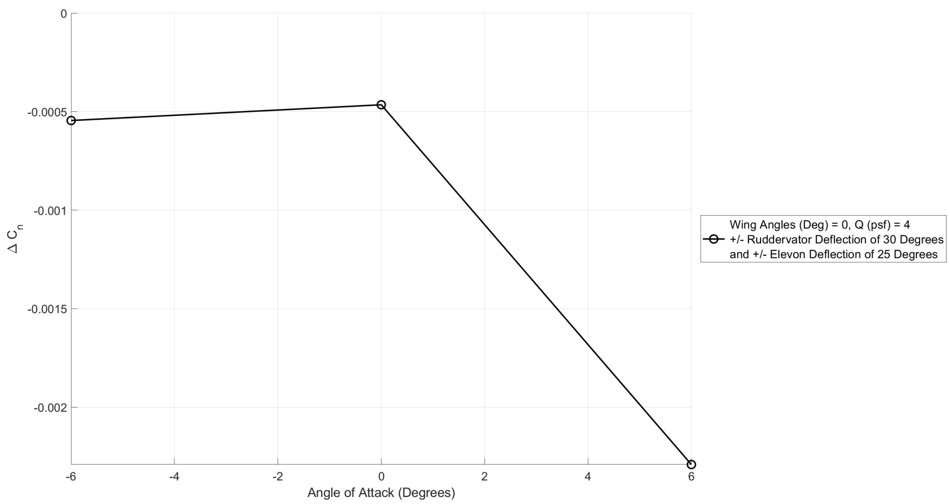

Figure 603. Forward flight trim point Δ C_n vs angle of attack for elevon and ruddervator deflection.

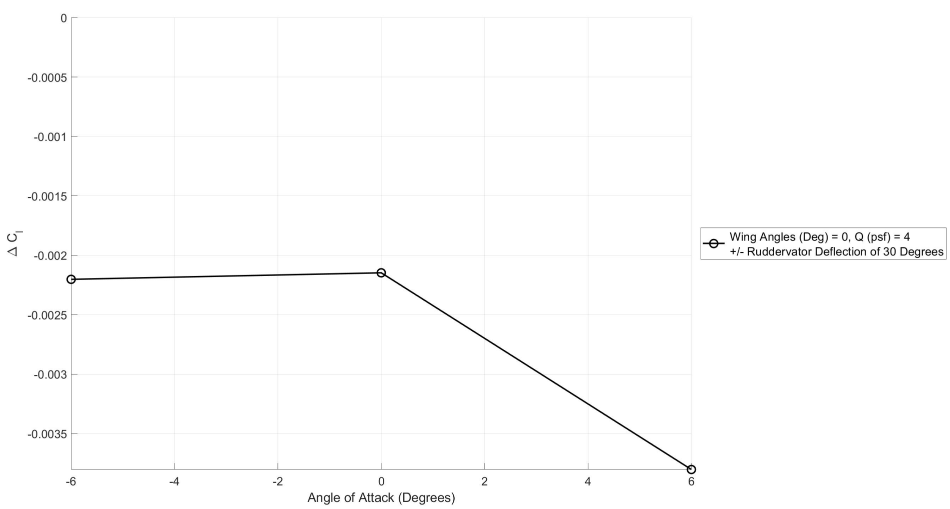

Figure 604. Forward flight trim point Δ C_l vs angle of attack for ruddervator deflection.

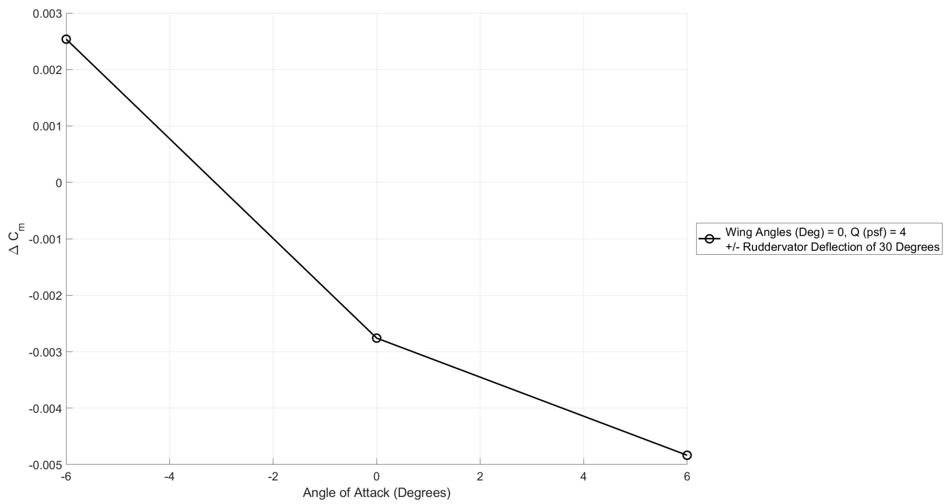

Figure 605. Forward flight trim point Δ C_m vs angle of attack for ruddervator deflection.

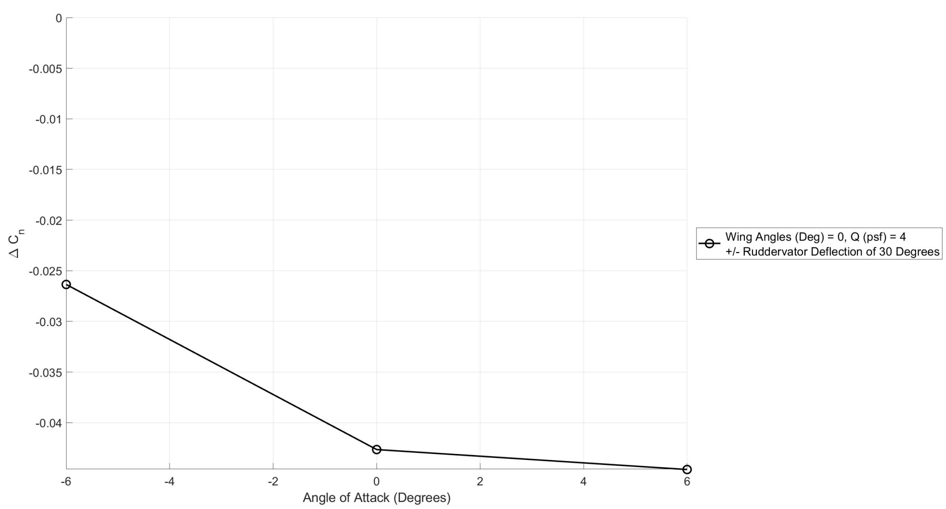

Figure 606. Forward flight trim point Δ C_n vs angle of attack for ruddervator deflection.

REPORT DOCUMENTATION PAGE	*Form Approved* *OMB No. 0704–0188*

1. REPORT DATE *(DD-MM-YYYY)*	**2. REPORT TYPE**	**3. DATES COVERED** *(From - To)*
01-06-2020	Technical Memorandum	

4. TITLE AND SUBTITLE	
Investigation of a Tandem Tilt-wing VTOL Aircraft in the NASA Langley 12-Foot Low-Speed Tunnel	**5a. CONTRACT NUMBER**
	5b. GRANT NUMBER
	5c. PROGRAM ELEMENT NUMBER
6. AUTHOR(S)	**5d. PROJECT NUMBER**
Steven C. Geuther, David D. North and Ronald C. Busan	**5e. TASK NUMBER**
	5f. WORK UNIT NUMBER 109492.02.07.01.10

7. PERFORMING ORGANIZATION NAME(S) AND ADDRESS(ES)	**8. PERFORMING ORGANIZATION REPORT NUMBER**
NASA	L–
9. SPONSORING/MONITORING AGENCY NAME(S) AND ADDRESS(ES)	**10. SPONSOR/MONITOR'S ACRONYM(S)**
National Aeronautics and Space Administration Washington, DC 20546-0001	NASA
	11. SPONSOR/MONITOR'S REPORT NUMBER(S) NASA/TM–2020–5003178

12. DISTRIBUTION/AVAILABILITY STATEMENT
Unclassified-Unlimited
Subject Category
Availability: NASA STI Program (757) 864-9658

13. SUPPLEMENTARY NOTES
An electronic version can be found at http://ntrs.nasa.gov.

14. ABSTRACT
The emerging Urban Air Mobility market imposes new design requirements on aircraft, including the ability to have vertical take-off and landing (VTOL) capabilities with the ability to transition into fast and efficient forward flight. Industry has proposed many different vehicle configurations, which have many different challenges. A primary challenge facing many of these concepts is flight through the transition corridor from vertical to horizontal flight and back. In an effort to better understand and help improve vehicle safety in the complex transition corridors, NASA Langley Research Center has proposed to characterize the transition corridor with wind tunnel and flight tests for a variety of unmanned aircraft system sized VTOL configurations. The first vehicle of this series is the Langley Aerodrome 8 (LA-8). LA-8 is a high-risk/high-reward tandem tilt-wing vehicle with distributed electric propulsion and a partially deflected slipstream aircraft. The LA-8 vehicle has gone through a preliminary wind tunnel test in NASA Langley's 12-Foot Low-Speed Wind Tunnel. The results of the aerodynamic data collected, including the longitudinal, lateral, and directional force and moment aerodynamic coefficients, from these tests uring different phases of flight are presented

15. SUBJECT TERMS
VTOL, Transition, Wind Tunnel, UAS, UAM

16. SECURITY CLASSIFICATION OF:			**17. LIMITATION OF ABSTRACT**	**18. NUMBER OF PAGES**	**19a. NAME OF RESPONSIBLE PERSON**
a. REPORT	**b. ABSTRACT**	**c. THIS PAGE**			STI Information Desk (help@sti.nasa.gov)
U	U	U	UU	343	**19b. TELEPHONE NUMBER** ***(Include area code)*** (757) 864-9658

Standard Form 298 (Rev. 8/98)
Prescribed by ANSI Std. Z39.18